Vivek Borse · Pranjal Chandra
Rohit Srivastava *Editors*

BioSensing, Theranostics, and Medical Devices

From Laboratory to Point-of-Care Testing

Springer

BioSensing, Theranostics, and Medical Devices

Vivek Borse • Pranjal Chandra • Rohit Srivastava
Editors

BioSensing, Theranostics, and Medical Devices

From Laboratory to Point-of-Care Testing

Springer

Editors
Vivek Borse
Department of Medical Devices
National Institute of Pharmaceutical
Education and Research (NIPER)
Hyderabad, Telangana, India

Pranjal Chandra
Department of Bioscience and Biochemical
Engineering
Indian Institute of Technology
Varanasi, Uttar pradesh, India

Rohit Srivastava
Department of Bioscience Bioengineering
Indian Institute of Technology Bombay
Mumbai, Maharashtra, India

ISBN 978-981-16-2781-1 ISBN 978-981-16-2782-8 (eBook)
https://doi.org/10.1007/978-981-16-2782-8

This Springer imprint is published by the registered company Springer Nature Singapore Pte Ltd.
The registered company address is: 152 Beach Road, #21-01/04 Gateway East, Singapore 189721, Singapore

Contents

About the Editors

Vivek Borse is working as a DST INSPIRE Faculty at the Department of Medical Devices, National Institute of Pharmaceutical Education and Research (NIPER), Hyderabad, Telangana, India. Earlier he was associated with the Centre for Nanotechnology, Indian Institute of Technology (IIT) Guwahati, Assam, India. He is a Graduate in Pharmacy with Gold Medal and University First Rank from North Maharashtra University, Jalgaon, Maharashtra. He has completed M. Tech. (Pharm.) from the National Institute of Pharmaceutical Education and Research (NIPER), Mohali. Further, he has completed PhD from the Department of Biosciences and Bioengineering, IIT Bombay, Mumbai. His thesis titled "Nanodiagnostics for Orthopedic Implant-associated Infection" was chosen for the "Award for Excellence in Thesis Work" for the year 2016–2018 for outstanding research contributions in PhD. The award was presented to Vivek Borse by the Hon. Prime Minister of India, Mr. Narendra Modi in the 56th Convocation of IIT Bombay.

Vivek Borse has published his research work in more than 20 international journals, 5 book chapters, and a book. He has expertise in the field of nanobiotechnology, nanodiagnostics, lateral flow immunoassay (LFIA), point-of-care devices, nanomaterials, polymers, biomaterials, novel drug delivery systems, and biomedical engineering. His research area includes an interdisciplinary field of nanotechnology, biotechnology, and pharmacy providing pertinent solutions to healthcare.

Pranjal Chandra is an Assistant Professor at the School of Biochemical Engineering, Indian Institute of Technology (BHU), Varanasi, India. He earned his Ph.D. from Pusan National University, South Korea and did post-doctoral training at Technion-Israel Institute of Technology, Israel. His research focus is highly interdisciplinary, spanning a wide range in biotechnology, nanobiosensors, material engineering, and nanomedicine. He has designed several commercially viable biosensing prototypes that can be operated for onsite analysis for biomedical diagnostics. He has published 10 books on various aspects of biosensors/ medical diagnostics from IET London, Springer Nature, and CRC Press, USA. He has also published more than 100 original research articles in journals of high repute. He is the recipient of many prestigious awards, coveted honors, and fellowships such as DST Ramanujan fellowship (Government of India); Early Carrier Research Award (ECRA) (DST, Government of India); BK-21 and NRF fellowship, South Korea; Technion Post-Doctoral Fellowship, Israel; Nano Molecular Society India Young Scientist Award; Biotech Research Society India (BRSI) Young Scientist Award; Young Engineers Award 2018; ACS/Elsevier Outstanding Reviewer Awards; Highly Cited Corresponding authors in the Royal Society of Chemistry (RSC), Cambridge, London; Top 10% cited article in the General Chemistry Section RSC Journal, Cambridge, London; Gandhian Young Technology Innovation Award (GYTI) 2020, Selected as Member of National Academy of Sciences (MNASc), India, etc. He is also listed among the World's Top 2% Scientist in a report by Stanford University, USA.

Rohit Srivastava is working as a Himanshu Patel Chair Professor and Head, Department of Biosciences and Bioengineering at the Indian Institute of Technology, Bombay. He has been awarded the prestigious Dr. Shanti Swarup Bhatnagar Prize 2021 for Medical Sciences. He completed his Bachelor of Engineering in Electronics Engineering from VNIT, Nagpur in 1999 and Master of Science and a Ph.D. in Biomedical Engineering from Louisiana Tech University, Ruston, LA, USA. His specialization lies in POC diagnostic

devices, biomedical microsystems devices (MEMS), nanoengineered biosensors, photothermal therapy in cancers, and nanoengineered orthopedic applications. His lab, in collaboration with Biosense Technologies Pvt. Ltd., has developed and commercialized "UChek," a portable urine analysis system based on the mobile platform and has also made a low-cost reader for quantitatively analyzing urine dipsticks for which he has received the DBT Biotech Process and Product Commercialization Award 2015 and the OPPI Young Investigator Award 2014. He has been awarded the prestigious Vasvik Award 2013 for Biological Sciences and Technology for Suchek, an indigenous, accurate, low-cost glucometer supported by the Indian Council of Medical Research. He is also the recipient of the prestigious Tata Innovation Fellowship Award from DBT for his translational work on diagnosing orthopedic implant-related infections. He has recently been awarded the prestigious DBT National Bioscience Award for translating technologies from the lab. He has recently been awarded the prestigious NASI Reliance Industries Platinum Jubilee Awards 2018 for Application Oriented Innovations in Physical Sciences. He has published more than 130 research articles in the journals of high repute and 100 international conference proceedings. He has been awarded INAE Abdul Kalam Technology Innovation Fellowship and elected as Fellow of National Academy of Science, India, Fellow of Royal Society of Chemistry (FRSC), and Fellow of Royal Society of Biology (FRSB), London.

Chapter 1
Gold Nanoclusters as Emerging Theranostic Interventions for Biomedical Applications

Kritika Sood and Asifkhan Shanavas

1.1 Introduction

Many recent advances in nanotechnology have provided a vast pool of functional nanomaterials that have been employed for various combinatorial biomedical applications like therapeutics, imaging, and diagnostic probes [1]. The advancements in the field of instrumentation and biosensing have led to highly sophisticated diagnostic techniques such as wearable sensors and smart-phone based point of care (POC) devices that have widely revolutionized the conventional biosensing platforms to aid portable and bed-side diagnosis [2]. Various nanomaterials such as quantum dots, carbon dots have recently been used utilized for synergistic theranostic applications. However, due to the leakage of toxic heavy metals in vivo and accumulation in different organs, these nanomaterials have limited applications [3]. Thus, the need of the hour is to develop highly biocompatible, photostable, and renal clearable materials for efficient biotracking and therapeutic purpose.

One such novel class of luminescent nanomaterials is the metallic nanoclusters (NCs), which have prospered tremendously over the last decades motivated by the increasing interest in studying the evolution of opto-electronic properties from the atomic level to the bulk solids as their size increases. Metal nanoclusters (NCs) which act as an intermediary link between the larger plasmonic metal nanoparticles and isolated metal atoms to form ultrasmall nanostructures (size usually <2 nm) are composed of a few tens or several hundreds of atoms and display a unique set of opto-electronic properties due to their strong quantum confinement effects [4]. Nanoclusters have a core–shell structure wherein the core metal atoms are

K. Sood · A. Shanavas (✉)
Inorganic & Organic Nanomedicine (ION) Lab, Institute of Nano Science and Technology, Mohali, Punjab, India
e-mail: kritika.ph17227@inst.ac.in; asifkhan@inst.ac.in

V. Borse et al. (eds.), *BioSensing, Theranostics, and Medical Devices*,
https://doi.org/10.1007/978-981-16-2782-8_1

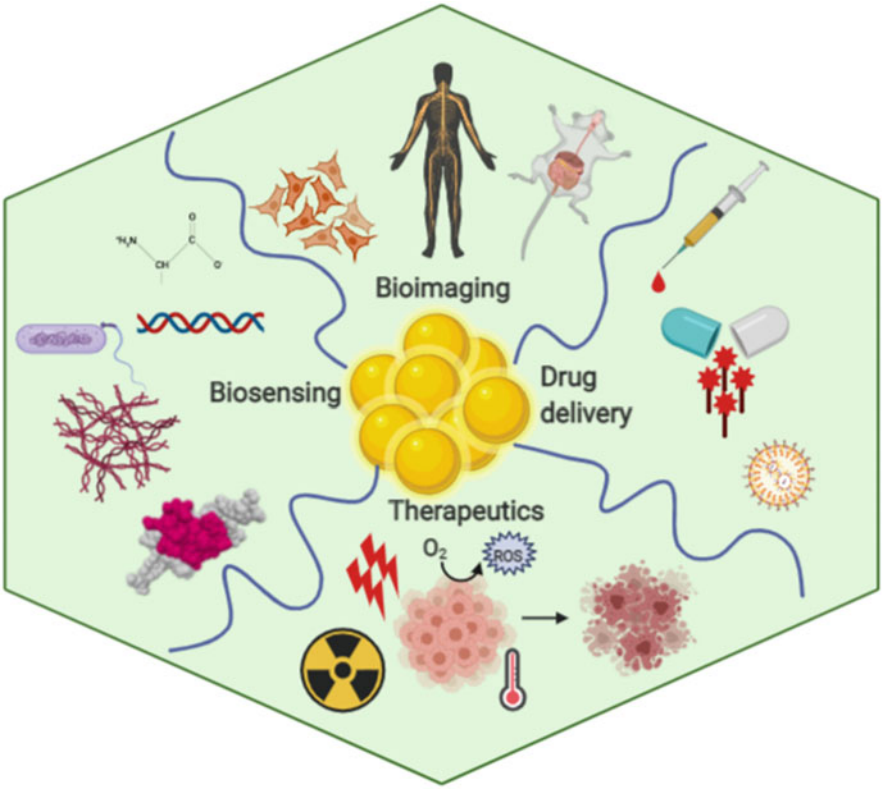

Fig. 1.1 Different biomedical applications of gold nanoclusters

surrounded by organic ligand groups that act as protecting agents to stabilize the metal core. The size of the nanoparticles limits the free movement of conduction electrons to the metal surface, which determines their size dependent optical characteristics SPR. However, as the size of these metal nanoparticles decreases to the Fermi wavelength of conduction electrons, as in the case of NCs, the band structure quantizes from continuous energy bands in nanoparticles, to discontinuous bands and breaks into discrete HOMO-LUMO energy levels. These quantized energy levels allow unique photoluminescent, electronic, and catalytic properties of metal NCs.

In the past few years, various noble metal NCs with different metallic cores (Au, Ag, Pt, Cu) have found substantial uses in theranostic applications due to their highly desirable properties [5–7]. Interestingly, the use of luminescent gold nanoclusters (AuNCs) has gained tremendous attention in various biomedical fields such as biosensing, therapeutics, and bioimaging which can be accredited to their high biocompatibility, relatively higher cellular uptake, higher renal clearance for in vivo applications, ease of conjugation for imparting various functionalities, relatively higher quantum yield than organic dyes, tunable emission in visible and IR region, and good photostability [5, 8].

This chapter mainly focusses on the role of gold nanoclusters in the field of biosensing and therapeutics for biomedical applications (Fig. 1.1). Additionally, various strategies employed for biosensing by gold nanoclusters along have also been discussed.

1.2 Synthesis of AuNCs

Various strategies have been employed for development of water-soluble; highly fluorescent AuNCs with high biocompatibility and quantum yield for their use in biomedical applications. Due to their ultrasmall size, the metallic core atoms can agglomerate to form larger nanoparticle, hence, the use of different ligands as stabilizing/capping agents is essential to stabilize the nanoclusters (Fig. 1.2). The two main techniques used for synthesis of AuNCs are:

(i) **Thiol-based approach**—Due to high strength of Au–S bonds, thiolated ligands have been successfully employed for the synthesis of AuNCs. The size, surface charge and hence their photoluminescent properties are dependent upon the nature of the thiolated molecule used. For e.g., Glutathione (GSH), 3-mercaptopropionic acid (MPA), D-penicillamine (DPA), 11-mercaptoundecanoic acid (11-MUA), etc. [9–12]. 11-MUA and DPA have been employed as both reducing and stabilizing agents, while GSH and MPA have been used along with different reducing agents such as sodium borohydride and THPC (tetrakis (hydroxymethyl) phosphonium chloride) for synthesis of AuNCs.

(ii) **Template-assisted approach**—This approach employs using various biomacromolecules (such as DNA, carbohydrates, etc.), peptides, proteins, enzymes, polymers, and dendrimers for scaffold/template based synthesis of AuNCs [13–17]. These biomolecules are generally employed along with a reducing agent for complete reduction of Au III to Au 0. The as synthesized highly biocompatible AuNCs are however embedded inside the scaffold mole-

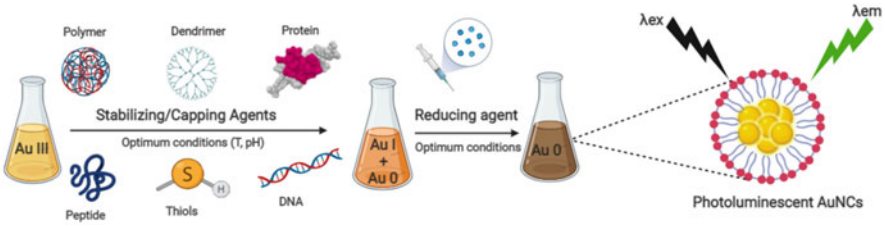

Fig. 1.2 Schematic depicting synthesis of AuNCs using different stabilizing/capping agents

cules which may lead to their decreased fluorescence and comparatively larger hydrodynamic size.

1.3 Gold Nanoclusters as Biosensors

Biosensors are precise and powerful analytical devices utilizing one or more biologic sensing elements with a transducer for specific detection of certain target bioanalyte (s) of interest. With the advent of nanomaterials, the nanobiosensors have employed for use in wide range applications such as medical diagnostics, biomedicine, drug discovery, food safety, environmental monitoring, defense as well as security. Nanobiosensors based on AuNCs have a great potential in the field of optical detection of sensitive bioanalytes due to their various unique properties such as larger Stokes shift, higher emission rates, water solubility, and excellent biocompatibility for both in vitro and in vivo sensing applications. The main strategies employed for biosensing via AuNCs as well as the recent advances of AuNCs in biosensing applications would be discussed in the later part of this chapter.

(a) Elements of a Biosensor

To better understand how a NC acts as a nanobiosensor works, it is important to highlight the mechanism behind and how the different components of a biosensor act

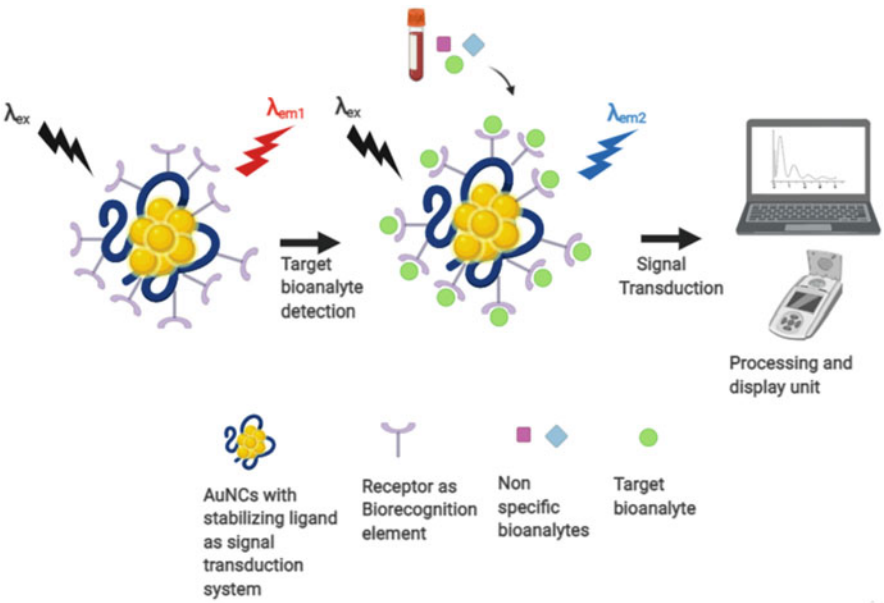

Fig. 1.3 Schematic of AuNCs as biosensors depicting different elements

in coherence to detect a readable output signal (Fig. 1.3). The major components of any biosensing system include the following:

1. **Bioanalyte**—It is the sample to be detected for specific detection by the biosensor (e.g., target bioanalytes from blood, urine, CSF, serum, etc.)
2. **Biological Recognition Element (Bio-receptor)**—which specifically detects the target sample or bioanalyte such as antibodies and aptamers.
3. **Signal Transducer System**—which records the physiochemical interaction (electrochemical, optical, mass and acoustic, etc.) between the bio-receptor and the target bioanalyte and converts the change occurred in the form of a measurable electric signal.
4. **Detector or Processing Unit**—which detects and processes the electrical signal into logical form and acts a as a graphical user interface for better understanding of system by the user.

Fluorescent AuNCs as biosensors function by capturing the change in their luminescent signals, for instance, the change in wavelength (Stokes shift) or in fluorescent intensity, to respond to the bioanalyte specifically and with an acceptable limit of detection (LOD). The interaction of fluorescent nanoclusters' ligand or core with the bioanalyte may lead to different phenomena such as charge transfer, electrostatic interactions, aggregation of NCs, or Förster resonance energy transfer (FRET) amongst various other possibilities, which may lead to a change in their properties thereby affecting the luminescent behavior. This change of luminescence is leveraged upon heavily for optical sensing, thereby bringing in light the promising role of fluorescent AuNCs as biosensors.

The biosensing efficiency of a system relies significantly on their specificity of interaction with the target bioanalyte. In a typical AuNC based biosensor, the surface functionalized ligand molecule acting as a bio-recognition element and the fluorescent AuNCs core acting as physicochemical transducer are the two intimately coupled parts responsible for producing an optical fluorescent signal upon interaction with the target bioanalyte. The functionalization of AuNCs via different strategies such as ligand exchange or conjugating with specific biomolecules (e.g., antibodies or aptamers) aid in selective bio-interaction that plays a crucial role for ultrasensitive detection for an efficient biosensing system. Therefore, selecting an appropriate functionalization or bioconjugation strategy is an important step to build a highly sensitive biosensor. With the rapid development of atomically precise NCs via facile synthetic procedures, the design of AuNCs has been made versatile to cater to the needs of a range of biosensing requirements. Therefore, over the years, the role of AuNCs has evolved rapidly as simple, highly sensitive, robust and integrated minimally sized biosensors for wide array of environmental and biomedical applications.

(b) Main Strategies for Biosensing Via Fluorescent AuNCs

Au NCs have been used in biosensing applications broadly based on either exclusively or a combination of the following main strategies:

1. Structure based Photoluminescent Sensing

The detection of analytes based on optical responses such as the absorption and the emission properties of NCs has been the most widely used sensing mechanism. However, the luminescent properties of NCs are not completely understood at the molecular level yet, since its photoluminescence properties depend on many factors such as cluster size surface ligands and cluster assembled structural changes, etc. Some of these mechanisms would be

(i) Size Effect

Due to the quantum confinement effect of metal NCs as their size approaches Fermi wavelength of electrons, the continuous energy band becomes discrete and the transition from metal to molecule ensues. Atomically precise metal NCs have been known to possess characteristic absorption characteristics that are distinguishable from each other based on their absorption profiles. It has been reported that as the size of the cluster decreases, the spacing between the discrete energy states increases which leads to a blue shift in the emission of the smaller NCs as compared to their larger counterparts [18]. Similarly, when the luminescence of Au NCs is solely attributed to the metal centered electron transition, the emission of Au NCs has been observed to undergo a red shift upon increasing their size and PL quenching in the visible region as the cluster size further increases (Fig. 1.4a) [19]. Such a size dependent quenching and shifting of emission wavelength is an important employable characteristic for biosensing mechanisms.

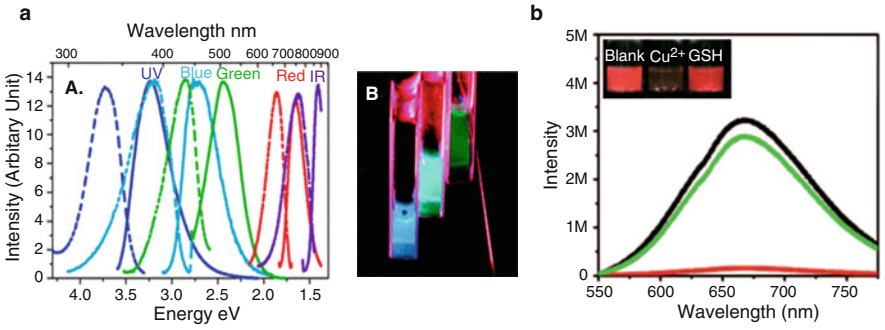

Fig. 1.4 Structure based Photoluminescent sensing: (**a**) Excitation (dashed) and emission (solid) spectra of different sized gold nanoclusters with UV (Au5), blue (Au8), green (Au13), red (Au23), and near IR (Au31) emission. The enclosed image shows Au5, Au8, and Au13 solutions (from left to right) under long-wavelength UV lamp irradiation. Reprinted with permission from Ref. [19]) © 2004 American Physical Society-PRL. (**b**) Recovery of the photoluminescence intensity of the BSA–AuNC+Cu^{2+} mixture after the addition of glutathione (GSH; black = cluster, red = cluster +Cu^{2+}, and green = cluster+Cu^{2+} +GSH). Inset: the corresponding photographs. Reprinted with permission from Ref. [20]) © 2010 Wiley

(ii) **Aggregation Induced Emission**

Aggregation Induced Emission (AIE) or Aggregation Induced Emission Enhancement (AIEE) is a self-assembly governed photoemission process depicted by various nanoclusters which has been exploited for design of novel biosensors. Luminescence of NCs depends on its surrounding environment. Various mechanistic studies have revealed that restriction of intramolecular motion (RIM), which includes both rotation (rotational intramolecular rotation or RIR) and vibration (rotational intramolecular vibration or RIV), in the aggregated state is the main cause for the AIE effect [21, 22]. AIE-type NCs have considerably enhanced PL in aggregated states. AuNCs have also recently emerged as AIEgens and have been employed for ultrasensitive and highly sensitive detection of amino acid, lysine. The AIE-active dual-emitting fluorescent GSH–AuNCs/lysine complex was used to ratiometrically detect the analyte molecule without the need of any conjugated fluorogen [23]. Alternatively, the inhibition of assembly of NCs to block fluorescence could also be employed as a sensing mechanism for analyzing bioanalytes. A similar system was adopted for the detection of heparin, an anticoagulating agent using mesoporous silica nanoparticles conjugated with gold nanoclusters (MSN-AuNCs) [24]. The electrostatic interaction between negatively charged heparin and positively charged MSN which inhibited the assembly of AuNCs; leading to de-enhancement in fluorescence leading to sensitive detection of heparin.

(iii) **Aggregation Induced Quenching and Chelation for "Turn ON-OFF" Sensors**

The recovery of photoluminescence on addition of chelators such as EDTA or divalent ions like Ca^{+2} can be used as a "turn on" sensor for various important biomolecules. Glutathione is one such rather important antioxidant biomolecule found in our body used to combat free radicals and reactive oxygen species and plays a pivotal role in HIV expression and cancer therapy. The luminescence of the BSA–AuNC has been exploited as a "turn off" sensor for Cu^{2+} ions and a "turn on" sensor for glutathione [20]. The interaction of Cu^{+2} ions with the BSA shell of the cluster results in the mediation of protein-protein interaction leading to the aggregation of clusters into larger sized nanostructures and thereby quenching their luminescent effect. This is another type of self-assembly governed photoemission phenomenon called the **aggregation induced quenching (AIQ) effect.** In this case, the reversible nature of this AIQ effect was observed upon adding GSH as a chelator. Since GSH is a better chelator of Cu^{+2} than BSA, hence, upon interaction with glutathione, the Cu^{+2} ions form a complex with GSH. Subsequently, this leads to deaggregation of BSA–AuNCs and their full luminescent recovery (Fig. 1.4b).

(iv) **Ligand Effect**

Ligands play a very significant role in the formation as well as stabilization of NCs, preventing the core metal atoms from aggregation and maintain their size dependent photoluminescent properties [25]. However, the surface ligands of AuNCs not only act as capping agents but also affect the luminescence of AuNCs

by transferring of charge from thiolated surface ligands to the gold core. This charge transfer from S atom of thiolated ligand to the Au metallic core is called the ligand-to-metal charge transfer (LMCT) effect. While the Au–Au aurophilic interactions, some Au^+ complexes containing thiolated ligands can also result in the ligand-to-metal-metal charge transfer (LMMCT) effect. Both LMCT and LMMCT produce luminescence which has a longer lifetime than luminescence occurring from electronic transactions in metal core. The charge transfer through LMCT/LMMCT also depends upon the electron donation ability (S atom to Au/S atom to Au–Au) of the ligand group [26].

The employment of ligands with stronger electron donation capability would result in enhancement of the fluorescence of the AuNCs. Therefore, ligand exchange of AuNCs with electron-rich atoms or groups has been found as a promising technique to enhance the fluorescence and thereby its quantum yield (QY) for sensitive detection of bioanalytes. Lots of researches have used this strategy for various applications like biolabeling and bioimaging in addition to biosensing applications.

(v) **Functionalization-based Biosensing Strategy**

Functionalization of fluorescent AuNCs further broadens their perspective for biomedical applications. Passivation of AuNPs interface by biomolecule conjugation has been extensively studied for increasing biocompatibility as well as imparting functionality for various clinical and biomedical applications [27]. Nano-surface engineering of sensing probes by functionalization is an important aspect to increase the specificity and sensitivity of any biosensor system [28]. The main strategies for functionalization include ligand exchange, bioconjugation, and noncovalent interactions [29]. Bioconjugation of AuNCs with specific biomolecules that could target specific cell types for receptor mediated endocytosis. For instance, folic acid (FA) is a commonly used conjugate for specifically targeting cancer cells with overexpressed folate receptors. Ultrasmall FA conjugated BSA–AuNCs loaded with anticancer drug doxorubicin (DOX) have been developed for highly targeted FA–AuNC–DOX for synergistic folate receptor positive tumor NIR fluorescence imaging and therapy [9]. Apart from biomolecules, various antibodies and aptamers have also been used for functionalization of AuNCs for highly specific and sensitive biosensing strategies [15, 30].

2. **Electrochemiluminescence-based Sensing**

Electrochemiluminescence (ECL) refers to the phenomenon of luminescence caused due to a high-energy electron transfer reaction between electrogenerated species on the surface of electrodes during a chemical reaction, which possesses the advantages of both the electrochemical and chemiluminescent methods. As compared to PL, it provides lower cost and improved signal to noise ratio. ECL produces luminescence only under electrochemical excitation, unlike chemiluminescence, and thus exhibits high sensitivity and fast response. ECL has also been employed in field of immunosensing assays and medical diagnostics for Alzheimer's and Parkinson's disease [31, 32]. AuNCs and CdTe nanocrystals have been

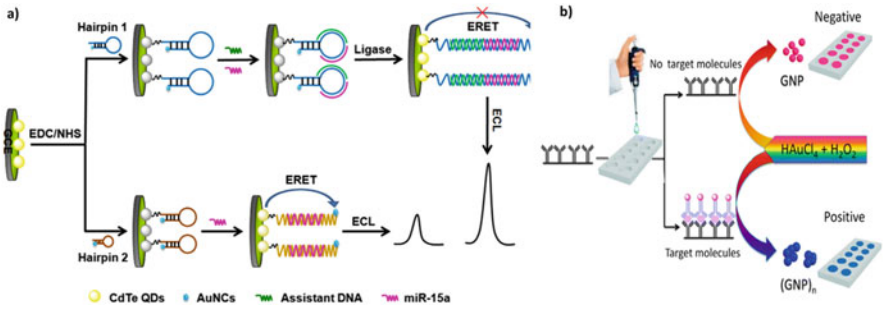

Fig. 1.5 Electrochemiluminescence and enzyme mimetics based sensing: (**a**) Schematic illustration of highly selective detection strategy of miRNA based on the distance-dependent ERET between CdTe nanocrystals and Au nanoclusters. Reprinted with permission from Ref. [33] ©2014 Elsevier. (**b**) Schematic representation of the plasmonic nanosensor. In sandwich structure, the target molecule is anchored to the substrate by capture antibodies and recognized by other antibodies labeled with AuNCs. Reprinted with permission from Ref. [34]) © 2016 American Chemical Society

employed for a distance-dependent electrochemiluminescence resonance energy transfer (ERET) system based sensing platform for highly selective "turn on" detection of microRNA by employing the ligase enzyme [33]. The AuNCs functionalized hairpin DNA electrode when conjugated with CdTe nanocrystals resulted in a strong interaction leading to the ECL quenching of CdTe. In the presence of microRNA and assistant DNA, the enzyme ligase ligates them both to form a DNA–RNA heteroduplex and the subsequent recovery of electrochemiluminescence due to blocking of ERET; thereby serving as a "turn on" sensor for miRNA (Fig. 1.5a).

3. Enzyme Mimetics-based Sensing

Nanozymes are next generation artificial mimetic enzymes which can catalyze a specific substrate reaction with catalytic efficiency and enzyme kinetics similar to natural enzymes, however, are more stable and resist physiological changes (like strong acid/basic pH or extreme temperature), unlike naturally occurring enzymes.

Interestingly, gold nanoclusters have been reported to possess intrinsic enzyme mimetic properties such as peroxidase (POD), catalase (CAT), and Glucose oxidase (GOD) which have been employed for various biomedical applications [35–37]. By integrating the enzymatic properties for catalytic functions and the characteristic photoluminescence feature of the NCs, various groups have studied these multifunctional NCs as nanoprobes for biosensing applications. For instance, BSA–AuNCs have been found to convert hydrogen peroxide into hydroxyl radicals. This POD like activity of BSA–AuNCs has been employed extensively in the field of biosensing. BSA–AuNCs have been employed in ELISA immunoassay for the design of an ultrasensitive plasmonic nanosensor for naked eye read out of multiple ultratrace bioanalytes such as protein avidin, thyroid hormone T3, cancer antigen

CA15-3, and methamphetamine (MA) which is a small molecule and abused drug [34]. The POD mimetic AuNCs were conjugated on the outer layer antibody to catalyze hydrogen peroxide decomposition which was used to reduce HAuCl4 into AuNPs for colorimetric naked eye detection of bioanalytes. While the AuNCs catalyze the decomposition of H_2O_2, the AuNP formation requires H_2O_2 to give a colorimetric detection in the presence of even ultratrace amounts of analytes (Fig. 1.5b). The Limit of Detection (LOD) was ultrasensitive towards MA standing at ~2.3×10^{-18} mg/mL.

(c) Bioanalyte Sensing with AuNCs

AuNCs have a great potential to function as sensitive optical reporters for sensitive detection of various bio macromolecules owing to their characteristics like strong photoluminescence, good water solubility, large stokes shift, and high photostability. Therefore, by utilizing these properties and the strategies of biosensing discussed previously, we will review the role of AuNCs as biosensors in this section.

(i) **Nucleic acids**

The detection of nucleic acid is an essential diagnostic tool for a number of harmful pathogens like bacteria and viruses, genetic mutations, and forensic applications. AuNCs have been exploited for detection of DNA by numerous electroluminescent based sensing strategies. AuNCs and CdTe nanocrystals employed for electrochemiluminescence resonance energy transfer (ERET) system based sensing platform for detection of microRNA by employing ligase have been explained in electrochemiluminescence based sensing strategy section (Fig. 1.5a) [33]. HIV DNA has been detected using a novel electrochemical biosensor using graphene stabilized gold nanoclusters (GR/AuNCs) based conductive platform with Exo III-assisted DNA recycling amplification based on aptamer rich in cytosine as a capture probe [38]. In the presence of target DNA, the cytosine rich probe was digested due to Au–N bond between cytosine and gold nanoclusters and the signal was decreased giving rise to an ultrasensitive signal-off electrical biosensor with limit of detection of 30 aM which allows early detection of AIDS in patient blood detected with HIV (Fig. 1.6a). Another electrochemical DNA biosensor designed by using streptavidin-horseradish peroxidase enzyme scaffolded gold nanoclusters (SA-HRP AuNCs) for highly specific and ultrasensitive detection of *Phanerochaete chrysosporium* manganese peroxidase gene using PCR and restriction endonuclease digestion with a LOD of 8.0×10^{-18} M [40]. In another interesting study, UV light assisted ssDNA (single stranded) consisting of polyadenosine stabilized A_{30}-AuNC-nucleation sequence and a hybridization sequence along with a combination of SYBR Green (SG), a double strand chelating dye, were used to design a ratiometric fluorescent probe for highly specific and sensitive detection of nucleic acid target sequences in human serum sample [39]. The UV light played a dual role of reducing Au^{+3} to Au^0 and decomposition of citrate ions as shown in Fig. 1.6b. Under single excitation conditions, the A_{30}-AuNC/SG-bearing ssDNA and perfectly matched DNA resulted

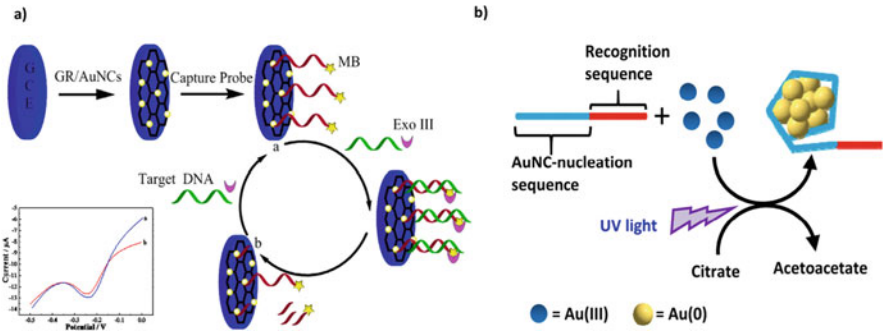

Fig. 1.6 Nucleic Acid sensing by AuNCs: (**a**) Schematic illustration of the proposed biosensor fabrication process wherein the initial signal obtained from capture probe and the final signal after incubation with target DNA and Exo III. Reprinted with permission from Ref. [38]) © 2015 American Chemical Society. (**b**) Schematic of ratiometric detection of specific nucleic acid target via the combination of SG and AuNC-bearing ssDNA. Reprinted with permission from Ref. [39]) © 2015 American Chemical Society

in fluorescence emission of 475 nm and 525 nm, respectively, to ratiometrically sense nucleic acid targets with LOD of 0.3 nM.

(ii) **Proteins**

Sensitive and specific detection of certain biomarkers, a special class of proteins, and their precise quantification is an important parameter for early diagnosis of various diseases as well as in evaluation of drugs and therapeutics. The functionalization of selective receptor molecules such as carbohydrates, antibodies, and aptamers on the surface of AuNCs has been used for sensing of various proteins. It takes into account the structural diversity and complexity of target proteins by incorporating the bio-recognition characteristic to target proteins as well as the exceptional optical properties of NCs. Triulzi et al. utilized the electrostatic interaction between the PAMAM-conjugated AuNCs and polyclonal goat derived antihuman IgG antibody for detection of the human IgG antigen via immunoassay [15]. Upon the electrostatic interaction, a quenching of fluorescence of AuNCs is observed based upon formation of antigen–antibody immunocomplexes thereby resulting in decreased fluorescence intensity. Chang et al. employed breast cancer marker protein platelet-derived growth factor AA for conjugation with AuNCs (PDGF AA-AuNCs) as fluorescent donor along with thiol-derivative PDGF binding aptamers modified AuNPs (Apt-AuNPs) as quencher, to develop a competitive fluorescence quenching assay for analyzing proteins PDGF and PDGF receptors [30]. The interaction between PDGF AA-AUNCs and Apt-AuNPs quenched the PL intensity of PDGF AA-AuNCs due to high affinity between Apt and PDGF. The PL quenching was suppressed in presence of PDGF and PDGF α-receptor due to competitive between PDGF and Apt-AuNPs which can be employed as a fluorescence "turn on" sensing mechanism for proteins PDGF and PDGF receptors with LOD of 80 pM and 0.25 nM, respectively. Protein kinases (PK) phosphorylate the

proteins playing a major role in cellular pathways especially those involved in signal transduction and hence their activity needs to be highly regulated for diagnosis of various diseases. Peptide template AuNCs have been used as fluorescent probes for highly sensitive detection of protein kinase activity based on phosphorylation and cleavage by carboxypeptidase Y [41]. Another peptide–AuNC was used for highly sensitive detection of another PK—casein kinase II (CK2) based on the aggregation quenching mechanism with LOD of 0.027 unit mL^{-1} [42]. Trypsin is another important digestive protease vital for the pancreatic exocrine regulation. Highly sensitive detection of trypsin in human urine samples by using BSA–AuNCs by a concentration dependent fluorescent quenching strategy has also been carried out [43]. Additionally other important proteins such as **IL-6** [44], **Human IgE** [45], **GST tagged proteins** [46], **human serum proteins** [47], **metalloproteinase** [48], **alkaline phosphatase** [49], **hemoglobin** [50], **ricin** [51], amongst various others have also been detected using AuNCs as biosensor.

(iii) **Small biomolecules**

Amino acids are involved in a myriad of biological processes such as protein synthesis, intracellular signaling, and homeostasis, Hence, any changes in their physiological levels manifest in various diseased conditions. Thiol containing amino acids such as cysteine (Cys) and homocysteine (Hcy) have a greater affinity towards AuNCs and can increase their stability by acting as protecting groups as well as influence their optical properties. The deficiency of Cys and Hcy is known risk factors in metabolic disorders and cardiovascular and neurodegenerative disorders. A ratiometric fluorescent probe BSA–AuNCs conjugated with NBD (7-nitro-2,1,3-benzoxadiazole) was developed for highly selective intracellular monitoring and imaging of Cys and Hcy in HeLa cells [52]. The AuNCs–NBD in presence of Cys and Hcy caused cleavage of thioether bond and generated free NBD which emitted at 540 nm while the red emission of AuNCs remained constant thereby ratiometrically determining Cys and Hcy with high specificity over GSH and other amino acids.

Another ratiometricfluorescence assay based on fluorescence quenching and enhancement effect of BSA–AuNCs was used to construct a sensor array for the fluorescent determination of amino acids Asp, Cys, and His through interaction with bound metal ions [53]. His-stabilized AuNCs have also been employed as "Turn On/Off sensors" for sensitive and selective detection of Cu^{+2} ions and His by utilizing the peroxidase-like nanozyme activity of AuNCs [54]. Upon the interaction of His–AuNCs with Cu^{+2} resulted in fluorescence quenching and upon subsequent addition of His underwent a fluorescent recovery due to high stability of His/Cu^{+2} complexation. The LOD for Cu^{+2} ions and His was 0.1 and 20 nM, respectively.

Hydrogen peroxide (H_2O_2) is another important analyte playing key roles in host defense, various oxidative biosynthesis, and signaling pathways. It is involved in various enzymatic reactions such as peroxidases and catalases and has been used in quantitative assessment of various enzymes and substrate molecules. 11-mercaptoundecanoic acid (polymer) stabilized AuNCs were developed by Shiang et al. for highly sensitive and selective detection of H_2O_2 and glucose based on luminescence quenching mechanism [12]. Glucose upon reaction with

enzyme glucose oxidase resulted in generation of H_2O_2 which upon interaction with the 11-MUA AuNCs leads to glucose detection (LOD = 1 μM). This is because the 11-MUA bound to AuNCs via the Au–S bond was oxidized in presence of H_2O_2 resulting in PL quenching leading to wide dynamic range detection (100 nM–1.0 mM) with LOD of 30 nM for H_2O_2 and subsequently for glucose. HRP functionalized AuNCs were first employed by Wen et al. for the highly sensitive detection of H_2O_2 with LOD of 30 nM by utilizing biomineralization process [55]. The HRP protein was used as a template for synthesis of fluorescent AuNCs which underwent a quenching mechanism upon the addition of H_2O_2 indicating the active enzymatic activity of HRP in the HRP–AuNCs.

Glucose is one of the most common bioanalytes in blood, urine samples which is essential for diagnosis of conditions like diabetes and hypoglycemia. The NCs have dual advantage of enzymatic activity and luminescence property which have been incorporated synergistically as a novel sensing mechanism. The enzymatic determination of glucose via fluorescent AuNCs seems to be the most important method of choice for highly sensitive and quick detection of glucose levels in body. BSA–AuNCs have been employed for glucose oxidase (GO_x) enabled highly sensitive determination of glucose in the range of 0.1 μM to 0.5 mM (LOD 5 μM) via similar mechanism of H_2O_2 degradation of AuNCs resulting in PL quenching mechanism as discussed above [56]. The enzyme capped GOx functionalized AuNCs were shown to be effective for linear range (2−140 μM) glucose detection with LOD 0.7 μM [37]. N-acetyl-l-cysteine-protected NAC–AuNCs were reported for Fenton reaction mediated FL quenching mechanism [57]. In presence of glucose oxidase enzyme, the glucose is converted into H_2O_2, which then using the Fenton reaction, is converted into highly toxic OH^- free radical which quenches the fluorescence of AuNCs and helps in detection of glucose with LOD 0.18 μM.

Dopamine is an important biomolecule, which functions as both a hormone and a neurotransmitter and is responsible for key roles in functioning of the CNS, cardiovascular, and renal systems of our body. Lower levels of dopamine (DA) in human body may lead to depression, hallucinations, and other various neurological disorders such as Parkinson's disease. BSA–AuNC mediated fluorometric and colorimetric dual channel probe was developed by Tao et al. for highly sensitive and selective detection of DA [58]. Upon electrostatic attachment of DA with BSA–AuNCs, the FL intensity of AuNCs increased due to photo-induced electron transfer process leading to a fluorometric detection of DA. Additionally, the peroxidase-like activity of AuNCs is inhibited in presence of DA, which was used for its highly specific colorimetric detection with LOD of 10 nM. BSA–AuNCs have also been used as Cu^{+2} mediated fluorometric "turn on" biosensors for dopamine in human serum and urine samples with LOD 0.01 μM [59]. The quenched fluorescence of BSA–AuNCs upon Cu^{+2} addition was retrieved specifically by the addition of DA over other biomolecules which can be attributed to the higher stability of the CuH_2 $(Dop)_2$ complex (Fig. 1.7). Modified BSA–AuNCs were employed to detect DA in cerebrospinal fluid (LOD 0.83 nM) via concentration dependent fluorescence quenching mechanism due to oxidation of DA into dopamine-O-quinone which accepts the electrons from BSA–AuNCs thereby leading to its fluorescence quenching [60]. A

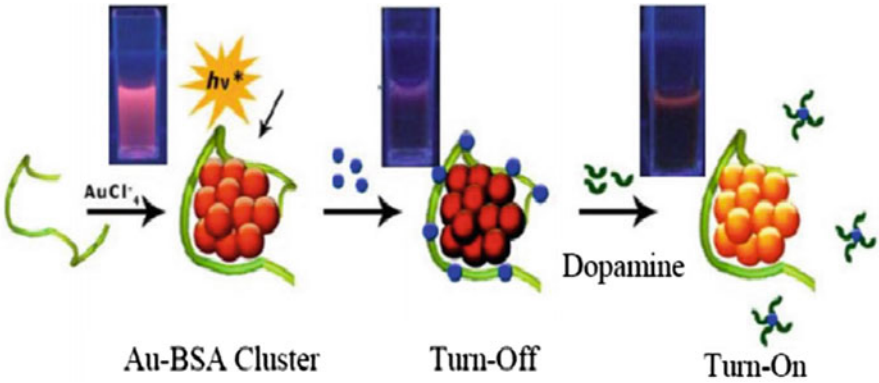

Fig. 1.7 Small biomolecule sensing by AuNCs: Schematic illustration of the Cu^{2+}–BSA–Au NCs for dopamine detection. Reprinted with permission from Ref. [59]) © 2014 Elsevier

simple label free ECL biosensor has also been developed using AuNCs immobilized on indium tin oxide (ITO) electrode along with a co-reactant $K_2S_2O_8$, for detection of DA in aqueous media possibly due to effective electron transfer from ITO conduction band towards the AuNCs [61].

Many other biomolecules that are vital for various biochemical processes and are key factors in analysis of various diseased states such as **folic acid** [62, 63], **GSH** [20, 64, 65], **urea** [66], **uric acid** [67], **ATP** [68, 69], **cholesterol** [70, 71], **heparin** [14, 72], amongst many others have also been detected by using AuNCs.

(iv) **Drug molecules**

Drug molecules screening is important for forensic analysis, anti-doping tests as well as to study the metabolic pathway of different drugs in living organisms or biological fluids. BSA–AuNCs were first utilized for simple, sensitive, and selective detection of vitamin B12 with LOD 100 ng mL^{-1} based upon the fluorescence quenching mechanism [73]. Methotrexate is an important chemotherapeutic agent and immune suppressant used for treatment of various types of cancer or rheumatoid arthritis. BSA–AuNCs were employed for sensitive detection of methotrexate by concentration dependent fluorescence quenching mechanism in human serum and urine samples [74]. Ciprofloxacin, an antibiotic, was successfully detected using BSA–AuNCs in human samples via Cu^{+2} mediated "turn off/on" mechanism. The addition of Cu^{+2} leads to fluorescence quenching of BSA–AuNCs which was then fully recovered in the presence of ciprofloxacin allowing its sensitive detection 0.4 to 50 ng mL^{-1} with 0.3 ng mL^{-1} LOD [75]. Certain drugs (e.g., ibuprofen, warfarin, phenytoin, and sulfanilamide) were screened by Yu et al. based on stabilizing effect of these drug ligands to serum albumin (BSA and HSA) from the relative fluorescence intensity of the resulting serum albumin AuNCs [76]. DNA templated AuNCs were utilized for a novel fluorescence enhancement system based on Eu^{3+}–Tetracycline complex (EuTC) for detection of tetracycline, another antibiotic, from human

urine and milk samples with LOD 4 nM [17]. This remarkable sensing system is probably promising for different biomedical applications due to its dramatically enhanced-fluorescence.

(v) **Heavy metal cations/inorganic anions**

Heavy metal contamination through occupational as well as polluted environmental sources are both predominant sources of exposure to humans and may result in asphyxia, gastro-intestinal disturbances, physical, muscular as well as neurological distress. Therefore, accurate and precise determination of heavy metal content in our body is essential for rapid and effective treatment. Hg^{+2} toxicity in aquatic and biological systems poses a severe damage risk to CNS, brain, and kidney at even very low concentrations and hence AuNCs have been extensively employed for its rapid fluorometric determination in various biological samples. Xie et al. first employed BSA–AuNCs to develop a highly selective and ultrasensitive and label free sensor for the detection of Hg^{+2} ions based on fluorescence quenching mechanism of AuNCs due to the high affinity of Hg^{+2}–Au^{+} interactions with very less LOD of 0.5 nM which is quite lower than maximum permitted Hg^{+2} levels of 10 nM as per US EPA [77]. This method can be easily transformed for a paper strip-based assay for routinely Hg^{+2} monitoring. Lin et al. developed Lysozyme VI stabilized AuNCs for the detection of Hg^{+2} and CH_3Hg^{+} in seawater based on fluorescence quenching mechanism due to the interaction between Hg^{+2}/CH_3Hg^{+} and Au^{+} on the Au surface with LOD 3 pM and 4 nM for Hg^{+2} and CH_3Hg^{+}, respectively [78]. The selectivity of this fluorescent probe was about 500x more for Hg^{+2} than any other metal ions for its ultrasensitive detection. Peptide template AuNCs were used as a highly specific biosensor for determination of intracellular Hg^{+2} via quenching mechanism with LOD 30 nM in aqueous solutions [79]. Microwave assisted dihydrolipoic acid capped DHLA–AuNCs were developed by Shang et al. for intracellular imaging and hence detection of Hg^{+2} ions in HeLa cells due to specific interactions between Hg^{+2} and Au^{+} with LOD 0.5 nM [80]. β-lactoglobulin stabilized AuNCs were synthesized for highly sensitive and selective Hg^{+2} detection in beverages, urine, and serum successfully [81]. Moreover, enzymes like esterases have also been used for templating AuNCs to rapidly detect Hg^{+2} in linear range 1–30 nM with LOD 0.88 nM for paper strip-based sensing technique [82]. Very recently electrospun fluorescent and robust fibers based on gold nanoclusters-loaded alginate were utilized as a novel, low cost, and highly selective sensors for $Hg^{+2}$and Cu^{+2} in aqueous solutions with LODs 82.14 nM and 187.99 nM, respectively [83]. 11-MUA capped AuNCs were used as "turn off" sensors for Hg^{+2} with good linearity ranging from 37.5 to 3750 nM and LOD 8.6 nM [84]. Apart from Hg^{+2}; Cu^{+2} has also been extensively investigated for determination by AuNCs for their role in environmental pollution as well as trace metal in biological systems. Lysine stabilized AuNCs (Lys-AuNCs) along with BSA–AuNCs were cooperatively used for highly selective detection of Cu^{+2} with 0.8×10^{-12} mol L^{-1} LOD [85]. Blue emitting AuNCs synthesized in presence of human hemoglobin were utilized as highly sensitive and selective fluorescent "turn off" sensors for Cu^{+2} due to formation of Hb–AuNCs/Cu^{+2} aggregates with LOD 28 Nm and "turn on" sensors for

Histidine with LOD 0.6 μM [86]. BSA–AuNCs were used as intracellular "turn off" sensors for live HeLa cancer cells with LOD 50 μM [87]. Precise atomic AuNCs with Au-510 core were used as highly sensitive detection of Pb^{+2} in drinking water over Au-590 core AuNCs with LOD 10 nM highlighting the size dependent fluorescence properties of AuNCs [88]. Cadmium is known to cause lung, kidney, and bone damage and is hence vital to detect in water and biosystem sources. Methionine capped AuNCs for selective and sensitive detection of Cd^{+2} in water and milk samples with LOD 12.25 nM based on Cd^{+2} aggregation induced enhanced emission (AIEE) strategy [89]. GSH capped AuNCs were reported as a novel single probe for discriminative detection of Hg^{+2} and Cd^{+2} via pH induced surface modulation of NCs resulting in a "turn off-on" sensor in environmental water samples [90]. Very recently, BSA–AuNCs have been utilized for sensing of two heavy metals Co^{+2} and Cd^{+2} based on their binding induced conformational change in protein AuNCs resulting in altering its fluorescence properties by inter system crossing and FRET mechanism and thereby detecting the metal ions in the wide range of 5–165 ng/mL and 20–1000 ng/mL for Co^{+2} and Cd^{+2}, respectively [91]. Additionally, Vancomycin capped AuNCs have been employed for a rapid, sensitive, and wide range detection of Fe^{+3} ions in different water sources with 1.4 μmol L^{-1} LOD [92].

Apart from heavy metals, other harmful anions such as **cyanide (CN^-)** from water samples [93], **highly reactive species from live cells** [94, 95], **sulphide (S^{-2})** [96, 97], and **nitrite (NO_2^-)** [98, 99] have also been detected from human urine and water samples using fluorescent AuNCs.

(vi) **Intracellular pH and temperature**

Temperature is one of the major parameters affecting various chemical and biological processes as well as their kinetics in vivo. pH helps regulate various cellular processes and is an important indicator of disease progression—primarily cancer. Therefore, both temperature and pH are important physiological tools that enable our understanding of cellular processes and medicine for various theranostic purposes. Yu et al. first prepared GSH and cysteamine coated negatively charged AuNCs which depicted pH-dependent adsorption on membranes of living cells, within a biological range, which could be used as a diagnostic and fluorescent imaging tool for cells that undergo pH changes [100]. BSA–AuNCs have also been employed for targeted imaging and highly sensitive ratiometric pH determination tools for folate rich HeLa cancer cells within broad pH (6.0–7.8) range [101]. This strategy can further be extended to construct ratiometric fluorescent biosensors for targeted drug delivery applications as well. Shang et al. reported ultrasmall NIR emitting fluorescent AuNCs with excellent thermal sensitivity for simultaneous intracellular thermometry over the physiological temperature range (15–45 °C) as well as imaging in HeLa cells [102]. GSH capped AuNCs developed by Kong et al. found to display temperature-dependent emission were used for fluorometric determination of temperature (0 to 60 °C range) and imaging of human cancer cells and bacterial cells [103].

1.4 Gold Nanoclusters as Therapeutics

The unique physicochemical and optical properties of AuNCs such as—enhanced photoluminescence and quantum yield, tunable photoemission, excellent biocompatibility, high solubility, effective renal clearance due to its ultrasmall size, ease of functionalization for selective targets approach, have made the AuNCs standout from their traditional noble metal NPs and heavy metal quantum dot counterparts for various biomedical applications. This section deals with various recent advances of fluorescent AuNCs towards different therapeutic applications.

(a) Gold Nanoclusters in Image Guided Cancer Therapeutics

(i) **Photothermal Therapy**

Photothermal therapy (PTT) is one of the most widely used and clinically accepted phototherapy that relies on the activation of a photosensitizing material by a laser irradiation source, usually NIR, for heat induced thermal ablation of cancer cells. PTT may also be referred to as hyperthermia in clinical settings. Gu et al. developed hybrid nano-carriers loaded with BSA–AuNCs and indocyanine green (ICG) dye for one-photon/two-photon fluorescence imaging and highly effective photothermal therapy [104]. Similarly, GSH–AuNCs were combined with porphyrin derivatives for tumor-targeted imaging guided in vitro and in vivo photothermal therapy due to their NIR fluorescence emission at ~710 nm, high biocompatibility, and excellent water solubility [105]. Recently, albumin-assisted polyallylamine capped BSA/PAH–AuNCs fabricated through ultrasonication procedure were reported to display excellent hyperthermal effects (~60 °C) upon NIR laser irradiation(~808 nm) in a 4 T1 breast cancer cell system in vitro and in 4 T1 cell tumor xenograft mice in vivo (Fig. 1.8), remarkably suppressed breast cancer growth by tumor ablation [106].

(ii) **Photodynamic Therapy**

Photodynamic therapy (PDT) is another kind of clinically approved phototherapy which employs lasers of specific wavelength to excite the photosensitizers and induces apoptosis of cancer cells and tumor ablation mediated by ROS and other free radicals generated during the process. AuNCs have been used as photosensitizers (PS) due to their high biocompatibility, non-toxicity, high photostability, and appropriate quantum yield and can be introduced into tumors and cancer cells and alone or with a drug molecule to synergistically kill the cancer cells through PDT-Chemo combinational therapy. NIR emitting lipoic acid capped AuNCs conjugated with FA (folic acid) and protoporphyrin IX (PFL–AuNCs) depicted excellent tumor reduction property for real time fluorescence image guided *in vivo* photodynamic therapy [107]. FA facilitated tumor targeting while protoporphyrin IX acted as PS and the resultant PFL–AuNCs were able to generate significantly higher amount of $^1O_2$ (singlet oxygen) at 1270 nm than the photosensitizer alone. Chlorin e6 (Ce6) photosensitizer conjugated SiO_2-coated multifunctional AuNCs (AuNCs@SiO_2-Ce6) were developed by Huang et al. for fluorescence image guided

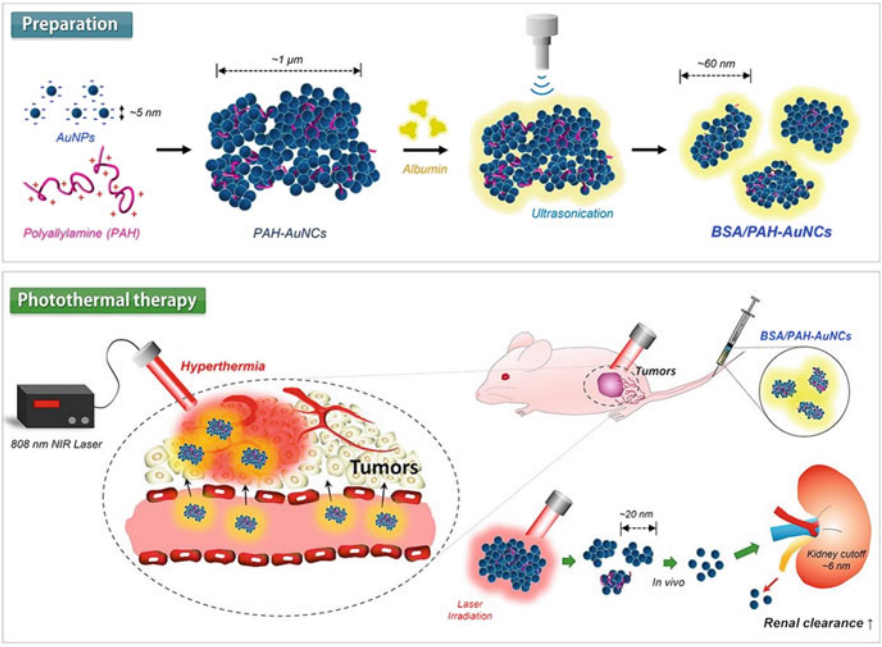

Fig. 1.8 AuNCs for Photothermal Therapy: Schematic illustration of the facile preparation and PTT of BSA/PAH–AuNCs. Reprinted with permission from Ref. [106]) © 2018 Elsevier

photodynamic therapy [108]. The AuNCs@SiO_2-Ce6 showed certain desirable features such as—high Ce6 loading, no non-specific release of Ce6 during circulation, enhanced cellular uptake, high water solubility, and good biocompatibility which facilitate its use in medical diagnostics such as CT and photoacoustic image guided PDT. Similarly, GSH capped AuNCs conjugated with FA and PEG (polyethylene glycol) were used for simultaneous fluorescence imaging and targeted PDT and were found to show superior penetration and retention in MGC-803 (gastric carcinoma) bearing mouse model [109]. Herein, Ce6 was trapped in PEG network and was used as PS for PDT. Peptide capped nucleus targeting TAT–AuNCs were designed as multifunctional nanomaterials for bioimaging, gene delivery and as photosensitizers in NIR activated targeted photodynamic therapy (980 nm) by sensitizing generation of $^1O_2$ without presence of additional organic photosensitizers to effectively destroy HeLa cancer cells [110] as shown in Fig 1.9a. Han et al. have recently developed a highly efficient in vivo two-photon PDT system utilizing dihydrolipoic acid coated DHLA–AuNCs as type I photosensitizing agents (Fig 1.9b) specifically for the treatment of deep seated or large tumors [111].

(iii) **Radiation therapy**

Radiation therapy is one amongst the most effective cancer therapeutics that uses high powered ionizing energy beams, such as protons or X-rays, to kill cancer cells by DNA and protein damage and shrinking the tumor sizes. Herein, the role of

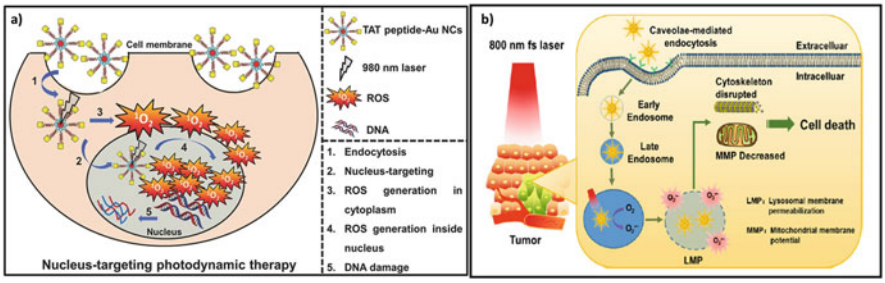

Fig. 1.9 AuNCs for Photodynamic Therapy: (**a**) Schematic representation for the nucleus targeting TAT peptide–AuNCs mediated PDT. Reprinted with permission from Ref. [110]) ©2015 Wiley. (**b**) Schematic illustration of the cancer therapy mechanism of AuNC@DHLA internalized via caveolae-mediated endocytosis for NIR fs laser irradiated PDT. Reprinted with permission from Ref. [111]) ©2019 American Chemical Society

radiosensitizers stands at utmost importance to effectively deal with the damage caused by radiation to healthy proximal cells and tissues. AuNCs have recently been used as radiosensitizers due to its high biocompatibility and ultrasmall size which enables efficient accumulation inside tumors for enhanced radiation effect as well as effective renal clearance for minimal toxic effects. GSH capped Au_{25} NCs designed by Zhang et al. inherited the strong radio sensitizing effect of Au core along with biocompatible GSH shell for enhanced cancer radiation therapy and effective renal clearance by utilizing the preferential accumulation of these GSH–Au_{25}NCs in tumors via enhanced permeability and retention (EPR) effect [112]. The GSH–Au25NCs were reported to exhibit stronger radiation enhancement than BSA–Au 25NCs, which could be attributed to the improved cell uptake of smaller GSH–Au 25 NCs (hydrodynamic size ~2.4 nm) as compared to that of BSA–Au 25 NCs (~6 nm) for tumor radiation therapy. Subsequently, different sized GSH stabilized AuNCs such as $Au_{10\text{-}12}(SG)_{10\text{-}12}$ [113] and $Au_{29\text{-}43}$ $(SG)_{27\text{-}37}$ [114] have been successfully employed as radiosensitizers with high tumor uptake and renal clearance leading to significant radiation enhancement effect. Furthermore, the effect of surface charge on GSH–Au_{33}NCs was studied and the negatively charged AuNCs were found to have highest tumor uptake and therefore pronounced radiotherapy sensitization over its positively charged and neutral counterparts thereby highlighting the importance of surface functionalization on the role of AuNCs in radiotherapeutics [115]. Recently, cyclic RGD (arginine–glycine–aspartic acid) peptide capped AuNCs were utilized as radiosensitizers as well as fluorescent probes αvβ3 integrin-positive cancer cells leading to enhanced radiation effect [13] as shown in Fig. 1.10a, b. Therefore, these results successfully envisage ultrasmall AuNCs as next generation biocompatible, metabolizable, and highly effective radiosensitizers for clinical use in cancer radiation therapy.

(iv) **Microwave and Radiofrequency assisted therapy**

Non-ionizing electromagnetic irradiation like microwave (MW) and radiofrequency (RF) have been gaining wide attention for hyperthermia as well as

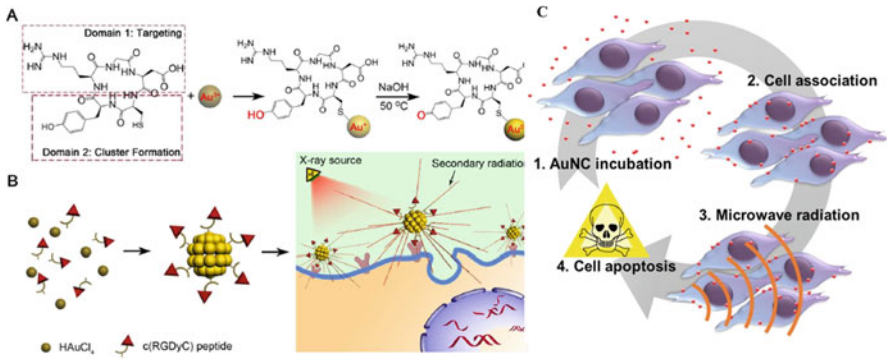

Fig. 1.10 AuNCs for ionizing and non-ionizing radiation based therapeutics: (**a**) Schematic illustration of c(RGDyC)-AuNCs formation and (**b**) c(RGDyC)-AuNCs accumulation in αvβ3 integrin-positive cancer cells and interaction with incident radiation intensively, generating secondary radiation, and leading to radiation enhancement effect. Reprinted with permission from Ref. [13]) ©2017 Elsevier. (**c**) Schematic of BSA–AuNC for microwave radiation assisted cytotoxicity for cancer therapy. Reprinted with permission from Ref. [116]) ©2017 American Chemical Society

triggered cancer therapeutics due to their deeper penetration ability and non-invasive modality. Cifuentes-Riuset al. studied the effect of BSA–AuNCs on different types of mammalian cells (fibroblasts, B-lymphocytes, glioblastoma, neuroblastoma, and prostate cancer cells) under 1 GHz microwave radiation which resulted in a specific-microwave dependent cytotoxicity caused by localized heating effect (Fig. 1.10c) suggesting their potential towards effective and safe cancer nanomedicines [116]. Similarly, Kharrazi et al. studied the response of 100 W radio frequency electric field (RF-EF) on mercaptosuccinic acid capped MSA–AuNCs in pancreatic cancer cells (MIA Paca-2) for in vitro hyperthermia applications [117]. The MSA–AuNCs generated 50 °C temperature rise and an effective RF-EF hyperthermia for successful eradication of pancreatic cancer cells. These studies show highly promising potential of AuNCs for electromagnetic therapy in a clinical setup in the near future.

(b) Neurodegenerative Diseases Therapeutics

The ultrasmall AuNCs with their unique physicochemical properties and high biocompatibility have successfully paved a way for their use in neurodegenerative disease therapeutics as they can easily penetrate the blood brain barrier (BBB) through the intracellular spaces. Recent studies have shown promising results of AuNCs in treatment of Parkinson's disease (PD). Gao et al. reported the use of N-isobutyryl-L-cysteine (L-NIBC) protected AuNCs for direct anti-PD activities by inhibiting the aggregation and fibrillation of α-Synuclein, a neuronal protein linked to neuropathology, as well as exhibited excellent neuroprotective activity against MPP+ (1-Methyl-4-phenylpyridine) induced neurotoxicity in cell PD model [118]. L-NIBC AuNCs also reported significant reversal of dopaminergic (DA) neuron loss in sick mice as shown in Fig. 1.11 which opens up novel avenues to develop anti-PD drugs using AuNCs in a clinical setup. Recently, the optimal

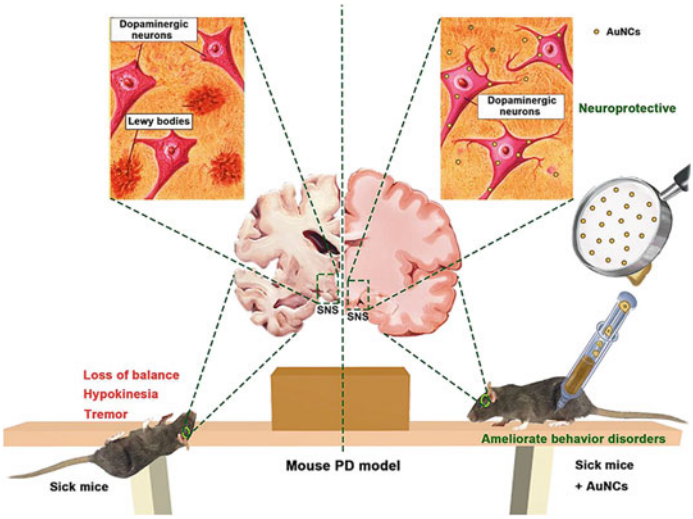

Fig. 1.11 AuNCs for neurodegenerative diseases therapeutics: Schematic illustration depicting that AuNCs prevent α-Synuclein aggregation and fibrillation and improve cell viability in MPP+ lesioned cell PD model. Reprinted with permission from Ref. [118]) ©2019 Elsevier

route of AuNCs administration in mice targeting PD was reported to be via intraperitoneal injection due to greatest bioavailability and the longest residence in brain by penetrating the BBB and excreted mainly through kidney [119]. Alzheimer's disease is another neurological disorder pathologically characterized mainly by the plaques of amyloid-β (Aβ) peptides and their fibrillation. During an experimental study by Gao et al., it was found that GSH–AuNCs can completely inhibit the Aβ peptides from aggregation in comparison to their larger AuNPs counterparts which reportedly accelerated the Aβ fibrillation process [120]. This work was able to highlight the significance of the size effect of AuNCs in therapeutics and presented a novel strategy for designing anti-amyloidosis drugs as well as in approaching the inhibition of Aβ fibrillation from a new perspective. Subsequently, hexapeptide CLVFFA conjugated CLVFFA-AuNCs were reported to inhibit aggregation, prolongation, and mature fibrils' disaggregation of Aβ40, a pivotal biomarker of Alzheimer's disease, even at low concentrations. Furthermore, dihydrolipoic acid capped DHLA–AuNCs have been successfully employed to regulate neuroinflammation and to improve neuronal regeneration in N2a (neuronal cell line) and ex vivo brain slice stroke model; thereby suggesting its use as a potent therapeutic agent in central nervous system disorders such as traumatic brain injury, strokes, and neurodegenerative diseases [121].

(c) Drug Delivery Applications

Gold nanoclusters due to their high tunable emission, photostability, non-toxicity, biocompatibility have been extensively used in combination with drug molecules for excellent theranostics. The ligands stabilizing the AuNCs may form Au–S or amide

bonds and conjugate drug molecules which act as prodrug nanocomposite for controlled release thereby reducing the side effects of free drugs. Doxorubicin (DOX) is one of the most commonly used anticancer drugs that has been used in cancer therapeutics. Lysozyme capped AuNCs loaded with DOX have been developed to efficiently deliver drug to cause highly selective killing of MCF-7 cancer cells with 90% efficiency in comparison to normal breast cells MCF-10A with 40% killing efficiency [122]. The intreacellular release of DOX was determined fluorometrically by FRET imaging of the cancer cells. Khandelia et al. developed an NIR fluorescent nanovehicle consisting of AuNCs in BSA nanoparticles for image guided delivery of DOX by one and two-photon excitations of the AuNCs to probe their cellular uptake and subsequent DOX release [123]. Li et al. developed a scalable method to encapsulate multifunctional AuNCs assemblies in a polyacrylic acid/calcium phosphate shell and utilized its aggregation enhanced emission properties for delivering a high payload of DOX and providing excellent bimodal CT/fluorescence contrast imaging for guided liver tumor ablation depicted through a hepatocarcinoma tumor xenograft model [124]. Recently, peptide protected AuNCs have been used as triggered drug delivery systems for Vancomycin, an antibiotic, with self-regulated drug loading and release properties for antimicrobial therapeutics. Upon interaction with bacteria, the vancomycin molecules are released in proportion to the amount of bacteria present result in fluorescence quenching of AuNCs [125]. Cisplatin is another chemotherapeutic agent that kills cancer cells by damaging and inhibiting DNA synthesis in solid tumors. Zhou et al. developed BSA–AuNCs conjugated with a cisplatin prodrug and folic acid (FA–AuNCs–Pt) for image guided targeted chemotherapy of breast cancer cells and inhibited the growth and lung metastasis of orthotopically implanted 4T1 breast tumors [126]. Cells with folate receptors can be specifically targeted by conjugating the carrier system with FA for a folate-receptor-mediated endocytosis thereby enabling a targeted drug delivery system. Subsequently, paclitaxel (PTX)-loaded AuNCs conjugated with FA-modified amphiphilic polymer (AuNCs/FA-PDNH) displayed much higher cytotoxicity than its contemporary PTX-loaded AuNCs/PDNH nanocomposite without FA modification in the folate overexpressed KB cells and hence acts as a model system for early theranostics for folate-overexpressing cancerous cells [127]. Thus, the development of specific drug delivery systems achieved by specific modifications of surface ligand groups of fluorescent AuNCs seems to be a promising avenue for enhanced therapeutic applications in times to come.

(d) SiRNA/Gene Delivery Applications

Gene delivery is the process of transferring foreign DNA to host cells for treating various genetic incurable diseases for therapeutic applications. Fluorescence AuNCs have been gaining popularly as non-viral gene delivery vectors due to its non-toxic, highly biocompatible, highly photostable, non-immunogenic nature, enhanced cellular uptake along with ideal fluorescent tracking properties to track transfection behavior. Cationic polymer layer polyethylenimine stabilized PEI–AuNCs have been employed as effective vectors for gene delivery wherein the biocompatible AuNCs decrease the cytotoxicity of PEI and simultaneously act as fluorescent probes

for tracking the transfection behavior whereas the cationic PEI layer enhances gene transfection efficiency in HepG2 cells [128]. Subsequently, highly fluorescent PEI Ag–Au alloys NCs were reported to show high gene transfection efficiency and low cytotoxicity in cancer cells B16F10, HeLa, and CHO cells for applications in image assisted gene delivery applications [129]. A similar fluorescent cationic BSA stabilized bimetallic Au–Ag alloy NCs have been utilized for synergistically delivering therapeutic suicide gene CD-UPRT with a visual fluorescent aid to HeLa cancer cells along with prodrug 5-FC induced ROS mediated apoptosis for therapeutics [130]. TAT peptide stabilized AuNCs can act as DNA nanocargoes due to its nucleus targeting properties and were utilized as multifunctional agents for NIR activated photodynamic therapy and in vivo and in vitro bioimaging agents [110]. The TAT peptide –AuNCs were reported to have ultrahigh cellular uptake and gene transfection efficiency (~81%) in HeLa cells and zebrafish. Apart from DNA, siRNA is another powerful tool for modifying gene expression through a process called RNAi (RNA interference) for gene silencing or gene knockdown therapy. Gold nanocluster assisted siRNA delivery of NGF (nerve growth factor) for its downregulation in pancreatic tumor cells as well as *in vivo* mice model, resulting in efficient NGF gene silencing has been successfully developed and is a promising approach towards pancreatic cancer therapy [131].

1.5 Conclusions and Future Prospects

Photoluminescent AuNCs are rapidly emerging as a promising class of nanotheranostic agents due to their ultrasmall size and unique opto-electronic properties, high biocompatibility, and good renal clearance. Bioconjugated AuNCs offer highly specific and sensitive biosensing platforms with exceptional limit of detection. The photoresponsive and fluorescence properties can be employed for PTT, PDT, and radiation therapy applications. The exemplary nanotheranostic properties of AuNCs and their present ongoing advancements highlight their potential in specific POC devices as well as potential clinical translation.

References

1. Palekar-Shanbhag, P., Jog, S. V., Chogale, M. M., & Gaikwad, S. S. (2013). Theranostics for cancer therapy. *Current Drug Delivery, 10*, 357–362.
2. Purohit, B., Kumar, A., Mahato, K., & Chandra, P. (2020). Smartphone-assisted personalized diagnostic devices and wearable sensors. *Current Opinion in Biomedical Engineering, 13*, 42–50.
3. Kulkarni, N. S., Guererro, Y., Gupta, N., Muth, A., & Gupta, V. (2019). Exploring potential of quantum dots as dual modality for cancer therapy and diagnosis. *Journal of Drug Delivery Science and Technology, 49*, 352–364.

4. Varnavski, O., Ramakrishna, G., Kim, J., Lee, D., & Goodson, T. (2010). Critical size for the observation of quantum confinement in optically excited gold clusters. *Journal of the American Chemical Society, 132*, 16–17.
5. Chen, L.-Y., Wang, C.-W., Yuan, Z., & Chang, H.-T. (2015). Fluorescent gold nanoclusters: Recent advances in sensing and imaging. *Analytical Chemistry, 87*, 216–229.
6. Shang, L., Dong, S., & Nienhaus, G. U. (2011). Ultra-small fluorescent metal nanoclusters: Synthesis and biological applications. *Nano Today, 6*(4), 401–418.
7. Zhang, L., & Wang, E. (2014). Metal nanoclusters: New fluorescent probes for sensors and bioimaging. *Nano Today, 9*, 132–157.
8. Palmal, S., & Jana, N. R. (2013). Gold nanoclusters with enhanced tunable fluorescence as bioimaging probes. *Wiley Interdisciplinary Reviews. Nanomedicine and Nanobiotechnology, 6*(1), 102–110.
9. Chen, H., Li, S., Li, B., Ren, X., Li, S., Mahounga, D. M., Cui, S., Gu, Y., & Achilefu, S. (2012). Folate-modified gold nanoclusters as near-infrared fluorescent probes for tumor imaging and therapy. *Nanoscale, 4*, 6050–6064.
10. Chen, T.-H., & Tseng, W.-L. (2012). (Lysozyme type VI)-stabilized Au8 clusters: Synthesis mechanism and application for sensing of glutathione in a single drop of blood. *Small, 8*, 1912–1919.
11. Shang, L., Dörlich, R. M., Brandholt, S., Schneider, R., Trouillet, V., Bruns, M., Gerthsen, D., & Nienhaus, G. U. (2011). Facile preparation of water-soluble fluorescent gold nanoclusters for cellular imaging applications. *Nanoscale, 3*, 2009–2014.
12. Shiang, Y.-C., Huang, C.-C., & Chang, H.-T. (2009). Gold nanodot-based luminescent sensor for the detection of hydrogen peroxide and glucose. *Chemical Communications, 23*, 3437–3439.
13. Liang, G., Jin, X., Zhang, S., & Xing, D. (2017). RGD peptide-modified fluorescent gold nanoclusters as highly efficient tumor-targeted radiotherapy sensitizers. *Biomaterials, 144*, 95–104.
14. Liu, P., Shang, L., Li, H., Cui, Y., Qin, Y., Wu, Y., Hiltunen, J. K., Chen, Z., & Shen, J. (2014). Synthesis of fluorescent α-chymotrypsin A-functionalized gold nanoclusters and their application to blot-based technology for Hg2+ detection. *RSC Advances, 4*, 31536–31543.
15. Triulzi, R. C., Micic, M., Giordani, S., Serry, M., Chiou, W.-A., & Leblanc, R. M. (2006). Immunoasssay based on the antibody-conjugated PAMAM-dendrimer–gold quantum dot complex. *Chemical Communications, 28*, 5068–5070.
16. Xie, J., Zheng, Y., & Ying, J. Y. (2009). Protein-directed synthesis of highly fluorescent gold nanoclusters. *Journal of the American Chemical Society, 131*, 888–889.
17. Yang, X., Zhu, S., Dou, Y., Zhuo, Y., Luo, Y., & Feng, Y. (2014). Novel and remarkable enhanced-fluorescence system based on gold nanoclusters for detection of tetracycline. *Talanta, 122*, 36–42.
18. Muhammed, M. A. H., Verma, P. K., Pal, S. K., Kumar, R. C. A., Paul, S., Omkumar, R. V., & Pradeep, T. (2009). Bright, NIR-emitting Au23 from Au25: Characterization and applications including biolabeling. *Chemistry – A European Journal, 15*, 10110–10120.
19. Zheng, J., Zhang, C., & Dickson, R. M. (2004). Highly fluorescent, water-soluble, size-tunable gold quantum dots. *Physical Review Letters, 93*, 77402.
20. Habeeb Muhammed, M. A., Verma, P. K., Pal, S. K., Retnakumari, A., Koyakutty, M., Nair, S., & Pradeep, T. (2010). Luminescent quantum clusters of gold in bulk by albumin-induced core etching of nanoparticles: Metal ion sensing, metal-enhanced luminescence, and biolabeling. *Chemistry – A European Journal, 16*, 10103–10112.
21. Leung, N. L. C., Xie, N., Yuan, W., Liu, Y., Wu, Q., Peng, Q., Miao, Q., Lam, J. W. Y., & Tang, B. Z. (2014). Restriction of intramolecular motions: The general mechanism behind aggregation-induced emission. *Chemistry – A European Journal, 20*, 15349–15353.

22. Mei, J., Hong, Y., Lam, J. W. Y., Qin, A., Tang, Y., & Tang, B. Z. (2014). Aggregation-induced emission: The whole is more brilliant than the parts. *Advanced Materials, 26*, 5429–5479.
23. Liu, G., Feng, D.-Q., Hua, D., Liu, T., Qi, G., & Wang, W. (2017). Fluorescence enhancement of terminal amine assembled on gold nanoclusters and its application to ratiometric lysine detection. *Langmuir, 33*, 14643–14648.
24. Ma, L., Zhang, M., Yang, A., Wang, Q., Qu, F., Qu, F., & Kong, R.-M. (2018). Sensitive fluorescence detection of heparin based on self-assembly of mesoporous silica nanoparticle–gold nanoclusters with emission enhancement characteristics. *Analyst, 143*, 5388–5394.
25. Wu, Z., & Jin, R. (2010). On the Ligand's role in the fluorescence of gold nanoclusters. *Nano Letters, 10*, 2568–2573.
26. Yang, T. Q., Peng, B., Shan, B. Q., Zong, Y. X., Jiang, J. G., Wu, P., & Zhang, K. (2020). Origin of the photoluminescence of metal nanoclusters: From metal-centered emission to ligand-centered emission. *Nanomaterials, 10*, 261.
27. Kumar, A., Purohit, B., Mahato, K., Mahapatra, S., Srivastava, A., & Chandra, P. (2020). Bio-nano-interface engineering strategies of AuNPs passivation for next-generation biomedical applications. In P. Chandra & L. M. Pandey (Eds.), *BT - Biointerface engineering: Prospects in medical diagnostics and drug delivery* (pp. 215–231). Singapore: Springer Singapore.
28. Purohit, B., Vernekar, P. R., Shetti, N. P., & Chandra, P. (2020). Biosensor nanoengineering: Design, operation, and implementation for biomolecular analysis. *Sensors International, 1*, 100040.
29. Song, X.-R., Goswami, N., Yang, H.-H., & Xie, J. (2016). Functionalization of metal nanoclusters for biomedical applications. *Analyst, 141*, 3126–3140.
30. Huang, C.-C., Chiang, C.-K., Lin, Z.-H., Lee, K.-H., & Chang, H.-T. (2008). Bioconjugated gold nanodots and nanoparticles for protein assays based on photoluminescence quenching. *Analytical Chemistry, 80*, 1497–1504.
31. Fan, Y., Chen, S., Wei, S., Guo, J., & Li, Y. (2020). A simple "on–off–on" ECL sensor for glucose determination based on Pd nanowires and Ag doped g-C3N4 nanosheets. *Analytical Methods, 12*, 8–17.
32. Xia, N., Wang, X., Zhou, B., Wu, Y., Mao, W., & Liu, L. (2016). Electrochemical detection of amyloid-β oligomers based on the signal amplification of a network of silver nanoparticles. *ACS Applied Materials & Interfaces, 8*, 19303–19311.
33. Cheng, Y., Lei, J., Chen, Y., & Ju, H. (2014). Highly selective detection of microRNA based on distance-dependent electrochemiluminescence resonance energy transfer between CdTe nanocrystals and Au nanoclusters. *Biosensors and Bioelectronics, 51*, 431–436.
34. Zhao, Q., Huang, H., Zhang, L., Wang, L., Zeng, Y., Xia, X., Liu, F., & Chen, Y. (2016). Strategy to fabricate naked-eye readout ultrasensitive plasmonic nanosensor based on enzyme mimetic gold nanoclusters. *Analytical Chemistry, 88*, 1412–1418.
35. Feng, J., Huang, P., Shi, S., Deng, K.-Y., & Wu, F.-Y. (2017). Colorimetric detection of glutathione in cells based on peroxidase-like activity of gold nanoclusters: A promising powerful tool for identifying cancer cells. *Analytica Chimica Acta, 967*, 64–69.
36. He, W., Zhou, Y.-T., Wamer, W. G., Hu, X., Wu, X., Zheng, Z., Boudreau, M. D., & Yin, J.-J. (2013). Intrinsic catalytic activity of Au nanoparticles with respect to hydrogen peroxide decomposition and superoxide scavenging. *Biomaterials, 34*, 765–773.
37. Xia, X., Long, Y., & Wang, J. (2013). Glucose oxidase-functionalized fluorescent gold nanoclusters as probes for glucose. *Analytica Chimica Acta, 772*, 81–86.
38. Wang, Y., Bai, X., Wen, W., Zhang, X., & Wang, S. (2015). Ultrasensitive electrochemical biosensor for HIV gene detection based on graphene stabilized gold nanoclusters with exonuclease amplification. *ACS Applied Materials & Interfaces, 7*, 18872–18879.
39. Li, Z.-Y., Wu, Y.-T., & Tseng, W.-L. (2015). UV-light-induced improvement of fluorescence quantum yield of DNA-templated gold nanoclusters: Application to ratiometric fluorescent sensing of nucleic acids. *ACS Applied Materials & Interfaces, 7*, 23708–23716.

40. Zhou, Y., Tang, L., Zeng, G., Chen, J., Wang, J., Fan, C., Yang, G., Zhang, Y., & Xie, X. (2015). Amplified and selective detection of manganese peroxidase genes based on enzyme-scaffolded-gold nanoclusters and mesoporous carbon nitride. *Biosensors and Bioelectronics, 65*, 382–389.
41. Song, W., Liang, R.-P., Wang, Y., Zhang, L., & Qiu, J.-D. (2015). Green synthesis of peptide-templated gold nanoclusters as novel fluorescence probes for detecting protein kinase activity. *Chemical Communications, 51*, 10006–10009.
42. Song, W., Wang, Y., Liang, R.-P., Zhang, L., & Qiu, J.-D. (2015). Label-free fluorescence assay for protein kinase based on peptide biomineralized gold nanoclusters as signal sensing probe. *Biosensors and Bioelectronics, 64*, 234–240.
43. Hu, L., Han, S., Parveen, S., Yuan, Y., Zhang, L., & Xu, G. (2012). Highly sensitive fluorescent detection of trypsin based on BSA-stabilized gold nanoclusters. *Biosensors and Bioelectronics, 32*, 297–299.
44. Yang, G.-H., Shi, J.-J., Wang, S., Xiong, W.-W., Jiang, L.-P., Burda, C., & Zhu, J.-J. (2013). Fabrication of a boron nitride–gold nanocluster composite and its versatile application for immunoassays. *Chemical Communications, 49*, 10757–10759.
45. Alonso, M. C., Trapiella-Alfonso, L., Fernández, J. M. C., Pereiro, R., & Sanz-Medel, A. (2016). Functionalized gold nanoclusters as fluorescent labels for immunoassays: Application to human serum immunoglobulin E determination. *Biosensors and Bioelectronics, 77*, 1055–1061.
46. Qin, L., He, X., Chen, L., & Zhang, Y. (2015). Turn-on fluorescent sensing of glutathione S-transferase at near-infrared region based on FRET between gold nanoclusters and gold nanorods. *ACS Applied Materials & Interfaces, 7*, 5965–5971.
47. Zhang, J., Sajid, M., Na, N., Huang, L., He, D., & Ouyang, J. (2012). The application of au nanoclusters in the fluorescence imaging of human serum proteins after native PAGE: Enhancing detection by low-temperature plasma treatment. *Biosensors and Bioelectronics, 35*, 313–318.
48. Nguyen, P.-D., Cong, V. T., Baek, C., & Min, J. (2017). Fabrication of peptide stabilized fluorescent gold nanocluster/graphene oxide nanocomplex and its application in turn-on detection of metalloproteinase-9. *Biosensors and Bioelectronics, 89*, 666–672.
49. Deng, H.-H., Deng, Q., Li, K.-L., Zhuang, Q.-Q., Zhuang, Y.-B., Peng, H.-P., Xia, X.-H., & Chen, W. (2020). Fluorescent gold nanocluster-based sensor for detection of alkaline phosphatase in human osteosarcoma cells. *Spectrochimica Acta Part A: Molecular and Biomolecular Spectroscopy, 229*, 117875.
50. Chen, L.-Y., Huang, C.-C., Chen, W.-Y., Lin, H.-J., & Chang, H.-T. (2013). Using photoluminescent gold nanodots to detect hemoglobin in diluted blood samples. *Biosensors and Bioelectronics, 43*, 38–44.
51. Selvaprakash, K., & Chen, Y.-C. (2017). Detection of ricin by using gold nanoclusters functionalized with chicken egg white proteins as sensing probes. *Biosensors & Bioelectronics, 92*, 410–416.
52. Yu, H., Liu, Y., Wang, J., Liang, Q., Liu, H., Xu, J., & Shao, S. (2017). A gold nanocluster-based ratiometric fluorescent probe for cysteine and homocysteine detection in living cells. *New Journal of Chemistry, 41*, 4416–4423.
53. Wang, M., Mei, Q., Zhang, K., & Zhang, Z. (2012). Protein-gold nanoclusters for identification of amino acids by metal ions modulated ratiometric fluorescence. *Analyst, 137*, 1618–1623.
54. Liu, Y., Ding, D., Zhen, Y., & Guo, R. (2017). Amino acid-mediated "turn-off/turn-on" nanozyme activity of gold nanoclusters for sensitive and selective detection of copper ions and histidine. *Biosensors & Bioelectronics, 92*, 140–146.
55. Wen, F., Dong, Y., Feng, L., Wang, S., Zhang, S., & Zhang, X. (2011). Horseradish peroxidase functionalized fluorescent gold nanoclusters for hydrogen peroxide sensing. *Analytical Chemistry, 83*, 1193–1196.

56. Jin, L., Shang, L., Guo, S., Fang, Y., Wen, D., Wang, L., Yin, J., & Dong, S. (2011). Biomolecule-stabilized Au nanoclusters as a fluorescence probe for sensitive detection of glucose. *Biosensors & Bioelectronics, 26*, 1965–1969.
57. Deng, H.-H., Wu, G.-W., He, D., Peng, H.-P., Liu, A.-L., Xia, X.-H., & Chen, W. (2015). Fenton reaction-mediated fluorescence quenching of N-acetyl-l-cysteine-protected gold nanoclusters: Analytical applications of hydrogen peroxide, glucose, and catalase detection. *Analyst, 140*, 7650–7656.
58. Tao, Y., Lin, Y., Ren, J., & Qu, X. (2013). A dual fluorometric and colorimetric sensor for dopamine based on BSA-stabilized aunanoclusters. *Biosensors and Bioelectronics, 42*, 41–46.
59. Aswathy, B., & Sony, G. (2014). Cu2+ modulated BSA–Au nanoclusters: A versatile fluorescence turn-on sensor for dopamine. *Microchemical Journal, 116*, 151–156.
60. Govindaraju, S., Ankireddy, S. R., Viswanath, B., Kim, J., & Yun, K. (2017). Fluorescent gold nanoclusters for selective detection of dopamine in cerebrospinal fluid. *Scientific Reports, 7*, 40298.
61. Li, L., Liu, H., Shen, Y., Zhang, J., & Zhu, J.-J. (2011). Electrogenerated chemiluminescence of Au nanoclusters for the detection of dopamine. *Analytical Chemistry, 83*, 661–665.
62. Hemmateenejad, B., Shakerizadeh-shirazi, F., & Samari, F. (2014). BSA-modified gold nanoclusters for sensing of folic acid. *Sensors and Actuators B: Chemical, 199*, 42–46.
63. Yan, X., Li, H., Cao, B., Ding, Z., & Su, X. (2015). A highly sensitive dual-readout assay based on gold nanoclusters for folic acid detection. *Microchimica Acta, 182*, 1281–1288.
64. Peng, H.-P., Jian, M.-L., Huang, Z.-N., Wang, W.-J., Deng, H.-H., Wu, W.-H., Liu, A.-L., Xia, X.-H., & Chen, W. (2018). Facile electrochemiluminescence sensing platform based on high-quantum-yield gold nanocluster probe for ultrasensitive glutathione detection. *Biosensors and Bioelectronics, 105*, 71–76.
65. Tian, D., Qian, Z., Xia, Y., & Zhu, C. (2012). Gold nanocluster-based fluorescent probes for near-infrared and turn-on sensing of glutathione in living cells. *Langmuir, 28*, 3945–3951.
66. Nair, L. V., Philips, D. S., Jayasree, R. S., & Ajayaghosh, A. (2013). A near-infrared fluorescent nanosensor (AuC@urease) for the selective detection of blood urea. *Small, 9*, 2673–2677.
67. Liu, Y., Li, H., Guo, B., Wei, L., Chen, B., & Zhang, Y. (2017). Gold nanoclusters as switch-off fluorescent probe for detection of uric acid based on the inner filter effect of hydrogen peroxide-mediated enlargement of gold nanoparticles. *Biosensors and Bioelectronics, 91*, 734–740.
68. Li, P.-H., Lin, J.-Y., Chen, C.-T., Ciou, W.-R., Chan, P.-H., Luo, L., Hsu, H.-Y., Diau, E. W.-G., & Chen, Y.-C. (2012). Using gold nanoclusters as selective luminescent probes for phosphate-containing metabolites. *Analytical Chemistry, 84*, 5484–5488.
69. Selvaprakash, K., & Chen, Y.-C. (2014). Using protein-encapsulated gold nanoclusters as photoluminescent sensing probes for biomolecules. *Biosensors and Bioelectronics, 61*, 88–94.
70. Chang, H.-C., & Ho, J. A. (2015). Gold nanocluster-assisted fluorescent detection for hydrogen peroxide and cholesterol based on the inner filter effect of gold nanoparticles. *Analytical Chemistry, 87*, 10362–10367.
71. Chen, X., & Baker, G. A. (2013). Cholesterol determination using protein-templated fluorescent gold nanocluster probes. *Analyst, 138*, 7299–7302.
72. Liu, J.-M., Chen, J.-T., & Yan, X.-P. (2013). Near infrared fluorescent trypsin stabilized gold nanoclusters as surface plasmon enhanced energy transfer biosensor and in vivo cancer imaging bioprobe. *Analytical Chemistry, 85*, 3238–3245.
73. Samari, F., Hemmateenejad, B., Rezaei, Z., & Shamsipur, M. (2012). A novel approach for rapid determination of vitamin B12 in pharmaceutical preparations using BSA-modified gold nanoclusters. *Analytical Methods, 4*, 4155–4160.
74. Chen, Z., Qian, S., Chen, X., Gao, W., & Lin, Y. (2012). Protein-templated gold nanoclusters as fluorescence probes for the detection of methotrexate. *Analyst, 137*, 4356–4361.

75. Chen, Z., Qian, S., Chen, J., Cai, J., Wu, S., & Cai, Z. (2012). Protein-templated gold nanoclusters based sensor for off-on detection of ciprofloxacin with a high selectivity. *Talanta, 94*, 240–245.
76. Yu, Y., New, S. Y., Xie, J., Su, X., & Tan, Y. N. (2014). Protein-based fluorescent metal nanoclusters for small molecular drug screening. *Chemical Communications, 50*, 13805–13808.
77. Xie, J., Zheng, Y., & Ying, J. Y. (2010). Highly selective and ultrasensitive detection of Hg2+ based on fluorescence quenching of Au nanoclusters by Hg2+–Au+ interactions. *Chemical Communications, 46*, 961–963.
78. Lin, Y.-H., & Tseng, W.-L. (2010). Ultrasensitive sensing of Hg2+ and CH3Hg+ based on the fluorescence quenching of lysozyme type VI-stabilized gold nanoclusters. *Analytical Chemistry, 82*, 9194–9200.
79. Li, Y., Yuan, M., Khan, A. J., Wang, L., & Zhang, F. (2019). Peptide-gold nanocluster synthesis and intracellular Hg2+ sensing. *Colloids and Surfaces A: Physicochemical and Engineering Aspects, 579*, 123666.
80. Shang, L., Yang, L., Stockmar, F., Popescu, R., Trouillet, V., Bruns, M., Gerthsen, D., & Nienhaus, G. U. (2012). Microwave-assisted rapid synthesis of luminescent gold nanoclusters for sensing Hg2+ in living cells using fluorescence imaging. *Nanoscale, 4*, 4155–4160.
81. Zang, J., Li, C., Zhou, K., Dong, H., Chen, B., Wang, F., & Zhao, G. (2016). Nanomolar Hg2+ detection using β-lactoglobulin-stabilized fluorescent gold nanoclusters in beverage and biological media. *Analytical Chemistry, 88*, 10275–10283.
82. Thakur, N. S., Mandal, N., & Banerjee, U. C. (2018). Esterase-mediated highly fluorescent gold nanoclusters and their use in ultrasensitive detection of mercury: Synthetic and mechanistic aspects. *ACS Omega, 3*, 18553–18562.
83. He, Y., Du, E., Zhou, X., Zhou, J., He, Y., Ye, Y., Wang, J., Tang, B., & Wang, X. (2020). Wet-spinning of fluorescent fibers based on gold nanoclusters-loaded alginate for sensing of heavy metal ions and anti-counterfeiting. *Spectrochimica Acta Part A: Molecular and Biomolecular Spectroscopy, 230*, 118031.
84. Xu, S., Li, X., Mao, Y., Gao, T., Feng, X., & Luo, X. (2016). Novel dual ligand co-functionalized fluorescent gold nanoclusters as a versatile probe for sensitive analysis of Hg2+ and oxytetracycline. *Analytical and Bioanalytical Chemistry, 408*, 2955–2962.
85. Yang, X., Yang, L., Dou, Y., & Zhu, S. (2013). Synthesis of highly fluorescent lysine-stabilized Au nanoclusters for sensitive and selective detection of Cu2+ ion. *Journal of Materials Chemistry C, 1*, 6748–6751.
86. Shamsipur, M., Molaabasi, F., Shanehsaz, M., & Moosavi-Movahedi, A. A. (2015). Novel blue-emitting gold nanoclusters confined in human hemoglobin, and their use as fluorescent probes for copper(II) and histidine. *Microchimica Acta, 182*, 1131–1141.
87. Durgadas, C. V., Sharma, C. P., & Sreenivasan, K. (2011). Fluorescent gold clusters as nanosensors for copper ions in live cells. *Analyst, 136*, 933–940.
88. Bain, D., Maity, S., Paramanik, B., & Patra, A. (2018). Core-size dependent fluorescent gold nanoclusters and ultrasensitive detection of Pb2+ ion. *ACS Sustainable Chemistry & Engineering, 6*, 2334–2343.
89. Peng, Y., Wang, M., Xiaoxia, W., Wang, F., & Liu, L. (2018). Methionine-capped gold nanoclusters as a fluorescence-enhanced probe for cadmium(II) sensing. *Sensors, 18*, 658.
90. Huang, P., Li, S., Gao, N., & Wu, F. (2015). Toward selective, sensitive, and discriminative detection of Hg2+ and Cd2+via pH-modulated surface chemistry of glutathione-capped gold nanoclusters. *Analyst, 140*, 7313–7321.
91. Akshath, U. S., Bhatt, P., & Singh, S. A. (2020). Differential interaction of metal ions with gold nanoclusters and application in detection of cobalt and cadmium. *Journal of Fluorescence, 30*, 537–545.
92. Yu, M., Zhu, Z., Wang, H., Li, L., Fu, F., Song, Y., & Song, E. (2017). Antibiotics mediated facile one-pot synthesis of gold nanoclusters as fluorescent sensor for ferric ions. *Biosensors and Bioelectronics, 91*, 143–148.

93. Liu, Y., Ai, K., Cheng, X., Huo, L., & Lu, L. (2010). Gold-nanocluster-based fluorescent sensors for highly sensitive and selective detection of cyanide in water. *Advanced Functional Materials, 20*, 951–956.
94. Chen, T., Hu, Y., Cen, Y., Chu, X., & Lu, Y. (2013). A dual-emission fluorescent nanocomplex of gold-cluster-decorated silica particles for live cell imaging of highly reactive oxygen species. *Journal of the American Chemical Society, 135*, 11595–11602.
95. Zhuang, M., Ding, C., Zhu, A., & Tian, Y. (2014). Ratiometric fluorescence probe for monitoring hydroxyl radical in live cells based on gold nanoclusters. *Analytical Chemistry, 86*, 1829–1836.
96. Cui, M.-L., Liu, J.-M., Wang, X.-X., Lin, L.-P., Jiao, L., Zheng, Z.-Y., Zhang, L.-H., & Jiang, S.-L. (2013) A promising gold nanocluster fluorescent sensor for the highly sensitive and selective detection of S^{2-}. *Sensors and Actuators B: Chemical 188,* 53–58
97. Yuan, Z., Peng, M., Shi, L., Du, Y., Cai, N., He, Y., Chang, H.-T., & Yeung, E. S. (2013). Disassembly mediated fluorescence recovery of gold nanodots for selective sulfide sensing. *Nanoscale, 5*, 4683–4686.
98. Liu, H., Yang, G., Abdel-Halim, E. S., & Zhu, J.-J. (2013). Highly selective and ultrasensitive detection of nitrite based on fluorescent gold nanoclusters. *Talanta, 104*, 135–139.
99. Unnikrishnan, B., Wei, S.-C., Chiu, W.-J., Cang, J., Hsu, P.-H., & Huang, C.-C. (2014). Nitrite ion-induced fluorescence quenching of luminescent BSA-Au25 nanoclusters: Mechanism and application. *Analyst, 139*, 2221–2228.
100. Yu, M., Zhou, C., Liu, J., Hankins, J. D., & Zheng, J. (2011). Luminescent gold nanoparticles with pH-dependent membrane adsorption. *Journal of the American Chemical Society, 133*, 11014–11017.
101. Ding, C., & Tian, Y. (2015). Gold nanocluster-based fluorescence biosensor for targeted imaging in cancer cells and ratiometric determination of intracellular pH. *Biosensors and Bioelectronics, 65*, 183–190.
102. Shang, L., Stockmar, F., Azadfar, N., & Nienhaus, G. U. (2013). Intracellular thermometry by using fluorescent gold nanoclusters. *Angewandte Chemie International Edition, 52*, 11154–11157.
103. Kong, L., Chu, X., Ling, X., Ma, G., Yao, Y., Meng, Y., & Liu, W. (2016). Biocompatible glutathione-capped gold nanoclusters for dual fluorescent sensing and imaging of copper (II) and temperature in human cells and bacterial cells. *Microchimica Acta, 183*, 2185–2195.
104. Gu, W., Zhang, Q., Zhang, T., Li, Y., Xiang, J., Peng, R., & Liu, J. (2016). Hybrid polymeric nano-capsules loaded with gold nanoclusters and indocyanine green for dual-modal imaging and photothermal therapy. *Journal of Materials Chemistry B, 4*, 910–919.
105. Zhang, Y., Li, J., Jiang, H., Zhao, C., & Wang, X. (2016). Rapid tumor bioimaging and photothermal treatment based on GSH-capped red fluorescent gold nanoclusters. *RSC Advances, 6*, 63331–63337.
106. Lee, S., Lee, C., Park, S., Lim, K., Kim, S. S., Kim, J. O., Lee, E. S., Oh, K. T., Choi, H.-G., & Youn, Y. S. (2018). Facile fabrication of highly photothermal-effective albumin-assisted gold nanoclusters for treating breast cancer. *International Journal of Pharmaceutics, 553*, 363–374.
107. Nair, L. V., Nazeer, S. S., Jayasree, R. S., & Ajayaghosh, A. (2015). Fluorescence imaging assisted photodynamic therapy using photosensitizer-linked gold quantum clusters. *ACS Nano, 9*, 5825–5832.
108. Huang, P., Lin, J., Wang, S., Zhou, Z., Li, Z., Wang, Z., Zhang, C., Yue, X., Niu, G., Yang, M., Cui, D., & Chen, X. (2013). Photosensitizer-conjugated silica-coated gold nanoclusters for fluorescence imaging-guided photodynamic therapy. *Biomaterials, 34*, 4643–4654.
109. Zhang, C., Li, C., Liu, Y., Zhang, J., Bao, C., Liang, S., Wang, Q., Yang, Y., Fu, H., Wang, K., & Cui, D. (2015). Gold nanoclusters-based nanoprobes for simultaneous fluorescence imaging and targeted photodynamic therapy with superior penetration and retention behavior in tumors. *Advanced Functional Materials, 25*, 1314–1325.

110. Vankayala, R., Kuo, C.-L., Nuthalapati, K., Chiang, C.-S., & Hwang, K. C. (2015). Nucleus-targeting gold nanoclusters for simultaneous in vivo fluorescence imaging, gene delivery, and NIR-light activated photodynamic therapy. *Advanced Functional Materials, 25*, 5934–5945.
111. Han, R., Zhao, M., Wang, Z., Liu, H., Zhu, S., Huang, L., Wang, Y., Wang, L., Hong, Y., Sha, Y., & Jiang, Y. (2019). Super-efficient in vivo two-photon photodynamic therapy with a gold nanocluster as a type I photosensitizer. *ACS Nano*. https://doi.org/10.1021/acsnano.9b05169.
112. Zhang, X.-D., Chen, J., Luo, Z., Wu, D., Shen, X., Song, S.-S., Sun, Y.-M., Liu, P.-X., Zhao, J., Huo, S., Fan, S., Fan, F., Liang, X.-J., & Xie, J. (2014). Enhanced tumor accumulation of Sub-2 nm gold nanoclusters for Cancer radiation therapy. *Advanced Healthcare Materials, 3*, 133–141.
113. Zhang, X.-D., Luo, Z., Chen, J., Shen, X., Song, S., Sun, Y., Fan, S., Fan, F., Leong, D. T., & Xie, J. (2014). Ultrasmall Au10−12(SG)10−12 nanomolecules for high tumor specificity and cancer radiotherapy. *Advanced Materials, 26*, 4565–4568.
114. Zhang, X.-D., Luo, Z., Chen, J., Song, S., Yuan, X., Shen, X., Wang, H., Sun, Y., Gao, K., Zhang, L., Fan, S., Leong, D. T., Guo, M., & Xie, J. (2015). Ultrasmall glutathione-protected gold nanoclusters as next generation radiotherapy sensitizers with high tumor uptake and high renal clearance. *Scientific Reports, 5*, 8669.
115. Wang, J.-Y., Chen, J., Yang, J., Wang, H., Shen, X., Sun, Y.-M., Guo, M., & Zhang, X.-D. (2016). Effects of surface charges of gold nanoclusters on long-term in vivo biodistribution, toxicity, and cancer radiation therapy. *International Journal of Nanomedicine, 11*, 3475–3485.
116. Cifuentes-Rius, A., Ivask, A., Das, S., Penya-Auladell, N., Fabregas, L., Fletcher, N. L., Houston, Z. H., Thurecht, K. J., & Voelcker, N. H. (2017). Gold nanocluster-mediated cellular death under electromagnetic radiation. *ACS Applied Materials & Interfaces, 9*, 41159–41167.
117. Amini, S. M., Kharrazi, S., & Jaafari, M. R. (2017). Radio frequency hyperthermia of cancerous cells with gold nanoclusters: An in vitro investigation. *Gold Bulletin, 50*, 43–50.
118. Gao, G., Chen, R., He, M., Li, J., Li, J., Wang, L., & Sun, T. (2019). Gold nanoclusters for Parkinson's disease treatment. *Biomaterials, 194*, 36–46.
119. Hu, J., Gao, G., He, M., Yin, Q., Gao, X., Xu, H., & Sun, T. (2020). Optimal route of gold nanoclusters administration in mice targeting Parkinson's disease. *Nanomedicine, 15*, 563–580.
120. Gao, G., Zhang, M., Gong, D., Chen, R., Hu, X., & Sun, T. (2017). The size-effect of gold nanoparticles and nanoclusters in the inhibition of amyloid-β fibrillation. *Nanoscale, 9*, 4107–4113.
121. Xiao, L., Wei, F., Zhou, Y., Anderson, G. J., Frazer, D. M., Lim, Y. C., Liu, T., & Xiao, Y. (2020). Dihydrolipoic acid–gold nanoclusters regulate microglial polarization and have the potential to alter neurogenesis. *Nano Letters, 20*, 478–495.
122. Chattoraj, S., Amin, A., Jana, B., Mohapatra, S., Ghosh, S., & Bhattacharyya, K. (2016). Selective killing of breast cancer cells by doxorubicin-loaded fluorescent gold nanoclusters: Confocal microscopy and FRET. *ChemPhysChem, 17*, 253–259.
123. Khandelia, R., Bhandari, S., Pan, U. N., Ghosh, S. S., & Chattopadhyay, A. (2015). Gold nanocluster embedded albumin nanoparticles for two-photon imaging of cancer cells accompanying drug delivery. *Small, 11*, 4075–4081.
124. Li, L., Zhang, L., Wang, T., Wu, X., Ren, H., Wang, C., & Su, Z. (2015). Facile and scalable synthesis of novel spherical au nanocluster assemblies@polyacrylic acid/calcium phosphate nanoparticles for dual-modal imaging-guided cancer chemotherapy. *Small, 11*, 3162–3173.
125. Li, Q., Pan, Y., Chen, T., Du, Y., Ge, H., Zhang, B., Xie, J., Yu, H., & Zhu, M. (2018). Design and mechanistic study of a novel gold nanocluster-based drug delivery system. *Nanoscale, 10*, 10166–10172.
126. Zhou, F., Feng, B., Yu, H., Wang, D., Wang, T., Liu, J., Meng, Q., Wang, S., Zhang, P., Zhang, Z., & Li, Y. (2016). Cisplatin prodrug-conjugated gold nanocluster for fluorescence imaging and targeted therapy of the breast cancer. *Theranostics, 6*, 679–687.

127. Chen, D., Luo, Z., Li, N., Lee, J. Y., Xie, J., & Lu, J. (2013). Amphiphilic polymeric nanocarriers with luminescent gold nanoclusters for concurrent bioimaging and controlled drug release. *Advanced Functional Materials, 23*, 4324–4331.
128. Tao, Y., Li, Z., Ju, E., Ren, J., & Qu, X. (2013). Polycations-functionalized water-soluble gold nanoclusters: A potential platform for simultaneous enhanced gene delivery and cell imaging. *Nanoscale, 5*, 6154–6160.
129. Wang, P., Lin, L., Guo, Z., Chen, J., Tian, H., Chen, X., & Yang, H. (2016). Highly fluorescent gene carrier based on Ag–Au alloy nanoclusters. *Macromolecular Bioscience, 16*, 160–167.
130. Dutta, D., Chattopadhyay, A., & Ghosh, S. S. (2016). Cationic BSA templated Au–Ag bimetallic nanoclusters as a theranostic gene delivery vector for HeLa cancer cells. *ACS Biomaterials Science & Engineering, 2*, 2090–2098.
131. Lei, Y., Tang, L., Xie, Y., Xianyu, Y., Zhang, L., Wang, P., Hamada, Y., Jiang, K., Zheng, W., & Jiang, X. (2017). Gold nanoclusters-assisted delivery of NGF siRNA for effective treatment of pancreatic cancer. *Nature Communications, 8*, 15130.

Chapter 2
Advances in Materials, Methods, and Principles of Modern Biosensing Tools

Mitali Basak, Shirsendu Mitra, and Dipankar Bandyopadhyay

2.1 Introduction

In the modern era, research and development in biosensing, therapeutics, diagnostics, and medical devices are rather interlinked. This is because, in many ways, they symbiotically cater to the needs of millions of people by enabling the detection of diseases to evaluate health conditions and provide treatment. Thus, of late, medical sciences and technologies are perhaps undergoing a confluence with the other multidisciplinary areas, for example, materials, electronics, micro/nanotechnology, biotechnology, to mention a few. Among these diverse directions of growth in medical research, one of the very important areas is the development of gen-next technologies at a lower price with higher efficacy and robustness [1]. In this regard, some of the examples can be the state-of-art progresses in genetic [2] or tissue engineering [3], robotic surgeries [4] or drug deliveries [5], digital electronics [6], internet of things (IoT) [7], artificial intelligence (AI) [8], among others. The objective has been to tap upon all the sci-tech resources efficiently and sustainably to engender a need-based delivery to the entire mankind at an affordable price [9].

Mitali Basak and Shirsendu Mitra contributed equally with all other contributors.

M. Basak
Centre for Nanotechnology, Indian Institute of Technology Guwahati, Guwahati, Assam, India

S. Mitra
Department of Chemical Engineering, Indian Institute of Technology Guwahati, Guwahati, Assam, India

D. Bandyopadhyay (✉)
Centre for Nanotechnology, Indian Institute of Technology Guwahati, Guwahati, Assam, India

Department of Chemical Engineering, Indian Institute of Technology Guwahati, Guwahati, Assam, India
e-mail: dipban@iitg.ac.in

V. Borse et al. (eds.), *BioSensing, Theranostics, and Medical Devices*,
https://doi.org/10.1007/978-981-16-2782-8_2

In particular, one of the key factors in the progress of sensor developments is the discovery of new materials. The other factor is the use of "less" amount of materials ushers the development of miniaturized technologies. Inventions of smart and advanced materials like carbon nanotubes [10], graphene [11], conducting polymers [12], metal nanoparticles (MNP) [13], metal/inorganic [14] or carbon/organic composites [15] have elevated the capabilities of sensing to the next level. Such materials are found to be versatile in the sense that all of them have suitable sensing properties while they can also be immobilized on diverse materials that are frequently used for such applications. Alongside the advancement on the discovery of novel smart materials, research on MNP has also widened the base of the sensor research by multiple factors. The MNP like gold (AuNP) [16], silver (AgNP) [17], and platinum (PtNP) [18] are among the frequently used ones for developing biosensors. The MNP are versatile because they can attach biomolecules like enzymes [19], antibodies [20], and aptamers [21], which can attract specific analytes, and the MNP show characteristic optical changes on the attachment of specific analytes. Alongside optical changes, the MNP also show a change in electrical conductivity [22], impedance [23], or capacitance [24] on the addition of analytes on it. Exploiting such variations in the physicochemical properties on the specific interactions with the analytes, sensors have been developed to satisfy the requirements of agriculture [25], food [26], diagnostics [27], point-of-care testing (POCT) [28, 29], and forensic [30] applications.

Among all the other varieties of sensors, of late, the biosensors have gained ample attention for their brilliance in judging the quality of human health. Advanced technologies like the design and development of microfluidic chips, single-cell identification platforms, portable spectrophotometers, wearable sensors, AI-based measurements, and high-throughput semiconductor devices have perhaps revolutionized this field. The researchers are now also focusing on storing such a huge pool of data generated through biosensing on the cloud interfaces to create the base for the use of big data analytics in medical diagnostics. The mission here is to integrate biosensors at the different levels of biomedical initiatives such as (a) detect diseases non-invasively but accurately, (b) store and analyze the results of the test using big data and AI platforms, (c) disseminate if required through IoT, and (d) provide solutions using AI-ML-IoT. Such structured and stepwise healthcare initiatives are perhaps enabling the biosensing field to move towards the lanes of tech-driven automated systems, replacing the conventional skill-driven ecosystem. The improved selectivity, sensitivity, and reliability of these tech-driven products has been well accepted in the medical world and soon become a handy tool in near furture.

However, presently, a large section of the medical laboratories across the globe is largely unequipped to welcome such a paradigm shift because of their inclination towards a skill-based ecosystem in technology usage. Figure 2.1 thematically shows the steps to the use of smart and advanced materials for fabricating miniaturized low-cost biosensors targeting the economic recognition of diseases, leading to the POCT for the detection of diseases at the patient's site. Integration of such devices with the ecosystem of a digital reading interface, wireless transfer of data, storage, and analysis using AI-ML-IoT platforms may enable the development of a

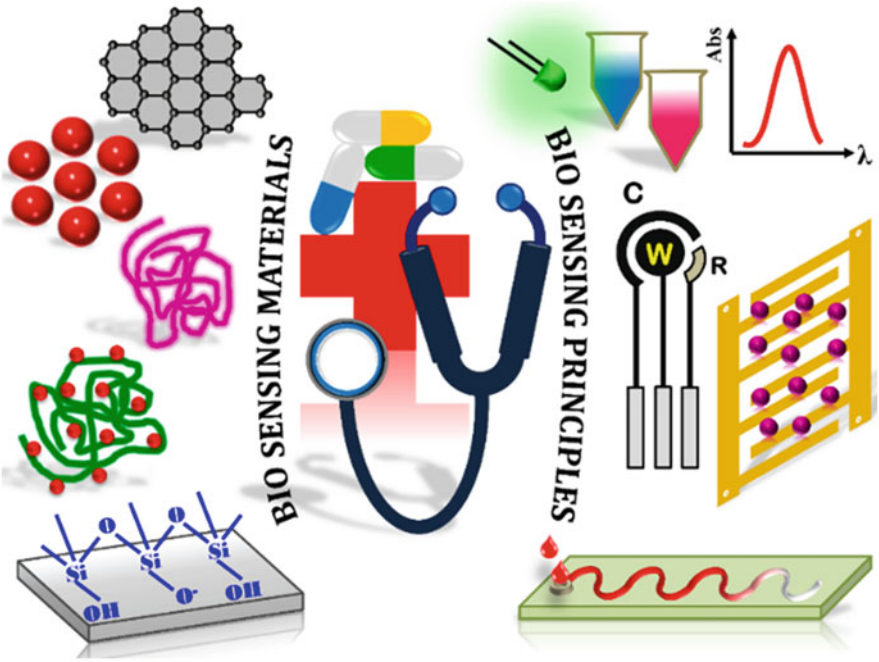

Fig. 2.1 Schematically shows different materials and principles of detection used in biosensors

tech-based ecosystem with minimal modification to the existing skill-based ecosystem. In this chapter, we plan to elaborate upon the finer details of such a skill-based ecosystem while exploring the roles of different types of modern-day biosensors enforcing such a revolutionizing change.

2.2 Materials for Biosensors

The research on materials science has close links with the research of biosensors. Different kinds of inorganic, organic, and composite materials are used for developing biosensors. Carbonaceous materials like graphene [11], single-walled carbon nanotubes [31], multiwalled carbon nanotubes [32], graphite [33], graphene dots [34], or carbon dots [35] are among the frequently used materials for developing electrochemical electrodes, resistive, capacitive, and impedance-based biosensors. Carbonaceous materials are among the forerunners for the development of biosensors. Apart from carbonaceous materials [11], conducting polymers [12], indium tin oxide (ITO) [36], graphene nanocomposites [37], metal modified nanoparticles [38], heterocyclic aromatic compounds are among the wide spectrum of materials used for making biosensors.

Carbon-based colorimetric sensors are generally developed exploiting carbon dots, graphene dots, and graphene oxide. A lot of previous reports hint that an ample amount of work was done on colorimetric biosensors, which were made exploiting carbon dots for the detection of hemoglobin [39], cholesterol [40], dopamine [41], glucose [42], DNA [43], cancer cells [44], and antibodies [45]. The previous report also suggests that carbon dots were also used as a fluorescent imaging probe [46]. Carbon quantum dots also appear as colorimetric biosensors for the development of sensors. Graphene oxides are proven to be a versatile reducing agent, and hence it was used as a reducing agent in a host of colorimetric sensors such as heparin [47], carcinogenic aromatic amine [48].

Due to the suitable conductivity of the carbonaceous materials, electrochemical, resistive, and capacitive sensors are more in practice and research as compared to the colorimetric sensors. Carbon-based electrochemical biosensors are very popular, and first-generation carbon-based electrochemical sensors have been developed using graphite [33], activated carbon [49], and activated carbon/inorganic composite [50] electrodes. After graphite [33] and activated carbon electrodes [49], glassy carbon [51] has gained technological and scientific importance, and a lot of electrochemical working electrodes have been made exploiting this class of materials. With the ubiquitous success of material science research, electrochemical biosensor development utilizing carbon nanotubes [31] and graphene oxide [52] has gained enormous popularity. Both carbon nanotube and graphene oxides have been widely employed to develop various electrochemical biosensors for bacteria detection [53], virus detection [54], detection of cholesterol [55], glucose [56], ketones [57], urea [58], or hemoglobin [59] in blood.

Although carbonaceous materials have been dominating the biosensor sector since the distant past, a lot of other kinds of developments have also been reported. Of late, electrochemical sensor developments based on ITO have gained careful attention. Immobilization of antibodies on top of the ITO surface to develop different kinds of immunosensors has become a trivial approach in recent times. Using ITO, similar kinds of biosensors have been developed to detect different analytes from blood serum [60], aqueous solutions [61], and other body fluids [62]. After the invention of electrically conducting polymers, such as polyaniline, it has been widely used to develop biosensors. Conducting polymers have an optimum conductivity and have different phases, which enable the material to be used as biosensor development material. In a different kind of approach, aromatic heterocyclic molecules [63] and azo compounds [64] are utilized for the development of biosensors. Alongside, many other materials such as silicon [65], alumina [66], magnetic micro/nanoparticles [67], molecularly imprinted polymer [68], nanoporous gold supported porous cobalt oxide [69], nanowire [70], zinc oxide microspheres [71], sol-gel materials [72], lipid bilayer [73], transition metal dichalcogenides [74] are also used for making biosensors.

Apart from these, the MNP based conducting materials are also extensively in operation for developing the most recent version of biosensors. For example, the efficacies of costly but versatile gold, silver, or platinum nanoparticles have been employed in diverse biosensor by the use of “less” amount of materials through the

miniaturization of the processes. The surface of gold and silver nanoparticles can be easily modified to immobilize different biomolecules like enzymes, antibodies, and aptamers. Attachment of such molecules on the surface of MNP subsequently helps in developing several biosensors to detect multiple analytes in blood serum, urine, and aqueous solutions. In some other reports, for efficient and sensitive detection of analytes, surface plasmon resonance (SPR) [75] and localized surface plasmon resonance (LSPR) [76] are in operation.

2.3 Principles of Biosensing

2.3.1 Colorimetric

Colorimetric sensors belong to the class of optical sensors, which changes color by an external stimulus. An external stimulus can be defined as any physicochemical change in the environment of the analyte surrounding the sensor. The designing of this type of sensor is decided on the basis of the target, i.e., the analyte. Colorimetric sensors have gained its popularity owing to user-friendliness, economical, easy analysis along with considerable sensitivity and specificity to various analytes. There are a number of strategies available for designing the colorimetric sensors, a few of them are summarized in the below sections:

2.3.1.1 Liquid Phase Biosensors

In the liquid phase detection principle, both the sensing material and the analyte are used in the liquid medium. This arrangement is advantageous for collective reasons like instantaneous sample preparation, homogeneity of the reagent used in the sensing procedure, exclusion of complexities of reagent immobilization on any surface. Due to such advantages, the methodology is preferred in most of the pathological laboratories or testing centers.

Moreover, this method is favored conventionally to carry out studies in various fields. In the field of liquid phase colorimetric detection, as conceptualized in Fig. 2.2, there are multiple technologies available.

The most recent technology, which can be thought of in liquid phase detection, is the localized surface plasmon resonance (LSPR) phenomenon of MNP. A number of works were done using this LSPR based spectroscopic technique [77]. The basic idea is to measure the shift in the wavelength and the enhancement in the intensity of the MNP spectrum, on the addition of a specific analyte into the system. Soomro et al. [78] fabricated a colorimetric biosensor to diagnose mercuric ions using copper nanoparticles (CuNP). Similarly, Shrivas et al. [79] developed a chemical sensor based on the lauryl sulfate modified AuNP for the detection of arsenic in different water samples. This technique was also extended to the biosensing sector for the development of multianalyte detection. LSPR based ampicillin sensor was

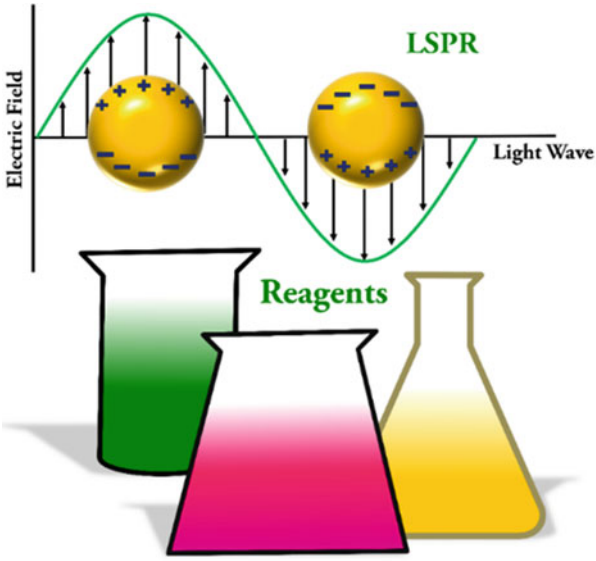

Fig. 2.2 Schematically shows liquid phase detection in the colorimetric based principle of detection in biosensors

developed by Shrivas et al. [80] using citrate capped silver nanoparticles to detect ampicillin from urine samples of the patients. This system changed color from yellow to shades of pink and showed a redshift in the LSPR spectrum of the silver nanoparticles. A glucose sensor was developed by Zhao et al. [81], exploiting the LSPR property of gold nanorods. Here, the authors showed that different concentration of glucose present in serum samples of the subjects produces various vivid colors on reaction with glucose oxidase and horse peroxidase immobilized on gold nanorods.

Many biosensors were also developed exploiting the colorimetric detection technique to identify the levels of various biomolecules or pathogen infection from different biological fluids. Ellairaja et al. [82] designed a biosensor using (2,2′-((1E,1′E)-((6-bromopyridine-2,3-diyl) bis(azanylylidene)) bis (-methanylylidenediphenol) (BAMD) targeted for the diagnosis of jaundice in humans. The developed sensor was aimed to detect the levels of bilirubin expressed in blood and urine samples of the patients to identify jaundice. Pourreza et al. [83] developed a hemoglobin sensor using curcumin nanoparticles from the blood samples of the subjects. They showed that on the attachment of hemoglobin molecules to the curcumin nanoparticles, the intensity of the nanoparticles diminishes, and this phenomenon has been targeted to quantify hemoglobin present in the blood samples of the patients.

The advent of metal nanoparticles accelerated the reliability and acceptance of colorimetric biosensors to a great extent. Thus, AuNP and AgNP become the most efficient sensing probe for the development of biosensors. Verma et al. [84] designed a biosensor to identify concentration of pathogens to check the health effects due to nosocomial, foodborne, and water-borne diseases using AuNP as the probe. They

showed a rapid color change of AuNP on the alteration of environmental conditions owing to the presence of the targeted pathogen. Similarly, Rajamanikandan et al. [85] designed a biosensor for the measurement of vitamin B1, using silver nanoparticles as the probe, from the blood and urine samples of the subjects. Nirala et al. [86] developed a cholesterol measuring unit using gold nanoparticles as the probe. Here, they immobilized cholesterol oxidase on the gold nanoparticles, which on interaction with the serum samples of the subject causes the color of gold nanoparticles to change from red to shades of blue with varying concentrations of cholesterol. Zhao et al. [81] developed a glucose sensor using gold nanorods, immobilized with glucose oxidase enzyme. The authors reported that on the reaction of glucose with glucose oxidase, which produces hydrogen peroxide, on further reaction with 3,3′,5,5′-tetramethylbenzidine produces various vivid colors ranging with the different concentrations of glucose.

With the modernization of the technologies, the sensing techniques have also been explored in many other substrates, as explained in the following sections.

2.3.1.2 Paper Biosensors

Paper-based biosensor, refers to thematic Fig. 2.3, is a type of colorimetric detection technique where the sensing material is immobilized on top of a paper substrate. Paper-based sensors or devices have received renewed interest in the fields of point-of-care technologies because of its simple, inexpensive, portable, and disposable characteristics. These sensors have diversified their applications ranging from environmental analysis to clinical diagnostics. Colorimetric techniques incorporated with paper-based devices are particularly attractive because of its user-friendliness, ability to provide semi-quantitative results without the use of complicated bulky

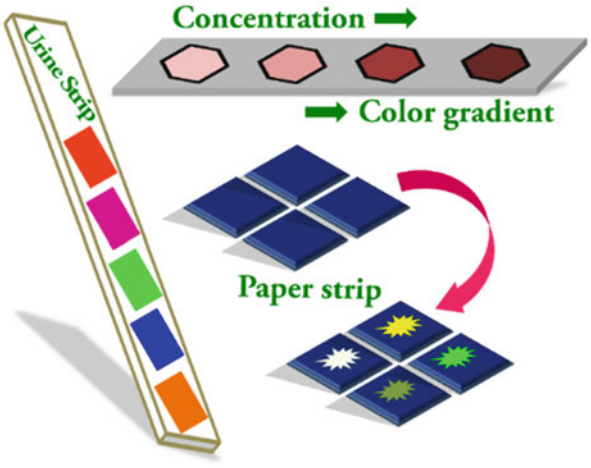

Fig. 2.3 Schematically shows colorimetric based detection in the paper as a substrate

instruments, or providing quantitative results with simple optical detectors like image processing software.

In the field of clinical diagnostics, colorimetric detection incorporating paper-based devices has proved to be advantageous diagnostic tools relative to other traditional methods due to its simplicity, sensitivity, and low-cost keys. Several biosensing techniques have been developed for efficient clinical diagnosis. Teengam et al. [87] developed a paper-based DNA detection colorimetric assay for the determination of MERS-CoV, MTB, and HPV oligonucleotides. They developed paper-based motifs immobilized with AgNP as the sensors. The detection principle shows the aggregation of nanoparticles by pyrrolidinyl peptide nucleic acid (PNA) if the complementary DNA is absent. However, if the complementary DNA is present, the DNA–PNA duplex caused the dispersion of AgNP which subsequently made a color change. Dutta et al. [88] reported a paper-based α-amylase quantification point-of-care testing device. Here, the authors coated the paper with starch iodine, which shows a deep blue color. On reaction with α-amylase, the starch hydrolysis caused the de-coloration of the paper, which is quantified against various concentrations of α-amylase from human blood serum.

In another work, Gabriel et al. [89] developed a paper-based colorimetric biosensor to quantify glucose levels from the human tear fluid. In this work, glucose oxidase was immobilized on the paper substrate, which on reaction with glucose gives hydrogen peroxide as a by-product and on further reaction with 3, 3′, 5, 5-′-tetramethylbenzydine (TMB) gives different shades of color. Similarly, Wang et al. [90] also developed glucose and uric acid monitoring paper-based sensors using chitosan, TMB, horseradish peroxidase (HRP), and the corresponding enzyme, i.e., glucose oxidase and uricase. The color shade developed was transduced with the help of a smartphone. The sensor was also tested with real serum and tear samples, which show relevant results.

2.3.1.3 Microfluidic Biosensors

The modernization of sophisticated high-end instruments has enabled the integration of biosensors with microfluidic systems, which has proved to be an efficient alternative to conventional laboratory methods. Figure 2.4 shows a glimpse of a microfluidic biosensor. Here, a channel of micron range is used as a modified probe for the detection of various targeted analytes. It offers a significant decrease in sample size, reagents used, effective energy consumption, waste production, cost and has also increased the detection specificity and sensitivity limit as compared to the conventional diagnostics method. The enhanced analytical performance of these microsystems has made detection adaptable to home-testing applications.

There are three types of microfluidic-based biosensing platforms [91]: (i) Continuous flow microfluidic system, where the system consists of two inlets, one for analyte addition, and other for reagent addition, and one outlet to collect the remnants. (ii) Droplet based microfluidic system where the analyte and the reagent from the two inlets meet at a T-junction and the output is obtained in the form of

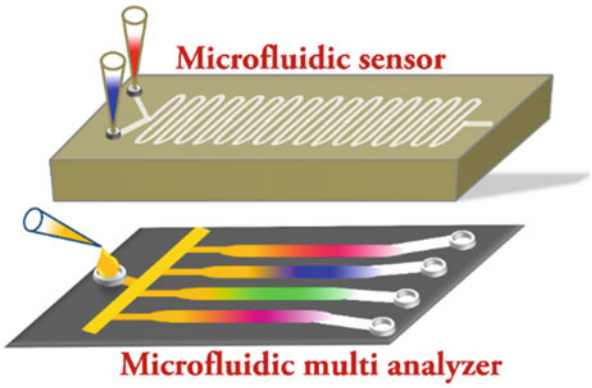

Fig. 2.4 Schematically shows colorimetric based detection in the microfluidic channel as a substrate

discrete droplets, which are then isolated with the help of immiscible fluid. (iii) New generation digital microfluidic systems, which create droplets on an array on top of electrostatically actuated electrodes as compared to the continuous flow systems. Some studies have already been done to develop microfluidic-based biosensors to detect various diseases and irregularities of specific biochemical reactions. Srinivasan et al. [92] developed a digital microfluidic platform for multianalyte detection like glucose, lactate, glutamate, and pyruvate using the principle of electrowetting integrated with an optical absorbance measurement system. In another work, Koh et al. [93] developed a microfluidic colorimetric sweat sensor for chloride and hydronium ions, glucose, and lactate. The reported sensor was claimed to be soft, flexible, and stretchable and measures pH, sweat rate, total sweat loss, and concentration of chloride and lactate.

Apart from these, Zhang et al. [94] reported a novel biosensor to diagnose *E. coli* from human serum samples using AuNP immobilized with antibodies against the target. The attachment of the target with the sample analyte produced a color change of the sensor from red to shades of blue, which was transduced for the quantification of the bacteria of interest. Fraser et al. [95] designed a portable microfluidic biosensor to measure Malaria from the human serum sample. The developed device was based on the aptamer tethered enzyme capture technology, which specifically recognizes *Plasmodium falciparum* lactate dehydrogenase (PfLDH) enzyme. It was claimed that the reported device is suitable for spot testing. Zaytseva et al. [96] developed a similar device for the detection of pathogenic organisms and viruses using PDMS based microchannels.

2.3.1.4 Microfluidic Paper Analytical Devices (μPADs)

Microfluidic analytical devices based on paper (μPADs), as portrayed in Fig. 2.5, has gained widespread acceptance, after its introduction in 2007 [97], owing to affordability, user-friendliness, ubiquitous nature, and since it does not need external instruments and easy fabrication processes. The μPADs consist of hydrophilic or

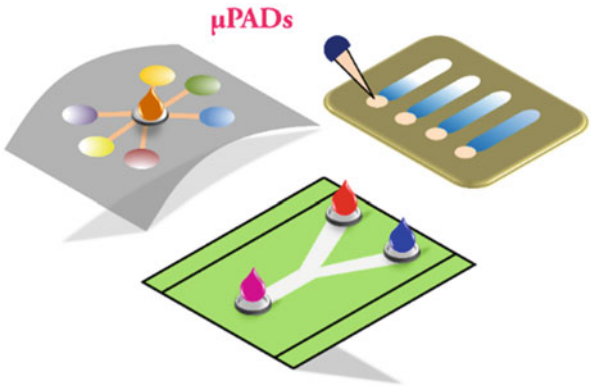

Fig. 2.5 Thematically shows colorimetric detection in µPADs as a substrate

hydrophobic microchannels on the paper, based on the requirement, fabricated using various methods like wax printing, inkjet printing, wax-screen printing, photolithography, and others. Two varieties of µPADs are there, the 2D and 3D fabrication. In 2D µPADs, the microchannels are fabricated on the part of the paper substrate to transport fluids in horizontal as well as vertical directions for various applications. In the case of 3D fabrication, an alternating stack of paper and water impermeable tape is made such that both the layers are patterned to permeate the flow of fluid within as well as between the layers of paper.

The microchannel networks and the associated analytical devices of the µPADs have enabled easier fluid handling and real-time quantitative analysis of various targets in the fields of medicine [98, 99], healthcare [98], and environment [100]. Gabriel et al. [101] designed chitosan modified µPADs to measure glucose and urea. They tested the glucose and urea concentration with high specificity from the blood samples of the patients. The authors also claimed that using this technique, they have identified different levels of glucose, non-invasively from the tear samples of some patients, which shows no variation with the standard results. In similar lines, Zhu et al. [102] also developed a µPAD based glucose sensor based on hybrid nanocomplex of glucose oxidase (GO_x), horseradish peroxidase (HRP), and $Cu_3(PO_4)_2$ which forms a flower-like structure. The authors claimed that the developed sensor can detect the glucose levels from blood serum as well as from whole blood. Cho et al. [103] developed a µPAD based immunosensor for the detection of urinary tract infection (UTI) and gonorrhea or sexually transmitted diseases (STD). The authors immobilized the antibodies for *E. coli* and STD at the center of the µPAD. The urine samples collected from the patient were first treated with Tween-80 and then loaded into the microchannel through the inlet. They showed a similar specificity as with the commercially available urine analysis strips. Vella et al. [104] have designed a µPAD for the identification of two biomarkers identified for unhealthy liver functioning, alkaline phosphatase (ALP), and aspartate aminotransferase (AST) and total serum protein. Apart from all these works, µPADs have also been developed for the easy detection of many common diseased conditions like HIV [105], Malaria [106], Hepatitis C [107], Tuberculosis [108], and many others.

2.3.2 *Colorimetric Assays*

Colorimetric assays are a particular variant of lateral flow assay (LFA), popularly known as test strips. Nowadays, with the advancement of the technologies in the field of biosensors, LFA based biosensors have become one of the critical elements of POCT techniques, widely accepted by medical practitioners as well as by the end-users owing to its properties of simplicity, rapidness, and cost-effectiveness [109]. Figure 2.6 shows the typical arrangement and operation of a flow assay. LFAs consist of a series of membranes arranged together to facilitate the flow of the sample. At first, a sample pad is placed where the sample is dropped. In a few cases, a filter member is also attached to this sample pad to filter the crude analyte samples as well as to control the amount of sample required. After the sample pad, a conjugate pad is placed where the antibodies with the label are immobilized. If the sample contains the target element, the targets attach to the antibodies immobilized on the conjugate pad which flows in forward direction. Afterward, a nitrocellulose membrane is placed where the binding reagents are immobilized, which binds to the target attached antibodies coming from the conjugate pad. This line is called the test line. In case, if the required targets are present in the analyte, the test line develops a color, where the intensity of the color developed signifies the quantity of the target present in the analyte used. A control line is also placed in the nitrocellulose membrane, which confirms the flow of the sample through the assay. Finally, an absorbent pad is placed, which absorbs the excess sample used, to complete the construction of the sandwich-type LFA.

In a competitive type LFA, the target is immobilized in the nitrocellulose membrane, whereas the antibody corresponding to that analyte with the label is immobilized on the conjugate pad. If the analyte dropped does not contain the target element, the antibodies with the label flow through the assay and attached to the target immobilized in the nitrocellulose membrane and increase the intensity of the initial color of the line. However, if the target is present in the analyte, the antibody in the conjugate pad attaches to the incoming target and thus is not free to attach with the target immobilized in the assay. This causes the intensity of the color to reduce. There are a number of LFAs developed for the quantification of various elements like for the detection of multiple cardiac biomarkers [110], creatine [111], influenza

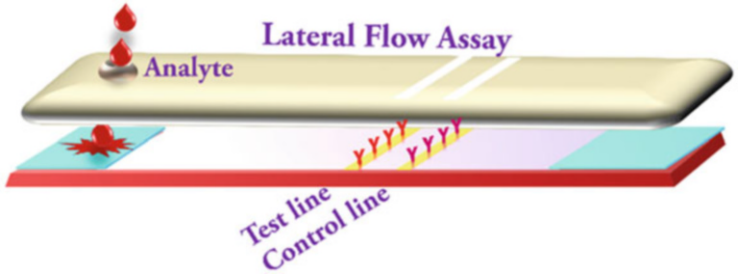

Fig. 2.6 Symbolically shows the working principle of a colorimetric assay

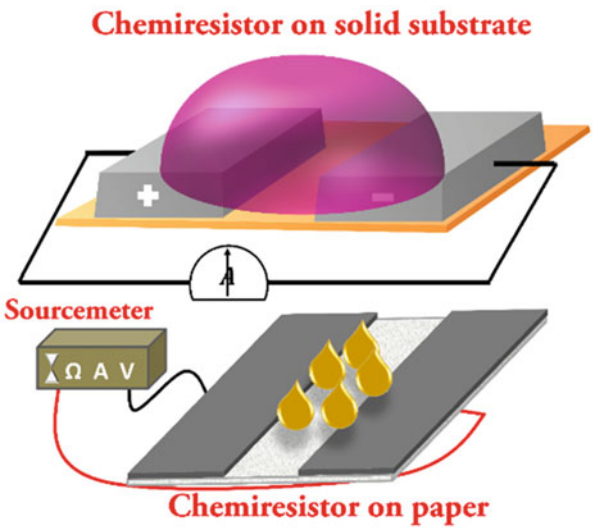

Fig. 2.7 Represents a typical chemiresistive based biosensor measurement arrangement

virus [112], interleukin-6 [113], detection of carcinoembryonic antigen [114], pneumolysin [115], etc.

2.3.3 Chemiresistive Biosensors

Chemiresistive biosensors are a class of biosensors, which changes its electrical resistance as a cause of any chemical change in the environment. It consists of a substrate for placing a sensing material and two electrodes for observing the electrical resistance change, as shown thematically in Fig. 2.7. In a basic prototype of a chemiresistor, the sensing material is positioned in between two electrodes. The sensing material has a resistance of its own, which is taken as the base resistance of the sensor. On the addition of the analyte to the sensing material, correspondingly the resistance of the system also changes. This change in the resistance can be easily measured using a multimeter or sourcemeter depending on the degree of resistance change. The relative change of the resistance, on the addition of an analyte, from the base resistance is marked as the signature of the presence of the target in the analyte. Moreover, in some cases, the resistance of the system changes proportionally to the amount of target present in the analyte, which helps in the quantitative analysis of the target. The explained chemiresistive system has significantly aided the development of biosensors for the healthcare sector. Several detection kits have been developed for the identification of foreign bodies like dengue [116], malaria [117], *E. coli* [118] to count a few. Chemiresistive sensors have also been explored for the detection of any biochemical imbalances like glucose [119], α-amylase [120], cholesterol [121], and alcohol breath analyzer [122].

2.3.4 *Electrochemical Biosensors*

Electrochemical biosensors are the subgroup of chemical sensors where the electrical signal generated from the chemical interaction of the capture molecule and the targeted analyte is transduced as a means of sensing mechanism. The symbolic image shown in Fig. 2.8 would guide the readers to get an idea about electrochemical biosensor along with working electrode chemistry. These sensors are advantageous in the areas where the analytes have meager detection limits of the target presence. The electrochemical sensors consist of a working electrode where the chemical interaction is meant to occur to produce an electrical signal, which is marked against a reference electrode to get the current or the potential values. A counter electrode is also placed, which provides a means of applying input potential to the working electrode. The three-electrode system is useful to characterize the electrochemical property of the analyte. It gives an understanding of the potential at which the required chemical reaction happens, which is not possible in a two-electrode system where none of the electrode's potential is fixed to measure the potential change. The amount of the electrical signal produced is proportional to the amount of the target of interest present in the analyte taken. The electrochemical sensors are also beneficial in terms of the usage of the sample. Since electrochemistry is a surface technique, it does not depend on reaction volume, and thus minimal amount also provides significant results [123].

Electrochemical sensors can further be classified into bio-catalytic devices and affinity sensors [123]. In bio-catalytic devices, enzymes, cells, or tissue sections are immobilized on the working electrode to recognize the target element and produce electroactive species like the detection of cholesterol from cholesterol oxidase [124]. However, in affinity devices, selective binding species modified working electrode are used for the detection of the targeted antigen, like antibody–antigen interaction or use of nucleic acids, such as detection of HIV [125], various kinds of cancer [126, 127], leukemia [128], detection of dengue [129], etc. An essential

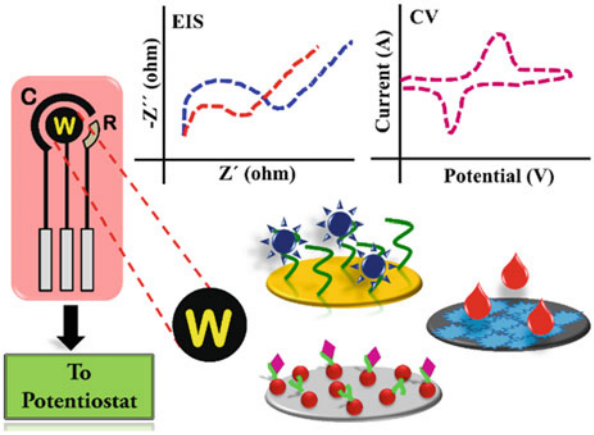

Fig. 2.8 Schematically shows various techniques and working electrodes used in an electrochemical biosensor

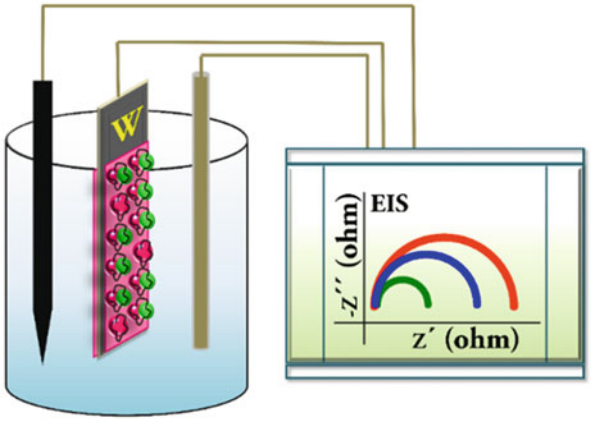

Fig. 2.9 Shows the principle of detection in impedance-based biosensors

requirement of an electrochemical sensor is the preparation of an ideal, specific, and sensitive working electrode aimed to detect the targeted biomolecule. There are many substrates and materials available nowadays for the fabrication of the working electrode [130]. Many electrochemical sensing techniques have been developed by fabricating the working electrode using silicon substrate [65], alumina [66], magnetic micro/nano particles [67], molecularly imprinted polymer [68], nanoporous gold supported porous cobalt oxide [69], nanowire [70], zinc oxide microspheres [71], sol–gel materials [72], lipid bilayer [73], transition metal dichalcogenides [74], etc. Recently, advancements have also been made in the fields of development of flexible [131] and disposable [132] electrochemical sensors or clinical applications to boost the healthcare sectors.

Impedance-based biosensors are a subgroup of electrochemical biosensors where both the reactance and the resistance of the system are measured for the detection of the targeted biomolecule. Figure 2.9 assists the readers to follow up with the impedance-based biosensing protocol. These systems consist of a substrate to place the sensing medium and electrodes to measure the reactance and resistance change. Both two-electrode and three-electrode systems can be used. The resistance and reactance are evaluated at the solid electrode/liquid analyte interface by observing the current response by applying a small AC voltage. A number of works have been done for the development of biosensors based on the detection of an enzyme, nucleic acid or DNA, antibodies, cells, or microorganisms [133]. Other than these, several studies have also been done for the development of detection kits for the identification of various foreign elements like bacterial cells [134], influenza virus [135], HIV [133], Hepatitis B [136] or for the monitoring of various biochemical imbalances like bio-electronic detection of various proteins [137], cholesterol [138], lipid [139] to count a few.

Capacitive biosensors are the subgroup of impedance-based biosensors. These biosensors evaluate the changes in dielectric properties and the dielectric layer thickness at the electrolyte/electrode interface. The capture molecules are immobilized on the surface of the electrode and on the addition of the analyte

containing the target element, an electrical capacitance is developed between the working electrode and the electrolyte [140]. The sensor arrangement can be of two-electrode system [141], interdigitated electrode systems [142] or capacitive arrays can also be used in this regard [143]. Capacitive sensors can be further classified into two sub-groups as faradaic and non-faradaic sensors on the basis of the transient current flow. A faradaic sensor requires redox species for the transfer of charges across the electrolyte/electrode interface, which is not the case with non-faradaic sensors. That is why non-faradaic sensors are more preferable for the point-of-care applications [24]. A number of biosensing procedures have been developed utilizing the capacitive measurement techniques such as for the detection of various irregularities originated from the imbalance of certain nutrients in the human body like for glucose [144], cholesterol [145], neurotransmitter dopamine [146], levels of C-reactive protein (CRP) as cardiac health biomarker [147] are among a few studies. Several works have also been done for the identification of pathogenic conditions invading the body like serodiagnosis of infectious disease [148]. Various works have also been performed in the fields of cancer diagnosis like detection of various levels of Tumor Necrosis Factor-alpha, B-type natriuretic peptide, Troponin-I, Serum Amyloid A, Fibrinogen, Interleukin 6 [142] and for the sensitive detection of vascular endothelial growth factor-165 (VEGF) in human serum [149].

2.3.5 *Semiconductor Biosensors*

The semiconductor-based biosensor is a category of biosensor where the detection of the target element is carried out with the help of semiconductor devices like field effect transistor (FET), surface acoustic devices (SAW), ion sensitive field effect transistor (ISFET), or others. The symbolic diagram as depicted in Fig. 2.10 shows a

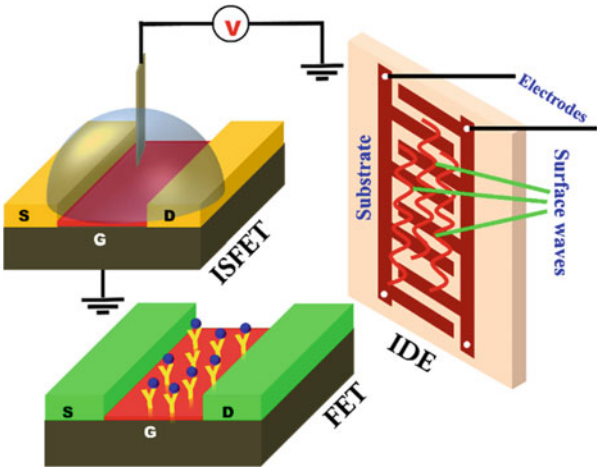

Fig. 2.10 Shows different conventional semiconductor devices which are used as biosensing principle

few of the existing semiconductor devices, which are being used as biosensors. In the case of FET based semiconductor devices, the sensing material is generally immobilized on the gate region, and the output current response of the device is evaluated after the addition of the analyte of interest. If the target to be detected is an ionic solution, ISFET is generally used. SAW devices exploit the horizontal polarization of the shear waves as a measure of the detection of various quantities of analytes, e.g., proteins.

The response of the device changes mainly because of the change in mass increase and viscoelastic property of the device surface [150]. The scope of semiconductor-based biosensors has widely extended from the detection of phytopathogen [151], detection of various microorganisms, e.g., Ebola virus [152], detection of biochemical imbalances in a body like cholesterol [153] to tumor marker detection in human serum [154] and cancer diagnostics like lung cancer [155].

2.4 Recent Trends of Biosensing and Device Fabrication

Multifarious efforts are being put forward for the advancements in the field of biosensing. A close look into the recent research on biosensing reveals that there are few characteristics, which are targeted for revamping and modernization of biosensors. First of all, unlike the conventional biosensors, miniaturization of the existing sensing techniques is on the rise. With the successful advancements of nanotechnology, paper-based devices, microfluidic devices, and paper-based microfluidics, and miniaturization have been flourished. Other important characteristics of modern biosensors are user-friendliness, portability, and low cost. Wide varieties of sensors, e.g., electrochemical, capacitive, resistive, impedance based are taken under consideration for their characteristic integration. The most important trend which is followed alongside miniaturization and portability is "no compromise" with selectivity, sensitivity, level of detection, and repeatability of biosensors.

The ultimate aim of the biosensing technologies is the fabrication of hand-held devices for instant and accurate measurements. In this regard, a close look into previous works reveals that considerable efforts have been made in POCT device fabrication. In making those POCT devices several technologies have been exploited such as electrochemical sensing, portable spectrophotometry, colorimetric flow assay, colorimetric strips, microfluidic based devices, μ-pads among others. Among the developed devices glucometer, both colorimetric and electrochemical, hemoglobin meter, urine strips, pregnancy kit, malaria kit, dengue kit, digital pressure monitoring device, pulse oximeter has become very popular in the global health market. Alongside these devices, a lot of efforts are put forward to develop non-invasive devices targeting glucose sensing, eye irregularities detection, internal imaging, and many more. It is interesting that leading companies like Google, Apple, or Samsung are working in the field of biosensing for coming up with technology solutions based on digitization, artificial intelligence, big data analysis, machine learning tools.

2.5 Future of Biosensing

One can straightaway project some of the salient features of future biosensors. In the era of digitization, analog measurements are not appreciated in most cases, especially in medical diagnostics sector. As a result, attention is paid to the digitization of biosensors and associated devices. The prime objectives of future biosensors are instant measurement techniques, digital reading, wireless reading transfer, cost-effectiveness, less energy consumption, and most importantly accuracy, sensitivity, selectivity, and robustness. Looking at the current scenario of medical diagnostics the most important features of future generation biosensors would definitely have the following features:

(a) High sensitivity and the time of detection should be as minimum as possible.
(b) The target would be zero tolerance with respect to the accuracy and selectivity of the biosensors.
(c) Along with digital reading, it will also be a mandate to have a wireless communication system for sending and storage of obtained data.
(d) Multiple measurements in a single device will be one of the peripheral targets.
(e) The need to be energy efficient and of high-power density.
(f) Miniaturization should lead to the use of high-power density, low power, energy efficient, and portable batteries.
(g) A high capacity is always targeted to cope with any emergency or some bacterial and viral outbreaks.
(h) AI-ML-IoT platforms will be targeted to integrate to analyze and predict probable treatment based on previously fed data during the latest measurement.

2.6 Summary

The present chapter summarizes various aspects of biosensing and biosensors development with special emphasis on recent advancements of biosensing techniques. It was also justified that holistic attempts are made for the development of portable devices which would be cost effective and user friendly. The chapter is summarized with the following key points:

(a) Different techniques of biosensing like colorimetry, electrochemical, resistive, capacitive, impedance based, and associated techniques have been discussed in detail.
(b) The use of the above-mentioned techniques for the development of paper based, microfluidic based, flow assay, and liquid phase sensors was discussed.
(c) The development of different kinds of electrochemical working electrodes for the development of the sensors is also taken into consideration.
(d) Alongside electrode development, different miniaturization techniques of the developed electrodes and integration of multiple working electrodes into one for simultaneous sensing were also discussed.

(e) Different devices, colorimetric assays, lab on a chip device, and other allied techniques for the development of tiny devices have been discussed.

Further, a few of the commercially available devices based on the discussed techniques of sensing are also cited in this chapter to give an insight into the health care market. Recent trends of biosensing and related advancements based on the detailed background have also been summarized. Conclusively, the present chapter assists readers from different fields of science and technology who are working in the field of biosensing and device development.

References

1. Purohit, B., Vernekar, P. R., Shetti, N. P., & Chandra, P. (2020). Biosensor nanoengineering: Design, operation, and implementation for biomolecular analysis. *Sensors International, 1*, 100040.
2. Nicholl, D. S. (2008). *An introduction to genetic engineering*. Cambridge, MA: Cambridge University Press.
3. Lanza, R., Langer, R., Vacanti, J. P., & Atala, A. (2020). *Principles of tissue engineering*. New York: Academic Press.
4. Chan, J. K., Gardner, A. B., Taylor, K., Thompson, C. A., Blansit, K., Yu, X., & Kapp, D. S. (2015). Robotic versus laparoscopic versus open surgery in morbidly obese endometrial cancer patients—A comparative analysis of total charges and complication rates. *Gynecologic Oncology, 139*, 300.
5. Alici, G. (2015). Towards soft robotic devices for site-specific drug delivery. *Expert Review of Medical Devices, 12*, 703.
6. Keyes, R. W. (1979). The evolution of digital electronics towards VLSI. *IEEE Journal of Solid-State Circuits, 14*, 193.
7. Tan, L., & Wang, N. (2010). *Future Internet: The Internet of things architecture, possible applications and key challenges*, IEEE
8. Russell, S., & Norvig, P. (2002). *Artificial intelligence: A modern approach*. Englewood Cliffs, NJ: Prentice Hall.
9. Purohit, B., Kumar, A., Mahato, K., & Chandra, P. (2020). Smartphone-assisted personalized diagnostic devices and wearable sensors. *Current Opinion in Biomedical Engineering, 13*, 42.
10. Yang, N., Chen, X., Ren, T., Zhang, P., & Yang, D. (2015). Carbon nanotube based biosensors. *Sensors and Actuators B: Chemical, 207*, 690.
11. Suvarnaphaet, P., & Pechprasarn, S. (2017). Graphene-based materials for biosensors: A review. *Sensors, 17*, 2161.
12. Ates, M. (2013). A review study of (bio) sensor systems based on conducting polymers. *Materials Science and Engineering: C, 33*, 1853.
13. Doria, G., Conde, J., Veigas, B., Giestas, L., Almeida, C., Assunção, M., Rosa, J., & Baptista, P. V. (2012). Noble metal nanoparticles for biosensing applications. *Sensors, 12*, 1657.
14. Liu, Z., Zhang, L., Poyraz, S., & Zhang, X. (2013). Conducting polymer-metal nanocomposites synthesis and their sensory applications. *Current Organic Chemistry, 17*, 2256.
15. Zhu, M., & Diao, G. (2011). Review on the progress in synthesis and application of magnetic carbon nanocomposites. *Nanoscale, 3*, 2748.
16. Elahi, N., Kamali, M., & Baghersad, M. H. (2018). Recent biomedical applications of gold nanoparticles: A review. *Talanta, 184*, 537.

17. Marin, S., Mihail Vlasceanu, G., Elena Tiplea, R., Raluca Bucur, I., Lemnaru, M., Minodora Marin, M., & Mihai Grumezescu, A. (2015). Applications and toxicity of silver nanoparticles: A recent review. *Current Topics in Medicinal Chemistry, 15*, 1596.
18. Claussen, J. C., Kumar, A., Jaroch, D. B., Khawaja, M. H., Hibbard, A. B., Porterfield, D. M., & Fisher, T. S. (2012). Nanostructuring platinum nanoparticles on multilayered graphene petal nanosheets for electrochemical biosensing. *Advanced Functional Materials, 22*, 3399.
19. Crespilho, F. N., Ghica, M. E., Florescu, M., Nart, F. C., Oliveira, O. N., Jr., & Brett, C. M. (2006). A strategy for enzyme immobilization on layer-by-layer dendrimer–gold nanoparticle electrocatalytic membrane incorporating redox mediator. *Electrochemistry Communications, 8*, 1665.
20. Sharma, A., Matharu, Z., Sumana, G., Solanki, P. R., Kim, C., & Malhotra, B. (2010). Antibody immobilized cysteamine functionalized-gold nanoparticles for aflatoxin detection. *Thin Solid Films, 519*, 1213.
21. Li, L.-D., Chen, Z.-B., Zhao, H.-T., Guo, L., & Mu, X. (2010). An aptamer-based biosensor for the detection of lysozyme with gold nanoparticles amplification. *Sensors and Actuators B: Chemical, 149*, 110.
22. Raguse, B., Chow, E., Barton, C. S., & Wieczorek, L. (2007). Gold nanoparticle chemiresistor sensors: Direct sensing of organics in aqueous electrolyte solution. *Analytical Chemistry, 79*, 7333.
23. Pingarrón, J. M., Yanez-Sedeno, P., & González-Cortés, A. (2008). Gold nanoparticle-based electrochemical biosensors. *Electrochimica Acta, 53*, 5848.
24. Altintas, Z., Kallempudi, S. S., & Gurbuz, Y. (2014). Gold nanoparticle modified capacitive sensor platform for multiple marker detection. *Talanta, 118*, 270.
25. Tothill, I. E. (2001). Biosensors developments and potential applications in the agricultural diagnosis sector. *Computers and Electronics in Agriculture, 30*, 205.
26. Luong, J. H., Bouvrette, P., & Male, K. B. (1997). Developments and applications of biosensors in food analysis. *Trends in Biotechnology, 15*, 369.
27. Malhotra, B. D., & Chaubey, A. (2003). Biosensors for clinical diagnostics industry. *Sensors and Actuators B: Chemical, 91*, 117.
28. Xianyu, Y., Wang, Q., & Chen, Y. (2018). Magnetic particles-enabled biosensors for point-of-care testing. *Trends in Analytical Chemistry, 106*, 213.
29. Chandra, P. (2016). *Nanobiosensors for personalized and onsite biomedical diagnosis*. London: The Institution of Engineering and Technology.
30. Yáñez-Sedeño, P., Agüí, L., Villalonga, R., & Pingarrón, J. (2014). Biosensors in forensic analysis. A review. *Analytica Chimica Acta, 823*, 1.
31. Wang, J. (2005). Carbon-nanotube based electrochemical biosensors: A review. *Electroanalysis, 17*, 7.
32. Luong, J. H., Hrapovic, S., & Wang, D. (2005). Multiwall carbon nanotube (MWCNT) based electrochemical biosensors for mediatorless detection of putrescine. *Electroanalysis, 17*, 47.
33. Torrinha, Á., Amorim, C. G., Montenegro, M. C., & Araújo, A. N. (2018). Biosensing based on pencil graphite electrodes. *Talanta, 190*, 235.
34. Zheng, P., & Wu, N. (2017). Fluorescence and sensing applications of graphene oxide and graphene quantum dots: A review. *Chemistry - An Asian Journal, 12*, 2343.
35. Wang, J., & Qiu, J. (2016). A review of carbon dots in biological applications. *Journal of Materials Science, 51*, 4728.
36. Aydın, E. B., & Sezgintürk, M. K. (2017). Indium tin oxide (ITO): A promising material in biosensing technology. *TrAC Trends in Analytical Chemistry, 97*, 309.
37. Dhand, V., Rhee, K. Y., Kim, H. J., & Ho Jung, D. (2013). A comprehensive review of graphene nanocomposites: Research status and trends. *Journal of Nanomaterials, 2013*.
38. Mallakpour, S., & Madani, M. (2015). A review of current coupling agents for modification of metal oxide nanoparticles. *Progress in Organic Coatings, 86*, 194.
39. Barati, A., Shamsipur, M., & Abdollahi, H. (2015). Hemoglobin detection using carbon dots as a fluorescence probe. *Biosensors and Bioelectronics, 71*, 470.

40. Bui, T. T., & Park, S.-Y. (2016). A carbon dot–hemoglobin complex-based biosensor for cholesterol detection. *Green Chemistry, 18*, 4245.
41. Jana, J., Chung, J. S., & Hur, S. H. (2019). ZnO-associated carbon dot-based fluorescent assay for sensitive and selective dopamine detection. *ACS Omega, 4*, 17031.
42. Zhai, H., Bai, Y., Qin, J., & Feng, F. (2019). Colorimetric and ratiometric fluorescence dual-mode sensing of glucose based on carbon quantum dots and potential UV/fluorescence of o-diaminobenzene. *Sensors, 19*, 674.
43. Teles, F., & Fonseca, L. (2008). Trends in DNA biosensors. *Talanta, 77*, 606.
44. Perfézou, M., Turner, A., & Merkoçi, A. (2012). Cancer detection using nanoparticle-based sensors. *Chemical Society Reviews, 41*, 2606.
45. Bagheri, S., Termeh Yousefi, A., & Mehrmashhadi, J. (2019). Carbon dot-based fluorometric optical sensors: An overview. *Reviews in Inorganic Chemistry, 39*, 179.
46. Ali, H., Ghosh, S., & Jana, N. R. (2020). Fluorescent carbon dots as intracellular imaging probes. *Wiley Interdisciplinary Reviews. Nanomedicine and Nanobiotechnology, 12*, e1617.
47. Fu, X., Chen, L., & Li, J. (2012). Ultrasensitive colorimetric detection of heparin based on self-assembly of gold nanoparticles on graphene oxide. *Analyst, 137*, 3653.
48. Qu, Z.-B., Lu, L.-F., Zhang, M., & Shi, G. (2018). Colorimetric detection of carcinogenic aromatic amine using layer-by-layer graphene oxide/cytochrome c composite. *ACS Applied Materials & Interfaces, 10*, 11350.
49. Kim, J.-H., Cho, S., Bae, T.-S., & Lee, Y.-S. (2014). Enzyme biosensor based on an N-doped activated carbon fiber electrode prepared by a thermal solid-state reaction. *Sensors and Actuators B: Chemical, 197*, 20.
50. Hayat, A., Rhouati, A., Mishra, R. K., Alonso, G. A., Nasir, M., Istamboulie, G., & Marty, J. L. (2016). An electrochemical sensor based on TiO2/activated carbon nanocomposite modified screen printed electrode and its performance for phenolic compounds detection in water samples. *International Journal of Environmental Analytical Chemistry, 96*, 237.
51. Niu, X., Yang, W., Wang, G., Ren, J., Guo, H., & Gao, J. (2013). A novel electrochemical sensor of bisphenol A based on stacked graphene nanofibers/gold nanoparticles composite modified glassy carbon electrode. *Electrochimica Acta, 98*, 167.
52. Lee, J., Kim, J., Kim, S., & Min, D.-H. (2016). Biosensors based on graphene oxide and its biomedical application. *Advanced Drug Delivery Reviews, 105*, 275.
53. Chen, Y., Michael, Z. P., Kotchey, G. P., Zhao, Y., & Star, A. (2014). Electronic detection of bacteria using holey reduced graphene oxide. *ACS Applied Materials & Interfaces, 6*, 3805.
54. Mandal, H. S., Su, Z., Ward, A., & Tang, X. S. (2012). Carbon nanotube thin film biosensors for sensitive and reproducible whole virus detection. *Theranostics, 2*, 251.
55. Wisitsoraat, A., Sritongkham, P., Karuwan, C., Phokharatkul, D., Maturos, T., & Tuantranont, A. (2010). Fast cholesterol detection using flow injection microfluidic device with functionalized carbon nanotubes based electrochemical sensor. *Biosensors and Bioelectronics, 26*, 1514.
56. Wang, S., Zhang, Q., Wang, R., & Yoon, S. (2003). A novel multi-walled carbon nanotube-based biosensor for glucose detection. *Biochemical and Biophysical Research Communications, 311*, 572.
57. Cavallari, M. R., Braga, G. S., da Silva, M. F., Izquierdo, J. E., Paterno, L. G., Dirani, E. A., Kymissis, I., & Fonseca, F. J. (2017). A hybrid electronic nose and tongue for the detection of ketones: Improved sensor orthogonality using graphene oxide-based detectors. *IEEE Sensors Journal, 17*, 1971.
58. Das, G., & Yoon, H. H. (2015). Amperometric urea biosensors based on sulfonated graphene/polyaniline nanocomposite. *International Journal of Nanomedicine, 10*, 55.
59. Anirudhan, T. S., & Alexander, S. (2017). A potentiometric sensor for the trace level determination of hemoglobin in real samples using multiwalled carbon nanotube based molecular imprinted polymer. *European Polymer Journal, 97*, 84.

60. Ansari, A. A., Kaushik, A., Solanki, P. R., & Malhotra, B. D. (2009). Electrochemical cholesterol sensor based on tin oxide-chitosan nanobiocomposite film. *Electroanalysis, 21*, 965.
61. Lin, Y., Peng, Y., & Di, J. (2015). Electrochemical detection of Hg (II) ions based on nanoporous gold nanoparticles modified indium tin oxide electrode. *Sensors and Actuators B, 220*, 1086.
62. Kim, S.-E., Kim, Y. J., Song, S., Lee, K.-N., & Seong, W. K. (2019). A simple electrochemical immunosensor platform for detection of apolipoprotein A1 (Apo-A1) as a bladder cancer biomarker in urine. *Sensors and Actuators B: Chemical, 278*, 103.
63. Bundy, J. G., Morriss, A. W., Durham, D. G., Campbell, C. D., & Paton, G. I. (2001). Development of QSARs to investigate the bacterial toxicity and biotransformation potential of aromatic heterocylic compounds. *Chemosphere, 42*, 885.
64. Smaniotto, A., Mezalira, D. Z., Zapp, E., Gallardo, H., & Vieira, I. C. (2017). Electrochemical immunosensor based on an azo compound for thyroid-stimulating hormone detection. *Microchemical Journal, 133*, 510.
65. Souteyrand, E., Martin, J., & Martelet, C. (1994). Direct detection of biomolecules by electrochemical impedance measurements. *Sensors and Actuators B: Chemical, 20*, 63.
66. Nguyen, B. T. T., Peh, A. E. K., Chee, C. Y. L., Fink, K., Chow, V. T., Ng, M. M., & Toh, C.-S. (2012). Electrochemical impedance spectroscopy characterization of nanoporous alumina dengue virus biosensor. *Bioelectrochemistry, 88*, 15.
67. Xu, Y., & Wang, E. (2012). Electrochemical biosensors based on magnetic micro/nano particles. *Electrochimica Acta, 84*, 62.
68. Gui, R., Jin, H., Guo, H., & Wang, Z. (2018). Recent advances and future prospects in molecularly imprinted polymers-based electrochemical biosensors. *Biosensors and Bioelectronics, 100*, 56.
69. Lang, X.-Y., Fu, H.-Y., Hou, C., Han, G.-F., Yang, P., Liu, Y.-B., & Jiang, Q. (2013). Nanoporous gold supported cobalt oxide microelectrodes as high-performance electrochemical biosensors. *Nature Communications, 4*, 1.
70. Wanekaya, A. K., Chen, W., Myung, N. V., & Mulchandani, A. (2006). Nanowire-based electrochemical biosensors. *Electroanalysis, 18*, 533.
71. Lu, X., Zhang, H., Ni, Y., Zhang, Q., & Chen, J. (2008). Porous nanosheet-based ZnO microspheres for the construction of direct electrochemical biosensors. *Biosensors and Bioelectronics, 24*, 93.
72. Wang, J. (1999). Sol–gel materials for electrochemical biosensors. *Analytica Chimica Acta, 399*, 21.
73. Tien, H. T., & Ottova, A. (1998). Supported planar lipid bilayers (s-BLMs) as electrochemical biosensors. *Electrochimica Acta, 43*, 3587.
74. Wang, Y.-H., Huang, K.-J., & Wu, X. (2017). Recent advances in transition-metal dichalcogenides based electrochemical biosensors: A review. *Biosensors and Bioelectronics, 97*, 305.
75. Guo, X. (2012). Surface plasmon resonance based biosensor technique: A review. *Journal of Biophotonics, 5*, 483.
76. Sepúlveda, B., Angelomé, P. C., Lechuga, L. M., & Liz-Marzán, L. M. (2009). LSPR-based nanobiosensors. *Nano Today, 4*, 244.
77. M. Basak, S. Mitra, S.K. Agnihotri, A. Jain, A. Vyas, M.L.B. Bhatt, R. Sachan, M. Sachdev, H.B. Nemade, D. Bandyopadhyay. (2021) ACS Applied Bio Materials, 4, 5378.
78. Soomro, R. A., Nafady, A., Memon, N., Sherazi, T. H., & Kalwar, N. H. (2014). L-cysteine protected copper nanoparticles as colorimetric sensor for mercuric ions. *Talanta, 130*, 415.
79. Shrivas, K., Shankar, R., & Dewangan, K. (2015). Gold nanoparticles as a localized surface plasmon resonance based chemical sensor for on-site colorimetric detection of arsenic in water samples. *Sensors and Actuators B: Chemical, 220*, 1376.

80. Shrivas, K., Sahu, J., Maji, P., & Sinha, D. (2017). Label-free selective detection of ampicillin drug in human urine samples using silver nanoparticles as a colorimetric sensing probe. *New Journal of Chemistry, 41*, 6685.
81. Lin, Y., Zhao, M., Guo, Y., Ma, X., Luo, F., Guo, L., Qiu, B., Chen, G., & Lin, Z. (2016). Multicolor colormetric biosensor for the determination of glucose based on the etching of gold nanorods. *Scientific Reports, 6*, 37879.
82. Ellairaja, S., Shenbagavalli, K., Ponmariappan, S., & Vasantha, V. S. (2017). A green and facile approach for synthesizing imine to develop optical biosensor for wide range detection of bilirubin in human biofluids. *Biosensors and Bioelectronics, 91*, 82.
83. Pourreza, N., & Golmohammadi, H. (2015). Hemoglobin detection using curcumin nanoparticles as a colorimetric chemosensor. *RSC Advances, 5*, 1712.
84. Verma, M. S., Rogowski, J. L., Jones, L., & Gu, F. X. (2015). Colorimetric biosensing of pathogens using gold nanoparticles. *Biotechnology Advances, 33*, 666.
85. Rajamanikandan, R., & Ilanchelian, M. (2017). Simple and visual approach for highly selective biosensing of vitamin B1 based on glutathione coated silver nanoparticles as a colorimetric probe. *Sensors and Actuators B: Chemical, 244*, 380.
86. Nirala, N. R., Saxena, P. S., & Srivastava, A. (2018). Colorimetric detection of cholesterol based on enzyme modified gold nanoparticles. *Spectrochimica Acta Part A: Molecular and Biomolecular Spectroscopy, 190*, 506.
87. Teengam, P., Siangproh, W., Tuantranont, A., Vilaivan, T., Chailapakul, O., & Henry, C. S. (2017). Multiplex paper-based colorimetric DNA sensor using pyrrolidinyl peptide nucleic acid-induced AgNPs aggregation for detecting MERS-CoV, MTB, and HPV oligonucleotides. *Analytical chemistry, 89*, 5428.
88. Dutta, S., Mandal, N., & Bandyopadhyay, D. (2016). Based α-amylase detector for point-of-care diagnostics. *Biosensors and Bioelectronics, 78*, 447.
89. Middya, S., Bhattacharjee, M., Mandal, N., & Bandyopadhyay, D. (2018). RGO-paper sensor for point-of-care detection of lipase in blood serum. *IEEE Sensors Letters, 2*, 1.
90. Wang, X., Li, F., Cai, Z., Liu, K., Li, J., Zhang, B., & He, J. (2018). Sensitive colorimetric assay for uric acid and glucose detection based on multilayer-modified paper with smartphone as signal readout. *Analytical and Bioanalytical Chemistry, 410*, 2647.
91. Luka, G., Ahmadi, A., Najjaran, H., Alocilja, E., DeRosa, M., Wolthers, K., Malki, A., Aziz, H., Althani, A., & Hoorfar, M. (2015). Microfluidics integrated biosensors: A leading technology towards lab-on-a-chip and sensing applications. *Sensors, 15*, 30011.
92. Srinivasan, V., Pamula, V., Pollack, M., & Fair, R. (2003). *A digital microfluidic biosensor for multianalyte detection*. Kyoto: IEEE.
93. Koh, A., Kang, D., Xue, Y., Lee, S., Pielak, R. M., Kim, J., Hwang, T., Min, S., Banks, A., & Bastien, P. (2016). A soft, wearable microfluidic device for the capture, storage, and colorimetric sensing of sweat. *Science Translational Medicine, 8*, 366ra165.
94. Zheng, L., Cai, G., Wang, S., Liao, M., Li, Y., & Lin, J. (2019). A microfluidic colorimetric biosensor for rapid detection of *Escherichia coli* O157: H7 using gold nanoparticle aggregation and smart phone imaging. *Biosensors and Bioelectronics, 124*, 143.
95. Fraser, L. A., Kinghorn, A. B., Dirkzwager, R. M., Liang, S., Cheung, Y.-W., Lim, B., Shiu, S. C.-C., Tang, M. S., Andrew, D., & Manitta, J. (2018). A portable microfluidic aptamer-tethered enzyme capture (APTEC) biosensor for malaria diagnosis. *Biosensors and Bioelectronics, 100*, 591.
96. Zaytseva, N. V., Goral, V. N., Montagna, R. A., & Baeumner, A. J. (2005). Development of a microfluidic biosensor module for pathogen detection. *Lab on a Chip, 5*, 805.
97. Xia, Y., Si, J., & Li, Z. (2016). Fabrication techniques for microfluidic paper-based analytical devices and their applications for biological testing: A review. *Biosensors and Bioelectronics, 77*, 774.
98. Rivet, C., Lee, H., Hirsch, A., Hamilton, S., & Lu, H. (2011). Microfluidics for medical diagnostics and biosensors. *Chemical Engineering Science, 66*, 1490.

99. Sriram, G., Bhat, M. P., Patil, P., Uthappa, U. T., Jung, H.-Y., Altalhi, T., Kumeria, T., Aminabhavi, T. M., Pai, R. K., & Kurkuri, M. D. (2017). Based microfluidic analytical devices for colorimetric detection of toxic ions: A review. *Trends in Analytical Chemistry, 93*, 212.
100. Almeida, M. I. G., Jayawardane, B. M., Kolev, S. D., & McKelvie, I. D. (2018). Developments of microfluidic paper-based analytical devices (μPADs) for water analysis: A review. *Talanta, 177*, 176.
101. Gabriel, E. F., Garcia, P. T., Cardoso, T. M., Lopes, F. M., Martins, F. T., & Coltro, W. K. (2016). Highly sensitive colorimetric detection of glucose and uric acid in biological fluids using chitosan-modified paper microfluidic devices. *Analyst, 141*, 4749.
102. Zhu, X., Huang, J., Liu, J., Zhang, H., Jiang, J., & Yu, R. (2017). A dual enzyme–inorganic hybrid nanoflower incorporated microfluidic paper-based analytic device (μPAD) biosensor for sensitive visualized detection of glucose. *Nanoscale, 9*, 5658.
103. Cho, S., San Park, T., Nahapetian, T. G., & Yoon, J.-Y. (2015). Smartphone-based, sensitive μPAD detection of urinary tract infection and gonorrhea. *Biosensors and Bioelectronics, 74*, 601.
104. Vella, S. J., Beattie, P., Cademartiri, R., Laromaine, A., Martinez, A. W., Phillips, S. T., Mirica, K. A., & Whitesides, G. M. (2012). Measuring markers of liver function using a micropatterned paper device designed for blood from a fingerstick. *Analytical Chemistry, 84*, 2883.
105. Rohrman, B. A., Leautaud, V., Molyneux, E., & Richards-Kortum, R. R. (2012). A lateral flow assay for quantitative detection of amplified HIV-1 RNA. *PLoS One, 7*, e45611.
106. Fu, E., Liang, T., Spicar-Mihalic, P., Houghtaling, J., Ramachandran, S., & Yager, P. (2012). Two-dimensional paper network format that enables simple multistep assays for use in low-resource settings in the context of malaria antigen detection. *Analytical Chemistry, 84*, 4574.
107. Mu, X., Zhang, L., Chang, S., Cui, W., & Zheng, Z. (2014). Multiplex microfluidic paper-based immunoassay for the diagnosis of hepatitis C virus infection. *Analytical Chemistry, 86*, 5338.
108. Tsai, T.-T., Huang, C.-Y., Chen, C.-A., Shen, S.-W., Wang, M.-C., Cheng, C.-M., & Chen, C.-F. (2017). Diagnosis of tuberculosis using colorimetric gold nanoparticles on a paper-based analytical device. *ACS Sensors, 2*, 1345.
109. Ye, H., & Xia, X. (2018). Enhancing the sensitivity of colorimetric lateral flow assay (CLFA) through signal amplification techniques. *Journal of Materials Chemistry B, 6*, 7102.
110. Zhang, D., Huang, L., Liu, B., Ni, H., Sun, L., Su, E., Chen, H., Gu, Z., & Zhao, X. (2018). Quantitative and ultrasensitive detection of multiplex cardiac biomarkers in lateral flow assay with core-shell SERS nanotags. *Biosensors and Bioelectronics, 106*, 204.
111. Zhang, J., Lv, X., Feng, W., Li, X., Li, K., & Deng, Y. (2018). Aptamer-based fluorometric lateral flow assay for creatine kinase MB. *Microchimica Acta, 185*, 364.
112. Hwang, S. G., Ha, K., Guk, K., Lee, D. K., Eom, G., Song, S., Kang, T., Park, H., Jung, J., & Lim, E.-K. (2018). Rapid and simple detection of Tamiflu-resistant influenza virus: Development of oseltamivir derivative-based lateral flow biosensor for point-of-care (POC) diagnostics. *Scientific Reports, 8*, 1.
113. de Souza Sene, I., Costa, V., Brás, D. C., de Oliveira Farias, E. A., Nunes, G. E., & Bechtold, I. H. (2020). A point of care lateral flow assay for rapid and colorimetric detection of interleukin 6 and perspectives in bedside diagnostics. *Journal of Clinical Medical Research, 2*, 1.
114. Liu, F., Zhang, H., Wu, Z., Dong, H., Zhou, L., Yang, D., Ge, Y., Jia, C., Liu, H., & Jin, Q. (2016). Highly sensitive and selective lateral flow immunoassay based on magnetic nanoparticles for quantitative detection of carcinoembryonic antigen. *Talanta, 161*, 205.
115. Blanco-Covián, L., Montes-García, V., Girard, A., Fernández-Abedul, M. T., Pérez-Juste, J., Pastoriza-Santos, I., Faulds, K., Graham, D., & Blanco-López, M. C. (2017). Au@Ag SERRS tags coupled to a lateral flow immunoassay for the sensitive detection of pneumolysin. *Nanoscale, 9*, 2051.

116. Zhang, G.-J., Zhang, L., Huang, M. J., Luo, Z. H. H., Tay, G. K. I., Lim, E.-J. A., Kang, T. G., & Chen, Y. (2010). Silicon nanowire biosensor for highly sensitive and rapid detection of Dengue virus. *Sensors and Actuators B: Chemical, 146*, 138.
117. Panigrahi, A. K., Singh, V., & Singh, S. G. (2017). A multi-walled carbon nanotube–zinc oxide nanofiber based flexible chemiresistive biosensor for malaria biomarker detection. *Analyst, 142*, 2128.
118. Li, F., & Kosel, J. (2013). A magnetic biosensor system for detection of *E. coli*. *IEEE Transactions on Magnetics, 49*, 3492.
119. Lai, J.-Y., Chen, Y.-T., Wang, T.-H., Chang, H.-S., & Lai, J.-L. (2007). *Biosensor integrated with transducer to detect the glucose*. Kyoto: IEEE.
120. Mandal, N., Bhattacharjee, M., Chattopadhyay, A., & Bandyopadhyay, D. (2019). Point-of-care-testing of α-amylase activity in human blood serum. *Biosensors and Bioelectronics, 124*, 75.
121. Tyagi, M., Chandran, A., Joshi, T., Prakash, J., Agrawal, V., & Biradar, A. (2014). Self assembled monolayer based liquid crystal biosensor for free cholesterol detection. *Applied Physics Letters, 104*, 154104.
122. Roy, N., Mitra, S., Das, N. M., Mandal, N., Bandyopadhyay, D., Nemade, H. B., & Mandal, T. K. (2019). Paper based enzymatic chemiresistor for POC detection of ethanol in human breath. *IEEE Sensors Journal*. https://doi.org/10.1109/jsen.2019.2952940.
123. Ricci, F., Adornetto, G., & Palleschi, G. (2012). A review of experimental aspects of electrochemical immunosensors. *Electrochimica Acta, 84*, 74.
124. Torres, A. C., Ghica, M. E., & Brett, C. M. (2012). Poly (neutral red)/cholesterol oxidase modified carbon film electrode for cholesterol biosensing. *Electroanalysis, 24*, 1547.
125. Zhang, D., Peng, Y., Qi, H., Gao, Q., & Zhang, C. (2010). Label-free electrochemical DNA biosensor array for simultaneous detection of the HIV-1 and HIV-2 oligonucleotides incorporating different hairpin-DNA probes and redox indicator. *Biosensors and Bioelectronics, 25*, 1088.
126. Topkaya, S. N., Azimzadeh, M., & Ozsoz, M. (2016). Electrochemical biosensors for cancer biomarkers detection: Recent advances and challenges. *Electroanalysis, 28*, 1402.
127. Wang, J. (2006). Electrochemical biosensors: Towards point-of-care cancer diagnostics. *Biosensors and Bioelectronics, 21*, 1887.
128. Ensafi, A. A., Taei, M., Rahmani, H., & Khayamian, T. (2011). Sensitive DNA impedance biosensor for detection of cancer, chronic lymphocytic leukemia, based on gold nanoparticles/gold modified electrode. *Electrochimica Acta, 56*, 8176.
129. Cecchetto, J., Carvalho, F. C., Santos, A., Fernandes, F. C., & Bueno, P. R. (2015). An impedimetric biosensor to test neat serum for dengue diagnosis. *Sensors and Actuators B: Chemical, 213*, 150.
130. Kumar, A., Purohit, B., Maurya, P. K., Pandey, L. M., & Chandra, P. (2019). Engineered nanomaterial assisted signal-amplification strategies for enhancing analytical performance of electrochemical biosensors. *Electroanalysis, 31*, 1615.
131. Reddy, A., Narakathu, B. B., Atashbar, M., Rebros, M., Hrehorova, E., & Joyce, M. (2010). *Printed electrochemical based biosensors on flexible substrates*. Kyoto: IEEE.
132. Janegitz, B. C., Cancino, J., & Zucolotto, V. (2014). Disposable biosensors for clinical diagnosis. *Journal of Nanoscience and Nanotechnology, 14*, 378.
133. Jiang, X., & Spencer, M. G. (2010). Electrochemical impedance biosensor with electrode pixels for precise counting of CD4+ cells: A microchip for quantitative diagnosis of HIV infection status of AIDS patients. *Biosensors and Bioelectronics, 25*, 1622.
134. Varshney, M., & Li, Y. (2009). Interdigitated array microelectrodes based impedance biosensors for detection of bacterial cells. *Biosensors and Bioelectronics, 24*, 2951.
135. Wang, R., Lin, J., Lassiter, K., Srinivasan, B., Lin, L., Lu, H., Tung, S., Hargis, B., Bottje, W., & Berghman, L. (2011). Evaluation study of a portable impedance biosensor for detection of avian influenza virus. *Journal of Virological Methods, 178*, 52.

136. Chen, C.-C., Lai, Z.-L., Wang, G.-J., & Wu, C.-Y. (2016). Polymerase chain reaction-free detection of hepatitis B virus DNA using a nanostructured impedance biosensor. *Biosensors and Bioelectronics, 77*, 603.
137. Rodriguez, M. C., Kawde, A.-N., & Wang, J. (2005). Aptamer biosensor for label-free impedance spectroscopy detection of proteins based on recognition-induced switching of the surface charge. *Chemical Communications, 2005*, 4267.
138. Arya, S. K., Prusty, A. K., Singh, S., Solanki, P. R., Pandey, M. K., Datta, M., & Malhotra, B. D. (2007). Cholesterol biosensor based on N-(2-aminoethyl)-3-aminopropyl-trimethoxysilane self-assembled monolayer. *Analytical Biochemistry, 363*, 210.
139. Bordi, F., Cametti, C., & Gliozzi, A. (2002). Impedance measurements of self-assembled lipid bilayer membranes on the tip of an electrode. *Bioelectrochemistry, 57*, 39.
140. Ertürk, G., & Mattiasson, B. (2017). Capacitive biosensors and molecularly imprinted electrodes. *Sensors, 17*, 390.
141. Berggren, C., Bjarnason, B., & Johansson, G. (2001). Capacitive biosensors. *Electroanalysis, 13*, 173.
142. Ceylan, O., Mishra, G. K., Yazici, M., Qureshi, A., Niazi, J. H., & Gurbuz, Y. (2018). A hand-held point-of-care biosensor device for detection of multiple cancer and cardiac disease biomarkers using interdigitated capacitive arrays. *IEEE Transactions on Biomedical Circuits and Systems, 12*, 1440.
143. Mattiasson, B., & Hedström, M. (2016). Capacitive biosensors for ultra-sensitive assays. *TrAC Trends in Analytical Chemistry, 79*, 233.
144. Hartono, A., Sanjaya, E., & Ramli, R. (2018). Glucose sensing using capacitive biosensor based on polyvinylidene fluoride thin film. *Biosensors, 8*, 12.
145. Aghaei, A., Hosseini, M. R. M., & Najafi, M. (2010). A novel capacitive biosensor for cholesterol assay that uses an electropolymerized molecularly imprinted polymer. *Electrochimica Acta, 55*, 1503.
146. Lu, M. S.-C., Chen, Y.-C., & Huang, P.-C. (2010). 5 × 5 CMOS capacitive sensor array for detection of the neurotransmitter dopamine. *Biosensors and Bioelectronics, 26*, 1093.
147. Qureshi, A., Gurbuz, Y., & Niazi, J. H. (2010). Label-free detection of cardiac biomarker using aptamer based capacitive biosensor. *Process Engineering, 5*, 828.
148. Li, S., Cui, H., Yuan, Q., Wu, J., Wadhwa, A., Eda, S., & Jiang, H. (2014). AC electrokinetics-enhanced capacitive immunosensor for point-of-care serodiagnosis of infectious diseases. *Biosensors and Bioelectronics, 51*, 437.
149. Qureshi, A., Gurbuz, Y., & Niazi, J. H. (2015). Capacitive aptamer–antibody based sandwich assay for the detection of VEGF cancer biomarker in serum. *Sensors and Actuators B: Chemical, 209*, 645.
150. Länge, K., Gruhl, F. J., & Rapp, M. (2013). *Surface Acoustic Wave (SAW) biosensors: Coupling of sensing layers and measurement*. New York: Springer.
151. Moreau, A. L., Janissen, R., Santos, C. A., Peroni, L. A., Stach-Machado, D. R., de Souza, A. A., de Souza, A. P., & Cotta, M. A. (2012). Highly-sensitive and label-free indium phosphide biosensor for early phytopathogen diagnosis. *Biosensors and Bioelectronics, 36*, 62.
152. Baca, J. T., Severns, V., Lovato, D., Branch, D. W., & Larson, R. S. (2015). Rapid detection of Ebola virus with a reagent-free, point-of-care biosensor. *Sensors, 15*, 8605.
153. Siddique, S., Iqbal, M. Z., & Mukhtar, H. (2017). Cholesterol immobilization on chemical vapor deposition grown graphene nanosheets for biosensors and bio FETs with enhanced electrical performance. *Sensors and Actuators B: Chemical, 253*, 559.
154. Cheng, S., Hotani, K., Hideshima, S., Kuroiwa, S., Nakanishi, T., Hashimoto, M., Mori, Y., & Osaka, T. (2014). Field effect transistor biosensor using antigen binding fragment for detecting tumor marker in human serum. *Materials, 7*, 2490.
155. Cheng, S., Hideshima, S., Kuroiwa, S., Nakanishi, T., & Osaka, T. (2015). Label-free detection of tumor markers using field effect transistor (FET)-based biosensors for lung cancer diagnosis. *Sensors and Actuators B: Chemical, 212*, 329.

Chapter 3
Evolution Towards Theranostics: Basic Principles

Pallavi Kiran, Amreen Khan, Suditi Neekhra, Pankaj Kumar, Barkha Singh, Shubham Pallod, Faith Dias, and Rohit Srivastava

3.1 Introduction

Nanotechnology is defined as the science of tiny particles lying within the scale of a few nanometers [1, 2]. The emerging fields in nanotechnology brought scientists together to develop a prognosis by merging diagnosis and therapeutics, leveraging their advantages. This provided insight into some major discoveries in effectively treating patients through early detection. Several deadly disorders including neurological and cardiovascular disorders could now be diagnosed and treated simultaneously [3, 4]. Moreover, personalized medicine for different diseases like cancer which shows heterogeneity has started to evolve with the developments in therapeutics modalities [5, 6]. To go deep into the approaches of many such case studies, we require an understanding of the phenomena behind the evolution of this therapy.

A single nanoparticle working as a diagnostic, therapeutic, and imaging agent can be substantiated in point-of-care testing. The term theranostic was proposed to define this aspect of treatment [7]. Surprisingly, although seems newly evolved, "Theranostic" was coined over 50 years ago when scientists struggled to determine a better way for simultaneous analysis and cure of thyroid cancer. The first treatment has been reported to incorporate nuclear medicine of Iodine-131 which is a radioisotope [8]. Undergoing various phases of development, it is now quite an effective

P. Kiran · S. Neekhra · P. Kumar · S. Pallod · F. Dias · R. Srivastava (✉)
Department of Biosciences and Bioengineering, Indian Institute of Technology Bombay, Powai, Mumbai, India
e-mail: rsrivasta@iitb.ac.in

A. Khan · B. Singh
Department of Biosciences and Bioengineering, Indian Institute of Technology Bombay, Powai, Mumbai, India

Centre for Research in Nanotechnology and Science, Indian Institute of Technology Bombay, Powai, Mumbai, India

V. Borse et al. (eds.), *BioSensing, Theranostics, and Medical Devices*,
https://doi.org/10.1007/978-981-16-2782-8_3

and safe method of treatment. This paved the way for the discovery of many nanotheranostic agents further enhancing the potential of medical care [9, 10].

In practice, not only theranostics but also theragnostics materials are being widely used in hospitals and various markets worldwide [11]. Several companies have many theranostic agents in the pipeline, and the future will bring innovative advances giving a detailed perspective on this type of technology. While many nanoparticle-based theranostic agents have FDA approval, a few are undergoing clinical trial licensing under specific categories of imaging or therapeutic agents [12]. However, to develop an effective, reliable, and well-designed theranostic medicine, science has still to go a long way. It is important to establish universally acceptable, safety, and toxicity profiles to get regulatory approvals for launching multifunctional theranostic materials as a point-of-care diagnosis in the market.

Through this chapter, we will be enhancing our primary understanding of theranostics as a point-of-care diagnostic and therapeutic platform. Further heading towards the characteristics and mechanisms involved with special emphasis on intrinsic properties. We also wish to provide insight into behavioral studies in biological environments based on toxicological fate. The chapter will take the reader through the challenges to the solution and a future scope ending on a summary of a point-of-care theranostic device.

Overall, the chapter sheds light on a topic of new found interest, wherein we see the seamless integration of theranostics and point-of-care devices. The basic concepts of theranostics have been introduced at first, initially advocating the need for constant monitoring and patient centered therapeutics, which is then followed by unraveling the components involved in theranostics and its applications in point-of-care devices. The chapter then focuses on the use of carriers in theranostics, particularly nanoparticles and their route of administration, followed by the targeting approaches involved in ensuring that the carrier reaches the site of the infected or diseased cells. Recent advancements in the field have been reviewed with a focus on the affordability of such devices, advantages of these technologies over the already existent conventional ones, and the challenges involved in developing and commercializing such technologies. With personalized medicine becoming a topic of major interest, point-of-care devices having theranostic potential is picking up as an area of research in the foreseeable future and the chapter aims in exploring this domain and identifying the pros and cons of this medically advanced diagnostic and therapeutic platform amalgamated in a single device. The chapter provides comprehensive information about the types of theranostic materials, their applications, advantages, and challenges.

3.2 Basic Principle of Theranostics in POC

Theranostics covers a wide range of topics that help optimize a vast range of therapies in the medical sector [13]. One such advancement of theranostics is its extension to real-time analysis which focuses on point-of-care testing. Point-of-care

testing is a type of healthcare made available on an immediate basis at any given point of time with the desired effect. Initially, this was utilized for an accurate on the spot diagnosis specific to a patient. However, with further development, therapy-based diagnosis has emerged for patient care in conjugation with professional consultation and advice. Since then many individually programmed kits have been utilized to rectify of a patient's disease and disorders [14]. The design, strategy, and novelty of such dynamic yet systemic approaches depend on deep apprehension and clinical proficiency. As we move towards the mechanism and different properties of nanoparticles used in POC, we have summarized the definition and the principle aspects of theranostics.

3.2.1 Fundamental Prospects

Biodistribution and therapeutic efficacy marked their occurrence soon after disease detection, where undesirable variation in therapy may have led to treatment failure. Medical imaging and therapeutics synergistically define theranostics as an integration of a biocompatible material package to diagnose and treat the patient. With theranostics, both the pharmacokinetic and pharmacodynamic fate of a drug inside the body can be traced and enhanced systematically [15]. The conceptual basis of theranostics in point-of-care testing is based on the principle interplay between pharmacogenetics, proteomics, and biomarker profiling of the patient. Pharmacogenetics assists in understanding the genomic sequence centralized on adequate biomarker response for an optimal outcome. A biomarker is a protein that acts as a biochemical indicator to monitor and diagnose every disease development stage during molecular treatment. This modulates designing a better drug moiety as a theranostic agent [16]. Moreover, the mechanisms of physiological pathways need to be determined for increasing the knowledge of an altered disease state. The changes in a gene sequence can adversely impact the drug binding and function [17]. Hence, another crucial part of patient care is predicting the protein infestations in revealing the encoded isoforms by the genome to get information about the physiological behavior of a cell. This provides the key to examine cellular function, localization, and expression of proteins. Different types of proteins behave differently in varying environments giving better prediction of variable biological information [18]. In contrast with community settings where generalized treatment is said to be dispersive, patient-centered treatment drifts evidence-based care improving accuracy and precision, possibly with the help of biomarker tracers. It includes molecular characterization, biomarker function, biomarker validation, and effective clinical utilization including bioinformatics tools [19].

The major concept behind extending these approaches has given a way to tackle physical clues associated with asymptomatic infections, supporting therapy. Organ-specific tests combined with electrical medical records and real-time image analysis have enhanced early detection of the target infestations [20]. Overall, this standardized shift from "one medicine for all" to a "fit for purpose" mindset has

revolutionized the healthcare sector. POC has principally been investigated to satisfy demand, seeking more improvised prognosis, diagnosis, and treatment [21].

3.2.2 Components

Due to their tiny characteristic dimensions, nanomaterials possess the ability to carry both the therapeutic and diagnostic agents along with the targeting moiety for drug delivery to a specific site. This has led to nanomaterials becoming an integral part of theranostics, which encouraged the use of the term "nanotheranostics". Nanotheranostics in conjugation with point-of-care devices aim to utilize the principles of nanotechnology in advanced theranostics. Characteristics of the therapeutic agent, diagnostic agent, effect, size, shape, and type of material define a theranostic, as shown in Fig. 3.1. Implementing all the properties in a single module for achieving effective treatment has brought about various nanoparticles and their chemical functionalization. Surface modified liposomes, dendrimers, metal and inorganic nanoparticles, carbon nanotubes, solid lipid nanoparticles, micelles, and biodegradable polymeric nanoparticles have been specifically designed to circumscribe patient-specific medicines. Also, recent developments in synthetic biology have propagated the use of cellular systems such as bacteria, viruses, and mammalian cells as theranostic agents. However, they require strong validation due to the characteristic cell-based therapies employed for individuals [22]. The advent behind the theranostic nanoparticles' design strategy is based on Ferrari's classification which comprises three major components, namely a biomedical payload, a carrier,

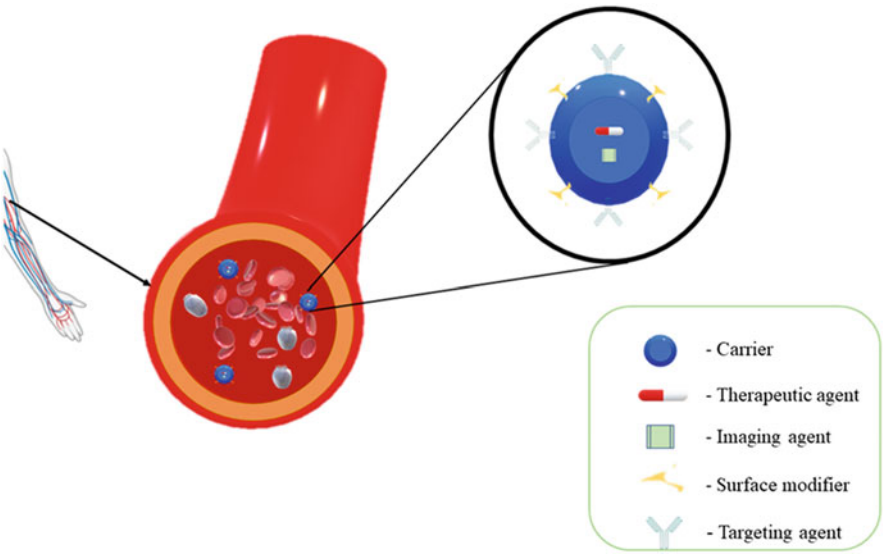

Fig. 3.1 Different constituents of a theranostic as a carrier system (created with Biorender.com)

and a surface modifier. The biomedical cargo consists of therapeutic agents, imaging agents, contrast agents, quantum dots, etc. After being processed, nanoparticles serve as carrier systems with inorganic or organic particles relinquishing sufficient protection to the therapeutic agent from biological invasion under physiological conditions for the therapeutic agent to be delivered efficiently. Surface modifiers increase the time of circulation by enhancing uptake and allowing easy penetration by crossing heterogeneous barriers for site-specific binding [13]. Upon further exploration, the types of technologies that come under the realm of point-of-care devices consist of label-free biosensors, microfluidic devices, lab on a chip technologies, lateral flow assays, smartphone-based applications, and wearable technologies. Gold nanoparticles used in lateral flow biosensors have contributed to improving the sensitivity of the methods as the formation of a sandwich occurs between the primary biomarker, the analyte, and the secondary biomarker tagged to a nanoparticle resulting in the appearance of color in the test zone. This could be attributed to the surface plasmon resonance effect. In the case of silver nanoparticles, the variation in nanoparticle morphology and associated optical properties results in different wavelengths, forming different tones of color in the testing zone which can be used in multiplex point-of-care tests. Electrochemical-based sensor nanoparticles have been explored to prepare inks for the fabrication of electrodes such as gold, silver, and carbon nanoparticle tubes. Also, magnetic nanoparticles employed in nuclear magnetic resonance imaging provide high precision diagnosis, owing to the low background signal. Nanowires of copper, nickel, platinum, gold, silver, and silicone are used in patient-centered medical support devices. The introduction of nanowires into paper substrates used for electrocardiogram monitoring depicts an application of using nanowires in POC devices [23].

Another aspect of theranostics has been the developing image-guided drug delivery by using imaging agents coupled with techniques like positron emission tomography (PET), fluorescence molecular tomography (FMT), and ultrasound. Apart from this, photothermal therapy (PTT) with magnetic resonance imaging (MRI) induces apoptotic cell death wherein near infra-red (NIR) visible light excites photoabsorber molecules and converts the energy of the incident light into heat by increasing temperature. Photodynamic therapy is another emerging modality where the reactive oxygen species produces a photo-necrotic effect at a suitable wavelength. The photosensitizer drug and the imaging moiety enable image-guided treatment of the diseased person, thus increasing the chance of better treatment [24].

3.2.3 Point-of-Care Devices

Point-of-care diagnosis technology has propelled the biomedical field towards engineering micro- and nanodevices amalgamating many clinical steps in a single build. Reliability, efficacy, portability, and affordability with ease of operation follow the basis of validation during clinical and personal use [25]. While many nanodiagnostic tools apply advanced optical, mechanical, electrical,

electrochemical, and mechanical concepts, there is no limit to improving the design of POC devices detection of diseases. Through nanoport technology, devising nanosensors with translating nucleic acids a lot of progress in the field of digitalization-based biosensors, for on the spot to recognizable electric signals and immediate mapping with already available datasets is possible [26]. Diseases like cancer whose tumor growth and development requires precise detection for effective treatment have also been explored as part of this domain. Antibodies carrying SERS (surface-enhanced Raman scattering/spectroscopy) nanotags with Raman reporters have been investigated to detect CD44, TGFbRII, and EGFR biomarkers during in vivo tumor targeting, showing active signals for a longer time. Detection techniques involving SERS offer higher specificity and multiplexing simultaneous detections capabilities in a single test [27]. Alternatively, quantum dots (QDs) [28] can assist in detecting changes in the pH of the body's physiological and acidic tumor microenvironment [29]. Recently, many lab-on-a-chip miniaturized nanoparticle-based devices for real-time analysis have been developed to diagnose and treat infectious diseases. Quantum dot-based fluorescent nanoparticles, such as iron oxide due to its magnetic and metallic properties when labeled with various biological targets have shown wide scope in increasing sensitivity for immunoassay POC devices already existent in the market. Many such approaches have been extended to readily available and extensively used devices in cell phone-based polarized light microassay platforms. Diagnostic based magnetic resonance systems offer nuclear magnetic resonance (NMR) based rapid multiplex detection. However, its application is limited due to its affordability and portability. Other metallic POC nanodiagnostic tools including paper and magnetic barcode-based systems utilize lateral flow microfluidics, effectively displaying visible readouts by simultaneous detection of multiple infections [30]. However, many criteria remain unfulfilled and the following sections reveal the importance of integrating this promising technology with various upcoming developments.

3.3 Biological Factors Involved in Theranostic Applications

The developments in nanoparticles for point-of-care applications need to consider variety of biological factors to transform into a functionalized personal medicine. While dealing with theranostic applications, the design scheme involves two basic precision steps in nanoparticle formulation. Firstly, for diagnosis purposes, the nanoparticle design is crucially important in disease identification and treatment progression after administration. It is combined with various techniques like NIR fluorescence, PET/SPECT, and MRI. Second factor is related to the use as therapeutic by photodynamic, chemotherapy, gene therapy, hyperthermia, and radiation therapies [21, 31].

3.3.1 Administration of Nanoparticles

Path guided nanoparticles targeting a specific site is highly dependent on the route of administration. This purpose is served mostly by localized and systemic administration. In localized administration, nanoparticles are injected directly into the disease-affected sites. Similarly, the drug is particularly delivered to the tumor microenvironment (intratumoral region). However, in the case of systemic treatment, the nanoparticles circulate through body fluids hence have to encounter and overcome many barriers to reach the desired site [32, 33].

The accumulation of nanoparticles at the target site depends on engineered nanoparticles conjugating ligands (antibodies, enzymes, aptamers, or small molecules). The type of surface modifications depends on molecular markers expressed on the disease or disorder being treated. The property of enhanced permeability and retention (EPR) shown in Fig. 3.2 should be presented by drug for effective cancer treatment [34].

The state of action is the disease microenvironment being biologically different from the normal tissues acting as a mode for the targeted delivery of nanoparticles. The targeted delivery can further be classified as active, passive, and physical briefly described [35].

3.3.1.1 Passive Targeting

In passive targeting, the nanoparticles are accumulated at the target site by an intrinsic property of the disease environment. The permeability factor is responsible for the crowding of nanoparticles. The neovasculature, developed due to angiogenesis at the diseased site, is different from that of the normal cells. They have high permeability. Such vascularization represents one characteristic property of blood

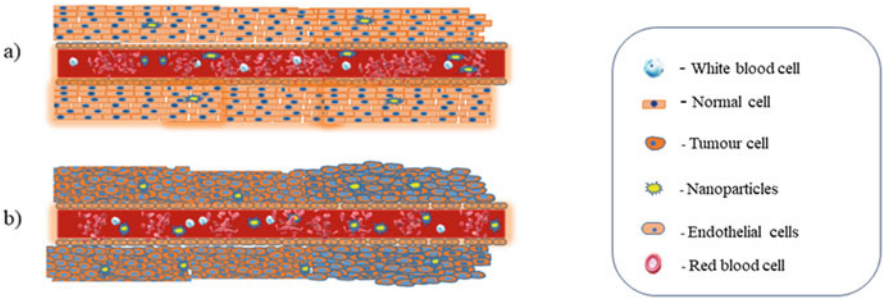

Fig. 3.2 The accumulation of nanoparticles is less in normal cells. (**a**) as compared to the tumor cells. (**b**) The event termed as enhanced permeability and retention (EPR) due to wrapped vessels surrounding the tumor

vessels at the tumor. This distinctive feature is known as EPR supporting the accumulation of nanoparticles at the target sites [35].

3.3.1.2 Active Targeting

Active targeting utilizes affinity interaction as a key player in nanoparticle accumulation at target sites. Active targeting is more specific than passive targeting as it increases the reliability of drug-loaded nanoparticles. This requires actual chemical moiety for surface changes of the nanoparticle to ease proper interaction with ligand. Some examples include the conjugated ligands acting against folate, transferring, and human epidermal receptors. Biologically dynamic conditions like angiogenesis factor, uncontrolled cell growth, and tumor target have also been studied. One development is designing the nanoparticles by inhibiting the growth factors for preventing tumor progression [35].

3.3.1.3 Physical Targeting

Nanoparticle delivery involving internally and externally assisted approaches to enhance penetration is stated as physical targeting. Electroporation, ultrasound, and magnetofection are few examples of externally employed physical techniques used in nanoparticle delivery. Different physical properties of body homeostasis can also be utilized to configure nanoparticles. Physiological properties of the disease environment ought to act as a stimulant for nanoparticles, thus improving the drug molecules' delivery. pH, temperature, light, and hypoxia are a few factors that have been explored in passive targeting [35].

3.3.2 The Journey of Nanoparticles to the Target Sites

The systematically injected nanoparticles before reaching the target site have to pass through multifaceted biological elements on its way. Sequential events involve corona formation, blood, extravasation, tumor penetration, and intracellular trafficking [36]. Introduced nanoparticle first interacts with the biomolecules of blood components forming structure known as "corona." The corona formation depends on the physicochemical property and travel time of nanoparticles. Proteins present in corona mask the function of the engineered surface of nanoparticles. This even restricts the antibody exposure, hence resulting in reduced release of encapsulated drug molecules at the target site. Additionally, this might also activate the cascading effect of the immune response leading to hypersensitivity. However, not all protein interactions hamper the activity of nanoparticles. Proteins like dysopsonin and albumins reduce the phagocytic capability of the immune response against nanoparticle facilitating its release. Half-life and effectiveness of circulating nanoparticle

depend on the permeability of tumor vasculature. A shorter half-life during circulation is sufficient for nanoparticle accumulation in the target site because of increased vascular permeability at the tumor environment. In contrast, a longer circulation time is required for those having low permeability of the vasculature. Polyethylene glycol (PEG), present on the surface of nanoparticles increases blood circulation time and hence shows more effect. Moreover, nanoparticle interaction with protein reduces due to steric hindrance, rendering it less prone to immune attacks. During cancer progression, the presence of arteries and veins formed by the process of angiogenesis possesses higher permeability than those of normal cells. "Dynamic vents" could be helpful in the intake of nanoparticles to the tumor. Dynamic vents open momentarily, assisting penetration depending on the tumor permeability, nanoparticle size, and other physicochemical properties. Also, the conjugated ligand antibody against the biomarker is beneficial for tumor penetration. The higher the affinity between antibody and biomarker, the more is the penetration. Strong interactions lead to internalization of nanoparticles, whereas weak interactions of the antibody have extensive diffusion within the tissues exposing to intracellular trafficking. Likewise, some of the nanoparticles are engineered with RNA interference (RNAi). RNAi requires a cytosolic environment to be functionally active. Overall, all the processes cause nanoparticle for further modifications and might interfere with actually intended properties, thus are required to be studied thoroughly [36].

3.4 Recent Advancements in Theranostics

The prospects of theranostics for various diseases have been extensively investigated worldwide for the last two decades. Herein a few of the recent concepts leading the researchers towards the multipurpose probes and tools for affordable developments are listed. Organic, inorganic, composites, biomimicking, and biomaterial-based are all utilized to meet these demands and serve efficacious therapy. Few examples are represented in Table 3.1.

Smart and demand-responsive integration of biomaterial science with imaging modalities and disease biology has built the strong platform of theranostics. They can detect, sense, image, trigger, activate, block, and convey according to their design approach sufficing the demands. Theranostic platforms have revolutionized the clinical conclusions of various diseases and also the traditional methods to treat them.

Moderation of the traditional techniques gives the advantage of providing quick treatment rendering sufficient time for other latest technologies to emerge and gain validation for advanced treatment. In radiotherapy and brachytherapy, there is enormous scope for modifications and improvements in the probes. Designing new theranostic probes can lead to improved cancer treatment [37, 38]. Similarly, the theranostic eye lens is an excellent example of a wearable theranostics, with surface modification of lens surface for diagnosis and providing antiviral treatment

Table 3.1 Overview of nanosystems for theranostic applications

S. no.	Targeted disease	Theranostic agents	Active agent	Platform implemented	References
1.	Cancer	64Cu-D3R-C18-DOTA And 64Cu-D3R-C16-DOTA	Cu and Lu	PET/CT scan-based imaging and then brachytherapy dosimetry	Wang et al. [37]
2.	Medulloblastoma Cancer	90Y-DOTA-tyr3-octreotide (90Y-DOTATOC) And 68Ga-DOTA-tyr3-octreotide (68Ga-DOTATOC)	Yttrium and gallium	Targeting cell surface with a peptide attached radio isotope for imaging via PET followed by radiotherapy	Waldherr et al. [38]
3.	Breast cancer TNBC	Bioresponsive hydrogel nanoprobes	5-FU drug	Nanodevice sense, silence the specific gene sequence, and release the active drug	Conde et al. [39]
4.	Eyes	Theranostic eye lenses	Antiviral poly-sulfonate	Theranostic lenses to defend eyes with help of antiviral coating and detect IL-1α	Mak et al. [40]
5.	Gastrointestinal stromal tumors (GIST)	Cancer theranostic H-dots	Imatinib loaded H-dots	Image-guided surgery of GIST, with lowered immune uptake and increased tumor suppression with efficient drug delivery	Kang et al. [41].
6.	Bacterial infections	Siderophore based DOTAM theranostic scaffold	Siderophore conjugated catechol and DOTAM scaffold	Imaging the bacterial growth via a fluorogen activating protein and treat the infection by the antibiotic loaded in the cargo	Ferreira et al. [42]
7.	MDR bacterial infections	Sonotheranostic based nanoliposomes for MDR	Purpurin loaded in $MLP_1$8 liposomes	Distinguish bacterial infection from inflammation or cancer site and treat resistant bacteria using a sonosensitizer	Pang et al. [43]
8.	MDR bacterial infections	Luminescent nanodrugs of ciprofloxacin	Ciprofloxacin based nanodrugs	Diagnosing the bacterial infection with help of nanoaggregates which are luminescent as well as antibacterial	Xie et al. [44]

9.	Bacterial infection	Fluorescent pH sensitive antimicrobial nanoparticles	Poly(poly-(ethylene glycol) methyl ether methacrylate)-*b*-poly (2-diisopropylamino) ethyl methacrylate-*co*—Hydroxyethyl methacrylate-chlorine e6 (PPEGMA-*b*-P(DPA-*co*-HEMA)- Ce6)	Antimicrobial and photodynamic therapy under acidic conditions (pH 6)	Liu et al. [45]
10.	Colon cancer	Theranostic fluorescent emitting bacteria	Salmonella strains	Bacterial fluorescence imaging of tumor used in compaction with immunotherapy	Woong et al. [46]
11.	Orthopedic implants	pH responsive drug depots in titanium nanotubes	Ampicillin loaded in titanium nanotubes	Release of drug from switchable PMMA gates, when pH drops due to bacterial growth	Chen et al. [47]
12.	Bacterial biofilm infected tissues	pH response based anti-microbial photosensitive nanosheets	MnO_2 nanosheets loaded with chlorine e6	Detection of bacterial infected tissues by fluorescence and treatment by photody-namic therapy	Xui et al. [48]
13.	CNS	Bipolymeric nanogels	HEC and linseed oil-based polyol	Drug delivery to CNS by crossing BBB	Vashist et al. [49]
14.	Cancer cells	Gold-silica nanoparticles	Silica nanoparticles coated with gold nanoparticles and monoclonal antibody of anti-CTLA-4	Mitochondrial imaging by enhanced upconversion luminescent, followed by photodynamic therapy and activating immune response to provide anticancer therapy	Lin et al. [50]
15.	Cancer tumors	Bacterial based nano-heaters and imaging agents	Bacterial OMV packing melanin and other cargo proteins including fluores-cent proteins and optoacoustic chromoproteins	Optoacoustic based imaging for diagno-sis and therapeutic treatment of tumor by photothermal therapy	Gujrati et al. [51]
16.	Diabetes wound healing	Bioactive antibacterial dressing material	Polyethylene glycol diacrylate (PEGDA) with bioactive glass nanoparticles containing copper and sodium alginate	Silica based hydrogel scaffold to enhance wound healing in diabetics by increasing HIF1α-VEGF expression	Li et al. [52]

(continued)

Table 3.1 (continued)

S. no.	Targeted disease	Theranostic agents	Active agent	Platform implemented	References
17.	Tuberculosis meningitis	Aptamer based theranostic molecules	G-quadruplex-(G4)-forming aptamer MS10-Trunc	Diagnosis and treatment of *Mycobacterium tuberculosis* (Mtb) MS-specific single-stranded DNA using G-quadruplex aptamers against them	Dhiman et al. [53]
18.	*Staphylococcus aureus* infections	Fluorescent vancomycin based nanoparticles	Vancomycin-silicon based nanoparticles	Diagnosis gram positive bacterial infections like *S. aureus* and effectively treat at lower concentrations than free vancomycin	Zhai et al. [54]

[40], while using sonotherapy to treat MDR bacterial infections has introduced a completely new treatment model [43].

Nanoparticles have great potential for various modifications, making them more preferable over others available for a wide range of clinical treatments. Photothermal therapy, photodynamic therapy, along with drug release and real-time imaging of the affected area, have been broad areas of research for the last two decades. Continuous efforts are being made to bring them to the hospitals, as they are much more cost-effective and have higher therapeutic efficacy with minimum side effects over other therapies in use. Gold–silica nanoparticles [50], antibiotic nanoaggregates [44], pH-dependent antimicrobial nanoparticles [45, 47, 48], bacterial based theranostics [42, 46, 51] are a few examples of a wide range of diseases. They provide therapy and diagnosis, in much more targeted and effective ways.

One among the stated, bacterial therapy is another mode of therapeutic treatment prevalent in research labs these days. To provide imaging and on-demand therapeutic efficacy, this mode of theranostics is being explored extensively as the delivery model for eventually targeting multidrug-resistant bacterial biofilms and infections, colon cancer models, etc. [42, 46, 51]. Nucleic acid-based sensors and delivery probes are a new mode of theranostics, which are the latest and least explored so far. Such sensitive point-of-care sensors have an enormous amount of opportunities for modification as they are more selective, sensitive, accuracy, and efficacy. Also, by activation, silencing, trigger, and blockade, drug delivery can be manipulated as per the requirement. For example, using DNA based active agents can help us sense the desired gene sequences, and then treat effectively [39, 53].

3.5 Advantages of Smart Theranostics Agents Over Conventional Therapy

The design strategy of theranostics depends mainly upon targeting selective areas, providing imaging capabilities, and delivering specific cargo with minimal side effects. Nanotheranostics present new opportunities to upgrade the safety and efficacy of conventional therapeutics and have shown promising applications in diseases like cancer, cardiovascular diseases, inflammatory diseases, and pathogenic infections. Nanoparticles exhibit superior theranostic performance, owing to their exceptional properties for efficient drug loading, easy surface functionalization, biocompatibility, prolonged circulation time, high fluorescence, and photostability for bio-imaging. Some of the most widely utilized nanomaterials are magnetic nanoparticles, gold nanoparticles, carbon nanomaterials, polymers, dendrimers, and liposomes. The advantages of such theranostic systems are described below: Few of the advantages of smart theranostics have been shown in Fig. 3.3.

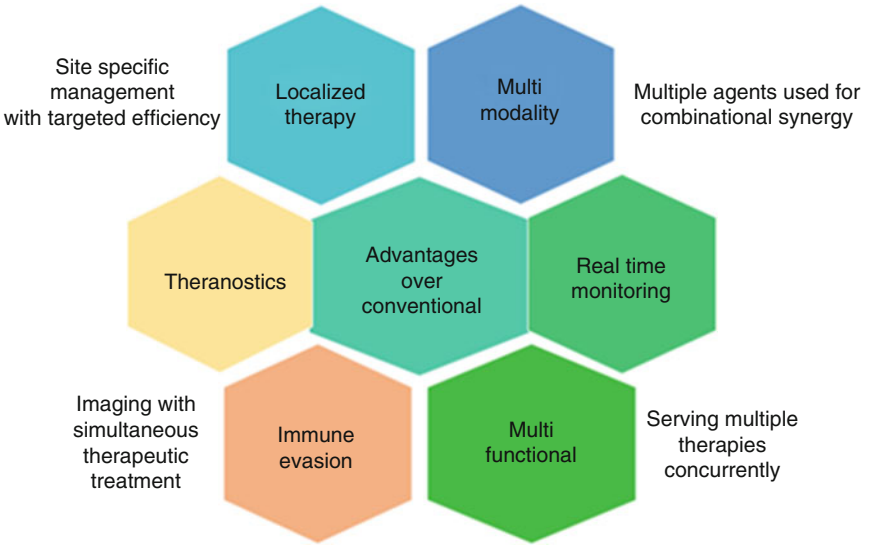

Fig. 3.3 A schematic of the advantages of smart theranostic agents over the conventional therapies

3.5.1 Localized Therapy

Localized therapy refers to the treatment that is directed towards particular cells, tissue, or organ. This may include surgery, topical treatment, laser therapy, cryotherapy, and radiation therapy. The delivery of therapeutic nanoparticles can be done be by active (utilizing site-specific biomolecules) or passive mode (using enhanced permeation effect). In the case of neurodegenerative disorders, one of the major challenges has been the transportation of drugs to cross the blood–brain barrier (BBB). For Alzheimer's, liposomal nanoparticles have shown successful crossing of BBB [3]. Dual functional PEG-PLGA nanoparticles present targeted delivery towards the amyloid plaque [55]. Generation of the long-lasting anti-coagulant surface over a freshly formed clot via thrombin targeted bivalirudin-functionalized perfluorocarbon nanoparticle provides site-specific management of acute thrombosis [56].

3.5.2 Multimodality

Combination therapy exploits the synergistic effect of more than one drug, which improves the efficiency of drugs and reduces side effects. This approach allows multiple agents to be delivered sequentially or simultaneously. For example, platinum-based lipid-coated nanoparticles encapsulated with mi-RNA is an excellent example of chemotherapy combined with gene therapy [57]. A tri-synergistic

approach (phototherapy–photodynamic therapy–chemotherapy) has been developed to overcome the chemotherapy resistance in tumor-bearing mice for breast cancer treatment [58]. AIE-based (aggregation-induced emission) based nanostructures and the derived systems show outstanding results in detection, differentiation, and killing various microbes. They also demonstrate the excellent application in image-guided PDI (photodynamic inactivation) for pathogenic infections [59].

3.5.3 Simultaneous Diagnosis and Therapy

Distinctive properties of plasmonic nanoparticles have been exploited for simultaneous diagnosis and therapy of different diseases. Electron rich surface of gold nanostructures makes them excellent contrast imaging agents. When combined with photothermal therapy, such a system can perform both functions. In theranostics, therapy with fluorescent imaging therapy has been utilized with metal nanoparticles like gold, iron oxide, silver nanoparticles, and quantum dot-based nanoparticles [60].

3.5.4 Multifunctionality

Bioactive molecules absorb near-infrared (NIR) region light, which has been a reliable tool for visualization, detection, and treatment of cancer [61]. Studies have shown the use of gold nanoparticles (AuNPs) as nanocarriers for drug delivery, photosensitizers for cancer diagnostics, and plasmonic photothermal (PPT)/photodynamic (PDT) therapy [62]. Similarly NIR active graphene shhet and quantom dot have been utilized for imaging, PDT and PTT [10].

3.5.5 Real-Time Monitoring

Upcoming treatment modalities in research insist on real-time monitoring of the position of malignancies in case of cancer or different parameters in case of other diseases. Sun et al. developed a vascular endothelial growth factor (VEGF) loaded-IR800 and conjugated with graphene oxide (GO-IR800-VEGF) nanoparticles for imaging angiogenesis of ischemic muscle in a mice hind limb model. This system was able to deliver VEGF to the injury site, and its efficiency was analyzed by positron emission tomography (PET) [63].

3.5.6 *Immune-Evasion*

Functionalization of nanotherapeutics with recognized antigens to increase their retention time is another emerging strategy. Specially designed formulations can induce biomimetic and bioinspired mechanisms. For example, PLGA coated with RBC membranes mimics both the surface and shape of the red blood cell membrane. In such molecules, both physical and chemical biomimicry act in synergy, mechanism that enhancing detoxification of nanoparticles. It further improves its survival rate in a mouse model of sepsis, resisting cellular uptake [64].

3.6 Challenges for Responsible Development

Development in theranostics is not immune to different challenges and limitations which demand further research. Nanomedicine offers numerous advantages over conventional drugs such as localized therapy, lower dosage, higher bioavailability, and an ability to dovetail diagnostics with a therapeutic agent. Even though this increasingly evolving field presents a promising alternative to conventional modalities of treatment, issues of stability, toxicity, and commerciality shown in Fig. 3.4 need to be addressed before considering them superior to existing drugs.

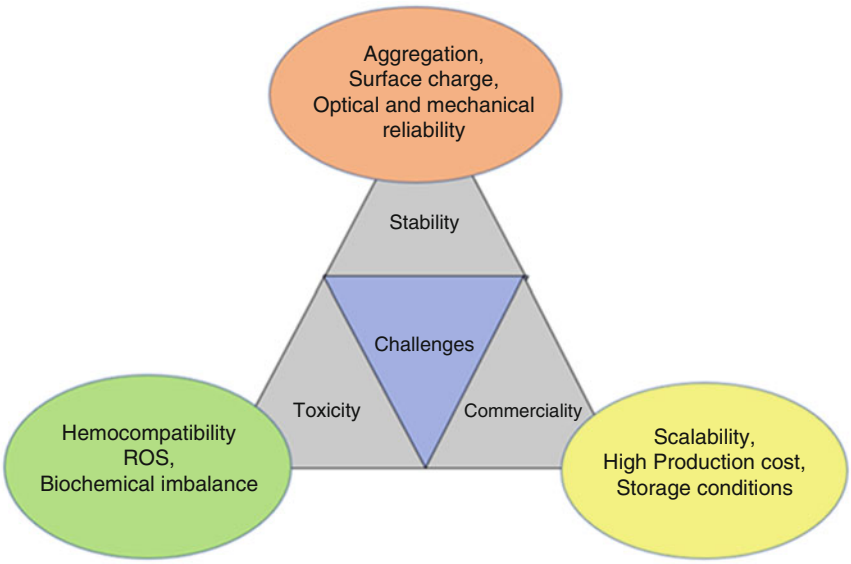

Fig. 3.4 Overview of the major challenges being faced in the development strategies of smart theranostics

3.6.1 Toxicity

When using materials for biological applications, they are imperative to be biocompatible. Nanoparticle-associated toxicity can arise from various properties such as chemical makeup, morphology, size, charge, and surface modifications. Even though gold and platinum are inert, a cytotoxic cationic surfactant, CTAB (N-cetyltrimethylammonium bromide), which is used as a soft template in the synthesis of gold nanorods, needs to be replaced with other polymers such as polyethylene glycol (PEG) [65]. Similarly, with appropriate surface modifications, the cytotoxicity of other nanoparticles can also be mitigated.

The size of nanoparticles has a complex relationship with toxicity. Toxicity can be induced by interaction with cell membrane proteins and reactive oxygen species (ROS) generation. It has been reported that TiO_2 nanoparticles with less than 10 nm and greater than 30 nm induce similar levels of ROS per surface area. However, ROS generation drastically increased upon the increasing size from 10 to 30 nm [66]. Nanoparticles of smaller size have a higher specific surface area. Hence, they interact more with cell membrane proteins, increasing their cellular uptake. The shape of the nanostructures also affects biocompatibility. Rod-shaped Fe_2O_3 and CeO_2 nanoparticles are stated as more cytotoxic than spherical nanoparticles [67, 68].

Moreover, the particles with higher positive surface charges are more toxic as they interact with negatively charged surface proteins. This leads to higher bioavailability due to enhanced endocytosis and a higher number of particles per cell remain cytotoxic. In literature, positively charged ZnO nanoparticles were found to be more cytotoxic than the negatively charged [69]. Different surface modifications can manipulate the surface charge. In one study [70], modifying surface of Fe_3O_4 nanoparticles with negatively charged oleic acid decreased their cytotoxicity.

Nanoparticles confer low toxic effects as compared to free drug treatment or traditional chemotherapy. However, toxicity from nanoparticle treatment should be at the level where the efficacy is maximum compared to toxic effects.

Some nanoparticles may be nephrotoxic like Gadolinium, whereas inorganic nanoparticles might cause cytokine fluctuation in the body. Silica and silver nanoparticles in mice have shown Alzheimer-like symptoms, which might affect the nervous system. Copper oxide has shown dose-dependent toxicity as well as DNA fragmentation in neural cells due to reactive oxygen species (ROS) that weakens the brain process of learning and memory storage. Iron nanoparticles have also shown (Alzheimer's disease) AD-like symptoms [71].

Toxicity due to various factors discourages the clinical applications of nanoparticles in theranostics. Because the mechanisms that cause cytotoxicity are poorly understood, current research is focused on identifying biochemical and molecular mechanisms underlying the toxicity of nanoparticles.

3.6.2 Stability

Nanoparticles are more reactive and less stable due to higher surface energy. The stability of nanoparticles can be defined in relation to shape, aggregation, size, and surface chemistry [72]. Aggregation of nanoparticles is caused due to interactions at short distances. Plasmonic nanoparticles such as gold and platinum illustrate the changes due to aggregation well. Due to peculiar optical properties of these materials, they exhibit a color change of solution leading to differed absorbance. Their clustering can be characterized by spectroscopy and electron microscopy. Aggregation can be prevented by reducing the probability of collision of particles. Methods to decrease the collision include reducing the storage time, the concentration of nanoparticles in the solution, or performing chemical changes like surface modifications, and adjusting pH.

The stability of nanoparticles in terms of shape and size can be defined as retaining the morphology, size of individual nanoparticles as well as size distribution during storage and experiments. As nanomaterial's chemical, mechanical, and optical properties strongly depend on size and shape, changes in these components lead to the deterioration of desired performance. The dimensionality of the nanoparticles can be preserved by maintaining the homogeneity of the original solution [73] and adding stabilizing agents.

3.6.3 Commerciality

The valuation of nanomedicine industry is estimated to reach approximately $334 billion by 2025. However, at present, the field is still in infancy and needs major transformation in terms of R&D and investments. For the translation of emerging healthcare technologies into the industry, factors such as superiority as compared to existing products, scalability, and costs are considered of paramount importance. The laboratory synthesis methods of nanomaterials consist of multiple steps, many of which involve the addition of reagents in stoichiometric proportions. After synthesis, purification methods and optimized parameters change from laboratory to industry.

Nanomaterials are synthesized by top to bottom approach in industries instead of the bottom to top approach in small scale synthesis. It enables enterprises to bypass the complex process of trace solvent removal. After scale-up, the desired properties of the material might be lost. For example, in the production of nanoparticles using the emulsion method, upon increasing impeller speed and agitation time, particle entrapment efficiency remained unchanged while nanoparticle size decreased [74].

Cost is also a significant factor in considering nanomedicine as an alternative to drug formulations. Nanotherapeutics are significantly expensive due to complex manufacturing processes, extremely lengthy, and more cost involved in the validation of concepts, difficult navigation through clinical trials, and sporadic

involvement of Big Pharma as compared to small and medium enterprises. For example, an anticancer drug Doxorubicin costs 8–9 times less than its nanoformulation, Doxil. However, it does not significantly increase the life span of patients. Some people justify the higher costs of nanoformulations due to their reduced side effects [75]. In the upcoming time, the increased involvement of large pharmaceutical companies and market-driven research can help overcome the current challenges faced by this industry.

3.7 Future Perspective

Currently, disease diagnosis and treatment encompass a single-target approach. Utilizing "multi-target combination" conjugated with multifaceted nanoparticles based multimode imaging system to treat complex disease will significantly improve treatment efficacy averting disease progression. Nucleic-acid based sensors and delivery probes are evolving as a mode of CNS and deep tissue disease theranostics expressing an enormous amount of opportunities in enhancing selectivity, sensitivity, and accuracy for POC devices. In-depth understanding of toxicity study synchronized nanoparticle modification will help in improving degradation and excretion rate. Further, finding ways to manufacture cost-effective miniaturization of nanodevices will aid a surgically placed prophylactic tool with routine monitoring and easy moderation. Also, intervening research will see new method optimization techniques, universally applicable diagnostic assay, improved universal safety guidelines, stability, and storage parameter advancements. Filling loopholes, these aspects can improve the current nanosystems leveraging human-based technologies.

3.8 Conclusion

The point-of-care in theranostic has been proved to be a dynamic domain where rapid advancement in precision and accuracy is liberating research and market value. Disease management has circumference early diagnosis, standardized therapy, and periodic monitoring. Delay in diagnosing, initiation of first-line therapy, and inability in detecting disease recurrence threaten life. Nanotheranostics concept of combining diagnosis and therapy in single multifunctional advent has evident "personalized medicine" allowing patient readout with maximum proximity and minimal intervention at individual latitude. The synergistic approach of nanotechnology actuated disease-specific molecular signatures has opened the possibilities of detailed visualization. Nanoparticles engineered surface modification and target functionalization have revealed the opportunity to transcend the immune system and increased molecules circulation time. Targeting specific biomarkers via active or passive mode further provides scope of enhanced cellular uptake of the active moiety reducing multidrug resistance and adverse side effects that would otherwise deter

efficient recovery. However, long term toxicity and stability remain a major challenge when adhering to better biocompatibility. Hence, health care offers nanotheranostic to explore with future advances in biomarker discoveries, diagnostics, drug-delivery systems, and biologics.

Acknowledgement The authors would like to thank Shweta Shinde for scientific discussion.

References

1. Hood, E. (2004). Nanotechnology: looking as we leap. *Environmental Health Perspectives, 112* (13), A740. https://doi.org/10.1289/ehp.112-a740.
2. Silva, G. A. (2004). Introduction to nanotechnology and its applications to medicine. *Surgical Neurology, 61*(3), 216–220. https://doi.org/10.1016/j.surneu.2003.09.036.
3. Ramanathan, S., et al. (2018). Theranostic applications of nanoparticles in neurodegenerative disorders. *International Journal of Nanomedicine, 13*, 5561–5576. https://doi.org/10.2147/IJN.S149022.
4. Tang, J., Lobatto, M. E., Read, J. C., Mieszawska, A. J., Fayad, Z. A., & Mulder, W. J. M. (2011). Nanomedical theranostics in cardiovascular disease. *Current Cardiovascular Imaging Reports, 5*(1), 19–25. https://doi.org/10.1007/s12410-011-9120-6.
5. Ma, Q., & Lu, A. Y. H. (June 2011). Pharmacogenetics, pharmacogenomics, and individualized medicine. *Pharmacological Reviews, 63*(2), 437–459. https://doi.org/10.1124/pr.110.003533.
6. Wang, A. Z., Langer, R., & Farokhzad, O. C. (2012). Nanoparticle delivery of cancer drugs. *Annual Review of Medicine, 63*(1), 185–198. https://doi.org/10.1146/annurev-med-040210-162544.
7. Landais, P., et al. (May 2009). Evaluation and validation of diagnostic tests for guiding therapeutic decisions. *Thérapie, 64*(3), 195–201. https://doi.org/10.2515/therapie/2009028.
8. Yordanova, A., et al. (2017). Theranostics in nuclear medicine practice. *OncoTargets and Therapy, 10*, 4821–4828. https://doi.org/10.2147/OTT.S140671.
9. Gawne, P. J., et al. (2020). PET imaging of liposomal glucocorticoids using 89Zr-oxine: Theranostic applications in inflammatory arthritis. *Theranostics, 10*(9), 3867–3879. https://doi.org/10.7150/thno.40403.
10. Kumawat, M. K., et al. (2019). Preparation of graphene oxide-graphene quantum dots hybrid and its application in cancer theranostics. *Materials Science and Engineering: C, 103*, 109774. https://doi.org/10.1016/j.msec.2019.109774.
11. Alexander, A. A., & Jotterand, F. (2014). Market considerations for nanomedicines and theranostic nanomedicines. *Cancer Theranostics*, 471–491.
12. Ventola, C. L. Progress in nanomedicine: Approved and investigational nanodrugs. *P T, 42*(12), 742–755.
13. Lim, E. K., Kim, T., Paik, S., Haam, S., Huh, Y. M., & Lee, K. (2015). Nanomaterials for theranostics: Recent advances and future challenges. *Chemical Reviews, 115*(1), 327–394. https://doi.org/10.1021/cr300213b.
14. Bartlett, G., Antoun, J., & Zgheib, N. K. (2012). Theranostics in primary care: Pharmacogenomics tests and beyond. *Expert Review of Molecular Diagnostics, 12*(8), 841–855. https://doi.org/10.1586/erm.12.115.
15. Santhosh Kalash R, Lakshmanan VK, Cho C-S, Park I-K (2016) 4.4 – Theranostics. https://doi.org/10.1016/B978-0-323-37127-8/00012-1
16. Siest, G., & Schallmeiner, E. (2013). Pharmacogenomics and theranostics in practice: A summary of the Euromedlab-ESPT (the European Society of Pharmacogenomics and Theranostics). *EJIFCC, 24*(3), 85–859.

17. Haga, S. B. (Sep 2016). Challenges of development and implementation of point of care pharmacogenetic testing. *Expert Review of Molecular Diagnostics, 16*(9), 949–960. https://doi.org/10.1080/14737159.2016.1211934.
18. Amiri-Dashatan, N., Koushki, M., Abbaszadeh, H.-A., Rostami-Nejad, M., & Rezaei-Tavirani, M. (2018). Proteomics applications in health: Biomarker and drug discovery and food industry. *Iranian Journal of Pharmaceutical Research, 17*(4), 1523–1536.
19. Marvell, L. (2017). Implementing the basic principles of biomarker use in oncology nursing: Enhancing knowledge and practice through an elearning module. *Canadian Oncology Nursing Journal, 27*(4), 401–402.
20. Mehta, R. L. (2017). Moderator's view: Patient-centered approaches for optimizing AKI management: The role of kidney biomarkers. *Nephrology, Dialysis, Transplantation, 32*(3), 419–422. https://doi.org/10.1093/ndt/gfx023.
21. Jeelani, S., Jagat Reddy, R. C., Maheswaran, T., Asokan, G. S., Dany, A., & Anand, B. (2014). Theranostics: A treasured tailor for tomorrow. *Journal of Pharmacy & Bioallied Sciences, 6*(1). https://doi.org/10.4103/0975-7406.137249.
22. Enrico, C. (2018). Nanotheranostics and theranostic nanomedicine for diseases and cancer treatment. In *Design of nanostructures for theranostics applications* (pp. 41–68). New York: Elsevier.
23. Quesada-González, D., & Merkoçi, A. (2018). Nanomaterial-based devices for point-of-care diagnostic applications. *Chemical Society Reviews, 47*(13), 4697–4709. https://doi.org/10.1039/c7cs00837f.
24. Mura, S., & Couvreur, P. (Oct 2012). Nanotheranostics for personalized medicine. *Advanced Drug Delivery Reviews, 64*(13), 1394–1416. https://doi.org/10.1016/j.addr.2012.06.006.
25. Park, J. Y., & Kricka, L. J. Role of nano-and microtechnologies in clinical point-of-care testing. [Online]. www.minimed.com
26. Kumar, A., et al. (2019). Nanotherapeutics. In *Nanotechnology in modern animal biotechnology: Concepts and applications* (pp. 149–161). New York: Elsevier.
27. Chandra, P., Tan, Y. N., & Singh, S. P. (2017). *Next generation point-of-care biomedical sensors technologies for cancer diagnosis*. Singapore: Springer Singapore.
28. Thakur, M., Kumawat, M. K., & Srivastava, R. (Jan 2017). Multifunctional graphene quantum dots for combined photothermal and photodynamic therapy coupled with cancer cell tracking applications. *RSC Advances, 7*(9), 5251–5261. https://doi.org/10.1039/c6ra25976f.
29. Chandra, P., & Prakash, R. (2020). *Nanobiomaterial engineering: Concepts and their applications in biomedicine and diagnostics*. Singapore: Springer Singapore.
30. Wang, Y., Yu, L., Kong, X., & Sun, L. (2017). Application of nanodiagnostics in point-of-care tests for infectious diseases. *International Journal of Nanomedicine, 12*, 4789–4803. https://doi.org/10.2147/IJN.S137338.
31. Ali, I., et al. (2020). Progress in polymeric nano-medicines for theranostic cancer treatment. *Polymers (Basel), 12*(3). https://doi.org/10.3390/polym12030598.
32. Bisht, S., et al. (2010). Systemic administration of polymeric nanoparticle-encapsulated curcumin (NanoCurc) blocks tumor growth and metastases in preclinical models of pancreatic cancer. *Molecular Cancer Therapeutics, 9*(8), 2255–2264. https://doi.org/10.1158/1535-7163.MCT-10-0172.
33. Li, L., et al. (2013). Improved intratumoral nanoparticle extravasation and penetration by mild hyperthermia. *Journal of Controlled Release, 167*(2), 130–137. https://doi.org/10.1016/j.jconrel.2013.01.026.
34. Yin, H., Liao, L., & Fang, J. (2014). Enhanced permeability and retention (epr) effect based tumor targeting: The concept, application and prospect. *JSM Clinical Oncology and Research, 2*(1), 1–5.
35. Arachchige, M. C. M., Reshetnyak, Y. K., & Andreev, O. A. (2015). Advanced targeted nanomedicine. *Journal of Biotechnology, 202*, 88–97. https://doi.org/10.1016/j.jbiotec.2015.01.009.

36. Shi, J., Kantoff, P. W., Wooster, R., & Farokhzad, O. C. (2017). Cancer nanomedicine: Progress, challenges and opportunities. *Nature Reviews. Cancer, 17*(1), 20–37. https://doi.org/10.1038/nrc.2016.108.
37. Wang, W., et al. (2020). Preclinical evaluation of cationic DOTA-triarginine-lipid conjugates for theranostic liquid brachytherapy. *Theranostics, 10*(3), 142–155. https://doi.org/10.7150/ntno.44562.
38. Martin, M., Schultz, M., Bushnell, D., Dick, D., Lehman, S., & Project Goals Schema. A *Phase II Theranostics Trial: Dosimetry-Guided Peptide Receptor Radiotherapy with Y-DOTA-tyr3-Octreotide (90 Y-DOTATOC) in Children and Adults with Neuroendocrine and other Somatostatin Receptor Expressing Tumors as determined by ^{68}Ga-DOTA-tyr3 -Octreotide (^{68}Ga-DOTATOC) PET/CT*.
39. Conde, J., Oliva, N., & Artzi, N. (2015). Implantable hydrogel embedded dark-gold nanoswitch as a theranostic probe to sense and overcome cancer multidrug resistance. *Proceedings of the National Academy of Sciences of the United States of America, 112*(11), E1278–E1287. https://doi.org/10.1073/pnas.1421229112.
40. Mak, W. C., Cheung, K. Y., Orban, J., Lee, C. J., Turner, A. P. F., & Griffith, M. (2015). Surface-engineered contact Lens as an advanced theranostic platform for modulation and detection of viral infection. *ACS Applied Materials & Interfaces, 7*(45), 25487–25494. https://doi.org/10.1021/acsami.5b08644.
41. Kang, H., et al. (2020). Renal clearable theranostic nanoplatforms for gastrointestinal stromal tumors. *Advanced Materials, 32*(6), 1–9. https://doi.org/10.1002/adma.201905899.
42. Ferreira, K., et al. (2017). Multivalent Siderophore–DOTAM conjugates as theranostics for imaging and treatment of bacterial infections. *Angewandte Chemie, International Edition, 56*(28), 8272–8276. https://doi.org/10.1002/anie.201701358.
43. Pang, X., et al. (2019). Bacteria-responsive nanoliposomes as smart sonotheranostics for multidrug resistant bacterial infections. *ACS Nano, 13*(2), 2427–2438. https://doi.org/10.1021/acsnano.8b09336.
44. Xie, S., et al. (2017). Design and synthesis of theranostic antibiotic nanodrugs that display enhanced antibacterial activity and luminescence. *Proceedings of the National Academy of Sciences of the United States of America, 114*(32), 8464–8469. https://doi.org/10.1073/pnas.1708556114.
45. Liu, P., Xu, L. Q., Xu, G., Pranantyo, D., Neoh, K. G., & Kang, E. T. (Nov 2018). PH-sensitive theranostic nanoparticles for targeting bacteria with fluorescence imaging and dual-modal antimicrobial therapy. *ACS Applied Nano Materials, 1*(11), 6187–6196. https://doi.org/10.1021/acsanm.8b01401.
46. Woong, S. (2019). In vivo monitoring of theranostic fluorescence bacteria in orthotopic fluorescence endoscopy. *Endoscopic Microscopy*. https://doi.org/10.1117/12.2509530.
47. Chen, J., et al. (2020). On-demand storage and release of antimicrobial peptides using Pandora's box-like nanotubes gated with a bacterial infection-responsive polymer. *Theranostics, 10*(1). https://doi.org/10.7150/thno.38388.
48. Xiu, W., et al. (2020). Biofilm microenvironment-responsive nanotheranostics for dual-mode imaging and hypoxia-relief-enhanced photodynamic therapy of bacterial infections. *Research*. https://doi.org/10.34133/2020/9426453.
49. Vashist, A., Atluri, V., Raymond, A., Kaushik, A., & Parira, T. (2020). Development of multifunctional biopolymeric auto-fluorescent micro- and nanogels as a platform for biomedical applications. *Frontiers in Bioengineering and Biotechnology, 8*, 1–16. https://doi.org/10.3389/fbioe.2020.00315.
50. Lin, B., Liu, J., Wang, Y., Yang, F., Huang, L., & Lv, R. (2020). Enhanced upconversion luminescence-guided synergistic antitumor therapy based on photodynamic therapy and immune checkpoint blockade. *Chemistry of Materials*. https://doi.org/10.1021/acs.chemmater.0c01031.

51. Li, Y., Xu, T., Tu, Z., Dai, W., Xue, Y., & Tang, C. (2020). Bioactive antibacterial silica-based nanocomposites hydrogel scaffolds with high angiogenesis for promoting diabetic wound healing and skin repair. *Theranostics, 10*(11). https://doi.org/10.7150/thno.41839.
52. Dhiman, A., et al. (2019). Theranostic application of a novel G-quadruplex-forming DNA aptamer targeting malate synthase of mycobacterium tuberculosis. *Molecular Therapy – Nucleic Acids, 18*, 661–672.
53. Zhai, X., Song, B., Chu, B., Su, Y., Wang, H., & He, Y. (2018). Highly fluorescent, photostable, and biocompatible silicon theranostic nanoprobes against Staphylococcus aureus infections. *Nano Research, 11*(12), 6417–6427.
54. Gujrati, V., et al. (2019). Bioengineered bacterial vesicles as biological nano-heaters for optoacoustic imaging. *Nature Communications*. https://doi.org/10.1038/s41467-019-09034-y.
55. Zhang, C., et al. (2014). Dual-functional nanoparticles targeting amyloid plaques in the brains of Alzheimer's disease mice. *Biomaterials*. https://doi.org/10.1016/j.biomaterials.2013.09.063.
56. Gupta, M. K., Lee, Y., Boire, T. C., Lee, J. B., Kim, W. S., & Sung, H. J. (2017). Recent strategies to design vascular theranostic nanoparticles. *Nano, 1*(2), 166–177. https://doi.org/10.7150/ntno.18531.
57. Yang, T., et al. (2016). Anti-tumor efficiency of lipid-coated cisplatin nanoparticles co-loaded with microRNA-375. *Theranostics, 6*(1), 142–154. https://doi.org/10.7150/thno.13130.
58. Wang, T., et al. (2016). Intracellularly acid-switchable multifunctional micelles for combinational photo/chemotherapy of the drug-resistant tumor. *ACS Nano, 10*(3), 3496–3508. https://doi.org/10.1021/acsnano.5b07706.
59. He, X., et al. (2019). AIE-based theranostic systems for detection and killing of pathogens. *Theranostics, 9*(11), 3223–3248. https://doi.org/10.7150/thno.31844.
60. Acharya, G., Mitra, A. K., & Cholkar, K. (2017). *Nanosystems for diagnostic imaging, biodetectors, and biosensors*. New York: Elsevier.
61. Kim, H., Chung, K., Lee, S., Kim, D. H., & Lee, H. (2016). Near-infrared light-responsive nanomaterials for cancer theranostics. *Wiley Interdisciplinary Reviews. Nanomedicine and Nanobiotechnology, 8*(1), 23–45. https://doi.org/10.1002/wnan.1347.
62. García Calavia, P., Bruce, G., Pérez-García, L., & Russell, D. A. (2018). Photosensitiser-gold nanoparticle conjugates for photodynamic therapy of cancer. *Photochemical & Photobiological Sciences, 17*(11), 1534–1552. https://doi.org/10.1039/c8pp00271a.
63. Sun, Z., et al. (2013). VEGF-loaded graphene oxide as theranostics for multi-modality imaging-monitored targeting therapeutic angiogenesis of ischemic muscle. *Nanoscale, 5*(15). https://doi.org/10.1039/c3nr01573d.
64. Ben-Akiva, E., Meyer, R. A., Yu, H., Smith, J. T., Pardoll, D. M., & Green, J. J. (2020). Biomimetic anisotropic polymeric nanoparticles coated with red blood cell membranes for enhanced circulation and toxin removal. *Science Advances, 6*(16). https://doi.org/10.1126/sciadv.aay9035.
65. Niidome, T., et al. (Sep 2006). PEG-modified gold nanorods with a stealth character for in vivo applications. *Journal of Controlled Release, 114*(3), 343–347. https://doi.org/10.1016/j.jconrel.2006.06.017.
66. Jiang, J., Oberdörster, G., Elder, A., Gelein, R., Mercer, P., & Biswas, P. (Jan 2008). Does nanoparticle activity depend upon size and crystal phase? *Nanotoxicology, 2*(1), 33–42. https://doi.org/10.1080/17435390701882478.
67. Forest, V., Leclerc, L., Hochepied, J.-F., Trouvé, A., Sarry, G., & Pourchez, J. (Feb 2017). Impact of cerium oxide nanoparticles shape on their in vitro cellular toxicity. *Toxicology in Vitro, 38*, 136–141. https://doi.org/10.1016/j.tiv.2016.09.022.
68. Lee, J. H., et al. (Dec 2014). Rod-shaped iron oxide nanoparticles are more toxic than sphere-shaped nanoparticles to murine macrophage cells. *Environmental Toxicology and Chemistry, 33*(12), 2759–2766. https://doi.org/10.1002/etc.2735.
69. Baek, M., et al. (July 2011). Factors influencing the cytotoxicity of zinc oxide nanoparticles: Particle size and surface charge. *Journal of Physics Conference Series, 304*, 012044. https://doi.org/10.1088/1742-6596/304/1/012044.

70. Kai, W., Xiaojun, X., Ximing, P., Zhenqing, H., & Qiqing, Z. (2011). Cytotoxic effects and the mechanism of three types of magnetic nanoparticles on human hepatoma BEL-7402 cells. *Nanoscale Research Letters, 6*(1), 480. https://doi.org/10.1186/1556-276X-6-480.
71. Karlsson, H. L., Cronholm, P., Gustafsson, J., & Möller, L. (2008). Copper oxide nanoparticles are highly toxic: A comparison between metal oxide nanoparticles and carbon nanotubes. *Chemical Research in Toxicology, 21*(9), 1726–1732. https://doi.org/10.1021/tx800064j.
72. Phan, H. T., & Haes, A. J. (July 2019). What does nanoparticle stability mean? *Journal of Physical Chemistry C, 123*(27), 16495–16507. https://doi.org/10.1021/acs.jpcc.9b00913.
73. Cao, G. (2011). *Nanostructures and nanomaterials* (2nd ed.). London: World Scientific.
74. Colombo, A. P., Briançon, S., Lieto, J., & Fessi, H. (Jan 2001). Project, design, and use of a pilot plant for nanocapsule production. *Drug Development and Industrial Pharmacy, 27*(10), 1063–1072. https://doi.org/10.1081/DDC-100108369.
75. Bosetti, R., & Jones, S. L. (June 2019). Cost–effectiveness of nanomedicine: Estimating the real size of nano-costs. *Nanomedicine, 14*(11), 1367–1370. https://doi.org/10.2217/nnm-2019-0130.

Chapter 4
Biosensor-Based Point-of-Care Devices: Metabolites and Pulse Oximetry

Inga M. Hwang, Xuwen A. Lou, Adam A. Toubian, and Daniel T. Kamei

4.1 Introduction

Rapid and accurate measurements of glucose, creatine, lipid levels, and hemoglobin (Hb) saturation are critical for multiple aspects of patient care, including diagnosis of various conditions and monitoring patients during and after surgery. Therefore, there is a rising demand for devices that perform these measurements at the point-of-care (POC).

POC glucose monitoring is used in both at-home and clinical care settings; roughly 463 million people have diabetes worldwide, and greater than 90% of patients experience stress-induced hyperglycemia in intensive care units [1, 2]. The reliability of devices for POC glucose measurement has increased; however, several challenges remain. For example, biomolecules including sugars, ascorbic acid, acetaminophen, mannitol, and dopamine often result in inaccurate glucose level measurements. Varying volume percentages of erythrocytes in blood can also affect glucose readings [1].

While POC glucose measurements are performed both inside and outside of clinical settings, creatine and creatinine measurements are typically performed in-clinic to detect post-surgical complications. For example, acute kidney injury (AKI) occurs in roughly 30% of cardiac surgery patients with varying severity; 1–2% of patients require dialysis, which increases their risk of post-surgical mortality approximately eightfold [3, 4]. AKI may also progress into chronic kidney disease, which causes deterioration of kidney function [5]. POC AKI detection can be accomplished using creatine, which is reversibly converted to creatinine by the enzyme creatinine amidohydrolase [6]. Serum creatine and creatinine levels are

I. M. Hwang · X. A. Lou · A. A. Toubian · D. T. Kamei (✉)
Department of Bioengineering, University of California, Los Angeles, Los Angeles, CA, USA
e-mail: imhwang97@engineering.ucla.edu; xuwen@g.ucla.edu; adamtoubian6@g.ucla.edu; kamei@seas.ucla.edu

V. Borse et al. (eds.), *BioSensing, Theranostics, and Medical Devices*,
https://doi.org/10.1007/978-981-16-2782-8_4

considered reliable predictors of AKI; one study found serum creatinine detected more AKI patients than another biomarker, cystatin C [7, 8]. Creatine and creatinine POC detection is still an emerging field, so this chapter will only discuss devices that have been subject to clinical study since 2010.

Similarly, lipid measurements are commonly performed in clinical settings to diagnose cardiovascular diseases (CVD), which accounted for over 17.9 million deaths in 2016. Over 75% of these deaths occur in countries with limited access to advanced healthcare and testing. Because early-stage diagnosis of cardiovascular diseases improves prognosis, widespread POC screening is crucial to lowering the mortality rate [9–11]. Although there are a variety of risk factors for CVD, the physiological cause is high levels of certain lipids in the blood. These lipids form deposits on arterial walls in a process referred to as atherosclerosis, leading to ischemia, heart attack, and stroke [9, 12]. Physicians generally use laboratory blood tests called full lipid profiles to diagnose CVD. Lipid panels measure the concentration of triglycerides (TG), total cholesterol (TC), high-density lipoproteins (HDL), and low-density lipoproteins (LDL). LDL levels are often calculated from HDL, TG, and TC levels using the Friedewald equation, as LDL is difficult to measure directly [13].

Pulse oximetry, which quantifies Hb saturation, is used in both pre-hospital and intensive care settings as a surrogate for arterial blood gas measurements (pCO_2 and pO_2) and allows for monitoring of gas exchange in the lungs [14]. Pulse oximetry is well-suited to POC settings because it is noninvasive, though it has several limitations. First, the accuracy of a pulse oximeter is governed by its pre-programmed calibration curve, often leading to systematic measurement bias. Additionally, compounds in whole blood including carboxyhemoglobin and bilirubin can interfere with readings. Finally, oximeter performance can be affected by skin pigmentation, though manufacturers have recently begun to address this limitation by using data from wider ranges of skin tones to generate their calibration curves [15–17]. Although numerous pulse oximeters designed solely for at-home, non-clinical use are commercially available, this section will only discuss pulse oximeters designed for clinical use that have been studied after 2013.

4.2 Glucose Measurement at the Point-of-Care

4.2.1 Methods of Measurement

Though the glucose meter is one of the first commercialized biosensors, its testing principle has remained relatively unchanged. The traditional fingerstick test requires application of a small blood sample to a test strip, where plasma glucose diffuses through several filter layers to react with immobilized enzymes. A typical glucose test strip is shown in Fig. 4.1. The exchange of electrons during the reaction generates an electrical current which is detected by an electrode embedded in the strip and is transduced to a glucose reading within seconds [19].

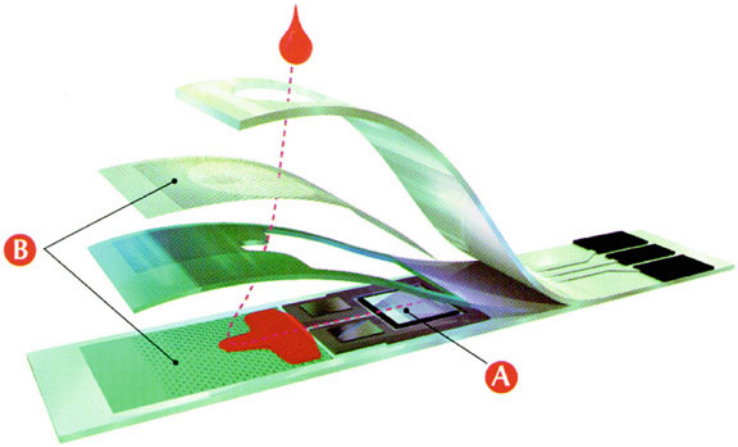

Fig. 4.1 Common structure of the glucose test strip found in commercial glucose meters. (**a**) An electrode system consisting of reference, counter, and working electrodes. (**b**) A hydrophobic layer that wicks the blood sample towards the electrodes. Reprinted with permission from Wang J. [18] Electrochemical Glucose Biosensors. Chemical Reviews 108:814–825. Copyright 2008 American Chemical Society

Commercial glucose meters typically use two major enzymes: glucose oxidase (GOx) and glucose dehydrogenase (GDH). GOx catalyzes the oxidation of glucose, and the products are gluconolactone and hydrogen peroxide. Levels of hydrogen peroxide, consumption of oxygen, and electron transfer during the GOx reaction can be used to measure glucose concentration [1]. The advantages of GOx include high specificity for glucose, low cost, and insensitivity to extreme pH and temperature. However, its primary disadvantage is the accuracy of readings fluctuates with oxygen levels. GDH, however, anaerobically catalyzes the oxidation of glucose, and it is paired with various cofactors such as NAD, FAD, and PQQ. Compared to GOx, GDH is more efficient and expensive [19].

4.2.2 Summary of Devices

4.2.2.1 Glucose Meters for At-Home Care

Before entering the market, most at-home glucose meters are evaluated using unenforced criteria. The most common set of criteria is the International Organization for Standardization (ISO 15197). Additionally, all manufacturers in the USA must comply with FDA guidance for over-the-counter glucose meters. Due to lack of regular assessment by independent studies and limited enforced regulation, the accuracy of at-home glucose meters remains in question; a 2018 review article found that among 143 studied at-home glucose meters, approximately two-thirds of them passed ISO 15197: 2003, and 40% passed ISO 15197:2013 [20].

Though numerous at-home glucose meters are commercially available, four companies have been sharing a majority of the glucose meter market: LifeScan, Abbott, Roche, and Ascensia [21–24]. Therefore, this section will only focus on currently available FDA-approved, handheld devices released after 2010 that are manufactured by these four companies.

The Accu-Chek Guide (Roche), Contour Next One (Ascensia), Freestyle Freedom Lite (Abbott), and One Touch Verio (LifeScan) are four commonly used at-home glucose meters. All four devices have been consistently and sufficiently accurate to comply with the more relaxed ISO 15197:2003 standard in numerous studies [20]. Specifically, one study demonstrated that 82% of Accu-Chek Guide's results were within 5% of the reference value, which exceeds the current ISO standard 15197:2013 [25]. Conversely, another study showed less than half of the One Touch Verio's results fall within 5% of the reference value, indicating its low precision within a smaller range of accuracy limits [26]. Consequently, the device exhibits conflicting results when evaluated against the more recent and stringent ISO 15197:2013 standard [20]. Another extensively studied device is Freestyle Freedom Lite. The Freedom Lite produces consistently accurate readings when blood samples of normal hematocrit level are used. However, its measurements are significantly affected by extreme hematocrit levels, indicating that it may not be suitable for patients with blood disorders or other contraindications. Of the four devices, the Contour Next One provides accurate measurements within the widest hematocrit range [27, 28].

Devices designed for long-term and ongoing glucose management are also available. The Freestyle Insulinx (Abbott), Contour Next Link (Ascensia), and Accu-Chek Aviva Expert (Roche) provide insulin dosage recommendations based on blood glucose results. The Contour Next USB (Ascensia), One Touch Verio Reflect (LifeScan), One Touch Verio Flex (LifeScan), Freestyle Precision Neo (Abbott), and Accu-Chek Guide Me (Roche) allow patients to transfer glucose measurements to other smart devices for better data management. The Contour Next and Contour Next EZ (Ascensia) provide "second chance" test strips that allow patients to reapply blood to the same strip in case of insufficient sample [29].

4.2.2.2 Glucose Meters for Clinical Care

Glucose meters intended for clinical care can be divided into two sub-categories: non-critical care and critical care. For the non-critical care sub-category, many at-home devices are re-marketed to hospitals since no regulation prohibits this.

Glucose meters intended for critical care, however, typically have higher accuracy thresholds. While ISO standards remain the same, these devices must comply with FDA guidance for prescription glucose meters and seek additional clearance for use in critical care settings. This section will focus on glucose meters released after 2010 that are not single-use tests and are intended for professional settings.

A well-established device is the Accu-Chek Inform II (Roche). This device utilizes a mutant variant of GDH, which eliminates interference from maltose and

xylose. Multiple clinical studies show this device's performance is consistent with ISO standards, and one study found that its accuracy significantly improves when the device is used by trained personnel [30–33]. However, a different study found that the Accu-Chek Inform II consistently tends to report hypoglycemia in newborns and another found icodextrin in patients receiving peritoneal dialysis significantly interferes with glucose readings [34, 35].

Another extensively studied device is the Biomedical StatStrip Glucose Hospital Monitoring system (Nova) [36]. This device gained much publicity as the first fingerstick glucose meter with FDA clearance for critically ill patients. However, very high concentrations of acetaminophen are reported to interfere with its measurements, and another study shows its accuracy is not consistent during and after cardiopulmonary bypass surgery (FDA, [37, 38]). In addition to critical care units, the Accu-Chek Inform II, StatStrip, and Freestyle Precision Pro (Abbott) have been evaluated in surgical intensive care settings and found to be less consistent than laboratory assays, providing another avenue for future glucose meter improvement [39]. For a comprehensive comparison of all the glucose meters discussed in this section, refer to Table 4.1.

4.3 Creatinine Measurement at the Point-of-Care

4.3.1 Methods of Measurement

Creatine and creatinine are most commonly detected amperometrically, using an enzymatic cascade to convert creatine into hydrogen peroxide, as shown in Fig. 4.2. A redox reaction occurs between a platinum anode and an Ag/AgCl cathode submerged in an electrolyte solution. Hydrogen peroxide is oxidized at the platinum anode, while reduction simultaneously occurs at the Ag/AgCl cathode. This pair of reactions generates a current proportional to the concentration of hydrogen peroxide and therefore to the concentration of creatine or creatinine in the sample [6, 40–46].

Creatine is also detected colorimetrically through an enzymatic reaction that produces a dye or chromophore. This reaction is performed either in solution or on a paper test strip and quantified by measuring the absorbance (solution) or reflectance (paper strip) [47, 48].

4.3.2 Summary of Devices

One handheld device is the StatSensor (Nova) [36] and its smaller counterpart, the StatSensor Xpress. Studies performed in hospital, trauma, and radiological settings indicate the StatSensor produces repeatable measurements in clinically relevant ranges [45, 49–51]. The StatSensor Xpress was also tested successfully in a clinic in Nicaragua and in an obstetric unit [52, 53]. Studies diverge when comparing the

Table 4.1 A summary of the discussed POC blood glucose measurement devices [29]

Manufacturer	Device name	Released	Setting	Enzyme	HCT range	Blood source
Abbott	Precision Pro	2013	Professional, multiple users	GDH	15–65%	Fresh capillary blood, venous whole blood, arterial whole blood, neonatal heelstick
Nova Biomedical	StatStrip	2018	Professional, multiple users	GOx	20–65%	Fresh capillary blood, venous whole blood, arterial whole blood, neonatal heelstick, neonatal arterial whole blood
Nova Biomedical	StatStrip Xpress	2018	Professional, multiple users	GOx	20–65%	Fresh capillary blood, venous whole blood, arterial whole blood, neonatal heelstick, neonatal arterial whole blood
Roche	Accu-Chek Inform II	2012	Professional, multiple users	Mut. Q-GDH	10–65%	Fresh capillary blood, venous whole blood, arterial whole blood, neonatal heelstick
Abbott	FreeStyle Freedom Lite	2010	Home, single user	GDH-FAD	15–65%	Fresh capillary blood, venous whole blood, alternative site testing
Abbott	FreeStyle Insulinx	2012	Home, single user	GDH-FAD	15–65%	Fresh capillary blood
Abbott	Freestyle Optium/ Precision Neo	2017	Home, single user	GDH-NAD	15–65%	Fresh capillary blood
Ascensia	Contour Next	2012	Home, single user	GDH-FAD	15–65%	Fresh capillary blood, alternative site testing
Ascensia	Contour Next One	2016	Home, single user	GDH-FAD	15–65%	Fresh capillary blood, alternative site testing, neonatal blood
Ascensia	Contour Next EZ	2014	Home, single user	GDH-FAD	15–65%	Fresh capillary blood, alternative site testing

(continued)

Table 4.1 (continued)

Manufacturer	Device name	Released	Setting	Enzyme	HCT range	Blood source
Ascensia	Contour Next Link	2012	Home, single user	GDH-FAD	15–65%	Fresh capillary blood, alternative site testing
Ascensia	Contour Link	2012	Home, single user	GDH-FAD	20–65%	Fresh capillary blood
Ascensia	Contour Next USB	2012	Home, single user	GDH-FAD	15–65%	Fresh capillary blood, alternative site testing
LifeScan	One Touch Verio Reflect	2020	Home, single user	GDH-FAD	20–60%	Fresh capillary blood
LifeScan	One Touch Verio Flex	2015	Home, single user	GDH-FAD	20–60%	Fresh capillary blood
LifeScan	One Touch Verio	2011	Home, single user	GDH-FAD	20–60%	Fresh capillary blood, alternative site testing
Roche	Accu-Chek Guide Me	2018	Unspecified, single user	GDH-FAD	10–65%	Fresh capillary blood, alternative site testing
Roche	Accu-Chek Guide	2016	Unspecified, single user	GDH-FAD	10–65%	Fresh capillary blood, alternative site testing
Roche	Accu-Chek Aviva Expert	2013	Home, single user	Mut. Q-GDH	10–65%	Fresh capillary blood

StatSensor to laboratory methods. One study found StatSensor measurements were reliable except when samples from diabetics with high glucose were used [54]. A second study found the StatSensor systematically overestimates creatine, and a third found the StatSensor systematically underestimates creatine [55, 56]. These conflicting results indicate the StatSensor's performance depends on the laboratory reference test used and the patient demographics tested.

A second handheld device is the i-STAT (Abbott), a handheld, cartridge-based device as shown in Fig. 4.3. The i-STAT measurements performed in clinical settings demonstrated stronger correlation with laboratory testing than the StatSensor, but weaker correlation than a benchtop POC device, the ABL800 Flex (Radiometer) [57–59]. However, the i-STAT's correlation to laboratory tests varies with the laboratory method used, as i-STAT results differed significantly from measurements obtained using isotope dilution mass spectrometry in a different study [60]. Additionally, studies indicate the i-STAT is prone to user error in emergency department settings, particularly during sample collection and handling [61, 62].

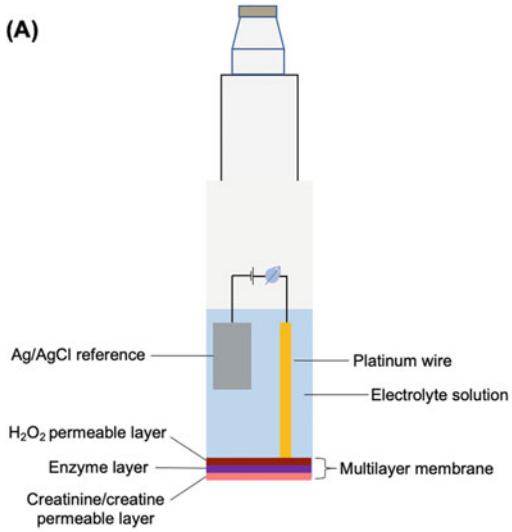

(B)

Creatinine + H_2O ↔ creatine	Creatinine amidohydrolase
Creatine + H_2O → sarcosine + urea	Creatinine amidohydrolase
Sarcosine + H_2O + O_2 → glycine + CH_2O + H_2O_2	Sarcosin oxidase

Fig. 4.2 Schematic representation of an electrode for amperometric detection of creatinine/creatine. Devices detecting both creatine and creatinine often require more than one electrode. (**a**) Creatinine and/or creatine in the sample enters the electrode through the bottom membrane layer. Enzymes stored in the middle layer convert creatine into hydrogen peroxide (H_2O_2). Finally, H_2O_2 diffuses into the electrolyte solution and is oxidized at the platinum anode. Ag cations are simultaneously reduced at the Ag/AgCl cathode, generating a current proportional to the concentration of H_2O_2 and therefore to the concentration of creatinine/creatine. (**b**) Summary of the enzymatic reactions occurring within the middle enzyme layer of the membrane [40]

In addition to handheld devices, several benchtop POC devices intended for rapid bedside patient monitoring are commercially available. One device is the Piccolo Xpress (Abaxis) [63] depicted in Fig. 4.3, which was found to be precise and accurate in clinically relevant ranges for all the analytes it measures. Creatine was found to be the Piccolo's least precise analyte; however, studies indicate this imprecision may result from user technique [64–66]. A second group of benchtop devices are the various ABL800 devices (Radiometer) [58]. One of these devices, the ABL800 Flex, was found to correlate well with laboratory enzymatic assays [67].

The devices best suited for POC use based on the World Health Organization (WHO) ASSURED criteria for POC devices are the i-STAT and the StatSensor, because they are handheld, rapid, and compatible with fingerstick sample collection [68]. However, the ABL 800 devices have the lowest minimum measurable

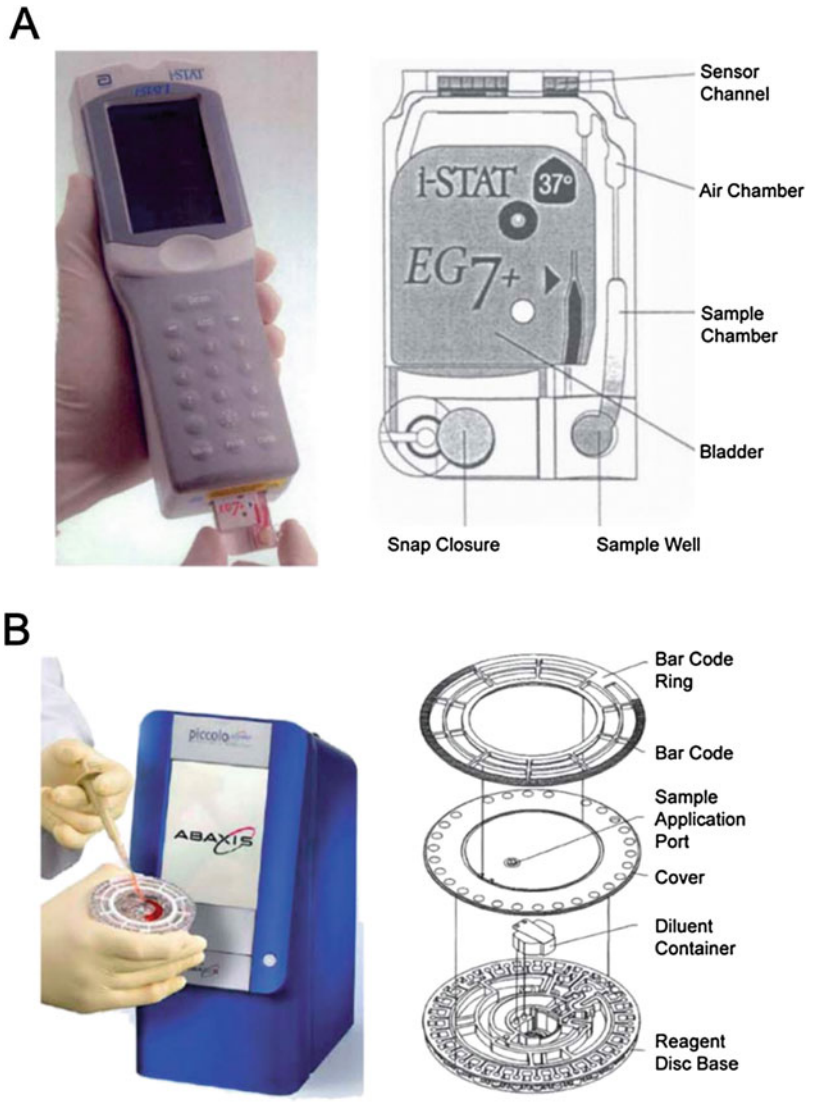

Fig. 4.3 (**a**) Photograph and schematic of the Abbott i-STAT. (**b**) Photograph and schematic of the Abaxis Piccolo. Republished with permission of the Royal Society of Chemistry from Commercialization of microfluidic point-of-care diagnostic devices, Chin et al., 12, 2012; permission conveyed through Copyright Clearance Center, Inc.

concentration and widest reportable range, while the Piccolo is the only device compatible with blood, serum, and plasma. A direct comparison of all creatine/creatinine measurement devices discussed in this section is shown in Table 4.2.

Table 4.2 Summary of the discussed POC devices for creatine/creatinine measurement in clinical settings

Device name	Manufacturer	Tabletop/ handheld	Recordable range (μmol/L)	Blood volume needed	Detection method	Sample type	Time to result
i-STAT [43]	Abbott	Handheld (0.7 kg)	18–1768	65 μL	Enzymatic + amperometric	Whole blood	120 s
StatSensor [36]	Nova	Handheld (0.22 kg)	27–1056	1.2 μL fingerstick	Enzymatic + amperometric	Whole blood	30 s
Piccolo Xpress	Abaxis	Benchtop (5.3 kg) [47]	18–1768 [41, 42]	100 μL [63]	Enzymatic + absorbance	Whole blood, serum, plasma [69]	12 min (complete panel of 14 tests) [41, 42]
IRMA TRUpoint [48]	ITC	Benchtop (2.381 kg)	18–1061	125–200 μL	Enzymatic + amperometric	Whole blood	90 s
ABL A800 Flex	Radiometer	Benchtop (33.2–35.1 kg) [40]	10–1800 [9]	30–250 μL [58]	Enzymatic + amperometric	Whole blood	80–150 s [58]

4.4 Lipid Measurement at the Point-of-Care

4.4.1 Mechanisms of Measurement

All devices discussed in this section use the following mechanisms to measure a full lipid profile from a whole blood sample. First, blood cells are separated from plasma using fiberglass paper or glass. The blood cells are left behind, while the plasma continues to flow through the device before being diverted into two paths: one path for TC and TG, and the other for HDL and glucose (if the device is equipped with glucose detection capabilities). The latter path is pretreated with certain reagents to precipitate out non-HDL cholesterol molecules like LDL and VLDL, which are left behind as the sample (now only containing HDL) continues to flow through the device. At this point, all paths proceed to their respective reaction zones, which contain the reagents and enzymes necessary to convert TC, TG, HDL, and glucose (if so equipped) into purple dye. These reactions are summarized in Fig. 4.4. Then, the device measures the reflectance of the reaction zones. The reflectance is converted to the concentration of purple dye, which correlates with the concentrations of TC, TG, and HDL in the original blood sample. Therefore, devices delivering full lipid profiles must contain a minimum of 3 reaction zones—one each for TC, TG, and HDL—and an additional zone for glucose, if so equipped. These values, and LDL value calculated using the Friedewald Equation, are displayed on a screen or sent directly to a printer for patients to take home their results [69, 71–73].

4.4.2 Summary of Devices

The first device we will highlight is the Cholestech LDX (Abbott). This device is a small tabletop model intended for use in clinics and physician offices. It uses glass cassettes containing the necessary testing reagents for a full lipid panel plus glucose. The cassettes require 2 drops of blood (about 40 μL) and the device displays the results in about 5 min. This device is intended for clinical use; as such, it is not FDA-approved for at-home use. The testing cassettes must be refrigerated and Abbott recommends calibrating the system using control cassettes at the beginning and end of the day, as well as every 20 tests [69]. In resource-poor settings, this could be an inconvenience, as clinics may not have access to refrigeration.

Another widely used POC lipid detection device is the CardioChek [72, 73]. This family of devices comes in 3 variants. The first, called the Cardiochek Home Cholesterol Test System, is a base model that measures TC, TG, and HDL. The second, called the CardioChek PA, measures a full lipid panel (TC, TG, HDL, and LDL) and can measure glucose using a separate test. The most expensive model, the CardioChek Plus, simultaneously measures a full lipid panel and glucose and also features Wi-Fi compatibility. All three models use paper test strips and require a

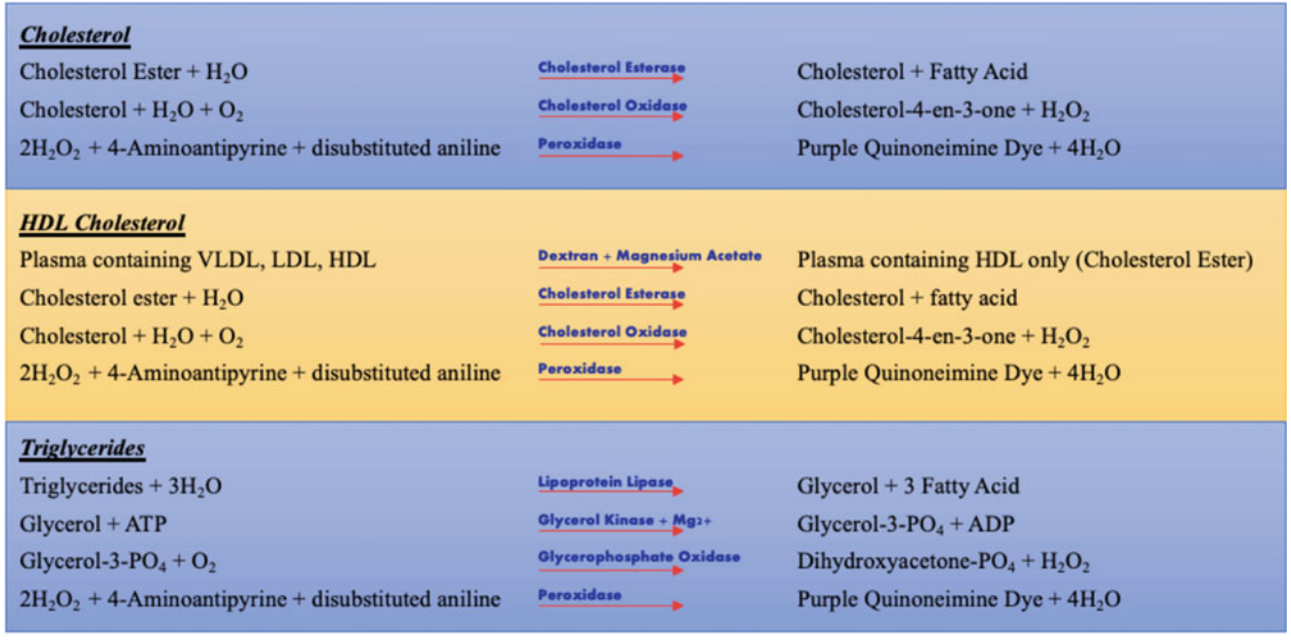

Fig. 4.4 A summary of the enzymatic reactions used to quantify the concentrations of various lipid molecules in the blood [70]. Lipid molecules in plasma are converted to purple dye before being read via reflectance photometry. Reflectance is converted to the concentration of dye which is related to the original concentration of the lipid in the patient sample

single drop of blood. This device is useful at the POC because the paper test strips do not need to be refrigerated and are cheaper than the Cholestech LDX cassettes. Additionally, all three devices are battery-operated, handheld, portable, and CLIA-waived, making them suitable for both at-home and clinic use [72, 73].

When comparing these devices to the laboratory gold standard, the Cholestech LDX outshines its competitors. The LDX overwhelmingly agreed with the laboratory reference method for determining lipid levels in 12 different studies [13, 74–85]. Both the precision and accuracy were found to agree with the lab method under intense statistical analysis, based on the guidelines for accurate lipid detection established by the National Cholesterol Education Program (NCEP) [77, 86]. In a similar fashion, devices from the CardioChek family were found to agree with laboratory methods in 6 different studies, based on NCEP guidelines [74, 80, 84, 85, 87, 88]. However, one 2007 study found significant differences between lipid levels measured by the CardioChek PA and a CDC-certified laboratory [83]. Another study, conducted in rural Kenya in 2006, deemed the CardioChek PA unsuitable for their POC needs after seeing very significant differences between device-measured and lab-measured lipid levels [89].

A separate study found that both the Cholestech LDX and CardioChek devices performed most accurately when used in conjunction with patient risk calculations instead of when directly comparing lipid levels. This is very beneficial at the POC since lipid levels are not stand-alone variables when determining risk for CVD. When taking into account patient history along with lipid levels measured using the Cholestech LDX and CardioChek analyzers, clinicians consistently grouped patients into low-risk, medium-risk, and high-risk categories for CVD [89]. This shows the effectiveness of both of these devices in the early diagnosis of CVD cases, which is ultimately the goal at the POC.

When compared head to head, the Cholestech LDX outperformed CardioChek devices in nearly all cases for nearly all analytes [74, 76, 83, 85, 90]. Although a few studies found that the CardioChek PA system was more accurate for HDL measurements, while the Cholestech system was more accurate for non-HDL measurements, this was not reflected in the majority of direct comparison studies published [90]. Consistently, the LDX was rated easier to use but more expensive than CardioChek systems [76, 84].

4.5 Pulse Oximetry Measurements at the Point-of-Care

4.5.1 Methods of Measurement

Pulse oximetry measurements are based on the principle that the transmittance of light through cutaneous vascular beds corresponds to the concentration of hemoglobin (Hb) in the blood. Pulse oximeters contain red and near-infrared LEDs on one side of the probe and a photodiode detector on the other. Oxygen saturation is calculated using the ratio of red-light absorbance to near-infrared light absorbance.

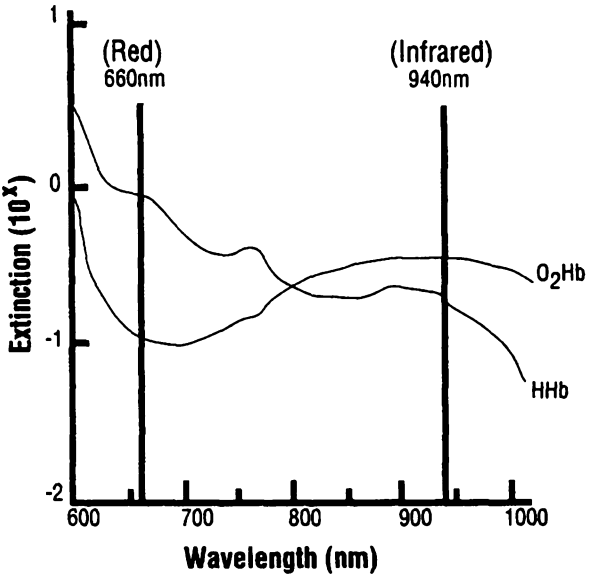

Fig. 4.5 Extinction curve of reduced hemoglobin (HHb) and oxyhemoglobin (O_2Hb). HHb has a higher extinction at 660 nm (red light) and a lower extinction at 940 nm (infrared light) than O_2Hb. Therefore, red light absorption is roughly proportional to HHb, while infrared absorption is roughly proportional to O_2Hb. The pulse oximeter uses the ratio of these two absorbances to determine Hb saturation. Reprinted from American Journal of Emergency Medicine 17(1), Sinex J., Pulse oximetry: Principles and Limitations, 59–66, Copyright [16], with permission from Elsevier

As shown in Fig. 4.5, red light absorbance is proportional to reduced Hb, while near-infrared light absorbance is proportional to oxygenated Hb [16].

4.5.2 Summary of Devices

Although many devices for blood gas, electrolyte, and metabolite measurement are also able to perform oximetry measurements, this section will only discuss pulse oximeters that have been subject to clinical study since 2013. Commercialized pulse oximeters range in size from tabletop to handheld and finger clip-style devices, though clinical studies only focus on handheld and tabletop oximeters.

One well-studied oximeter is the NBM200 (Orsense) [91], a portable tabletop monitor. Unlike traditional oximeters, which use a clip-style probe, this device uses a cuff that fits around the thumb and inflates to obstruct blood flow during collection of optical measurements [91]. Clinical studies conducted on potential blood donors, as well as pregnant and adolescent women in rural India, suggest the NBM200 systematically overestimates total hemoglobin relative to direct blood measurements. Additionally, the device exhibited variability in repeated measurements, though one study notes the measurement averages did not differ significantly from those of the reference [92–96].

The Pronto-7 (Masimo) [107] oximeter uses a clip-style probe attached to a handheld device. Studies indicate the effectiveness of this device varies between clinical settings. When tested on cardiac surgical outpatients, the Pronto-7 accurately measured total hemoglobin in most patients, but systematically overestimated it in

patients with an implanted HeartMate II left ventricular assist device (Abbott). The Pronto-7 was also not deemed suitable for emergency settings because it does not accurately measure low hemoglobin concentrations [99]. In a pediatric ICU, studies indicate it is suitable to screen for anemia in neonates, but it should be used in conjunction with blood-based laboratory tests to ensure accuracy [100, 101]. Finally, a study in potential blood donors found the Pronto's measurements exhibited moderate correlation with laboratory methods and strong repeatability. This study concluded the Pronto-7 is well-suited for screening of potential donors, especially in resource-poor areas [102].

A second handheld device is the Radical-7 (Masimo) [97, 98]. This device is marketed as multipurpose, as it can be used as a handheld monitor or mounted into a docking station for use at the patient bedside [102]. In a study on patients undergoing surgery, the Radical-7's accuracy improved with peripheral perfusion, indicating low perfusion affects its measurements of total hemoglobin [103]. Similarly, a study in trauma patients found low perfusion led to a high failure rate and lack of correlation between the Radical-7 and laboratory measurements [104]. Several studies with emergency patients found the Radical-7 exhibited a non-statistically significant negative bias relative to laboratory methods. Additionally, one study concluded the device was not sufficiently accurate for emergency department use, and a second suggested the device could be used reliably during drug administration [105].

A third handheld device is the Nellcor (Medtronic) [106], which was found suitable for continuous respiratory rate monitoring in hospitals but had poor accuracy when measuring oxygenated hemoglobin in cyanotic children [108, 109]. Table 4.3 compares all of the pulse oximeters discussed in this section.

Table 4.3 Summary of the discussed POC devices for pulse oximetry measurement in clinical settings

Device name	Manufacturer	Handheld, finger clip or tabletop	Pulse rate measurable range	Total Hb measurable range (SpHb)	SpO2 measurable range
NBM200 [92, 93]	Orsense	Tabletop (1 kg)	30–240 bpm	7–17 g/dL	1–100%
Pronto-7 [107]	Masimo	Handheld (0.367 kg)	25–240 bpm	8–17 g/dL	70–100%
Radical-7	Masimo	Handheld (0.54 kg) [97]	25–240 bpm [98]	0–25 g/dL [98]	0–100% [98]
Nellcor PM10N [106]	Medtronic	Handheld (0.274 kg)	20–250 bpm	–	1–100%

4.6 Conclusion

Although POC measurement of glucose, creatine/creatinine, lipid levels, and Hb saturation are successful fields, there is still progress to be made. The primary limitation of devices for POC glucose measurement is regulation. Manufacturing of glucometers for at-home and non-critical care settings is not regularly assessed by independent studies and follows looser guidelines than glucometers for critical care settings. Therefore, the demand for more accurate at-home tests, as well as in-clinic tests more resistant to interfering biomolecules, continues to rise.

Unlike glucose measurement, POC creatinine testing is still a relatively new field. The majority of devices available are used for bedside monitoring in clinics, and studies indicate that results from available handheld devices deviate more from laboratory tests than their tabletop counterparts. Future work in this field will likely focus on improving the accuracy of handheld devices and developing assays compatible with a wider range of biological media [110].

Both devices for POC lipid measurement discussed in this chapter performed well in measuring plasma lipid levels, as indicated by clinical studies. Physicians can consistently diagnose patients with early-stage CVD using these devices, allowing ample time for lifestyle changes to improve the prognosis.

Finally, this chapter examined pulse oximetry as a POC substitute for arterial blood gas measurements. Blood gas measurements are typically conducted in-hospital, while pulse oximetry is used both in-clinic and during hospital care. Although both methods provide similar information about the condition of the patient, they cannot be used interchangeably. Studies indicate direct blood gas measurements, while more invasive are better suited for surgical and critical care environments than pulse oximetry. Advances in pulse oximetry have and will continue to address its limitations, including interference from skin pigmentation and various biomolecules in whole blood.

References

1. Narla, N., Jones, M., Hermayer, K. L., & Zhu, Y. (2016). Critical care glucose point-of-care testing. *Advances in Clinical Chemistry, 76*, 97–121.
2. Saeedi, P., Petersohn, I., Salpea, P., Malanda, B., Karuranga, S., Unwin, N., Colagiuri, S., Guariguata, L., Motala, A. A., Ogurtsova, K., Shaw, J. E., Bright, D., William, R., & Diabetes Atlas Committee, I. D. F. (2019). Global and regional diabetes prevalence estimates for 2019 and projections for 2030 and 2045: Results from the international diabetes federation diabetes atlas, 9th edition. *Diabetes Research and Clinical Practice, 157*, 107843.
3. Freundlich, R., Maile, M., Sferra, J., Jewell, E., Kheterpal, S., & Engoren, M. (2018). Complications associated with mortality in the National Surgical Quality Improvement Program database. *Anesthesia and Analgesia, 127*, 55–62.
4. Karkouti, K., Wijeysundera, D., Yau, T., Callum, J., Cheng, D., Crowther, M., Dupuis, J., Fremes, S., Kent, B., Laflamme, C., Lamy, A., Legare, J., Mazer, C., McCluskey, S., Rubens,

F., Sawchuk, C., & Beattie, W. (2009). Acute kidney injury after cardiac surgery. *Circulation, 119*, 495–502.
5. Venkatachalam, M., Griffin, K., Lan, R., Geng, H., Saikumar, P., & Bidani, A. (2010). Acute kidney injury: A springboard for progression in chronic kidney disease. *American Journal of Physiology. Renal Physiology, 298*, F1078–F1094.
6. Mohabbati-Kalejahi, E., Azimira, V., Bahrami, M., & Ganbari, A. (2012). A review on creatinine measurement techniques. *Talenta, 97*, 1–8.
7. Ho, J., Reslerova, M., Gali, B., Nickerson, P., Rush, D., Sood, M., Bueti, J., Komenda, P., Pascoe, E., Arora, R., & Rigatto, C. (2012). Serum creatinine measurement immediately after cardiac surgery and prediction of acute kidney injury. *American Journal of Kidney Diseases, 60*, 196–201.
8. Spahillari, A., Parikh, C., Sint, K., Koyner, J., Patel, U., Edelstein, C., Passik, C., Thiessen-Philbrook, H., Swaminathan, M., Shlipak, M., & TRIBE-AKI Consortium. (2012). Serum cystatin C versus creatinine-based definitions of acute kidney injury following cardiac surgery: A prospective cohort study. *American Journal of Kidney Diseases, 60*, 922–929.
9. Ference, B., Graham, I., Tokgozoglu, L., & Catapano, A. (2018). Impact of lipids on cardiovascular health. *Journal of the American College of Cardiology, 72*, 1141–1156.
10. Lu, S., Yu, T., Wang, Y., Liang, L., Chen, Y., Xu, F., & Wang, S. (2017). Nanomaterial-based biosensors for measurement of lipids and lipoproteins towards point-of-care of cardiovascular disease. *Analyst, 142*, 3309–3321.
11. WHO. (2017). *Cardiovascular diseases (CVD)*. Accessed April 21, 2020, from https://www.who.int/news-room/fact-sheets/detail/cardiovascular-diseases-(cvds)
12. Munson, K. (2019). Cholestech standard operating procedure. Gunderson Health Systems. Accessed April 21, 2020, from https://www.gundersenhealth.org/app/files/public/6631/Lab-Policies-Cholestech-Lab-8788.pdf
13. Jain, A., Persaud, J., Rao, N., Harvey, D., Robertson, L., Nirmal, L., Nirmal, D., Thomas, M., Mikhailidis, D., & Nair, D. (2011). Point of care testing is appropriate for national health service health check. *Annals of Clinical Biochemistry, 48*, 159–165.
14. Chad, P., Leathley, M., London, R., McLean, S., Phang, P., Priestley, R., Rosenberg, F., Singer, J., Anis, A., & Dodek, P. (1997). Practice guidelines for arterial blood gas measurement in the intensive care unit decreases numbers and increases appropriateness of tests. *Critical Care Medicine, 25*, 1308–1313.
15. Haessler, R., Brandl, F., Zeller, M., Briegel, J., & Peter, K. (1992). Continuous intra-arterial oximetry, pulse oximetry and co-oximetry during cardiac surgery. *Journal of Cardiothoracic and Vascular Anesthesia, 6*, 668–673.
16. Sinex, J. (1999). Pulse oximetry: Principles and limitations. *The American Journal of Emergency Medicine, 17*, 59–66.
17. Zeballos, R., & Weisman, I. (1991). Reliability of noninvasive oximetry in black subjects during exercise and hypoxia. *The American Review of Respiratory Disease, 144*, 1241–1244.
18. Wang, J. (2008). Electrochemical glucose biosensor. *Chemical Reviews, 108*, 814–825.
19. Yoo, E. H., & Lee, S. Y. (2010). Glucose biosensors: An overview of use in clinical practice. *Sensors (Basel), 10*, 4558–4457.
20. King, F., Ahn, D., Hsiao, V., Porco, T., & Klonoff, D. C. (2018). A review of blood glucose monitor accuracy. *Diabetes Technology & Therapeutics, 20*, 843–856.
21. DarioHealth Corp (2017) United states securities and exchange commission form 10-K. Accessed May 26, 2020, from https://www.sec.gov/Archives/edgar/data/1533998/000114420418015415/tv487753_10k.htm
22. Dexcom Inc. (2015). *United states securities and exchange commission form 10-K*. Accessed May 26, 2020, from https://www.sec.gov/Archives/edgar/data/1093557/000109355716000432/dxcm-12312015x10k.htm
23. Klatman, E. L., Jenkins, A. J., Ahmedani, M. Y., & Ogle, G. D. (2019). Blood glucose meters and test strips: Global market and challenges to access in low-resource settings. *The Lancet Diabetes and Endocrinology, 7*, 150–160.

24. Ojha, U., & Mohammed, R. (2018). Disruption in the diabetic device care market. *Medical Devices (Auckland, NZ), 11*, 51–56.
25. Pleus, S., Baumstark, A., Jendrike, N., Mende, J., Link, M., Zschornack, E., Haug, C., & Freckmann, G. (2020). System accuracy evaluation of 18 CE-marked current-generation blood glucose monitoring systems based on EN ISO 15197:2015. *BMJ Open Diabetes Research & Care, 8*, e001067.
26. Freckmann, G., Schmid, C., Baumstark, A., Pleus, S., Manuela, L., & Haug, C. (2012). System accuracy evaluation of 43 blood glucose monitoring systems for self-monitoring of blood glucose according to DIN EN ISO 15197. *Journal of Diabetes Science and Technology, 6*, 1060–1107.
27. Musholt, B., Schipper, C., Thomé, N., Ramljak, S., Schmidt, M., Forst, T., & Pfützner, A. (2011). Dynamic electrochemistry corrects for hematocrit interference on blood glucose determinations with patient self-measurement devices. *Journal of Diabetes Science and Technology, 5*, 1167–1175.
28. Ramljak, S., Lock, J. P., Schipper, C., Musholt, P. B., Forst, T., Lyon, M., & Pfützner, A. (2013). Hematocrit interference of blood glucose meters for patient self-measurement. *Journal of Diabetes Science and Technology, 7*, 179–189.
29. FDA 510(k). *Premarket Notification Database*. Accessed May 26, 2020, from https://www.accessdata.fda.gov/scripts/cdrh/cfdocs/cfPMN/pmn.cfm
30. Dunne, N., Viggiani, M. T., Pardo, S., Robinson, C., & Parkes, J. L. (2015). Accuracy evaluation of CONTOUR(®)PLUS compared with four blood glucose monitoring systems. *Diabetes Therapy, 6*, 377–388.
31. Freckmann, G., Jendrike, N., Baumstark, A., Pleus, S., Liebing, C., & Haug, C. (2018). User performance evaluation of four blood glucose monitoring systems applying ISO 15197:2013 accuracy criteria and calculation of insulin dosing errors. *Diabetes Therapy, 9*, 683–697.
32. Guimont, C., Desjobert, H., Fonfréde, M., Vitoux, D., Benoist, J. F., Launay, J. M., Peoc'h, K., & Lefévre, G. (2015). Multicentric evaluation of eight glucose and four ketone blood meters. *Clinical Biochemistry, 48*, 1310–1316.
33. Hermayer, K. L., Loftley, A. S., Reddy, S., Narla, S. N., Epps, N. A., & Zhu, Y. (2015). Challenges of inpatient blood glucose monitoring: Standards, methods, and devices to measure blood glucose. *Current Diabetes Reports, 15*, 10.
34. Dogan, K., Kayalp, D., Ceylan, G., Azak, A., Senes, M., Duranay, M., & Yucel, D. (2016). Falsely elevated glucose concentrations in peritoneal dialysis patients using icodextrin. *Journal of Clinical Laboratory Analysis, 30*, 506–509.
35. Thomas, F., Signal, M., Harris, D. L., Weston, P. J., Harding, J. E., Shaw, G. M., Chase, J. G., & CHYLD Study Group. (2014). Continuous glucose monitoring in newborn infants: How do errors in calibration measurements affect detected hypoglycemia? *Journal of Diabetes Science and Technology, 8*, 543–550.
36. Nova. (2020). *Meters: StatSensor*. Accessed May 3, 2020, from https://www.novabio.us/statstrip-creatinine/
37. Chenoweth, J. A., Dang, L. T., Gao, G., & Tran, N. K. (2020). Acetaminophen interference with Nova StatStrip® glucose meter: Case report with bench top confirmation. *Clinical Toxicology*. https://doi.org/10.1080/15563650.2020.1732404.
38. Nakadate, Y., Sato, H., Roque, P., Sato, T., Matsukawa, T., Wykes, L., Kawakami, A., & Schricker, T. (2019). Accuracy of blood glucose measurements using the NOVA StatStrip® glucometer during cardiac surgery: A prospective observational study. *Canadian Journal of Anaesthesia, 66*, 943–952.
39. Claerhout, H., Prins, M. D., Mesotten, D., Van De Berghe, G., Mathieu, C., Van Eldere, J., & Vanstapel, F. (2016). Performance of strip-based glucose meters and cassette-based blood gas analyzer for monitoring glucose levels in a surgical intensive care setting. *Clinical Chemistry and Laboratory Medicine, 54*, 169–180.
40. Radiometer. (2008). *ABL A800 Flex reference manual*. Accessed April 28, 2020, from http://www.healthandcareni.net/stlabs/webhb/poct/documents/poct%20abl800%20man.pdf

41. Abaxis. (2015). *Piccolo kidney check*. Accessed April 28, 2020, from https://www.abaxis.com/sites/default/files/resource-packages/Kidney%20Check%20Package%20Insert-EN_0.pdf
42. Abaxis. (2015). *Piccolo Xpress chemistry analyzer*. Accessed May 3, 2020, from https://www.abaxis.com/sites/default/files/resource-brochures/piccolo_888-3010_rev_k_xpressflyer_ss.pdf
43. Abbott. (2017). *Procedure manual for the i-STAT System*. Accessed April 28, 2020, from https://www.lagaay.com/Catalogus/Product%20information/215720/Procedure%20Manual%20I-STAT.pdf
44. IRMA. (2014). *TruPoint blood analysis system user manual*. Accessed April 28, 2020, from https://www.lifehealthmed.com/wp-content/uploads/2016/05/441116LH_0715.pdf
45. Kosack, C., Kieviet, W., Bayrak, K., Milovic, A., & Page, A. (2015). Evaluation of the Nova StatSensor Xpress creatine point-of-care handheld analyzer. *PLoS One, 10*, e0122433.
46. Shephard, M. (2011). Point-of-care testing and creatinine measurement. *Clinical Biochemist Reviews, 32*, 109–114.
47. Abaxis. (2013). *Piccolo Xpress chemistry analyzer operator's manual*. Accessed April 28, 2020, from https://www.activeforever.com/pdf/chemistry-analyzer-owner-manual.pdf
48. Roche. (2010). *Reflotron Plus training manual*. Accessed April 28, 2020, from http://bosch.test.med.usyd.edu.au/facilities/molecular-biology/reflotron%20training%20manual.pdf
49. Carden, A., Salcedo, E., Tran, N., Gross, E., Mattice, J., Shepard, J., & Galante, J. (2016). Prospective observational study of point-of-care creatinine in trauma. *BMJ, 1*, 1–4.
50. Inoue, A., Nitta, N., Ohta, S., Imoto, K., Yamasaki, M., Ikeda, M., & Murata, K. (2017). StatSensor-i point-of-care creatinine analyzer may identify patients at high-risk contrast-induced nephropathy. *Experimental and Therapeutic Medicine, 13*, 3503–3508.
51. Schnabl, K., Bagherpoor, S., Diker, P., Cursio, C., DuBois, J., & Yip, P. (2010). Evaluation of the analytical performance of the Nova StatSensor creatinine meter and reagent strip technology for whole blood testing. *Clinical Biochemistry, 43*, 1026–1029.
52. Glasmacher, S., Bonongwe, P., & Stones, W. (2016). Point-of-care lactate and creatinine analysis for sick obstetric patients at Queen Elizabeth Central Hospital in Blantyre Malawi: A feasibility study. *Malawi Medical Journal, 28*, 15–18.
53. Minnings, K., Kerns, E., Fiore, M., Fiore, M., Parekh, R., DuBois, J., Isbell, T., Ferguson, R., & Fiore, L. (2015). Chronic kidney disease prevalence in Rivas, Nicaragua: Use of a field device for creatinine measurement. *Clinical Biochemistry, 48*, 456–458.
54. Srihong, C., Pangsapa, K., Chuaboonmee, K., Kotipan, Y., Charuruks, N., & Path, F. R. C. (2012). Evaluation of the analytical performance of the Nova StatSensor creatinine meter for blood testing. *Journal of the Medical Association of Thailand, 95*, 1225–1231.
55. Shephard, M., Peake, M., Corso, O., Shephard, A., Mazzachi, B., Spaeth, B., Barbara, J., & Mathew, T. (2010). Assessment of the Nova StatSensor whole blood point-of-care creatinine analyzer for the measurement of kidney function in screening for chronic kidney disease. *Clinical Chemistry and Laboratory, 48*, 1113–1119.
56. Spaeth, B., Shephard, A., Shephard, M., & Mathew, T. (2015). Assessment of a point-of-care device for measuring creatinine in a community screening program for chronic kidney disease. *Medical Research Archives, 3*, 1–6.
57. Dimeski, G., Tilley, V., Jones, B., & Brown, N. (2013). Which point-of-care creatinine analyzer for radiology: Direct comparison of the i-STAT and StatStrip creatinine methods with different sample types. *Annals of Clinical Biochemistry, 50*, 47–52.
58. Radiometer. (2020). *ABL 800 Flex blood gas analyzer*. Accessed May 3, 2020, from https://www.radiometeramerica.com/en-us/products/blood-gas-testing/abl800-flex-blood-gas-analyzer
59. Snaith, B., Harris, M., Shinkins, B., Jordaan, M., Messenger, M., & Lewington, A. (2018). Point-of-care creatinine testing for kidney function measurement prior to contrast-enhanced diagnostic imaging: Evaluation of the performance of three systems for clinical utility. *Clinical Chemistry and Laboratory Medicine, 56*, 1269–1278.

60. Moreno, M., Schwartz, A., & Dvorkin, R. (2015). The accuracy of point-of-care creatinine testing in the emergency department. *Advances in Emergency Medicine, 2015*, 965368.
61. Martin, C. (2010). i-STAT - combining chemistry and haematology in PoCT. *Clinical Biochemist Reviews, 31*, 81–84.
62. Yeo, C., Ngo, A., Ng, W., Lim, S., & Jacob, E. (2011). Assessing performance of the i-STAT at the point of care in the emergency room. *Proceedings of Singapore Healthcare, 20*, 157–161.
63. Abaxis. (2020). *Piccolo Xpress chemistry analyzer*. Accessed May 3, 2020, from https://www.abaxis.com/medical/piccolo/function?language_content_entity=en
64. Lee-Lewandrowski, E., Flood, J., Zak, R., Griggs, D., & Lewandrowki, K. (2017). Evaluation of the Abaxis Piccolo point-of-care chemistry analyzer. *Point of Care, 16*, 102–104.
65. Jang, Y., Su, N., Kim, H., Cho, Y., Sun, H., Shim, Y., Son, D., & Park, P. (2011). Clinical usefulness of point-of-care test chemistry analyzer in neonatal intensive care unit. *Journal of the Korean Society of Neonatology, 18*, 301–309.
66. Murata, K., Glaser, L., Nardiello, M., Richardson, S., Ramanathan, L., & Carlow, D. (2015). Analytical performance of the Abaxis Piccolo Xpress point of care analyzer in whole blood, serum and plasma. *Clinical Biochemistry, 48*, 1344–1346.
67. Bargnoux, A., Beaufils, O., Oguike, M., Lopasso, A., Dupuy, A., Sebbane, M., Badiou, S., Fesler, P., & Cristol, J. P. (2018). Point-of-care testing in patients receiving contrast-enhanced computed tomography scan. *Clinica Chimica Acta, 478*, 111–113.
68. Kosack, C., Page, A., & Klatser, P. (2017). A guide to aid the selection of diagnostic tests. *Bulletin of the World Health Organization, 95*, 639–645.
69. Abbott. (2020). *Cholestech LDX analyzer*. Accessed April 21, 2020, from https://www.alere.com/en/home/product-details/cholestech-ldx-system.html
70. Allain, C. C., Poon, L. S., Chan, C. S., Richmond, W., & Fu, P. C. (1974). Enzymatic determination of total serum cholesterol. *Clinical Chemistry, 4*, 470–475.
71. Anaokar, S., Crispino, M., & Crabtree, E. (2009). *Method for determining concentration of multiple analytes in a single fluid sample*. US7494818
72. Polymer Technology Systems. (2020). *CardioChek plus analyzer accuracy and precision for lipid and glucose presentation*. Accessed April 21, 2020, from https://ptsdiagnostics.com/cardiochek-plus-analyzer/
73. Polymer Technology Systems. (2020). *CardioChek products overview*. Accessed April 21, 2020, from https://ptsdiagnosticscom/cardiochek-products-overview/
74. Bastianelli, K., Ledin, S., & Chen, J. (2016). Comparing the accuracy of 2 point-of-care lipid testing devices. *Journal of Pharmacy Practice, 30*, 490–497.
75. Carey, M., Markham, C., Gaffney, P., Boran, G., & Maher, V. (2006). Validation of a point of care lipid analyser using a hospital-based reference laboratory. *Irish Journal of Medical Science, 175*, 30–35.
76. Dale, R., Jensen, L., & Krantz, M. (2008). Comparison of two point-of-care lipid analyzers for use in global cardiovascular risk assessments. *The Annals of Pharmacotherapy, 42*, 633–639.
77. Issa, J. S., Strunz, C., Giannini, S. D., Forti, N., & Diament, J. (1996). Precision and accuracy of blood lipid analyses by a portable device (Cholestech-LDX). *Arquivos Brasileiros de Cardiologia, 66*, 339–342.
78. Jain, A., Rao, N., Sharifi, M., Bhatt, N., Patel, P., Nirmal, D., Persaud, J., Nair, D. (2016). Evaluation of the point of care Afinion AS100 analyser in a community setting. *Annals of Clinical Biochemistry, 54*, 331–341.
79. Ose, L., Aass, B., & Christophersen, B. (1995). A rapid analysis of the lipid profile. A comparative study of different analytical methods for determination of blood lipids. *Journal of the Norwegian Medical Association, 115*, 3487–3489.
80. Panz, V., Raal, F., Paiker, J., Immelman, R., & Miles, H. (2005). Performance of the CardioChek PA and Cholestech LDX® point-of-care analysers compared to clinical diagnostic laboratory methods for the measurement of lipids. *Cardiovascular Journal of South Africa, 16*, 112–117.

81. Parikh, P., Mochari, H., & Mosca, L. (2009). Clinical utility of a fingerstick technology to identify individuals with abnormal blood lipids and high-sensitivity C-reactive protein levels. *American Journal of Health Promotion, 23*, 279–282.
82. Santee, J. (2012). Accuracy and precision of the cholestech LDX system in monitoring blood lipid levels. *American Journal of Health-System Pharmacy, 59*, 1774–1779.
83. Shephard, M. D., Mazzachi, B. C., & Shephard, A. K. (2007). Comparative performance of two point-of-care analysers for lipid testing. *Clinical Laboratory, 53*, 561–566.
84. Whitehead, S., Ford, C., & Gama, R. (2013). A combined laboratory and field evaluation of the Cholestech LDX and CardioChek PA point-of-care testing lipid and glucose analysers. *Annals of Clinical Biochemistry, 51*, 54–67.
85. Whitehead, S., Ford, C., & Gama, R. (2014). The impact of different point-of-care testing lipid analysers on cardiovascular disease risk assessment. *Journal of Clinical Pathology, 67*, 535–539.
86. National Cholesterol Education Program Expert Panel on Detection, Evaluation, and Treatment of High Blood Cholesterol in Adults (Adult Treatment Panel III). (2002). Third report of the National Cholesterol Education Program (NCEP) expert panel on detection, evaluation, and treatment of high blood cholesterol in adults (adult treatment panel III) final report. *Circulation, 106*, 3143–3421.
87. Ferreira, C., França, C., Januário, C., Zucker, M., Andriolo, A., & Scartezini, M. (2015). Clinical correlation between a point-of-care testing system and laboratory automation for lipid profile. *Clinica Chimica Acta, 446*, 263–266.
88. Gao, Y., Zhu, C. G., Wu, N. Q., Guo, Y. L., Liu, G., Dong, Q., & Li, J. J. (2016). Study on the reliability of CardioChek PA for measuring lipid profile. *Journal of Peking University* (abstract)
89. Park, P., Chege, P., Hagedorn, I., Kwena, A., Bloomfield, G., & Pastakia, S. (2016). Assessing the accuracy of a point-of-care analyzer for hyperlipidaemia in western Kenya. *Tropical Medicine & International Health, 21*, 437–444.
90. Donato, L., Deobald, G., Wockenfus, A., Hornseth, J., Saenger, A., & Karon, B. (2015). Comparison of two point of care devices for capillary lipid screening in fasting and postprandial adults. *Clinical Biochemistry, 48*, 174–176.
91. Orsense. *NBM 200: Non-invasive measurement of Hemoglobin*. Accessed May 6, 2020, from http://www.orsense.com/files/files/NBM%20200%20product%20brochure-website.pdf
92. Ahankari, A., Fogarty, A. W., Tata, L. J., Dixit, J. V., & Myles, P. R. (2016). Assessment of a non-invasive haemoglobin sensor NBM 200 among pregnant women in rural India. *BMJ Innovations, 2*, 70–77.
93. Ahankari, A., Dixit, J. V., Fogarty, A. W., Tata, L. J., & Myles, P. R. (2016). Comparison of the NBM 200 non-invasive haemoglobin sensor with Sahli's haemometer among adolescent girls in rural India. *BMJ Innovations, 2*, 144–148.
94. Malukani, P., Gajjar, M., Gonsai, R., Bhatnagar, N., & Goswami, H. (2014). Study of newer invasive and non-invasive methods of haemoglobin estimation in blood donor screening - a study on 200 donors. *International Journal of Current Research and Review, 6*, 26–30.
95. Pagliaro, P., Belardinelli, A., Boko, V., Salamon, P., Manfroi, S., & Tazzari, P. (2014). A non-invasive strategy for haemoglobin screening of blood donors. *Blood Transfusion, 12*, 458–463.
96. Singh, A., Dubey, A., Sonker, A., & Chaudhary, R. (2015). Evaluation of various methods of point-of-care testing of haemoglobin concentration in blood donors. *Blood Transfusion, 13*, 233–239.
97. Masimo. (2018). *Radical-7 pulse co-oximeter*. Accessed May 6, 2020, from https://www.masimo.com/siteassets/us/documents/pdf/plm-10014b_product_information_radical-7_us.pdf
98. Masimo. (2019). *Radical-7 operator's manual*. Accessed May 6, 2020, from http://www.frankshospitalworkshop.com/equipment/documents/pulse_oximeter/user_manuals/Masimo%20Radical%207%20Pulse%20Oximeter%20-%20User%20manual%20(2019).pdf

99. Bruells, C., Menon, A., Rossaint, R., Goetzenich, A., Czaplik, M., Zoremba, N., Autschbach, R., & Schaelete, G. (2013). Accuracy of the Masimo Pronto-7 system in patients with left ventricular assist devices. *Journal of Cardiothoracic Surgery, 8*, 159.
100. Hsu, D., French, A., Madson, S., Palmer, J., & Gidvani-Diaz, V. (2016). Evaluation of a noninvasive hemoglobin measurement device to screen for anemia in infancy. *Maternal and Child Health Journal, 20*, 827–832.
101. Phillips, M., Khoury, A., Bortsov, A., Marzinsky, A., Short, K., Cairns, B., Charles, A., Joyner, B., & McLean, S. (2015). A noninvasive hemoglobin monitor in the pediatric intensive care unit. *The Journal of Surgical Research, 195*, 257–262.
102. Al-Khabori, M., Al-Riyami, A., Al-Farsi, K., Al-Huneini, M., Al-Hashim, A., Al-Kemyani, N., & Daar, S. (2014). Validation of a non-invasive pulse CO-oximetry based hemoglobin estimation in normal blood donors. *Transfusion and Apheresis Science, 50*, 95–98.
103. Isosu, T., Obara, S., Hosono, A., Ohashi, S., Nakano, Y., Imaizumi, T., Mogami, M., & Murakawa, M. (2013). Validation of continuous and noninvasive hemoglobin monitoring by pulse CO-oximetry in Japanese surgical patients. *Journal of Clinical Monitoring and Computing, 27*, 55–60.
104. Moore, L., Wade, C., Vincent, L., Podbielski, J., Camp, E., del Junco, D., Radhakrishnan, H., McCarthy, J., Gill, B., & Holcomb, J. (2013). Evaluation of noninvasive hemoglobin measurements in trauma patients. *American Journal of Surgery, 206*, 1041–1047.
105. Sjöstrand, F., Rodhe, P., Berglund, E., Lundström, N., & Svensen, C. (2013). The use of a noninvasive hemoglobin monitor for kinetic analysis in an emergency room setting. *Anesthesia and Analgesia, 116*, 337–342.
106. Medtronic. (2018). *Nellcor portable SpO2 patient monitoring system, PM10N*. Accessed May 6, 2020, from https://www.medtronic.com/content/dam/covidien/library/us/en/product/pulse-oximetry/nellcor-portable-spo2-patient-monitoring-system-sell-sheet.pdf
107. Masimo. (2018). *Pronto pulse co-oximeter*. Accessed May 6, 2020, from https://www.masimo.com/siteassets/us/documents/pdf/plm-10077b_product_information_pronto.pdf
108. Bergese, S., Mestek, M., Kelley, S., McIntyre, R., Uribe, A., Sethi, R., Watson, J., & Addison, P. (2017). Multicenter study validating accuracy of a continuous respiratory rate measurement derived from pulse oximetry: A comparison with capnography. *Anesthesia and Analgesia, 124*, 1153–1159.
109. Kim, E., Lee, J., Song, I., Kim, H., Jang, Y., Yoo, S., & Kim, J. (2019). Accuracy of pulse oximeters at low oxygen saturations in children with congenital cyanotic heart disease: An observational study. *Pediatric Anesthesia, 29*, 597–603.
110. Canovas, R., Cuartero, M., & Crespo, G. (2019). Modern creatine (bio)sensing: Challenges of point-of-care platforms. *Biosensors & Bioelectronics, 130*, 110–124.

Chapter 5
Biosensor-Based Point-of-Care Devices: Detection of Infectious Diseases and Cancer

Inga M. Hwang, Cassandra M. Cantu, Rohan Chawla, and Daniel T. Kamei

5.1 Introduction

Cancer and infectious diseases account for a combined total of almost 20 million deaths each year. Low- and middle-income countries are even more severely affected, accounting for approximately 70% of cancer deaths [1]. Moreover, 81% of infectious disease deaths occur in the African, South Asian, and Mediterranean countries [2]. Early diagnosis of these health conditions can significantly improve prognosis. When detected in its early stages, cancer is more likely to respond to treatment, resulting in a higher probability of survival. Early diagnosis of infectious diseases can also increase likelihood of recovery and prevent outbreaks. Unfortunately, most current gold-standard detection methods for cancer and infectious diseases, such as biopsies, imaging, polymerase chain reaction (PCR), and enzyme-linked immunosorbent assays (ELISA), are poorly suited to low-resource settings. They are typically time-consuming, expensive, and often require trained personnel or laboratory equipment [3]. Therefore, there is a need for affordable, rapid, and accurate devices capable of diagnosing these health conditions at the point-of-care (POC). Although some reviews have been published which discuss non-commercial POC diagnostics [4–7], this review will focus on commercially available POC tests.

In a report discussing the current progress towards achieving the United Nations' Sustainable Development Goals, the World Health Organization (WHO) identified HIV, tuberculosis, malaria, and sexually transmitted infections (STIs) as some of the most critical infectious diseases to treat. Therefore, this chapter will focus on these diseases when discussing devices for POC pathogen detection. We will also limit our

I. M. Hwang · C. M. Cantu · R. Chawla · D. T. Kamei (✉)
Department of Bioengineering, University of California, Los Angeles, Los Angeles, CA, USA
e-mail: imhwang97@engineering.ucla.edu; casscantu@g.ucla.edu; rohanchawla@g.ucla.edu; kamei@seas.ucla.edu

V. Borse et al. (eds.), *BioSensing, Theranostics, and Medical Devices*,
https://doi.org/10.1007/978-981-16-2782-8_5

discussion of STIs to syphilis, chlamydia, and gonorrhea, which, along with trichomoniasis, make up the only four currently curable STIs [2]. We chose not to include trichomoniasis as there are few commercially available POC devices which detect it. However, it should be noted that there are a multitude of highly accurate POC devices on the market which detect diseases we chose not to cover, like the well-known CrAg LFA [8] which detects bacterial meningitis [8]. We also chose not to discuss multiplex devices, which detect multiple diseases from a single sample.

POC cancer detection is limited by low sensitivity and specificity, as testing for a single biomarker often does not provide sufficient information for definitive diagnosis. While a multiplex test could address this issue, none are currently available [9]. Therefore, commercially available POC cancer devices typically require another test conducted in tandem or further confirmatory testing.

While over 200 types of cancer exist, we will limit our discussion of commercial POC devices to the world's top ten most common cancers [10, 11]. Out of the top ten, the types that have commercial POC tests available are prostate, colorectal, liver, and bladder cancer. Although omitted from this chapter, it is important to acknowledge that commercial POC devices do exist for other cancers.

5.2 Pathogen Detection at the Point-of-Care

5.2.1 Methods of Detection

There are two main categories of devices used for POC pathogen detection: lateral-flow immunoassays (LFAs) and nucleic acid amplification technology (NAAT)-based sensors.

The paper-based LFA utilizes antibody–antigen binding for the detection of biomarkers. Its setup, in order of direction of flow, includes a sample pad, conjugate pad, nitrocellulose membrane with a printed test line and control line, and absorbent pad. For a detailed schematic of a typical LFA, please refer to Fig. 5.1. The sample is first introduced to the sample pad and re-solubilizes the dehydrated nanoprobes on the conjugate pad. Common probes consist of bio-conjugated colloidal gold or monodisperse latex particles tagged with colored or fluorescent dyes. In the case of a sandwich LFA, these particles are conjugated with biomarker-specific antibodies which interact with any antigens present in the sample. The nanoprobes and sample are wicked via capillary action to the detection zone, which contains test and control lines. The appearance of the test line, which consists of immobilized biomarker-specific antibodies, indicates the target analyte is present. The appearance of the control line, which consists of immobilized secondary antibodies, confirms the validity of the test. Lastly, the absorbent pad facilitates flow, wicks excess reagents, and prevents backflow. LFA results are generally qualitative or semi-quantitative, where semi-quantitative LFAs have additional lines to approximate analyte concentrations in certain ranges. In addition, electronic readers can assess test line intensity and determine quantitative estimates of target concentrations [13]. In general, LFAs

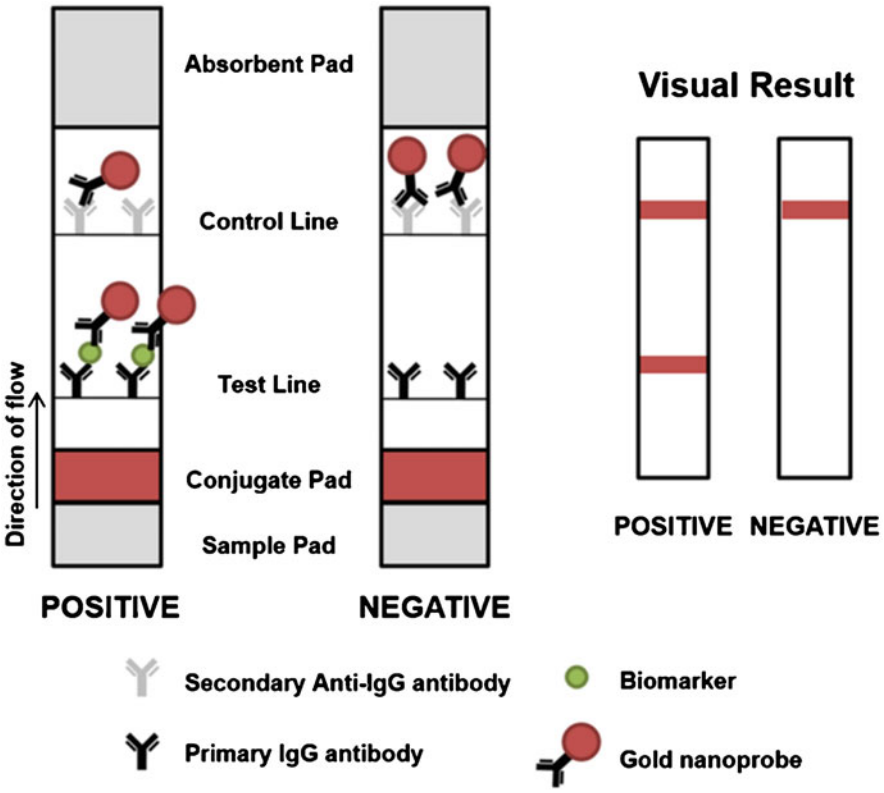

Fig. 5.1 Visual representation of a sandwich LFA using bio-conjugated colloidal gold nanoparticles to detect a biomarker. As shown in the right panel, the presence of two lines indicates a positive result, and the presence of one line indicates a negative result. Reprinted by permission from Mosley et al.: Springer Nature, Microchimica Acta, Improved lateral-flow immunoassays for chlamydia and immunoglobulin M by sequential rehydration of two-phase system components within a paper-based diagnostic, Mosley et al. [12], Copyright 2017

are cheap, portable, and rapid tests well-suited to the POC. However, they suffer from low sensitivity, lowering the accuracy of results and limiting their applications to select diseases.

NAAT-based devices detect pathogens by amplifying nucleic acid fragments present in samples. Although the amplification process varies between devices, the most commonly used method is PCR. A typical workflow consists of sample processing, amplification, and detection, which is visually depicted in Fig. 5.2. Nucleic acid fragments are extracted from the sample, transported to a reaction zone, and amplified. The amplified product is then detected, typically by fluorescent probes [15]. Finally, the fluorescent data is analyzed, with some devices performing melt-curve analyses to determine mutations in the original pathogenic DNA or RNA [16]. The advantage of NAAT-based devices over LFAs is a high degree of accuracy coupled with a relatively rapid test-to-response time (though, NAAT-based devices

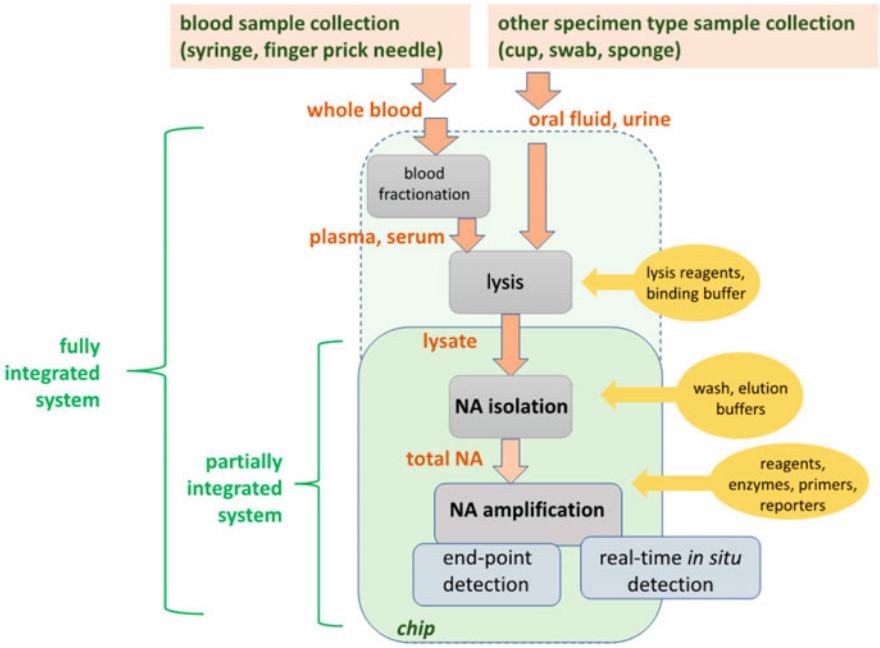

Fig. 5.2 Schematic of the typical workflow for a NAAT device. Whole blood samples are fractionated, typically via centrifugation, and red blood cells are removed. Next, the lysate is purified to remove amplification inhibitors and the released nucleic acids are amplified, usually via PCR. The amplified products are detected through various methods, including gel electrophoresis, fluorescent reporter probes, and colored dyes. Reprinted with permission from Mauk et al. [14] Simple Approaches to Minimally-Instrumented, Microfluidic-Based Point-of-Care Nucleic Acid Amplification Tests. Biosensors 8:1-30. Open access copyright 2018 MDPI

still produce slower results than LFAs). However, the primary disadvantage of NAAT-based devices is that they can be expensive and bulky, rendering them less well-suited to POC settings.

Although there are many devices in development which involve other technologies and mechanisms of detection, such as wearable biosensors and engineered nanomaterials, none are commercially available at this time. For more information on these devices, see Purohit et al. [6], Kumar et al. [5], Chandra and Pandey [4].

5.2.2 Summary of Devices

5.2.2.1 HIV

Current gold-standard diagnostics for HIV detection, which include ELISA for antibodies and PCR to measure viral RNA, are not well-suited for POC settings because they require expensive laboratory equipment [17]. Because the majority of

high-risk populations live in low-resource settings, POC tests are essential to combat this pandemic. While there are three major categories of devices available (CD4 technologies, NAAT-based tests, and LFAs), this section will only discuss devices which have received WHO Prequalification for use as in vitro diagnostic products [18]. WHO Prequalification is a mark of approval by the WHO which guarantees a product meets a certain quality standard. The WHO requires all prequalified tests to be commercially available and intended for use in low-resource settings. Manufacturers undergo a rigorous assessment, involving site inspections and accuracy tests, before they are approved [19].

Measurements of CD4 cells can be used to diagnose HIV because the disease decreases CD4 cell counts [20]. The two main portable devices using this method of diagnosis are the Pima Analyzer (Abbott) and the BD FACSPresto Near-Patient CD4 Counter (BD Biosciences). The Pima Analyzer quantifies CD4 cells using flow cytometry, while the FACSPresto uses fluorescence microscopy. Although both devices are portable and almost entirely automated, they are very expensive, with prices in the thousands of dollars [21, 22]. Thus, CD4 technologies show great promise as POC diagnostic tools, but are currently too expensive for widespread use.

The second category is NAAT-based devices. While many PCR-based assays are commercially available, there are only a limited number of automated, portable devices capable of nucleic acid amplification and detection. There are two such devices that use WHO Prequalified reagents for the detection of HIV: the GeneXpert Omni (Cepheid) and the m-Pima Analyzer (Abbott) [18]. The Omni is a portable version of Cepheid's renowned GeneXpert technology and detects viral RNA in patient blood samples using the PCR [23]. The m-Pima is a similar product made by Abbott, and costs $15,000, limiting the widespread use of this device [24]. However, if a particular clinic can purchase these devices, they have the advantage of not being single use tests. Instead, they use individual cartridges containing disease-specific reagents, allowing for detection of a wide range of diseases at a more reasonable price: $25/cartridge in the case of the m-Pima [25].

The final category of devices is LFAs. Current LFAs for HIV detection fall into two groups: antibody tests and antibody–antigen tests. In general, antibody tests are highly accurate, with sensitivities and specificities close to 100% [22]. There are also four antibody tests suitable for at-home self-testing: the Mylan HIV Self-Test (Mylan), the SURE CHECK HIV 1/2 Assay (Chembio), the OraQuick InHome HIV (OraSure Technologies), and the INSTI HIV self-test (INSTI). These tests are well-suited to the POC because they are highly accurate, portable, cheap, and user-friendly, with the OraQuick even capable of analyzing oral samples [26]. However, one disadvantage of antibody tests is the disease must progress significantly before the body starts producing antibodies. Some antibody-antigen tests can overcome this challenge by detecting the virus directly through the p24 antigen. Because p24 is a membrane protein, it allows for detection of HIV before antibodies are produced and when it is most contagious. Unfortunately, p24 antigen tests typically have low sensitivities, meaning they will not always be able to give a definitive negative test result [20, 27–29].

Overall, there are several promising methods of POC HIV diagnosis. While CD4 technologies and NAAT-based devices produce results comparable to laboratory tests, their usefulness in low-resource settings is limited by their high costs. LFAs are the devices best-suited to HIV detection at the POC because they are fast, cheap, portable, easy to use, and accurate.

5.2.2.2 Tuberculosis

The current gold-standard method of POC tuberculosis detection is smear microscopy, which is not ideal for POC settings because it requires expensive equipment and trained personnel [30].

There are only three major commercialized LFAs available for tuberculosis diagnosis: the Alere Determine TB LAM Ag (Abbott), the ASSURE TB Rapid Test (MP Biomedicals), and the SD Bioline TB Ag MPT64 Rapid (Standard Diagnostics). The Alere Determine and SD Bioline tests are both antigen tests with different targets, while the ASSURE test is an antibody test [31–33]. Although the SD Bioline test is the most accurate, it requires culture samples, which can take up to 10 days to grow [34]. This long time-to-result is a major disadvantage when considering a POC setting, where same day results are preferred. Both the ASSURE and Alere Determine tests have performed better than microscopy in studies but suffer from low sensitivities [35, 36]. The Alere Determine also performs best in patients with low CD4 counts, limiting its usefulness to HIV patients in critical condition [33]. While LFA tests have been developed for tuberculosis detection, none can truly be considered suitable for the POC as they lack both accuracy and speed.

The most promising POC tests for tuberculosis are NAAT-based. There are three portable, automated devices with assays capable of tuberculosis detection: the GeneXpert Omni (Cepheid), the Truelab Uno Dx Real Time Qualitative micro PCR Analyzer (Molbio Diagnostics), and the EasyNat TB IAD/Automatic CPA Nucleic Acid Analyzer TB (Ustar Biotechnologies). The Uno Dx uses PCR for amplification and the EasyNat uses isothermal cross priming amplification in its workflow [37, 38]. The Xpert assay and the Truenat MTB-Rif Dx (for use with the Uno Dx) are endorsed by the WHO as tuberculosis diagnostics, and both are capable of measuring resistance to the antibiotic rifampin [39]. It is unclear whether the Omni can perform melt-curve analysis to determine rifampin resistance, but the Uno Dx is capable of doing so. However, studies have demonstrated the Xpert assay has a higher sensitivity and specificity than the Uno Dx [39]. With its rapid time-to-result (<80 min), high accuracy, and limited sample preparation, the Xpert assay seems best-suited for a POC setting [40]. Although the Omni device may be expensive, each individual cartridge is in fact relatively cheap—only around $10—further increasing the device's appeal as a POC diagnostic [30].

5.2.2.3 Malaria

The pathogenic cause of malaria is the *Plasmodium* parasite, which enters the body via mosquito bites. The two most common parasitic strains are *P. falciparum* and *P. vivax*. Malaria is currently diagnosed in POC settings using microscopy, which is not ideal because it requires expensive laboratory equipment and trained personnel [41]. Although there are a multitude of LFAs available for malaria diagnosis, we will limit our discussion to those that have received WHO Prequalification [18].

The majority of commercialized LFAs are antigen tests which detect *Plasmodium* lactate dehydrogenase (pLDH) or histidine-rich protein II (HRP-II). There are also some tests that detect aldolase, but none are WHO Prequalified. Parasite lactate dehydrogenase is an enzyme present in all *Plasmodium* species, but HRP-II is a *P. falciparum*-specific antigen, allowing tests to distinguish between strains of parasites. Tests can also determine the type of pLDH present to distinguish between a wider range of parasites. The WHO published a report in 2018 comparing more than 300 LFAs for malaria diagnosis. By their metrics, the Alere Malaria Ag Pf (Abbott) and the CareStart Malaria PAN (pLDH) Ag RDT (AccessBio) are the most accurate tests for detecting *P. falciparum* samples. The First Response Malaria Ag. P.f./P.v. Card (Premier Medical) was the most accurate WHO Prequalified test for detecting *P. vivax* samples, and the CareStart Malaria PAN test was the most accurate WHO Prequalified test for detecting both parasite strains. This report shows malarial LFAs are highly accurate and reliable for use in low-resource clinical settings. For more in-depth results and comparisons, see Table 5.1 and the WHO Malaria RDT Product Evaluations Report [18, 94].

5.2.2.4 Syphilis

Bacterial syphilis is currently diagnosed by performing blood tests to detect antibodies. These tests are not suitable for the POC because they require expensive equipment and multiple liquid-handling steps [95]. Therefore, automated or handheld devices are needed for resource-poor settings.

We will only cover the three devices with active applications for WHO Prequalification in this section, though there are others available for purchase. The three devices in this category are the Alere Determine TP (Abbott), the First Response Syphilis Anti-TP Test Card (Premier Medical), and STANDARD Q Syphilis Ab Test (Standard Diagnostics) [96]. All three antibody tests are LFAs. The Determine TP and STANDARD Q have both been clinically evaluated, with relatively high sensitivities and specificities. While the Determine TP had a larger range of sensitivities, both tests were found to be accurate in whole blood [74, 78]. The First Response Syphilis test has not been clinically evaluated, but the manufacturer states it has a sensitivity of 99.1% and a specificity of 99.6% [75]. In general, these three tests are equivalent by most metrics, with the Determine TP and STANDARD Q gaining a slight advantage because their accuracy is clinically

Table 5.1 A summary of the discussed pathogen detection devices

Name	Manufacturer	Disease	Biomarker	Detection method	Sample	Cost (USD)	User	Time	Size	Sensitivity and specificity
INSTI HIV Self Test (flow-through) [42]	bioLytical Laboratories Inc.	HIV	Ab[a]	LFA (vertical flow-through)	Whole blood	$3.09/test [43]	At-home user	~1 min	Handheld	Sens: 99.8% Spec: 99.5%
OraQuick In-Home HIV [44]	OraSure Technologies, Inc.	HIV	Ab	LFA	Oral samples	$3.00/test [45]	At-home user	20 min	Handheld	Sens: 99.4% Spec: 99.0%
Mylan HIV Self-Test [46]	Mylan	HIV	Ab	LFA	Whole blood	$4.50/test [47]	At-home user	~15 min	Handheld	Sens: 99.8% Spec: 99.8%
SURE CHECK HIV Self-Test[b] [48]	ChemBio Diagnostic Systems, Inc	HIV	Ab	LFA	Whole blood	$2.10/test [49]	At-home user	~15 min	Handheld	Sens: 97% Spec: 100%
Pima CD4 Analyzer Cartridge (for use with the Pima CD4 Analyzer) [50]	Abbott (formerly Alere)	HIV	CD3/CD4 Cells	CD4	Whole blood	$5.95/cartridge [51]	Clinicians	20 min [52]	Benchtop	See WHO Prequalification Public Report for Performance Evaluation [50]
BD FACSPresto Cartridge (For use with BD FACSPresto Near-Patient CD4 Counter) [53]	Becton, Dickinson and Company	HIV	CD4 Cells	CD4	Whole blood	$8.80/cartridge [54]	Clinicians	20–30 min [55]	Benchtop	See WHO Prequalification Public Report for Performance Evaluation [53]
m-PIMA HIV-1/2 VL Cartridge (for use with m-PIMA Analyser) [56]	Abbott	HIV	RNA	NAAT	Whole blood	$25 [25]	Clinicians	<70 min	Benchtop	Sens: 95.1% Spec: 99.4%
Xpert HIV-1 Qual Assay (For use with GeneXpert Omni) [57]	Cepheid	HIV	RNA	NAAT	Whole blood	$14.90/cartridge [58]	Clinicians	95 min	Benchtop	Sens: 98.69% Spec: 100% LoD: 350 copies/mL
BD FACSPresto Near-Patient CD4		HIV	CD4 Cells	CD4	Whole blood	$7,910 [21]	Clinicians	–		–

Counter System (Device) [53]	Becton, Dickinson and Company								Benchtop (7 kg) [55]	
m-PIMA Analyser (Device) [56]	Abbott	HIV	RNA	NAAT	Whole blood	$15,000 [24]	Clinicians	–	Benchtop (8 kg)	–
Pima CD4 Analyzer (Device) [50]	Abbott (formerly Alere)	HIV	CD3/CD4 Cells	CD4	Whole blood	$6,095 [59]	Clinicians	–	Benchtop (2.54 kg)	–
GeneXpert Omni [23]	Cepheid	Multiple	Nucleic Acid	NAAT	Whole blood	Inquired	Clinicians	–	Benchtop (1 kg) [22]	–
Cobas Liat System [60]	Roche Diagnostics	Multiple (HIV)	Nucleic Acid	NAAT	Whole blood	$25,000	Clinicians	–	Benchtop (3.76 kg) [61]	–
Truelab Uno Dx Real Time Quantitative micro PCR Analyzer [37]	Molbio Diagnostics	Multiple	Nucleic Acid	NAAT	Whole blood	–	Clinicians	–	Benchtop	–
Alere Determine TB LAM Ag [33]	Abbott (formerly Alere)	TB	Ag[c] (LAM)[d]	LFA	Urine		Clinicians (for HIV patients in critical condition)	25 min	Handheld	Sens: 42% Spec: 91% [35]
ASSURE TB Rapid Test [31]	MP Biomedicals	TB	Ab	LFA	Whole blood, plasma, and serum	–	Clinicians	15 min	Handheld	Sens: 60.2% Spec: 82.3% [36]
SD Bioline TB Ag MPT64 Rapid [32]	Standard Diagnostics, Inc	TB	Ag (MPT64)	LFA	Culture	$2.23/ test [62]	Clinicians	15 min (8–12 days for a culture sample)	Handheld	Sens: 100% Spec: 96.4–100% [34, 62]
Xpert MTB/RIF Ultra Cartridge (For use with GeneXpert System) [40]	Cepheid	TB	DNA	NAAT	Whole blood, pleural fluid, nasopharyngeal, sputum, stool, gastric, urine	$9.98/ cartridge [63]	Clinicians	<80 min	Handheld	Sens: 46–97% Spec: 71–100% [39]

(continued)

Table 5.1 (continued)

Name	Manufacturer	Disease	Biomarker	Detection method	Sample	Cost (USD)	User	Time	Size	Sensitivity and specificity
Truenat MTB Plus Cartridge (For use with Truelab Uno Dx) [64]	Molbio Diagnostics	TB	DNA	NAAT	Whole blood	–	Clinicians	60 min	Handheld	Sens: 89% Spec: 98% [39]
EasyNat TB IAD/Automatic CPA Nucleic Acid Analyzer TB [38]	Ustar Biotechnologies	TB	DNA	NAAT (CPA)	Whole blood, sputum	–	Clinicians	–	Benchtop	Sens: 84–93% Spec: 87–99% [65]
Alere Malaria Ag P.f [66]	Abbott (Formerly Alere)	Malaria	Ag (Pf HRP2)[e]	LFA	Whole blood	$1.10/ test [67]	Clinicians	20 min	Handheld	Sens: 99% Spec: 98.6% PDS[f] Pf: 98%
First Response Malaria Ag. P.f./ P.v. Card Test [68]	Premier Medical Corporation Limited	Malaria	Ag (Pf HRP2 and Pv pLDH)	LFA	Whole blood	$0.30/ test [69]	Clinicians	20 min	Handheld	Sens: 100% Spec: 100% PDS Pf: 94% PDS Pv: 100%
CareStart Malaria PAN (pLDH) Ag RDT[g] [70]	Access Bio, Inc	Malaria	Ag (Pan pLDH)	LFA	Whole blood	$0.50/ test [71]	Clinicians	20 min	Handheld	Sens: 96–97% Spec: 98.5% PDS Pf: 84% PDS Pv: 88.6%
Alere Determine TP [72]	Abbott	Syphilis	Ab	LFA	Whole blood, plasma, and serum	$1.45/ test [73]	Clinicians	15 min	Handheld	Sens: 59.6–100% Spec: 95.7–100% [74]
First Response Syphilis Anti-TP Test Card [75]	Premier Medical Corporation Limited	Syphilis	Ab	LFA	Whole blood, plasma, and serum	$0.03/ test [76]	Clinicians	20 min	Handheld	Sens[h]: 99.1% Spec: 99.6%
STANDARD Q Syphilis Ab Test [77]	SD Biosensor	Syphilis	Ab	LFA	Whole blood, plasma, and serum	Inquired	Clinicians	5–20 min	Handheld	Sens: 85–91% Spec: 97–98% [78]

ACON Chlamydia [79]	ACON Laboratories	Chlamydia	Ag	LFA	Urine and cervical/vaginal swab	–	Clinicians	–	Handheld	Sens: 22.7–66.7% Spec: 91.3–100%
BioRapid Chlamydia Ag Test [79]	Biokit, Spain	Chlamydia	Ag	LFA	Vaginal swab	–	Clinicians	–	Handheld	Sens: 17.3% Spec: 93.5%
Chlamydia Rapid Test SAS [79, 80]	Diagnostics for the Real World	Chlamydia	Ag	LFA (Uses Signal Amplification)	Urine and vaginal swab	–	Clinicians	25 min	Handheld	Sens: 41.2–82.6% Spec: 89–98.8%
Clearview Chlamydia [79]	Abbott	Chlamydia	Ag	LFA	Vaginal/cervical swab	–	Clinicians	15 min [81]	Handheld	Sens: 31.1–53.5% Spec: 95.2–99.2%
Chlamydia Test Card [79, 82]	UltiMed Products	Chlamydia	Ag	LFA	Endocervical swab	–	Clinicians	15 min	Handheld	Sens: 63% Spec: 99.6%
QuickVue Chlamydia [79]	Quidel Corporation	Chlamydia	Ag	LFA	Cervical/vaginal swab	$10.40/ test [83]	Clinicians	10–15 min	Handheld	Sens: 25–37.7% Spec: 99.4–99.7%
aQcare Chlamydia Rapid Test [79, 84]	MEDISENSOR, INC	Chlamydia	Ag	LFA (Uses fluorescent nanoparticles, and requires a portable reader)	Urine and endocervical/ urethral swab	–	Clinicians	15 min	Handheld	Sens: 88.2–93.8% Spec: 94.7–96.8%
Handilab-C [79, 85]	Handilab	Chlamydia	Peptidase 123CBV enzyme	Enzyme Detection	Vaginal swab	–	Clinicians	–	Handheld	Sens: 11.6–17.9% Spec: 90.6–91.9%
Xpert CT/NG Cartridge (For use with the GeneXpert System) [86]	Cepheid	Chlamydia/ Gonorrhea	DNA	NAAT	Urine, vaginal/ endocervical/ pharyngeal/rectal swabs	$16.20/ test [87]	Clinicians	90 min	Handheld	Sens: 86–97% Spec: ~99% [88, 89]

(continued)

Table 5.1 (continued)

Name	Manufacturer	Disease	Biomarker	Detection method	Sample	Cost (USD)	User	Time	Size	Sensitivity and specificity
ACON CT/NG DUO Test [90]	ACON Laboratories	Chlamydia/ Gonorrhea	Ag	LFA	Endocervical swabs	–	Clinicians	–	Handheld	Sens: 12.5% Spec: 99.8%
ACON NG Test [90]	ACON Laboratories	Gonorrhea	Ag	LFA	Endocervical swabs	–	Clinicians	–	Handheld	Sens: Unquantifiable (No True Positives in Clinical Study) Spec: 97.2%
PATH GC-Check [91]	PATH	Gonorrhea	Ag	LFA	Vaginal/cervical swabs	–	Clinicians	20 min	Handheld	Sens: 70% Spec: 97.2%
OneStep Gonorrhea RapiCard InstaTest [92]	Cortez Diagnostics	Gonorrhea	Ag	LFA	Endocervical/ urethral swab	–	Clinicians	15 min	Handheld	Sens: 32.4–33.3% Spec: 96–97.9%
BinaxNOW Gonorrhea [93]	Abbott	Gonorrhea	Ag	LFA	Urine	–	Clinicians	15 min	Handheld	Sens: 94.1% Spec: 95.8%

[a] *Ab* antibody
[b] For complete list of WHO Prequalified HIV LFAs, see WHO List of Prequalified in vitro Diagnostic Products [18]
[c] *Ag* antigen
[d] *LAM* lipoarabinomannan
[e] Pf, *P. falciparum*; Pv, *P. vivax*, Pan represents all *Plasmodium* species
[f] PDS stands for Panel Detection Score, which is a metric used by the WHO to evaluate Malaria rapid tests, considered more stringent than Sensitivity/Specificity. See WHO Malaria RDT Product Evaluations Report for more info [94]
[g] For complete list of WHO Prequalified Malaria LFAs, see WHO List of Prequalified in vitro Diagnostic Products [18]
[h] Not clinically verified

verified. Since all three tests are LFAs, they are also portable, cheap, and suitable for use in POC environments.

5.2.2.5 Chlamydia and Gonorrhea

We will cover chlamydia and gonorrhea in the same section because they are caused by similar pathogens and their diagnostic tools have similar limitations. As a result, we will include devices that can detect both chlamydia and gonorrhea.

Most laboratory-based diagnostic tests for these two bacterial infections utilize nucleic acid amplification [97, 98]. These tests are accurate and have low limits of detection but are not ideal for resource-poor settings because they require expensive equipment and trained personnel. There are several clinically evaluated, commercialized devices capable of chlamydia/gonorrhea detection at the POC, with most falling into two categories: LFAs and NAAT-based devices.

Many commercially available chlamydia LFAs detect the infection-causing bacteria using antigen tests. Since chlamydia is a localized infection, all LFAs use urethral/vaginal swabs or urine as the sample media. As a result, most LFAs require sample processing beforehand; typically, several liquid-handling steps to lyse and dilute the bacteria in the sample. While these steps are relatively trivial, they require trained staff, limiting the use of these LFAs in resource-poor settings. Some tests even require centrifugation, which utilizes equipment not available at many low-resource clinics [99].

The majority of POC chlamydia detection methods suffer from low sensitivities. For example, the non-LFA Handilab-C (Handilab), which detects the chlamydial Peptidase 123CBV from vaginal/urethral swab samples, has been clinically shown to have a sensitivity of 10–20% [85]. Most explanations for this low sensitivity reference small bacterial loads in samples, which may be a difficult problem to overcome. However, the aQcare Chlamydia TRF LFA (MEDISENSOR) uses fluorescent nanoparticles in conjunction with a portable reader to improve its sensitivity [79, 100]. While the aQcare Chlamydia TRF does show promise, the requirement of a portable reader limits its utility in POC settings. LFAs which detect gonorrhea also face similar limitations.

There are only a few commercialized LFAs for gonorrhea detection. All are antigen tests using cervical/urethral swab samples, and most have been shown to have low sensitivities in clinical studies. An exception is the BinaxNOW (Abbott), which has been shown to have a high sensitivity and specificity in a clinical study [93]. However, the majority of gonorrhea LFAs are not widely used because of their low accuracy.

The Xpert CT/NG cartridge, which is used with the GeneXpert Omni, is the only commercially available NAAT-based assay we found that diagnoses chlamydia and/or gonorrhea in POC settings. The Omni is well-suited for POC settings because of its portability and speed. This assay is also more accurate than most non-NAAT devices, as it demonstrated high sensitivity and specificity (>85%) in several clinical studies [88, 89]. Thus, the Xpert CT/NG when used with the GeneXpert Omni is

currently the best device for POC detection of chlamydia and gonorrhea, though the device itself likely has a high upfront cost.

5.3 Cancer Detection at the Point-of-Care

5.3.1 Methods of Detection

The majority of commercialized POC cancer devices are sandwich LFAs. As aforementioned, conventional LFAs present qualitative readouts while variations in the LFA can produce semi-quantitative results. Additionally, electronic readers can convert LFA signal intensities into quantitative results.

An emerging technology in POC cancer detection is microfluidic devices, with one device recently approved by the FDA [102–104]. Its mechanism is shown in Fig. 5.3. Similar to the LFA, the sample solution first re-solubilizes the dehydrated biomarker-specific antibody probes, followed by binding of the probes to the target molecules. The sample solution, driven by the analyzer's vacuum, flows through the microfluidic portion of the cassette, which includes a test zone, negative control zone, and a positive control zone. After binding occurs at these regions, the device automatically removes unbound particles with several wash steps and sequentially applies an enhancement solution to increase signal intensities. Lastly, the analyzer converts the optical density to biomarker concentration [105].

It should be noted that there are devices in development that utilize more advanced technologies, like the nanomaterials found in cancer cytosensors. However, no commercially available device currently employs these mechanisms of detection. For more information on these devices, see Purohit et al. [7].

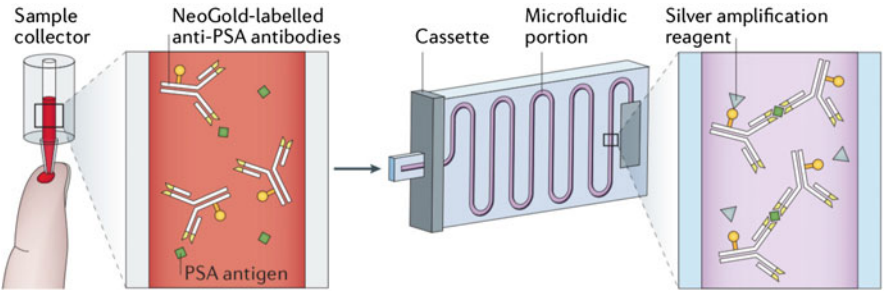

Fig. 5.3 Schematic of the Sangia Total PSA Test, a microfluidic device for prostate cancer detection. In the sample collector, PSA antigens in blood bind to the present NeoGold-labeled anti-PSA antibodies. The sample collector is inserted into the cassette, and the solution flows through the microfluidic channel for silver amplification. The cassette is then placed into an analyzer that converts optical density to biomarker concentration (not shown). Reprinted with permission from Mejía-Salazar et al. [101] Microfluidic Point-of-Care Devices: New Trends and Future Prospects for eHealth Diagnostics. Sensors 20:1–19, 1951. Open access copyright 2020 MDPI

5.3.2 *Summary of Devices*

5.3.2.1 Prostate Cancer

Prostate-specific antigen (PSA) tests are commonly utilized for prostate cancer detection and monitoring. However, PSA levels can be affected by nonmalignant tumors, age, body mass index, race, and/or other health conditions, decreasing the overall accuracy of these tests [106]. Therefore, PSA tests are not definitive and are recommended to be followed by or combined with a digital rectal exam, transrectal ultrasound-guided biopsy, and/or traditional biopsy if needed [107].

A multitude of conventional and semi-quantitative LFAs for PSA are commercially available. However, since these have not been validated through independent studies, we will only cover quantitative LFA tests. The PSAwatch with BioScan (MediWatch), CancerCheck PSA with Concile Ω100 Reader (Concile GmbH), and the ichroma PSA system (Boditech Med) are all tests that utilize electronic readers [108–110]. The PSAwatch and CancerCheck PSA employ colloidal gold nanoprobes, while the i-CHROMA uses fluorescent probes. A broad summary of these devices' mechanisms is shown in Fig. 5.4. While all three devices demonstrated good correlation (r-squared values ranging from 0.72 to 0.96) with laboratory tests in their respective studies, it should be noted that the size and high cost of these analyzers may limit POC use. In addition, the i-CHROMA PSA system consistently reported above the true value [110–113]. The PSAwatch with BioScan appears to have the highest correlation with traditional laboratory tests, but there has been no direct comparison between the three devices [112].

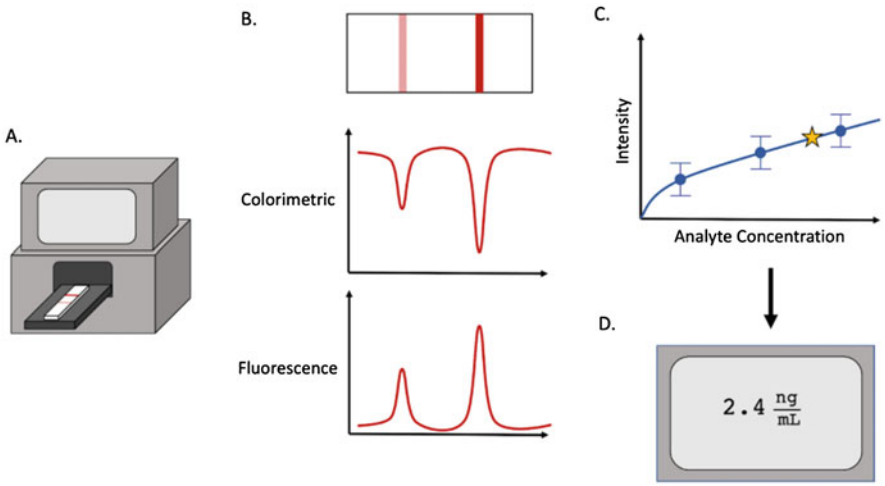

Fig. 5.4 General overview for obtaining quantitative LFA results with use of an electronic reader. (**a**) LFA is inserted into a desktop-size or portable electronic reader. (**b**) LFA signal intensities are mapped accordingly depending on LFA type (colorimetric or fluorescence). (**c**) Analyte concentration is determined by use of a standard curve. (**d**) Readout of results

Lastly, the Silver Amplified NeoGold ImmunoAssay (Sangia) Total PSA Test (OKPO Diagnostics) is a recent FDA-approved POC microfluidic device for PSA. In whole blood samples, the device accurately detects down to 0.08 ng/mL PSA and exhibits equivalent results to an FDA-approved standard test. This device is currently awaiting a CLIA waiver [102, 103, 114].

PSA tests have been proven to be viable options for POC prostate cancer detection when used in conjunction with other tests, despite debate about their usefulness.

5.3.2.2 Colorectal Cancer

POC colorectal cancer tests most commonly detect fecal occult blood (FOB) through two main formats: guaiac FOB tests (gFOB) and fecal immunochemical testing (FIT). While both tests typically require mailed-in patient samples, they are considered POC as they do not require a centralized laboratory. The gFOB test depends on the pseudo-peroxidase activity of hemoglobin in FOB, while FIT relies on antibody–antigen binding. For both tests, a colonoscopy recommendation is given after a positive result. However, many countries have replaced gFOB with FIT in practice and guidelines because it does not require patients to diet before testing, detects cancers of the lower gastrointestinal tract, and delivers more rapid and accurate results [115, 116]. Additionally, other POC colorectal cancer devices test for carcinoembryonic antigen (CEA), but their use has not been validated. The specificity of this biomarker is also limited as levels can be elevated by other cancers and factors [120]. Therefore, we will focus our discussion on POC colorectal tests to the FIT format.

One study compared qualitative FITs ImmunoCARE-C (CARE Diagnostica) [118], FOB Advanced (Ult Med), PreventID CC (Preventis), bioNexia FOBplus (bioMerieux), and QuickVue iFOB Test (Quidel) to three laboratory-based quantitative FITs and found wide variance in performance. Out of these six, the ImmunoCARE-C and FOB advanced were the best-performing; nevertheless, all tests suffered from relatively low sensitivities. However, the study did not fully reflect real-life conditions as samples were frozen before testing [119]. In another study with both POC and non-POC FITS, the researchers found that all devices were generally in agreement and listed sensitivities ranging from 87.2% to 98.4%, and specificities ranging from 80.8% to 99.4% for the POC FIT devices. This includes the Hemoccult ICT (Beckman Coulter), Hemosure iFOBT (Hemosure), hema-screen SPECIFIC (Immunostics), Clearview Ultra FOB (Wampole Laboratories), OC-Light iFOB (Polymedco), and QuickVue iFOB Test (Quidel) [120]. For further specifications on test performances, see Table 5.2.

POC fecal immunochemical testing (FIT) is the predominantly used FOB test that, in conjunction with colonoscopy, can detect colorectal cancer. POC CEA tests can potentially be used for patient monitoring; however, they still await evaluation.

Table 5.2 A summary of the discussed cancer detection devices

Device name	Manufacturer	Type of cancer detected	Biomarker	Detection method	Sample	Time-to-Result	Size	Cost (USD)	Sensitivity and specificity
CancerCheck PSA with Concile Ω100 Reader [109]	concile GmbH	Prostate cancer	Prostate-specific antigen (PSA)	LFA (Quantitative with reader)	Plasma, serum	20 min	Portable tabletop analyzer	–	Sens:85.7% Spec: 66.7% [113]
ichroma PSA system [110]	Boditech Med Inc	Prostate cancer	Prostate-specific antigen (PSA)	LFA (Quantitative with reader)	Whole blood, serum, plasma	15 min	Portable tabletop analyzer	Test strip: N/A Analyzer: $1590.87[a]	Sens:N/A Spec: N/A
PSAwatch with BioScan [108]	MediWatch	Prostate cancer	Prostate-specific antigen (PSA)	LFA (Quantitative with reader)	Whole blood	10 min	Handheld analyzer	Test strip : $6.21 Analyzer: $2235 [112]	Sens:N/A Spec: 99.5%[b] [108]
Silver Amplified NeoGold ImmunoAssay (Sangia) Total PSA Test with Claros 1 Analyzer [106, 121]	OPKO Diagnostics	Prostate cancer	Prostate-specific antigen (PSA)	Microfluidic device	Whole blood	15 min	Portable tabletop analyzer	Test cassette: $15 Analyzer: $2500	Sens: 85.4%, 91.0%[c] Spec: 30.3%, 21.9%[c] [103]
Clearview Ultra FOB Test [122]	Wampole Laboratories	Colorectal cancer	Fecal occult blood (FOB)	LFA	Stool	5 min	Handheld	–	Sens: 91.6% Spec: 94.1% [120]
bioNexia FOBplus [123]	bioMerieux	Colorectal cancer	Fecal occult blood (FOB)	LFA	Stool	5 min	Handheld	–	Sens: 35.8% Spec: 81.9% [119]
FOB Advanced [124]	Ulti med	Colorectal cancer	Fecal occult blood (FOB)	LFA	Stool	5–10 min	Handheld	–	Sens:18% Spec: 92.9% [119]
ImmunoCARE-C [118]	CARE Diagnostica	Colorectal cancer	Fecal occult blood (FOB)	LFA	Stool	5–10 min	Handheld	$1.16%[d]	Sens:11.4% Spec: 96.7% [119]

(continued)

Table 5.2 (continued)

Device name	Manufacturer	Type of cancer detected	Biomarker	Detection method	Sample	Time-to-Result	Size	Cost (USD)	Sensitivity and specificity
hema-screen SPECIFIC [125]	Immunostics	Colorectal cancer	Fecal occult blood (FOB)	LFA	Stool	5 min	Handheld	$5.31 [126]	Sens: 98.1% Spec: 99.4% [120]
Hemoccult ICT [127]	Beckman Coulter	Colorectal cancer	Fecal occult blood (FOB)	LFA	Stool	5 min	Handheld	$5.77 [128]	Sens: 98.2% Spec: 98.1% [120]
Hemosure iFOBT [129]	Hemosure	Colorectal cancer	Fecal occult blood (FOB)	LFA	Stool	5 min	Handheld	$6.30 [130]	Sens: 94.4% Spec: 91.2% [120]
OC-Light iFOB (also called OC-Light S FIT) [131]	Polymedco	Colorectal cancer	Fecal occult blood (FOB)	LFA	Stool	5 min	Handheld	$15.21 [132]	Sens: 98.4% Spec: 98.3% [120]
PreventID CC [133]	Preventis	Colorectal cancer	Fecal occult blood (FOB)	LFA	Stool	10 min	Handheld	$16.27 [133]	Sens: 29.6% Spec: 81.8% [119]
QuickVue iFOB Test [134]	Quidel Corporation	Colorectal cancer	Fecal occult blood (FOB)	LFA	Stool	5–10 min	Handheld	$8.90 [135]	Sens: 45.2–98.3% Spec: 70.2–99.0% [119, 120]
AFP One-step Rapid Detection Kit [136]	Shanghai Outdo Biotech Co	Liver cancer	Alpha fetoprotein (AFP)	LFA	Whole blood	N/A	Handheld	–	Sens: 41–65% Spec: 80–94% [136]
Alere NMP22 Bladderchek [137]	Abbott	Bladder cancer	Nuclear matrix protein (NMP22)	LFA	Urine	30 min	Handheld	–	Sens: 12.9% Spec: 100% [138]

Bladder Tumor Antigen (BTA) STAT [139]	Polymedco	Bladder cancer	Human complement factor H related protein	LFA	Urine	5 min	Handheld	$16.58 [140]	Sens: 58.0–82.8% Spec: 68.0–72.0% [141]
UBC Rapid with Concile Ω100 Reader [142]	IDL Biotech	Bladder cancer	Cytokeratin 8 and 18	LFA (Quantitative w/electronic reader)	Urine	10 min	Portable tabletop analyzer	–	Sens: 61.3%, 64.5%[e] Spec: 77.3%, 81.8%[e] [138]

[a]From Amazon
[b]With digital rectal exam (DRE)
[c]Not clinically verified
[d]Personal correspondence
[e]With electronic reader

5.3.2.3 Liver Cancer

Alpha fetoprotein (AFP) is a widely used biomarker for detecting liver cancer. While AFP levels can be persistently high in patients with cirrhosis, especially when caused by hepatitis B or C, they can also be indicative of malignancy. Thus, numerous expert groups generally recommend AFP testing with ultrasonography every 6 months for high-risk patients as well as CT and MRI scans when necessary [143].

Numerous POC AFP LFAs are commercially available, such as the AFP One-step Rapid Detection Kit (Shanghai Outdo Biotech), which have demonstrated excellent agreement with an AFP ELISA kit [136]. Nevertheless, many POC AFP tests are not formally validated despite their use in clinical settings.

5.3.2.4 Bladder Cancer

Although different biomarkers are utilized in both laboratory and POC bladder cancer tests, the low sensitivities and specificities associated with their measurement preclude recommendation of POC diagnostics for detection and monitoring of bladder cancer. Thus, bladder cancer is primarily diagnosed through traditional means such as urine cytology, cystoscopy, and/or biopsies [143].

POC bladder cancer LFAs include the Bladder Tumor Antigen (BTA) stat (Polymedco), the Alere NMP22 Bladderchek (Abbott), and the UBC Rapid with Concile Ω100 (IDL Biotech) which test for complement factor H and related proteins, nuclear matrix protein 22, and cytokeratins 8 and 18, respectively [137, 139, 142]. In a study involving all three devices, BTA stat consistently produced false positive results for macrohematuria and microhematuria with high erythrocyte densities due to cross-reactivity. Since patients testing for bladder cancer commonly experience macrohematuria and/or microhematuria, BTA stat is not a suitable test [144]. In another study comparing NMP22 Bladderchek and UBC Rapid with Concile Ω100, UBC Rapid exhibited overall higher sensitivity. However, even the best combination of UBC Rapid with cytology demonstrated a sensitivity of only 77.4%, meaning this method cannot replace traditional bladder cancer testing [138].

Poor performance has hindered widespread use of these devices and thus, improvement is first needed to move towards POC testing of bladder cancer.

5.4 Conclusion

Many accurate, low-cost, and rapid diagnostics are available for detection of pathogenic diseases and cancers at the POC. The most commonly used device format for both cancer and disease detection is the LFA. Most LFAs are limited by low sensitivity; however, several diagnostics have overcome this limitation using electronic readers and various signal enhancement techniques. NAAT-based assays are

primarily used for pathogen detection, though they suffer from high costs. However, cancer diagnostics focus on detection of biomarkers instead of genetic material, so NAAT assays are not often used. Current research into POC cancer detection focuses on microfluidic devices, with one recently FDA approved. Multiplex tests able to simultaneously detect multiple biomarkers have also been developed, though none are commercially available [145].

One recent application of POC pathogen detection is diagnostic testing for the SARS-CoV-2 virus. The greatest threat of the virus is its ability to overwhelm hospitals, and the 2020 pandemic has strained healthcare systems worldwide, producing shortages of vital equipment such as ventilators [146]. The virus also spreads rapidly, necessitating the development of POC diagnostics allowing for expansive, rapid testing, while minimizing the resource burden on hospitals and clinics. This chapter does not discuss SARS-CoV-2 diagnostics because the existing tests are still being extensively examined at this time. However, several LFA antibody tests and NAAT-based devices have been developed, such as the ID NOW (Abbott) [137, 147].

POC pathogen and cancer diagnostics allow for early detection and timely treatment, improving the prognosis of patients in resource-poor settings without access to laboratory testing. However, they are not without limitations. POC pathogen diagnostics are commonly limited by low sensitivities and accuracies. Additionally, there are still many diseases that lack commercial POC diagnostics. For example, the WHO compiled a list of Neglected Tropical Diseases which include schistosomiasis and foodborne trematodiases [148]. Cancer diagnostics are also limited by their sensitivities and specificities, and physicians are advised to verify their results with confirmatory testing before making clinical decisions. Current research is focused on addressing these limitations, and there are currently several promising devices available for both pathogen and cancer detection at the POC.

References

1. WHO. (2018). *Cancer*. Accessed April 22, 2020, from https://www.who.int/news-room/fact-sheets/detail/cancer
2. Weltgesundheitsorganisation. (2015). *Health in 2015: From MDGs, millennium development goals to SDGs, sustainable development goals*. World Health Organization.
3. Gaikwad, P. S., & Banerjee, R. (2018). Advances in point-of-care diagnostic devices in cancers. *Analyst, 143*, 1326–1348.
4. Chandra, P., & Pandey, L. M. (Eds.). (2020). *Biointerface engineering: Prospects in medical diagnostics and drug delivery*. Springer Singapore.
5. Kumar, A., Purohit, B., Mahato, K., & Chandra, P. (2019). Chapter 11: Advance engineered nanomaterials in point-of-care immunosensing for biomedical diagnostics. In *Immunosensors* (pp. 238–266). The Royal Society of Chemistry.
6. Purohit, B., Kumar, A., Mahato, K., & Chandra, P. (2020). Smartphone-assisted personalized diagnostic devices and wearable sensors. *Current Opinion in Biomedical Engineering, 13*, 42–50.

7. Purohit, B., Kumar, A., Mahato, K., Roy, S., & Chandra, P. (2019). Chapter 9 - Cancer cytosensing approaches in miniaturized settings based on advanced nanomaterials and biosensors. In P. K. Maurya & S. Singh (Eds.), *Nanotechnology in modern animal biotechnology* (pp. 133–147). Elsevier.
8. IMMY. (2019). *IMMY CrAg LFA*. Accessed April 28, 2020, from https://www.immy.com/crag
9. Hanash, S. M., Pitteri, S. J., & Faca, V. M. (2008). Mining the plasma proteome for cancer biomarkers. *Nature, 452*, 571–579.
10. National Cancer Institute. (1980). *A to Z list of cancer types*. Accessed April 22, 2020, from https://www.cancer.gov/types
11. Word Cancer Research Fund. (2018). *Worldwide cancer data*. Accessed April 22, 2020, from https://www.wcrf.org/dietandcancer/cancer-trends/worldwide-cancer-data
12. Mosley, G. L., Pereira, D. Y., Han, Y., Lee, S. Y., Wu, C. M., Wu, B. M., & Kamei, D. T. (2017). Improved lateral-flow immunoassays for chlamydia and immunoglobulin M by sequential rehydration of two-phase system components within a paper-based diagnostic. *Microchimica Acta, 184*, 4055–4064.
13. Wong, R., & Tse, H. (2009). *Lateral flow immunoassay*. Humana Press.
14. Mauk, M. G., Song, J., Liu, C., & Bau, H. H. (2018). Simple approaches to minimally-instrumented, microfluidic-based point-of-care nucleic acid amplification tests. *Biosensors, 8*, 17.
15. Tanriverdi, S., Chen, L., & Chen, S. (2010). A rapid and automated sample-to-result HIV load test for near-patient application. *The Journal of Infectious Diseases, 201*, S52–S58.
16. Horne, D. J., Kohli, M., Zifodya, J. S., Schiller, I., Dendukuri, N., Tollefson, D., Schumacher, S. G., Ochodo, E. A., Pai, M., & Steingart, K. R. (2019). Xpert MTB/RIF and Xpert MTB/RIF Ultra for pulmonary tuberculosis and rifampicin resistance in adults. *Cochrane Database of Systematic Reviews, 6*, CD009593.
17. UCSF. (2020). *HIV diagnosis*. Accessed May 3, 2020, from https://www.ucsfhealth.org/conditions/hiv/diagnosis
18. WHO. (2020). *WHO list of prequalified in vitro diagnostic products*. Accessed May 26, 2020, from https://www.who.int/diagnostics_laboratory/evaluations/200501_prequalified_product_list_vl.pdf?ua=1
19. WHO. (2020). *WHO What We Do | WHO - Prequalification of medicines programme*. Accessed May 13, 2020, from https://extranet.who.int/prequal/content/what-we-do
20. CDC. (2019). *About HIV/AIDS | HIV Basics | HIV/AIDS | CDC*. Accessed May 3, 2020, from https://www.cdc.gov/hiv/basics/whatishiv.html
21. UNICEF. (2018). *FACSPresto CD4abs% counter with startkit*. Accessed May 6, 2020, from https://supply.unicef.org/s0002000.html
22. Unitaid. (2018). *Market and technology landscape: HIV rapid diagnostic tests for self-testing*, 4th ed. Unitaid, Geneva. Accessed May 26, 2020, from https://unitaid.org/assets/HIVST-landscape-report.pdf
23. Cepheid. (2020). *Cepheid | About Us*. Accessed May 3, 2020, from https://www.cepheid.com/en_US/about
24. UNICEF. (2018). *m-PIMA complete*. Accessed May 6, 2020, from https://supply.unicef.org/s0000598.html
25. UNICEF. (2018). *m-PIMA HIV-1/2 VL cartridge, kit/50*. Accessed May 6, 2020, from https://supply.unicef.org/s0000598.html
26. OraSure. (2016). *OraQuick in Home HIV Test | OraQuick*. Accessed May 6, 2020, from http://www.oraquick.com/What-is-OraQuick/OraQuick-In-Home-HIV-Test
27. Branson, B. M. (2010). The future of HIV testing. *Journal of Acquired Immune Deficiency Syndromes, 55*, S102–S105.
28. Fox, J., Dunn, H., & O'Shea, S. (2011). Low rates of p24 antigen detection using a fourth-generation point of care HIV test. *Sexually Transmitted Infections, 87*, 178–179.

29. Gray, E. R., Bain, R., Varsaneux, O., Peeling, R. W., Stevens, M. M., & McKendry, R. A. (2018). p24 revisited: a landscape review of antigen detection for early HIV diagnosis. *AIDS (London, England), 32*, 2089–2102.
30. Boyle, D. (2017). *Tuberculosis: Diagnostics technology landscape* (5th ed.). World Health Organization.
31. MP Biomedicals. (2016). *ASSURE TB rapid test manual*. Accessed May 26, 2020, from https://www.mpbio.com/media/productattachment/DX072016-EN-ASSURE-TB-Rapid-Test-CE-0743500-Manual.pdf
32. Standard Diagnostics, Inc (2016) SD Product Catalog 4
33. Abbott. (2019). *Alere Determine TB LAM Ag Test Brochure.*
34. Orikiriza, P., Nyehangane, D., Atwine, D., Kisakye, J. J., Kassaza, K., Amumpaire, J.-M., & Boum, Y. (2017). Evaluation of the SD bioline TB ag MPT64 test for identification of *Mycobacterium tuberculosis* complex from liquid cultures in southwestern Uganda. *African Journal of Laboratory Medicine, 6*, a383.
35. Bjerrum, S., Schiller, I., Dendukuri, N., Kohli, M., Nathavitharana, R. R., Zwerling, A. A., Denkinger, C. M., Steingart, K. R., & Shah, M. (2019). Lateral flow urine lipoarabinomannan assay for detecting active tuberculosis in people living with HIV. *Cochrane Database of Systematic Reviews, 10*, CD011420.
36. Mukhopadhyay, A., Guan, M., Chen, H. Y., Lu, Y., & Lim, T. K. (2006). Prospective study of a new serological test (ASSURE TB rapid test) for the diagnosis of pulmonary tuberculosis. *The International Journal of Tuberculosis and Lung Disease Official Journal of the International Union Against Tuberculosis Lung Disease, 10*, 620–626.
37. Molbio Diagnostics. (2020). *Truelab Uno Dx Real Time Qualitative micro PCR analyzer manual*.
38. Ustar Biotechnologies. (2018). *Ustar EasyNAT Brochure*. Accessed May 28, 2020, from http://www.bioustar.com/EN/downfile.aspx?CateId=178&CId=164
39. WHO. (2020). Molecular assays intended as initial tests for the diagnosis of pulmonary and extrapulmonary TB and rifampicin resistance in adults and children: Rapid communication. World Health Organization, Geneva. Accessed May 26, 2020, from https://apps.who.int/iris/bitstream/handle/10665/330395/9789240000339-eng.pdf?sequence=1&isAllowed=y
40. Cepheid. *Xpert MTB/RIF Ultra Brochure*. Accessed May 26, 2020, from https://p.widencdn.net/sihiwi/Cepheid-Xpert-MTB-RIF-Ultra-Brochure-CE-IVD-3098-English
41. WHO. (2020). *Malaria*. Accessed April 13, 2020, from https://www.who.int/en/news-room/fact-sheets/detail/malaria
42. WHO. (2018). *WHO prequalification of in vitro diagnostics public report: INSTI HIV self-test*. World Health Organization.
43. UNICEF. (2018). *INSTI HIV Self-Test, kit/1T*. Accessed May 6, 2020, from https://supply.unicef.org/s0003846.html
44. WHO. (2016). *WHO prequalification of in vitro diagnostics public report: OraQuick HIV self-test*. World Health Organization.
45. UNICEF. (2018). *Oraquick HIV self-test, Kit/50*. Accessed May 6, 2020, from https://supply.unicef.org/s0001657.html
46. WHO. (2019). *WHO prequalification of in vitro diagnostics public report: Mylan HIV self-test*. World Health Organization.
47. UNICEF. (2018). *Mylan HIV self-test, kit/1T*. Accessed May 6, 2020, from https://supply.unicef.org/s0003847.html
48. WHO. (2019). *WHO prequalification of in vitro diagnostics public report: SURE CHECK HIV self-test*. World Health Organization.
49. UNICEF. (2018). *Sure Check HIV 1/2, kit/25*. Accessed May 6, 2020, from https://supply.unicef.org/s0003764.html
50. WHO. (2013). *WHO prequalification of in vitro diagnostics public report: Pima CD4 test*. World Health Organization.

51. UNICEF. (2018). *PoC CD4 [abs] cartridge kit,100 tests*. Accessed May 26, 2020, from https://supply.unicef.org/s0001223.html
52. Abbott. (2019). *Pima CD4 reaching further brochure.*
53. WHO. (2019). *WHO prequalification of in vitro Diagnostics public report: BD FACSPresto near-patient CD4 counter system*. World Health Organization.
54. UNICEF. (2018). *FACSPresto CD4 abs%, cartridges kit/100*. Accessed May 6, 2020, from https://supply.unicef.org/s0002002.html
55. BD Biosciences. (2014). *BD FACSPresto near-patient CD4 counter instructions for use*. Accessed May 26, 2020, from https://www.bdbiosciences.com/ds/europe/tds/23-12808.pdf
56. WHO. (2019). *WHO prequalification of in vitro diagnostics public report: m-PIMA HIV-1/2 VL*. World Health Organization.
57. WHO. (2019). *WHO prequalification of in vitro Diagnostics public report: Xpert HIV-1 Qual assay*. World Health Organization.
58. UNICEF. (2018). *GeneXpert HIV1 Qual EID cartridge kit/10*. Accessed May 6, 2020, from https://supply.unicef.org/s0002147.html
59. UNICEF. (2018). *PoC CD4 [abs],counter with start kit*. Accessed May 26, 2020, from https://supply.unicef.org/s0001224.html
60. Scott, L., Gous, N., Carmona, S., & Stevens, W. (2015). Laboratory evaluation of the Liat HIV quant (IQuum) whole-blood and plasma HIV-1 viral load assays for point-of-care testing in South Africa. *Journal of Clinical Microbiology, 53*, 1616–1621.
61. Roche. (2018). *cobasLiat System Brochure*. Accessed May 26, 2020, from https://www.cobasliat.com/app/uploads/2019/07/cobas_Liat_System_Brochure_PP-GBL-00380_0418.pdf
62. Arora, J., Kumar, G., Verma, A. K., Bhalla, M., Sarin, R., & Myneedu, V. P. (2015). Utility of MPT64 antigen detection for rapid confirmation of *Mycobacterium tuberculosis* complex. *Journal of Global Infectious Diseases, 7*, 66.
63. UNICEF. (2018). *Xpert MTB/RIF Ultra Assay, kit/50*. Accessed May 7, 2020, from https://supply.unicef.org/s0001690.html
64. Molbio Diagnostics Truenat MTB Plus Package Insert. Accessed May 26, 2020, from http://www.molbiodiagnostics.com/uploads/product_download/20190927.152146~Truenat-MTB-Plus-packinsert.pdf
65. Deng, S., Sun, Y., Xia, H., Liu, Z., Gao, L., Yang, J., Zhao, Y., Huang, F., Feng, J., Wang, L., Huan, S., & Zhan, S. (2019). Accuracy of commercial molecular diagnostics for the detection of pulmonary tuberculosis in China: A systematic review. *Scientific Reports, 9*, 1–11.
66. WHO. (2019). *WHO Prequalification of In Vitro Diagnostics Public Report Alere Malaria Ag P.f.* World Health Organization, Geneva
67. UNICEF. (2018). *Alere Mal AgPf safety lancet,1T/kitx25*. Accessed May 7, 2020, from https://supply.unicef.org/s0003859.html
68. WHO. (2018). *WHO Prequalification of in vitro diagnostics public report: First Response® Malaria Ag*. P.f. / P.v. Card Test. World Health Organization, Geneva
69. UNICEF. (2018). *FirstResponseMalAgPf/PvCardTest,kit/30*. Accessed May 7, 2020, from https://supply.unicef.org/s0003864.html
70. WHO. (2018). *WHO prequalification of in vitro diagnostics public report: CareStartTM malaria PAN (pLDH) Ag RDT*. World Health Organization.
71. UNICEF. (2018). *CareStart Malaria pLDH (PAN), kit/25*. Accessed May 7, 2020, from https://supply.unicef.org/s0003782.html
72. Abbott. (2019). *Alere Determine Syphilis TP Quick Reference Guide.*
73. UNICEF. (2018). *Alere Determine, Syphilis RDT, kit/100*. Accessed May 5, 2020, from https://supply.unicef.org/all-materials/diagnostic-test-kits/syphilis-test-kits/syphilis-simplerapid/s0003550.html
74. Mabey, D., Peeling, R. W., Ballard, R., Benzaken, A. S., Galbán, E., Changalucha, J., Everett, D., Balira, R., Fitzgerald, D., Joseph, P., Nerette, S., Li, J., & Zheng, H. (2006). Prospective, multi-centre clinic-based evaluation of four rapid diagnostic tests for syphilis. *Sexually Transmitted Infections, 82*, v13–v16.

75. Premier Medical Corporation Ltd. (2012). *First response syphilis anti-TP card test package insert*. Accessed May 26, 2020, from http://premiermedcorp.com/wp-content/uploads/2013/08/product_documents/Infectious_Diseases/I08FRC30-1.pdf
76. India Mart. (2020). *First Response Syphilis Anti Tp Card Test Kit*. Accessed May 7, 2020, from https://www.indiamart.com/proddetail/first-response-syphilis-anti-tp-card-test-kit-19120495033.html
77. SD Biosensor. (2013). *Products - STANDARD Q Syphilis Ab*. Accessed May 7, 2020, from http://sdbiosensor.com/xe/product/2628?category=2309
78. Lubis, R., Sirait, S., Agustin, T., & Indriatmi, W. (2019). P748 syphilis diagnostic test of STANDARDTM Q syphilis AB using fingerprick whole blood and serum on high risk populations. *Sexually Transmitted Infections, 95*, A322–A323.
79. Kelly, H., Coltart, C. E. M., Pai, N. P., Klausner, J. D., Unemo, M., Toskin, I., & Peeling, R. W. (2017). Systematic reviews of point-of-care tests for the diagnosis of urogenital chlamydia trachomatis infections. *Sexually Transmitted Infections, 93*, S22–S30.
80. Nadala, E.-C., Goh, B. T., Magbanua, J.-P., Barber, P., Swain, A., Alexander, S., Laitila, V., Michel, C.-E., Mahilum-Tapay, L., Ushiro-Lumb, I., Ison, C., & Lee, H. H. (2009). Performance evaluation of a new rapid urine test for chlamydia in men: Prospective cohort study. *BMJ, 339*, b2655.
81. Trans Continental Medical Products. (2014). *Clearview® Chlamydia MF Test* |. Accessed May 8, 2020, from http://www.transcontinentalmedicalproducts.com/product/clearview-chlamydia-mf-test/
82. Sabidó, M., Hernández, G., González, V., Vallès, X., Montoliu, A., Figuerola, J., Isern, V., Viñado, B., Figueroa, L., & Casabona, J. (2009). Clinic-based evaluation of a rapid point-of-care test for detection of chlamydia trachomatis in specimens from sex workers in Escuintla, Guatemala. *Journal of Clinical Microbiology, 47*, 475–476.
83. CLIAwaived Quidel QuickVue Chlamydia Tests. Accessed May 8, 2020, from https://www.cliawaived.com/quidel-quickvue-chlamydia-test.html
84. Ham, J. Y., Jung, J., Hwang, B.-G., Kim, W.-J., Kim, Y.-S., Kim, E.-J., Cho, M.-Y., Hwang, M.-S., Won, D. I., & Suh, J. S. (2015). Highly sensitive and novel point-of-care system, aQcare chlamydia TRF kit for detecting chlamydia trachomatis by using Europium (Eu) (III) chelated nanoparticles. *Annals of Laboratory Medicine, 35*, 50–56.
85. Schachter, J. (2016). Point-of-care tests using enzyme detection to diagnose chlamydia trachomatis infection do not work. But when they fail in clinical trials, they reappear under different names. *Sexually Transmitted Infections, 92*, 406–407.
86. Cepheid. (2019). *Xpert CT/NG Package Insert*. Accessed May 26, 2020, from https://www.cepheid.com/Package%20Insert%20Files/Xpert-CTNG-US-ENGLISH-Package-Insert-301-0234%2D%2DRev-K.pdf
87. UNICEF. (2018). *Xpert CT/NG Assay, kit/10*. Accessed May 7, 2020, from https://supply.unicef.org/s0001685.html
88. Gaydos, C. A., Van Der Pol, B., Jett-Goheen, M., Barnes, M., Quinn, N., Clark, C., Daniel, G. E., Dixon, P. B., & Hook, E. W. (2013). Performance of the Cepheid CT/NG Xpert rapid PCR test for detection of chlamydia trachomatis and *Neisseria gonorrhoeae*. *Journal of Clinical Microbiology, 51*, 1666–1672.
89. Goldenberg, S. D., Finn, J., Sedudzi, E., White, J. A., & Tong, C. Y. W. (2012). Performance of the GeneXpert CT/NG assay compared to that of the Aptima AC2 assay for detection of rectal chlamydia trachomatis and *Neisseria gonorrhoeae* by use of residual Aptima samples. *Journal of Clinical Microbiology, 50*, 3867–3869.
90. Nuñez-Forero, L., Moyano-Ariza, L., Gaitán-Duarte, H., Ángel-Müller, E., Ruiz-Parra, A., González, P., Rodríguez, A., & Tolosa, J. E. (2016). Diagnostic accuracy of rapid tests for sexually transmitted infections in symptomatic women. *Sexually Transmitted Infections, 92*, 24–28.

91. Alary, M., Gbenafa-Agossa, C., Aïna, G., Ndour, M., Labbé, A. C., Fortin, D., Steele, M., & Peeling, R. W. (2006). Evaluation of a rapid point-of-care test for the detection of gonococcal infection among female sex workers in Benin. *Sexually Transmitted Infections, 82*, v29–v32.
92. Abbai, N. S., Moodley, P., Reddy, T., Zondi, T. G., Rambaran, S., Naidoo, K., & Ramjee, G. (2015). Clinical evaluation of the OneStep gonorrhea RapiCard InstaTest for detection of *Neisseria gonorrhoeae* in symptomatic patients from KwaZulu-Natal, South Africa. *Journal of Clinical Microbiology, 53*, 1348–1350.
93. Suzuki, K., Matsumoto, T., Tateda, K., Yamaguchi, K., Murakami, H., & Ishii, N. (2004). Evaluation of a rapid antigen detection test for *Neisseria gonorrhoeae* in urine sediment for diagnosis of gonococcal urethritis in males. *Journal of Infection and Chemotherapy, 10*, 208–211.
94. WHO. (2018). *Malaria rapid diagnostic test performance: Results of WHO product testing of malaria RDTs: Round 8 (2016–2018)*. World Health Organization.
95. CDC. (2019). *STD Facts - Syphilis (Detailed)*. Accessed May 6, 2020, from https://www.cdc.gov/std/syphilis/stdfact-syphilis-detailed.htm
96. WHO. (2020). *Syphilis Rapid Tests: Progress of the active applications in the prequalification of IVDs assessment pipeline*. Accessed May 26, 2020, from https://www.who.int/diagnostics_laboratory/syphilis_rapid_test.pdf?ua=1
97. CDC. (2019). *Detailed STD Facts - Chlamydia*. Accessed May 6, 2020, from https://www.cdc.gov/std/chlamydia/stdfact-chlamydia-detailed.htm
98. CDC. (2019). *Detailed STD Facts - Gonorrhea*. Accessed May 6, 2020, from https://www.cdc.gov/std/gonorrhea/stdfact-gonorrhea-detailed.htm
99. Stratton, N. J., Hirsch, L., Harris, F., de la Maza, L. M., & Peterson, E. M. (1991). Evaluation of the rapid CLEARVIEW chlamydia test for direct detection of chlamydiae from cervical specimens. *Journal of Clinical Microbiology, 29*, 1551–1553.
100. Medisensor Inc. (2018). aQcareTM Chlamydia TRF-S_us. In *medi*. Accessed May 6, 2020, from http://medi-sensor.com/en/aqcare-chlamydia-trf-s_us/
101. Mejía-Salazar, J., Cruz, K., Vásques, E., & de Oliveira, J. O. (2020). Microfluidic point-of-care devices: New trends and future prospects for eHealth diagnostics. *Sensors, 20*, 1–19.
102. FDA. (2019). *Sangia Total PSA Test - P170037*. Accessed April 22, 2020, from https://www.fda.gov/medical-devices/recently-approved-devices/sangia-total-psa-test-p170037
103. FDA. (2019). *Summary of safety and effectiveness data (SSED)*. Accessed May 6, 2020, from https://www.accessdata.fda.gov/cdrh_docs/pdf17/p170037b.pdf
104. Zhang, Z., & Nagrath, S. (2013). Microfluidics and cancer: Are we there yet? *Biomedical Microdevices, 15*, 595–609.
105. OPKO Diagnostics. (2019). *Instructions for use*. Accessed April 22, 2020, from https://www.accessdata.fda.gov/cdrh_docs/pdf17/p170037c.pdf
106. Lilja, H., Ulmert, D., & Vickers, A. J. (2008). Prostate-specific antigen and prostate cancer: Prediction, detection and monitoring. *Nature Reviews. Cancer, 8*, 268–278.
107. Barry, M. J. (2001). Prostate-specific-antigen testing for early diagnosis of prostate cancer. *The New England Journal of Medicine, 344*, 1373–1377.
108. Mediwatch. *Bioscan PSAwatch*. Accessed April 22, 2020, from https://itarmed.org/files/product/636092906854064473-Analizatori-mochi-PSA-BioScan-Mediwatch.pdf
109. Concile. (2017). *CancerCheck PSA*. Accessed May 6, 2020, from https://www.concile.de/en/produkte/quantitative-rapid-tests/cancercheck-psa/
110. Boditech. (2015). *ichroma PSA*. Accessed May 6, 2020, from http://genius-diagnostics.al/site/wp-content/uploads/2015/08/INS-PS-EN-PSA_Rev.17_150701.pdf
111. Beltran, L., Leach, E., Fonseka, S., Bolodeoku, J., & Chinegwundoh, F. (2018). An evaluation of the novel i-CHROMA™ point-of-care testing (POCT) method for the analysis of prostate-specific antigen (PSA) in serum. *BJSTR, 9*, 4.
112. Karim, O., Rao, A., Emberton, M., Cochrane, D., Partridge, M., Edwards, P., Walker, I., & Davidson, I. (2007). Point-of-care PSA testing: An evaluation of PSAwatch. *Prostate Cancer and Prostatic Diseases, 10*, 270–273.

113. Rausch, S., Hennenlotter, J., Wiesenreiter, J., Hohneder, A., Heinkele, J., Schwenter, C., Stenzl, A., & Todenhöfer, T. (2016). Assessment of a new point-of-care system for detection of prostate specific antigen. *BMC Urology, 16*, 26785797.
114. Meyer, A. R., & Gorin, M. A. (2019). First point-of-care PSA test for prostate cancer detection. *Nature Reviews. Urology*. Accessed May 6, 2020, from https://www.nature.com/articles/s41585-019-0179-1
115. Kościelniak-Merak, B., Radosavljević, B., Zając, A., & Tomasik, P. J. (2018). Faecal occult blood point-of-care tests. *Journal of Gastrointestinal Cancer, 49*, 402–405.
116. Nicholson, B. D., Thompson, M., Price, C. P., Heneghan, C., & Plüddemann, A. (2015). Home-use faecal immunochemical testing: Primary care diagnostic technology update. *The British Journal of General Practice, 65*, 156–158.
117. Perkins, G. L., Slater, E. D., Sanders, G. K., & Prichard, J. G. (2003). Serum tumor markers. *American Family Physician, 68*, 1075–1082.
118. CARE Diagnostica. *immoCARE-C*. Accessed May 8, 2020, from https://www.care.co.at/en/products/immocare-c
119. Hundt, S. (2009). Comparative evaluation of immunochemical fecal occult blood tests for colorectal adenoma detection. *Annals of Internal Medicine, 150*, 162.
120. Daly, J. M., Bay, C. P., & Levy, B. T. (2013). Evaluation of fecal immunochemical tests for colorectal cancer screening. *Journal of Primary Care and Community Health, 4*, 245–250.
121. Eclipse Product Development. (2020). *Life Sciences*. Accessed May 8, 2020, from https://eclipsepd.com/areas/life-sciences
122. Wampole Laboratories. (2004). *Clearview ULTRA FOB test*. Accessed May 8, 2020, from http://www.diagnosticsdirect2u.com/images/PDF/Clearview%20FOB%20Test%20Brochure.pdf
123. bioMerieux. *bioNexia FOBplus*. Accessed May 8, 2020, from https://www.biomerieux.com.br/sites/subsidiary_br/files/9305153-008-gb-a-bionexia-fob-plus.pdf
124. Ulti med. *Early colorectal cancer diagnosis by FOB Advanced*. Accessed May 8, 2020, from http://www.omegairl.com/pdf/010A210-20_FOB_cassette_GB_advanced_oct2009.pdf
125. Immunostics. *hema-screen SPECIFIC with DEVEL-A-TAB*. Accessed May 8, 2020, from https://129082f9-e06f-6c6b-89d6-60fb1687ba08.filesusr.com/ugd/8a6edf_9d1fbbc9cbaa4894a68c9d416fe2afd2.pdf
126. Tiger Medical. (2020). *Immunostics HSSPCAS-25 hema-screen SPECIFIC tubes and cassettes*. Accessed May 8, 2020, from https://www.tigermedical.com/Products/Hema-Screen-Specific-Tubes-and-Cassettes__IMMHSSPCAS-10-.aspx?invsrc=adwords_tm&gclid=CjwKCAjwte71BRBCEiwAU_V9h_vLSkRmmpRhpo8q2RMPsH_hCcQGKpjnQpHSpn4ly4u7hyYvEppl9BoC7TIQAvD_BwE
127. Beckman Coulter. (2018). *Hemoccult ICT*. Accessed May 8, 2020, from https://wwwbeckmancoultercom/download/file/wsr-158616/395095AB?type=pdf
128. Medex Supply. (2020). *Beckman Coulter Hemoccult ICT test device kit*. Accessed May 8, 2020, from https://www.medexsupply.com/diagnostic-tests-blood-fecal-occult-tests-beckman-coulter-hemoccult-ict-test-device-kit-20-bx-x_pid-42093.html
129. Hemosure. (2013). *Hemosure one-step immunological fecal occult blood test*. Accessed May 8, 2020, from http://hemosure.com/wp-content/uploads/2013/10/Product-Insert-1.pdf
130. CLIAwaived. *Hemosure one-step fecal occult Blood Tests (FOB)*. Accessed May 8, 2020, from https://www.cliawaived.com/hemosure-one-step-fecal-occult-blood-test-fob.html
131. Polymedco. (2020). *What is OC-Light® S FIT?* Accessed May 8, 2020, from https://www.polymedco.com/what-is-oc-lights-fit.php
132. VWR. OC-Light® S FIT Test Kits, Polymedco. Accessed May 8, 2020, from https://us.vwr.com/store/product/27484137/oc-light-s-fit-test-kits-polymedco
133. Preventis. (2020). *Prevent ID CC colorectal cancer screening*. Accessed May 8, 2020, from https://www.preventis.com/products/preventid%c2%ae-cc
134. Quidel. *QuickVue iFOB Test*. Accessed May 8, 2020, from https://www.quidel.com/sites/default/files/product/documents/quickvue_ifob_sales_sheet.pdf

135. CLIAwaived. *Quidel QuickVue iFOB Test kit*. Accessed May 8, 2020, from https://www.cliawaived.com/quickvue-quidel-ifob-test-kit.html
136. Jin, J., Zhang, X. Y., Shi, J. L., Xue, X. F., Lu, L. L., Lu, J. H., Jiang, X. P., Hu, J. F., Duan, B. S., Yang, C. Q., Lu, D. R., Lu, D. L., Chen, J. G., & Gao, H. J. (2017). Application of AFP whole blood one-step rapid detection kit in screening for HCC in Qidong. *American Journal of Cancer Research, 7*, 1384–1388.
137. Abbott. (2020). *Alere NMP22 Bladderchek*. Accessed May 12, 2020, from https://www.alere.com/en/home/product-details/nmp22-bladderchek.html
138. Pichler, R., Tulchiner, G., Fritz, J., Schaefer, G., Horninger, W., & Heidegger, I. (2017). Urinary UBC rapid and NMP22 test for bladder cancer surveillance in comparison to urinary cytology: Results from a prospective single-center study. *International Journal of Medical Sciences, 14*, 811–819.
139. Polymedco. (2020). *What is the BTA stat test?* Accessed May 12, 2020, from https://www.polymedco.com/what-is-bta-stat-test.php
140. CLIAwaived. *BTA STAT - Rapid Test for Recurrent Bladder Cancer*. Accessed May 8, 2020, from https://www.cliawaived.com/bta-stat-rapid-test-for-recurrent-bladder-cancer.html
141. Greene, K. L., Berry, A., & Konety, B. R. (2006). Diagnostic utility of the immunoCyt/uCyt+ test in bladder cancer. *Revista de Urología, 8*, 190–197.
142. IDL Biotech. *UBC rapid for bladder cancer detection*. Accessed May 12, 2020, from https://idlbiotech.com/wp-content/uploads/2019/12/UBC-Rapid-91-657-07_1910.pdf
143. Sturgeon, C. M., & Diamandis, E. (2010). *Use of tumor markers in liver, bladder, cervical, and gastric cancers* (Vol. 3–15, pp. 17–21). American Association for Clinical Chemistry.
144. Lüdecke, G., Pilatz, A., Hauptmann, A., Bschleipfer, T., & Widner, W. (2012). Comparative analysis of sensitivity to blood in the urine for urine-based point-of-care assays (UBC rapid, NMP22 BladderChek and BTA-stat) in primary diagnosis of bladder carcinoma. Interference of blood on the results of urine-based POC tests. *Anticancer Research, 32*, 2015–2018.
145. Hayes, B., Murphy, C., Crawley, A., & O'Kennedy, R. (2018). Developments in point-of-care diagnostic technology for cancer detection. *Diagnostics, 8*, 39.
146. Meng, L., Qiu, H., Wan, L., Ai, Y., Xue, Z., Guo, Q., Deshpande, R., Zhang, L., Meng, J., Tong, C., Liu, H., & Xiong, L. (2020). Intubation and ventilation amid the COVID-19 outbreak: Wuhan's experience. *Anesthesiology*. https://doi.org/10.1097/ALN.0000000000003296
147. Abbott. (2020). *Abbott ID NOWTM COVID-19 - Alere is now Abbott*. Accessed May 17, 2020, from https://www.alere.com/en/home/product-details/id-now-covid-19.html
148. WHO. (2020). *WHO neglected tropical diseases*. Accessed May 26, 2020, from http://www.who.int/neglected_diseases/diseases/en/

Chapter 6
Non-invasive Cellular Characterization Using Bioimpedance Sensing

Debanjan Das and Soumen Das

6.1 Introduction

Understanding of cell physiology plays a crucial role in the diagnosis and prevention of complex diseases especially in cancer research. Normal cell properties such as morphology, biochemical composition, adhesion, motility, apoptosis, etc. are modified during the cancer development. Thus, for diagnosis and treatment of cancer, it is important to study the characteristics of cancer cells from different origin in relation to its normal counterpart. In medical pathology especially in oncology, very often cells and different cellular activities and behaviors such as cell adhesion, growth, proliferation, cell–cell interaction, and cell toxicity are examined to identify disease with the help of biological assay, phase contrast microscopy, fluorescence imaging, etc. In general, these conventional techniques very often require costly chemicals, fluorescent or radioactive labeling as a part of experimental procedure. Therefore, there exists a great demand for a label-free, non-invasive, and cost-effective method for cancer detection and characterization. Literature survey reveals that during the advancement of a cell from a healthy normal stage towards malignancy, its electrical, mechanical, and optical characteristics [1–4] associated with biophysical properties modify along with its biological changes. Therefore, there is a possibility to open an alternative path for label-free detection of the cancer diseases by identifying and measuring these non-biological parameters of the cells which may carry the signature of cancer disease. Out of various techniques, recently, electric impedance based measurement has become one of the preferred potential techniques

D. Das
Department of ECE, IIIT Naya Raipur, Raipur, India
e-mail: debanjan@ieee.org

S. Das (✉)
School of Medical Science and Technology, IIT Kharagpur, Kharagpur, India
e-mail: sou@smst.iitkgp.ac.in

V. Borse et al. (eds.), *BioSensing, Theranostics, and Medical Devices*,
https://doi.org/10.1007/978-981-16-2782-8_6

to monitor live cell behavior in real time in terms of passive electrical parameters [5, 6].

Bioimpedance offers continuous, non-destructive, non-invasive, and label-free measurements and quantitatively characterizes biological cells, which is more efficient, inexpensive, sensitive, and simple compared to existing microscopic or optical observation technique [5]. Cellular bioimpedance measurements are typically performed in microchip-based systems in two different ways. First approach includes bioimpedance measurement during cell culture on microfabricated electrodes [7]. An alternate way is to measure while cells are transported through microfluidic channels [8, 9]. The most common form of the cell impedance technique is electric cell-substrate impedance sensing (ECIS) [10, 11], first developed by Giaever and Keese [12] for studying cell response in real time. Electrical impedance spectroscopy of living cells provides continuous and non-invasive measurements, which is more efficient, inexpensive, sensitive, and simple compared to existing microscopic or optical observation technique.

Impedance spectroscopy has been extensively used to study the cellular behavior either at a given time with a frequency sweep or in real time at a known frequency. However, a major challenge in impedance based assay is interpretation of impedance spectra. Traditionally frequency swept impedance data with group of cells is predominantly interpreted by equivalent circuit modeling via fitting methods or theoretical analysis. The parameter extraction by theoretical modeling can handle long data sets by taking care of geometric corrections. This theoretical modeling may also extend the utilization of impedance spectroscopy data for estimating the equivalent single cell parameters by avoiding complex methodology of single cell trapping in microchannel. The present chapter is an inspiration for developing a label-free impedimetric technique and analysis methods to characterize cancer and normal cells in correspondence with other biophysical characteristics.

6.2 Principle

6.2.1 Cell-Substrate Impedance

When cells attach and spread onto the surface of the electrode, the measured impedance increases because the cell membranes act as insulators and block current flow. A schematic of the current flow path in cell culture medium with cells at low and high frequency is shown in Fig. 6.1. Under small signal configuration, a minor amount of current is passed through the electrodes, thus making the measurements non-invasive and non-destructive to the cells. The impedance (Z) of ECIS system is determined as the ratio of voltage phasor to current phasor by Ohm's law:

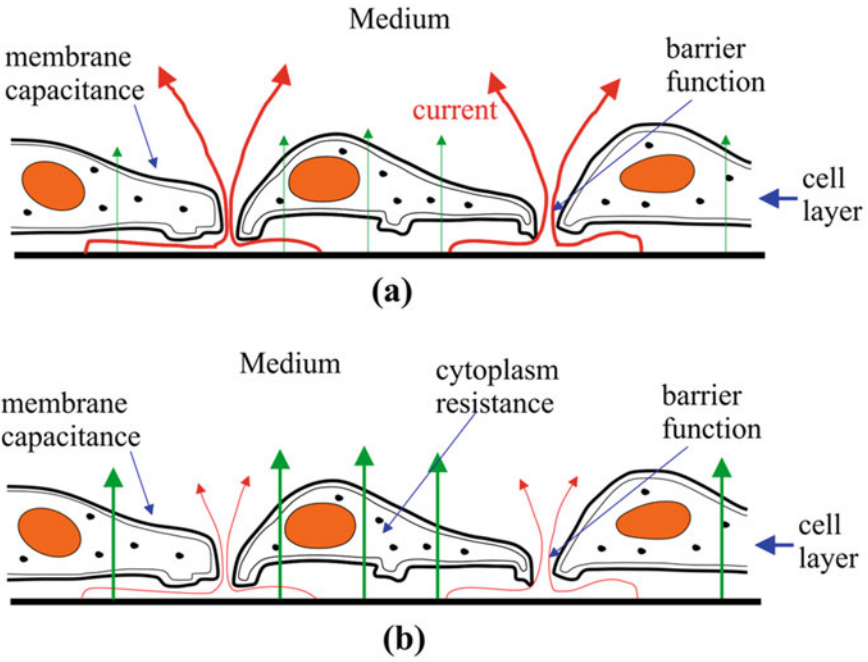

Fig. 6.1 Schematic of current flow in cell culture medium with cells. (**a**) At low AC frequency current is bypassed via paracellular pathways and (**b**) at high AC frequency current flows via transcellular pathways

$$Z(j\omega) = \frac{V(j\omega)}{I(j\omega)} = Z_r(\omega) + jZ_i(\omega), \tag{6.1}$$

where I is the applied alternating current, V is the resulting voltage, $j = \sqrt{-1}$, $\omega = 2\pi f$, ω is the angular frequency, and f is the applied alternating current (AC) frequency. The magnitude ($|Z|$) and phase angle (θ) of the impedance are determined from real part of impedance ($Z_r(\omega)$) and imaginary part of impedance ($Z_i(\omega)$). When cells inoculated inside a media are added to the bioimpedance sensing device, current flow path alters leading to change in impedance value. Thus, by comparing the impedance values of only media and that of cells plus media one can extract the information about the cells only. With proper analysis the measured impedance ($|Z|$, θ) can be split into its components (R, C) and quantitative information about the media and cells can be obtained to characterize a particular cell. Different system parameters of attached group of cells on electrode surface such as solution resistance, double layer capacitance, equivalent resistance, and capacitance of group of cells are extracted and quantified by analyzing the equivalent circuit models or fitting with commercial curve fitting software.

6.2.2 *Design and Simulation of Sensor Configuration*

The bioimpedance measurements are usually performed using two [13, 14], three [15], or four electrodes configurations [6] as shown in Fig. 6.2. In two-electrode mode Working (W) and Working Sense (WS) are connected to a (working) electrode and Reference (R) and Counter (C) are connected to a second (aux) electrode. In three-electrode setup, the Reference lead is separated from the Counter and placed as separate near to working electrode, whereas in four-electrode mode all four placed separately. Four-electrode setup measures only the in-between solution, whereas two-electrode setup incorporates solution and other barriers. Therefore, there- and four-electrode modes are more useful for electrochemical analysis, whereas two-electrode mode is more popular for measuring general impedance of any system. In bioimpedance study also two-electrode measurement has become

most practical technique and has been debuted as a commercially available technique (BioPhysics). Here, the bioimpedance sensor consists of six separate mini-culture wells having an individual circular working electrode (WE) and a counter electrode (CE), which is common in two wells as shown in Fig. 6.3a. The cross-sectional view of the sensor as depicted in Fig. 6.3b shows that WE and part of CE electrode are in contact with sample during impedance measurement. The diameter of circular working electrode is 3 mm, the width of semi-circular counter

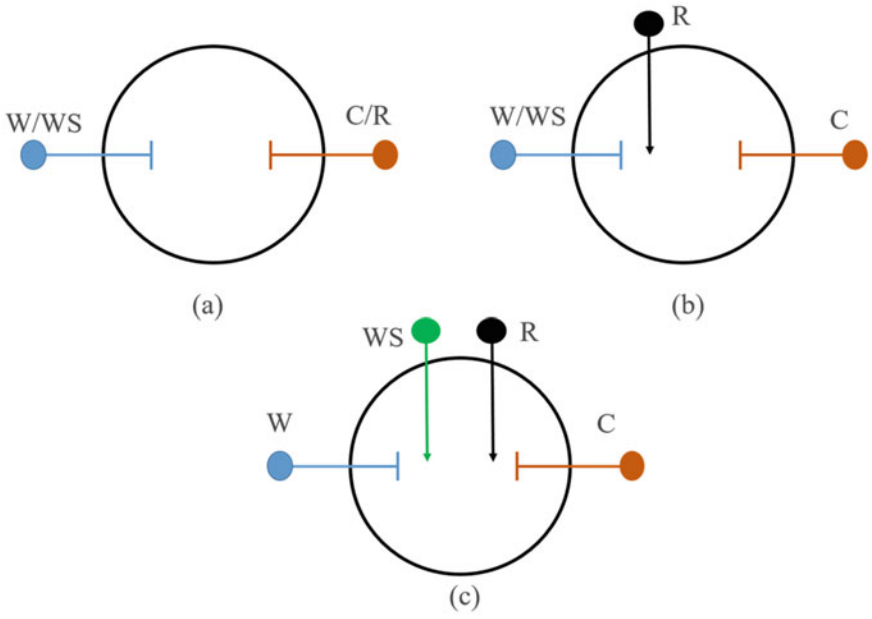

Fig. 6.2 Schematic representation of different electrode configurations: (**a**) two-electrode, (**b**) three-electrode, and (**c**) four-electrode setup. *W* working, *WS* working sense, *R* reference, *C* counter electrode

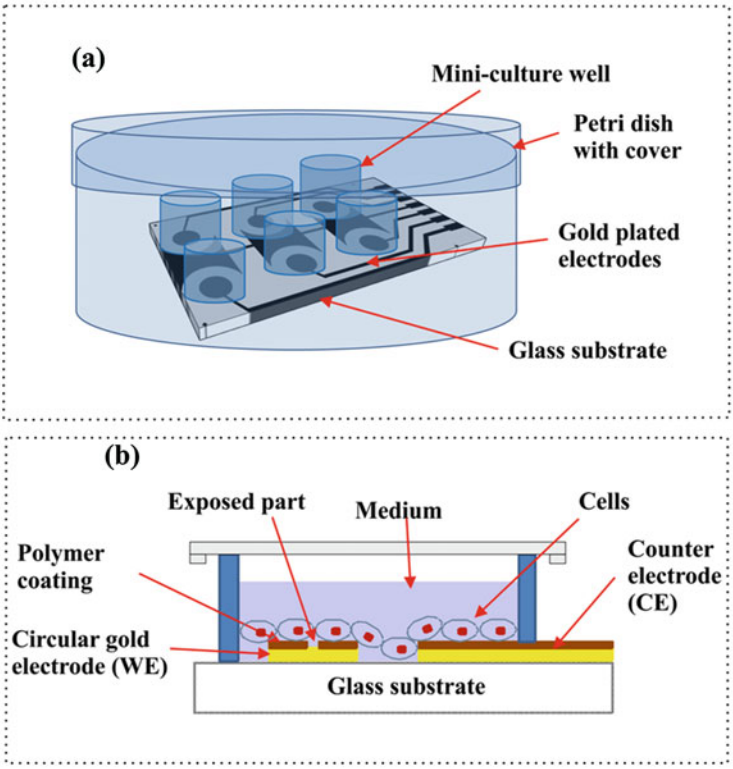

Fig. 6.3 Schematic diagram of (**a**) proposed bioimpedance sensor having six mini-culture wells, (**b**) cross-sectional view of one of the microwell

electrode is 2.8 mm, and gap between WE and CE is 1.5 mm. Each well has substrate area of 0.8 cm^2.

An electrical double layer capacitance is developed at the interface between WE and its surrounding electrolyte [16]. In order to reduce the dominancy of double layer capacitance, the top surface of working electrode is coated with a 2 μm thick polymer. However, a small circular portion of diameter 250 μm of patterned gold metal at the center of WE is exposed. The coated polymer on the entire WE electrode except the circular exposed metal pattern at the central region will act as a charge barrier forming a coating capacitance in the range of nF/cm^2 and therefore blocks the current flow. Finally, the entire device is housed inside a cell-culture grade petri dish to avoid further contamination.

The potential and electric field distribution for the designed electrodes configuration were numerically simulated in COMSOL Multiphysics 4.4a to characterize the effect of applied frequency on cellular study. The field line simulation will help to select the operating frequency zone. The 3D geometrical model was built in electric current (ec) interface under the AC/DC module using Eq. (6.1).

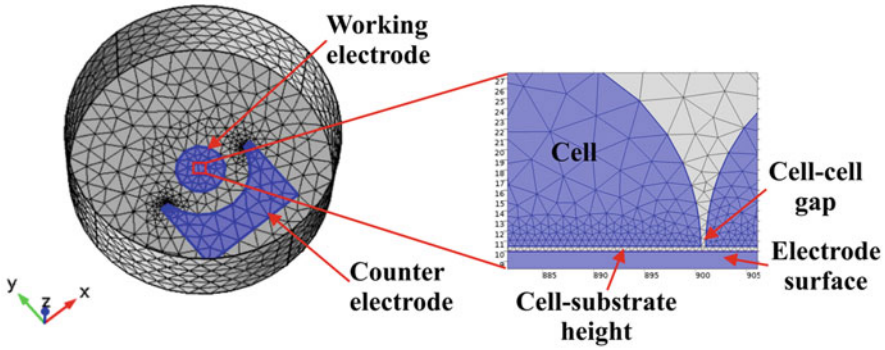

Fig. 6.4 Finite element layout of one well with electrodes and a layer of cells on the electrode surface

$$\begin{aligned} \nabla \cdot J &= Q_j \\ E &= -\nabla V \\ D &= \varepsilon_0 \varepsilon_r E \\ J &= \sigma E + j\omega D + J_e, \end{aligned} \tag{6.2}$$

where Q_j is the charge density, σ is the conductivity, ω is the angular frequency, D is the electric displacement field, V is the potential, and J_e is an external generated current density. Figure 6.4 shows the model layout of the system after meshing in COMSOL. Electrical insulating boundary conditions were enforced on all the boundaries, except the electrodes area. Both electrodes were modeled as perfect conductors by considering as equipotential surfaces. The boundary condition of the working electrode has been imposed as voltage terminal and a potential of 10 mV was applied whereas zero potential was applied to counter electrode. The insulating well was filled up with 400 μl of medium of conductivity 1.5S/m and a relative dielectric constant of 136.

A layer of cells with 0.5 μm gap between two neighboring cells was modeled considering individual cell as semi-ellipsoidal solid object having radius of 20 μm. The separation between cell-layer and bottom electrode substrate was assumed as 0.5 μm. Typical dielectric property of cells was applied to individual cell geometry [17]. The entire geometry was meshed using fine triangular mesh element and computed at different frequencies.

The electric potential and field distribution inside the well will assist to characterize effect of applied frequency on cellular study and to select the operating frequency zone. The finite element simulation was performed with frequency sweep of 100 Hz–10 MHz having 10 mV excitation voltage. Figure 6.5 describes the field lines distribution at 1 kHz and 40 kHz. It is also depicted that at 1 kHz field lines only passed through intercellular pathway. At lower frequency, cells behave as insulators due to dielectric nature of cell membrane and field lines cannot penetrate the cell membrane. Thus, lower frequency measurement is mainly dominated by

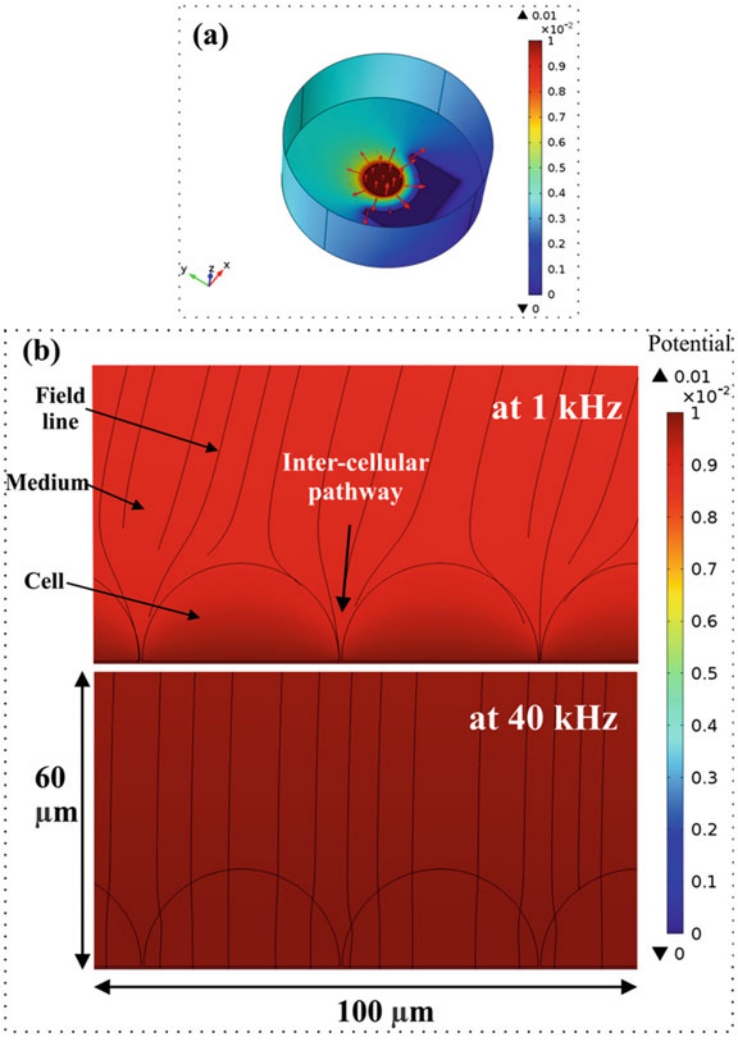

Fig. 6.5 (**a**) Electric field distribution with 10 mV potential, (**b**) electric field line distribution at two different frequencies—1 and 40 kHz. At 1 kHz field lines only pass through the gap between two cells, while at 40 kHz it penetrates through cells

gap-junction and electrode–electrolyte interfaced properties. Whereas, at higher frequency electric field lines can easily penetrate and go through the intra-inter cellular portions of cell, therefore can provide cellular electrical properties. It has been found that at mid-frequency range (~40 kHz) field lines were distributed in the entire cell-layer (both cell membrane and intercellular pathway).

6.3 Bioimpedance Sensor and Impedance Measurement

6.3.1 Device Fabrication

The present bioimpedance device was realized by two mask process using the conventional microfabrication technology on a glass substrate. The entire fabrication process consists of initial electrode patterning on the substrate, followed by selective coating of thin polymer and placing of cloning cylinder, and finally packing of the device. Figure 6.6 shows the basic steps involved in the device fabrication process and corresponding assembling of the device.

The process starts with cleaning of glass substrate in piranha solution (H_2O_2: H_2SO_4: 1:1) for 20 min followed by dehydrating in oven at 150 °C for 30 min. Chrome (0.01 μM) and gold (0.2 μM) were deposited onto the cleaned glass by DC sputtering technique for electrodes realization (Fig. 6.6b). Subsequently, the photolithography steps were performed to define the electrodes. Positive photoresist (HPR 504, Fujifilm) was spin-coated (Fig. 6.6c) at 3000 rpm for 20 s and soft baked at 90 °C for 30 min. The sample was then exposed to UV radiation for 7 s inside a UV-Mask aligner (Fig. 6.6d) through the mask containing the electrode patterns. Subsequently, the resist was developed in HPRD 429 for 35 s to achieve the patterned structure followed by post baking for 30 min at 120 °C. The gold and chrome layer were then etched using gold and chrome etchant, respectively, at room temperate for 3 min and the remaining photoresist was stripped off in acetone (Fig. 6.6f) to attain the electrode pattern.

After realizing the electrode patterns, a thin polymer layer was coated on the electrode surface and lithographically patterned to protect the electrode surface leading to reduced double layer capacitance and open the required bond pads for electrical connection. Initially, the sample was treated under oxygen plasma with a power of 40 W for 30 s (Fig. 6.6g) to remove any resist residue and enhance the surface adhesion for the subsequent process. Photosensitive polymer SU 8-5 was coated (Fig. 6.6h) on the sample at 4000 rpm for 20 s and pre-heated on a hot plate at 65 °C for 1 min and 95 °C for 3 min. Subsequently, the sample was properly aligned with the mask containing the patterns of bond pad opening using the mask aligner instrument (Fig. 6.6i) and the sample was exposed to UV light for 12 s to open a circular portion having a diameter of 250 μm. In the next step, the SU-8 layer was hard baked at 65 °C for 1 min and at 95 °C for 1 min successively, followed by treatment in its developer solution for 1 min (Fig. 6.6k).

Finally, pyrex cloning cylinders with outer diameter of 8 mm were bonded on the glass covering the individual WE-CE electrodes pair. The open cylinders were covered with a transparent cover. Consequently, the final packaged bioimpedance device as shown in Fig. 6.7 was glued on a cleaned PCB with necessary arrangement for electrical connections and the whole device was placed inside a Petri plate to protect from contamination.

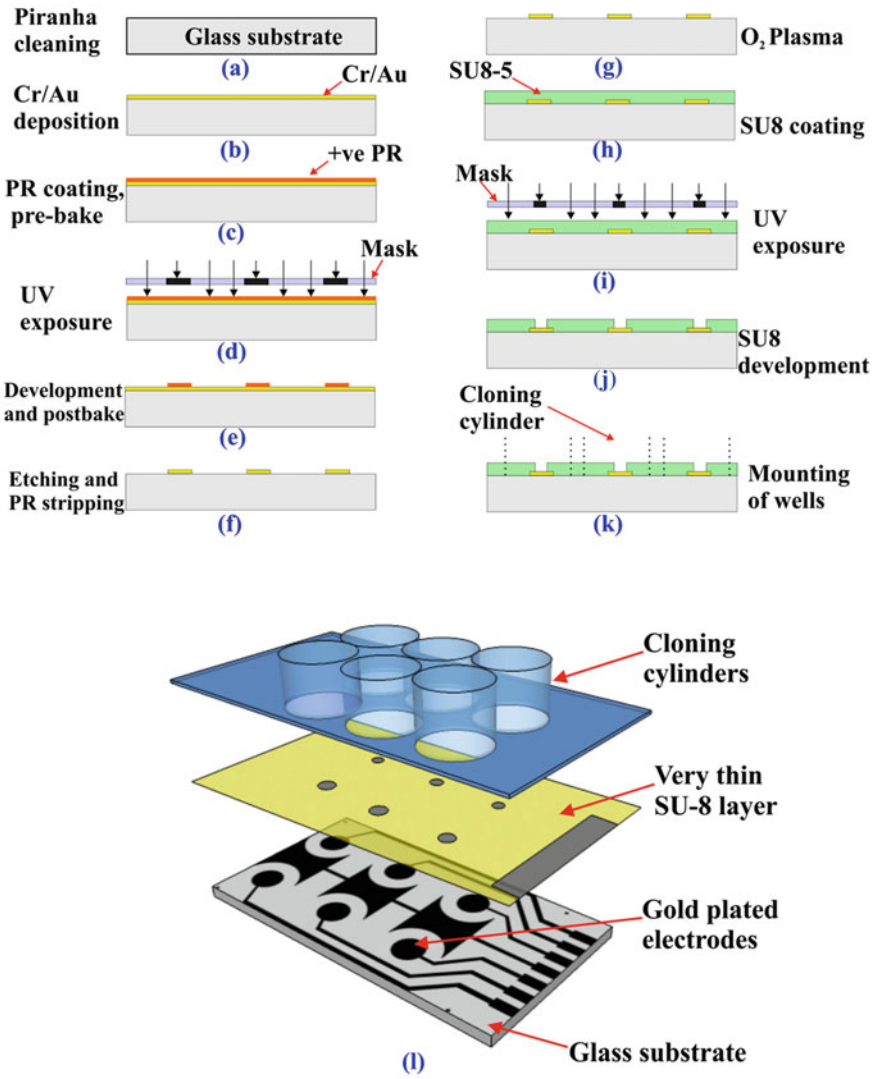

Fig. 6.6 (**a**–**k**) Schematic representation of realization of the device, (**l**) the 3D assembly steps

6.3.2 Cleaning and Surface Modification of the Sensor

Before using in cell culture, the packaged sensor was cleaned and sterilized properly under UV light. The fabricated device can be used several times with accurate sensing capability. At first, all the culture wells were cleaned with ethanol and finally rinsed with DI water. Subsequently, the surface of the sensor was functionalized by dilute Poly-L-Lysine for 5 min at room temperature. Afterward, the wells were air

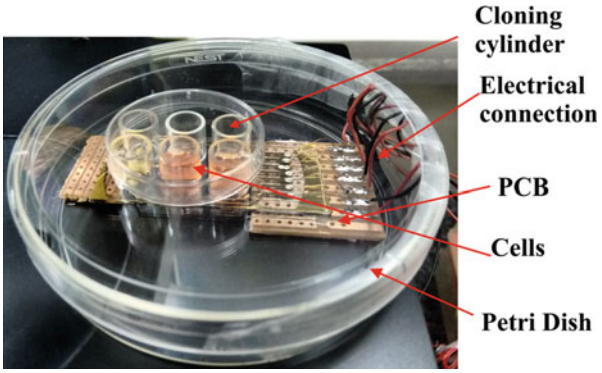

Fig. 6.7 Photograph of the final fabricated and packaged sensor

dried at room temperature for overnight and finally, the device was ready to use. Before seeding the cells inside the wells, the surface of the wells was rinsed again with DI water and dried properly.

6.3.3 Experimental Setup

The whole packaged bioimpedance chip was placed inside a humidified CO_2 incubator at 37 °C in the presence of 5% CO_2. The electrical contact wires were carefully taken out from the incubator and connected with an impedance analyzer. In the present work, Agilent precision impedance analyzer 4294-A interfaced with computer was utilized for bioimpedance measurement. Figure 6.8 shows the schematic of experimental setup. To overcome the effect of unwanted impedance data during measurement, short and open circuit compensations were performed as per standard procedure [18].

6.3.4 Cell Culture and Cell Seeding Inside the Chip

The cells were grown in T25 tissue culture flasks and incubated in a humidified atmosphere containing 5% carbon dioxide at 37 °C. The confluent cell population was harvested by treating with 0.25% trypsin and 0.02% EDTA for 5 min. The trypsin was deactivated by adding fresh media. The cells were pelleted by centrifuging at 3000 rpm for 5 min and re-suspended in 1 ml of fresh media/PBS (HiMedia) having NaCl (9000 mg/L), Na_2HPO_4 (795 mg/L), NaH_2PO_4 (144 mg/L), and pH 7.4. Cell concentration was diluted to 1,00,000 cells in 400 µl and seeded inside each well. Afterward, the whole chip was kept inside the incubator and the impedance data of cells were recorded after 7 h when all the cells attached on the electrode surface.

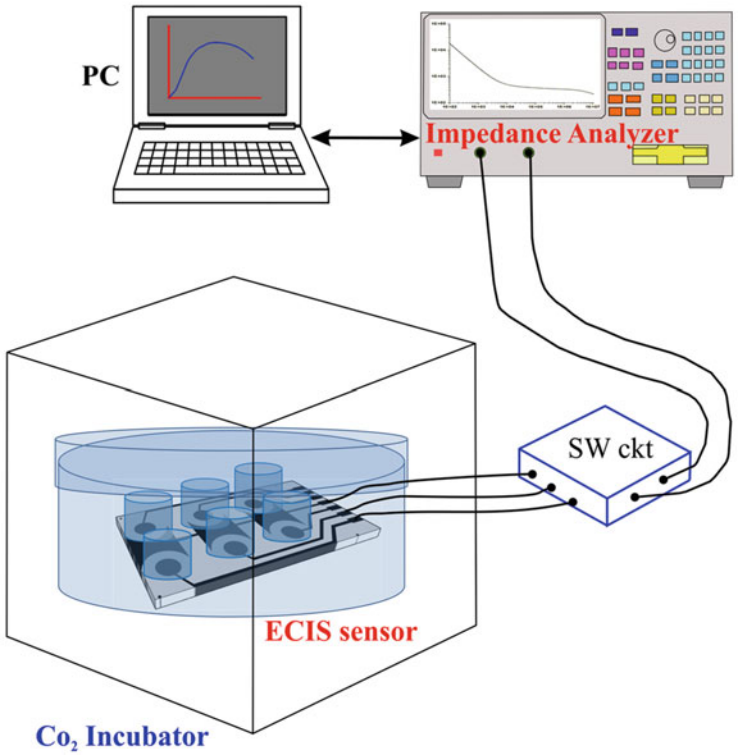

Fig. 6.8 Schematic of the experimental setup for bioimpedance measurement

6.3.5 Bioimpedance Measurement

Agilent precision impedance analyzer 4294-A was used to record the impedance data. The impedance value of growing cells was measured with a frequency sweep of 100 Hz–10 MHz having 167 data points and 10 mV excitation voltage. Initially, 400 µl of culture medium was added into one of the wells of the fabricated device and impedance and admittance values were measured for adjusted frequency range. Subsequently, same volume of medium with immersed cells was added into the well and the measurement was repeated. Each measurement was also repeated for three times without disturbing the system to get the average reading with standard deviation (SD).

Figure 6.9 represents the experimentally measured variation of average impedance modulus and phase angle along with their SD vs. frequency conducted for PBS media in devices with and without HeLa cells. It may be observed in Fig. 6.9 that the impedance value decreases with frequency up to medium frequency range followed by a constant region and again starts falling at very high frequency. The effects of adding HeLa cells to the PBS media on impedance data are also shown in Fig. 6.9.

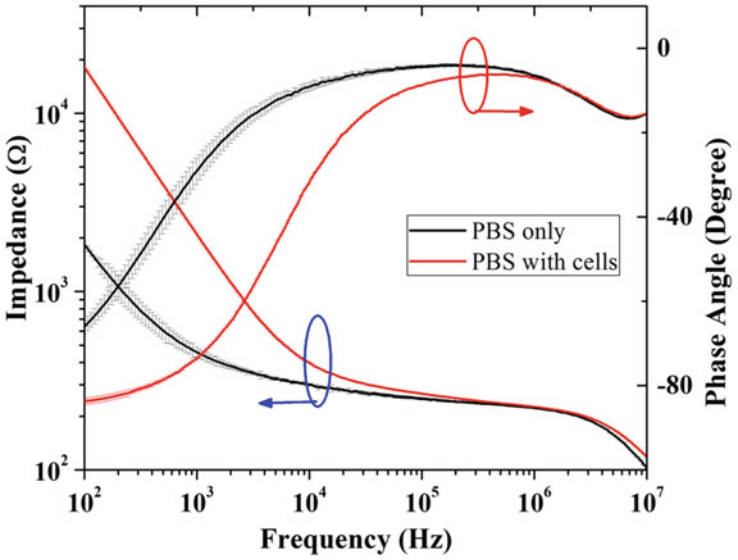

Fig. 6.9 Variation of impedance and phase angle with frequency of system in the absence and presence of cells suspended in PBS solution

The Bode diagram indicates that the overall impedance value increases abruptly at the starting frequency on adding the cells to the media as compared to only PBS and decreases steadily with the increase of frequency up to 10 kHz. However, the impedance plots of both the cases coincide above the frequency of 100 kHz.

6.4 Theoretical Analysis

6.4.1 Electrical Equivalent Model of the System

The bioimpedance sensor realized in a thick polymer substrate consists of patterned individual working electrode (WE) and common counter electrode (CE) made of gold metal. A rectangular well made up of polymer is placed on the substrate and located in such a way that WE and part of CE electrodes are in contact with sample during impedance measurement. The schematic of cross-sectional view of the device is shown (Fig. 6.10) [5]. The top surface of WE is coated with a thin polymer layer with an exposure of a small gold area at its center to prevent artifacts due to immersion of gold interconnects in the electrolyte. This leads to developing a coating capacitance and pore resistance contributed by fine pores available on the polymer surface. Exposed gold portion of the WE contributes in the formation of exposed electrode resistance and double layer capacitance at the electrode–electrolyte interface. Now, in a simple way a cell can be pictured as a single shell consisting of

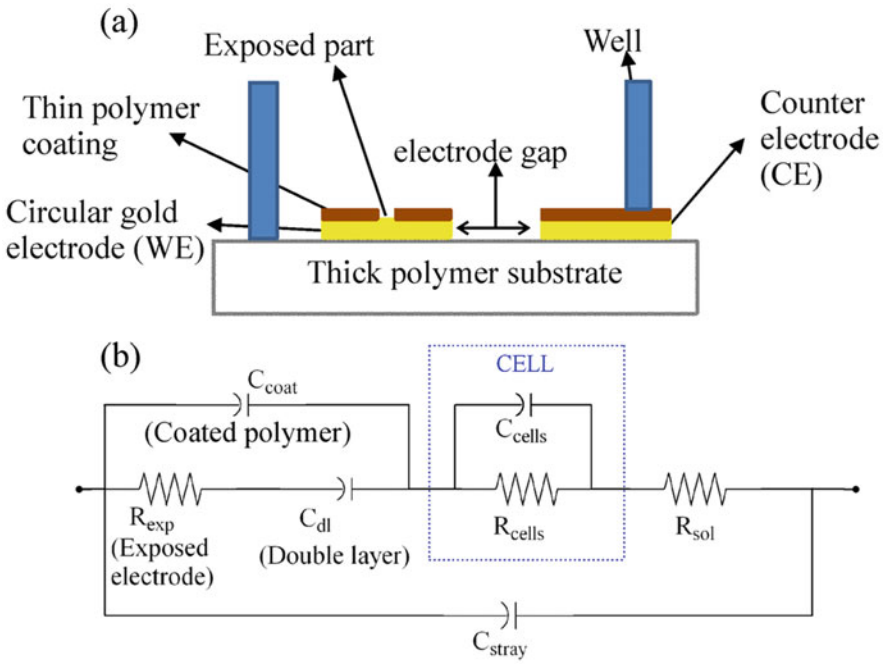

Fig. 6.10 (**a**) Schematic of cross-sectional view of one microwell of bioimpedance sensor, (**b**) electrical equivalent circuit of entire system (taken from [5])

cytoplasm and cell membrane. The cytoplasm may be approximated as highly conducting ionic solution with a large concentration of dissolved organic material which is considered to be a resistive pathway to the electrical signal in the electrical equivalent of the system. However, cell membrane consists of a thin phospholipid bilayer which acts as a dielectric material and thus offers a capacitive pathway to the system. In the device, cells sitting over the electrode surface are modeled as cell membrane capacitance and its cytoplasmic resistance offered by individual cell and intercellular resistance offered by media available between two adjacent cells. Due to low conductivity of cell membrane only high frequency current will flow through it, while low frequency current will pass through extracellular gap between the cells. Hence, collection of the cells forming a monolayer on the bottom surface of the system may be assumed to be parallel combination of equivalent resistance and equivalent capacitance. On the basis of these concepts the equivalent circuit of the system, consisting of cell immersed in phosphate buffer saline (PBS) media, is modeled as shown in Fig. 6.10b. Here R_{exp}, C_{coat}, C_{dl} are the resistance, coating capacitance, and double layer capacitance of exposed portion of working electrode along with coating pore resistance, respectively. R_{sol} is the solution resistance of the media. The contribution of the cells is modeled in the form of parallel combinations of resistance and capacitance of cell membrane and extracellular gap and intercellular resistance, respectively. The resistance of the membrane and

capacitance of the cytoplasm are negligible as discussed earlier, so they are neglected for the equivalent model analysis. In simple way, cells forming a monolayer over the electrode can be modeled as R_{cell} and C_{cell} as shown in Fig. 6.10b. Stray capacitance contributed by parallel gold electrodes is negligible (10 pF range) and thus neglected in the present study due to their dominance in very high frequency (>50 MHz) which is beyond the scope of present study.

6.4.1.1 Estimation of Equivalent Model Parameters

Different system parameters such as solution resistance, double layer capacitance, cell membrane capacitance, intercellular resistance, electrode resistance can be extracted and quantified by analyzing these equivalent circuit models or fitting with commercially available curve fitting software. In literature, these parameters were calculated using finite element modeling software and spice simulation [19], quantitative analysis and parameters fitting of the equivalent circuit model based on the Levenberg–Marquardt (LEVM) algorithm [20], equivalent circuit models and complex nonlinear least squares (CNLS) fitting [14], etc. Therefore, it shows that parameter extraction is mostly performed using equivalent model simulation and fitting software. These software fit the measured impedance data utilizing numerical minimization algorithms by iterative procedure. However, an initial guess is compulsory to start the algorithm which iterates the values accurately only if the initial conditions are chosen to be close to the final value [21–23]. Alternately, modeling the system based on measurement process and analysis of result through theoretical approach will provide more flexibility, accurate estimation of data, and in depth information of the extracted data. The theoretical data analysis also leads to detailed modeling of the complex biological systems and helps to estimate the single cell component value. The theoretically calculated data may provide an initial idea about the range of parameter values and may be utilized as initial guess for fitting software. The subsequent sections demonstrate an alternate approach based on fragmental frequency analysis method to theoretically estimate different parameters of an equivalent electrical circuit for the bioimpedance sensor as compared to available fitting software.

6.4.1.2 Fragmental Frequency Analysis Method to Extract the Model Parameters

In the proposed fragmental frequency analysis method the entire frequency range is segregated into different zones. The electrical equivalent circuits shown in Fig. 6.10b have been modified for those frequency ranges based on the dominance of the individual parameters at that frequency zone. The measured frequency zone is divided into three frequency ranges: lower frequency (<1 kHz), medium frequency (1–100 kHz), and high frequency (>100 kHz) range. The experimental data are

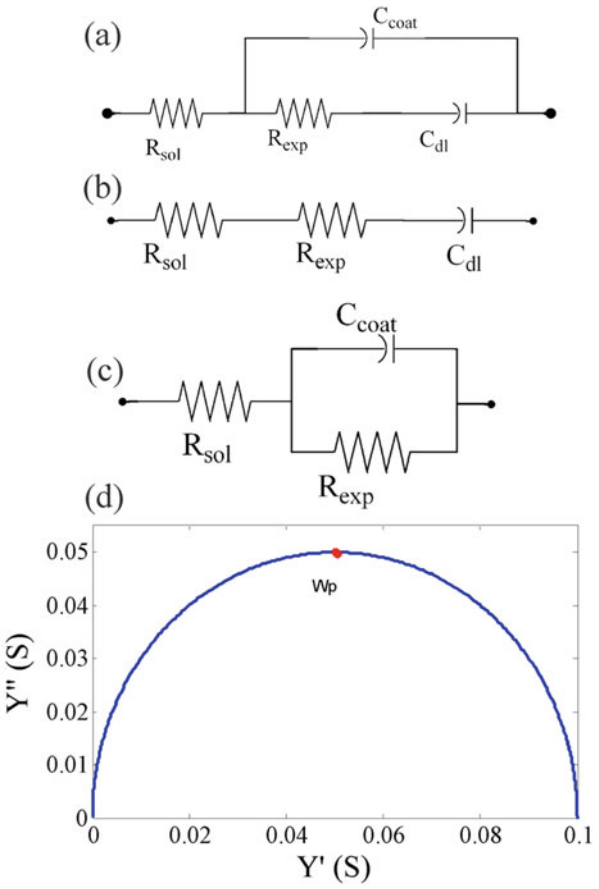

Fig. 6.11 (**a**) Electrical equivalent circuit of ECIS system with media only, (**b**) equivalent circuit at lower frequency range neglecting C_{coat}, (**c**) equivalent circuit at higher frequency range neglecting C_{dl}, (**d**) a typical admittance Nyquist plot for finding peak frequency (taken from [5])

represented by Bode and Nyquist curves and parameter values are calculated by theoretically analyzing the individual range.

(a) Electrode and Media Parameters

Considering the presence of only media in device the equivalent circuit of Fig. 6.10b can be modified as shown in Fig. 6.11a for extracting the electrical properties of electrodes and media. Figure 6.11b, c shows the new equivalent circuits at lower and higher frequency zone, respectively. Since the value of double layer capacitance is in μF range [16], its effect is negligible and acts as short circuit path above 100 kHz frequency. Accordingly the circuit is modified as shown in Fig. 6.11c and the corresponding impedance magnitude and phase for this circuit are expressed as:

$$|Z| = \sqrt{\left(R_{\text{sol}} + \frac{R_{\text{exp}}}{1 + \omega^2 R_{\text{exp}}^2 C_{\text{coat}}^2}\right)^2 + \left(\frac{\omega R_{\text{exp}}^2 C_{\text{coat}}}{1 + \omega^2 R_{\text{exp}}^2 C_{\text{coat}}^2}\right)^2}. \tag{6.3}$$

$$Z_{\text{r}}(\omega) = R_{\text{sol}} + \frac{R_{\text{exp}}}{1 + \omega^2 R_{\text{exp}}^2 C_{\text{coat}}^2}. \tag{6.4}$$

$$\theta = -\tan^{-1} \frac{\omega R_{\text{exp}}^2 C_{\text{coat}}}{R_{\text{sol}} + R_{\text{exp}} + 1 + \omega^2 R_{\text{sol}} R_{\text{exp}}^2 C_{\text{coat}}^2}. \tag{6.5}$$

Equation (6.4) depicts that the real part of impedance converges to R_{sol} as the frequency becomes higher which shows that the real part of impedance magnitude ($Z_r(\omega)$) becomes relatively constant at higher frequencies. This concept was explored to find out the value of resistance of the media. Phase angle approaches towards zero at lower as well as higher frequency, which indicates that phase attains a peak value in between the frequency range as shown in a typical admittance plot in Fig. 6.11d for the above circuit.

The angular frequency corresponding to the peak point in the Fig. 6.11d is expressed mathematically as:

$$\omega_{\text{p1}} = \frac{1}{R_{\text{exp}} C_{\text{coat}}} \left(1 + \frac{R_{\text{exp}}}{R_{\text{sol}}}\right). \tag{6.6}$$

And the value of imaginary part of admittance ($Y(j\omega)$) at this peak angular frequency is given as:

$$Y\left(j\omega_{\text{p}}\right) = \frac{R_{\text{sol}}}{2R_{\text{exp}}\left(R_{\text{exp}} + R_{\text{sol}}\right)}. \tag{6.7}$$

Since at higher frequency, the equivalent circuit behaves like the circuit as shown in Fig. 6.11c, Eqs. (6.6) and (6.7) can be used to calculate the coating capacitance as well as the resistance of the exposed part of the electrode and the pore resistance. The value of the coating capacitance is in nF range and double layer capacitance is in μF range [14]. Thus at lower frequencies, reactance of coating capacitance is very high which makes it behave like open circuit. Hence, the modified circuit diagram in this frequency range would look like as shown in Fig. 6.11b. This is simple RC series circuit whose impedance magnitude and phase response are given by Eqs. (6.8) and (6.9).

$$|Z| = \sqrt{\left(R_{\text{sol}} + R_{\text{exp}}\right)^2 + \left(\frac{1}{\omega C_{\text{dl}}}\right)^2}. \tag{6.8}$$

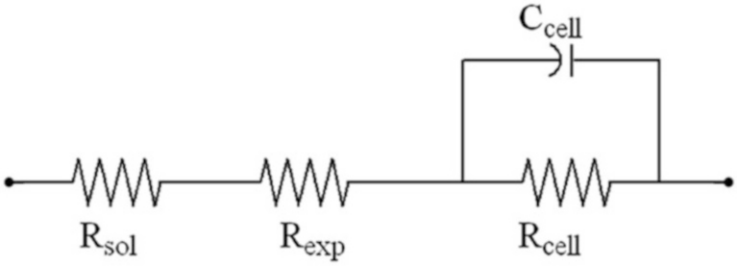

Fig. 6.12 Electrical equivalent circuit of ECIS system with cells suspended in solution at medium frequency zone (1–50 kHz) (taken from [5])

$$\theta = -\tan^{-1}\frac{1}{\omega C_{\mathrm{dl}}\left(R_{\mathrm{sol}} + R_{\mathrm{exp}}\right)}. \tag{6.9}$$

It is clear from the above mathematical expressions that impedance magnitude decreases and phase approaches to zero from its negative value as the frequency increases. The peak angular frequency in the Nyquist curve of RC circuit corresponds to

$$\omega_{\mathrm{p2}} = \frac{1}{\left(R_{\mathrm{exp}} + R_{\mathrm{sol}}\right)C_{\mathrm{dl}}}. \tag{6.10}$$

This leads to estimate the value of double layer capacitance (C_{dl}) by substituting the R_{sol} from Eq. (6.4).

(b) Cell Parameters

It may be assumed that adding the cells to the media has negligible effect on the total resistance value of the media, as total volume of PBS media with HeLa cells remains nearly same as that of media without cells. Other parameters such as resistance of the exposed part of the electrode and coating capacitance also do not change much on adding the cells to the media. The double layer capacitance only dominates below 1 kHz due to its high value (μF range) [24]. Considering the negligible effect of double layer capacitance and coating capacitance in medium frequency range (1–100 kHz), the equivalent circuit model of PBS solution with HeLa cells is modified as shown in Fig. 6.12. The Nyquist curve of this circuit will have a peak corresponding to angular frequency ω_{p} that is given in Eq. (6.11).

$$\omega_{\mathrm{p3}} = \frac{1}{\left(R_{\mathrm{exp}} + R_{\mathrm{sol}}\right)C_{\mathrm{cell}}}\left(1 + \frac{R_{\mathrm{cell}}}{R_{\mathrm{exp}} + R_{\mathrm{sol}}}\right). \tag{6.11}$$

The value of imaginary part of admittance at this peak frequency is expressed by Eq. (6.12).

$$Y\left(j\omega_{\mathrm{p}} \right) = \frac{R_{\mathrm{exp}} + R_{\mathrm{sol}}}{2R_{\mathrm{cell}}\left(R_{\mathrm{cell}} + R_{\mathrm{exp}} + R_{\mathrm{sol}}\right)}. \tag{6.12}$$

Now, putting the values of already calculated R_{exp} and R_{sol}, the cell parameters R_{cell}, C_{cell} can be estimated using Eqs. (6.11) and (6.12).

6.4.2 *Extracting the Single Cell Property from Measurement of Group of Cells*

Analysis of electrical properties of a single cell has become a new trend to correlate cellular events for understanding complex physiological processes. Electrical attributes of single cell analysis provide information about bio-physiological properties of cell which is sensitive to biophysical changes in cell. However, this technique suffers from several challenges, which need to be overcome. Handling of a single cell in microchannel is complicated and requires trapping mechanisms in the microchannel for single cell impedance measurement [25, 26]. The throughput of cell capturing devices is limited unless large numbers of traps are available in the microchannel [27, 28]. The integration of electrodes together with multiplexed impedance measurements increases the complexity of the system. For large arrays of traps, complex active matrix method is needed to measure the signals from multiple electrodes. Moreover, polarization of microelectrodes is also significant and needs special attention to extenuate the effect [29, 30]. Due to heterogeneity of biological system, it is expected that cells show its natural characteristics in a colony of similar cells rather than its individual environment. These shortcomings play major difficulties when the electrical properties are utilized to distinguish between normal and cancerous cells through single cell analysis. Alternatively, electrical properties of a single cell can be estimated through the bioimpedance measurement of cells in suspensions using well-established Maxwell's mixture theory [31] without interfering the above issues. The analysis relates the complex permittivity of the suspension to the complex permittivity of the particle, the suspending media, and the volume fraction. Therefore, the proposed technique provides a comparatively easy alternative way to extract the single cell parameters without involving the complex technology required for single cell analysis in microchannel.

The present study introduces a simple and detailed analysis technique to extract electrical properties of single cell from impedance spectroscopy data of group of cells in suspension using Maxwell's mixture theory.

6.4.2.1 Maxwell's Mixture Theory

The suspended biological cells in media form a heterogeneous system and its dielectric properties are generally described by Maxwell's mixture theory [31]. For

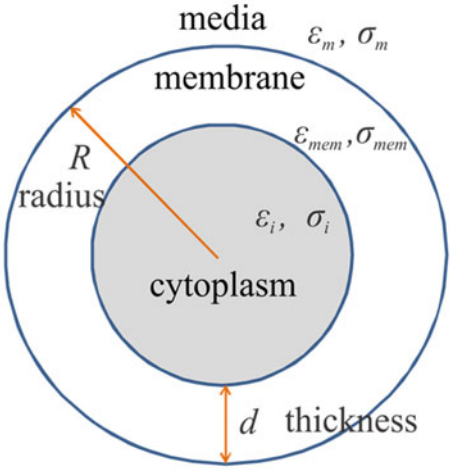

Fig. 6.13 Schematic diagram of single-shell model of cell in suspension (taken from [17])

a spherical particle dispersed in a suspending medium at a low volume fraction, the Maxwell's mixture theory provides an equivalent complex dielectric permittivity of the cells in the frequency domain according to Eq. (6.13) [17].

$$\widetilde{\varepsilon}_{mix} = \widetilde{\varepsilon}_m \frac{1 + 2\varphi\tilde{f}_{\text{cm}}}{1 - \varphi\tilde{f}_{\text{cm}}} \lim_{x\to\infty}, \tag{6.13}$$

where $\tilde{f}_{\text{cm}}$ is the complex Clausius–Mossotti factor

$$\tilde{f}_{\text{cm}} = \frac{\widetilde{\varepsilon}_p - \widetilde{\varepsilon}_m}{\widetilde{\varepsilon}_p + 2\widetilde{\varepsilon}_m}. \tag{6.14}$$

The subscripts "mix," "p," and "m" refer to mixture, particle, and media, respectively, and $\widetilde{\varepsilon}$ is the complex permittivity and represented as $\widetilde{\varepsilon} = \varepsilon - j\frac{\sigma}{\omega}$, where $j = \sqrt{-1}$, ε, σ, ω, and φ are permittivity, conductivity, and angular frequency and the volume fraction of the cells in suspension, respectively.

Although Maxwell's theory is valid only for low volume fraction ($\varphi < 10\%$), later Hanai et al. [32, 33] extended the theory for all volume fractions which is depicted in Eq. (6.15).

$$1 - \varphi = \left(\frac{\widetilde{\varepsilon}_{\text{mix}} - \widetilde{\varepsilon}_p}{\widetilde{\varepsilon}_m - \widetilde{\varepsilon}_p}\right)\left(\frac{\widetilde{\varepsilon}_m}{\widetilde{\varepsilon}_{\text{mix}}}\right)^{1/3}. \tag{6.15}$$

In terms of single shelled spherical cell model in suspension as shown in Fig. 6.13, the complex permittivity of the cell is [31]:

$$\widetilde{\varepsilon}_p = \widetilde{\varepsilon}_{\text{mem}} \frac{\gamma^3 + 2\left(\frac{\widetilde{\varepsilon}_i - \widetilde{\varepsilon}_{\text{mem}}}{\widetilde{\varepsilon}_i + 2\widetilde{\varepsilon}_{\text{mem}}}\right)}{\gamma^3 - \left(\frac{\widetilde{\varepsilon}_i - \widetilde{\varepsilon}_{\text{mem}}}{\widetilde{\varepsilon}_i + 2\widetilde{\varepsilon}_{\text{mem}}}\right)}, \tag{6.16}$$

with $\gamma = R + d/R$, where $\widetilde{\varepsilon}_{\text{mem}}$ and $\widetilde{\varepsilon}_i$ are the complex permittivity of cell membrane and cytoplasm, respectively; R is the radius of cell; and d is the membrane thickness. Thus, the complex permittivity of the cell is a function of dielectric properties of membrane, internal properties (mainly cytoplasm), and size of the individual cell. The complex bioimpedance ($\tilde{Z}_{\text{mix}}$) of cells in suspension is related to the equivalent complex permittivity of the mixture and the geometrical parameters of the measurement system by [31]

$$\tilde{Z}_{\text{mix}} = \frac{1}{j\omega\widetilde{\varepsilon}_{\text{mix}} G}, \tag{6.17}$$

where G is a geometric constant, which is the ratio of electrode area (A) to gap (g), A/g between the electrodes. In this study, impedance spectroscopy of cells suspended in media is carried out using ECIS based device with known geometric constant. Subsequently, complex impedance and equivalent complex permittivity of mixture of suspended cells are found out using Eq. (6.17).

6.4.2.2 Equivalent Electrical Model of Single Cell

In general, an equivalent electrical circuit model analogous to physical model is utilized to describe the electrical properties of suspended cells. Although it is quite complex to analyze the equivalent circuit model, the conductivity of membrane and the permittivity of the cytoplasm were considered to be very low in the present study to get simple mathematical expression as stated in Eqs. (6.18) and (6.19).

$$\widetilde{\varepsilon}_i = -j\sigma_i/\omega. \tag{6.18}$$

$$\widetilde{\varepsilon}_{\text{mem}} = \varepsilon, \tag{6.19}$$

where σ_i is the conductivity of cytoplasm and ε is the permittivity of membrane. Putting the above assumptions in Eq. (6.16) it can be simplified in Eqs. (6.20) and (6.21) [17].

$$\widetilde{\varepsilon}_p = \varepsilon \frac{\gamma^3 + 2\left(\frac{-j\sigma_i/\omega - \varepsilon}{2\varepsilon - j\sigma_i/\omega}\right)}{\gamma^3 - \left(\frac{-j\sigma_i/\omega - \varepsilon}{2\varepsilon - j\sigma_i/\omega}\right)}. \tag{6.20}$$

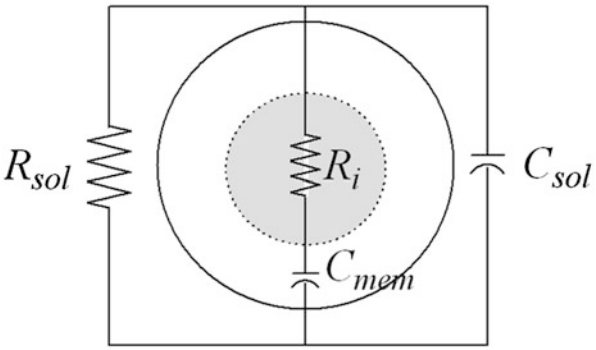

Fig. 6.14 Simplified equivalent circuit model of a single cell in suspension (taken from [17])

$$\left(\frac{\mathrm{Re}\left[\widetilde{\varepsilon}_{\mathrm{p}}\right]+j\mathrm{Im}\left[\widetilde{\varepsilon}_{p}\right]}{\varepsilon}\right)=\left(\frac{2b\varepsilon^{2}+a(\sigma_{i}/\omega)^{2}}{b^{2}\varepsilon^{2}+(\sigma_{i}/\omega)^{2}}\right)+j\left(\frac{\varepsilon\sigma_{i}/\omega(2-ab)}{b^{2}\varepsilon^{2}+(\sigma_{i}/\omega)^{2}}\right), \tag{6.21}$$

where $a=\left(\frac{\gamma^{3}+2}{\gamma^{3}-1}\right)$, $b=\left(\frac{2\gamma^{3}+1}{\gamma^{3}-1}\right)$ with $\gamma=\frac{R+d}{R}$.

On dividing the real and imaginary part of $\widetilde{\varepsilon}_{\mathrm{p}}$ in Eq. (6.21), a quadratic equation is formed as:

$$\frac{a}{\omega}(\sigma_{i}/\varepsilon)^{2}-K(2-ab)(\sigma_{i}/\varepsilon)+2b\omega=0, \tag{6.22}$$

where $K=\left(\frac{\mathrm{Re}\left[\widetilde{\varepsilon}_{\mathrm{p}}\right]}{\mathrm{Im}\left[\widetilde{\varepsilon}_{\mathrm{p}}\right]}\right)$..

By assuming the $l=\sigma_{i}/\varepsilon$ and equating with the imaginary part of Eq. (6.21), the permittivity of single cell is obtained as

$$\varepsilon=\left(\frac{b^{2}+(l/\omega)^{2}}{(l/\omega)(2-ab)}\right)\mathrm{Im}\left[\widetilde{\varepsilon}_{p}\right]. \tag{6.23}$$

Using Eq. (6.22) value of l is calculated, then the relative permittivity (ε) is obtained from Eq. (6.23), and finally conductivity (σ_i) is incurred through $\sigma_i = l \times \varepsilon$.

The impedance of cell suspension consists of impedance of the medium represented by a parallel combination of resistance and capacitance and impedance of cells. According to Foster and Schwan [34], a single cell is approximated to a cytoplasm resistor (R_i) in series with a membrane capacitor (C_{mem}) as represented in Fig. 6.14. The cell membrane consists of a thin phospholipid bilayer having very low conductivity and acts as a dielectric material offering a capacitive pathway to the system

The cell cytoplasm can be approximated as a highly conducting ionic solution with a large concentration of dissolved organic material which is considered to be resistive pathway to the electrical signal in the electrical equivalent of the system. The values of simplified frequency dependent cell parameters are determined by the

dielectric and conductivity properties of cell and medium, cell size, volume fraction, and geometric constant of the system [31]:

$$C_{\text{mem}}(\omega) = \frac{9\varphi R\varepsilon}{4d} G. \tag{6.24}$$

$$R_i(\omega) = \frac{4\left(\frac{1}{2\sigma_m} + \frac{1}{\sigma_i}\right)}{9\varphi G}. \tag{6.25}$$

The frequency dependent relative permittivity (ε) and conductivity (σ_i) of single cell obtained in Eqs. (6.22) and (6.23) are used in Eqs. (6.24) and (6.25) to extract the single cell membrane capacitance and cytoplasm resistance.

6.5 Applications

6.5.1 Calculation of Equivalent Parameters of HeLa Cells Using Fragmental Frequency Analysis

6.5.1.1 Resistance of the PBS Media

At high frequency double layer capacitance can be considered shorted and the equivalent circuit of the PBS media without HeLa cells would look like Fig. 6.12c. The plot of real part of impedance data of PBS media with frequency is shown in Fig. 6.15.

According to Eq. (6.4), the real part of impedance converges to R_{sol} at higher frequency range. The graph demonstrates that the real part of impedance becomes relatively constant at higher frequencies, i.e., above 100 kHz and R_{sol} was found to be approximately 220 Ω.

6.5.1.2 Resistance R_{exp}

According to proposed fragmental analysis, it is required to present the data in admittance curve to extract the value of resistance of the exposed part of the electrode. The peak point of the admittance plot of impedance data of media without cells provides information about the exposed resistance of the electrode. Nyquist plot of the experimental PBS data is shown in Fig. 6.16 having two peaks, where G and B are conductance and susceptance in Siemens (S), respectively. The first peak at lower frequency corresponds to the double layer capacitance since the coating capacitance acts as open circuited in this frequency range. Considering the equivalent circuit as given in Fig. 6.12c for high frequency range, the value of imaginary part of admittance at the peak frequency is governed by Eq. (6.6). Since R_{sol} is known from the previous calculation, the value of resistance of exposed part of the

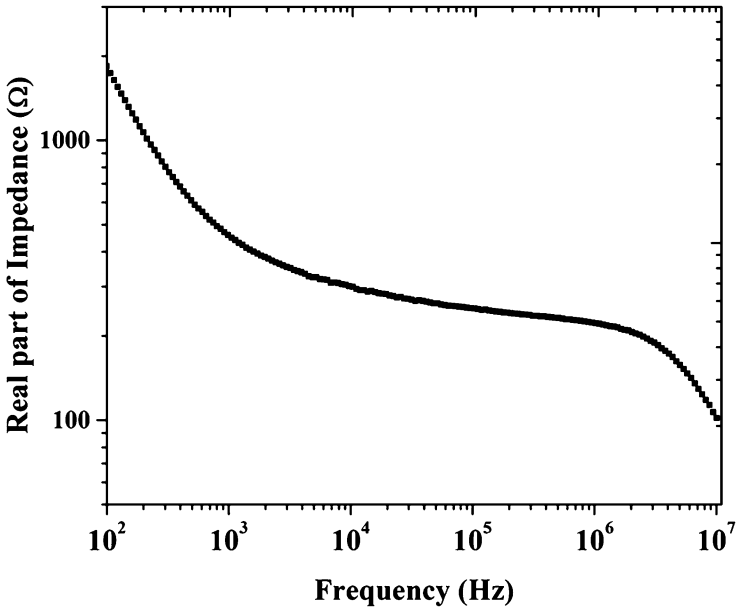

Fig. 6.15 Variation of real part of impedance data of media without cells with frequency (taken from [5])

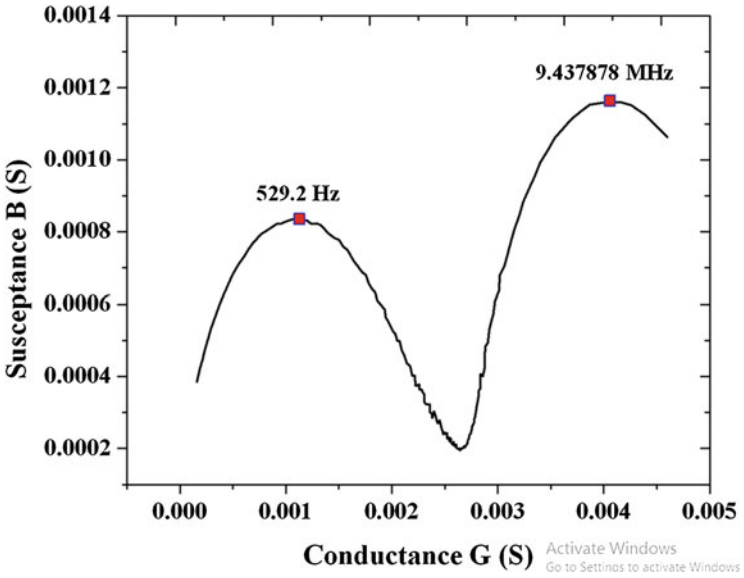

Fig. 6.16 Nyquist plot of admittance data with only PBS solution (taken from [5])

electrode may be estimated using Eq. (6.7). In this case, the frequency corresponding to the second peak is found to be 9.437 MHz, and the magnitude of imaginary part of admittance at this frequency is found to be 0.0012 S. Using R_{sol} as 220 Ω in Eq. (6.7) the resistance of the exposed part R_{exp} of the electrode is calculated to be 217.76 Ω.

6.5.1.3 Coating Capacitance

Considering the resistance of the PBS media, the exposed part of electrode, and the frequency corresponding to the second peak of the curve obtained in Fig. 6.16, the value of coating capacitance was subsequently calculated using Eq. (6.11) to be approximately 0.154 nF.

6.5.1.4 Double Layer Capacitance

At lower frequency the equivalent circuit looks like the resistance of the PBS media in series with the double layer capacitance as given in Fig. 6.12b and the corresponding lower frequency peak is a function of C_{dl}, R_{sol}, and R_{exp}. In the experimental Nyquist curve as shown in Fig. 6.16, the lower peak frequency is found to be 529.2 Hz. Using the already extracted values of R_{sol} and R_{exp} in Eq. (6.10) the double layer capacitance C_{dl} was found out to be 0.687 μF.

6.5.1.5 Equivalent Parameters of the HeLa Cells

To extract equivalent electrical parameters of cells, it is assumed that resistance of the exposed part of the electrode and coating capacitance do not alter on adding the cells to the media. Figure 6.13 describes the electrical equivalent circuit of HeLa cells suspended in PBS solution at medium frequency. The circuit has two time constants corresponding to two peaks in the Nyquist curve of admittance spectrum as shown in Fig. 6.17. It has been observed from Fig. 6.17 that adding the cells to the media, lower peak frequency in the Nyquist curve changes, while the peak at higher frequency remains at same position as compared to Fig. 2.16 because only coating capacitance dominates at higher frequency, which remains same for both the cases. As depicted from Fig. 6.17 that the position of lower frequency peak obtained at 6.0103 kHz is higher than frequency observed for PBS media as shown in Fig. 6.16. However, the peak at higher frequency occurs at same frequency at 9.437 MHz for both the cases. The higher frequency peak obtained from measured impedance result corresponds to 9.437 MHz which matches closely with the theoretically calculated frequency considering the already extracted parameters $C_{coat} = 0.154$ nF, $R_{sol} = 220$ Ω, and $R_{exp} = 217.76$ Ω validating the present method at high frequency zone. Double layer capacitance is not affected appreciably on adding the cells to media and the reactance of double layer at frequency 6.0103 kHz is 38.54 Ω. Hence, the double layer capacitance may be considered shorted around this frequency and validated the

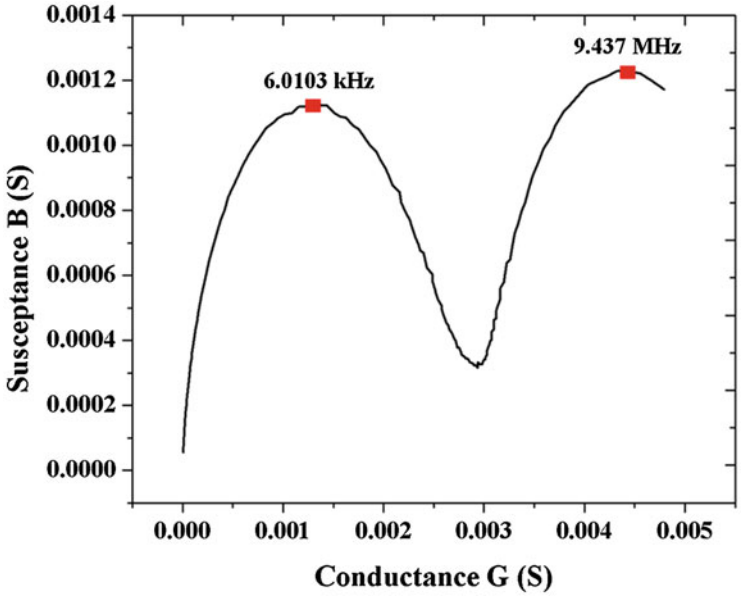

Fig. 6.17 Nyquist plot of admittance data of system with HeLa cells suspended in PBS solution (taken from [5])

equivalent circuit model at medium frequency (1–100 kHz) as depicted in Fig. 6.17. Considering the lower peak frequency at Fig. 6.17 the calculated values of cell parameters R_{cell} and C_{cell} are found to be 272.05 Ω and 0.010 μF using Eqs. (6.11) and (6.12).

The above studies provide a systematic pathway for estimating various electrical parameters initially by extracting the parameters, e.g., double layer, coating capacitance, and resistance of exposed part of the electrode from impedance spectroscopy data of PBS media without HeLa cells and subsequently use these parameters to calculate the equivalent parameters of HeLa cells from the impedance spectroscopy data of PBS media with cells. Table 6.1 summarizes the theoretically extracted parameters along with its comparison with data extracted using LEVM-based fitting software. However, the above results are achieved by assuming the parameters extracted from media data do not change on adding the cells to the media. It is expected that the double layer capacitance changes on adding the cells to the media because of redistribution of ions at the electrode–electrolyte interface, while other parameters do not change appreciably. Thus, it is desirable to study cell behavior at slightly higher frequency range to avoid the effect of change in double layer capacitance.

Table 6.1 Comparison between values of different parameters extracted theoretically and using LEVM based fitting software

Parameters	Theoretically calculated	Using fitting software
R_{sol}	220 Ω	201 ± 2.903 Ω
R_{exp}	217.76 Ω	191 ± 6.303 Ω
C_{coat}	0.154 nF	0.32 ± 0.02 nF
C_{dl}	0.687 μF	0.77 ± 0.05 μF
R_{cell}	272.05 Ω	267 ± 32.04 Ω
C_{cell}	0.010 μF	0.0136 ± 0.0013 μF

6.5.2 *Extraction of Single Cell Parameters of HeLa Cells*

Maxwell's mixture theory has been explored for single cell analysis utilizing the impedance data measured at various voltages. In this approach, volume fraction of 1 million HeLa cells suspended in a total volume of 400 μl is represented as

$$\varphi = \frac{10^6 \times \left(\frac{4}{3}\right)\pi R^3}{400 \times 10^{-6} \times 10^{-3}} \approx 0.0104 < 0.1, \tag{6.26}$$

considering the average radius of a HeLa cell (R) as 10 μm, while the typical thickness of membrane (d) is 5 nm [9]. The geometric constant ($G = A/g$) of the device as mentioned in Eq. (6.26) is not easy to find because of nonlinear electric field. However, the approximate value of G is found out by substituting the area of the electrode (A) equal to 1 cm^2 and average gap between the electrodes (g) to 3 mm. The measured relative permittivity of PBS medium used in the experiment is 136, and the conductivity of the media is 1.56 S/m. Hence, the complex permittivity of PBS may be expressed as Eq. (6.27).

$$\widetilde{\varepsilon}_m = 136\varepsilon_0 + j\frac{1.56}{\omega}, \tag{6.27}$$

where ε_0 =8.854 × 10^{-12} F/m and ω is angular frequency. Using impedance spectroscopy data obtained from the experiment, the complex permittivity of mixture $\left(\widetilde{\varepsilon}_{mix}\right)$ was calculated using Eq. (6.17). Subsequently $\widetilde{\varepsilon}_{mix}$, $\widetilde{\varepsilon}_m$, and φ were substituted in Eq. (6.15) to estimate the complex permittivity $\left(\widetilde{\varepsilon}_p\right)$ of single HeLa cell. Figures 6.18a, b illustrate the variation of conductivity and permittivity of the single HeLa cell, respectively, with the frequency sweep from 100 Hz to 10 MHz for various operational voltages in the range of 1 mV–1 V. The results show that both the conductivity and relative permittivity of equivalent single HeLa cell increase with higher operational voltage at lower frequency range. From Fig. 6.14a it may be observed that, at lower frequency, the conductivity of single HeLa cell increases from 0.13 to 0.23 S/m as the voltage increased from 10 mV to 1 V. The results indicate that the higher electric field opens up more ionic channels in the cell membrane and thus enhances the charge exchange process between cytoplasm and

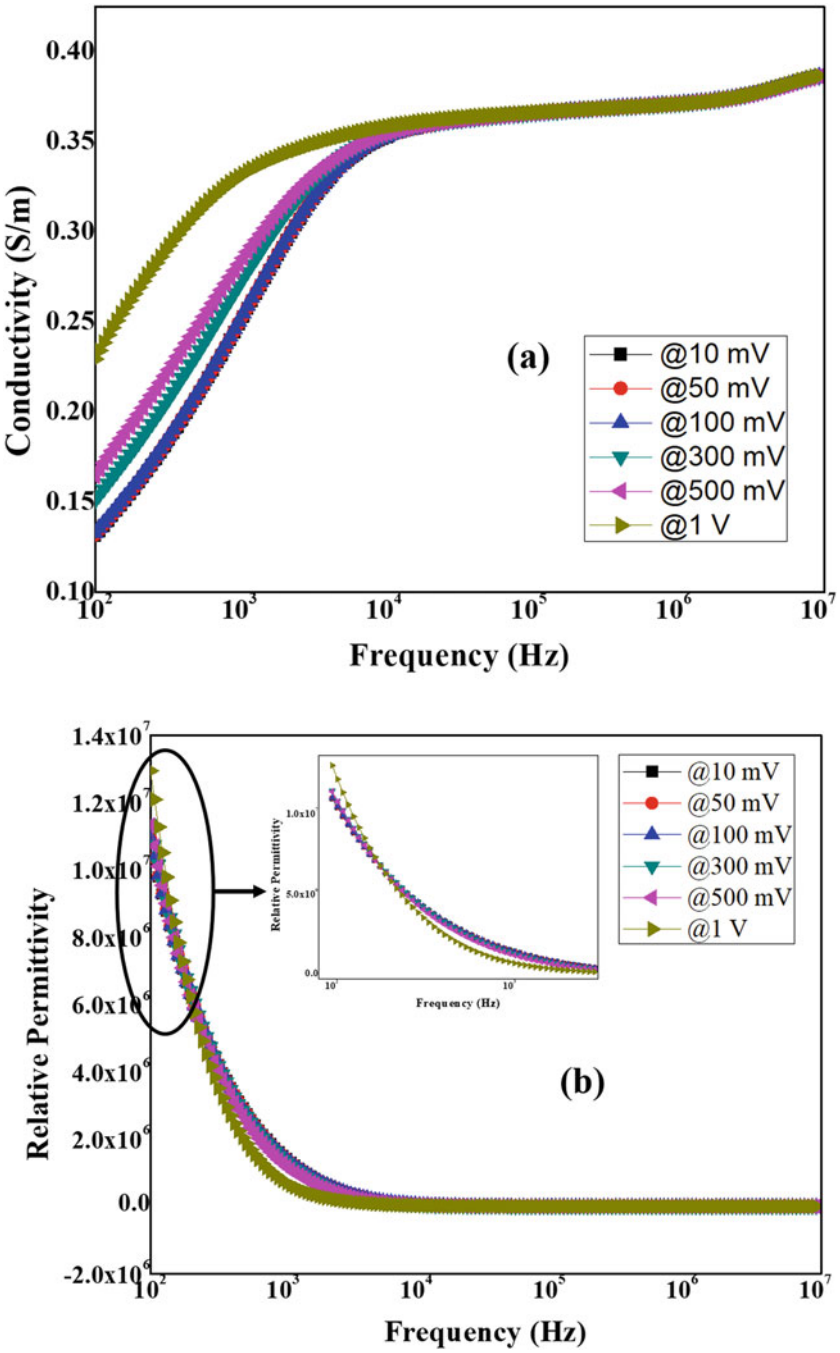

Fig. 6.18 Variation of (**a**) conductivity, (**b**) relative permittivity of single HeLa cell with frequency at different voltages. Inset shows the magnified image of circled portion of (**b**) (taken from [17])

extracellular solution. This phenomenon allows higher current to flow through the cell membrane and cytoplasm leading to increase of conductivity. Availability of ionic channel enhances the charge exchange between the cytoplasm and extracellular solution. Wang et al. [9] showed similar variation of permittivity and conductivity for different voltages measured by trapping a single HeLa cell inside the microchannel. Figure 6.18b shows that the measured relative permittivity of single HeLa cell is nearly same for different operating voltage up to 300 mV. At higher applied voltage above 300 mV, the slope of relative permittivity of cell is sharper than lower voltage data up to 4 kHz and thereafter all the permittivity data remain nearly same for entire operating voltages. Under higher electric field the capacitance representing the cell membrane may be fully charged at lower operating frequency, whereas at higher frequency zone it is unable to fully charge within one cycle [9, 35]. This demonstrates the decrease in relative permittivity of HeLa cell with increasing frequency at higher operating potential. The above experimental facts depict that the relative permittivity and conductivity of single HeLa cell are function of applied potential and frequency. These information may be useful for electroporation of cell membrane and characterization of different diseased cells.

Additionally, the parameters such as cell membrane capacitance and cytoplasm resistance of a cell may be utilized for identification of cell type and may also be explored for diagnostic and prognostic applications correlating with the disease progression. Therefore, extraction of membrane capacitance and cytoplasm resistance of single cell has emerged as major requirement to get the detailed insight of the disease and characterize them. The already extracted relative permittivity (ε) and conductivity (σ_i) of single cell are further used to obtain the membrane capacitance and cytoplasm resistance of single HeLa cell using Eqs. (6.24) and (6.25) and its variation with frequency is shown in Fig. 6.19a, b, respectively. Since the permittivity of membrane decreases continuously with the frequency, the membrane capacitance shows similar variation as observed in Fig. 6.19a. Its value decreases from 50 nF/cm^2 at 100 Hz to 9 pF/cm^{2}at 1 MHz. In β-dispersion range (above 100 kHz) the membrane capacitance becomes almost constant in the range of few nF/cm^2, which matches closely with the generally accepted value of single HeLa cell membrane capacitance obtained by cell trapping [26]. As depicted from the Fig. 6.19b cytoplasm resistance decreases with frequency in lower frequency range while it becomes almost constant (35 kΩ cm^2) in β-dispersion range which is also congruent with the generally accepted values of single HeLa cell cytoplasm resistance obtained by the method of cell trapping [26]. Table 6.2 shows a comparison between the extracted cell membrane capacitance and cytoplasm resistance through single cell trapping method by Wang et al. [9] and the present method of impedance measurement of colony of suspended cells. Thus, the experimental and theoretical analysis technique presented in this chapter demonstrate that electrical properties of single cell may be evaluated through the bioimpedance measurement of a colony of cells in suspensions using the Maxwell's mixture theory without complicated single cell trapping technique. It is expected that the extracted parameters will provide more realistic and practical information about the cell because its measurement has been conducted in close resemblance to practical conditions.

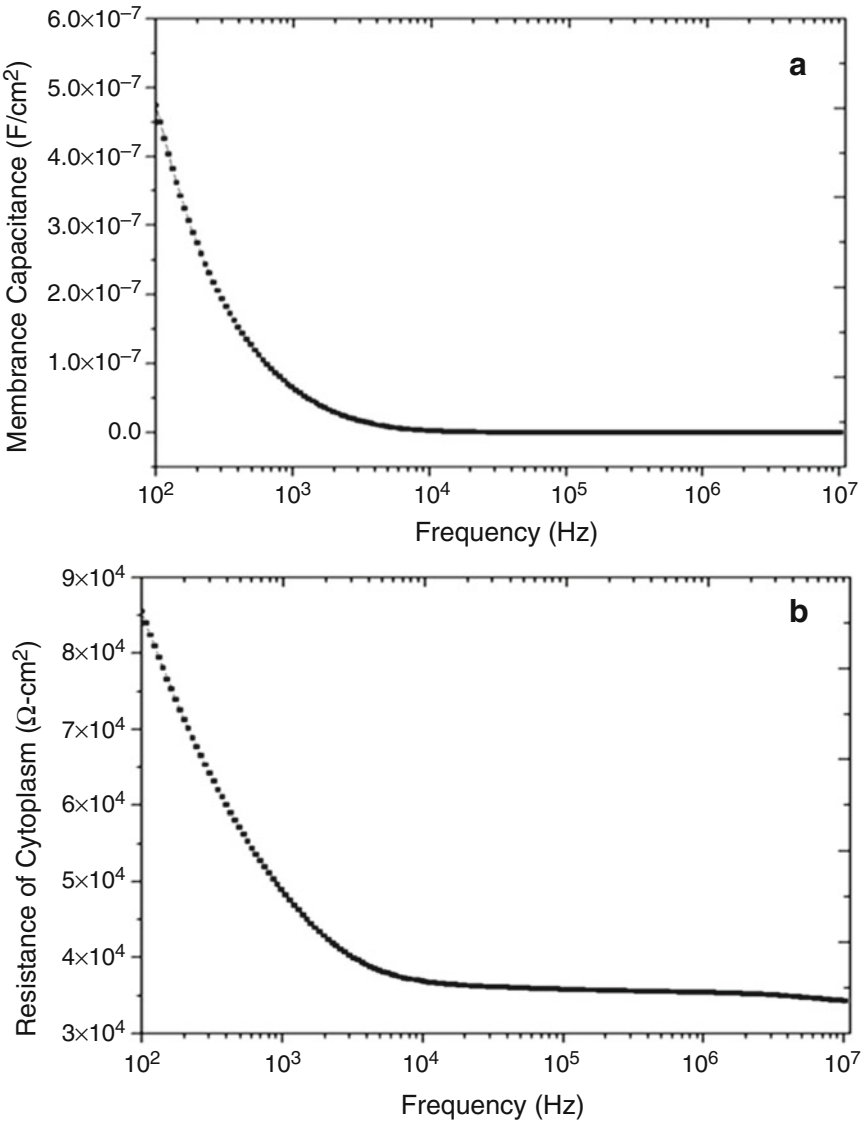

Fig. 6.19 Variation of (**a**) membrane capacitance, (**b**) cytoplasm resistance with respect to frequency (taken from [17])

6.6 Summary

A miniaturized bioimpedance sensor for on-chip cell culture and electrical equivalent model of the cell–electrode system to characterize biological cells has been presented in this chapter. The device has been fabricated using microfabrication

Table 6.2 Comparison of extracted single cell parameters

Single cell parameters	By single cell trapping method (Wang et al.)	By cells suspension method (analysis using present technique)
Resistance of cytoplasm (Ω cm^2)	6.0×10^4	3.5×10^4
Membrane capacitance (F/cm^2)	2.5×10^{-9}	3.9×10^{-9}

technology considering the biocompatibility issues and it demonstrates successful cell culture and corresponding impedance change. Subsequently, based on the experiment, an equivalent circuit model has been developed considering coating capacitance, double layer capacitance, exposed electrode resistance, and resistance–capacitance of group of growing cells on the electrode surface. Utilizing proposed fragmental analysis method with equivalent circuit model in different frequency ranges the simplified mathematical models are formulated to evaluate the parameter values theoretically. The extracted parameter values are further compared with the standard LEVM based fitting software EIS Spectrum Analyzer. Thus, the present study will provide an alternative way to evaluate the information of electrical equivalent parameters of electrode and cells of the system with a better understanding of complex mechanism in bioimpedance measurement.

Further, the importance of single cell measurement and existing methods with its limitations is discussed. In this chapter, a technique to extract the electrical properties of single HeLa cell through bioimpedance analysis of its colony of cells in suspension by Maxwell's mixture theory has been presented. Using the bioimpedance spectroscopy data of HeLa cells in PBS medium at different voltages, complex permittivity of the mixture was calculated which was further analyzed to extract the permittivity and conductivity of single HeLa cell. The experimental observation reveals that the relative permittivity and conductivity of single HeLa cell is a function of applied potential and frequency. At low frequency, the conductivity of single cell increases which is attributed for opening of more ion channels of membrane at higher electric field, allowing higher current to flow through the cell membrane and cytoplasm leading to increase of conductivity. At lower frequencies the relative permittivity of cell membrane decreases with the voltage. The relative permittivity of single HeLa cell is almost constant at the entire frequency range at lower operating voltage of 10–300 mV, while at higher applied voltage at 500 mV and 1 V, it reduces rapidly with increasing frequency. This indicates that under higher electric field the capacitance representing the cell membrane may be fully charged at lower operating frequency, whereas at higher frequency zone it may be unable to be fully charged within one cycle**.** In β-dispersion range, the membrane capacitance and cytoplasm resistance were calculated to be in 3.9 nF/cm^2 and 35 kΩ cm^2, respectively, which matches closely with the value obtained from cell trapping method found in literature.

Therefore, the present chapter provides an alternative technique to theoretically calculate the model parameters of group of cells on electrode surface. Further

extraction of electrical properties of a single cell from the bioimpedance spectroscopy of a colony of cells by avoiding the complexity of single cell capturing and impedance measurement in microchannel led to fundamental contribution to the future study of cellular bioimpedance.

References

1. Chen, J. (2014). Nanobiomechanics of living cells: A review. *Interface Focus, 4*(2), 20130055.
2. Rehman, A., Firdous, S., Nawaz, M., & Ahmad, M. (2012). Optical parameters measurement for diagnostic and photodynamic therapy of human cervical adenocarcinoma (HeLa) cell line. *Laser Physics, 22*(1), 322–326. https://doi.org/10.1134/s1054660x12010161
3. Yang, L., Arias, L. R., Lane, T., Yancey, M., & Mamouni, J. (2011). Real-time electrical impedance-based measurement to distinguish oral cancer cells and non-cancer oral epithelial cells. *Analytical and Bioanalytical Chemistry, 399*(5), 1823–1833. https://doi.org/10.1007/s00216-010-4584-9
4. Kumar, A., Purohit, B., Maurya, P. K., Pandey, L. M., & Chandra, P. (2019). Engineered nanomaterial assisted signal-amplification strategies for enhancing analytical performance of electrochemical biosensors. *Electroanalysis, 31*(9), 1615–1629.
5. Das, D., Kamil, F. A., Agrawal, S., Biswas, K., & Das, S. (2014). Fragmental frequency analysis method to estimate electrical cell parameters from bioimpedance study. *IEEE Transactions on Instrumentation and Measurement, 63*(8), 1991–2000.
6. Sarró, E., Lecina, M., Fontova, A., et al. (2012). Electrical impedance spectroscopy measurements using a four-electrode configuration improve on-line monitoring of cell concentration in adherent animal cell cultures. *Biosensors & Bioelectronics, 31*(1), 257–263. https://doi.org/10.1016/j.bios.2011.10.028.
7. Rahman, A. R. A., Lo, C.-M., & Bhansali, S. (2006). A micro-electrode array biosensor for impedance spectroscopy of human umbilical vein endothelial cells. *Sensors and Actuators B: Chemical, 118*(1–2), 115–120. https://doi.org/10.1016/j.snb.2006.04.060.
8. Gawad, S., Schild, L., & Renaud, P. (2001). Micromachined impedance spectroscopy flow cytometer for cell analysis and particle sizing. *Lab on a Chip, 1*(1), 76–82. https://doi.org/10.1039/b103933b.
9. Wang, M.-H., & Jang, L.-S. (2009). A systematic investigation into the electrical properties of single HeLa cells via impedance measurements and COMSOL simulations. *Biosensors & Bioelectronics, 24*(9), 2830–2835. https://doi.org/10.1016/j.bios.2009.02.012.
10. Asphahani, F., Wang, K., Thein, M., et al. (2011). Single-cell bioelectrical impedance platform for monitoring cellular response to drug treatment. *Physical Biology, 8*(1), 015006.
11. Giaever, I., & Keese, C. R. (1993). A morphological biosensor for mammalian cells. *Nature, 366*(6455), 591.
12. Giaever, I., & Keese, C. R. (1991). Micromotion of mammalian cells measured electrically. *Proceedings of the National Academy of Sciences, 88*(17), 7896–7900.
13. Lo, C. M., Keese, C. R., & Giaever, I. (1995). Impedance analysis of MDCK cells measured by electric cell-substrate impedance sensing. *Biophysical Journal, 69*(6), 2800–2807. https://doi.org/10.1016/S0006-3495(95)80153-0.
14. Rahman, A. R. A., Chun-Min, L., & Bhansali, S. (2009). A detailed model for high-frequency impedance characterization of ovarian Cancer epithelial cell layer using ECIS electrodes. *IEEE Transactions on Biomedical Engineering, 56*(2), 485–492. https://doi.org/10.1109/tbme.2008.2008488.
15. Pradhan, R., Mitra, A., & Das, S. (2012). Impedimetric characterization of human blood using three-electrode based ECIS devices. *Journal of Electrical Bioimpedance, 3*(1), 12–19.

16. Orazem, M. E., & Tribollet, B. (2008). *Electrochemical impedance spectroscopy*. Hoboken, NJ: Wiley-VCH.
17. Das, D., Kamil, F. A., Biswas, K., & Das, S. (2014). Evaluation of single cell electrical parameters from bioimpedance of a cell suspension. *RSC Advances, 4*(35), 18178–18185.
18. Agilent. (2002). *Agilent 4294A precision impedance analyzer operation manual*.
19. Gawad, S., Henschkel, M., Leung-Ki, Y., et al. (2000). Fabrication of a microfluidic cell analyzer in a microchannel using impedance spectroscopy. In 1st *Annual International, Conference On 2000 Microtechnologies in Medicine and Biology*, pp. 297–301.
20. Wegener, J., Zink, S., Rosen, P., & GAlla, H. (1999). Use of electrochemical impedance measurements to monitor B-adrenergic stimulation of bovine aortic endothelial cells. *Pflügers Archiv - European Journal of Physiology, 437*, 925–934.
21. Gill, P. E., & Murray, W. (1978). Algorithms for the solution of the nonlinear least-squares problem. *SIAM Journal on Numerical Analysis, 15*(5), 977–992. https://doi.org/10.2307/2156716.
22. Nocedal, J., & Wright, S. J. (1999). *Numerical optimization*. New York: Springer.
23. Pujol, J. (2007). The solution of nonlinear inverse problems and the Levenberg-Marquardt method. *Geophysics, 72*(4), W1–W16. https://doi.org/10.1190/1.2732552.
24. Lvovich, V. F. (2012). *Impedance spectroscopy: Applications to electrochemical and dielectric phenomena*. Boca Raton, FL: Wiley.
25. Han, A., Yang, L., & Frazier, A. B. (2007). Quantification of the heterogeneity in breast Cancer cell lines using whole-cell impedance spectroscopy. *Clinical Cancer Research, 13*(1), 139–143. https://doi.org/10.1158/1078-0432.ccr-06-1346.
26. Jang, L.-S., & Wang, M.-H. (2007). Microfluidic device for cell capture and impedance measurement. *Biomedical Microdevices, 9*(5), 737–743. https://doi.org/10.1007/s10544-007-9084-0.
27. Skelley, A., Kirak, O., Suh, H., Jaenisch, R., & Voldman, J. (2009). Microfluidic control of cell pairing and fusion. *Nature Methods, 6*(2), 147–152.
28. Carlo, D. D., Wu, L. Y., & Lee, L. P. (2006). Dynamic single cell culture array. *Lab on a Chip, 6*(11), 1445–1449. https://doi.org/10.1039/b605937f.
29. Abdur Rahman, A. R., Price, D. T., & Bhansali, S. (2007). Effect of electrode geometry on the impedance evaluation of tissue and cell culture. *Sensors and Actuators B: Chemical, 127*(1), 89–96. https://doi.org/10.1016/j.snb.2007.07.038.
30. Schwan, H. P. (1992). Linear and nonlinear electrode polarization and biological materials. *Annals of Biomedical Engineering, 20*(3), 269–288. https://doi.org/10.1007/bf02368531.
31. Sun, T., & Morgan, H. (2010). Single-cell microfluidic impedance cytometry: A review. *Microfluidics and Nanofluidics, 8*(4), 423–443. https://doi.org/10.1007/s10404-010-0580-9.
32. Hanai, T., Asami, K., & Koizumi, N. (1979). Dielectric theory of concentrated suspensions of shell-spheres in particular reference to the analysis of biological cell suspensions. *Bulletin of the Institute for Chemical Research, 57*, 297–305.
33. Hanai, T., Koizumi, N., & Irimajiri, A. (1975). A method for determining the dielectric constant and the conductivity of membrane-bounded particles of biological relevance. *Biophysics of Structure and Mechanism, 1*(4), 285–294. https://doi.org/10.1007/bf00537642.
34. Foster, K. R., & Schwan, H. P. (1989). Dielectric properties of tissues and biological materials: A critical review. *Critical Reviews in Biomedical Engineering, 17*(1), 25–104.
35. Orjan, G., & Martinsen, S. G. (2008). *Bioimpedance and bioelectricity basics* (2nd ed.). London: Academic Press.

Chapter 7
Research Aspects and Strategies for the Development of Biosensors for Renal Disease Diagnosis

Akshay Srivastava and Gopal Agarwal

7.1 Point-of-Care Devices and their Importance in Renal Diseases Diagnosis

Point-of-care (POC) devices are designed to test and provide relevant information in a clinical setting during patient consultation for immediate action. The POC can also be performed at the bedside, home, or in paramedical support as well as in secondary and tertiary settings (Vashist, Luppa, Yeo, Ozcan, & Luong, 2015). For resource-constrained settings, WHO sets ideal characteristic for POC to be "ASSURED (Affordable, Sensitive, Specific, User-friendly, Rapid and robust, Equipment free, and Deliverable to end-users)" for developing diagnostic test [1].

The incidence of kidney disease is constantly growing but the limited sensitivity and specificity of available diagnostics for early stage detection possess obstacles in providing timely treatment. The global burden of deaths related to kidney-associated disease was estimated at nearly 1.2 million populations in 2017. Patients suffering from kidney injury requiring renal replacement are estimated to be 5.4 million by 2030. Hence, there is an urgent need for the early assessment of acute and chronic kidney injury [2]. Chronic kidney disease (CKD) is defined as the dysfunction of the healthy kidney to filter and remove the waste from a body. When it is progressed to the end-stage failure, a massive level of fluids and electrolytes accumulates in the body [3]. Thirty million people in the USA have been suffering from CKD and around 96% of the population are not aware of the kidney damage. In the Indian population, diabetes has risen to 7.1% and 28% in urban and rural areas, respectively [4] which has become the main concern in developing CKD. Approximately 1 in 3 diabetic adults is also diagnosed with CKD [5]. In 2017, a study suggested that the

A. Srivastava (✉) · G. Agarwal
National Institute of Pharmaceutical Education and Research, Ahmedabad, Gujarat, India
e-mail: akshay.srivastava@niperahm.res.in

V. Borse et al. (eds.), *BioSensing, Theranostics, and Medical Devices*,
https://doi.org/10.1007/978-981-16-2782-8_7

global prevalence of chronic kidney disease (CKD) was 9.1% (697.5 million cases), of which nearly one-third cases were from India and China [6]. Irreversible kidney failure persists as the leading cause of high mortality in critically ill patients. The global ranking of CKD was around 12th in causing common death and approximately 17th in causing disability [7]. Acute kidney injury (AKI) is also possessing a threat in the progression towards end-stage renal disease. Timely diagnosis of AKI would also permit prediction of severity of AKI, course of timely treatment, and safety assessment during drug treatment. Needle biopsy is the current gold standard technique for the diagnosis of different types of kidney dysfunction. However, renal biopsy can lead to complications like bleeding, infections, and sometimes death. Furthermore, other techniques like ultrasound imaging and magnetic resonance imaging are routinely used to assess the kidney function but it is costly, time-consuming, and difficult [8]. Thus, the development of POC devices for early assessment of AKI and CKI can aid in the treatment of kidney disease.

Consider the following scenario; Wheelchair-bound elderly patient visiting nephrologists or general physician for a treatment related to kidney disease. The doctor may recommend her to get it tested for the proper functioning of the kidney. It would be difficult for the patient to go to the pathological center due to immobility, lack of car parking, access for wheelchairs, and probably endless wait for an appointment. Then, there would be a delay in receiving the pathology report and a follow-up visit to the doctor to discuss the treatment based on the report. Consider how much easier for the patient it would be if a kidney test could be done on-site and get the result within a few minutes in clinical setup and receive treatment. Similarly, a diabetic patient visits a doctor for a routine check-up and ensuring medications related to diabetes management. The doctor suggested changes in medicine and instructed a strict diet for diabetes management to avoid secondary complications such as kidney damage, etc. As usually diabetes patients do not visit the doctor so often and keep taking the same medicine for long without noticing the damage it may have caused to the kidney. Consider how much vigilant a patient can become if POC device is easily available to him for constant monitoring of kidney health at home. Thus, access to the POC device may address all these issues related to daily healthcare systems related to kidney health.

7.2 Various Biomarkers for Kidney Disease Diagnosis

Biomarkers play a crucial role in the diagnoses of renal disease at an early stage. Biomarkers can be measured as an indicator of biological processes in normal and disease states. There are several types of biomarkers: diagnostic, monitoring, pharmacodynamics, predictive, safety, prognostic, and susceptibility [9]. The readily available source of kidney disease biomarkers for the diagnosis is urine (non-invasive method) and blood (slightly invasive method). Both of these sources have their advantage and disadvantage, where urine provides an understanding of renal pathologies is less complex compared to serum, and can be easily collected at

home. However, the handling of urine greatly affects the stability of proteins present within. The serum is more stable than urine and is less prone to contamination as compared to urine. However, serum biomarkers represent the systemic response of disease, rather than organ-specific response, and also a large amount of protein presents in serum samples makes it difficult to estimate the desired protein [10]. The biomarkers in renal disease can be related to two stages of kidney disease, i.e. acute kidney injury (AKI) and chronic kidney injury (CKI). AKI is defined as an unexpected decrease in glomerular filtration rate that includes both loss of function and structural damage and consequently retention of nitrogenous waste products and dysregulation in exchange of extracellular volume and electrolytes. As per "Risk, Injury, Failure, Loss, and End-Stage Renal disease criteria (RIFLE)," the term AKI includes the entire spectrum of disease from the early stage of renal failure to the end-stage requiring renal replacement therapy. However, in 2007, acute kidney injury network (AKIN) proposed the more sensitive AKI diagnostic criteria. The proposed definition of AKI states that AKI is diagnosed by a sudden increase in serum creatinine of approximately 0.3 mg/dL (26.5 μmol/L) within 48 hours a 50% increase in serum creatinine level from baseline within 7 days or having urine volume less than 0.5 ml/kg/h for at least 6 h [11]. U.S.F.D.A approved biomarkers for AKI diagnosis include β_2 microglobulin, α_1 microglobulin, retinol-binding protein, cystatin C, microalbumin, clusterin, neutrophils gelatinase-associated lipocalin, kidney injury molecule-1 (KIM-1), asymmetric dimethylarginine (ADMA), interleukin-18, cysteine rich protein, osteopontin, fatty acid binding protein, sodium and hydrogen exchanger isoform, and fetuin A (Fig. 7.1). However, single marker may not be able to detect the development of CKD and its progression due to complex pathomechanism. A combination of markers would be required to map all the changes occurring in the progression of kidney disease [12]. However,

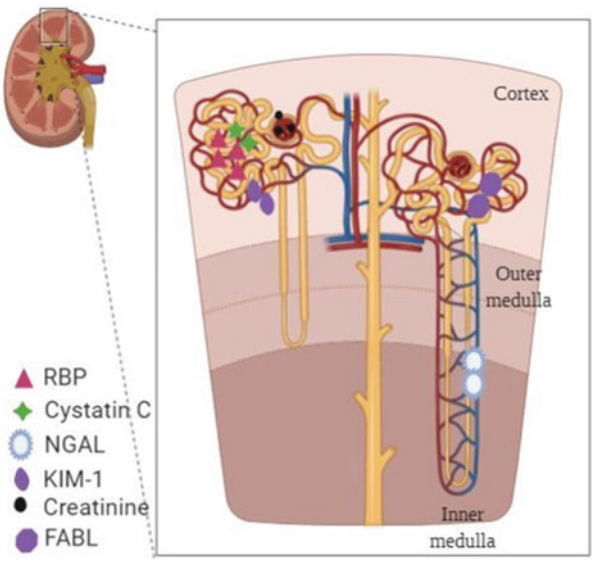

Fig. 7.1 Schematic illustration showing various regions of biomarkers present in different regions of the kidney

many studies to date have solely concentrated on serum creatinine and blood urea nitrogen (BUN) levels for detection of AKI [13]. eGFR can be calculated from the estimation of creatinine (CRE) concentration in blood or serum. However, variation in serum creatinine measurements can be influenced by age, sex, size of the body, total muscle mass, consumption of food, drugs, and other biological variation. International guidelines define chronic kidney injury (CKI) as a decrease in glomerular filtration rate $<$ 60 mL/min per 1.73 m^2 and/or having markers of kidney damage or both for at least 6 months. The main clinical manifestation of CKI is renal fibrosis, which is characterized by glomerulosclerosis, interstitial fibrosis, and tubular atrophy [3]. Diagnosis of CKI relies on the measurement of glomerular filtration rate and albuminuria. Based on the GFR, the CKI is classified into five different stages: stage I (GFR $>$ 90 ml/min), stage II (GFR $>$ 60–89 ml/min), stage IIIa (GFR 45–59 ml/min), stage IIIb (GFR 30–44 ml/min), stage IV (GFR 15–29 ml/min), and stage V (GFR $<$15 ml/min). We have summarized the occurrence of the prominent biomarkers of AKI, sample source, significance and limitations of detection in Table 7.1.

Albumin is another important biomarker that represents more than 80% of the protein content in the urine. The albumin:creatinine concentration ratio is the most widely used measurement for the detection of kidney damage. Urine dipstick is a qualitative measurement of protein usually involved in analyzing crude estimates of albumin with low sensitivity [14]. Incorporation of immunoassay principles in dipsticks has enabled the semi-quantitative measurement of urine microalbumin and/or albumin:creatinine ratio Nagrebetsky et al. (2013) McTaggart et al. (2012). The POC devices that provide quantitative measurement of urine albumin along with albumin:creatinine ratio utilize the principles of immuno and/or colorimetric assay [15–17]. However, the presence of albumin in urine involves biological variations. Transient increase in albumin concentration in several other conditions such as urinary tract infection, postural changes, hypertension, hyperglycemia, etc. in urine also leads to false-positive measurements [14, 18, 19]. These conventional markers may be replaced with newly discovered markers as discussed above and will be useful for the development of POC devices but their efficacy, sensitivity, specificity, and cost-effectiveness should be fully explored.

7.3 Point-of-Care Devices for Kidney Injury Diagnosis

Various biomarkers have been reported for AKI estimation; however, most of the POC devices for AKI are based on the estimation of creatinine level. Creatinine is the most commonly analyzed biomolecule for CKD [20]. Concentrations of creatinine greater than 150μM may demonstrate a risk of CKD but additional analytical tests would be required to exclude any such risk. However, creatinine values above 500μM advise serious renal impairment that may require dialysis or kidney transplantation in extreme cases [21]. Therefore, clinically sustainable and accurate detection of creatinine at POC may ensure individual well-being with an affordable

Table 7.1 AKI biomarkers and their significance

Biomarker	Source of biomarker detection	Significance of the biomarker in detection	Limitation of the biomarker in the detection of AKI
Retinol-binding protein (RBP)	Urine	Indicator of tubular function and glomerular filtration	
Cystatin C	Urine/ serum	Tubular injury cell marker and is released by all nucleated cells, indicates impaired GFR	Thyroid dysfunction, obesity, use of corticosteroid, inflammatory agent, old age, male gender, smoking affects the cystatin C level
Kidney injury molecule-1 (KIM-1)	Urine	High levels are released by damaged proximal tubular cells	
Neutrophils gelatinase-associated lipocalin (NGAL)	Urine/ plasma/ serum	Released from leukocytes, Henle's loop and collecting tubule, and indicator of inflammation	Stress and sepsis patient has a higher level of NGAL
Interleukin-18 (IL-18)	Urine	High levels indicator of renal inflammation and is released by monocytes, dendritic cells, and macrophages	
Fatty acid binding protein (FABL)	Urine	Released from proximal tubular cells, indicates proximal tubular injury and oxidative damage	
Creatinine	Serum/ urine	Indicates damage to kidney nephrons and change in glomerular filtration rate	The serum level depends upon muscle mass, age, sex
Tissue inhibitor of metalloproteinase 2 (TIMP) and Insulin-like growth factor-binding protein 7 (IGFBP7)	Urine	Indicates cellular stress or injury, markers of cell cycle arrest	Limited information regarding the biological role and factors affecting these biomarkers level

healthcare system and monitor advanced stages of CKD patients. Recently, POC has been developed for the analysis of creatinine in hospitals and pathology laboratories [22]. Colorimetric and voltammetry-based approaches have shown true POC devices that can replace older methods involving large sophisticated instrumentation [23–25]. A growing interest in utilizing the concept of voltammetry and amperometry for creatinine detection is observed in the last 10 years. Some of the marketed POC devices for the estimation of creatinine levels are i-STAT (Abbott, USA), epoc (Siemens, USA), StatSensor (Nova Biomedical, USA), ABL90 Flex Plus (Radiometer Benelux, The Netherlands), and STAT Profile Prime+ (Nova Biomedical, USA) (Fig. 7.2). The comparison of various POC devices for AKI is illustrated in Table 7.2. Mostly, these FDA approved POC devices for the measurement of

Fig. 7.2 Various marketed POC available for kidney function analysis. (**a**) Novastat sensor: (**b**) i-STAT, (**c**) epoc, (**d**) ABL800 Flex, (**e**) DRI-CHEM NX500, (**f**) Piccolo express

Table 7.2 Various marketed POC available for the estimation of creatinine level

POC	Type of sample analyzed	Minimum amount of sample required for detection	Method of detection	Limit of detection of POC	Time taken for detection
Nova stat sensor	Whole blood	1.2µl	Enzymatic, electrochemical biosensor strip	0.3–12 mg/dL	30 s
i-STAT	Whole blood, plasma, serum	100µl	Enzymatic, electrochemical biosensor strip	0.2–20 mg/dL	200 s
Epoc	Venous, arterial, and whole blood	92µl	Enzymatic, electrochemical biosensor strip	0.3–15 mg/dL	35 s
ABL800 FLEX	Whole blood, plasma, and serum	125µl	Enzymatic, electrochemical biosensor strip	10–2000 mg/dL	120 s
DRI-CHEM NX500 (Fujifilm)	Plasma, serum, and whole blood	10µl	Colorimetric	0.2–24 mg/dL	300 s
Piccolo Xpress (Abott)	Whole blood, serum, plasma	100µl	Enzymatic, colorimetric	0.2–20 mg/dL	720 s

creatinine levels are based on an enzymatic electrochemical biosensor. These POC devices involve *Creatinine Amidohydrolase* or *Creatine Amidinohydrolase* or *Sarcosine Oxidase* that converts the creatinine present in the sample into hydrogen peroxide, subsequently detected by redox-mediated horseradish-peroxidase (HRP)-catalyzed reduction on a gold electrode. Furthermore, the background creatinine is converted to water and oxygen and the outer diffusion barrier facilitates the rapid transport of oxygen to the oxidase enzyme to assure the sensor response is linear and proportional to the concentration of creatinine in the test fluid. The amount of eGFR is then calculated based on the creatinine levels. StatSensor is a handheld creatinine analyzer that quantitatively measures creatinine in capillary, venous, and whole blood. It was seen that StatSensor was not able to detect creatinine level accurately for children below 10 years of age and tends to underestimate the high value of creatinine (<600μmol/L) [1]. Furthermore, in a study by Heijden et al., it was seen that StatSensor gave more clinical errors and did not meet any criteria of creatinine for eGFR measurements as compared to i-Stat and epoc [26]. I-STAT is a cartridge-based analyzer that works on the transformation of electrical signals into human-readable results. The creatinine and urea level estimation can be done by a miniaturized version of traditional electrode technology [27]. It was seen that i-STAT provides high precision and linearity with comparable data to that of the routinely used chemistry and hematology analyzer [28].

These devices exhibit varying degrees of sensitivity and accuracy at a lower concentration of creatinine (<120μmol/L) depending upon age, sex, and disease condition [29]. Creatinine measurement in whole blood possesses serious challenges due to the presence of interfering molecules. There is a dire need for an analytically sound POC device for the identification of CKD at an early stage. The current requirement for the development of POC is sampling, quick results, automatic eGFR calculation, and error-free analytical performance to establish the risk of CKD and AKI. No device fulfills all these requirements in the current clinical setup and hence the opportunities remain in the development of creatinine-based POC in clinical settings. The establishment of other biomarkers has also been proposed to detect CKD and AKI, e.g. urinary neutrophil gelatinase-associated lipocalin (NGAL), urinary kidney injury molecule-1 (KIM-1), and cystatin C, [30, 31]. Some of these markers now utilized in POC devices are under development, e.g. Eurolyser SMART and CUBE devices utilize cystatin C and albumin, Alere Triage® using NGAL, the RenaStick based on urinary KIM-1 [32, 33]. RenaStick provides a novel and economic test for the detection of AKI. It can monitor the kidney damage at an early stage using FDA approved KIM-1 marker with greater sensitivity. It has shown a higher intensity of urinary KIM-1 in the patients suffering from acute kidney injury compared to healthy volunteers [33].

7.4 New Avenues in Developing POC for Renal Diseases

The basic principle in developing a biosensor mostly involves selecting a suitable matrix for antibody immobilization, and then the addition of the sample having the analyte and its detection using different principles (Fig. 7.3). The ultrasensitive sensor was fabricated for detection of chronic kidney disease, where papain enzyme was immobilized on carboxy functionalized multi-walled carbon nanotubes, using EDC/NHS chemistry. Interaction between cystatin C (present in urine samples) and papain enzymes was detected by cyclic voltammetry (CV) and differential pulse voltammetry (DPV) in less than 10 min. The sensitivity of these biosensors for detection of cystatin C in urine is 1583.49μA $cm^{-2}μg^{-1}$, detecting a lower amount of 0.58 ng/L of the biomarker [34]. Trindande et al. fabricated an electrochemical biosensor for the detection of cystatin C by the conjugation of graphene oxide (GO) with aminoferrocene that developed a catalytic nanocomposite and detects the biomarkers (with LOD 0.03 ng/ml) detection through antibody anchored to the nanocomposite [35]. The detection of cystatin C can also be done using combined surface-enhanced Raman spectroscopy and electrochemistry where the biomolecules extracted from the blood plasma using an extractor chip reduced via disulfide bond breakage and immobilized on a conductive gold-coated silicon nanopillar substrate. Such an oriented immobilization allowed reproducible surface-enhanced Raman spectrophotometer (SERS) and differential pulse voltammetry (DPV) results. Initially, SPR measurement was done, following which DPV is made to desorb analyte

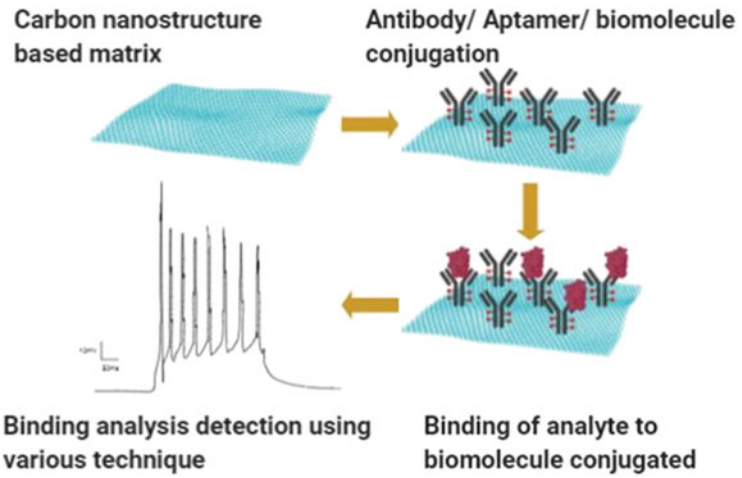

Fig. 7.3 Schematic representation depicting the basic principle for detection of an analyte in biosensors: The carbon nanostructure-based scaffolds are conjugated either with antibody, aptamers, or other biomolecules (enzyme, polymers) and then upon the addition of sample (having analyte), the analyte binds specially to the biomolecules, and this binding between analyte and biomolecules is detected using various techniques like cyclic voltammetry, differential pulse voltammetry, surface-enhanced Raman scattering, and others

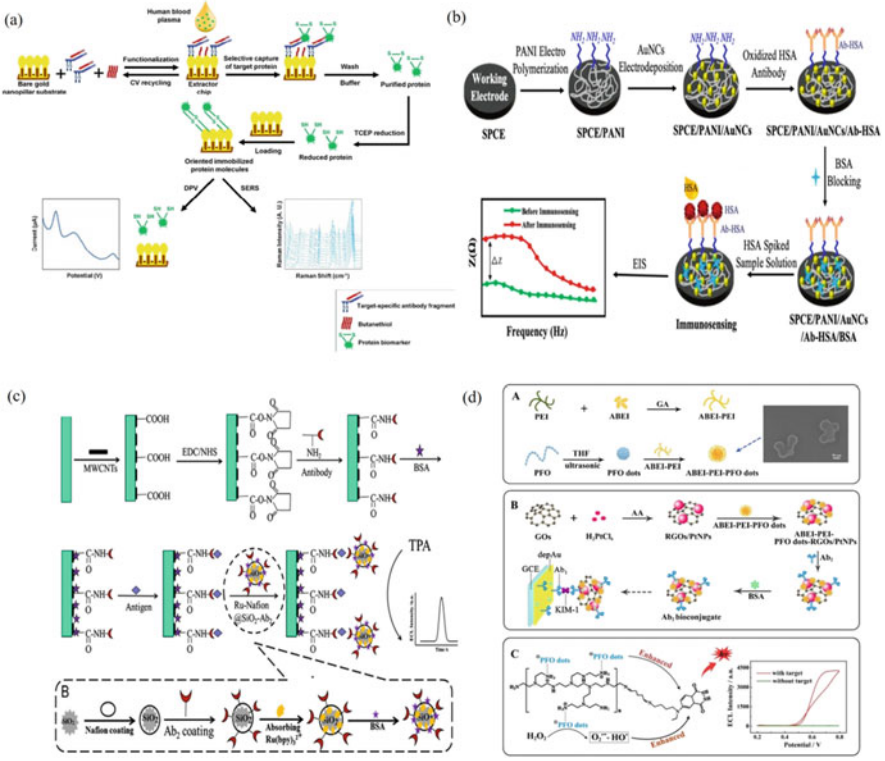

Fig. 7.4 Various strategies used in developing a biosensor to detect various biomarkers for the renal disease: (**a**) cystatin C (taken with permission from [36]), (**b**) KIM-1 (taken with permission from [39, 40]), (i) preparation of ECL emitter, (ii) construction of immunosensor, (iii) signal-enhanced mechanism, (**c**) retinol-binding protein 4 (taken with permission from [38]), (**d**) human serum albumin (taken with permission from [41, 42])

from the substrate and measure its concentration based on the reduced current. The developed biosensor has shown a sensitivity of 1pM and 62.5 nM, detected by SERS and DPV, respectively (Fig. 7.4a) [36].

Torabi et al. fabricated an immune sandwich-based POC device for the detecting RBP4 in the range of 0.001–2 ng/mL. The ultrasensitive sensor was also developed by immobilization of biotinylated RBP4 aptamers on streptavidin-coated polystyrene microwells. RBP4 present in human samples binds to the aptamers and the detection was made using luminol antibody. The chemical luminescence can be recorded from the oxidation using hydrogen peroxide as oxidant and Au^{+3} as catalyst [37]. Wu et al. have fabricated an enhanced chemiluminescence (ECL) based biosensor to detect RBP4, where MWCNTs were used as a substrate to anchor a large amount of the primary antibody on the glassy carbon electrode surface. A mesoporous silica nanoparticle capped with Nafoin ($Ru(bpy)_3^{+2}$) was modified with a secondary antibody on the surface (as shown in Fig. 7.4c). Enhanced ECL signal

was then observed on the exposure to RBP4 present in urine samples in the presence of tripropylamine (TPA) [38].

NGAL detection was also demonstrated using a label-free photoelectrochemical biosensor where oriented immobilization of NGAL nanobody was achieved on streptavidin-coated 2,9,16,23-tetraaminophthalocyanine (CoPc)-sensitized TiO_2 electrode. The binding of NGAL causes steric hindrance resulting in a decrease in photocurrent. The sensitivity of the fabricated biosensor was found to be 0.6 pg/ml [43]. Yukird et al. fabricated electrosprayed graphene/polyaniline modified screen-printed electrode for the detection of NGAL using cyclic voltammetry. The presence of polyaniline increases the number of amino groups for antibody immobilization. NGAL present in human serum was detected with LOD of 21.1 ng/ml using a minimal 10μl of a sample [44]. Furthermore, a Prussian blue nanoparticle having redox activity was deposited on graphitic C_3N_4 nanosheet by *in situ* reductions, which was further conjugated with polyclonal NGAL antibody. A screen-printed electrode was modified with a monoclonal antibody against NGAL. Upon addition of NGAL, a sandwich formed at the screen-printed electrode causes the conversion of Prussian blue to Prussian white, which can be observed by voltammetry. The fabricated biosensor was able to detect as low as 2.8 pg/ml concentration [45]. Furthermore, Kannan et al. fabricated an electrochemical immunosensor, where rabbit polygonal lipocalin-2 antibody on gold nanoparticles is initially developed, which is then attached on generation-1 polyamidoamine (PAMAM) dendrimer (LA2/AuNPs/PAMAM) immobilized on the gold electrode. The detection of the NGAL was achieved by the oxidation and current enhancement upon the antigen–antibody interactions. This biosensor has demonstrated a sensitivity to detect up to 1 ng/ml of the analyte in the sample [46].

KIM-1 detection was achieved using N-(aminobutyl)-N-(ethylisoluminol) (ABEI)-polyethylenimine (PEI)-poly (9,9-dioctylfluorenyl-2,7-diyl) (PFO) dots as a novel ECL emitter. The obtained ABEI-PEI-PFO dots with high ECL efficiency were due to the dual amplified property of PFO dots. Platinum (Pt) nanoparticles supported reduced graphene oxide (RGO) nanosheet was used as the loading platform of ABEI-PEI-PFO dots, to increase the electron transfer efficiency. The non-specific binding sites were blocked with bovine serum albumin (BSA), resulting in composites (ABEI-PEI-PFO dots-RGOs/PtNPs) with high-efficiency luminescence. This was further used as a nano-carrier for the detection of antibody (Ab_2) forming ABEI-PEI-PFO dots-RGOs/PtNPs-Ab_2-BSA complex (Ab_2 bioconjugates). Also, Au nanoparticle (AuNPs) was captured with an antibody (Ab_1). And through sandwiched immunoreaction among Ab_2, KIM-1, and Ab_1, a high-sensitive ECL (capable to detect 16.7 fg/ml) immune sensor was constructed for KIM-1 detection. (Fig. 7.4b) [39, 40]. A biosensor for the detection of human serum albumin was developed using the principle of electrochemical impedance spectroscopy (EIS). The carbon electrode (SPCE) was electropolymerized with polyaniline (PANI) for the deposition of gold nanocrystals (AuNC). Furthermore, conjugation of oxidized human serum antibody on polyaniline and gold nanocrystals composite have shown enhanced sensitivity for human serum albumin in the range of 3-300μg/ml (Fig. 7.4d) [41, 42]. The same research group has later developed

another electrochemical immunosensor consisting of silver nanoshells with polystyrene nanoparticle core covalently conjugated to human serum albumin (HSA) antibodies. These nanoprobes were then deposited on the electrode using electrophoresis. Each immunosensor consisted of two sensing sites: one for the test sample and another for control [41, 42]. Furthermore, Esentruk et al. fabricated a biosensor that can detect 0.7 pM of HSA, using surface plasma resonance. HSA imprinted screen electrode consisting of N-methacryloyl-L-leucine methyl ester, ethylene glycol dimethacrylate, as a crosslinker, and functional monomer was drop casted onto surface plasma resonance chips. It was found to be capable of the detection and quantification of albumin present in human urine samples [47]. Using the same principle of detection of surface plasma resonance, Liu et al. have fabricated a biosensor that can detect albumin up to 4μg/ml [48]. Furthermore, immobilization of silver nanoparticles loaded with albumin on a glass substrate has shown an enhanced interaction with anti-human albumin antibody, and these interactions of albumin present on the nanoparticles with antibody were detected using surface plasma resonance. The fabricated biosensor was able to detect 1 ng/ml of the analyte [49]. A screen-printed carbon electrode chronoamperometric based biosensor was also developed for the detection of albumin. Anti-human albumin was immobilized on the carbon electrode which has shown a sensitivity of 9.7μg/ml [50]. Biosensor fabricated by using colloidal gold nanoparticles and polyvinyl alcohol (PVA) has demonstrated the detection of urine albumin up to 25 ng/ml. The gold nanoparticles conjugated with human albumin antibody were deposited on PVA modified screen-printed carbon electrode and the quantitative detection was made using DPV and square wave voltammetry [51]. Now, with the advancement of technology, the patients can themselves detect the albumin present in their urine using smartphones. Akaraa et al. fabricated uTester that can conduct rapid and reliable quantification of human serum albumin. The biosensor is based on aggregation-induced emission nanomaterials bioprobe BSPOTPE [52]. The bioprobe is non-emissive in the absence of albumin, however, in the presence of albumin, the bioprobe emits fluorescence due to its aggregation, caused by the restriction of intramolecular rotation. Further, Raman spectroscopy has also been successful for the detection of albumin in human urine. Huang et al. have encapsulated human albumin antibodies into self-polymerizing dopamine, which can react with human albumin antigen. A sandwich was then developed between dopamine–albumin and 4 mercapto-pyridine SERS tag. This interaction was further analyzed by SERS with limit of detection around 0.2 mg/L [53].

A fluorescent biosensor dependent on the estimation of pH and urea in urine samples was also fabricated in the form of POC. The biosensor consists of fluorescein iso-thiocyanate dextran (FD)/FD-urease encapsulated alginate microcarriers as a ratio or single fluorometric biosensors. The radiometric sensor was developed by layer-by-layer (LBL) self-assembly of polystyrene sulfonate and polystyrene sulfonate with RuBpy over (FD)/FD-urease encapsulated alginate microcarriers. The presence of FD and RuBpy functioned as the indicator and reference fluorophores, respectively. The sensitivity of the developed biosensor was found to be pH units of 6–8 and urea within 0-50 mM [54]. Furthermore, Yang et al. have fabricated self-

implantable electronics-skin for *in situ* body fluid analyzer, which works on the principle of enzymatic reaction coupling of ZnO nanowires array. It has been demonstrated the analysis of urea/uric ratio in the body fluids. The developed biosensors convert the mechanical energy of the body into a piezoelectric impulse, which can be detected as a piezoelectric signal indicating the urea/uric acid concentration in body fluids [39, 40]. Further advancement in the simultaneous detection of urea and creatinine was achieved using Kretschmann-based surface plasma resonance. In a study by Menon et al., a biosensor based on the Kretschmann-based surface plasma resonance principle was developed for the detection of urea and creatinine levels up to 50–800 mM and 10–200 mM, respectively. Kretschmann-based surface plasma resonance involves a confined electromagnetic wave of surface plasmon polariton to propagate in the nearby region of dielectric metal interface. The illumination of polarized light on the metal surface excites the surface plasmon waves at the metal dielectric interface. Further, the energy from the incident light transfers to the surface plasmon and causes a sharp dip in the SPR response curve [55]. Similarly, the detection of urea can be made using a smartphone-based RGB profiling principle. Soni et al. have fabricated a sensor having co-immobilization of urease and pH indicator on a filter paper that changes the color upon interaction with salivary urea. The change in color correlates with the urea concentration that can be estimated using RGB coloring in the smartphone. The fabricated biosensor is capable to detect urea with LOD up to 10.4 mg/dL [56].

Multiwall carbon nanotubes paste (MWCNT)-TiO_2 and inulin bionanocomposite based biosensor was also developed for the detection of creatinine. The presence of TiO_2 has shown a significant involvement in the detection of creatinine. Ti^{+4} interacts with the hydroxyl group (–OH) group of inulin on one side and amino (–NH_2) group of creatinine on another side, thereby helping in the detection of creatinine. Also, TiO_2 stabilizes the hydroxylamine formed by the oxidation of creatinine on the electrochemical surface. The fabricated biosensor can detect up to 60 nM of creatinine using differential pulse voltammetry [57]. Furthermore, Dasgupta et al. have detected serum creatinine through ferric chloride using differential pulse voltammetry. The creatinine present in the sample is made to interact with $FeCl_3$, which leads to a decrease in the current signal due to the low availability of free $FeCl_3$. The reduction in the current signal is inversely correlated with the creatinine level [58]. The presence of creatininase, creatinase, and sarcosine oxidase nanoparticles on the glassy carbon electrode was also able to detect the presence of creatinine in human serum of healthy and renal dysfunction using cyclic voltammetry. The creatinine level of 0.01μM to 12μM was detected [24]. Similarly, Yadav et al. have fabricated a biosensor using creatininase, creatinase, and sarcosine oxidase mobilized on iron oxide nanoparticles that were co-immobilized on chitosan grafted polyaniline film. The developed film was further electrodeposited on a platinum wire through glutaraldehyde coupling. The developed biosensor was able to detect even 1μM of creatinine in human urine samples within 2 s time frame [59]. The sensitivity of the developed biosensor was further improved by using zinc oxide nanoparticles biosensor, instead of iron oxide, and has demonstrated the creatinine detection limit up to 0.5μMwithin 10 s [60, 61]. Further, to improve the

sensitivity of detection and long term storage stability, all the three enzymes were immobilized on a gold electrode and found an improvement in the detection limit up to 0.1μM of creatinine [62]. Also, when these enzymes were immobilized on the carboxylated MWCNT (multi-walled carbon nanotube)/polyaniline nanocomposite deposited on the platinum electrode, they have demonstrated the detection of creatinine in human sera up to 0.1μM using EIS [60, 61]. Biosensors based on the potentiometric determination of creatinine in urine have been explored for the detection of kidney biomarkers to enhance the sensitivity of the POC devices. The detection is based on an ionophore (Calix (4) pyrrole), which strongly interacts with creatinine. The developed sensor can detect creatinine up to $10^{-6.2}$M [63]. Raman spectroscopy-based creatinine detection has also led to the detection of 1.45 mg/L of the analyte in the human urine. Such detection is based upon agglomeration assay, where gold based nanoparticles interact with the creatinine present in human urine and form agglomerates, which is then analyzed using Raman spectrophotometer [64]. Besides this, the detection of creatinine can also be done by the interaction with hydrogen peroxide. The reaction of creatinine with H_2O_2 in the presence of cobalt (Co^{2+}) generates an unstable tetrahedral spirodioxetane intermediate, which further decomposes into an excited-state species with the elimination of CO_2. It has shown the detection of 7.2×10^{-8} mol/L of creatinine in urine samples [65]. Thus, various techniques employed to detect various renal biomarkers are constantly increasing the sensitivity of POC with lesser time. The sensitivity of various diagnostic technique principles as discussed in Table 7.3 helps to detect the smallest amount of analyte in the samples. However, if we compare and analyze the most frequently and reliable method for detection of these renal biomarkers, the amperometric based biosensor is more predominantly explored in recent time (Fig. 7.5). However, based on the gathered literature, it reflects that surface plasma resonance, Raman spectroscopy, and chemiluminescence have also been much capable of detecting the biomarkers, even in lower amount up to pictogram. Thus, in future, we can vision to have a large number of biosensors based on these novel techniques, which will entirely depend on the miniaturization of detection system for the development of POC.

.

7.5 Conclusion

Renal disease is a progressive disorder, which requires timely diagnosis to prevent chronic kidney failure. In that perspective, POC devices provides the advantage of a faster and reliable diagnosis required clinically. These devices are available from a benchtop system to smartwatch dimensions and type. Recent advancement in POC devices shows that amperometric and chemiluminescence based principles are most employed, which also provides required sensitivity for the detection of renal based biomarker analyte. However, other techniques like surface-enhanced Raman spectroscopy and surface-enhanced plasma resonance are more sensitive for the detection of an analyte. Thus, in future POC devices based on these principles can hold an edge over the existing technology.

Table 7.3 New principles of detection for kidney biomarkers

Biomarker detected	Principle of detection	Limit of detection	References
Cystatin C	Amperometric	0.58 ng/L	[34]
	Amperometric	0.03 ng/L	[35]
	Surface-enhanced Raman spectroscopy	1 pM	[36]
	Amperometric	62.5 nM	[36]
Retinol-binding protein 4	Chemical luminescence	0.001–2 ng/mL	[37]
	Enhanced chemical luminescence	78-5000 ng/mL	[38]
NGAL	Photoelectrochemical	0.6 pg/mL	[43]
	Amperometric	21.1 ng/mL	[44]
	Potentiometric	2.8 pg/mL	[45]
		1 ng/ml	[46]
KIM-1	Enhanced chemical luminescence	16.7 fg/mL	[39, 40]
Albumin	Amperometric	3-300μg/ml	[43]
	Surface plasma resonance	0.7 pM	[47]
		4μg/ml	[48]
		1 ng/ ml	[49]
	Chronoamperometric	9.7μg/ml	[50]
	Amperometric	25 ng/ml	[51]
	Aggregation-induced emission nanomaterials bioprobe	30-100 mg/dL	[52]
	Surface-enhanced Raman spectrophotometer	0.2 mg/L	[53]
Urea	Fluorescence	0-50 mM	[54]
	Piezo-enzymatic reaction	2.5-80 mM	[39, 40]
	RGB profiling	10.4 mg/dL	[56]
Urea and creatinine	Surface plasma resonance	50–800 mM for urea samples and 10–200 mM for creatinine samples.	[55]
Creatinine	Amperometric	60 nM	[57]
		0.2-5 mg/dL	[58]
		0.01μM to 12μM	[24]
		1μM	[59]
		0.5μM	[60, 61]
		0.1μM	[62]
		0.1μM	[60, 61]
	Potentiometric	$10^{-6.2}$M	[63]
	Raman spectroscopy	1.45 mg/L	[64]
	Chemiluminescence	7.2×10^{-8} Mol/L	[65]

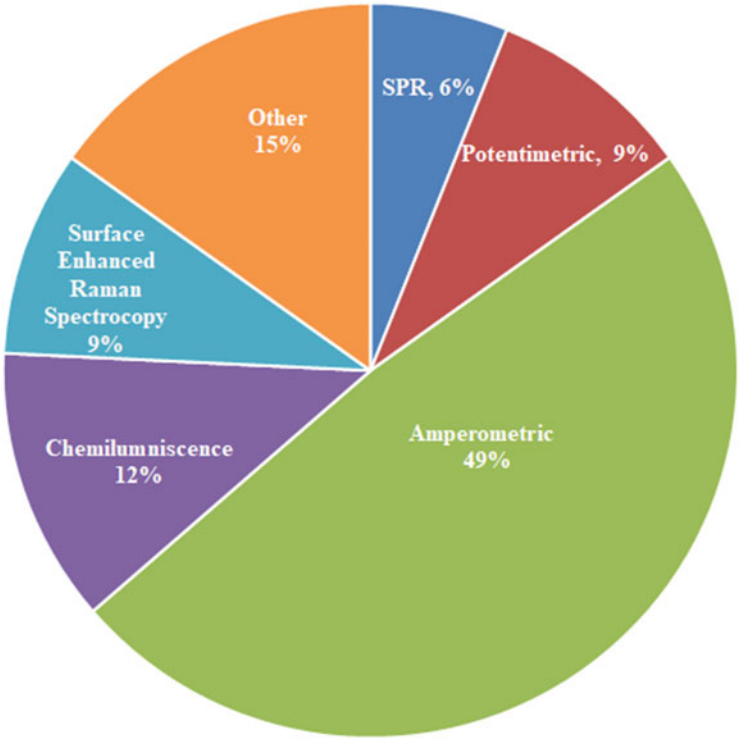

Fig. 7.5 Graph showing the percentage of most commonly reported principles for detection for various renal biomarkers

Acknowledgments The authors would like to acknowledge the Department of Pharmaceuticals, Ministry of Chemical and Fertilizers, Government of India for providing financial support.

References

1. Kosack, C. S., de Kieviet, W., Bayrak, K., Milovic, A., & Page, A. L. (2015). Evaluation of the Nova stat sensor® Xpress TM creatinine point-of-care handheld analyzer. *PLoS One, 10*(4), e0122433.
2. Bikbov, B., Purcell, C. A., Levey, A. S., Smith, M., Abdoli, A., Abebe, M., Adebayo, O. M., Afarideh, M., Agarwal, S. K., Agudelo-Botero, M., & Ahmadian, E. (2020). Global, regional, and national burden of chronic kidney disease, 1990–2017: A systematic analysis for the global burden of disease study 2017. *Lancet, 395*(10225), 709–733.
3. Levey, A. S., & Coresh, J. (2012). Chronic kidney disease. *Lancet, 379*(9811), 165–180.
4. Varma, P. (2015). Prevalence of chronic kidney disease in India-where are we heading? *Indian Journal of Nephrology, 25*(3), 133.
5. Stats, F. (2017). *National chronic kidney disease fact sheet*

6. Carney, E. F. (2020). The impact of chronic kidney disease on global health. *Nature Reviews. Nephrology, 16*(5), 251–251.
7. Veerappan, I., & Abraham, G. (2013). *Chronic kidney disease: Current status, challenges and management in India*. Ch*,* 130, 593-597
8. Hollis, E., Shehata, M., Khalifa, F., Abou El-Ghar, M., El-Diasty, T., & El-Baz, A. (2017). Towards non-invasive diagnostic techniques for early detection of acute renal transplant rejection: A review. *The Egyptian Journal of Radiology and Nuclear Medicine, 48*(1), 257–269.
9. Califf, R. M. (2018). Biomarker definitions and their applications. *Experimental Biology and Medicine, 243*(3), 213–221.
10. Bennett, M. R., & Devarajan, P. (2011). Characteristics of an ideal biomarker of kidney diseases. In *Biomarkers of kidney disease* (pp. 1–24). Elsevier.
11. Makris, K., & Spanou, L. (2016). Acute kidney injury: Definition, pathophysiology and clinical phenotypes. *The Clinical Biochemist Reviews, 37*(2), 85.
12. Rysz, J., Gluba-Brzózka, A., Franczyk, B., Jabłonowski, Z., & Ciałkowska-Rysz, A. (2017). Novel biomarkers in the diagnosis of chronic kidney disease and the prediction of its outcome. *International Journal of Molecular Sciences, 18*(8), 1702.
13. Vaidya, V. S., Ferguson, M. A., & Bonventre, J. V. (2008). Biomarkers of acute kidney injury. *Annual Review of Pharmacology and Toxicology, 48*, 463–493.
14. Sacks, D. B., Arnold, M., Bakris, G. L., Bruns, D. E., Horvath, A. R., Kirkman, M. S., Lernmark, A., Metzger, B. E., & Nathan, D. M. (2011). Guidelines and recommendations for laboratory analysis in the diagnosis and management of diabetes mellitus. *Clinical Chemistry, 57*(6), e1–e47.
15. Heerspink, H. J. L., Witte, E. C., Bakker, S. J., De Jong, P. E., De Zeeuw, D., & Gansevoort, R. T. (2008). Screening and monitoring for albuminuria: The performance of the Hemo Cue point-of-care system. *Kidney International, 74*(3), 377–383.
16. Omoruyi, F. O., Mustafa, G. M., Okorodudu, A. O., & Petersen, J. R. (2012). Evaluation of the performance of urine albumin, creatinine and albumin–creatinine ratio assay on two POC analyzers relative to a central laboratory method. *Clinica Chimica Acta, 413*(5-6), 625–629.
17. Sarafidis, P. A., Riehle, J., Bogojevic, Z., Basta, E., Chugh, A., & Bakris, G. L. (2008). A comparative evaluation of various methods for microalbuminuria screening. *American Journal of Nephrology, 28*(2), 324–329.
18. Martin, H. (2011). Laboratory measurement of urine albumin and urine total protein in screening for proteinuria in chronic kidney disease. *The Clinical Biochemist Reviews, 32*(2), 97.
19. Miller, W. G., Bruns, D. E., Hortin, G. L., Sandberg, S., Aakre, K. M., McQueen, M. J., Itoh, Y., Lieske, J. C., Seccombe, D. W., Jones, G., & Bunk, D. M. (2009). Current issues in measurement and reporting of urinary albumin excretion. *Clinical Chemistry, 55*(1), 24–38.
20. Joffe, M., Hsu, C.-Y., Feldman, H. I., Weir, M., Landis, J., & Hamm, L. L. (2010). Variability of creatinine measurements in clinical laboratories: Results from the CRIC study. *American Journal of Nephrology, 31*(5), 426–434.
21. Killard, A. J., & Smyth, M. R. (2000). Creatinine biosensors: Principles and designs. *Trends in Biotechnology, 18*(10), 433–437.
22. Cánovas, R., Cuartero, M., & Crespo, G. A. (2019). Modern creatinine (bio) sensing: Challenges of point-of-care platforms. *Biosensors & Bioelectronics, 130*, 110–124.
23. Dal Dosso, F., Decrop, D., Pérez-Ruiz, E., Daems, D., Agten, H., Al-Ghezi, O., Bollen, O., Breukers, J., De Rop, F., Katsafadou, M., & Lepoudre, J. (2018). Creasensor: SIMPLE technology for creatinine detection in plasma. *Analytica Chimica Acta, 1000*, 191–198.
24. Kumar, P., Jaiwal, R., & Pundir, C. (2017). An improved amperometric creatinine biosensor based on nanoparticles of creatininase, creatinase and sarcosine oxidase. *Analytical Biochemistry, 537*, 41–49.
25. Tseng, C.-C., Yang, R.-J., Ju, W.-J., & Fu, L.-M. (2018). Microfluidic paper-based platform for whole blood creatinine detection. *Chemical Engineering Journal, 348*, 117–124.
26. van der Heijden, C., Roosens, L., Cluckers, H., Van Craenenbroeck, A. H., & Peeters, B. (2019). Analytical and clinical performance of three hand-held point-of-care creatinine

analyzers for renal function measurements prior to contrast-enhanced imaging. *Clinica Chimica Acta, 497*, 13–19.
27. Martin, C. L. (2010). I-stat–combining chemistry and haematology in POC. *The Clinical Biochemist Reviews, 31*(3), 81.
28. Oh, Y., Koo, S. H., & Kwon, G. C. (2016). Evaluation of the i-STAT point-of-care Analyser. *Journal of Laboratory Medicine and Quality Assurance, 38*(4), 225–233.
29. Shephard, M., & Mathew, T. (2016). 11 Pointofcare testing for kidney. *A Practical Guide to Global Point-of-Care Testing*
30. Coca, S., Yalavarthy, R., Concato, J., & Parikh, C. R. (2008). *Biomarkers for the diagnosis and risk stratification of acute kidney injury: A systematic review*. *Kidney International, 73*, 1008–1016.
31. Martinez Lomakin, F., & Tobar, C. (2014). Accuracy of point-of-care serum creatinine devices for detecting patients at risk of contrast-induced nephropathy: A critical overview. *Critical Reviews in Clinical Laboratory Sciences, 51*(6), 332–343.
32. Parikh, C. R. (2009). A point-of-care device for acute kidney injury: A fantastic, futuristic, or frivolous 'measure'? *Kidney International, 76*(1), 8–10.
33. Vaidya, V. S., Ford, G. M., Waikar, S. S., Wang, Y., Clement, M. B., Ramirez, V., Glaab, W. E., Troth, S. P., Sistare, F. D., Prozialeck, W. C., & Edwards, J. R. (2009). A rapid urine test for early detection of kidney injury. *Kidney International, 76*(1), 108–114.
34. Desai, D., Kumar, A., Bose, D., & Datta, M. (2018). Ultrasensitive sensor for detection of early stage chronic kidney disease in human. *Biosensors & Bioelectronics, 105*, 90–94.
35. Trindade, E. K., Silva, B. V., & Dutra, R. F. (2019). A probeless and label-free electrochemical immunosensor for cystatin C detection based on ferrocene functionalized-graphene platform. *Biosensors & Bioelectronics, 138*, 111311.
36. Hassanain, W. A., Izake, E. L., & Ayoko, G. A. (2018). Spectroelectrochemical nanosensor for the determination of cystatin C in human blood. *Analytical Chemistry, 90*(18), 10843–10850.
37. Torabi, R., & Ghourchian, H. (2020). Ultrasensitive nano-aptasensor for monitoring retinol binding protein 4 as a biomarker for diabetes prognosis at early stages. *Scientific Reports, 10*(1), 1–10.
38. Wu, B., Hu, C., Hu, X., Cao, H., Huang, C., Shen, H., & Jia, N. (2013). Sensitive ECL immunosensor for detection of retinol-binding protein based on double-assisted signal amplification strategy of multiwalled carbon nanotubes and Ru (bpy) 32+ doped mesoporous silica nanospheres. *Biosensors & Bioelectronics, 50*, 300–304.
39. Yang, H., Wang, H., Xiong, C., Chai, Y., & Yuan, R. (2018a). Highly sensitive electrochemiluminescence immunosensor based on ABEI/H2O2 system with PFO dots as enhancer for detection of kidney injury molecule-1. *Biosensors & Bioelectronics, 116*, 16–22.
40. Yang, W., Han, W., Gao, H., Zhang, L., Wang, S., Xing, L., Zhang, Y., & Xue, X. (2018b). Self-powered implantable electronic-skin for in situ analysis of urea/uric-acid in body fluids and the potential applications in real-time kidney-disease diagnosis. *Nanoscale, 10*(4), 2099–2107.
41. Shaikh, M. O., Srikanth, B., Zhu, P.-Y., & Chuang, C.-H. (2019a). Impedimetric Immunosensor utilizing polyaniline/gold nanocomposite-modified screen-printed electrodes for early detection of chronic kidney disease. *Sensors, 19*(18), 3990.
42. Shaikh, M. O., Zhu, P.-Y., Wang, C.-C., Du, Y.-C., & Chuang, C.-H. (2019b). Electrochemical immunosensor utilizing electrodeposited au nanocrystals and dielectrophoretically trapped PS/ag/ab-HSA nanoprobes for detection of microalbuminuria at point of care. *Biosensors & Bioelectronics, 126*, 572–580.
43. Li, H., Mu, Y., Yan, J., Cui, D., Ou, W., Wan, Y., & Liu, S. (2015). Label-free photoelectrochemical immunosensor for neutrophil gelatinase-associated lipocalin based on the use of nanobodies. *Analytical Chemistry, 87*(3), 2007–2015.
44. Yukird, J., Wongtangprasert, T., Rangkupan, R., Chailapakul, O., Pisitkun, T., & Rodthongkum, N. (2017). Label-free immunosensor based on graphene/polyaniline nanocomposite for neutrophil gelatinase-associated lipocalin detection. *Biosensors & Bioelectronics, 87*, 249–255.

45. Zhang, F., Zhong, H., Lin, Y., Chen, M., Wang, Q., Lin, Y., & Huang, J. (2018). A nanohybrid composed of Prussian blue and graphitic C 3 N 4 nanosheets as the signal-generating tag in an enzyme-free electrochemical immunoassay for the neutrophil gelatinase-associated lipocalin. *Microchimica Acta, 185*(7), 327.
46. Kannan, P., Tiong, H. Y., & Kim, D.-H. (2012). Highly sensitive electrochemical determination of neutrophil gelatinase-associated lipocalin for acute kidney injury. *Biosensors & Bioelectronics, 31*(1), 32–36.
47. Esentürk, M. K., Akgönüllü, S., Yılmaz, F., & Denizli, A. (2019). Molecularly imprinted based surface plasmon resonance nanosensors for microalbumin detection. *Journal of Biomaterials Science. Polymer Edition, 30*(8), 646–661.
48. Liu, J.-T., Lin, P.-S., Hsin, Y.-M., Tsai, J.-Z., & Chen, W.-Y. (2011). Surface plasmon resonance biosensor for microalbumin detection. *Journal of the Taiwan Institute of Chemical Engineers, 42*(5), 696–700.
49. Lai, T., Hou, Q., Yang, H., Luo, X., & Xi, M. (2010). Clinical application of a novel sliver nanoparticles biosensor based on localized surface plasmon resonance for detecting the microalbuminuria. *Acta Biochimica et Biophysica Sinica, 42*(11), 787–792.
50. Tsai, J.-Z., Chen, C.-J., Settu, K., Lin, Y.-F., Chen, C.-L., & Liu, J.-T. (2016). Screen-printed carbon electrode-based electrochemical immunosensor for rapid detection of microalbuminuria. *Biosensors & Bioelectronics, 77*, 1175–1182.
51. Omidfar, K., Dehdast, A., Zarei, H., Sourkohi, B. K., & Larijani, B. (2011). Development of urinary albumin immunosensor based on colloidal AuNP and PVA. *Biosensors & Bioelectronics, 26*(10), 4177–4183.
52. Akraa, S., Tam, A. P. T., Shen, H., Tang, Y., Tang, B. Z., Li, J., & Walker, S. (2018). A smartphone-based point-of-care quantitative urinalysis device for chronic kidney disease patients. *Journal of Network and Computer Applications, 115*, 59–69.
53. Huang, Z., Zhang, R., Chen, H., Weng, W., Lin, Q., Deng, D., Li, Z., & Kong, J. (2019). Sensitive polydopamine bi-functionalized SERS immunoassay for microalbuminuria detection. *Biosensors & Bioelectronics, 142*, 111542.
54. Chaudhari, R., Joshi, A., & Srivastava, R. (2017). pH and urea estimation in urine samples using single fluorophore and ratiometric fluorescent biosensors. *Scientific Reports, 7*(1), 1–9.
55. Menon, P. S., Said, F. A., Mei, G. S., Berhanuddin, D. D., Umar, A. A., Shaari, S., & Majlis, B. Y. (2018). Urea and creatinine detection on nano-laminated gold thin film using Kretschmann-based surface plasmon resonance biosensor. *PLoS One, 13*(7), e0201228.
56. Soni, A., Surana, R. K., & Jha, S. K. (2018). Smartphone based optical biosensor for the detection of urea in saliva. *Sensors and Actuators B: Chemical, 269*, 346–353.
57. Kalaivani, G. J., & Suja, S. (2019). Enzyme-less sensing of the kidney dysfunction biomarker creatinine using an inulin based bio-nanocomposite. *New Journal of Chemistry, 43*(15), 5914–5924.
58. Dasgupta, P., Kumar, V., Krishnaswamy, P., & Bhat, N. (2018). Development of biosensor for detection of serum creatinine. *CSI Transactions on ICT, 6*(1), 5–10.
59. Yadav, S., Devi, R., Bhar, P., Singhla, S., & Pundir, C. (2012). Immobilization of creatininase, creatinase and sarcosine oxidase on iron oxide nanoparticles/chitosan-g-polyaniline modified Pt electrode for detection of creatinine. *Enzyme and Microbial Technology, 50*(4-5), 247–254.
60. Yadav, S., Devi, R., Kumar, A., & Pundir, C. (2011a). Tri-enzyme functionalized ZnO-NPs/CHIT/c-MWCNT/PANI composite film for amperometric determination of creatinine. *Biosensors & Bioelectronics, 28*(1), 64–70.
61. Yadav, S., Kumar, A., & Pundir, C. (2011b). Amperometric creatinine biosensor based on covalently coimmobilized enzymes onto carboxylated multiwalled carbon nanotubes/polyaniline composite film. *Analytical Biochemistry, 419*(2), 277–283.

62. Kumar, P., Kamboj, M., Jaiwal, R., & Pundir, C. (2019). Fabrication of an improved amperometric creatinine biosensor based on enzymes nanoparticles bound to Au electrode. *Biomarkers, 24*(8), 739–749.
63. Guinovart, T., Hernández-Alonso, D., Adriaenssens, L., Blondeau, P., Rius, F. X., Ballester, P., & Andrade, F. J. (2017). Characterization of a new ionophore-based ion-selective electrode for the potentiometric determination of creatinine in urine. *Biosensors & Bioelectronics, 87*, 587–592.
64. Zhu, W., Wen, B. Y., Jie, L. J., Tian, X. D., Yang, Z. L., Radjenovic, P. M., Luo, S. Y., Tian, Z. Q., & Li, J. F. (2020). Rapid and low-cost quantitative detection of creatinine in human urine with a portable Raman spectrometer. *Biosensors & Bioelectronics, 154*, 112067.
65. Hanif, S., John, P., Gao, W., Saqib, M., Qi, L., & Xu, G. (2016). Chemiluminescence of creatinine/H2O2/Co2+ and its application for selective creatinine detection. *Biosensors & Bioelectronics, 75*, 347–351.

Chapter 8
From Natural to Artificial Biorecognition Elements: From Antibodies to Molecularly Imprinted Polymers

Jaroslava Bezdekova, Tomas Rypar, Marcela Vlcnovska, Marketa Vaculovicova, and Mirek Macka

8.1 Introduction

The observation of nature that surrounds us and the effort to simplify everyday tasks led hand in hand to the discovery of many inventions and novel technologies, many of which are based on natural principles. But why should they be limited only to objects of a macroscopic world that can be seen by the naked eye? With the progress in science and discoveries of processes taking place in living cells, people started to be interested how life works. Consequently, they realized that life is based on specific interactions among cells and molecules, which exhibit some kind of molecular complementarity. They found out that molecular recognition is crucial in a number of processes, such as: (1) cell recognition where the protein-based surface

J. Bezdekova · M. Vaculovicova
Department of Chemistry and Biochemistry, Mendel University in Brno, CZ, Brno, Czech Republic

Central European Institute of Technology, Brno University of Technology, Brno, Czech Republic

T. Rypar · M. Vlcnovska
Department of Chemistry and Biochemistry, Mendel University in Brno, CZ, Brno, Czech Republic

M. Macka (✉)
Department of Chemistry and Biochemistry, Mendel University in Brno, CZ, Brno, Czech Republic

Central European Institute of Technology, Brno University of Technology, Brno, Czech Republic

School of Natural Sciences and Australian Centre for Research on Separation Science (ACROSS), University of Tasmania, Hobart, Australia
e-mail: Miroslav.Macka@ceitec.vutbr.cz

V. Borse et al. (eds.), *BioSensing, Theranostics, and Medical Devices*,
https://doi.org/10.1007/978-981-16-2782-8_8

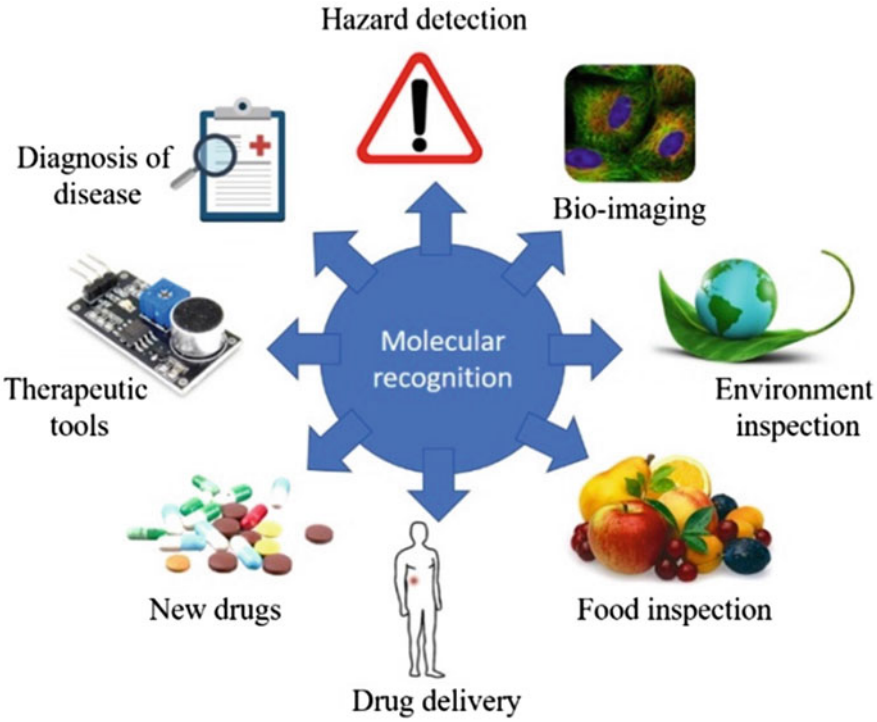

Fig. 8.1 Schematic overview of areas of applications of molecular recognition

receptors are able to recognize and respond to external stimuli; (2) catalytic activity of enzymes, which recognize substrate and enable to implementation of a wide range of reactions; (3) defensive ability of antibodies that are able to recognize antigens and trigger various protective processes; (4) cell division where specific proteins are able to recognize certain part of DNA and initiated replication; (5) cell differentiation which is based on recognition of stimuli leading to changes in gene expression and finally to specialized cells. So, why should not we get inspired by biological processes occurring in living cells and try to apply them in technologies that make our life easier?

The role of molecular recognition between biomolecules was first described as a "lock-and-key" mechanism by E. Fisher in 1894. Nowadays, molecular recognition draws a lot of attention in many scientific disciplines (e.g., efficient purification, analytical methods, imaging and clinical applications, etc.). Moreover, understanding and use of molecular recognition lead not only to the creation of novel assays and sensors but also to the development of new materials for drug delivery and treatment. The overview of scientific fields in which molecular recognition is important is schematically shown in Fig. 8.1.

Initially, biological macromolecules (such as antibodies or aptamers) have been widely used in molecular recognition-based technology. However, their limitations,

such as high production costs and low stability, lead to the development of other completely novel recognition components that are able to overcome the limitations of biological macromolecules.

In this chapter, the molecular elements (specifically antibodies, aptamers, and molecularly imprinted polymers) that have an enormous potential to be used as antibody alternatives in chemistry and medicine are discussed in detail.

8.2 Development and Production of Recognition Elements

8.2.1 Antibodies

Antibodies (Abs) are Y-shaped glycoprotein molecules formed by two heavy and two light polypeptide chains. They are produced by B-cells to recognize and neutralize antigens such as a variety of pathogens [1]. Abs were discovered in 1890 by Emil von Behring along with K. Shibasaburo, who for the first time described the presence of "neutralizing substances" in the blood, which could counter infections [2]. At the beginning of the twentieth century, antibodies were labeled by Paul Ehrlich as "magic bullets" that selectively target an area of disease in the human organism, and he predicted their application in medical therapy [3].

However, the first experiments focused on medical therapies that were performed with **polyclonal antibodies** (PAbs) were not as effective as predicted [4]. The majority of antigens have a highly sophisticated structure and contain several epitopes that can be recognized by different lymphocytes. As each lymphocyte produces an antibody against a different epitope, the resulting antibody response was polyclonal. This means that obtained PAbs are a mixture of heterogeneous antibodies, which are able to recognize and interact with a variety of epitopes within a single antigen. Because of low specificity and significant cross-reactivity, PAbs are not suitable for antibody-based therapy in medicine. Nevertheless, PAbs are applicable in the detection of unknown antigens, so, for example, they are utilized as primary antibodies in many immunoassays (incl. ELISA, Western blotting, etc.) or are useful in immunohistochemistry [5].

In 1975, Kohler and Milstein demonstrated a process of production of **monoclonal antibodies** (MAbs) [6]. MAbs are generated by a single B-lymphocyte clone, and thus they have a monovalent affinity and are able to recognize only one specific and always identical epitope (small antigen part) of an antigen [5]. The production of MAbs is based on an administration of the chosen antigen into an appropriate organism (e.g., mouse). After the development of the immune response within the animal, B-lymphocytes are extracted from the spleen. Subsequently, the isolated B-cells are fused with a myeloma cell line, resulting in the creation of immortalized B-cell/myeloma hybridomas. The created hybridomas have properties of both the fused cells; they are capable of fast continuous growth in a culture like a myeloma cell line and also of production of Abs as B-cells. Finally, hybridomas producing only one clone of antibodies (MAbs) are separated from the culture and used for the

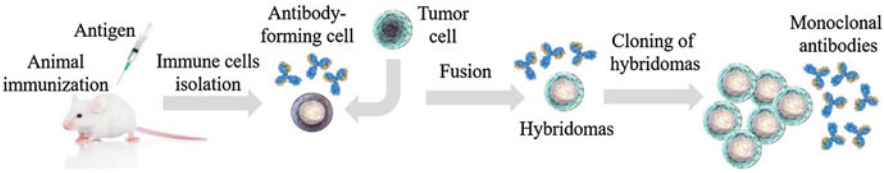

Fig. 8.2 Scheme of the procedure leading to the preparation of monoclonal antibodies

production of chosen MAbs [7]. For easier understanding of the process, preparation of MAbs is schematically shown in Fig. 8.2. Unfortunately, the main drawback of the hybridoma technology is the risk that the hybridoma cells lose the ability to produce the desired antibodies over time, or the antibodies may undergo unwanted changes, which may affect their functionality [8].

It was widely believed that these MAbs would be ideal reagents for imaging, drug delivery, and/or therapy. However, due to their animal origin, these MAbs were recognized as alien and eliminated by the patient's immune system when they were used as therapeutics. Notwithstanding, MAbs enable very selective or specific separation and identification of a wide range of different targets, and they are indispensable tools in many analytical approaches such as ELISA, Western blot, affinity chromatography, antibody-based sensors, and so on [9].

Recombinant phage antibodies (RAbs) are small proteins that consist of domains with variable heavy and light chains, and they may be connected via a flexible peptide chain. These antibody fragments retain the ability to recognize and bind the target epitope of an antigen. A major breakthrough in the field of RAbs was reported in 1990 by McCafferty et al., who presented the display of protein fragments on the surface of a filamentous bacteriophage. The filamentous phage is a virus-like particle that can infect bacteria (commonly *Escherichia coli*). Upon infection, the bacterial cells start to produce the phage particles with antibody fragments on their surface and secrete them into the culture media. RAbs produced by this way have several benefits compared to traditional MAbs (e.g., small penetrable size, high standard of specificity, low immunogenicity, and rapid production) [10]. Currently, RAbs are utilized in a number of clinical trials for diagnostic as well as therapeutic purposes [11]. Characterized RAbs can be used as chemicals to replace standard MAbs used for flow cytometry or immunohistochemistry. Thanks to their low immunogenicity, they are also applicable in cell targeting and imaging, as well as in vaccine development [12]. However, it is necessary to realize that in the case of RAbs there is only one antigen binding site (in comparison with two sites in the case of native antibodies), and therefore the affinity to antigen must be very high to avoid losses during the purification process [10]. Another limitation due to the small size of antibody fragments rests in their shorter in vivo half-lives, and therefore a more frequent drug dosing is necessary, which can increase the risks of undesirable effects.

The high immunogenicity of MAbs was one of the problems for their utilization in clinical use. However, progress in gene engineering enabled the partial

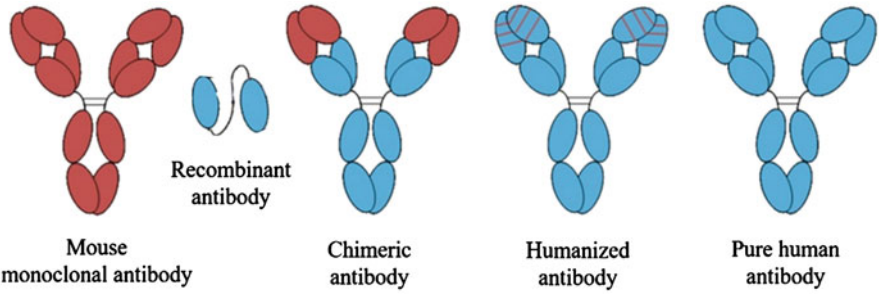

Fig. 8.3 Differences between a variety of types of antibodies. Scheme available at [16]

replacement of immunogenic sites in mouse MAb with the appropriate fragments of human antibodies. In 1984, chimeric Abs were developed by Morisson et al. to overcome the immunogenicity of MAbs [13]. Chimerization permits the connection of the whole antigen-specific domain of a mouse antibody with constant domains of a human antibody. These **chimeric Abs** are recognized as of own body and therefore are not eliminated by the immune system, and thus can be used in medical therapy [14]. Later, **humanized MAbs** were produced by gene engineering: here, only sites enabling selective interaction with antigen are of mouse origin. And finally, **pure human MAbs** began to be manufactured using transgenic mice producing human immunoglobulins. The approach takes advantage of the ability to replace mouse antibody gene locuses with their corresponding human genome sites [15]. Differences between the above-mentioned Abs are shown in Fig. 8.3.

The discovery of chimerization and humanization of antibodies led to a new era of antibody-based therapeutics. It has been expected that by 2020 approximately 70 MAbs products will be commercialized for therapeutic purposes, mainly for therapy of cancer and immune disorders [17] based on the fact that a total of 61 MAbs were approved by the end of 2017, which demonstrates the enormous impact of this technology.

The first MAbs-based therapeutic (Orthoclone OKT3) was approved by the Food and Drug Administration (FDA) in 1986 [18]. Since then, a wide range of other antibodies and antibody derivatives have been developed and approved for use, and new ones are still being developed. An overview of Abs-based drugs approved by FDA is presented in Table 8.1.

Moreover, George P. Smith and Gregory P. Winter were awarded Nobel Prize in Chemistry in 2018 for the development of their contributions to antibody therapy by utilization of Phage display technology [19, 20]. For a very detailed overview, readers should refer to [21].

Nevertheless, MAb-based treatments still face several obstacles that limit their widespread application as therapeutics. The main limitation is given by the high production costs associated with the need of mammalian cell cultures for the fabrication of MAbs, followed by a cleaning process under the Good Manufacturing Practice regime. This process is very time-consuming and expensive, which limits

Table 8.1 The overview of Abs-based drugs approved by FDA or EMA (The European Medicines Agency)

International name	Brand name	Target	Format	Disease	EMA approval	FDA approval
Sacituzumab govitecan	TRODELVY	TROP-2	Humanized IgG1	Breast cancer	NA	2020
Isatuximab	Sarclisa	CD38	Chimeric IgG1	Multiple myeloma	NA	2020
Eptinezumab	VYEPTI	CGRP	Humanized IgG1	Migraine prevention	NA	2020
Teprotumumab	Tepezza	IGF-1R	Human IgG1	Thyroid eye disease	NA	2020
[fam-]trastuzumab deruxtecan	Enhertu	HER2	Humanized IgG1	Metastatic breast cancer	NA	2019
Enfortumab vedotin	Padcev	Nectin-4	Human IgG1	Urothelial cancer	NA	2019
Crizanlizumab	Adakveo	CD62	Humanized IgG2	Sickle cell disease	In review	2019
Brolucizumab	Beovu	VEGF-A	Humanized scFv	Neovascular age-related macular degeneration	2020	2019
Romosozumab	Evenity	Sclerostin	Humanized IgG2	Osteoporosis	2019	2019
Polatuzumab vedotin	Polivy	CD79b	Humanized IgG1	Diffuse large B-cell lymphoma	2020	2019
Risankizumab	Skyrizi	IL-23 p19	Humanized IgG1	Plaque psoriasis	2019	2019
Caplacizumab	Cablivi	von Willebrand factor	Humanized nanobody	Acquired thrombotic thrombocytopenic purpura	2018	2019
Moxetumomab pasudotox	Lumoxiti	CD22	Murine IgG1 immunotoxin	Hairy cell leukemia	In review	2018
Emapalumab	Gamifant	IFN	Human IgG1	Primary hemophagocytic lymphohistiocytosis	In review	2018
Ibalizumab	Trogarzo	CD4	Humanized IgG4	HIV infection	2019	2018
Ravulizumab	Ultomiris	C5	Humanized IgG2	Paroxysmal nocturnal hemoglobinuria	2019	2018
Fremanezumab	Ajovy	CGRP	Humanized IgG2	Migraine prevention	2019	2018
Tildrakizumab	Ilumya	IL-23	Humanized IgG1	Plaque psoriasis	2018	2018
Mogamulizumab	Poteligeo	CCR4	Humanized IgG1	Mycosis fungoides or Sézary syndrome	2018	2018

Lanadelumab	Takhzyro	Plasma kallikrein	Human IgG1	Hereditary angioedema attacks	2018	2018
Burosumab	Crysvita	FGF23	Human IgG1	X-linked hypophosphatemia	2018	2018
Galcanezumab	Emgality	CGRP	Humanized IgG4	Migraine prevention	2018	2018
Erenumab	Aimovig	CGRP receptor	Human IgG2	Migraine prevention	2018	2018
Gemtuzumab	Mylotarg	CD33	Humanized IgG4	Acute myeloid leukemia	2018	2017
Durvalumab	IMFINZI	PD-L1	Human IgG1	Bladder cancer	2018	2017
Benralizumab	Fasenra	IL-5R α	Humanized IgG1	Asthma	2018	2017
Ocrelizumab	OCREVUS	CD20	Humanized IgG1	Multiple sclerosis	2018	2017
Emicizumab	Hemlibra	Factor Ixa	Humanized IgG4	Hemophilia A	2018	2017
Avelumab	Bavencio	PD-L1	Human IgG1	Merkel cell carcinoma	2017	2017
Sarilumab	Kevzara	IL-6R	Human IgG1	Rheumatoid arthritis	2017	2017
Guselkumab	TREMFYA	IL-23 p19	Human IgG1	Plaque psoriasis	2017	2017
Inotuzumab	BESPONSA	CD22	Humanized IgG4	Acute lymphoblastic leukemia	2017	2017
Dupilumab	Dupixent	IL-4R α	Human IgG4	Atopic dermatitis	2017	2017
Brodalumab	Siliq	IL-17R	Human IgG2	Plaque psoriasis	2017	2017
Obiltoxaximab	Anthim	*B. anthracis*	Chimeric IgG1	Prevention of inhalational anthrax	In review	2016
Atezolizumab	Tecentriq	PD-L1	Humanized IgG1	Bladder cancer	2017	2016
Bezlotoxumab	Zinplava	*Clostr. difficile* enterotoxin B	Human IgG1	Prevention of *Clostr. difficile* infection recurrence	2017	2016
Olaratumab	Lartruvo	PDGFRα	Human IgG1	Soft tissue sarcoma	2016	2016
Reslizumab	Cinqaero	IL-5	Humanized IgG4	Asthma	2016	2016
Ixekizumab	Taltz	IL-17a	Humanized IgG4	Psoriasis	2016	2016
Elotuzumab	Empliciti	SLAMF7	Humanized IgG1	Multiple myeloma	2016	2015
Daratumumab	Darzalex	CD38	Human IgG1	Multiple myeloma	2016	2015
Alirocumab	Praluent	PCSK9	Human IgG1	High cholesterol	2015	2015
Mepolizumab	Nucala	IL-5	Humanized IgG1	Severe eosinophilic asthma	2015	2015
Secukinumab	Cosentyx	IL-17a	Human IgG1	Psoriasis	2015	2015
Dinutuximab	Unituxin	GD2	Chimeric IgG1	Neuroblastoma	2015	2015

(continued)

Table 8.1 (continued)

International name	Brand name	Target	Format	Disease	EMA approval	FDA approval
Necitumumab	Portrazza	EGFR	Human IgG1	Cell lung cancer	2015	2015
Idarucizumab	Praxbind	Dabigatran	Humanized Fab	Reversal of dabigatran-induced anticoagulation	2015	2015
Evolocumab	Repatha	PCSK9	Human IgG2	High cholesterol	2015	2015
Alemtuzumab	Lemtrada	CD52	Humanized IgG1	Multiple sclerosis	2013	2014
Blinatumomab	Blincyto	CD19, CD3	Murine bispecific tandem scFv	Acute lymphoblastic leukemia	2015	2014
Pembrolizumab	Keytruda	PD1	Humanized IgG4	Melanoma	2015	2014
Nivolumab	Opdivo	PD1	Human IgG4	Melanoma, non-small cell lung cancer	2015	2014
Vedolizumab	Entyvio	α4β7 integrin	Humanized IgG1	Ulcerative colitis, Crohn disease	2014	2014
Ramucirumab	Cyramza	VEGFR2	Human IgG1	Gastric cancer	2014	2014
Siltuximab	Sylvant	IL-6	Chimeric IgG1	Castleman disease	2014	2014
Obinutuzumab	Gazyva	CD20	Humanized IgG1	Chronic lymphocytic leukemia	2014	2013
Raxibacumab	Pending	*B. anthracis*	Human IgG1	Anthrax infection	NA	2012
Ado-trastuzumab	Kadcyla	HER2	Humanized IgG1	Breast cancer	2013	2012
Pertuzumab	Perjeta	HER2	Humanized IgG1	Breast cancer	2013	2012
Brentuximab vedotin	Adcetris	CD30	Chimeric IgG1	Hodgkin lymphoma, systemic anaplastic large cell lymphoma	2012	2011
Ipilimumab	Yervoy	CTLA-4	Human IgG1	Metastatic melanoma	2011	2011
Belimumab	Benlysta	BLyS	Human IgG1	Systemic lupus erythematosus	2011	2011
Denosumab	Prolia	RANK-L	Human IgG2	Bone loss	2010	2010
Tocilizumab	RoActemra	IL-6R	Humanized IgG1	Rheumatoid arthritis	2009	2010
Ofatumumab	Arzerra	CD20	Human IgG1	Chronic lymphocytic leukemia	2010	2009
Golimumab	Simponi	TNF	Human IgG1	Rheumatoid and psoriatic arthritis, ankylosing spondylitis	2009	2009

Canakinumab	Ilaris	IL-1β	Human IgG1	Muckle-Wells syndrome	2009	2009
Ustekinumab	Stelara	IL-12/23	Human IgG1	Psoriasis	2009	2009
Certolizumab pegol	Cimzia	TNF	Humanized Fab	Crohn disease	2009	2008
Eculizumab	Soliris	C5	Humanized IgG2	Paroxysmal nocturnal hemoglobinuria	2007	2007
Ranibizumab	Lucentis	VEGF	Humanized IgG1 Fab	Macular degeneration	2007	2006
Panitumumab	Vectibix	EGFR	Human IgG2	Colorectal cancer	2007	2006
Natalizumab	Tysabri	a4 integrin	Humanized IgG4	Multiple sclerosis	2006	2004
Bevacizumab	Avastin	VEGF	Humanized IgG1	Colorectal cancer	2005	2004
Cetuximab	Erbitux	EGFR	Chimeric IgG1	Colorectal cancer	2004	2004
Omalizumab	Xolair	IgE	Humanized IgG1	Asthma	2005	2003
Ibritumomab	Zevalin	CD20	Murine IgG1	Non-Hodgkin lymphoma	2004	2002
Adalimumab	Humira	TNF	Human IgG1	Rheumatoid arthritis	2003	2002
Trastuzumab	Herceptin	HER2	Humanized IgG1	Breast cancer	2000	1998
Infliximab	Remicade	TNF	Chimeric IgG1	Crohn disease	1999	1998
Palivizumab	Synagis	RSV	Humanized IgG1	Prevention of respiratory syncytial virus infection	1999	1998
Basiliximab	Simulect	IL-2R	Chimeric IgG1	Prevention of kidney transplant rejection	1998	1998
Rituximab	MabThera	CD20	Chimeric IgG1	Non-Hodgkin lymphoma	1998	1997
Abciximab	Reopro	GPIIb/IIIa	Chimeric IgG1 Fab	Prevention of blood clots in angioplasty	1995	1994

Data were obtained from https://www.antibodysociety.org/

the widespread use of this type of medicaments [9]. Moreover, Abs very often suffer from batch-to-batch variations [22].

Other issues are the elimination of mAb therapeutics that can occur in the body and the fact that antibody-drug antibodies (ADAs) can be formed, binding competitively to the active site of the therapeutic MAbs, thus compromising the drug efficacy. Also, the drug pharmacokinetic properties, biological effects, and the toxicity can be unpredictably changed by ADAs [23]. Another issue is a misleading prediction of human response using animals due to the different levels of immunogenicity between animal models and humans [24].

Last but not least, enzymatic degradation may arise. It is generally known that MAbs may undergo enzymatic degradation, which may occur either at the site of the administration or in the bloodstream. Owing to the presence of high concentrations of enzymes in the gastrointestinal tract, oral delivery systems are challenging to develop [24]. Therefore, the means of administration of MAbs drugs is usually the parenteral injection. However, MAbs can still suffer from enzymatic degradation (e.g., by proteases or hydrolases) because they are abundant throughout the body [17].

Despite the high potential of Abs in medical therapy, these limitations lead to efforts to develop some novel recognition elements which will be more stable and less expensive.

8.2.2 APTAMERs

In 1990, two ground-breaking studies were performed simultaneously and independently confirmed that ligands of nucleic acids can selectively interact with virtually any protein. A.D. Ellington and J. W. Szostak isolated those RNA subpopulations from a population of RNA molecules with random sequences that specifically interacted with a variety of organic dyes and named them aptamers [25]. At the same time, C. Tuerk and L. Gold created an RNA chain that was able to selectively bind to T4DNA polymerase and used the term SELEX (Systematic Evolution of Ligands by Exponential Enrichment) for the process of its selection [26].

Aptamers are usually short single-stranded chains of DNA or RNA (50–100 base-long) that are able to bind to protein targets by folding into a three-dimensional conformation [27]. The above-mentioned SELEX is a process that enables the identification of an aptamer selective for a chosen target. The process consists of three main repetitive steps: selection, partitioning, and amplification (see Fig. 8.4). The entire procedure begins with the creation of a large "library" containing a variety of nucleotide sequences, which can theoretically adopt a specific three-dimensional structure.

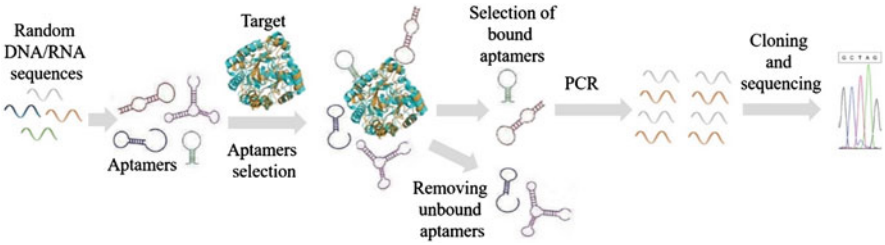

Fig. 8.4 Scheme of a process called SELEX, which ensures the choice of specific aptamers against the desired target

- In the **selection phase**, the nucleotide sequences from the "library" are incubated in the presence of the target for a required period of time. The sequences with weak or no affinity for the target remain unbound in solution, in difference to those with a higher ability to interact with the target that will be attracted to it.
- The **partitioning phase** ensures the physical separation of the aptamer–target complexes from the unreacted components of the mixture.
- In the **amplification phase**, the bound aptamers are released from the target. The captured and purified sequences are amplified by polymerase chain reaction (PCR) to generate a new "library" of aptamers that contains increased amounts of those effectively binding the target.

To reduce the very large number of unique sequences (in the order of trillions) to a small number of unique sequences that are able to selectively interact with the target, the whole process is repeated with a new "library" enriched in each step, repeated ca 5–15 times. The individual aptamers are subsequently extracted and sequenced. Their binding affinity and specificity are also determined [28] (Fig. 8.4).

In 2004, the first aptamer-based medicament was approved by the FDA (Macugen), focusing on the vascular endothelial growth factor and the therapy of age-related macular degeneration [29]. Unfortunately, no other aptamer-based drug has been developed since then, which is likely caused by insufficient knowledge of their structure, target interactions, and pharmacokinetics.

During the last few years, a wide range of experiments were carried out that led to improvements in the stability and efficiency of aptamers. This opens multiple new directions for therapeutic applications of aptamers. In this part of the chapter, we will discuss the benefits and limitations of aptamers, their significance for therapeutic applications, as well as the advances and directions of future research.

Aptamers are characterized by high affinity and excellent specificity toward desired targets [30], and therefore they offer new very attractive prospects in diagnostics [31], sensors [32], (bio)analytical assays [33], and also in medicine, where they have opened novel avenues for the development of therapeutics [34], and targeted drug delivery [35].

In contrast to Abs, they have a number of benefits, such as the possibility of automation and monitoring of the SELEX process that allow to produce specific aptamers with high selectivity and prevent batch-to-batch variability

[36]. Nevertheless, achieving required aptamer properties is challenging due to the short in vivo half-life, risk of immunogenicity, and entrapment in cellular organelles [37].

The first challenge to overcome was the short half-life of aptamers *in vivo*. It was expected that the small size of aptamers will allow to achieve higher aptamer penetration into tumors, in comparison with the structurally larger Abs. However, the majority of aptamers have sizes in the range of 5–30 kDa (the average diameter of aptamers is less than 5 nm), and thus they are susceptible to renal clearance [38]. One possible way to overcome the rapid renal excretion may be an increase of their total size through linkage with some suitable high molecular weight moieties (e.g., polyethylene glycol [39], cholesterol [40, 41], some proteins [42], or nanomaterials [43]).

Another limitation is due to nucleases (enzymes cleaving phosphodiester bonds of oligonucleotides) abundantly present in biological fluids that cause aptamer decay in several minutes [38]. An improvement in the stability of aptamers in serum can be resolved by their chemical modification. For example, locked nucleic acids that contain a 2-O, 4-C methylene bridge can be used. This modification has a high resistance to nucleases [44]. Another possibility is based on the replacement of the -OH group of ribose for amino [45] or -fluoro [46] moiety that can increase the resistance of aptamers.

On the one hand, the above-mentioned modifications protect the aptamers against degradation and extend their in vivo half-life, but, on the other hand, modified aptamer sequences may resemble pathogen-associated molecular patterns and activate the innate immune system, and thus they could cause immunogenicity or toxicity [47]. In some cases (e.g., in cancer treatment), it might be even beneficial because aptamers have a dual effect—they serve as the delivery agents of a chemotherapeutic drug and simultaneously, they re-activate the anti-tumor immunity. However, the risk of undesirable and harmful side effects is increased. Moreover, aptamers can accumulate in some organs (such as in the liver, kidney, or spleen) and might cause toxicity [37]. Therefore, deeper investigations of the correlation between the aptamer structure, the administration route, and adverse effects in vivo are urgently needed.

The most serious impediment in effective aptamer-based treatments is probably due to cellular organelles. The aptamers specific for cell-surface receptors are often endocytosed and trapped in the endo-lysosomal vesicle. For the endosomal escape, a number of approaches can be applied, such as a combination of aptamers with other delivery vehicles (liposomes [35], viruses [48], etc.), or aptamer attachment to a protein part that disrupts the endosome membrane [49]. Unfortunately, these strategies are not applicable for therapeutic aptamers because they might be toxic or immunogenic [37]. Therefore, it is necessary to develop non-toxic molecules enhancing the ability of endosomal escape compatible with the aptamer drug formulation.

Recently, a number of potential aptamers-based drugs that can be used in the treatment of infectious diseases started to appear. Among very promising works are those of application of aptamers as inhibitors of viral nucleic acid replication. So far, a cholesterol-conjugated aptamer able to enter into the cell

Table 8.2 Examples of aptamer-based drugs, which are currently in the phase of clinical trials

Aptamer	Molecular target	Disease	Phase
Blood and heart disease			
ARC1779	Specific inhibitor of Von Willebrand factor	Von Willebrand disease	II
ARC19499	Inhibitor of tissue factor pathway inhibitor	Hemophilia	I
NOX-H94	Inhibitor of hepcidin	Anemia of chronic disease	I
NU172	Inhibitor of thrombin	Heart disease	II
REG1	Inhibition of factor IX in the coagulation cascade	Coronary artery disease	II
Ophthalmology			
ARC1905	Inhibitor of factor C5 of the complement cascade	Age-related macular degeneration	I
E10030	Inhibitor of platelet-derived growth factor	Age-related macular degeneration	II
Cancer treatment			
NOX-A12	Inhibitor of cell-derived factor-1	Multiple myeloma; chronic lymphocytic leukemia	II
AS1411	Inhibitor of nucleolin	Leukemia, myeloid	II

Data were obtained from https://clinicaltrials.gov/

infected by Hepatitis C virus has been developed, and currently, this aptamer is investigated as a promising anti-viral drug [40, 41]. The aptamer inhibited virus RNA replication while not changing the gene expression profiles including genes related to innate immune response. Another promising study in the area of treatment of virus diseases was focused on the inhibition of HIV replication by using aptamers which were able to block viral protein Rev essential to the regulation of HIV protein expression [50].

In recent years, enormous progress has been made in the development of aptamers for anticoagulant, antithrombotic, and prohemostatic indications, and several aptamer-based medicaments are currently in the phase of clinical trials [51]. Another immensely important area of potential aptamer application is that in cancer treatment. So far, a wide range of aptamers capable of targeting different cancer cell biomarkers has been developed and reached the phase of clinical trials [30]. An overview of some selected promising aptamers in clinical trials is summarized in Table 8.2. The large number of aptamers-based medicaments is predicted soon to compete with antibody-based drugs for therapeutic applications.

8.2.3 Molecularly Imprinted Polymers (MIPs)

In 1931, M. V. Polyakov performed an experiment that led to the discovery of novel artificial materials with recognition ability. He found out that polymers prepared in the presence of another molecule were able to recognize and selectively interact with

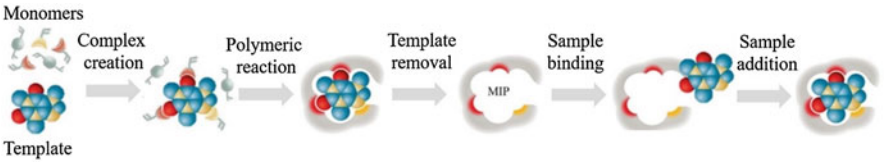

Fig. 8.5 Scheme of preparation and application of MIPs. Information available at [63]

this molecule [52]. It was the beginning of MIPs era. Due to their unique features, MIPs are sometimes dubbed artificial antibodies, enzyme mimic or synthetic receptors. Owing to their excellent physical and chemical stability, tuneable properties, and low production cost, they came to be competitors to commonly used biological macromolecules—antibodies [53].

Initially, the interest in molecular imprinting remained quite low. However, a discovery of non-covalent imprinting by Mosbach et al. in 1984 allowed a significant simplification in the preparation of MIPs, which led to an enormous upswing of this scientific field and exponential growth of publications in this area [54]. During the last decade, the progress in molecular imprinting enabled the development of novel types of diagnostic tools, sensors [55, 56], and assays [57, 58]. In addition, recently, the vast potential of molecular imprinting was discovered in therapeutic use (cell recognition [59], drug delivery [60], and regulation of cell behavior [61], etc.).

Molecular imprinting is a process that includes co-polymerization of functional monomers and cross-linkers in the presence of a template (the imprinted molecule). The functional monomers bind the template predominantly by non-covalent bonds and form a template–monomers complex. After initiation, the polymerization step leads to the creation of a highly cross-linked polymeric net. In the next step, template removal reveals the binding sites complementary to the imprinted molecules in terms of spatial structure as well as chemical availability of functional moieties. The obtained polymer matrix has molecular memory and enables rebinding of the imprinted molecule (analyte) with a very high specificity [62]. The principle of MIP preparation and subsequent application is schematically shown in Fig. 8.5**.**

In spite of the tremendous progress in the technology of imprinted polymers, imprinting of larger structures such as proteins, bacteria, viruses, etc., is still quite a big challenge. The main reason is that in the case of these structures creation of polyclonal MIPs with a broad range of binding sites with different affinities and specificities may occur. This may be caused by difficulties in maintaining the conformation and space orientation of native protein during the polymerization process. Besides, the large size of the imprinted structure causes difficulties in the template removal from the polymerized net, and the large binding sites may have reduced selectivity features because a range of smaller polypeptides can interact with them [64, 65].

In 2000, a completely new strategy termed epitope imprinting was discovered [66]. The epitope imprinting is based on imprinting of a small analyte/template fragment which is characteristic for the chosen large template instead of the

imprinting of the whole template structure [67]. In principle, this approach is very similar to the recognition of antigen by antibody, where the antibody is able to recognize only an epitope (small antigen part) and not the whole antigen structure. Imprinting of epitope in comparison with the whole protein imprinting permits relatively easy removal of the template ensures a uniform production of binding sites (because the small fragments have a less complicated structure and so maintaining their conformation during the polymerization is easier), and the synthesis cost is reduced, especially in the case of expensive protein templates [68]. The main drawback is associated with the identification of appropriate epitopes for the large molecule that requires detailed knowledge of template conformations [69].

However, recently, a novel protocol for protein epitopes identification suitable for molecular imprinting has been reported. The protocol is based on the synthesis of MIP nanoparticles in the presence of a whole target protein. The low concentration of polymeric mixture leads to the formation of MIP particles only around small parts of the protein. Partial proteolysis of the protein causes proteolytic cleavage of parts of the protein that are not protected by the created MIPs. The peptides surrounded by the polymer net are subsequently released and sequenced [70]. In brief, this approach enables the identification of surface protein regions appropriate for recognition by imprinted polymers.

Conventional polymerization approaches (e.g., bulk, emulsion, or suspension polymerization) exploit templates that are dissolved in the polymerization solution. These templates can rotate and freely move in the solution, which leads to the creation of random binding sites that suffer from heterogeneous polyclonal distribution and problematic batch-to-batch reproducibility. However, these drawbacks may be overcome by introducing an approach called solid-phase synthesis [62].

In this approach, the template is linked to a solid support (the most common are glass beads). This ensures its consistent orientation and leads to a decrease in polyclonality of the imprinted sites. Subsequently, the solid supports with covalently bound template molecules are incubated with a mixture of functional monomers, cross-linkers, and initiator, and the polymeric reaction is initiated. The unreacted components of the polymerization mixture and MIPs particles with low affinity are eluted at room temperature; meantime, the high affinity MIP nanoparticles stay bound to the template, and they are eluted in the next step by increasing the temperature. The obtained MIP particles have monoclonal binding sites, and therefore can be applicable to the preparation of commercially available MIPs [71, 72].

In spite of all the benefits that MIPs offer, the number of MIP-based commercial products is largely confined to a handful of products predominantly intended for selective solid-phase extraction and a few sensors. For the commercial application of MIPs, it is necessary to control the fabrication process and optimize it in such a manner that the obtained MIPs have a good batch-to-batch reproducibility, which was initially quite problematic. Therefore, it was necessary to focus on novel tools enabling to overcome bottlenecks in the production and characterization of MIPs-based materials. In 2013, an automated chemical reactor for solid-phase synthesis of MIP NPs in an aqueous environment was developed by the research group of

S. Piletsky [72]. The developed device was able to produce "ready to use" MIP nanoparticles with sub-nanomolar affinity in only 4 hours. Significant advantages of this automated chemical reactor rest in its full automation that enable the reactor to operate for 24 h, which eliminates human error and ensures high batch-to-batch reproducibility [72, 73]. These new advances may be the first step in the spread of commercial MIP-based products.

MIPs as artificial receptors in the field of medical therapy have a number of benefits in comparison with natural biorecognition materials. The major advantages are the possibility of automatized fabrication allowing rapid and low-cost production, batch-to-batch uniformity [72], and fast and homogenous functionalization by different probes providing unique features (e.g., fluorescence, magnetic properties, electric conductivity, etc.) [74]. Another enormous advantage is the possibility to design MIPs tailor made for almost any target from ions and small molecules to larger structures such as proteins by using computational modeling [75]. Their extremely high stability makes MIPs compatible with thermal sterilization and ensures their resistance against enzymatic or pH-dependent degradation, which is also beneficial [76].

Clearly, the potential of MIPs in cell biomedical fields is huge, spanning across many areas such as recognition or regulation of cell behavior. However, so far, the main interest has been in the creation of adsorption or separation materials and sensing tools and the application of MIPs in the therapeutic area was rarely reported. Nevertheless, in the last years, the interest in MIPs has been consistently growing, and the numbers of research publications in the area of MIPs have been increasing. MIPs, as well as various other nanomaterials, have been successfully used in medicine as part of diagnostic devices [77, 78] and sensors [79], drug delivery elements [77, 78], and cell imaging probes [80]. However, it has been found that only MIPs could also be used as medicaments. This means that the huge potential of MIPs in the therapeutic area is still in their infancy. The following part provides an overview of several ground-breaking works focused on the utilization of MIPs as pharmaceuticals, which can change the main areas of their traditional application.

The work published in 2010 by Hoshino and his co-workers completely changed the view of MIPs' utilization and directed many researchers to investigate the potential of MIPs in finding and creating novel medicaments. The authors utilized for the first time MIPs as an anti-venom, when MIPs they developed allowed to capture and clear a target bee peptide toxin from the bloodstream of living mice [81]. Since then, other studies on MIPs-based anti-venom have begun to appear [82].

The first study confirming the possibility of MIPs' application as anti-virotics was performed in 2019 by Xu et al. The study focused on the preparation of MIPs targeting a specific peptide motif situated on the surface of the human immunodeficiency virus (HIV). This structure is responsible for the decline of $CD4^+$ T-cells and the resulting deterioration of the immune system during HIV infection. Blocking the function of this peptide by the developed MIP nanoparticles is a promising therapeutical approach for counteracting HIV [61].

Currently, studies focusing on MIPs that may have the potential to be applied as immunotherapeutic or sensitizing agents to improving chemotherapeutic anti-tumor effects appear highly attractive. These MIPs may, namely, participate in the establishment of a novel therapeutic platform in cancer treatment. For example, the approach published by Rangel and co-workers in 2020 seems to be very promising. This work is based on MIPs that could block the function of cadherins and thus completely disrupt three-dimensional tumor spheroids as well as inhibit invasion of healthy cells [83].

In spite of the impressive results, the applications of MIPs in medical therapy are still in their infancy, and there is a long way to achieve their commercial utilization in medicine. There are many unanswered questions to which solutions are needed to be found and many issues that need to be resolved before successful practical applications of MIPs. These issues include safety and biodegradability, which have to be investigated in detail, and the optimal properties for their biodistribution and clearance have to be found. However, it is very likely that MIPs will attract progressively more attention and perhaps in a few years maybe will be available as first MIP-based medicaments approved by FDA.

8.3 Conclusions

Currently, the most utilized recognition elements in medicine are Abs, and a number of Abs-based medicaments are commercially available. However, the treatment by Abs-based drugs is very expensive. Besides, Abs still suffer from several issues that limit the widespread use of this type of medicaments. Therefore, there is a huge effort in finding some Abs alternatives that enable to overcome these limitations. Aptamers and MIPs seem to be very promising candidates. In the case of aptamers, one aptamer-based medicament has been already approved by FDA. However, insufficient understanding of the structure, target interactions, and pharmacokinetics led to the production of novel aptamer-based drugs having been halted for some time. Nowadays, there is a number of promising pharmaceuticals based on aptamers in the clinical phase, which predicts that most likely they will soon compete with Abs-based drugs for therapeutic applications. As for MIPs, owing to their excellent physical and chemical stability, tuneable properties, and low production costs, they seem to be very attractive as Abs alternatives. In the last years, interest in these therapeutics has been growing, and the number of research publications focused on this topic has been increasing as well. Despite many excellent laboratory results, there is a wide range of unanswered questions and unsolved issues that have to be resolved before MIPs practical therapeutic application. A summary of the properties of the individual recognition elements is shown in Table 8.3.

Table 8.3 Comparison of different recognition elements

Production			
Characteristics	Antibodies	MIPs	Aptamers
Formation	Immune response in animal host	Computational modeling	SELEX
Manufacture	Mammalian cell systems	Chemical synthesis	Chemical synthesis
Batch-to-batch variability	Very high	Low (in the case of automated reactor)	Low
Average lead time (incl. development, production, validation)	>6–8 months	2–4 weeks (usually one day for production)	2–4 months (few days for production)
Cost for development of a new entity	15,000–25,000 $	4000–13,000 $ (depending on template cost)	6000–10,000 $
Production cost	Very high	Low	Medium
Range of targets	Medium	Wide	Wide
Ease of functionalization	Low	Very high	Very high
Availability of monomers	Limited to the number of amino acids	>4000 of variety functional monomers	Limited to the number of nucleic bases
Properties			
Characteristics	**Antibodies**	**MIPs**	**Aptamers**
Size (nm)	10–20	10–300 (hydrodynamic)	2–8
Affinity	Pico- to nanomolar	Pico- to nanomolar	Pico- to nanomolar
Immunogenicity	High	Unknown	Low
Thermal stability	Low	Very high	High
Organic solvent stability	Low	Very high	Low
pH stability	Low	Very high	Low
Enzyme stability	Low	Very high	Low

References

1. Yunus, G. (2019). Biosensors: An enzyme-based biophysical technique for the detection of foodborne pathogens. In *Enzymes in Food biotechnology* (pp. 723–738). Elsevier.
2. Linton, D. S. (2005). *Emil von Behring: Infectious disease, immunology, serum therapy*. American Philosophical Society.
3. Brodsky, F. M. (1988). Monoclonal antibodies as magic bullets. *Pharmaceutical Research, 5*, 1–9.
4. Oriuchi, N. & Yang, D. J. (2001). Antibodies for targeted imaging: Properties and radiolabeling. *Targeted Molecular Imaging in Oncology*, (Springer), pp. 83–87
5. Lipman, N. S., Jackson, L. R., Trudel, L. J., & Weis-Garcia, F. (2005). Monoclonal versus polyclonal antibodies: Distinguishing characteristics, applications, and information resources. *ILAR Journal, 46*, 258–268.

6. Köhler, G., & Milstein, C. (1975). Continuous cultures of fused cells secreting antibody of predefined specificity. *Nature, 256*, 495–497.
7. Rajewsky, K. (2019). *The advent and rise of monoclonal antibodies*. Nature Publishing Group.
8. Little, M., Kipriyanov, S., Le Gall, F., & Moldenhauer, G. (2000). Of mice and men: Hybridoma and recombinant antibodies. *Immunology Today, 21*, 364–370.
9. Chames, P., Van Regenmortel, M., Weiss, E., & Baty, D. (2009). Therapeutic antibodies: Successes, limitations and hopes for the future. *British Journal of Pharmacology, 157*, 220–233.
10. Smith, K., Nelson, P. N., Warren, P., Astley, S., Murray, P. G., & Greenman, J. (2004). Demystified... recombinant antibodies. *Journal of Clinical Pathology, 57*, 912–917.
11. Souriau, C., & Hudson, P. J. (2001). Recombinant antibodies for cancer diagnosis and therapy. *Expert Opinion on Biological Therapy, 1*, 845–855.
12. Yusibov, V., Streatfield, S. J., & Kushnir, N. (2011). Clinical development of plant-produced recombinant pharmaceuticals: Vaccines, antibodies and beyond. *Human Vaccines, 7*, 313–321.
13. Morrison, S. L., Johnson, M. J., Herzenberg, L. A., & Oi, V. T. (1984). Chimeric human antibody molecules: Mouse antigen-binding domains with human constant region domains. *Proceedings of the National Academy of Sciences of the United States of America, 81*, 6851–6855.
14. Ribatti, D. (2014). From the discovery of monoclonal antibodies to their therapeutic application: An historical reappraisal. *Immunology Letters, 161*, 96–99.
15. Deyev, S., & Lebedenko, E. (2009). Modern technologies for creating synthetic antibodies for clinical application. *Acta Naturae, 1*, 32–50.
16. https://absoluteantibody.com/antibody-resources/antibody-engineering/humanisation/
17. Awwad, S., & Angkawinitwong, U. (2018). Overview of antibody drug delivery. *Pharmaceutics, 10*, 83.
18. Food, U. S., & Administration, D. (1993). *FDA papers*. U.S. Food and Drug Administration.
19. McCafferty, J., Griffiths, A. D., Winter, G., & Chiswell, D. J. (1990). Phage antibodies–filamentous phage displaying antibody variable domains. *Nature, 348*, 552–554.
20. Smith, G. P. (1985). Filamentous fusion phage–novel expression vectors that display cloned antigens on the virion surface. *Science, 228*, 1315–1317.
21. Lu, R. M., Hwang, Y. C., Liu, I. J., Lee, C. C., Tsai, H. Z., Li, H. J., & Wu, H. C. (2020). Development of therapeutic antibodies for the treatment of diseases. *Journal of Biomedical Science, 27*.
22. Voskuil, J. (2014). Commercial antibodies and their validation. *F1000Res, 3*, 232.
23. Shankar, G., Shores, E., Wagner, C., & Mire-Sluis, A. (2006). Scientific and regulatory considerations on the immunogenicity of biologics. *Trends in Biotechnology, 24*, 274–280.
24. Gebauer, M., & Skerra, A. (2009). Engineered protein scaffolds as next-generation antibody therapeutics. *Current Opinion in Chemical Biology, 13*, 245–255.
25. Ellington, A. D., & Szostak, J. W. (1990). In vitro selection of RNA molecules that bind specific ligands. *Nature, 346*, 818–822.
26. Tuerk, C., & Gold, L. (1990). Systematic evolution of ligands by exponential enrichment: RNA ligands to bacteriophage T4 DNA polymerase. *Science, 249*, 505–510.
27. Keefe, A. D., Pai, S., & a Ellington A. (2010). Aptamers as therapeutics. *Nature Reviews. Drug Discovery, 9*, 537–550.
28. Ferreira, C. S., & Missailidis, S. (2007). Aptamer-based therapeutics and their potential in radiopharmaceutical design. *Brazilian Archives of Biology and Technology, 50*, 63–76.
29. https://www.accessdata.fda.gov/ https://www.accessdata.fda.gov/drugsatfda_docs/nda/2004/21-756_Macugen.cfm
30. Sun, H., Zhu, X., Lu, P. Y., Rosato, R. R., Tan, W., & Zu, Y. (2014). Oligonucleotide aptamers: New tools for targeted cancer therapy. *Molecular Therapy–Nucleic Acids, 3*, e182.
31. Brody, E. N., & Gold, L. (2000). Aptamers as therapeutic and diagnostic agents. *Journal of Biotechnology, 74*, 5–13.

32. Song, S., Wang, L., Li, J., Fan, C., & Zhao, J. (2008). Aptamer-based biosensors. *Trends in Analytical Chemistry, 27*, 108–117.
33. Toh, S. Y., Citartan, M., Gopinath, S. C., & Tang, T.-H. J. B. (2015). Aptamers as a replacement for antibodies in enzyme-linked immunosorbent assay. *Biosensors & Bioelectronics, 64*, 392–403.
34. Osborne, S. E., Matsumura, I., & Ellington, A. D. (1997). Aptamers as therapeutic and diagnostic reagents: Problems and prospects. *Current Opinion in Chemical Biology, 1*, 5–9.
35. Cao, Z., Tong, R., Mishra, A., Xu, W., Wong, G. C., Cheng, J., & Lu, Y. (2009). Reversible cell-specific drug delivery with aptamer-functionalized liposomes. *Angewandte Chemie (International Ed. in English), 48*, 6494–6498.
36. Wu, Y. X., & Kwon, Y. J. (2016). Aptamers: The "evolution" of SELEX. *Methods, 106*, 21–28.
37. Hassel, S., & Mayer, G. (2019). Aptamers as therapeutic agents: Has the initial euphoria subsided? *Molecular Diagnosis & Therapy, 23*, 301–309.
38. Morita, Y., Leslie, M., Kameyama, H., Volk, D. E., & a Tanaka T. (2018). Aptamer therapeutics in cancer: Current and future. *Cancers, 10*, 80.
39. Boomer, R. M., Lewis, S. D., Healy, J. M., Kurz, M., Wilson, C., & McCauley, T. G. (2005). Conjugation to polyethylene glycol polymer promotes aptamer biodistribution to healthy and inflamed tissues. *Oligonucleotides, 15*, 183–195.
40. Lee, C. H., Lee, S.-H., Kim, J. H., Noh, Y.-H., Noh, G.-J., & Lee, S.-W. (2015a). Pharmacokinetics of a cholesterol-conjugated aptamer against the hepatitis C virus (HCV) NS5B protein. *Molecular Therapy–Nucleic Acids, 4*, e254.
41. Lee, C. H., Lee, S.-H., Kim, J. H., Noh, Y.-H., Noh, G.-J., & Lee, S.-W. (2015b). Pharmacokinetics of a cholesterol-conjugated aptamer against the hepatitis C virus (HCV) NS5B protein. *Molecular Therapy–Nucleic Acids, 4*, e254.
42. Kuhlmann, M., Hamming, J. B., Voldum, A., Tsakiridou, G., Larsen, M. T., Schmøkel, J. S., Sohn, E., Bienk, K., Schaffert, D., & Sørensen, E. S. (2017). An albumin-oligonucleotide assembly for potential combinatorial drug delivery and half-life extension applications. *Molecular Therapy–Nucleic Acids, 9*, 284–293.
43. Liu, Q., Jin, C., Wang, Y., Fang, X., Zhang, X., Chen, Z., & Tan, W. (2014). Aptamer-conjugated nanomaterials for specific cancer cell recognition and targeted cancer therapy. *NPG Asia Materials, 6*, e95.
44. Ni, S., Yao, H., Wang, L., Lu, J., Jiang, F., Lu, A., & Zhang, G. (2017). Chemical modifications of nucleic acid aptamers for therapeutic purposes. *International Journal of Molecular Sciences, 18*, 1683.
45. Yan, X., Gao, X., & Zhang, Z. (2004). Isolation and characterization of 2′-amino-modified RNA aptamers for human TNFα. *Genomics, Proteomics & Bioinformatics, 2*, 32–42.
46. Khati, M., Schüman, M., Ibrahim, J., Sattentau, Q., Gordon, S., & James, W. (2003). Neutralization of infectivity of diverse R5 clinical isolates of human immunodeficiency virus type 1 by gp120-binding 2′ F-RNA aptamers. *Journal of Virology, 77*, 12692–12698.
47. Ganson, N. J., Povsic, T. J., Sullenger, B. A., Alexander, J. H., Zelenkofske, S. L., Sailstad, J. M., Rusconi, C. P., & Hershfield, M. S. (2016). Pre-existing anti–polyethylene glycol antibody linked to first-exposure allergic reactions to pegnivacogin, a PEGylated RNA aptamer. *The Journal of Allergy and Clinical Immunology, 137*, 1610–1613. e1617.
48. Tong, G. J., Hsiao, S. C., Carrico, Z. M., & Francis, M. B. (2009). Viral capsid DNA aptamer conjugates as multivalent cell-targeting vehicles. *Journal of the American Chemical Society, 131*, 11174–11178.
49. Liu, H. Y., & Gao, X. (2013). A universal protein tag for delivery of SiRNA-aptamer chimeras. *Scientific Reports, 3*, 1–8.
50. Dearborn, A. D., Eren, E., Watts, N. R., Palmer, I. W., Kaufman, J. D., Steven, A. C., & Wingfield, P. T. (2018). Structure of an RNA aptamer that can inhibit HIV-1 by blocking rev-cognate RNA (RRE) binding and rev-rev association. *Structure, 26*, 1187–1195. e1184.

51. Chabata, C. V., Frederiksen, J. W., Sullenger, B. A., & Gunaratne, R. (2018). Emerging applications of aptamers for anticoagulation and hemostasis. *Current Opinion in Hematology, 25*, 382–388.
52. Polyakov, M. V. (1931). Adsorption properties and structure of silica gel. *Zhurnal Fizieskoj Khimii/Akademiya SSSR, 2*, 799–805.
53. Ye, L. (2015). Synthetic strategies in molecular imprinting. In *Molecularly imprinted polymers in biotechnology* (pp. 1–24). Springer.
54. Andersson, L., Sellergren, B., & Mosbach, K. (1984). Imprinting of amino acid derivatives in macroporous polymers. *Tetrahedron Letters, 25*, 5211–5214.
55. Ahmad, O. S., Bedwell, T. S., Esen, C., Garcia-Cruz, A., & Piletsky, S. A. (2019). Molecularly imprinted polymers in electrochemical and optical sensors. *Trends in Biotechnology, 37*, 294–309.
56. Selvolini, G., & Marrazza, G. (2017). MIP-based sensors: Promising new tools for cancer biomarker determination. *Sensors, 17*, 718.
57. Baggiani, C., Anfossi, L., & Giovannoli, C. (2013). MIP-based immunoassays: State of the art, limitations and perspectives. *Mol Impr, 1*, 41–54.
58. Tang, S.-P., Canfarotta, F., Smolinska-Kempisty, K., Piletska, E., Guerreiro, A., & Piletsky, S. J. (2017). A pseudo-ELISA based on molecularly imprinted nanoparticles for detection of gentamicin in real samples. *Analytical Methods, 9*, 2853–2858.
59. Pan, J., Chen, W., Ma, Y., & Pan, G. (2018). Molecularly imprinted polymers as receptor mimics for selective cell recognition. *Chemical Society Reviews, 47*, 5574–5587.
60. Alvarez-Lorenzo, C., & Concheiro, A. J. (2004). Molecularly imprinted polymers for drug delivery. *Journal of Chromatography. B, Analytical Technologies in the Biomedical and Life Sciences, 804*, 231–245.
61. Xu, J., Merlier, F., Avalle, B., Vieillard, V., Debré, P., Haupt, K., & Bui, B. T. S. (2019). Molecularly imprinted polymer nanoparticles as potential synthetic antibodies for immunoprotection against HIV. *ACS Applied Materials & Interfaces, 11*, 9824–9831.
62. Canfarotta, F., Cecchini, A. & Piletsky, S. (2018). *Nano-sized molecularly imprinted polymers as artificial antibodies*
63. https://www.sigmaaldrich.com/technical-documents/articles/analytical/food-beverage/analysis-aminoglycosides-pork.html
64. Ertürk, G., & Mattiasson, B. (2017). Molecular imprinting techniques used for the preparation of biosensors. *Sensors, 17*, 288.
65. Verheyen, E., Schillemans, J. P., Van Wijk, M., Demeniex, M.-A., Hennink, W. E., & Van Nostrum, C. F. (2011). Challenges for the effective molecular imprinting of proteins. *Biomaterials, 32*, 3008–3020.
66. Rachkov, A., & Minoura, N. J. (2000). Recognition of oxytocin and oxytocin-related peptides in aqueous media using a molecularly imprinted polymer synthesized by the epitope approach. *Journal of Chromatography. A, 889*, 111–118.
67. Kryscio, D. R., & Peppas, N. A. (2012). Critical review and perspective of macromolecularly imprinted polymers. *Acta Biomaterialia, 8*, 461–473.
68. Refaat, D., Aggour, M. G., Farghali, A. A., Mahajan, R., Wiklander, J. G., Nicholls, I. A., & Piletsky, S. A. (2019). Strategies for molecular imprinting and the evolution of MIP nanoparticles as plastic antibodies—synthesis and applications. *International Journal of Molecular Sciences, 20*, 6304.
69. Stolp, Z. D. (1914). *A high throughput multiplexed platform for monitoring proteolysis in the classical secretory pathway-search for novel antivirals*. (Sciences)
70. Piletsky, S., Piletska, E., Canfarotta, F. & Jones D. (2018). *Methods and kits for determining binding sites*. (WO Patent 2,018,178,629)
71. Ambrosini, S., Beyazit, S., Haupt, K., & Bui, B. T. S. (2013). Solid-phase synthesis of molecularly imprinted nanoparticles for protein recognition. *Chemical Communications, 49*, 6746–6748.

72. Poma, A., Guerreiro, A., Whitcombe, M. J., Piletska, E. V., Turner, A. P., & Piletsky, S. A. (2013). Solid-phase synthesis of molecularly imprinted polymer nanoparticles with a reusable template–"plastic antibodies". *Advanced Functional Materials, 23*, 2821–2827.
73. Poma, A., Guerreiro, A., Caygill, S., Moczko, E., & Piletsky, S. (2014). Automatic reactor for solid-phase synthesis of molecularly imprinted polymeric nanoparticles (MIP NPs) in water. *RSC Advances, 4*, 4203–4206.
74. Moczko, E., Poma, A., Guerreiro, A., de Vargas Sansalvador, I. P., Caygill, S., Canfarotta, F., Whitcombe, M. J., & Piletsky, S. (2013). Surface-modified multifunctional MIP nanoparticles. *Nanoscale, 5*, 3733–3741.
75. Nicholls, I. A., Andersson, H. S., Charlton, C., Henschel, H., Karlsson, B. C., Karlsson, J. G., O'Mahony, J., Rosengren, A. M., Rosengren, K. J., & Wikman, S. J. B. (2009). Theoretical and computational strategies for rational molecularly imprinted polymer design. *Biosensors & Bioelectronics, 25*, 543–552.
76. Svenson, J., & Nicholls, I. A. (2001). On the thermal and chemical stability of molecularly imprinted polymers. *Analytica Chimica Acta, 435*, 19–24.
77. Kumar, A., Purohit, B., Mahato, K., & Chandra, P. (2019a). Advance engineered nanomaterials in point-of-care immunosensing for biomedical diagnostics. In *Immunosensors* (pp. 238–266).
78. Kumar, A., Roy, S., Srivastava, A., Naikwade, M. M., Purohit, B., Mahato, K., Naidu, V., & Chandra, P. (2019b). Nanotherapeutics: A novel and powerful approach in modern healthcare system. In *Nanotechnology in modern animal biotechnology* (pp. 149–161). Elsevier.
79. Purohit, B., Kumar, A., Mahato, K., Roy, S., & Chandra, P. (2019). Cancer Cytosensing approaches in miniaturized settings based on advanced nanomaterials and biosensors. In *Nanotechnology in modern animal biotechnology* (pp. 133–147). Elsevier.
80. Shankar, S. S., Ramachandran, V., Raj, R. P., Sruthi, T., & Kumar, V. S. (2020). Carbon quantum dots: A potential candidate for diagnostic and therapeutic application. In *Nanobiomaterial engineering* (pp. 49–70). Springer.
81. Hoshino, Y., Koide, H., Urakami, T., Kanazawa, H., Kodama, T., Oku, N., & Shea, K. J. (2010). Recognition, neutralization, and clearance of target peptides in the bloodstream of living mice by molecularly imprinted polymer nanoparticles: A plastic antibody. *Journal of the American Chemical Society, 132*, 6644–6645.
82. Piszkiewicz, S., Kirkbride, E. A., Doreng-Stearns, N., Henderson, B. R., Lenker, M. A., Tang, E., Kawashiri, L. H., Nichols, C. S., Moore, S. C., & Sogo, S. G. (2013). Molecularly-imprinted nanoparticles that recognize Naja mossambica cytotoxins: Binding studies and biological effects. *Chemical Communications, 49*, 5954–5956.
83. Medina Rangel, P. X., Moroni, E., Merlier, F., Gheber, L. A., Vago, R., Tse Sum Bui, B., & Haupt, K. (2020). Chemical antibody mimics inhibit cadherin-mediated cell–cell adhesion: A promising strategy for cancer therapy. *Angewandte Chemie (International Ed. in English), 59*, 2816–2822.

Chapter 9
Design and Development of a Bed-Side Cardiac Health Monitoring Device

Sudipta Ghosh, Jayanta Mukhopadhyay, and Manjunatha Mahadevappa

9.1 Introduction

Living objects adapt to environmental changes, and various demands garnered by the activity of an organism. This ability to adapt is due to a series of complex control processes that affect the organism at the systemic, molecular, and cellular levels. Impairments in regulatory processes are the results or outcomes of many systemic diseases.

Out of several methods for evaluating the effectiveness of regulatory mechanisms, the most commonly employed technique is to analyze the footprints that characterize the response of a particular system to different stimuli during the transient changes between two stable states. There are two possibilities: reaction generated by an act of provocation (e.g., exercise or human tilt test) or transient phase response due to the organism's normal activity, caused by an unknown factor, to be identified by expert clinicians (e.g. cardiac arrhythmia, ischemia, etc.).

An effective control of the blood flow is of paramount importance for the proper development of various physiological processes. Two effectors that control the flow of blood are: the heart and the vascular system. Both of these systems (together known as the cardiovascular system) are controlled by an autonomous system, and various processes of local self-regulation. Many examinations related to the proper functioning of cardiovascular system are carried out in humans, including orthostatic maneuver, handgrip test, dynamic exercise, and cold pressure test. Each of these

S. Ghosh · M. Mahadevappa (✉)
School of Medical Science & Technology, IIT, Kharagpur, India
e-mail: mmaha2@smst.iitkgp.ac.in

J. Mukhopadhyay
Department of Computer Science & Engineering, IIT, Kharagpur, India

V. Borse et al. (eds.), *BioSensing, Theranostics, and Medical Devices*,
https://doi.org/10.1007/978-981-16-2782-8_9

tests helps in the evaluation and analysis of a particular system's dysfunction or inability to adapt. An advanced performance diagnosis method, performed in humans is outpatient monitoring of a range of varied physiological parameters, which are obtained during the habitual activity of an organism. Increasing prevalence of cardiovascular-related diseases throughout the world as well as the continuing fragility of the cardiovascular system in intensive care patients calls attention to the need for accurate methods of assessing system health. Hemodynamic monitoring which encompasses the study of development and propagation of flow and pressure pulses, including but not limited to: systemic, pulmonary arterial, and venous pressures and cardiac output, has traditionally serviced this need. However, hemodynamic monitoring methods are mostly invasive in nature. Consequently, they require on-site expert supervision, are costly, and suffer the risks of surgical complications [1]. An alternative non-invasive method, impedance cardiography (ICG) was first proposed by [2] in the thoracic region. An alternating current flows through the body fluid which has very low electrical resistance when applied to human body. When the electric potential is applied to the human body, the tissue exhibits electrical property called the Bio-Impedance. Compared to bone, fat, or air, current flows easily through those parts of the body which are composed mostly of water (blood, urine, and muscle). The electric current flows easily through water with ions which human body is composed of. The amount of resistance the body tissue exhibits to the small amount of current applied (less than 10 mA) is measured by the BIA (Bio-Impedance Analysis) [3].

Biological tissue's electrical properties are dependent on the presence of body fluids. In addition, these properties could be different for analyzing the same tissue in vivo and in vitro. The solid part of the tissue is mainly based on the isolating properties of cell membranes. The presence in the same tissue of conductive fluid part and solid, isolating component affects the anisotropic, electrical properties of the living tissue. There are three major frequency ranges that describe the relative permittivity changes called dispersion α, β, and γ. However in some tissues, all the frequency ranges are not properly represented. Dispersion α, which occurs in lower frequencies (in the vicinity of 100 Hz), is responsible for interfacial polarization and transport of ions across cell membranes. The β dispersion occurring in the frequency range of 10 kHz to 10 MHz traces its origin to the capacitive charging of cellular membranes and membrane-bound intracellular bodies [4]. The relaxation of excess water in tissues gives rise to the γ dispersion, which occurs at frequencies above 100 MHz [4]. Using impedance spectroscopy technique, the electrical properties of tissues are analyzed. It enables people to differentiate between different tissues and level of degeneration caused by the pathological processes, e.g. lesion development, arrhythmias, and the transplanted organ rejection mechanism [5, 6]. During the International Conference on Electrical Bio-Impedance (ICEBI), organized worldwide every third year since the first meeting in 1969, the mainstream research on bio-impedance methods is regularly presented. The fundamental research achievements in this field were presented in Martinsen et al. [7].

Impedance cardiography applications tend to use the frequency range of 15 to 100 kHz. The thin cellular membranes that separate the conductive fluids create

Table 9.1 Resistivity values of various tissues [9]

Type of Tissue	Resistivity (Ω-cm)
Blood plasma	63
Blood (for hematocrit, Ht = 47%)	150
Skeletal muscle (longitudinal)	300
Skeletal muscle (transverse)	700
Heart muscle (dog)	750
Lungs (dog)	1200
Saline 0.9%	57
Fat	2.180

electrical capacitance of up to 1 μ F/cm^2. This results in a resistive and capacitive character of the biological tissue's electrical properties, with the absence of inductive component symptoms. In terms of resistivity, blood plasma exhibits the lowest value with resistivity of 63 Ω-cm. However for tissues related to human being, blood has the lowest, and fat has the highest resistivity. The resistivity values of blood and fat are 150 Ω-cm and 1275 Ω-cm, respectively. Blood resistivity plays a major role in cardiac performance measurement using methods of impedance. Blood resistivity was assumed to have isotropic properties under static conditions, but there are suggestions that flowing blood is characterized by a relative decrease in resistivity of up to 10%. In addition, some authors based on experimental studies and model analysis also claim that the anisotropic properties of flowing blood are highly pronounced that we initially assumed and suggested using the resistivity tensor [8].

The resistivity of various biological tissues and fluids based on Geddes and Baker [9] compendium is presented in Table 9.1. The main conclusion drawn from the resistivity data presented in Table 9.1 is that in impedance cardiography the change of the impedance signal is generated mainly by changes caused by the blood volume translocations. Other tissues do not change the volume of blood or have resistivity values which are at least twice as high, compared to various other biological tissues. It is even 5 times higher in the case of the heart muscle, which leads to the conclusion that the heart isolates the blood that is accumulated within it.

9.1.1 Tissue as a Conductor

Tissues of a human body could be modeled as a finite, inhomogeneous volume conductor [10]. In case of impedance cardiography applications it can also be assumed to be a sourceless medium. The impedance of human tissues could be characterized by a three-element circuit model with a single time constant. The three circuit elements are: a low frequency resistor, R_0, a high frequency resistor, R_∞, and a constant phase element (CPE), as shown in Fig. 9.1. The function could be represented by the Cole-Cole model [11]. The function mentioned below represents

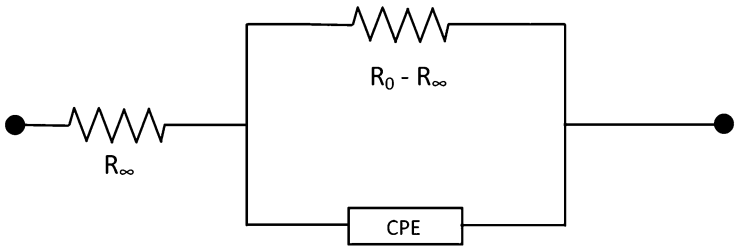

Fig. 9.1 Three element model for tissue impedance

impedance *Z*, as a function of frequency, having real *(R)* and imaginary components *(jX)*

$$Z(f) = R + jX \tag{9.1}$$

On expanding the above equation it can be written as:

$$Z(f) = R_\infty + \frac{R_0 - R_\infty}{1 + (j\varpi\tau)^\alpha} \tag{2}$$

where *Z(f)* is the impedance as function of frequency, R_0 is the resistance at frequency f = 0, *R* is the resistance at frequency f= ∞, and $\tau = [(R_0 - R_\infty)C]^{1/\alpha}$ is the time constant. The impedance of CPE could be written as $Z_{CPE} = 1/(j\varpi C)^\alpha$, where *C* is the capacitance and α is its order ($0 < \alpha \leq 1$), and $\varpi = 2\,\pi$ f.

9.2 Evolution of Bio-Impedance: Impedance Cardiography

Blood is attributed as a human tissue which has the highest conductivity. The resistivity of blood (130–160 Ω-cm) is much lower than the resistivity of muscle tissue (determined to be 300 Ω-cm) [9, 12]. This biophysical property of blood means that the impedance between the sensing electrodes is caused primarily by the blood volume contained within a particular segment of the human body. The formula of Nyboer [13, 14] (explained) was a mathematical description of a simple model of changes in the chest's blood vessels during the heart cycle. It presented the chest as a uniform cylinder filled with blood in which there was a single blood vessel with a specific diameter. During contraction, blood ejection from the heart to the aorta was simulated as a rapid extension of this vessel (uniform diameter increase) and a similarly fast, uniform return after the aortic valve was closed. The time of the extension of the vessel was equal to the time of ejection. Boer et al. [15], Porter et al. [16], Ito et al. [17], and Keim et al. [18], criticized this simplified model of heart hemodynamics phenomena and its consequences while calculating SV. This

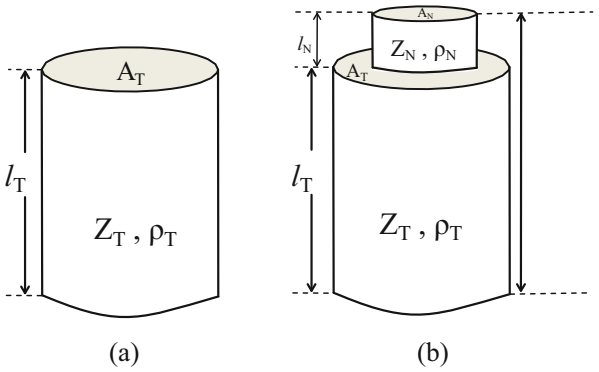

Fig. 9.2 (**a**) Single cylinder model, (**b**) Serially connected double cylinder model [26]

A_T, A_N = Cross section area (cm^2); Z_T, Z_N = Impedance (Ω);

ρ_T, ρ_N = Specific Resistivity (Ω-cm); l_T, l_N, l = Length

criticism was an inspiration for studies which [19–25] evaluated the impact of specific components on the ICG signal.

Raaijmakers [26] questioned the validity of the one-cylinder model, suggesting instead a serially connected two-cylinder model. They studied the length of the impedance parameters (distance between the receiving electrodes) Z_0, $\left(dz/dt\right)$, and stroke volume (SV) in both the models. It has been shown that all parameters are directly proportional to the length within a single-cylinder model. Whereas if the thorax and neck volume conductions are modeled separately, Z_0 and $\left(dz/dt\right)$ are expected to be linearly dependent onlength, whereas SV is non-linearly dependent onthe length. These expectations were compared with the results of measurements in vivo [26] using an array of electrodes placed on the thorax. Except for small distances, the results showed an almost linear relationship between the ICG parameters and the length. The linear part's regression analysis revealed statistically significant intercepts ($p < 0.05$). When stroke volume was calculated using Kubicek's equation [2], a single-cylinder model could not explain either the intercept or the non-linear part, whereas the experimental results were accurately described by a model consisting of two serially connected cylinders. Thus, they concluded that one-cylinder SV estimation is biased due to the invalid one-cylinder model and suggested corrections for the Kubicek equation using their two-cylinder model [26]. The single-cylinder model and the serially connected double cylinder model have been figuratively represented in Fig. 9.2.

It can be assumed that, when the alternating current passes through the chest, the following mechanical phenomena occur during the cardiac cycle and impact the impedance cardiography signal:

- Extension of the aorta and neck artery due to arterial pulse pressure.
- Extension of the pulmonary vessel.
- Changes in heart volume and blood filling volume.

Table 9.2 Origin of the impedance signal in impedance cardiography [28]

Contributing Organ	Contribution (%)
Pulmonary artery & lungs	+60
Aorta & thoracic musculature	+60
Right ventricle	−30
Left ventricle	−30
Pulmonary vein & left atrium	+20
Vena cava & right atrium	+20

- Changes in blood volume of the pulmonary vessels resulting in increased conductivity of the lungs.
- Changes in blood resistivity in large vessels resulting from the reorientation of blood cells as a function of blood velocity.
- Changes in resistivity of the skeletal muscle due to the pulsatile flow of blood.

Shankar et al. [24], Kosicki et al. [21], and Patterson [22] presented a mathematical model of chest impedance changes occurring during the heart cycle. Kim et al. [20] based on the model of the finite element and analyzed the impact of the factors set out in points 1, 3, 4, and 5. They concluded that impedance changes are proportional to the aorta's extension and that modifying the resistivity of the lung has an eight-fold less impact than that of the aorta. The impact on base impedance of the heart signal was significant but not proportional to heart volume changes. Kosicki et al. [21], who presented a cylindrical chest model with non-coaxial positioning of the chest organs, confirmed these findings. They noticed the aortic signal's small phase compared to changes in blood flow resistivity. They also showed the magnitude and phase shift of the impedance signal's particular components. However, on the basis of a three-dimensional model of resistors, Patterson [22] concluded that the impact on the impedance signal of specific components was: the pulmonary component (61%), the main arteries (23%), the skeletal muscle (13%), and other sources (3%). Most of these papers were theoretical and only checked on physical models of "phantom." Thomsen, [25] who experimentally found a higher correlation between impedance SV and aortic blood pressure ($r = 0.63$) than between SV and pulmonary artery blood pressure ($r = 0.26$), solved the issue of whether the impact of the aortic or pulmonary artery is higher. In addition, Bonjer's et al. [27] experiments on dogs (insulating the heart and lungs in a rubber bag) have shown that the heart muscle has a negligible impact on the ICG signal.

Several theoretical and experimental studies have been carried out in order to determine the origin of the impedance signal. Based on several studies, Penney [28] summarized the contribution to impedance cardiography signals of the size and function of anatomical structures. Table 9.2 presents the outcome of this resume.

After analyzing several hypotheses about the origin of impedance cardiography signals, Mohapatra [29] concluded that the impedance changes were caused by cardiac hemodynamics alone. He suggested that both a change in blood velocity and a change in blood volume are reflected in the signal. In addition, the variable

speed of ejection affects the systolic part, whereas the variable volume (mainly the atria and large veins) affects the diastolic part of the impedance curve. Amid the controversy over the unclear source of impedance cardiography signal, pointed out again by Mohapatra [29] and some other researchers, there are acceptable levels of correlation coefficients between the values obtained by ICG and reference methods. The observations from various studies are summarized below:

- The ICG signal is complex and the phase and direction of its components are not synchronized.
- It is not well defined the proportions between its components.
- The ICG signal depends on changes in aorta, neck arteries, and pulmonary vessels diameter and on the resistivity of flowing blood caused by reorientation of blood cells (only in large vessels).
- The ICG signal does not seem to depend on the volume of the heart and the amount of blood therein (isolating heart muscle properties in relation to blood resistivity).
- The ICG signal does not depend on the extension of the pulmonary artery for typically positioned electrodes.

9.3 Significance of Non-Invasive Recording of Cardiac Parameters

Easy access to health monitoring, without the use of sophisticated instruments is one of the primary essences of personalized point-of-care (POC) devices. [30–33] Initially observed from a pulse, the heart rate (HR) was the first parameter to be identified as describing the heart condition. The most important vital signal in intensive care units is HR detected from an electrocardiogram (ECG). ECG also describes the heart muscle state and is the main source of information on the propagation of electrical stimulation and cardiac neural control. The stroke volume (SV) is one of the important physiological parameters that are not fully available to clinicians (due to the necessary invasive procedures) or underestimated (when using non-invasive methods). This parameter and its changes in response to physiological or pharmacological stimuli may be an excellent tool for assessing the heart's mechanical efficacy. An indicator of effective cardiac work may be a reliable measurement of SV and its mean, e.g. in atrial fibrillation or in the presence of extra systole. As a product of HR and SV, cardiac output (CO) and changes in it are the physiological parameters that describe the efficiency of the heart and its capacity to undertake a load. It is also essential for monitoring treatment in cases of acute myocardial anomalies. Without accurate estimation of both blood pressure and CO, the analysis of hypertension cannot be taken seriously. The parameters that describe the heart contractility are systolic time intervals (STI), left ventricular ejection time (LVET), and pre-ejection period (PEP). Numerous studies have shown an abnormal STI in patients with myocardial disease (low ejection fraction or other left ventricular

performance measurements) [34–39]. This suggests that if invasive procedures are not available, the STI measurement may be used as contractility indices in part. Continuous measurement of blood pressure [40] is now also available in an outpatient version (Portapres). This signal is essential to cardiovascular system comprehensive analysis, e.g. in the evaluation of hypertension or baroreflex sensitivity.

9.4 Physiological and Clinical Applications of Impedance Cardiography

The ICG method has been applied in many different studies, starting with those reported by Miyamoto et al. [41–43], Miles et al. [44], to evaluate changes in cardiac output during exercise. Bogaard et al. [45] published review of ICG's hemodynamic measurement possibilities during exercise. They concluded that while ICG's calculation of the derived stroke volume was based on several debated assumptions, numerous validation studies showed good accuracy and reproducibility, including during exercise. In addition, Rosenberg et al. [46] in their review stated that impedance cardiography becomes an accepted method for safe, reliable, and reproducible evaluation of various hemodynamic parameters, related to cardiovascular functioning.

The controversies [47–50] surrounding ICG verification resulted in a skeptical approach to this technique by health authorities, which used to be considered a research method rather than a clinical one. Accordingly, Medicare and Medicaid Services and U.S. health insurance companies did not reimburse the cost of using ICG. This approach has been changed (as of 1 July 1999) and revised US policy on electrical impedance cardiac output monitoring now allows for limited coverage of cardiac monitoring using electrical bio-impedance, a form of plethysmography (impedance cardiography), for six uses:

- Suspected cardiovascular disease.
- Fluid management.
- Cardiogenic differentiation from pulmonary causes of acute dyspnea.
- Optimization of the atrioventricular interval of the pacemaker.
- Determination of the need for inotropic IV therapy.
- Post-transplant patients with myocardial biopsy.

Following the U.S. Medicare and Medicaid Services decision, the respective national health institutions in other countries decided to allow the cardiography impedance diagnosis to be refunded, initially in very limited areas, e.g. only in intensive care units. These decisions are certainly stimulating for ICG equipment manufacturers and hopefully will affect the development of hemodynamic outpatient monitoring systems based on impedance cardiography method.

9.5 Designing an Electrode - Skin Model for Simulation Studies

When electric current is applied, it flows at different rates depending mainly on the fat composition at various parts of the body which is the principle of bio-impedance analysis. Impedance is mainly the drop across the two electrodes placed on the body surface when a small constant current with a fixed frequency is applied across the electrodes. Bio-impedance analysis involves application of alternating current, which generates an electric potential directly proportional to the impedance across the recording/sensing electrodes. Alternating current is chosen over direct current to avoid charge accumulation around the excitation electrodes, which poses serious health risks and also contributes to the impedance around the electrodes. Finite Element Method (FEM) simulations have been used to depict the normalized current density, resistive loss, normalized electric field displacement, and the flow of current across the human skin [51]. The simulations have been carried out in finite element method solver (COMSOL Multiphysics, 5.2). Early detection and prevention of any imbalance in the body composition is important and BIA helps in the early detection. It also indicates the level of improvement the person is going through to improve the health. Thus to maintain proper functioning of the body, for healthy ageing and for reduced risk of illness BIA measurement is an appropriate solution. The effect of stimulating copper electrodes in a tetrapolar configuration, for impedance analysis is investigated using FEM (finite element method) solver (COMSOL Multiphysics, 5.2). COMSOL is used to numerically solve the partial differential equations given by Maxwell for a non-magnetic material, such as a biological tissue (skin). Maxwell's equations [52] can be written as:

$$\nabla \times H = J + \frac{\partial D}{\partial t} \tag{3}$$

$$\nabla \cdot B = 0 \tag{4}$$

$$\nabla \times E = -\frac{\partial B}{\partial t} \tag{5}$$

$$\nabla \cdot D = \rho(r, t) \tag{6}$$

$$\nabla \cdot J = -\frac{\partial \rho(r, t)}{\partial t} \tag{7}$$

where $\rho(r, t)$ is the charge density, J is the conduction current density, E is the electric field, B is the magnetic field, and H is the magnetic intensity. Since we are dealing with bio-potentials over a non-magnetic material (skin), the following assumptions are made: (a) the external magnetic field, B, is negligible, (b) $\frac{\partial D}{\partial t} = 0$, i.e. displacement current is zero [52], (c) the surface of the conducting or excitation electrodes is an equipotential surface, and (d) the electric field intensity (static) at the surface is directed toward the normal of the surface.

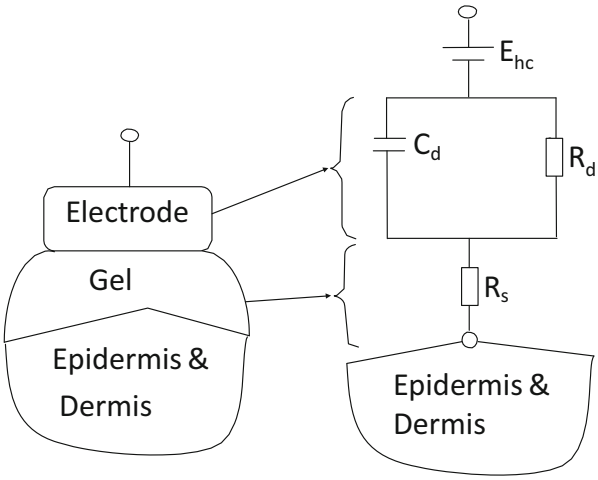

Fig. 9.3 Generalised skin-electrode model[a]

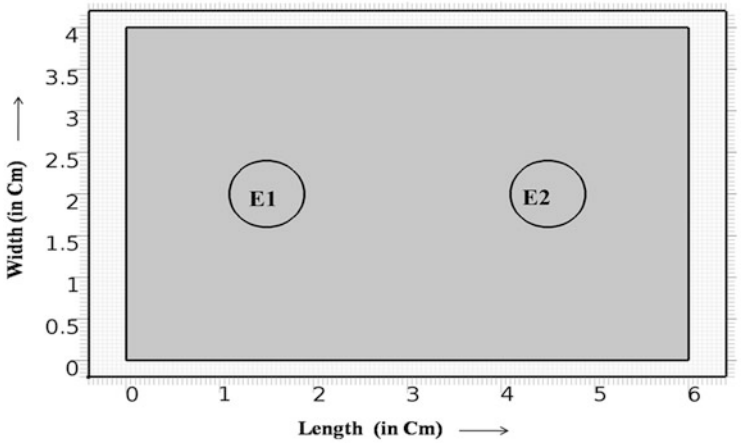

Fig. 9.4 Proposed skin-electrode model for impedance analysis[b]

In a tetrapolar arrangement, two electrodes are used for excitation and two electrodes are used for recording the change in voltage, which further enables us to calculate the impedance. We have characterized the electrical properties of an electrode on application of excitation current. The generalized electrode model is shown in Fig. 9.3, where E_{hc} is the electrode half-cell potential, R_d, C_d is the electrode impedance, and R_s is the gel related impedance [53]. The proposed model consists of 6 cm × 4 cm patch of human skin, on which two copper electrodes, of radius 0.4 cm, are positioned. Figure 9.4 shows us the rectangular patch of skin, along with the two copper electrodes (marked as E1 and E2), as designed in COMSOL. The human skin has an electrical conductivity (σ) of 0.343 S/m, and relative permittivity ($\in_r$) of 18,768 [54]. In the proposed model the depth of

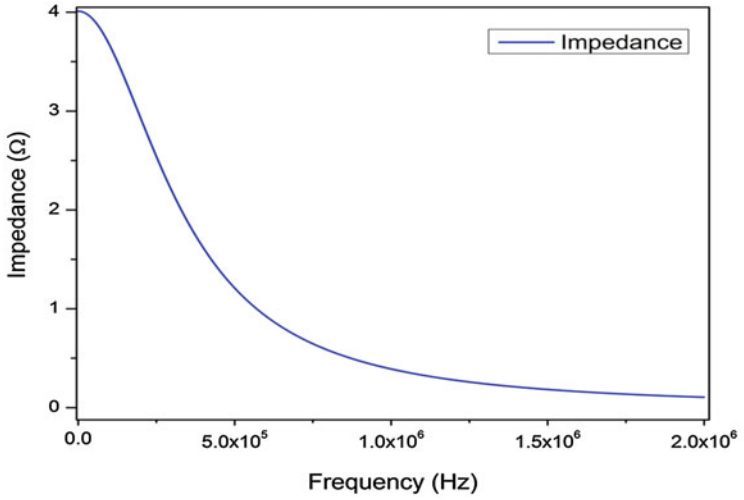

Fig. 9.5 Electrode-skin Impedance response for a wide range of frequency[c]

Table 9.3 Boundary conditions

Domain/Boundary Name	Type of condition	Equation(s)
Skin and electrodes	Current conservation	$\nabla.J = Q_j$ $J = (\sigma + j\omega\in_0\in_r)E + \mathrm{j}_e$ $E = -\nabla V$
Edges of the skin	Electric insulation	$n.J = 0$
Electrode boundary	Contact impedance	$n.J_1 = {}^1(V_1 - V_2)$ $n.J_2 = {}^1(V_2 - V_1)$

the skin perpendicular to the surface (d_s) is taken as 5 mm. The copper electrodes used have an electrical conductivity (σ) of 58.1×10^6 S/m and relative permittivity ($\in_r$) of 6.

The skin-electrode impedance decreases as the frequency increases. So, in impedance cardiography applications frequencies above 10 kHz are used [53]. It is also desirable to use currents above 1 mA, at higher frequencies such that stimulating shocks and perception of current could be avoided. In our proposed model copper electrodes were used as stimulating electrodes and a sinusoidal A.C. wave of frequency 15 kHz, and a current of 3 mA was passed through them. Figure 9.5 shows us the skin-electrode impedance curve, recorded over a wide range of frequency (100 Hz to 2 MHz).

Tetrapolar arrangement is chosen over bipolar configuration for impedance analysis, as it is easier to differentiate the contributing contact impedance of one electrode from the other. With the help of proposed model we have studied the variation in normalized current density, normalized electric field displacement, and resistive losses. First, a single cycle of sine wave was used for excitation, and the results were observed. After that, a continuous sine wave for one second was used

for excitation. All the boundary conditions that have been used for designing the proposed model are shown in Table 9.3.

9.5.1 Current Density

The model proposed is a classic example of a problem with a dielectric-conductor surface. The human skin acts as a dielectric and the copper electrodes as conductor. Current density is a vector, denoted by J (measured in A/m^2). Current through any closed surface is given by:

$$I = \oint_S J \cdot dS = \int_{vol} (\nabla \cdot J) dv \tag{8}$$

Each and every dielectric material has the capacity to store electric energy. Figure 9.6 shows the normalized current density distribution obtained as a result of a single excitation pulse. So when a single pulse of excitation voltage is given, the skin behaves like a capacitor. The value of current density increases and decreases as per the applied signal. Excitation of skin results in some instantaneous changes, as a result of a process known as electroporation of skin [55]. Electroporation of skin results in an increment of membrane permeability to potassium (K^+) ions and molecules when exposed to electric field, as a result of which the tissue conductance (G_e) increases. The tissue conductance is inversely proportional to the contact impedance. This physiological phenomenon results in an exponential decay in current density around the electrodes.

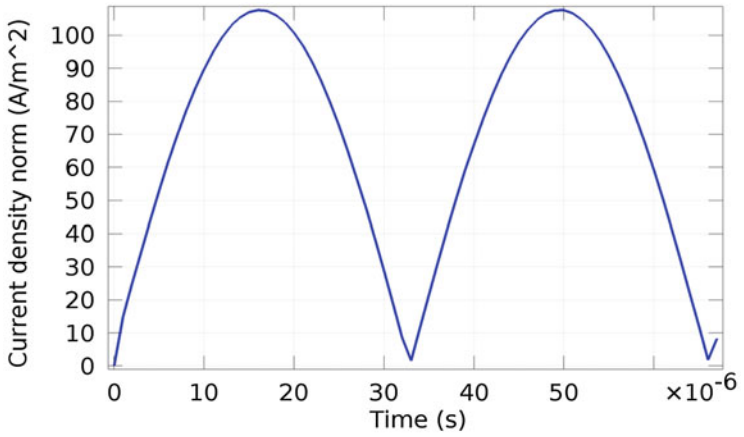

Fig. 9.6 Current density distribution obtained for a single pulse[d]

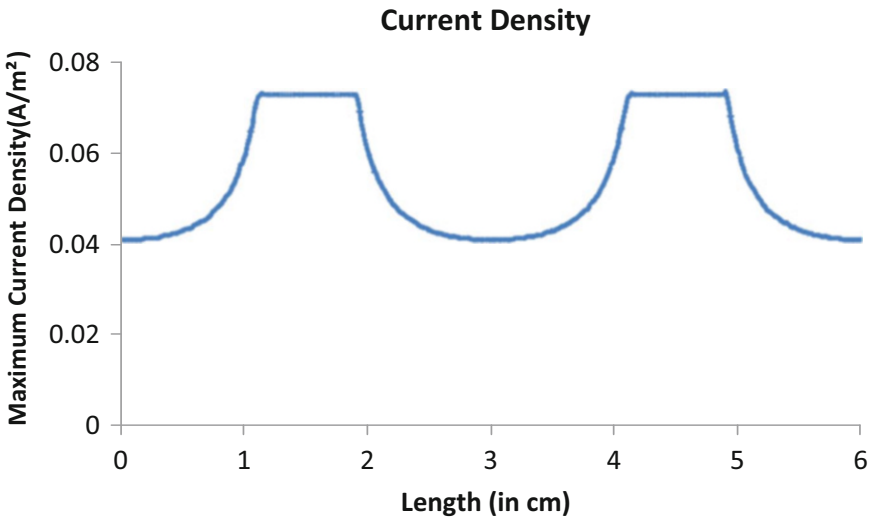

Fig. 9.7 Current density distribution obtained for continuous excitation[e]

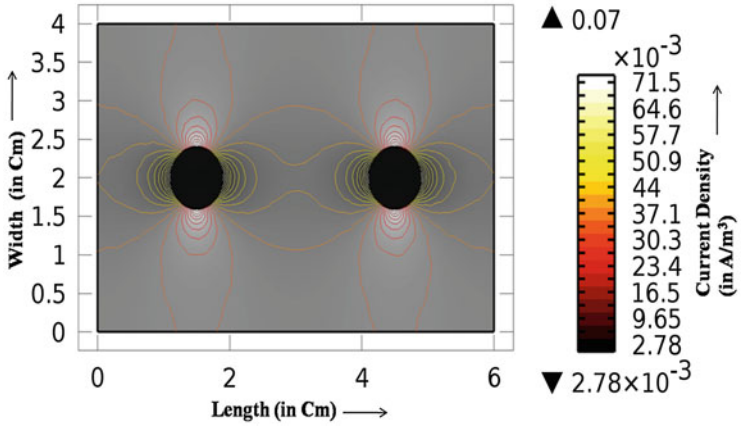

Fig. 9.8 Field line distribution of current density[f]

The current density values obtained along the line, for continuous stimulation, has been graphically shown in Fig. 9.7. The value of the current density is at its peak at the point where the electrodes are positioned, but as we move away from the electrodes, its value starts decreasing exponentially. We have used circular electrodes for excitation. Because of the circular geometry of the electrode the current density remains constant within each electrode. Rectangular electrodes have sharp edges, as a result of which more surface area is exposed per unit volume. This increases the current density at the edges. But a circular electrode acts as an equipotential surface. In our simulation the minimum value obtained is

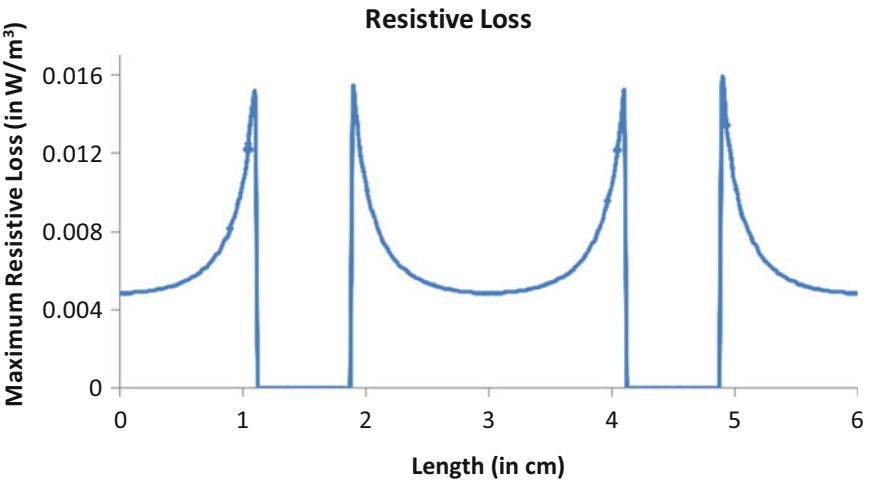

Fig. 9.9 Resistive loss obtained for continuous excitation[g]

approximately 0.04 A/m^2. The field lines of the current density distribution along the entire surface area of the skin, of our proposed model, are shown in Fig. 9.8.

9.5.2 Resistive Loss

The flow of electric current through a resistive material results in production of heat. This resistive heating is due to the friction created by retarding forces and collisions involving the charge carriers. The power loss incurred as a result of this heating is known as the resistive loss. The resistive loss is given by the following equation:

$$P = VI = I^2R \tag{9}$$

where P is the resistive power loss, V is the voltage applied, I is the value of current through a resistor, and R is the value of resistance. The amount of power loss at a constant voltage is more dependent on the amount of current change than the change in resistance. Hence as the current density decreases, the amount of power loss also decreases and vice versa. This statement holds good when the material is a dielectric, but when it is a conductor, the pattern of resistive loss changes. It is known that the conductance is inverse of the contact impedance. So in case of copper electrodes conductance is maximum and resistance is minimum (almost zero). This implies that

resistive loss is also minimum (almost zero). The resistive loss pattern obtained from our proposed model is shown graphically in Fig. 9.9.[1]

9.5.3 *Electric Field Displacement*

A dielectric (skin), in presence of an external field acts as a free-space arrangement of dipoles. The centers of these dipoles do not necessarily coincide. These dipoles not being free charge have negligible contribution in the conduction process. Since they are bound in their place by atomic and molecular forces, the dipoles only shift their positions in response to externally applied field [56]. These dipoles are bound charges and these determine conductivity. Every type of dipole is described by a dipole moment, p, given by:

$$\mathrm{p} = \mathrm{Q} \times \mathrm{d} \tag{9.10}$$

where Q is the positive charge of the two bound charges of the dipole and d is the distance between the positive and negative charge. The unit of p is coulomb-meters (C-m).

Since we have an entire volume that is full of dipoles, we could consider that there are n dipoles per unit volume. In that case the total dipole moment is given as:

$$p_{total} = \sum_{i=1}^{n\Delta v} p_i \tag{9.11}$$

Using Eq. 9.1.11 we define polarization P, as the dipole moment per unit volume, with unit coulombs per square meter (C/m^2). Polarization, P, is expressed as:

$$P = \lim_{\Delta v \to 0} \frac{1}{\Delta v} \sum_{i=1}^{n\Delta v} p_i \tag{12}$$

The polarization factor, P, is used to compute the electric field displacement (in C/m^2). The excitation electrodes, E1 and E2 were excited with a continuous 12 V, A.C. signal of 15 kHz. Then the corresponding electric field displacement (in C/m^2) was observed. Based on the above equations, the maximum and minimum values of electric field displacement were found to be 34.5×10^{-9} C/m^{2}and 8.42×10^{-10} C/m^2 (respectively). The observed electric displacement field pattern is shown in

[1] a,b,c,d,e,f,g,h,i Reprinted from,"A 2d electrode-skin model for electrical & contact impedance characterization of bio impedance", by S. Ghosh, M. Mahadevappa and J. Mukhopadhyay, 2016 IEEE Region 10 Conference (TENCON), pp. 2292–2295, IEEE, 2016, with permission from IEEE, (licence No.: 4943680947059)

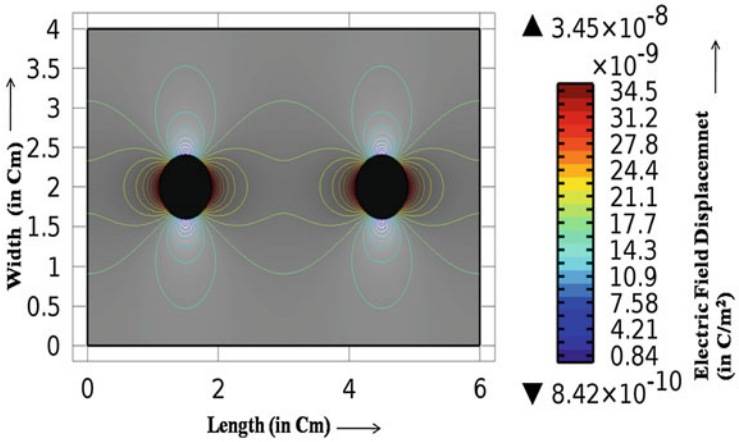

Fig. 9.10 Electric field displacement obtained after continuous excitation[h]

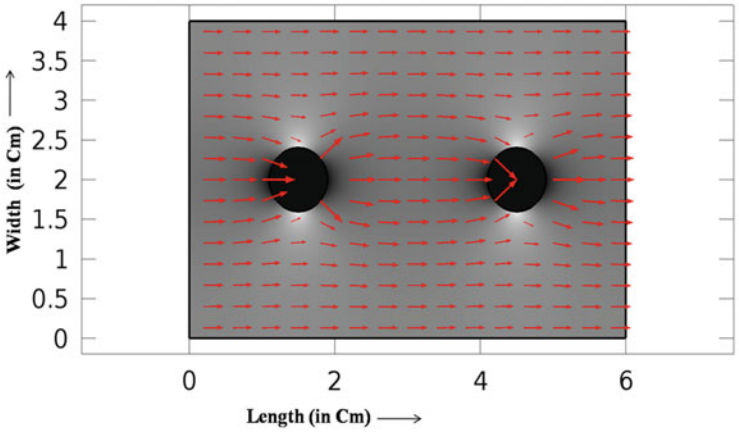

Fig. 9.11 Direction of electric field displacement[i]

Fig. 9.10. The direction of electric field due to the excitation current is from E1 to E2, as shown in Fig. 9.11.

9.6 ICG Acquisition

9.6.1 Frequency and Current Values

In cases related to impedance cardiography applications, frequencies in the range of 20–100 kHz and sinusoidal current between 1 and 5 mA [53, 57] are usually used.

Table 9.4 Physiological effects of cuurent(A.C.) at f = 60 hz, for 1 to 3 seconds [53]

Below 1 mA	Generally not perceptible
1 mA	Faint tingle
5 mA	Slight shock felt, not painful but disturbing; Average individual can let go; strong involuntary reactions
6 to 25 mA (women)	Painful shock, loss of muscular control
9 to 30 mA (men)	The freezing current, exterior muscles are stimulated
50 to 150 mA	Extreme pain, respiratory arrest
1000 to 4300 mA	Heart ceases pumping
10,000 mA	Cardiac arrest, severe burns, death

However lower values of current and frequencies have also been used by some researchers. The values of current and frequency areto be chosen in a manner, which provides with sufficient signal-to-noise ratio, and at the same time prevents the subjects from any adverse physiological effects. The skin-electrode impedance at 100 kHz is 100 times lower than that at low frequencies. Higher frequency value also helps in diminishing any unwanted impact on skin-electrode impedance, occurring due to subject's motion, while impedance cardiography signals are being monitored. However, increasing frequency of the applied current above 100 kHz may also produce stray capacitances. The physiological effect of current (A.C.) at a frequency of 60 hz, for 1 to 3 seconds, on a human subject is tabulated in Table 9.4.

9.6.2 ICG Measurement Methods

The two major methods of impedance cardiography (ICG)/bio-impedance measurements are: (a) bipolar and (b) tetrapolar modes of measurement. In bipolar mode, two electrodes are used, which serve the purpose of both, excitation as well and voltage reception. Current density in the neighborhood of the electrodes is higher in comparison withthe other surrounding region. This results in a non-uniform distribution of the total bio-impedance to be measured. The total bio-impedance signal is a superposition of two components: the skin-electrode impedance (modified by blood flow-induced movement) and the original signal (e.g. caused by the blood flow). A schematic representation of the bipolar mode of bio-impedance measurement is shown in Fig. 9.12a. In tetrapolar mode of bio-impedance measurement, two different sets of electrodes are used (four electrodes in total). One set of electrodes serve as the application (excitation) electrodes and the other set of electrodes act as the voltage receiving electrodes. Figure 9.12b shows a schematic representation of the tetrapolar mode of bio-impedance measurement. In tetrapolar mode of ICG measurements, a constant amplitude current is injected using the excitation electrodes (C), and the changes in voltage are received by the voltage sensing electrodes (R). The constant amplitude current generates a voltage which is proportional to the impedance of the tissue segment wherein the current is applied. In general the

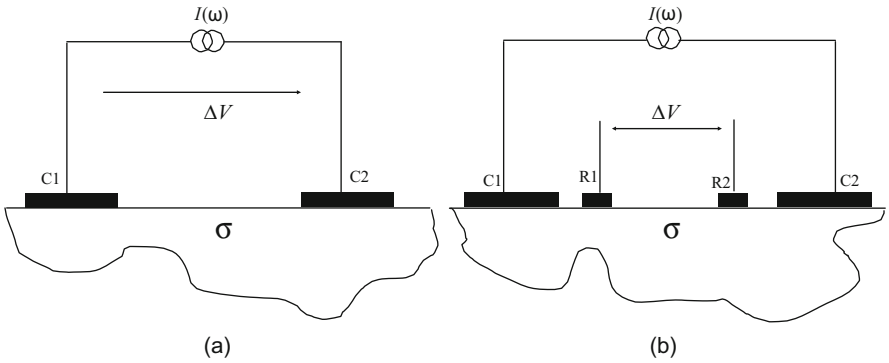

Fig. 9.12 (**a**) Bipolar Arrangement and (**b**) Tetrapolar Arrangement of electrodes

tetrapolar mode is preferred over bipolar mode of bio-impedance measurement, as the current density is uniformly distributed in case of the tetrapolar mode of measurement.

9.7 ICG Device Fabrication

A cost-effective, easy-to use impedance cardiography (ICG) device for recording ICG signals from subjects is proposed. The basic block diagram of the implemented circuit is shown in Fig. 9.13. The device is designed for use on the subject's forearm, with the aid of tetrapolar configuration. The device uses a function generator to generate a biphasic sinusoidal wave of 50% duty cycle. The generated signal is found to be oscillating about a value much higher than D.C. zero, so the generated sine wave is fed into a subtractor in order to receive a signal which oscillates about D.C. zero. The generated signal has to have 50% duty cycle such that there is no charge accumulation on the skin surface of the subject. Charge accumulation has to be zero so that there is no risk of skin burn to the subject. The signal thus generated is then amplified using an operational amplifier based non-inverting amplifier and fed into a voltage to current converter. The voltage to current converter is designed in a floating ground configuration. The output of the voltage to current converter is then fed into two excitation electrodes, placed on the forearm of the subject. The specifications of the excitation pulse injected through the excitation electrodes are as follows:

- Frequency: 15 kHz.
- Current: 3 mA.
- Source type: Sine Wave.

The voltage sensing electrodes (R1, R2), on a subject's forearm are placed in between the two excitation electrodes (C1, C2). The positioning of the electrodes is

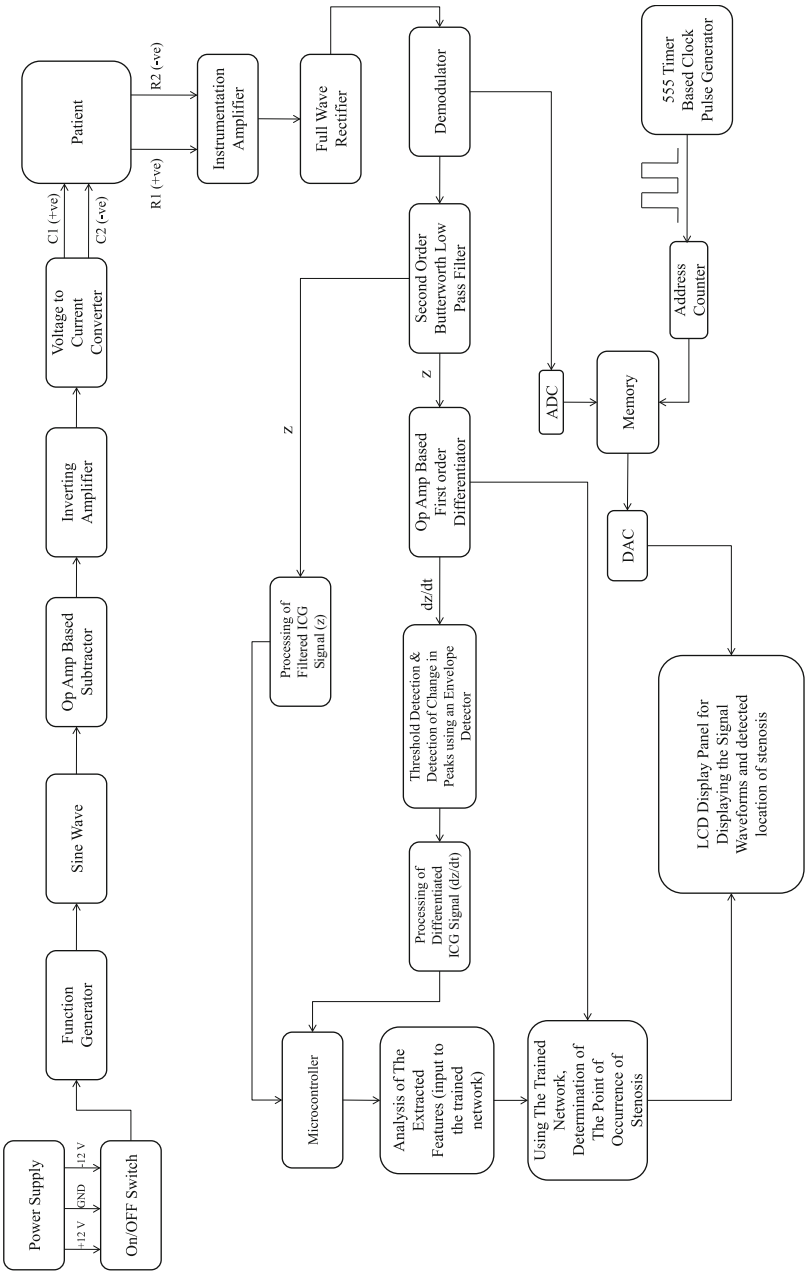

Fig. 9.13 Block diagram of the implemented circuit

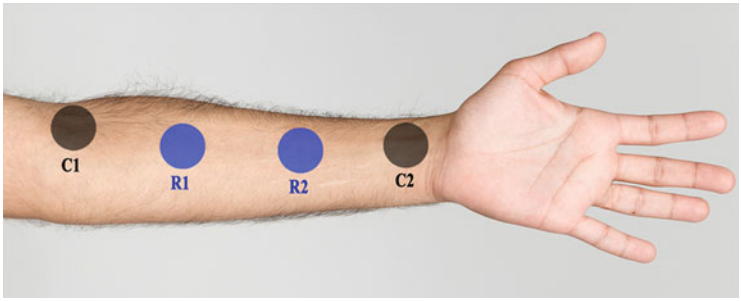

Fig. 9.14 Electrode placement on the fore-arm of the subject[1]

Table 9.5 Features extracted from the ICG signal

Type	Description
Pressure features	Systolic blood pressure Diastolic blood pressure Peak systolic pressure Peak diastolic pressure Mean blood pressure
Time features	Heart rate Systolic duration Diastolic duration Cardiac cycle
Area features	Area under one cardiac cycle Systolic area Diastolic area Area under differentiated wave
Amplitude features	Difference of first two peaks of the extracted cardiac cycle (P1-P2) difference of next two peaks of the extracted cardiac cycle (P3-P4) augmentation index (*AIx*)

shown in Fig. 9.14, where R1, R2 are the voltage sensing electrodes and C1, C2 are the excitation electrodes. The voltage signal received by the electrodes R1 and R2 is fed into an instrumentation amplifier, which is further rectified using a full wave rectifier. The full wave rectified signal is further fed into a demodulator which eliminates the 15 kHz carrier wave from the sensed signal. Once the signal is demodulated, it is passed through a second order low-pass Butterworth filter, with a cut-off frequency of 250 Hz (Table 9.5, and Fig. 9.15).

The filtered signal is further bifurcated into two channels. One of the channels carries the filtered signal onto a separate circuit designed only for the processing of filtered signal (marked as "Processing of filtered ICG signal (z)", in Fig. 9.13). Whereas the other channel feeds the filtered signal onto an operational amplifier based first order differentiator. The differentiator provides us with the first order differentiated ICG signal (dz/dt), which is then sent to an envelope detector for

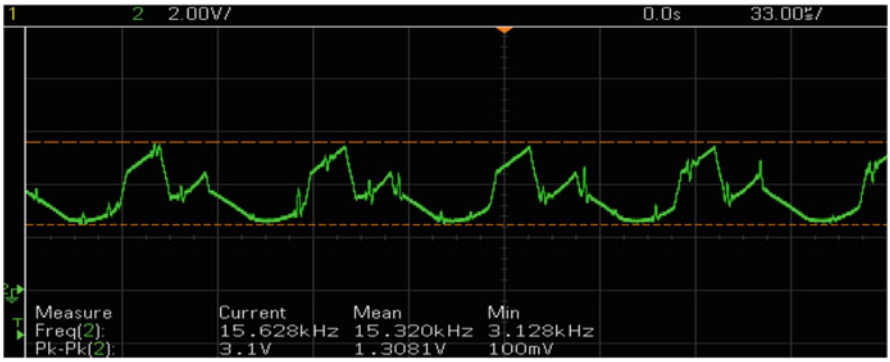

Fig. 9.15 Actual ICG signal recorded before filtering (raw signal)[2]

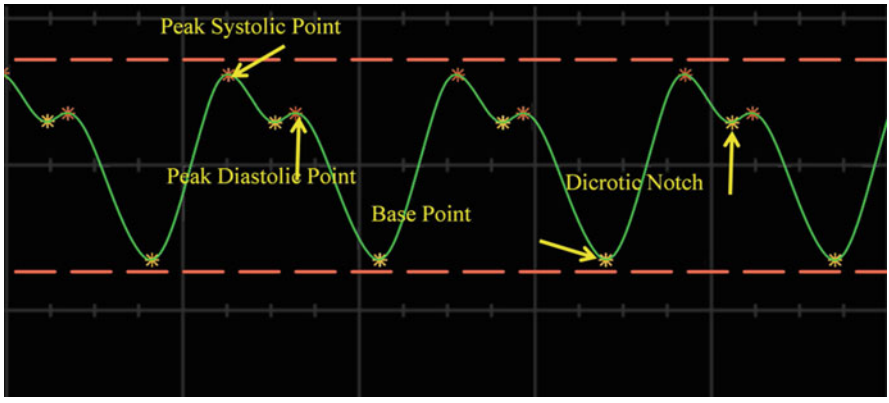

Fig. 9.16 Filtered ICG signal obtained after passing the raw signal through a low pass butterworth filter[3]

detection of various peaks in the signal based on threshold values. The envelope detector further advances the signal to a separate circuitry designed only for the processing of first order differentiated signal (marked as "Processing of filtered ICG signal (*dz/dt*)", in Fig. 9.13). The circuitry designed for processing of the filtered signal (z) helps us in the identification of various feature points in the ICG signal related to cardiac cycle of the recruited subject. The filtered signal is also further processed using envelope detector and an adaptive thresholding in order to identify the best available cardiac cycles. This signal is also used to identify peak systolic point, peak diastolic point, dicrotic notch, and base point as shown in Fig. 9.16.

The circuitry designed for processing the differentiated signal (*dz/dt*) is used for extraction of a feature called "Augmentation Index" (*AIx*). In order to obtain *AIx* the differentiated signal is again passed through a differentiator, and a Butterworth

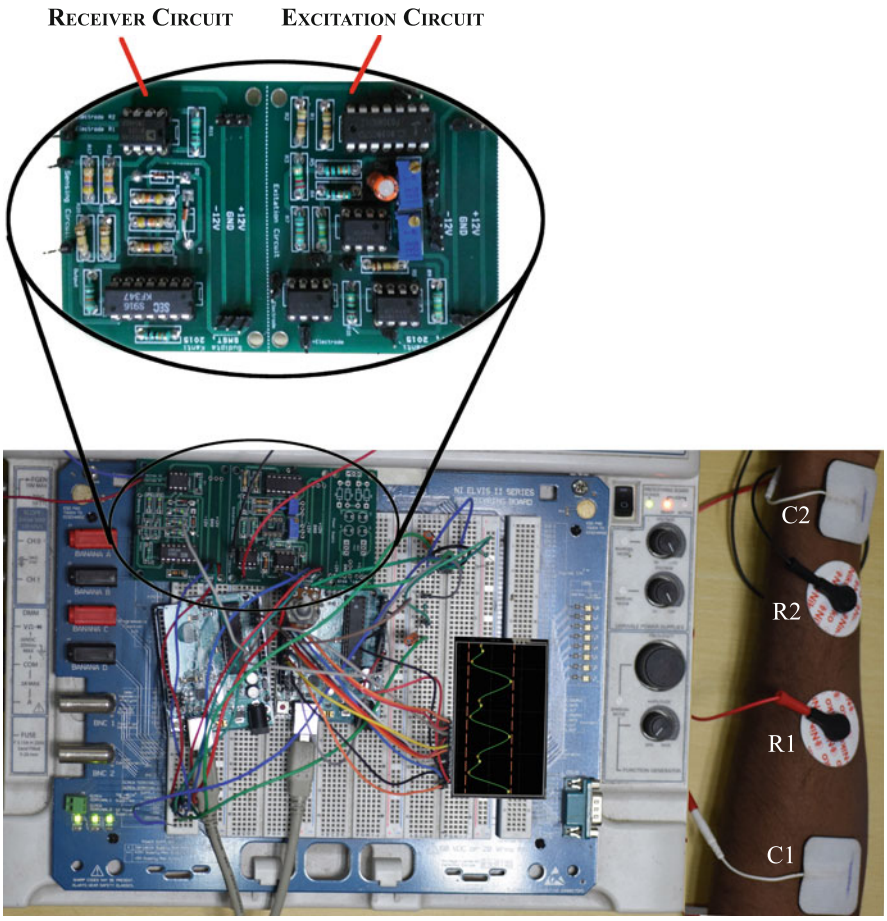

Fig. 9.17 Illustrative image of the prototype developed with electrodes placed on the arm[4]

low-pass filter of order 2 and a cutoff frequency of 250 Hz. The first order and the second order differentiated signals are individually passed through two different envelope detectors in order to identify the peaks required for calculation of *AIx*. Figure 9.17[2] shows a snapshot of the device acquiring ICG signal from a subject.

[2 1,2,3,4]Reprinted from,"Estimation of echocardiogram parameters with the aid of impedance cardiography and artificial neural networks", by S. Ghosh, B. P. Chattopadhyay, R. M. Roy, J. Mukherjee, and M. Mahadevappa, Artificial intelligence in medicine, vol. 96, pp. 45–58, 2019, with permission from Elsevier, (Licence No.: 4943690013102)

9.8 Conclusion

The aim of this chapter is to discuss a method for designing a cost-effective solution for monitoring one's cardiac health. The discussed methodology leads to the development of a bedside cardiac health monitoring device that could be used by any individual without the requirement of any expert supervision. The features extracted from the ICG signal could be used for prediction of various hemodynamic parameters like: Stroke Volume, Left Ventricular Ejection Fraction, Myo-cardial Performance Index, etc. Researchers have conducted various studies [58, 59] wherein the disscused methodology has been used for acquiring ICG signal, and therein predicting various hemodynamic parameters related to cardiac functioning.[3]

References

1. Bigatello, L., & George, E. (2002). Hemodynamic monitoring. *Minerva Anestesiologica, 68*(4), 219–225.
2. Kubicek, W. G. (1966). Development and evaluation of an impedance cardiac output system. *Aerospace Medicine, 37*, 1208–1212.
3. Dehghan, M., & Merchant, A. T. (2008). Is bioelectrical impedance accurate for use in large epidemiological studies? *Nutrition Journal, 7*(1), 26.
4. Batyuk, L., & Kizilova, N. (2018). Modeling of dielectric permittivity of the erythrocytes membrane as a three-layer model. In *Development trends in medical science and practice: the experience of countries of Eastern Europe and prospects of Ukraine: monograph* (pp. 18–37).
5. Palko, T., & Galwas, B. (1999). Electrical properties of biological tissues, their mea- surements and biomedical applications. *Automedica, 17*(4), 343.
6. Wtorek, J., Polinski, A., Stelter, J., & Nowakowski, A. (1998). Cell for measurements of biological tissue complex conductivity. *Technology and Health Care, 6*(2), 177–193.
7. Martinsen, O. G., & Grimnes, S. (2011). *Bioimpedance and bioelectricity basics*. Academic Press.
8. Wtorek, J., & Polinski, A. (2005). The contribution of blood-flow-induced conductivity changes to measured impedance. *IEEE Transactions on Biomedical Engineering, 52*(1), 41–49.
9. Geddes, L. A., & Baker, L. E. (1967). The specific resistance of biological material–a compendium of data for the biomedical engineer and physiologist. *Medical & Biological Engineering, 5*(3), 271–293.
10. Malmivuo, J., Plonsey, R., et al. (1995). *Bioelectromagnetism: principles and applications of bioelectric and biomagnetic fields*. Oxford University Press.
11. Charloux, A., Lonsdorfer-Wolf, E., Richard, R., Lampert, E., Oswald-Mammosser, M., Mettauer, B., Geny, B., & Lonsdorfer, J. (2000). A new impedance cardio- graph device for the non-invasive evaluation of cardiac output at rest and during exercise: comparison with the "direct" fick method. *European Journal of Applied Physiology, 82*(4), 313–320.
12. Geddes, L., & Sadler, C. (1973). The specific resistance of blood at body temperature. *Medical & Biological Engineering, 11*(3), 336–339.
13. Nyboer, J. (1950). Plethysmography. Impedance. *Medical Physics, 2*, 736–743.

[3]The authors declare that a patent has been filed for the device discussed in this chapter, vide application number KOL/201831001822

14. Nyboer, J., Kreider, M. M., & Hannapel, L. (1950). Electrical impedance plethysmog- raphy: a physical and physiologic approach to peripheral vascular study. *Circulation, 2*(6), 811–821.
15. Boer, P., Roos, J., Geyskes, G., & Mees, E. (1979). Measurement of cardiac out- put by impedance cardiography under various conditions. *The American Journal of Physiology - Heart and Circulatory Physiology, 237*(4), H491–H496.
16. Porter, J., & Swain, I. (1987). Measurement of cardiac output by electrical impedance plethysmography. *Journal of Biomedical Engineering, 9*(3), 222–231.
17. Ito, H., Yamakoshi, K., & Togawa, T. (1976). Transthoracic admittance plethysmo- graph for measuring cardiac output. *Journal of Applied Physiology, 40*(3), 451–454.
18. Keim, H. J., Wallace, J. M., Thurston, H., Case, D. B., Drayer, J., & Laragh, J. H. (1976). Impedance cardiography for determination of stroke index. *Journal of Applied Physiology, 41* (5), 797–799.
19. Anderson, F., Penney, B., Patwardhan, N., & Wheeler, H. (1980). Impedance plethysmography: the origin of electrical impedance changes measured in the human calf. *Medical & Biological Engineering & Computing, 18*(2), 234–240.
20. Kim, D. W., Baker, L., Pearce, J., & Kim, W. K. (1988). Origins of the impedance change in impedance cardiography by a three-dimensional finite element model. *IEEE Transactions on Biomedical Engineering, 35*(12), 993–1000.
21. Kosicki, J., Chen, L.-h., Hobbie, R., Patterson, R., & Ackerman, E. (1986). Contribu- tions to the impedance cardiogram waveform. *Annals of Biomedical Engineering, 14*(1), 67–80.
22. Patterson, R. P. (1985). Sources of the thoracic cardiogenic electrical impedance signal as determined by a model. *Medical & Biological Engineering & Computing, 23*(5), 411–417.
23. Sakamoto, K., Muto, K., Kanai, H., & Iizuka, M. (1979). Problems of impedance cardiography. *Medical & Biological Engineering & Computing, 17*(6), 697–709.
24. Shankar, T., Webster, J., & Shao, S. (1986). The contribution of vessel volume change to the electrical impedance pulse. *IEEE Transactions on Biomedical Engineering, 1*, 42–47.
25. Thomsen, A. (1979). Impedance cardiography. *Intensive Care Medicine, 5*(4), 206–206.
26. Raaijmakers, E., Faes, T., Goovaerts, H., De Vries, P., & Heethaar, R. (1997). The inaccuracy of kubicek's one-cylinder model in thoracic impedance cardiography. *IEEE Transactions on Biomedical Engineering, 44*(1), 70–76.
27. Bonjer, F., Van Den Berg, J., & Dirken, M. (1952). The origin of the variations of body impedance occurring during the cardiac cycle. *Circulation, 6*(3), 415–420.
28. Penney, B. C. (1986). Theory and cardiac applications of electrical impedance measure- ments. *Critical Reviews in Biomedical Engineering, 13*(3), 227–281.
29. Mohapatra, S. N. (1981). *Non-invasive cardiovascular monitoring by electrical impedance technique*. Pitman Med.
30. P. Chandra, Nanobiosensors for personalized and onsite biomedical diagnosis. The Institution of Engineering and Technology, 2016
31. P. Chandra and L. M. Pandey, "Biointerface engineering: prospects in medical diagnostics and drug delivery," 2020
32. Purohit, B., Kumar, A., Mahato, K., & Chandra, P. (2020). Smartphone-assisted person- alized diagnostic devices and wearable sensors. *Current Opinion Biomed Eng, 13*, 42–50.
33. Purohit, B., Vernekar, P. R., Shetti, N. P., & Chandra, P. (2020). Biosensor nanoengi- neering: design, operation, and implementation for biomolecular analysis. *Sensors International*, 100040.
34. Arshad, W., Duncan, A. M., Francis, D. P., O'sullivan, C. A., Gibson, D. G., & Henein, M. Y. (2004). Systole-diastole mismatch in hypertrophic cardiomyopathy is caused by stress induced left ventricular outflow tract obstruction. *American Heart Journal, 148*(5), 903–909.
35. G. P. Cybulski, Dynamic impedance Cardiography-the system and its applications. Polish Society of Medical Physics, 2005
36. Frey, M., & Doerr, B. (1983). Correlations between ejection times measured from the carotid pulse contour and the impedance cardiogram. *Aviation, Space, and Environmental Medicine, 54* (10), 894–897.

37. Lewis, R. P., Boudoulas, H., Leier, C. V., Unverferth, D. V., & Weissler, A. M. (1982). Usefulness of the systolic time intervals in cardiovascular clinical cardiology. *Transactions of the American Clinical and Climatological Association, 93*, 108.
38. Weissler, A. M., Harris, W. S., & Schoenfeld, C. D. (1968). Systolic time intervals in heart failure in man. *Circulation, 37*(2), 149–159.
39. Weissler, A. M., Peeler, R. G., & Roehll, W. H., Jr. (1961). Relationships between left ventricular ejection time, stroke volume, and heart rate in normal individuals and patients with cardiovascular disease. *American Heart Journal, 62*(3), 367–378.
40. Penaz, J., Voigt, A., & Teichmann, W. (1976). Contribution to the continuous indirect blood pressure measurement. *Zeitschrift fur die gesamte innere Medizin und ihre Grenzgebiete, 31* (24), 1030–1033.
41. Miyamoto, Y., Higuchi, J., Abe, Y., Hiura, T., Nakazono, Y., & Mikami, T. (1983). Dy- namics of cardiac output and systolic time intervals in supine and upright exercise. *Journal of Applied Physiology, 55*(6), 1674–1681.
42. Miyamoto, Y., Hiura, T., Tamura, T., Nakamura, T., Higuchi, J., & Mikami, T. (1982). Dynamics of cardiac, respiratory, and metabolic function in men in response to step work load. *Journal of Applied Physiology, 52*(5), 1198–1208.
43. Miyamoto, Y., Takahashi, M., Tamura, T., Nakamura, T., Hiura, T., & Mikami, M. (1981). Continuous determination of cardiac output during exercise by the use of impedance plethysmography. *Medical & Biological Engineering & Computing, 19*(5), 638–644.
44. Miles, D. S., Sawka, M. N., Hanpeter, D. E., Foster, J. E., Jr., Doerr, B. M., & Frey. (1984). Central hemodynamics during progressive upper-and lower-body ex- ercise and recovery. *Journal of Applied Physiology, 57*(2), 366–370.
45. Bogaard, H., Woltjer, H., Postmus, P., & De Vries, P. (1997). Assessment of the haemodynamic response to exercise by means of electrical impedance cardiography: method, validation and clinical applications. *Physiological Measurement, 18*(2), 95.
46. Rosenberg, P., & Yancy, C. W. (2000). Noninvasive assessment of hemodynamics: an emphasis on bioimpedance cardiography. *Current Opinion in Cardiology, 15*(3), 151–155.
47. Jensen, L., Yakimets, J., & Teo, K. K. (1995). A review of impedance cardiography. *Heart & Lung: The Journal of Acute and Critical Care, 24*(3), 183–193.
48. Lorne, E., Mahjoub, Y., Diouf, M., Sleghem, J., Buchalet, C., Guinot, P.-G., Petiot, S., Kessavane, A., Dehedin, B., & Dupont, H. (2014). Accuracy of impedance cardiography for evaluating trends in cardiac output: a comparison with oesophageal doppler. *British Journal of Anaesthesia, 113*(4), 596–602.
49. Sadauskas, S., Naudziuunas, A., Unikauskas, A., et al. (2016). Applicability of impedance cardiography during heart failure flare- ups. *Medical Science Monitor: International Medical Journal of Experimental and Clinical Research, 22*, 3614.
50. Silva, L. D. S., Reis, F. F., Silva, M. E. S., & Lima, D. V. M. D. (2018). Accuracy of impedance cardiography in acute myocardial infarction: a literature review. *Int J Cardiovascular Sci, 31*(3), 282–289.
51. Ghosh, S., Mahadevappa, M., & Mukhopadhyay, J. (2016). A 2d electrode-skin model for electrical & contact impedance characterization of bio impedance. In *2016 IEEE region 10 conference (TENCON), pp. 2292–2295*. IEEE.
52. Cardu, R., Leong, P. H., Jin, C. T., & McEwan, A. (2012). Electrode contact impedance sensitivity to variations in geometry. *Physiological Measurement, 33*(5), 817.
53. Webster, J. G. (2009). *Medical instrumentation application and design*. John Wiley & Sons.
54. D. Andreuccetti, (2012). "*An internet resource for the calculation of the dielectric prop- erties of body tissues in the frequency range 10 hz-100 ghz*," http://niremf.ifac.cnr.it/tissprop/
55. Luna, J. L. V., Krenn, M., Ramırez, J. A. C., & Mayr, W. (2015). Dynamic impedance model of the skin-electrode interface for transcutaneous electrical stimulation. *PLoS One, 10*(5), e0125609.

56. Hayt, W. H., Buck, J. A., et al. (1981). *Engineering electromagnetics* (Vol. 6). McGraw-Hill.
57. Ghosh, S., Giri, S., Kruthika, R., Chabhra, G. S., Mahadevappa, M., & Mukhopadhyay, J. (2016). Electrical impedance plethysmography based device for aortic pulse monitoring. In *Systems in Medicine and Biology (ICSMB), 2016 Interna- tional conference on* (pp. 124–127). IEEE.
58. Ghosh, S., Chattopadhyay, B. P., Roy, R. M., Mukherjee, J., & Mahadevappa, M. (2019). Estimation of echocardiogram parameters with the aid of impedance cardiog- raphy and artificial neural networks. *Artificial Intelligence in Medicine, 96*, 45–58.
59. Ghosh, S., Chattopadhyay, B. P., Roy, R. M., Mukhopadhyay, J., & Ma-hadevappa, M. (2018). Stroke volume, ejection fraction and cardiac health monitoring us- ing impedance cardiography. In *2018 40th annual international conference of the IEEE engineering in medicine and biology society (EMBC)* (pp. 4229–4232). IEEE.

Chapter 10
Tailoring Multi-Functional 1D or 2D Nanomaterials: An Approach towards Engineering Futuristic Ultrasensitive Platforms for Rapid Detection of Microbial Strains

Preetam Guha Ray, Baisakhee Saha, Pravin Vaidya, Hema Bora, Krishna Dixit, Asmita Biswas, and Santanu Dhara

10.1 Introduction

The associated surge in complexity of regular activities surrounding the environment have not only facilitated our lifestyle but also induced significant changes in genomic architecture of the microbial community as well. The re-alignment of demographic needs with changing decades has not only revolutionized technological accreditation of the civilized society but also aroused global obligations associated with it. Although certain changes were beneficial and worked symbiotically, however, unwanted mutation also provoked evolution of immolating malicious microbes which had huge social-economic impacts leading to dreadful epidemic or pandemic situations, the current manifestation of COVID-19 pandemic being the worst of all. Simultaneously, the research world had been witnessing a paradigm shift in the fields of information technology, electronic devices, homeland security, medicines, transportation, energy, and others, with the advent of technological solutions associated with nanoparticles [1–3]. The saga of such application can only be forecasted to advance rapidly in combination with upcoming technological advancements. Similar effects were also witnessed in healthcare sector wherein significant developments were observed in subjects related to tissue engineering, in vivo imaging, in vitro diagnostics, drug delivery, or molecular therapeutics [4, 5].

Nano-engineered systems are already being deployed as advanced drug carrier in the application of targeted drug delivery or components of such system have also been utilized for therapeutics in direct physical destruction of malignant tissues [4]. Several nanofibrous scaffolds are undergoing substantial clinical trials for

P. Guha Ray · B. Saha · P. Vaidya · H. Bora · K. Dixit · A. Biswas · S. Dhara (✉)
Biomaterials and Tissue Engineering Laboratory, School of Medical Science and Technology (SMST), Indian Institute of Technology Kharagpur, Kharagpur, India
e-mail: sdhara@smst.iitkgp.ac.in

V. Borse et al. (eds.), *BioSensing, Theranostics, and Medical Devices*,
https://doi.org/10.1007/978-981-16-2782-8_10

possible therapy in regenerative applications [6, 7]. Furthermore, in nano-bio-sensing, such nano-engineered systems have shown promising implications in contributing effectively in current medical practices [8]. A lot of such concepts related to diagnostics applications were grown on the concept of metal/metal oxide nanoparticles exploiting their surface-enhanced properties, perpetuating their significant contribution in the above areas [9]. In the past decade, 1D or 2D nanomaterials have gained much attention in fabricating electrical/electrochemical devices for rapid and ultrasensitive label-free detection of biomolecules. Finally, easy in-solution process-ability makes it an attractive alternative for fabrication of micro to nanoscale electronic devices thus improving its performance. 1D or 2D nanomaterials are those wherein one or two dimensions are particularly outside the nanoscale, for example, nanowires, nanotubes, and nanofibers often represent 1D nanomaterials, while graphene, layered double hydroxides, graphitic carbon nitride (g-C_3N_4), hexagonal boron nitride (hBN), layered metal/metal oxides, and transition metal dichalcogenides (TMDs) often represent the family of 2D nanomaterial [1]. There are several advantages of using these lower dimensional nanomaterials owing to their unexpected properties such as room temperature carrier mobility, excellent electrical properties. Along with superior charge carrying properties they also possess other physico-chemical properties including quantum Hall effect, ultra-high specific area, higher young's modulus, and superior optical transparency ensures stability for practical applications [1]. Its ability to confine electrons and its ballistic transport in 1D or 2D nanomaterials promotes their excellent electrical properties, making them ideal for application in ultrasensitive detection procedures (Fig. 10.1). Subsequently, an apparently ultra-high surface area renders ample opportunity for surface modifications or functionalization in order to modify it accordingly to suit any heterogeneous bio-affinitive reactions. High surface area also increases the number of capture probes thus increasing possibility of bio-affinitive reaction with the target analyte, thus allowing easy regulation of its surface properties. For example, electrochemical sensor has been prepared using SWCNTs treated with polyethylene amine for attaching monoclonal anti-carcinoembryonic antigen antibodies to detect carcinoembryonic antigen in saliva and serum [10]. Furthermore, graphene oxide (GO) possesses high affinity towards adsorbing (single stranded) nucleic acids via pi–pi stacking through interaction between ring structures of the hexagonal cells of graphene and nucleotide bases [11]. Similar to carbon nanotubes, GO also have its own fluorescence quenching property owing to its nanoscale fluorescence resonance energy transfer (FRET) property [12]. Together, these two properties lead to the utilization of GO in fluorescent based DNA detection [13].

However, it is essential to understand the bitter truth that even after continuous development of several technologies worth billions of dollars, still only few of them could actually be taken to patient's bed side. Although there were some extremely successful point-of-care (POC) technologies that made it to the commercial market and are very popular. For instance, the first concept of point-of-care bio-sensing technology was first published in the year 1962, by Clark and Lyons wherein enzymatic oxidation of glucose by glucose oxidase (GOx) was carried out using

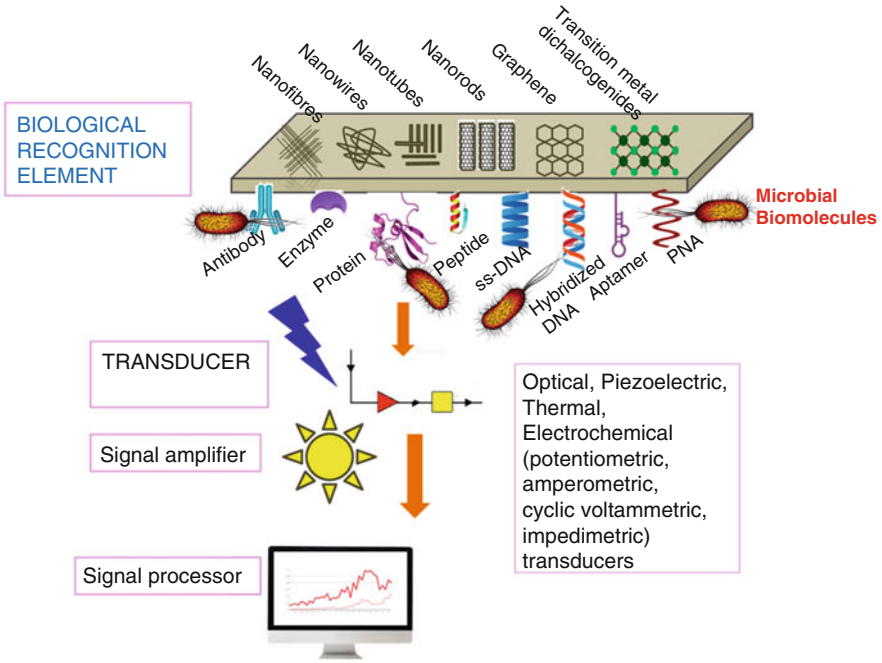

Fig. 10.1 Ultrasensitive biosensor platform with multi-functional 1D or 2D nanomaterials for rapid detection of microbial strains

Clark's oxygen electrode as selective transducer [14]. Ever since invention of the above technology, glucose biosensors have gathered much attention and compact units of such devices are made available commercially as the most used on-site and rapid diagnostic kit, available over the counter. It is being more than 50 years now and still many advance researches are going on in the same field to detect glucose from tear fluid in order to promote non-invasive detection of the analyte. Further even glucose sensor units integrated with insulin pumps are also explored for practical application. Another significant advancement in the field of bio-sensing technology came in the year 1969, when Margaret M Crane filed the patent for a diagnostic kit capable of detecting pregnancy and eventually got accepted for patenting in the year 1971 [15]. The presence of human chorionic gonadotropin (hCG) in the test sample of a female's urine is tested using a lateral flow system. hCG is a hormone, secreted by the placenta and it is supposed to be only present when a female is pregnant. The lateral flow device utilized in conducting the above test generally consists of at least two zones where primarily the bio-affinitive reactions occur. In the presence of hCG, the bound monoclonal antibodies-hCG complex will certainly mobilize polyclonal anti-hCG antibodies and the color reagent, which eventually appear as a colored stripe or dot in the test zone thus indicating pregnancy. The above narrated device is a classic example of biomolecule

immobilization using a surface functionalized test strip and subsequent availability of these biomolecules to react with the test analyte.

The introduction of DNA microarray technology endowed benefits in advent of several molecular biology tools, however, its fluorescence based optical detections system confronted several inherent shortcomings, owing to photo-bleaching of fluorescence dyes or ambiguous spectral cross-talk between dyes. Moreover, the process requires PCR for amplification and sample processing thus involving usage of bulky optical scanners limiting its deployment as a point-of care technology (POCT) [16, 17]. Apparently, it was essential to fabricate an electronic alternative of the same in order to attain enhanced sensitivity or selectivity. The development of such electronic alternatives not only facilitate in label-free detection of the microbes but their miniaturized architecture also enforces the possibility for developing multiplexed detection system for high-throughput screening [18]. Such system also possess possibility to be integrated as on-chip devices coupled to standard signal processing circuitry for signal acquisition, amplification, and detection. Metal submicron wire barcodes were used in conjunction with existing fluorescent based DNA detection assays for possible multiplexed detection procedures [19]. Thus, justifying the fact that nanoparticles could be deployed for DNA detection assays, however, in contrast to these optical methods, nanowires (NWs) or nanotubes (NTs) can also be used for label-free, ultrasensitive real-time electrical detection of biomolecule binding [20, 21].

On the horizon of biosensors for clinical diagnostics, food and beverage quality monitoring in industrial analysis enjoys a niche position in global economic market. As of year 2000, a market survey by Frost & Sullivan forecasted a market size of US $ 895 million in the field of biomedical engineering and of which medical devices account for close to US$ 300 million in sales. The radical growth in bio-sensing industry is estimated to be CAGR of 8.84% and touch USD 27.06 billion by 2022. The above statistics definitely projected amplifying demand of biosensors in the areas of quality monitoring of food and beverages, biodefense, healthcare or environmental monitoring worldwide.

10.2 1D or 2D Nanomaterials and its Sensing Application

10.2.1 1D Nanomaterials

10.2.1.1 Nanofibers

Nanofibers (NF), commonly fabricated by the process of electrospinning, claim importance owing to their larger surface area and high aspect ratio which provides a better signal-to-noise ratio and biochemical binding of the sensor [22]. Air pockets in electrospun NFs provide greater hydrophobicity while their porosity imparts high contact angle. Droplet and fluorescence based immunoassay was performed on “sticky” NF surface of electrospun polycaprolactone fibers of indium-tinoxide

glass for dual detection of S*almonella typhimurium* and *E. coli*-K12 by smartphones. The sticky surface provides a non-slip surface for droplet adhesion, while NFs provide local hydrophilicity (74°) facilitating the same [23]. Nanofibrous nitrocellulose membrane functionalized with respective antibodies functions as a low-cost biosensor for both viral and bacterial pathogens—bovine viral diarrhea virus (BVDV) and *Escherichia coli* O157:H7 with detection time of 8 mins and detection limits of 103 CCID/mL and 61 CFU/mL for the viral and bacterial samples, respectively. Oxygen plasma treatment further enhanced the capillary action of the NF membrane [24]. NF-light addressable potentiometric sensor (LAPS) was utilized separately for pH-sensitive hydrogel based has been developed for antigen-antibody detection. LAPS was integrated with electrospun polyacrylic acid/PVA (PAA/PVA) nanofibers as sensing layer (NF-LAPS) for detecting pH change in media while using *E. coli* to ferment sugar molecules. Furthermore, N-butyl acetate functionalized nano/microfibers of naturally occurring eggshell membrane was also deployed with efficient detection of E. coli O157/ H7 bacterial DNA responsible for producing Shiga toxin [25]. Also high sensitivity towards detection of *E. coli* was also achieved using d-mannose functionalized NFs. It selectively sensed mannose specific lectins belonging to *E. coli* rendering super-Nernstian response of 74 mV/pH change which could be related to a detection limit of 20 CFU/ml [26]. Analyte capture and concentration is also specifically done by NFs for better purification and detection. On-chip concentration of bacterial cells, *E. coli* K12, has been carried out by attaching anti-*E. coli* K12 antibodies on PVA NF mats with –COOH groups via EDC/NHS chemistry, which could retain negatively charged bacteria with non-specific electrostatic interactions and antibody-dependent specific capture [27].

10.2.1.2 Nanowires

Nanowires (NW) are solid fibers with diameter in the nanoscale range generally having length to width ratio $>$ 1000. These excellent electrical tools are being exploited as sensors since these can detect the binding events due to change in charge density on their surface upon binding of biomolecules like proteins, nucleic acids, peptide-nucleic acids (PNA), DNA-DNA hybridization, and also due to cell membrane potential and biomolecular charges [18, 28]. Any perturbation of electric fields on the surface of NW Field Effect Transistors (FET) bring about a large electrostatic modulation of carrier density owing to their higher surface area in order to create a Debye length screening [29]. An exponential decay in electrostatic potential was observed with distance, since net positive charges were neutralized by net negative charges on the NW [30]. Even a single biomolecule on the surface of the NW brings about perturbation in the electric field to cause either a charge accumulation or depletion, deep into the whole NW and consequently changes the flow of current in the channel [31]. Thus, NWs are aptly tailored to serve as highly sensitive biosensors. Metal oxide NWs with diameter range within tens of nanometers are quasi-1D crystalline structures with very high surface-to-volume ratio with bulk of atoms on the surface thereby enhancing the sensing ability via surface phenomenon.

Moreover, since these are almost fixed single crystals, hence there is minimum instability due to penetration and movement of signal molecules. In NW-mediated lysis method, for Gram-positive (*Bacillus subtilis*) and negative bacteria (*E. coli*) or yeast, cells are entangled within 30 nm diameter nanowires (SnO_2 or SiO_2). SiO_2 has better bacterial adsorption and biocompatibility and SnO_2 has better bacterial recovery rate. The membrane between the nanowires is ruptured by the shear force. A potential of 500 V/cm was applied for DNA extraction. Integration of this technique with loop-mediated isothermal amplification (LAMP) provides a single step rapid, detection assay for visual chromatic microbial cells [32]. Silicon nanowire (SiNW) array based biointerface is able to sense and exhibit high capture capacity for *E. coli* and *S. aureus* in drinking water at 8.6 and 5.5 $\times$ 10^6 cells per cm^2 in 40 min, respectively, by providing attachment sites for bacterial adhesins. SiNWs-Au@Ag interface directly captures bacteria, and was identified with laser induced breakdown spectroscopy (LIBS) mapping without any aiding biomolecules.

For the rapid, sensitive, and specific screening of viable food-borne pathogen like *Listeria monocytogenes* in ready-to-eat foods, TiO_2 NW bundle microelectrode-based impedance immunosensor has been applied wherein immobilized monoclonal antibodies on the surface of the NW bundle were used for capture. Concentration of *L. monocytogenes* as low as 4.7 $\times$ 10^2cfu/mL could be detected from the change in impedance due to the NW—antibody−bacteria complex within 50 min without any significant interference from other food-borne pathogens [33]. A miniature honeycomb-patterned silicon NWs based FET nanosensor could determine bacterial growth kinetics and metabolism by quantifying the changes in the source–drain current due to pH variation in response to antibiotics. The fabricated device had four groups of nanosensors, each consisting of an array of 8 transistors. Integration of multiple sensor platform in a single device paves its path through multiplexing and provides a high-throughput method of screening or diagnosis. Each nanosensor shared one reference electrode [34]. NW silicon on insulator films have been used to detect Ebola virus VP40 protein by its immune complex with specific monoclonal antibodies in real time of ∼200–300 s per test sample [35]. H1N1 influenza virus can adsorb 200 nm thick silicon NW while keeping the distance between NWs around 100–200 nm. This causes wavelength shifts in the Fabry–Perot fringes of the reflection spectrum of visible light from the NWs. This feature may form the basis of filters and sensors for viral binding and detection [36].

10.2.1.3 Nanotubes

Nanotubes are cylindrical structures with diameters in the nanoscale range (1–100 nm). Among all other types, like carbon, lipid, boron nitride, titanium oxide, silicon carbide, etc., carbon nanotube (CNT) steals the show due to its high mechanical tensile strength with light weight, very high aspect ratio, good thermal conductivity, fast electron transfer kinetics, exposed functional groups, chemical inertness, binder, carrier and immobilization properties for antibodies, DNA, RNA,

and aptamers [37]. Prieto-Simon et al., have tailored SWCNTs into immunosensors to detect MS2 bacteriophage, a contaminating agent in sewage impacted water supplies by covalently attaching SWCNTs to a cysteamine-modified gold electrode through electron communication. In another approach, antibodies were immobilized on iron oxide NP decorated SWCNTs via hydrazone coupling. These magnetic immune-carriers provided high number of antibody binding sites to minimize non-specific adsorptions. The detection limit in river water was 9.8 pfu/mL and subsequently improved to 39 pfu/mL in the second approach [38]. A brief is mentioned is Table 10.1.

10.2.1.4 Nanorods

Nanorods (NR) are the nanostructures with lengths between 10 and 120 nm with aspect ratios between 3 and 5. They can be metallic, carbon, semiconductor or oxides nanorods. When molecules get adsorbed on the surfaces of metallic nanostructures, a localized surface plasmon is generated due to the resonance of the oscillation frequency of the nanosurface electrons and the incident wavelength resulting in the enhancement of electromagnetic fields and giving rise to the phenomenon of Surface-Enhanced Raman Spectroscopy (SERS). To achieve high quality SERS effect, Ag-NRs generated by oblique angle deposition method are very useful, specifically the ones with length and diameter in the range of ~800–900 nm and 80–90 nm, respectively, with ~150 nm spacing between each adjacent NRs [39]. Dual functional peptide, P937, conjugated to gold NR (Au@P937) by Au–S bonds via terminal cysteine of the peptide started aggregating upon contact with bacterial surfaces, leads to their detection by change in the surface plasmonic absorbance intensity of the NRs sensitive to the bacterial concentration. The LOD for *E. coli* and *S. aureus* was 46 cfu/mL and 89 cfu/mL, respectively [40]. Ag-NR array based SERS has aided in the identification and differentiation of respiratory syncytial virus (RSV) mutants and strains (A2, A/Long, and B/1) detection of a cell wall-less prokaryote that causes respiratory ailments, *Mycoplasma pneumonia*, from the clinical throat swab specimens [44]; identification of food-borne pathogens like *S. epidermidis, E. coli* O157:H7, *E. coli* DH 5α, *S. aureus*, and *Salmonella typhimurium* and bacteria mixtures [45]; identification of different forms of mycolic acid (α-, methoxy-, and keto-forms) a tuberculosis biomarker from *Mycobacterium tuberculosis* [46].

10.2.2 2D Nanomaterials

10.2.2.1 Graphene

Both graphene and its derivatives like reduced graphene and n-doped graphene have potential bio-sensing applications. For bacterial sensor platforms, the lowest limit of

Table 10.1 Types of nanomaterials leading to detection of varying micro-organisms

Type of Nanomaterial		Organism	Reference
Nanofibers	Polycaprolactone fibers on indium-tin-oxide glass	*Salmonella typhimurium* and *E. coli*-K12	[16]
	Antibody functionalized nitro-cellulose membrane	Bovine viral diarrhea virus (BVDV) and *E. coli* O157:H7	[17]
	D-mannose functionalized NFs of polyacrylic acid/PVA (PAA/PVA) with integrated LAPS	*E. coli*	[18]
Nanowires	SnO_2/ SiO_2 core shell nanowires	*Gram positive (Bacillus subtilis),* gram negative (*E. coli*), and yeast cells	[24]
	TiO_2 NW bundle microelectrode-based imped-ance immunosensor	*Listeria monocytogenes,* a food-borne pathogen	[25]
	Silicon NWs nanosensor	Bacterial growth kinetics and metabolism	[26]
	NW silicon on insulator films	Ebola virus	[27]
	Silicon nanowires	H1N1 influenza virus	[28]
Nanotubes	SWCNTs attached to cysteamine-modified gold electrode	MS2 bacteriophage	[30]
	SWCNTs decorated with iron oxide NP	MS2 bacteriophage	[30]
Nanorods	Peptide conjugated au-NR	*E. coli*, *S. aureus*	[32]
	Ag-NR arrays	Respiratory syncytial virus, *Mycoplasma pneumonia*e *S. epidermidis, E. coli* O157: H7, *E. coli* DH 5α, *S. aureus*, and *Salmonella typhimurium, Mycobacterium tuberculosis*.	[35]
Graphene	Graphene and GO	Microbial toxins like botuli-num, staphylococcal toxin B, *Clostridium difficile* toxin, mycotoxin, aflatoxin, ochratoxin	[37]
	GO-based FET device passiv-ated with an ultrathin alumina layer overlaid with gold NPs with functionalized antibodies against microbial surface proteins	*E. coli* sensor platform	[39]
	Graphene nanoplatelets and monolayers interfaced with specific antimicrobial antibody functionalized array of gold microelectrode capacitors	*E. coli* O157:H7	[40]

(continued)

Table 10.1 (continued)

Type of Nanomaterial		Organism	Reference
Transition metal dichalcogenides	WS2 TMD nanosheet based fluorescence biosensor	MicroRNAs	[41]
Nano/ microgaps	Planar gap modified with NPs, with capture probes complementary to target DNA,	Capture of biomolecules like DNA and its point mutations	[42, 43]

detection for graphene and GO is 10 times less as compared to reduced-GO while for viral platforms, graphene modified with silver and gold NPs can detect as low as pg/mL of viral load [41]. Graphene derivatives have also been utilized for detection of microbial toxins like botulinum, staphylococcal toxin B, *Clostidium difficile* toxin, mycotoxin, aflatoxin, and ochratoxin, as excellently reviewed by Li et al. [47] Graphene based FET demonstrated current-voltage characteristics of graphene and exhibits strong increase in conductance upon exposure to *E. coli* at 10^5 cfu/ml concentration [48]. In another method, GO-based FET device passivated with an ultrathin alumina layer overlaid with gold NPs with functionalized antibodies against surface proteins of outer membrane have been used as *E. coli* sensor platform. Here both GO and alumina contribute holes and electrons as charge carriers. The positive charge of the antibodies is countered by the adsorption of negatively charged *E. coli* to reduce the current flow between the source and drain [49].

Graphene nanoplatelets and monolayers interfaced with anti-*E. coli* O157:H7 antibody functionalized array of gold microelectrode capacitors were used as label-free biosensor platforms for these pathogens. The capacitance response upon capture of the pathogen on-chip increased with the increase in the cell numbers due to graphene's charge carrier mobility upon capture on-chips, contribution of electro-negativity of the cell-wall phospholipids and ionizable groups, the cells' internal bioactivity and polarization of captured cell-surface charges. The LOD was 10–10^7 cells/ml in a tiny droplet of 5 μl within 30 mins [42]. Lin et al., developed an impedimetric immunosensor from nanocomposite film of reduced graphene doped chitosan, tagged with antibodies for the facile and sensitive detection of marine, pathogenic sulfate-reducing bacteria. FTIR results showed that the bonding between $–NH_2$ groups of chitosan and –COOH groups of reduced graphene resulted in the formation of the film. A linear correlation between I/V characteristics of the redox couple, ΔRct, and bacterial concentration was observed within the logarithmic limit of 1.8×10^2 to 1.8×10^7cfu/ml.

10.2.2.2 Transition Metal Dichalcogenides

Transition metal dichalcogenides (TMDs) belong to the emerging category of 2D materials which are direct band gap semiconductors as opposed to graphene [43]. TMD nanosheets are promising candidates as biosensors due to their higher surface area which could be deployed to adhere large number of sensing molecules,

and due to their super fluorescence-quenching properties. TMDs and GO bind single-stranded DNA by van der Waals forces and pi–pi interactions between the nucleobases and the surface, respectively, but both repel the double-stranded DNA [50]. Purines adsorb more strongly than pyrimidines on TMDs. When a fluorescent probe gets adsorbed to basal plane, its fluorescence signal is quenched which is, however, regained upon complexation with either complementary DNA or protein as the complex gets dislodged from the surface [51]. DNA adsorption on TMD surfaces is weaker and hence desorption due to DNA-specific hybridization is more prominent here. For MoS_2 and WS_2, the high MW surfactants, Triton-X100 and Tween-80 facilitate more desorption using stronger van der Waals forces of their tails to displace DNA [45]. WS2 TMD nanosheet based fluorescence biosensor has been designed for microRNA detection from cancer cell lines which may well be extrapolated to infectious diseases (as mentioned in Table 10.1). MicroRNA detection using TMD is highly sensitive with improved single-base mismatch discrimination, low fluorescence background, and low cost due to higher fluorescence quenching [52].

10.3 Functionalization Routes towards Microbial Detection

Biosensors are commonly used in healthcare settings to detect disease-causing agents or pathogens in biological samples. These biosensors detect electrochemical, optical or fluorescent signals generated by probe-target interactions as shown in Fig. 10.1. Nanomaterials have diverse properties which are exploited by scientists for their use in bio-sensing applications to fasten the process of microbial detection. Two-dimensional materials like carbon nanotubes have a highly porous network which can anchor high amount of receptor molecules to increase the sensitivity of detection, e.g. redox enzyme alone or in the combination of cofactors for efficient electron transfers [53].

The covalent functionalizations of nanomaterials are accomplished via chemically attaching carboxyl groups on sidewalls of nanotubes which interact with the functional groups on biomolecules to prepare capture probes for biosensors [54, 55]. The carbodiimide compound like N-ethyl-N′-(3-dimethylaminopropyl) carbodiimide hydrochloride (EDC) can activate the carboxyl groups to react with amine molecules in target biomolecules. The poly-L-Lysine (PLL) linkers are also employed owing to the presence of large number of active amino groups which are sufficient for reacting with carboxyl groups of SWNTs as well as linking SWNTs and biomolecules. Zhang et al. immobilized Horseradish peroxidase effectively on SWNT using PLL cross-linker and EDC cross-linking agent for sensing hydrogen peroxide [56]. In another instance, an immuno-biosensor was designed using EDC as cross-linking agent to attach anti-rotavirus antibodies on carboxyl groups of graphene oxide for detection of rotavirus [57]. Glutaraldehyde cross-linking method is also very effective to covalently immobilize monoclonal anti-CEA antibodies on polyethyleneimine wrapped multiwalled carbon nanotubes for the detection of

carcinoembryonic antigen in saliva and serum [58]. Jaiswal et al. used glutaraldehyde to cross-link amine terminal of probe DNA on electrophoretic assembly of ZnO nanorods for detection of the DNA of *E coli* [59].

On the other hand, non-covalent modifications are achieved via pi–pi, van der Waals, ionic interactions, and hydrogen bonding between nanomaterials and biomolecules through the use of polymers [60], enzymes [61, 62], and metal oxide or nanoparticles [63, 64]. Non-covalent functionalizations are relatively convenient and do not affect the structure and intrinsic properties of nanomaterials and biomolecules [65]. Bifunctional linker molecules can be used to functionalize nanomaterials, e.g. 1-pyrenebutanoic acid succinimidyl ester (PBSE) has pyrene group and succinimidyl ester which bind to graphene via pi–pi interaction and amines on antibody, respectively [66]. Such PSBE mediated graphene biosensor was used to detect *Escherichia coli* [67]. The carboxylated MWCNTs were acylated to make polyethyleneimine (PEI) functionalized MWCNTs [68] which were used for immobilization of T2 phage particle to detect the *Escherichia coli* [69]. The more detailed non-covalent functionalization of nanomaterials is reviewed here [70]. Various other molecules like enzyme, receptors, lectins, whole cells, peptides, and molecularly imprinted polymers can be used for functionalization [71] to identify the targets in various bio-sensing approaches.

10.4 1D or 2D Nanomaterials in Nano/Micro-Gap Based Sensing Devices

The above narrated 1D or 2D nanomaterials can also be strategically deployed to fabricate ultrasensitive detection platforms. Bridging of nano or micro-gap or emulate a bio-field effect transistor (bio-FET) has been used as powerful technique in increasing selectivity and sensitivity of such bio-devices for ultrasensitive detection of small biomolecules [72]. Often materials possessing excellent conductivity are deployed for fabrication of such sensitive devices owing to their enhanced electrical conductivity, higher sensitivity or easy read out characteristics. Thus, 1D or 2D nanomaterials enjoy a special place in fabricating such devices by virtue of their inherent physico-electro or chemical properties. In general, micro-devices are extremely helpful in the detection of biomolecules using electrical signals, for eg. resistance/impedance, field-effect, or capacitance/dielectric [72]. The nanogaps are often categorized into planar or vertical gaps. Amidst the considerable research done in this aspect, label-free detection of biomolecules using gold nanoparticles (Au-NP) or carbon based 1D or 2D nanomaterials have gathered much attention. Some examples depicting fabrication of such sensing devices and its plausible applications are narrated below.

10.4.1 Planar Gaps

Nano or micro-gap based devices usually follow a principle of filling the gap or bridging it with appropriate signaling probe as a signal to convey the presence of target analyte. In a planar system, the gap between electrodes are surface functionalized with capture probes corresponding to the target analyte, which can be a possible protein, a sequence of oligo, a whole cell or biomolecule tagged nanoparticles. In an approach, aminosilane functionalization was used to form a sub-monolayer of colloidal Au-NPs in order to fabricate an electronic transistor for detection of biomolecules (Fig. 10.2a) [74]. It was used to bridge a gap of 30 nm, created using e-beam lithography, between source and drain of the device. Alternatively, a self-assembly of Au-NPs was also used to bridge the gap using ac trapping and it was found that the devices portrayed a variation in resistance from 100 kΩ to a few tens of MΩ across the platform (Fig. 10.2b) [75]. Fabrication of such platforms were motivational for the development of next generation medical devices.

The above work was followed by a path breaking research done by Mirkin and co-workers wherein they deployed nanoparticles like Au-NPs for detection of biomolecules using a direct signal transduction pathway (Fig. 10.2c) [73]. Here, the gap was modified with capture probes complementary to target DNA, and further in presence of target DNA the gap was bridged using Au-NPs to complete the signal transduction path. In order to enhance the output signal, the process of metallization was adopted with silver ion to amplify the output signal. The process reported an excellent limit of detection (LOD) down to 500 fM while possessing a selectivity of ~100,000:1 for point mutation selectivity. Alternative strategies were further

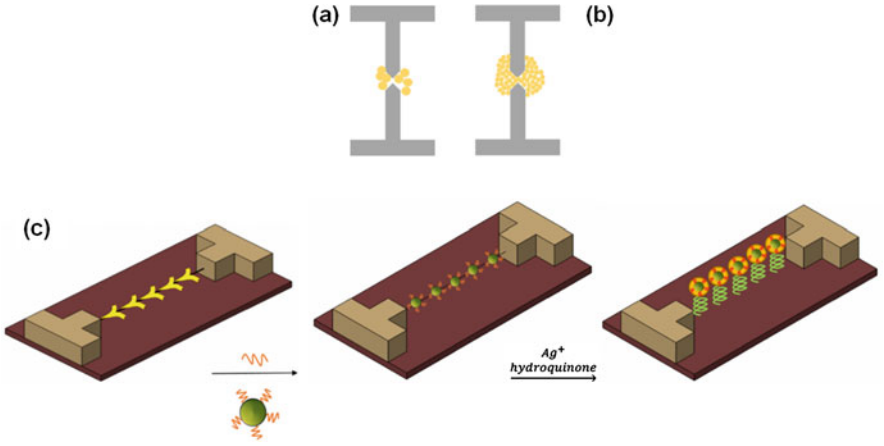

Fig. 10.2 Scheme portrays the usage of Au-NP as labels to bridge and fabricate efficient nano/micro-devices. (**a**) & (**b**) portray development of the concept of electron transition using Au-NP chain as bridge between the gap. (**b**) reveals the iconic work done by Mirkin and his group for electrical detection of DNA using Au-NP functionalized oligos and subsequent metallization with silver to enhance conductivity of the signal associated with the binding events of target-probe [73]

developed by other groups wherein alteration in electrical conductance was observed with changing DNA conformation [76]. It was witnessed that the system present low conductivity on presence of single-stranded DNA, however, the presence of double-stranded DNA enhanced the electrical conductivity. The above approach to confirm presence of target analyte surely increases specificity or selectivity and usage of electro-active conducting materials enhances the signal-to-noise ratio. Au-NPs are used extensively as choice for designing signaling probe for above applications. A monolayer or multi-layered system was deployed to analyze the same. For instance, devices functionalized with 1 nM concentration of capture DNA across a monolayer of Au-NPs covering a 72 nm gap were able to detect target DNA down to 1 fM concentration.

10.4.2 Planar Gap Based FET Devices

Reduced graphene oxide (R-GO) suspension was used to bridge the gap between micro-electrodes to form a liquid gate field effect transistor (FET) for detection of target DNA molecules using complementary PNA as the capture probe (Fig. 10.3) [77]. The model was extremely efficient to detect target DNA down to 100 fM concentration with excellent selectivity. Moreover, the system was efficacious enough to effectively differentiate between one-base mismatch sequences or the presence of non-complementary DNA. The ultra-sensitivity of the devised platform was also accompanied with excellent regeneration property in order to address re-usability of the platform for multiple measurements.

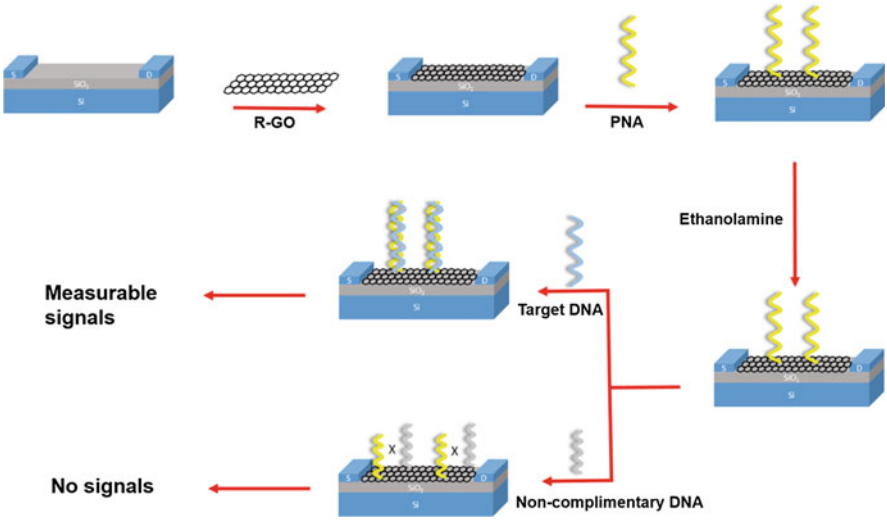

Fig. 10.3 Scheme showing the concept of fabricating RGO based bio-FET to detect target DNA using PNA as the capture probe, a concept adopted by Cai et al., 2014 [77]

10.4.3 Vertical Gap

Alternatively, Gao and co-workers were able to design a vertical nanogap, apparently different from the conventional one wherein the nanogap basically constitute of an oxide layer sandwiched between two micro-electrodes to form a nano-metal/insulator/metal multilayer (nanoMIM) nano-device (Fig. 10.4) [78]. The two micro-electrodes were further modified with different capture probes complementary to the 3′ & 5′ termini of the target DNA, respectively. Paradoxical to the conventional bridging technique, herein the target DNA bridges the complementary micro-electrodes followed by simple metallization of the DNA backbone with Ag + ions as briefed above to enhance the conductivity. The device was able to amplify conductance of the system by ~2 orders of magnitude to 2.1 × 104% with a cleaner background (<1.0 pS). A linear relationship between DNA concentration and conductance was observed in the I/V pattern when sweeped across a concentration range from 1.0 fM to 1.0 pM.

10.5 Sample Preparation

Sample preparation is one of the critical steps in downstream applications for identification and detection of microbial strains in a particular setup, e.g. food, healthcare, and forensics. The technological advancement in both hardware and software has developed highly sensitive equipment/or techniques such as biosensors, lab-on-chip and rapid diagnostic kits; moreover, in such techniques the purity and integrity of starting material (DNA/RNA/proteins) are of utmost importance, as even the minor contaminants can affect the final results. Thus, not only the biological applications such as genomic analysis, genetic and epigenetic analysis, and microbial (virus/bacterial) identification are highly sophisticated but also the human interface such as sample collection and preparation is critical issue. Sample preparation is dependent on the types of specimens available for molecular analysis, for

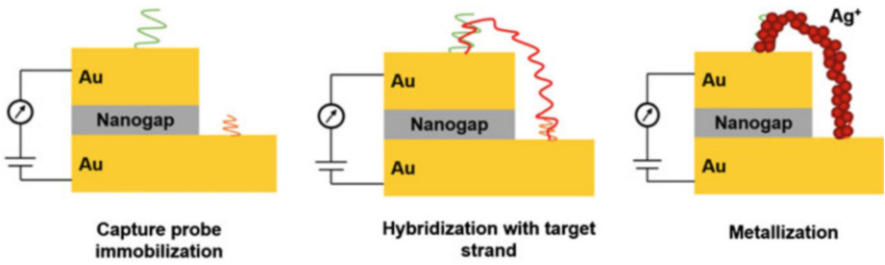

Fig. 10.4 Scheme showing fabrication of vertical nanogap (nanoMIM) having two termini and its plausible application in DNA sensing via electronic transduction mechanism as adopted by Roy et al., 2009 [78]

example, field or diagnostic samples can be collected in the form of tissue, culture, blood/serum/plasma, swabs, and others.

10.5.1 Cultures

Cultured microbes can be easily used for DNA or plasmid isolation and do not require large scale culturing making them quite convenient for downstream processing such as strain identification.

10.5.2 Tissues

In case of handling tissues, high quality nucleic acid (NA) isolation is observed in frozen tissues [79]. However, in majority of cases, e.g. hematopathological studies are conducted in fixed tissue samples and the associated procedures (immune-phenotyping and morphological characterization) are well sorted. Fixed samples can be stored for number of years and are great source of biomarker discovery in clinical settings utilizing the omics strategies to unravel information about the diseases. Tissue fixation can be done through chemicals (formaldehyde, glutaraldehyde, methanol, ethanol, and acetone) or microwave irradiation or natural cross-linker (genipin) [80]. Every method has its pros and cons associated, e.g. microwave methods lyse the red blood cells but it allows the cross-linking reagent to infiltrate the tissue making it useful in ultrastructural studies [81]. The most commonly prepared tissues are formalin fixed and paraffin embedded (FFPE) owing to easy handling and long-term storage. In addition, more steps and utmost care are needed to extract nucleic acids form FFPE tissues [82]. Presently, commercially available reagents (e.g. RNAlater; Ambion, Austin, Texas) are efficient to stabilize RNA and must be added immediately after sample collection [83].

10.5.3 Blood/Serum/Plasma

The most common way of collecting samples is blood or its constituents like plasma or serum. Blood samples were often collected in supplementation with anticoagulant such as acid citrate dextrose, heparin or ethylenediaminetetraacetic acid (EDTA) depending on the downstream processing. Heparin binds to DNA and inhibits the Taq polymerase enzymes needed in PCR applications [84]. Magnesium ions concentration is important for high molecular weight DNA isolation. Higher concentrations of EDTA have been proven beneficial for long-term storage of DNA [85]. Depending on whether the microorganism is intracellular or intercellular, samples are processed, e.g. malarial parasites resides in red blood cells so white

blood cells are removed and parasite-infected red blood cells (pRBCs) are separated for downstream processing [86]. Plasma is the choice for the analysis of viral load, hence need to be separated from blood sample. Commercial plasma preparation tubes (PPT) (BD Vacutainer) are available and widely used in the sample collection. In field studies, blood samples can be collected on filter paper of Whatman® Grade 903 and Ahlstrom Grade 226. These are frequently used for spotting of blood followed by drying and can be stored at room temperature for few hours to ease transportation [87, 88].

10.6 Extraction of Biological Molecules for Molecular Detection

Molecular detection of biological sample is the most commonly used method in the diagnosis of infectious disease or screening of genetic disorders and is based on the selection of targets such as DNA, RNA or protein. In addition, with the advent of modern technologies (as discussed in later sections), Nucleic acid (NA) based pathogen detection is highly sensitive and specific as compared to the classical microbiological techniques. This is mainly a three-step process comprising of sample preparation, amplification, and detection. It is quite essential to prepare the sample without the cellular components like membrane, organelles, and proteins for the smooth downstream processing. There are few steps which need to be followed for NA extraction from collected specimen: (a) cell lysis, (b) removal of lipids and proteins, and (c) DNA extraction followed by recovery and concentration as shown in Fig. 10.5.

Cell lysis process can be accomplished by simple use of salts or detergents (sodium dodecyl sulfate), enzymes (lysozyme), or by mechanical and physical methods (sonication/boiling/freeze thawing). In addition, various cell lysis methods are very well reviewed here [89]. Some cells like cancer cells, being soft can be lysed by puncturing mediated by nanowires [90] whereas bacterial cells do have a thick outer layers need different approach. In this regard, Yasui*et. al.* rupture the cells via stretching the cell membrane that comes between nanowire (bacteria compatible and flexible) by shear force [32].

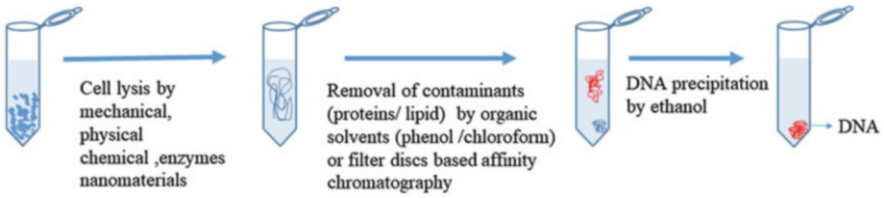

Fig. 10.5 DNA extraction via standard protocol followed in order of cell lysis, removal of contaminants and precipitation steps

10.6.1 Nucleic Acid Extraction

To extract the nucleic acids, either solvent extraction (SE) or solid-phase extraction (SPE) is used. Former is based on the fact that DNA/RNA lose solubility in organic solvents; after cell lysis and digestion of protein with proteinase K and SDS, when sample is treated with isoamyl-alcohol:chloroform:phenol (1:24:25), the DNA comes in aqueous phase leaving lipids, proteins, and cellular debris in organic phase. Later the DNA is recovered by ethanol precipitation [91]. This method produces highly purified NA but is very time consuming and cannot be considered for high-throughput needs. Additionally, it requires trained personal to handle liquid by pipettes to avoid the loss; organic solvents need proper disposal protocols.

Solid-phase extraction (SPE) method is more common nowadays owing to easy handling, automation, throughput capabilities, low cost and no need of skilled technicians. This semi-automated method utilize solid particles (replacing the phenol from SE) that can bind to proteins with high affinity and nucleic acids with low affinity for easy elution of nucleic acids. SPE is based on chromatographic techniques (size exclusion, ion exchange, and affinity) and is in the form of spin column with designed filter for appropriate needs. For example, Sephadex filter is used for size exclusion based SPE to purify DNA from low sized molecules, whereas Chelex resin based kits are used for ionic exchange SPE to clean DNA from the unwanted ions present [87, 92]. The most commonly used is the affinity based SPE wherein silica filter are used for specific binding of nucleic acids under high concentration of chaotropic salt and pH below 7 [93]. The commercial spin column mainly uses four steps of lysis, binding, washing, and elution utilizing the centrifuge at lower speed [94]. In cases, where samples (blood) are thick and can clog filters, beads or particles are used which can be directly mixed with the sample. The beads made of materials with magnetic or paramagnetic properties such as zirconia are widely used in separation techniques [95]. Magnetic beads can be coated with oligodT to specifically extract mRNA from total RNA sample [96].

10.6.2 Protein Extraction

Proteins can be obtained from a wide variety of clinical specimens (cells, tissues or blood). However, working with protein is not as easy as nucleic acids owing to low amounts available and difficulty in isolating specific proteins. Like nucleic acids, proteins cannot be amplified and are not as stable as DNA (RNA and proteins are both easily degraded), hence need lot of care and technical skills for handling samples [97]. Protein can be extracted by lysing through different means such as bead beating, sonication, heat treatment in detergent based buffer [98, 99]. The concentration or precipitation step is required to enrich the extracted protein and can be achieved using salts and precipitating reagents such as ethanol, acetone, etc. or through isoelectric precipitation [100–102]. Similar to nucleic acid extraction,

protein can be separated using chromatographic techniques (size exclusion, ion exchange, and affinity based). Recently, IgG-modified Fe_3O_4 magnetic beads have been used to identify pathogenic bacteria in human samples based on the fact that IgG can bind to protein A, protein G, protein L, and glycans on the surface of bacterial cells [103].

1D or 2D nanomaterials are quite versatile owing to their intrinsic properties as mentioned above. Studies also suggest that magnetic-NPs or CNTs have been explored for isolation of biological molecules. Shakhmaeva et al. reported that nanosized negatively charged MWCNTs was used to purify plasmid DNA from water suspension [104]. In another instance, graphene oxide nanoplatelets (GONPs) or hydrazine-reduced GONPs (rGONPs) were explored for isolation of genomic RNA and DNA from embryonic stem cells or plasmid DNA from bacteria [105]. The above interaction was supported by van der Waals forces, π–π stacking, or hydrogen bond of graphene with NAs [106]. The polyethylenimine-conjugated magnetic polypyrrole nanowires (PEI-mPpy NWs) have been utilized to extract human papilloma virus DNA from the minimal amount of urine sample [107]. Graphene and its derivatives have been successfully used as a sorbent to extract and concentrate proteins [108–110]. Uzzaman et al. have used graphene and graphene oxide to extract membrane associated proteins from cell lines and found to be more efficient than the commercial kits [111].

10.6.3 Automated Nucleic Acid Extraction Methods

The biomarkers of disease-causing microbes are low in concentration in biological samples and identified by techniques such as PCR and ELISA; the presence of contaminants or inhibitors can compromise the efficacy of the assay. Many researchers and companies are in the process of generating automated methods to scale up their research for high reproducibility with short-time span. After all, automation refers to simplicity, convenience, less human involvement, minimal cross contamination, and reproducibility. The amazing technologies such as microfluidics or nanomaterials have been coupled with advanced molecular techniques like isothermal DNA amplification, quantitative real-time PCR or ELISA to meet the expectation.

Hukari et al. designed a system utilizing a self-contained multicomponent sample cartridge with automated addition of enzymes and other buffers, mixing of components, capturing and eluting the analyte along with additional features for temperature sensitive process making it capable of NA extraction from different sample types such as whole blood, plasma, and water [112]. In another approach, workstation is designed where lysis and homogenization has been performed by magnetically-induced vortexing using glass beads and a magnetic stir disk with incorporating a pressurized air drying system to remove the residual buffer [113]. Rossetti *et al.* designed a diagnostic platform which helps in automated molecularly imprinted based solid-phase extraction (MISPE) of proteins in cancer

model [114]. Another functionalized magnetic beads based device helps in the extraction of NA and protein markers in one system. In this system, sample is mixed with the magnetic beads specific for the RNA, DNA, or protein biomarker and transported in a tube carrying corresponding solution to the biomarkers through the use of external magnet and assays showed biomarker recovery quite comparable to that of the tedious manual process [115].

Upon comparison with the manual or semi-automated sample preparation, automated workstation demonstrated equivalent performance [116–118]. Apart from lab based automation devices, commercial automated workstation are available in market. The magnetic bead based automated system are conveniently used in the laboratory research settings, e.g. AnaPrep (BioChain Institute, Inc., Newark, Calif.), MagNA Pure Compact, and the MagNA Pure LC instruments (Roche Applied Science, Indianapolis, IN) that can process 8–32 samples at one time. Recently, an automated method has been developed to extract nucleic acid from tissue samples used previously for histochemistry (e.g. immunohistochemistry, in situ hybridization) and staining (e.g., H&E) [119]. Such methods are promising in cases where sample types and sizes are limited.

Microfluidic approach has been extended to different fields including biology, medicine because of its various advantages like low sample volume, quick analysis, and automation [120]. Song et al. generated bipolar electrode (BPE) based microfluidic device to simultaneously concentrate and separate DNAs by attaching a streptavidin tag at one end of the DNA to enable the end-labeled free-solution electrophoresis (ELFSE) [121]. Microfluidic channel has been prepared by growing aligned carbon nanotubes having 93% porosity in order to allow the smaller molecules such as albumin to pass, while trapping blood cells with an efficiency of ~80% [122]. Microfluidics is explained in the following section of the chapter.

10.7 Fluid Kinetics for Detection Systems

Diversity in the target molecules makes bio-sensing a challenging as well as emerging domain of research due to the intricate or complex bio-affinitive reactions involved. Each target molecule has its unique way of detection and transduction [123, 124]. Typically, microfluidic and detection integrated on the same platform. However, integrating detection system with the biosensor platform possesses a major challenge in developing a practical device design for real-life application. Nevertheless, a device design typically depends on fluid transport mechanism such as continues flow, droplet or arrays of mixed fluids. The most important design parameter in all biosensors is detection time, which ultimately depends on measuring mechanism and fluidic system. However, with single molecular detection biosensor it is possible to achieve the higher specificity and grater efficacy with lower volume. These expediencies have led the scientist and engineers to design platforms that are able to detect single target molecule or class of biochemical to emerge a technology called micro total analysis system (μ-TAS) or Lab-on-Chip (LoC)

[124]. Microfluidics usually points out to a study of fluidic systems with critical functional lengths in 1–100 μm range, whereas nano-fluidic systems critical length varies from 1 to 100 nm. Both micro- and nano-fluidic systems are referred by surface area to volume ratio (SA/V). It is generally considered as higher the ratio higher the detection efficiency of the biosensor. There are two methods for fluid flow inside the channel, viz.; pressure driven and electro-kinetic. For micro-fluidic systems, the pressure driven mechanism can be use, however, with reduction in channel dimensions the pressure driven system becomes challenging. Hence in most of the cases the electro-kinetic driven fluid system is often used. In some cases, electro-osmosis method is used to drive liquid droplets into the channel [125].

Instead of above advantages, sufficient concentration of targeted molecules for detection puts limitation due to fundamental mass transport and reaction time. Consequently, detention time scale, t_c, is dependent on the flow of target molecule through the channel and mass diffusion with the transduction mechanism. Therefore, it is necessary to express the t_c in terms of characteristics length l_c and mass diffusivity of the target molecule or species of interest. Characteristic length is defined by the ratio of volume to surface, however, in general for circular cross sections, the diameter is considered as the characteristic length. The detection time is expressed as,

$$t_c = \frac{{l_c}^2}{D} \tag{1}$$

The eq. (1) indicates that smaller the characteristic length represents shorter detection time. Therefore, for smaller detection time the diameter of the channel should be as small as possible indicating lower volume to surface area ratio [125]. The characteristic length plays an important role in viscus forces. Consequently, wall–fluid interactions become interestingly important at low V/SA ratio (Approx. 10^{-9} m^{-1}). Dimensionless Reynolds number is defined as the ratio of inertial force to the viscus force. The equation is given by,

$$Re = \frac{\rho v l_c}{\mu} \tag{2}$$

where, ρ is the density of fluid to be tested, v is the average velocity of fluid, and μ is the viscosity of fluid. Since the equation owing to small characteristics length the Reynolds number becomes very small indicating viscus forces dominates inertial forces. Since most of the micro-fluids containing ions, colloid, biomolecules, etc. interact with the channel wall. The fluid–wall interaction is occurring mainly because of electrostatics or columbic forces F_{cu}, van der wall forces F_{vdw} and hydrodynamic forces F_{hy}. The columbic force for an infinite flat surface (here we are considering for infinitesimally small circular channel) is given as,

$$F_{el} = -\frac{2\pi RL_c}{\varepsilon\varepsilon_0}\left[2\sigma_S\sigma_P \exp\left(-\frac{l_c}{\lambda_D}\right) + \left(\sigma_S^2 + \sigma_P^2\right)\exp\left(-\frac{2l_c}{\lambda_D}\right)\right] \tag{3}$$

where, λ_D is the Debye length and σ_S and σ_P are the surface charge density of the sample and particle, respectively. Van der wall force is given as,

$$F_{vdw} = \frac{A_H R}{6l_c^2} \tag{4}$$

where, A_H is the Hamaker constant that indicates particle–particle interaction (here in blood). The Hamaker constant varies from substance to substance therefor, readers are asked to go in details depending on the target molecules by themselves. Moreover, the hydrodynamic force,

$$F_{hy} = b_s V = -f^* \frac{6\pi\mu R^2 V}{l_c} \tag{5}$$

where, b_s is the hydrodynamic damping coefficient, μ is the viscosity of fluid, f^* is the boundary slip coefficient. For no slip condition $f^* = 1$, and if slip exist $f^* < 1$. Usually, slip lengths are determined by applying eq. (5) utilizing a colloidal AFM probe tip. As an evidence from eqs. (3, 4, and 5) the columbic force shows the exponential dependence on characteristic length l_c, whereas van der wall forces and hydrodynamic force show inverse quadratic and inverse liner dependence on l_c. Therefore, it is very essential to understand the importance of characteristic length and its effect on solid (channel) walls–liquid (target molecule) interaction. Usually wall surfaces which come in contact with the target molecules acquire the net surface charges. These surface charges play an important role in ion absorption or mass diffusion with the coated wall surface in order to achieve the accurate measurement. Because of the charges on surface and target molecules there is a formation of layer called Stern layer. The distance between diffused particle layer on surface and stern layer is known as Debye length also known as screening length. The Debye length is given as,

$$\lambda_D = \sqrt{\frac{\varepsilon_e RT}{F^2 z_i^2 c_i}} \tag{6}$$

where, ε_e is the electric permittivity of the medium, R is the gas constant, T is the temperature (k), F is Faraday's constant, Z_i is the valence of the i^{th} species, and c_i is the concentration of the i^{th} species.

The Debye length ranges from 0.1 to 100 nm and it is an indication of the target molecule concentration in the solution. Typically, larger the Debye length smaller the concentration required. Since Debye lengths are important to determine Coulombic forces, it is inverse exponentially proptional to force. This leads to selection

of proper channel for microfluidic systems [125]. The above interpretation defines the limits to design microfluidic interfacing of bio-sensing devices. The diameter of channels and flow rate should be ascertained following the choice of detection sample in order to obtain desired results. Even functionalization of microfluidic channels can also be done in order to minimize channel clogging. Furthermore, acquaintance with a self-sustaining microfluidic platform will open up opportunities for real-time application of such detection system.

10.8 1D or 2D Material Based Optical Detection of Microbial Strains

Optics plays a crucial role in sensing microbes, proteins or DNA. Microbial biosensors have adopted few conventional technologies that made them very popular in the field of optical imaging. The principle behind designing the microbial sensor is the microbial architecture and lies upon the interaction of microbes with such analytes which results in a specific change that allows reporters to emit a signal. Furthermore, these signals are quantified by various means such as fluorescence microscopy that provides in situ imaging as well as analyses the signal. Different types of conventional optics include bioluminescence, fluorescence, sensory regulated, and electrochemical. Various techniques used for tracking are bacterial cells may include atomic force microscopy, flow cytometry, polymerase chain reaction, nucleic acid detection fluorescence microscopy, and Raman spectroscopy [126–129]. However, all of the above techniques require sophisticated knowledge of antibodies and are more expensive. Nanotechnology-based biosensors are cost-effective, accurate, specific, and are straightforward with respect to data acquisition and analysis. Based on mechanisms, optical biosensors has been further classified into phosphorescence, fluorescence, UV/VIS spectroscopy, Raman spectroscopy, and Forster resonant energy transfer (FRET). Herein, we are elaborating on the different modes utilized during designing the sensor.

10.8.1 Fluorescent Biosensor

Fluorescence exhibit features like less response time with higher sensitivity and specificity, also the efficiency of the fluorophore to get excited upon local interaction, made its popularity in the diagnostic field. Fluorescence hybridization in situ (FISH) allows the detection of microbes in blood cultures. Earlier, organic fluorophore was used, however, it possessed various limitations like photobleaching and blinking [130]. In this respect, various polymeric fluorophores have been created for tuning its optical property as well as improving its sensing mechanisms for designing and functioning biosensors. Recently, use of fluorescence

microscopy for detection of metal ions has been reported [131]. The conjugated polymer as a macromolecule used in a fluorescence helps in both energy harvesting system as well as providing a delocalizing signal. Moreover, protein based surface modifications were adopted to functionalize the nanostructured materials, in order to prepare them as promising alternative for device fabrication. Further peptide modified devices were used for fluorescent based detection techniques wherein a cumulative signal is acquired thus revealing the fact that distribution of functional moieties plays an essential role in the detection of biomolecules through optical response route.

10.8.2 FRET-Based Biosensors

FRET-based biosensors presents a fluorescence resonant effect to the degree of sensing elements such that it can be integrated into biosensors [132]. The primary property includes change of the non-radiative energy transfer process in the fluorophore excited state lifetimes. Different compounds having disturbed excited states could contribute to several detection techniques. FRET is often used for detecting DNA, aptamer, or protein corresponding to the target analyte by interpreting luminescent signals revealed during the process [133, 134]. FRET offers a unique experimental advantage for determining molecular distances that corresponds to the efficient energy transfer between donor and acceptor separated within a limited range of 10–80 Å.

10.8.3 Raman Based Sensor

Raman spectroscopy has been widely used for studying the biological related sample. In Raman spectroscopy, a spectrometer together with the optical microscope allows excitation and also enables the collection of spectra formed by Raman. Further spatial resolution was improved by improving the optical axis by using a confocal setup. Interestingly, it has also reduced the volume of sample required for characterization. Development of infra-red laser which can detect wavelengths around 800 nm, has been deployed for the usage of such microscopy to image live cells [108]. Such lasers provides dual benefit, firstly they reduced the background noise produced by molecular fluorescence, as well as reduces energy to get into transition. Secondly, it results in less photo-damage as compared to the UV lasers. For pathogen detection, various approaches of Raman spectroscopy have been employed, namely, non-resonant Raman, surface-enhanced Raman spectroscopy, UV resonance Raman, and non-linear Raman spectroscopy [135, 136]. Inactivation of pathogen spores and further imaging with Raman allows identification of species-specific peak. Recently, surface-enhanced Raman spectroscopy has been constructed

to monitor the cellular activity via direct and indirect manner, and also providing a strong platform for the detection of the molecule.

10.8.4 DNA Based Sensor

In DNA based sensor, high sensitivity detection and real-time information are needed. Mainly fluorescence from optical mode is exploited for the detection of DNA. DNA in cells are stained with Acridine orange, which was excited to a certain wavelength for developing DNA based sensor system for detection of DNA hybridization [137]. Optofluidic chip with a nanopore has been used in patch-clamp technique for the detection of ssDNA. The electrical output corresponds to fluorescent intensity with respect to the position of amino acids. Optical fiber also has been evolving in the field of detecting DNA [138]. This device works on acquiring the transition of reflected infrared wavelength, thus allowing the detection of DNA.

10.9 Summary and Future Work

The development of highly selectivity and ultrasensitive bio-sensing devices or methods always had much attention to it and nonetheless owing to realm of the present scenario, it is never been that imperative to innovate self-sustaining POC devices that may be used for mass application. 1D or 2D nanomaterials may play a pivotal role in devising such state-of-art devices, owing to their exceptional physico-electrical properties. High mechanical stability accompanied by ballistic conduction of electrons through their high surface area with excellent optical properties always opens a plethora of opportunity to develop bio-sensing devices capable of catering to a wide range of critical illnesses. Especially with a suitable extraction method coupled to an efficient fluidic system, devices prepared with 1D or 2D nanomaterials always open up opportunities to detect target at extremely minute concentration. Especially with the advent of bio-electronics, devices involving direct electrical conductance or a FET based conduction system provide a window to even monitor the smallest of alteration.

The devices which have been developed until date are ultrasensitive, however, their clinical intervention still needs to be tested. In order to successfully do so, it is imperative to develop strategies for even tailoring interface of the developed 1D or 2D materials. Often it is witnessed that such devices fail to keep up to the expectation due to bio-fouling of the micro-devices when exposed to real samples like blood serum, as they essentially contain proteins that tends to interact with the nanoparticle counterfeit. Thus, a well-devised functionalization strategy may not only overcome the process of bio-fouling but also make the device re-usable. The same could also be addressed by developing a better extraction process to selectively separate the target biomolecule from rest of the components. Nevertheless, a self-sustaining

microfluidic system is always a challenge to develop which may again help in processing and channeling target molecules to the reaction zone thus increasing chances of a successful bio-affinitive reaction. Thus, it is apparent that a well-tailored sensing platform coupled with well-engineered fluidic system may always lead the path for successful fabrication of an exceptional biosensor device.

References

1. Tan, C., Cao, X., Wu, X.-J., He, Q., Yang, J., Zhang, X., Chen, J., Zhao, W., Han, S., & Nam, G.-H. (2017). Recent advances in ultrathin two-dimensional nanomaterials. *Chemical Reviews, 117*(9), 6225–6331.
2. Purohit, B., Kumar, A., Mahato, K., & Chandra, P. (2020). Smartphone-assisted personalized diagnostic devices and wearable sensors. *Current Opinion in Biomedical Engineering, 13*, 42–50.
3. Purohit, B., Vernekar, P. R., Shetti, N. P., & Chandra, P. (2020). Biosensor nanoengineering: Design, operation, and implementation for biomolecular analysis. *Sensors International, 1*, 100040.
4. Chen, G., Roy, I., Yang, C., & Prasad, P. N. (2016). Nanochemistry and nanomedicine for nanoparticle-based diagnostics and therapy. *Chemical Reviews, 116*(5), 2826–2885.
5. Chandra, P., & Pandey, L. M.. "Biointerface Engineering: Prospects in Medical Diagnostics and Drug Delivery." (2020). (3) Zhang, S.; Geryak, R.; Geldmeier, J.; Kim, S.; Tsukruk, V. V. (2017). Synthesis, assembly, and applications of hybrid nanostructures for biosensing. *Chemical Reviews, 117*(20), 12942–13038.
6. Preetam, G. R., Pal, P., Srivas, P. K., Basak, P., Roy, S., & Dhara, S. (2018). Surface modification of eggshell membrane with electrospun chitosan/polycaprolactone nanofibers for enhanced dermal wound healing. *ACS Applied Bio Materials, 1*(4), 985–998.
7. Guha, R. P., Biswas, S., Roy, T., Ghosh, S., Majumder, D., Basak, P., Roy, S., & Dhara, S. (2019). Sonication assisted hierarchical decoration of ag-NP on zinc oxide nanoflower impregnated eggshell membrane: Evaluation of antibacterial activity and in vitro cytocompatibility. *ACS Sustainable Chemistry & Engineering, 7*(16), 13717–13733.
8. Zhang, S., Geryak, R., Geldmeier, J., Kim, S., & Tsukruk, V. V. (2017). Synthesis, assembly, and applications of hybrid nanostructures for biosensing. *Chemical Reviews, 117*(20), 12942–13038.
9. Ray, P. G., Das, M., Wan, M., Jacob, C., Roy, S., Basak, P., & Dhara, S. (2020). Surfactant and catalyst free facile synthesis of Al-doped ZnO nanorods–an approach towards fabrication of single nanorod electrical devices. *Applied Surface Science, 512*, 145732.
10. Viswanathan, S., Rani, C., Anand, A. V., & Ho, J.-A. A. (2009). Disposable electrochemical immunosensor for carcinoembryonic antigen using ferrocene liposomes and MWCNT screen-printed electrode. *Biosensors & Bioelectronics, 24*(7), 1984–1989.
11. He, S., Song, B., Li, D., Zhu, C., Qi, W., Wen, Y., Wang, L., Song, S., Fang, H., & Fan, C. (2010). A graphene nanoprobe for rapid, sensitive, and multicolor fluorescent DNA analysis. *Advanced Functional Materials, 20*(3), 453–459.
12. Swathi, R., & Sebastian, K. (2008). Resonance energy transfer from a dye molecule to graphene. *The Journal of Chemical Physics, 129*(5), 054703.
13. Qian, Z. S., Shan, X., Chai, L., Ma, J., Chen, J., & Feng, H. (2014). A universal fluorescence sensing strategy based on biocompatible graphene quantum dots and graphene oxide for the detection of DNA. *Nanoscale, 6*(11), 5671–5674.
14. Clark, L. C., Jr. (1962). Electrode systems for continuous monitoring in cardiovascular surgery. *Annals of the New York Academy of Sciences, 102*, 29–45.
15. Crane, M. M. (1971). *Diagnostic test device*. Google Patents.

16. Lewis, E. K., Haaland, W. C., Nguyen, F., Heller, D. A., Allen, M. J., Mac Gregor, R. R., Berger, C. S., Willingham, B., Burns, L. A., & Scott, G. B. (2005). Color-blind fluorescence detection for four-color DNA sequencing. *PNAS, 102*(15), 5346–5351.
17. Kumar, A., Purohit, B., Maurya, P. K., Pandey, L. M., & Chandra, P. (2019). Engineered nanomaterial assisted signal-amplification strategies for enhancing analytical performance of electrochemical biosensors. *Electroanalysis, 31*(9), 1615–1629.
18. Cui, Y., Wei, Q., Park, H., & Lieber, C. M. (2001). Nanowire nanosensors for highly sensitive and selective detection of biological and chemical species. *Science, 293*(5533), 1289–1292.
19. Nicewarner-Pena, S. R., Freeman, R. G., Reiss, B. D., He, L., Peña, D. J., Walton, I. D., Cromer, R., Keating, C. D., & Natan, M. J. (2001). Submicrometer metallic barcodes. *Science, 294*(5540), 137–141.
20. Star, A., Gabriel, J.-C. P., Bradley, K., & Grüner, G. (2003). Electronic detection of specific protein binding using nanotube FET devices. *Nano Letters, 3*(4), 459–463.
21. Cui, Y., Duan, X., Hu, J., & Lieber, C. M. (2000). Doping and electrical transport in silicon nanowires. *The Journal of Physical Chemistry. B, 104*(22), 5213–5216.
22. Rajasekaran, R., Seesala, V. S., Sunka, K. C., Ray, P. G., Saha, B., Banerjee, M., & Dhara, S. (2020). Role of nanofibers on MSCs fate: Influence of fiber morphologies, compositions and external stimuli. *Materials Science and Engineering, C 107*, 110218.
23. Nicolini, A. M., Fronczek, C. F., & Yoon, J.-Y. (2015). Droplet-based immunoassay on a 'sticky'nanofibrous surface for multiplexed and dual detection of bacteria using smartphones. *Biosensors & Bioelectronics, 67*, 560–569.
24. Luo, Y., Nartker, S., Miller, H., Hochhalter, D., Wiederoder, M., Wiederoder, S., Setterington, E., Drzal, L. T., & Alocilja, E. C. (2010). Surface functionalization of electrospun nanofibers for detecting E. coli O157: H7 and BVDV cells in a direct-charge transfer biosensor. *Biosensors & Bioelectronics, 26*(4), 1612–1617.
25. Guha, R. P., & Roy, S. (2016). Eggshell membrane: A natural substrate for immobilization and detection of DNA. *Materials Science and Engineering, C 59*, 404–410.
26. Shaibani, P. M., Jiang, K., Haghighat, G., Hassanpourfard, M., Etayash, H., Naicker, S., & Thundat, T. (2016). The detection of Escherichia coli (E. coli) with the pH sensitive hydrogel nanofiber-light addressable potentiometric sensor (NF-LAPS). *Sensors and Actuators B: Chemical, 226*, 176–183.
27. Matlock-Colangelo, L., Coon, B., Pitner, C. L., Frey, M. W., & Baeumner, A. J. (2016). Functionalized electrospun poly (vinyl alcohol) nanofibers for on-chip concentration of E. coli cells. *Analytical and Bioanalytical Chemistry, 408*(5), 1327–1334.
28. Ebara, M. (2016). *Biomaterials Nanoarchitectonics*. William Andrew.
29. Zhou, W., Dai, X., & Lieber, C. M. (2016). Advances in nanowire bioelectronics. *Reports on Progress in Physics, 80*(1), 016701.
30. Stern, E., Wagner, R., Sigworth, F. J., Breaker, R., Fahmy, T. M., & Reed, M. A. (2007). Importance of the Debye screening length on nanowire field effect transistor sensors. *Nano Letters, 7*(11), 3405–3409.
31. Zhang, A., & Lieber, C. M. (2016). Nano-bioelectronics. *Chemical Reviews, 116*(1), 215–257.
32. Yasui, T., Yanagida, T., Shimada, T., Otsuka, K., Takeuchi, M., Nagashima, K., Rahong, S., Naito, T., Takeshita, D., & Yonese, A. (2019). Engineering nanowire-mediated cell lysis for microbial cell identification. *ACS Nano, 13*(2), 2262–2273.
33. Wang, R., Ruan, C., Kanayeva, D., Lassiter, K., & Li, Y. (2008). TiO2 nanowire bundle microelectrode based impedance immunosensor for rapid and sensitive detection of listeria monocytogenes. *Nano Letters, 8*(9), 2625–2631.
34. Ibarlucea, B., Rim, T., Baek, C., De Visser, J., Baraban, L., & Cuniberti, G. (2017). Nanowire sensors monitor bacterial growth kinetics and response to antibiotics. *Lab on a Chip, 17*(24), 4283–4293.
35. Generalov, V., Naumova, O., Fomin, B., P'yankov, S., Khlistun, I., Safatov, A., Zaitsev, B., Zaitseva, E., & Aseev, A. (2019). Detection of Ebola virus VP40 protein using a nanowire SOI biosensor. *Optoelectronics, Instrumentation and Data Processing, 55*(6), 618–622.

36. Gonchar, K. A., Agafilushkina, S. N., Moiseev, D. V., Bozhev, I. V., Manykin, A. A., Kropotkina, E. A., Gambaryan, A. S., & Osminkina, L. A. (2020). H1N1 influenza virus interaction with a porous layer of silicon nanowires. *Mater Research Express, 7*(3), 035002.
37. Baughman, R. H., Zakhidov, A. A., & De Heer, W. A. (2002). Carbon nanotubes–the route toward applications. *Science, 297*(5582), 787–792.
38. Prieto-Simón, B., Bandaru, N., Saint, C., & Voelcker, N. (2015). Tailored carbon nanotube immunosensors for the detection of microbial contamination. *Biosensors & Bioelectronics, 67*, 642–648.
39. Negri, P., & Dluhy, R. A. (2013). Ag nanorod based surface-enhanced Raman spectroscopy applied to bioanalytical sensing. *Journal of Biophotonics, 6*(1), 20–35.
40. Chen, Q., Zhang, L., Feng, Y., Shi, F., Wang, Y., Wang, P., & Liu, L. (2018). Dual-functional peptide conjugated gold nanorods for the detection and photothermal ablation of pathogenic bacteria. *Journal of Materials Chemistry B, 6*(46), 7643–7651.
41. Peña-Bahamonde, J., Nguyen, H. N., Fanourakis, S. K., & Rodrigues, D. F. (2018). Recent advances in graphene-based biosensor technology with applications in life sciences. *J Nanobiotechnology, 16*(1), 75.
42. Pandey, A., Gurbuz, Y., Ozguz, V., Niazi, J. H., & Qureshi, A. (2017). Graphene-interfaced electrical biosensor for label-free and sensitive detection of foodborne pathogenic E. coli O157: H7. *Biosensors & Bioelectronics, 91*, 225–231.
43. Chhowalla, M., Shin, H. S., Eda, G., Li, L.-J., Loh, K. P., & Zhang, H. (2013). The chemistry of two-dimensional layered transition metal dichalcogenide nanosheets. *Nature Chemistry, 5*(4), 263–275.
44. Shanmukh, S., Jones, L., Zhao, Y.-P., Driskell, J., Tripp, R., & Dluhy, R. (2008). Identification and classification of respiratory syncytial virus (RSV) strains by surface-enhanced Raman spectroscopy and multivariate statistical techniques. *Analytical and Bioanalytical Chemistry, 390*(6), 1551–1555.
45. Chu, H., Huang, Y., & Zhao, Y. (2008). Silver nanorod arrays as a surface-enhanced Raman scattering substrate for foodborne pathogenic bacteria detection. *Applied Spectroscopy, 62*(8), 922–931.
46. Perumal, J., Dinish, U., Bendt, A. K., Kazakeviciute, A., Fu, C. Y., Ong, I. L. H., & Olivo, M. (2018). Identification of mycolic acid forms using surface-enhanced Raman scattering as a fast detection method for tuberculosis. *International Journal of Nanomedicine, 13*, 6029.
47. Li, Z., Li, X., Jian, M., Geleta, G. S., & Wang, Z. (2020). Two-dimensional layered nanomaterial-based electrochemical biosensors for detecting microbial toxins. *Toxins, 12*(1), 20.
48. Akbari, E., Buntat, Z., Afroozeh, A., Zeinalinezhad, A., & Nikoukar, A. (2015). Escherichia coli bacteria detection by using graphene-based biosensor. *IET Nanobiotechnology, 9*(5), 273–279.
49. Thakur, B., Zhou, G., Chang, J., Pu, H., Jin, B., Sui, X., Yuan, X., Yang, C.-H., Magruder, M., & Chen, J. (2018). Rapid detection of single E. coli bacteria using a graphene-based field-effect transistor device. *Biosensors & Bioelectronics, 110*, 16–22.
50. Lu, C., Liu, Y., Ying, Y., & Liu, J. (2017). Comparison of MoS2, WS2, and graphene oxide for DNA adsorption and sensing. *Langmuir, 33*(2), 630–637.
51. Zhou, X., Sun, H., & Bai, X. (2020). Two-dimensional transition metal Dichalcogenides: Synthesis, biomedical applications and biosafety evaluation. *Frontiers in Bioengineering and Biotechnology, 8*.
52. Xi, Q., Zhou, D.-M., Kan, Y.-Y., Ge, J., Wu, Z.-K., Yu, R.-Q., & Jiang, J.-H. (2014). Highly sensitive and selective strategy for microRNA detection based on WS2 nanosheet mediated fluorescence quenching and duplex-specific nuclease signal amplification. *Analytical Chemistry, 86*(3), 1361–1365.
53. Silveira, C. M., et al. (2010). Enhanced direct electron transfer of a multihemic nitrite reductase on single-walled carbon nanotube modified electrodes. *Electroanalysis, 22*(24), 2973–2978.

54. Yu, W., et al. (2020). Progress in the functional modification of graphene/graphene oxide: A review. *RSC Advances, 10*(26), 15328–15345.
55. Singh, C., et al. (2013). Carboxylated multiwalled carbon nanotubes based biosensor for aflatoxin detection. *Sensors and Actuators B: Chemical, 185*, 258–264.
56. Zhang, Y., et al. (2004). Poly-L-lysine functionalization of single-walled carbon nanotubes. *The Journal of Physical Chemistry B, 108*(39), 15343–15346.
57. Jung, J. H., et al. (2010). A graphene oxide based immuno-biosensor for pathogen detection. *Angewandte Chemie, 122*(33), 5844–5847.
58. Viswanathan, S., et al. (2009). Disposable electrochemical immunosensor for carcinoembryonic antigen using ferrocene liposomes and MWCNT screen-printed electrode. *Biosensors & Bioelectronics, 24*(7), 1984–1989.
59. Jaiswal, N., et al. (2020). An impedimetric biosensor based on electrophoretically assembled ZnOnanorods and carboxylated graphene nanoflakes on an indium tin oxide electrode for detection of the DNA of Escherichia coli O157: H7. *Microchimica Acta, 87*(1), 1.
60. Koval'chuk, A. A., et al. (2008). Effect of carbon nanotube functionalization on the structural and mechanical properties of polypropylene/MWCNT composites. *Macromolecules, 41*(20), 7536–7542.
61. Patel, S. K., et al. (2017). Eco-friendly composite of Fe3O4-reduced graphene oxide particles for efficient enzyme immobilization. *ACS Applied Materials & Interfaces, 9*(3), 2213–2222.
62. Palanisamy, S., et al. (2017). A novel laccase biosensor based on laccase immobilized graphene-cellulose microfiber composite modified screen-printed carbon electrode for sensitive determination of catechol. *Scientific Reports, 7*(1), 1–1.
63. Dong, H., Zhu, Z., Ju, H., & Yan, F. (2012). Triplex signal amplification for electrochemical DNA biosensing by coupling probe-gold nanoparticles–graphene modified electrode with enzyme functionalized carbon sphere as tracer. *Biosensors & Bioelectronics, 33*(1), 228–232.
64. Huang, J., et al. (2016). Silver nanoparticles coated graphene electrochemical sensor for the ultrasensitive analysis of avian influenza virus H7. *Analytica Chimica Acta, 913*, 121–127.
65. Liu, Y., Dong, X., & Chen, P. (2012). Biological and chemical sensors based on graphene materials. *Chemical Society Reviews, 41*(6), 2283–2307.
66. Huang, Y., et al. (2010). Nanoelectronic biosensors based on CVD grown graphene. *Nanoscale, 2*(8), 1485–1488.
67. Huang, Y., et al. (2011). Graphene-based biosensors for detection of bacteria and their metabolic activities. *Journal of Materials Chemistry, 21*(33), 12358–12362.
68. Li, R., et al. (2013). Surface charge and cellular processing of covalently functionalized multiwall carbon nanotubes determine pulmonary toxicity. *ACS Nano, 7*(3), 2352–2368.
69. Zhou, Y., et al. (2017). Charge-directed immobilization of bacteriophage on nanostructured electrode for whole-cell electrochemical biosensors. *Analytical Chemistry, 89*(11), 5734–5741.
70. Georgakilas, V., et al. (2016). Noncovalent functionalization of graphene and graphene oxide for energy materials, biosensing, catalytic, and biomedical applications. *Chemical Reviews, 116*(9), 5464–5519.
71. Labib, M., Sargent, E. H., & Kelley, S. O. (2016). Electrochemical methods for the analysis of clinically relevant biomolecules. *Chemical Reviews, 116*(16), 9001–9090.
72. Chen, X., Guo, Z., Yang, G.-M., Li, J., Li, M.-Q., Liu, J.-H., & Huang, X.-J. (2010). Electrical nanogap devices for biosensing. *Materials Today, 13*(11), 28–41.
73. Park, S.-J., Taton, T. A., & Mirkin, C. A. (2002). Array-based electrical detection of DNA with nanoparticle probes. *Science, 295*(5559), 1503–1506.
74. Sato, T., Ahmed, H., Brown, D., & Johnson, B. F. (1997). Single electron transistor using a molecularly linked gold colloidal particle chain. *International Journal of Applied Physics, 82*(2), 696–701.
75. Amlani, I., Rawlett, A. M., Nagahara, L. A., & Tsui, R. K. (2002). An approach to transport measurements of electronic molecules. *Applied Physics Letters, 80*(15), 2761–2763.

76. Chen, C.-C., Ko, F.-H., Chang, E. Y., Chang, F.-C., & Kuo, S.-W. (2008). Hybridization sensing by electrical enhancement with nanoparticles in nanogap. *Journal of Vacuum Science & Technology, B: Microelectronics and Nanometer Structures–Processing, Measurement, and Phenomena, 26*(6), 2572–2577.
77. Cai, B., Wang, S., Huang, L., Ning, Y., Zhang, Z., & Zhang, G.-J. (2014). Ultrasensitive label-free detection of PNA–DNA hybridization by reduced graphene oxide field-effect transistor biosensor. *ACS Nano, 8*(3), 2632–2638.
78. Roy, S., Chen, X., Li, M.-H., Peng, Y., Anariba, F., & Gao, Z. (2009). Mass-produced nanogap sensor arrays for ultrasensitive detection of DNA. *JACS, 131*(34), 12211–12217.
79. Shabihkhani, M., Lucey, G. M., Wei, B., Mareninov, S., Lou, J. J., Vinters, H. V., Singer, E. J., Cloughesy, T. F., & Yong, W. H. (2014). The procurement, storage, and quality assurance of frozen blood and tissue biospecimens in pathology, biorepository, and biobank settings. *Clinical Biochemistry, 47*(4–5), 258–266.
80. Donczo, B., & Guttman, A. (2018). Biomedical analysis of formalin-fixed, paraffin-embedded tissue samples: The holy grail for molecular diagnostics. *J Pharmaceut Biomed, 155*, 125–134.
81. Leong, A. S. Y., Daymon, M. E., & Milios, J. (1985). Microwave irradiation as a form of fixation for light and electron microscopy. *The Journal of Pathology, 146*(4), 313–321.
82. Bonin, S., Hlubek, F., Benhattar, J., Denkert, C., Dietel, M., Fernandez, P. L., Höfler, G., Kothmaier, H., Kruslin, B., & Mazzanti, C. M. (2010). Multicentre validation study of nucleic acids extraction from FFPE tissues. *Virchows Archiv, 457*(3), 309–317.
83. Kohl, C., Wegener, M., Nitsche, A., & Kurth, A. (2017). Use of RNALater® preservation for virome sequencing in outbreak settings. *Frontiers in Microbiology, 8*, 1888.
84. Holland, N. T., Smith, M. T., Eskenazi, B., & Bastaki, M. (2003). Biological sample collection and processing for molecular epidemiological studies. *Mutation Research, Reviews in Mutation Research, 543*(3), 217–234.
85. Lahiri, D. K., & Schnabel, B. (1993). DNA isolation by a rapid method from human blood samples: Effects of MgCl 2, EDTA, storage time, and temperature on DNA yield and quality. *Biochemical Genetics, 31*(7–8), 321–328.
86. Huy, N. T., Kariu, T., Tajima, K., & Kamei, K. (2004). One-step concentration of malarial parasite-infected red blood cells and removal of contaminating white blood cells. *Malaria Journal, 3*(1), 7.
87. Polski, J., Kimzey, S., Percival, R., & Grosso, L. (1998). Rapid and effective processing of blood specimens for diagnostic PCR using filter paper and Chelex-100. *Molecular Pathology, 51*(4), 215.
88. Mei, J. V., Alexander, J. R., Adam, B. W., & Hannon, W. H. (2001). Use of filter paper for the collection and analysis of human whole blood specimens. *The Journal of Nutrition, 131*(5), 1631S–1636S.
89. Shehadul Islam, M., Aryasomayajula, A., & Selvaganapathy, P. R. (2017). A review on macroscale and microscale cell lysis methods. *Micromachines, 8*(3), 83.
90. Kim, J., Hong, J. W., Kim, D. P., Shin, J. H., & Park, I. (2012). Nanowire-integrated microfluidic devices for facile and reagent-free mechanical cell lysis. *Lab on a Chip, 12*(16), 2914–2921.
91. Sambrook, J., Fritsch, E. F., & Maniatis, T. (1989). *Molecular cloning: A laboratory manual*. Cold spring harbor laboratory press.
92. Adeli, K., & Ogbonna, G. (1990). Rapid purification of human DNA from whole blood for potential application in clinical chemistry laboratories. *Clinical Chemistry, 36*(2), 261–264.
93. McCormick, R. M. (1989). A solid-phase extraction procedure for DNA purification. *Analytical Biochemistry, 181*(1), 66–74.
94. Gjerde, D. T., Hoang, L., Hornby, D. (2009). RNA extraction and analysis. *RNA purification and analysis.*
95. He, J., Huang, M., Wang, D., Zhang, Z., & Li, G. (2014). Magnetic separation techniques in sample preparation for biological analysis: A review. *Journal of Pharmaceutical and Biomedical, 101*, 84–101.

96. Lee, H., Jung, J., Han, S.-I., & Han, K.-H. (2010). High-speed RNA microextraction technology using magnetic oligo-dT beads and lateral magnetophoresis. *Lab on a Chip, 10*(20), 2764–2770.
97. Lee, C.-H. (2017). A simple outline of methods for protein isolation and purification. *Endocrinology and Metabolism, 32*(1), 18–22.
98. Swarge, B. N., Roseboom, W., Zheng, L., Abhyankar, W. R., Brul, S., de Koster, C. G., & de Koning, L. J. (2018). One-pot sample processing method for proteome-wide analysis of microbial cells and spores. *Proteomics. Clinical Applications, 12*(5), 1700169.
99. Tanca, A., Biosa, G., Pagnozzi, D., Addis, M. F., & Uzzau, S. (2013). Comparison of detergent-based sample preparation workflows for LTQ-O rbitrap analysis of the E scherichia coli proteome. *Proteomics, 13*(17), 2597–2607.
100. Speda, J., Johansson, M. A., Carlsson, U., & Karlsson, M. (2017). Assessment of sample preparation methods for metaproteomics of extracellular proteins. *Analytical Biochemistry, 516*, 23–36.
101. Zhang, X., Li, L., Mayne, J., Ning, Z., Stintzi, A., & Figeys, D. (2018). Assessing the impact of protein extraction methods for human gut metaproteomics. *Journal of Proteomics, 180*, 120–127.
102. Novák, P., & Havlíček, V. (2016). Protein extraction and precipitation. In *Proteomic profiling and analytical chemistry* (pp. 51–62). Elsevier.
103. Yi, J., Qin, Q., Wang, Y., Zhang, R., Bi, H., Yu, S., Liu, B., & Qiao, L. (2018). Identification of pathogenic bacteria in human blood using IgG-modified Fe 3 O 4 magnetic beads as a sorbent and MALDI-TOF MS for profiling. *Microchimica Acta, 185*(12), 542.
104. Shakhmaeva, I. I., Bulatov, E. R., Bondar, O. V., Saifullina, D. V., Culha, M., Rizvanov, A. A., & Abdullin, T. I. (2011). Binding and purification of plasmid DNA using multi-layered carbon nanotubes. *Journal of Biotechnology, 152*(3), 102–107.
105. Hashemi, E., Akhavan, O., Shamsara, M., Valimehr, S., & Rahighi, R. (2014). DNA and RNA extractions from eukaryotic and prokaryotic cells by graphene nanoplatelets. *RSC Advances, 4*(105), 60720–60728.
106. Varghese, N., Mogera, U., Govindaraj, A., Das, A., Maiti, P. K., Sood, A. K., & Rao, C. (2009). Binding of DNA nucleobases and nucleosides with graphene. *Chem Phys Chem, 10*(1), 206–210.
107. Lee, H., Choi, M., Hwang, S.-H., & Cho, Y. (2018). A versatile nanowire platform for highly efficient isolation and direct PCR-free colorimetric detection of human papillomavirus DNA from unprocessed urine. *Theranostics, 8*(2), 399.
108. Luo, J., Jiang, S., & Liu, X. (2013). Efficient one-pot synthesis of mussel-inspired molecularly imprinted polymer coated graphene for protein-specific recognition and fast separation. *The Journal of Physical Chemistry C, 117*(36), 18448–18456.
109. Chen, X., Hai, X., & Wang, J. (2016). Graphene/graphene oxide and their derivatives in the separation/isolation and preconcentration of protein species: A review. *Analytica Chimica Acta, 922*, 1–10.
110. Wei, X.-Q., Hao, L.-Y., Shao, X.-R., Zhang, Q., Jia, X.-Q., Zhang, Z.-R., Lin, Y.-F., & Peng, Q. (2015). Insight into the interaction of graphene oxide with serum proteins and the impact of the degree of reduction and concentration. *ACS Applied Materials & Interfaces, 7*(24), 13367–13374.
111. Uzzaman, A., Shang, Z., Qiao, Z., Cao, C.-X., & Xiao, H. (2018). Graphene and graphene oxide as a solid matrix for extraction of membrane and membrane-associated proteins. *MCA, 185*(2), 123.
112. Hukari, K. W., Shultz, M., Isely, N., Milson, R., & West, J. A. (2011). A completely automated sample preparation instrument and consumable device for isolation and purification of nucleic acids. *JALA: Journal of the Association for Laboratory Automation, 16*(5), 355–365.

113. Thakore, N., Garber, S., Bueno, A., Qu, P., Norville, R., Villanueva, M., Chandler, D. P., Holmberg, R., & Cooney, C. G. (2018). A bench-top automated workstation for nucleic acid isolation from clinical sample types. *Journal of Microbiological Methods, 148*, 174–180.
114. Rossetti, C., Świtnicka-Plak, M. A., Halvorsen, T. G., Cormack, P. A., Sellergren, B., & Reubsaet, L. (2017). Automated protein biomarker analysis: On-line extraction of clinical samples by molecularly imprinted polymers. *Scientific Reports, 7*, 44298.
115. Bitting, A. L., Bordelon, H., Baglia, M. L., Davis, K. M., Creecy, A. E., Short, P. A., Albert, L. E., Karhade, A. V., Wright, D. W., & Haselton, F. R. (2016). Automated device for asynchronous extraction of RNA, DNA, or protein biomarkers from surrogate patient samples. *Journal of Laboratory Automation, 21*(6), 732–742.
116. Dundas, N., Leos, N. K., Mitui, M., Revell, P., & Rogers, B. B. (2008). Comparison of automated nucleic acid extraction methods with manual extraction. *JMD, 10*(4), 311–316.
117. Dauphin, L. A., Hutchins, R. J., Bost, L. A., & Bowen, M. D. (2009). Evaluation of automated and manual commercial DNA extraction methods for recovery of Brucella DNA from suspensions and spiked swabs. *JCM, 47*(12), 3920–3926.
118. Yera, H., Ménégaut, L., Brenier-Pinchart, M.-P., Touafek, F., Bastien, P., Dalle, F., Cassaing, S., Delhaes, L., Filisetti, D., & Ménotti, J. (2018). Evaluation of five automated and one manual method for toxoplasma and human DNA extraction from artificially spiked amniotic fluid. *CMI, 24*(10), 1100–e7-1100. e11.
119. Day, W., & Peccarelli, M. C. (2019). *Fully automated nucleic acid extraction methods for tissue samples*. Google Patents.
120. Whitesides, G. M. (2006). The origins and the future of microfluidics. *Nature, 442*(7101), 368–373.
121. Song, H., Wang, Y., Garson, C., & Pant, K. (2015). Concurrent DNA preconcentration and separation in bipolar electrode-based microfluidic device. *Analytical Methods, 7*(4), 1273–1279.
122. Yeh, Y.-T., Lin, Z., Zheng, S.-Y., & Terrones, M. (2018). A carbon nanotube integrated microfluidic device for blood plasma extraction. *Scientific Reports, 8*(1), 1–8.
123. Luka, G., Ahmadi, A., Najjaran, H., Alocilja, E., DeRosa, M., Wolthers, K., Malki, A., Aziz, H., Althani, A., & Hoorfar, M. (2015). Microfluidics integrated biosensors: A leading technology towards lab-on-a-chip and sensing applications. *Sensors, 15*(12), 30011–30031.
124. Nikoleli, G.-P., Siontorou, C. G., Nikolelis, D. P., Bratakou, S., Karapetis, S., & Tzamtzis, N. (2018). Biosensors based on Microfluidic devices lab-on-a-Chip and Microfluidic technology. In *Nanotechnology and biosensors* (pp. 375–394). Elsevier.
125. Prakash, S., Pinti, M., & Bhushan, B. (1967). Theory, fabrication and applications of microfluidic and nanofluidic biosensors. *Philosophical Transactions of The Royal Society A Mathematical Physical and Engineering Sciences, 2012*(370), 2269–2303.
126. Rubio, E., Zboromyrska, Y., Bosch, J., Fernandez-Pittol, M. J., Fidalgo, B. I., Fasanella, A., Mons, A., Román, A., Casals-Pascual, C., & Vila, J. (2019). Evaluation of flow cytometry for the detection of bacteria in biological fluids. *PLoS One, 14*(8), e0220307.
127. Rozman, U., & Turk, S. Š. (2016). PCR technique for the microbial analysis of inanimate hospital environment. In *Polymerase chain reaction for biomedical applications* (pp. 119–134). UK: InTech.
128. Rudi, K., Moen, B., Drømtorp, S. M., & Holck, A. L. (2005). Use of ethidium monoazide and PCR in combination for quantification of viable and dead cells in complex samples. *AEM, 71*(2), 1018–1024.
129. Masakiyo, Y., Yoshida, A., Takahashi, Y., Shintani, Y., Awano, S., Ansai, T., Sawayama, S., Shimakita, T., & Takehara, T. (2010). Rapid LED-based fluorescence microscopy distinguishes between live and dead bacteria in oral clinical samples. *The Journal of Biomedical Research, 31*(1), 21–26.
130. Abdu-Aguye, M. T., Cordes, T. *Fluorophore stabilization and applications in the life-sciences*

131. Hao, L., Li, J., Kappler, A., & Obst, M. (2013). Mapping of heavy metal ion sorption to cell-extracellular polymeric substance-mineral aggregates by using metal-selective fluorescent probes and confocal laser scanning microscopy. *AEM, 79*(21), 6524–6534.
132. Ko, S., & Grant, S. A. (2006). A novel FRET-based optical fiber biosensor for rapid detection of salmonella typhimurium. *Biosensors & Bioelectronics, 21*(7), 1283–1290.
133. Fijen, C., Silva, A. M., Hochkoeppler, A., & Hohlbein, J. (2017). A single-molecule FRET sensor for monitoring DNA synthesis in real time. *PCCP, 19*(6), 4222–4230.
134. Wang, E., Zhang, Y., Cai, J., Cai, W., & Gao, T. (2011). Aptamer-based fluorescent biosensors. *Current Medicinal Chemistry, 18*(27), 4175–4184.
135. Wood, B. R., Caspers, P., Puppels, G. J., Pandiancherri, S., & McNaughton, D. (2007). Resonance Raman spectroscopy of red blood cells using near-infrared laser excitation. *Analytical and Bioanalytical Chemistry, 387*(5), 1691–1703.
136. López-Díez, E. C., & Goodacre, R. (2004). Characterization of microorganisms using UV resonance Raman spectroscopy and chemometrics. *Analytical Chemistry, 76*(3), 585–591.
137. Chen, X., Zhang, X.-E., Chai, Y.-Q., Hu, W.-P., Zhang, Z.-P., Zhang, X.-M., & Cass, A. E. (1998). DNA optical sensor: A rapid method for the detection of DNA hybridization. *Biosensors & Bioelectronics, 13*(3–4), 451–458.
138. Hine, A. V., Chen, X., Hughes, M. D., Zhou, K., Davies, E., Sugden, K., Bennion, I., & Zhang, L. (2009). *Optical fibre-based detection of DNA hybridization*. Portland Press Ltd..

Chapter 11
Clinical Validation of the Medical Devices: A General Prospective

Sumanta Ghosh, Dipesh Shah, Namdev More, Mounika Choppadandi, Deepak Ranglani, and Govinda Kapusetti

11.1 Introduction

Medical devices are a key component in modern-day health care for a better quality of life. Medical devices are employed for a wide range of applications, including simple medical examinations such as thermistors and stethoscopes to highly sophisticated devices like artificial pacemakers and vascular stents [1, 2]. As defined by Global Harmonization Task Force (GHTF) the term "medical device" means ". . .any instrument, apparatus, implement, machine, appliance, implant, in vitro reagent or calibrator, software, material or other similar or related article intended by the manufacturer to be used, alone or in combination, for human beings for one or more of the specific purpose(s) of diagnosis, prevention, monitoring, treatment or alleviation of disease or diagnosis, monitoring, treatment, alleviation of or compensation for an injury or investigation, replacement, modification, or support of the anatomy or of a physiological process or supporting or sustaining life or control of conception or disinfection of medical devices or providing information for medical or diagnostic purposes by means of in vitro examination of specimens derived from the human body; and which does not achieve its primary intended action in or on the human body by pharmacological, immunological or metabolic means, but which may be assisted in its intended function by such means. . ." [3].

The medical device regulations are highly needed to contain the devices with poor quality as drugs. However, except for developed countries, very few countries follow strict regulations [4, 5]. Therefore, there is a compulsion to draft regulatory policies for all other countries to examine the quality, safety, and efficacy of medical devices before entering the market. Countries' dissimilar regulations on medical devices obstructed access to high-quality, safe, and efficacious medical devices to

S. Ghosh · D. Shah · N. More · M. Choppadandi · D. Ranglani · G. Kapusetti (✉)
Department of Medical Devices, National Institute of Pharmaceutical Education and Research (NIPER)-Ahmedabad, Gandhinagar, Gujarat, India

V. Borse et al. (eds.), *BioSensing, Theranostics, and Medical Devices*,
https://doi.org/10.1007/978-981-16-2782-8_11

the end-users. Hence, there is a need to homogenize regulations to curtail the hurdles to enter the device in various markets. Among all, clinical validation's regulatory guidelines are the utmost important aspect to scrutinize the safety, quality, and efficacy of the medical devices.

In simple terms, clinical validation means the process of justifying all the clinical assessment study reports related to the device's performance, quality, safety, and efficacy with the regulatory compliance of any targeted markets. Usually, the final clinical validation is done by the highest regulatory authority of those countries. However, the need and types of clinical validation vary from device to device or class to class. The process of clinical confirmatory is a never-ending procedure for high risk associated devices, as per the implementation of post marketing clinical follow-up (PMCF), post-market surveillance (PMS), and periodic safety update report (PSUR) by the regulatory authorities of various countries. In recent days, various regulatory bodies have included another important regulation related to software across the globe. So, in a broader prospect, the clinical validation process for the clinical investigation plan and its results become mandatory regulatory compliance for every device.

Key Definitions Related to Clinical Validation (According to Indian MDR, 2017)

1. **Investigational medical device:** "A medical device (i) which does not have its predicate device or (ii) which is claimed for the new intended use or new population or new material or major design change; and is being assessed for safety or performance or effectiveness in a clinical investigation."
2. **Predicate device:** "A device, first time and first of its kind, approved for manufacture for sale or import and has the similar intended use, material of construction, and design characteristics as the device which is proposed for a license."
3. **Clinical evidence**: Defined as "(i) An in vitro diagnostic medical device, is all the information derived from a specimen collected from a human which supports the scientific validity and performance for its intended use; (ii) a medical device, the clinical data and the clinical evaluation report that supports the scientific validity and performance for its intended use."
4. **Clinical investigation**: "The systematic study of an investigational medical device in or on human participants to assess its safety, performance, or effectiveness."
5. **Clinical investigation plan**: "A document which contains the information about the rationale, aims and objective, design and the proposed analysis, conduct, methodology including performance, management, adverse event, withdrawal and statistical consideration and record-keeping pertaining to clinical investigation."
6. **Clinical performance evaluation:** "The systematic performance study of a new in vitro diagnostic medical device on a specimen collected from human participants to assess its performance."

7. **Clinical benefit:** "The positive impact of a device on the health of an individual, expressed in terms of a meaningful, measurable, patient-relevant clinical outcome (s), including outcome(s) related to diagnosis, or a positive impact on patient management or public health' as per the article 2(53) of the MDR."

A special wing of USFDA, i.e., Center for Devices and Radiological Health (CDRH), is accountable for regulating the manufacture, sale, distribution, re-label, and/or import of medical devices to the USA. According to USFDA, the devices are classified into three classes, i.e., Class I, II, or III, based on the risk associated with the devices. Class I devices possess no risk to the user's life, and thus they are subjected to some common controls and least regulations. Class II devices require some special controls and the general controls for receiving the market approval. Class III devices are those that support and sustain human life [6, 7]. Hence, it requires the demonstration of safety and efficacy through clinical trial studies before entering the market.

European Union (EU) acquires a decentralized system to achieve the marketing authority for the medical devices. Notified bodies in the EU acquire the quality assurance certificate and confirm post-approval obedience to quality management system (QMS) [6, 7]. Medical devices are classified and regulated by their respective country regulatory bodies to ensure their safety and efficacy before being commercialized. EU classifies devices into three main classes, i.e., Class I, IIa, IIb, and III depending on the risk. The device classification criteria are the duration of the contact, source of energy for the device, and the invasiveness of the device. Brief classification is presented as follows with some examples:

Class I: Hospital bed and blood pressure cuff
Class IIa: Hearing aid and X-ray diagnostic device
Class IIb: Ventilator and blood bags
Class III: Drug-eluting coronary stents

Various directives regulate the safety and marketing of medical devices in Europe, such as the Medical Device Directive (MDD 93/42/EEC), Active Implantable Medical Device Directive (AIMDD 90/42/EE), In vitro Diagnostic Medical Device Directive (IVDMDD 98/79/EC), etc.

In India, the medical device section of the Central Drugs Standards Control Organization (CDSCO) acts as the highest regulating authority for medical devices and in vitro diagnostic. The CDSCO controls the medical device regulations through the Central Licensing Authority (CLA) and State Licensing Authority (SLA). Under the third schedule of MDR, notified bodies shall be registered with CDSCO and shall be audited by CDSCO and accredited by NABCB (National Accreditation Board for Certification Bodies) or Quality Council of India (QCI). According to Indian MDR 2017, the medical devices and in vitro diagnostics are classified into four classes (Class A, B, C, and D) under the new framework MDR 2017, where Class A and B shows the least risk and Class C and D devices show the higher risk to patients. The new framework was darted in consideration with USFDA and EU-MDR. The notified bodies and SLA are responsible for regulating and verifying the QMS of

Table 11.1 The recalled medical devices in various markets through clinical validation [9]

Name of the devices	Manufacturer	Recalled country	Date of Recall	Reason for recall
Dual-chamber pacemakers (Adapta™)	Medtronics	USA	January 2019	Due to circuit failure
Cardiac resynchronization therapy defibrillators (CRT-ds)	Abbott	USA	August 2017	Due to premature battery depletion complaints caused by lithium deposition
Chemolock™	ICU Medical	Worldwide	February 2019	Due to the presence of plastic burr
Continuous glucose monitoring (CGM) systems	Dexcom	USA	February 2016	Due to a faulty auditory alarm
8100 model Alaris pump modules along with air-in-line (AIL) sensor kits	Becton Dickinson's subsidiary carefusion	CANADA	December 2016	Due to faulty alarm
Catheters with Beacon® tip technology	Cook Medical	USA	April 2016	Polymer degradation of the catheter tip
Vial2Bag fluid transfer systems	West Pharmaceutical	Worldwide	January 2019	Due to functioning issues
Leadcare blood lead testing systems	Magellan Diagnostics	Worldwide	May 2017	Gives inaccurate test results

Class A and B devices. The CLA is responsible for checking and granting import or manufacturer licenses for Class C and D. The permission for conducting the clinical investigation should be taken from CDSCO in the respective form. It is also notifying that CLA can cross-check and verify all the clinical evidence and other QMS compliances of any class of device, a sale in the Indian market. According to the MDR provisions, the approval for clinical investigation plan, device performance report should be done by the CLA and PMS should be done by the manufacturer but should be verified by the CDSCO at the time of audits.

The strong regulatory guidelines of medical devices can drive the development of quality devices, among the clinical validation process is the key paramater. A clinical trial sponsor typically performs clinical validation to facilitate the development of a new product. The goal of clinical validation is to demonstrate the device acceptably identifies, measures, or predicts the clinical, biological, physical, functional state, or experience in the defined context of use [8]. In simple terms, the entire procedure provides a legal defense against the malpractices on the medical devices. In this chapter, we will discuss required clinical validation protocols and detailed procedures for validation in contrast with safety and type of device (new or existed similar device). Apart from this, the reader will also get an idea about validation procedures in various countries by their classes. Table 11.1 shows some of the recent recalled devices went through the clinical validation in various markets.

11.2 What Is Clinical Evaluation?

11.2.1 Definition

"Clinical evaluation is the systematic approach for assessing and analyzing clinical data by conducting the literature search of scientific data and/or by conducting the clinical trial of medical devices. Clinical evaluation is mandatory for the compliance of safety, clinical performance, and effectiveness [8, 10]."

There is always a great confusion between clinical evaluation and clinical trials (clinical investigation). The clinical trial is one of the clinical evaluation steps, whereas clinical evaluation requires final verification and validation of medical devices [11]. Generally, the clinical evaluation is dependent on the design and innovativeness of the medical device. For instance, if the device has a similar configuration as the available marketed product, it is also known as substantially equivalent devices and does not require clinical investigation [8, 10]. Suppose the device is predicted to substantially equivalent devices, e.g., a bone screw or cardiac stents. In that case, the clinical evaluation will be carried out from the literature search by identifying the scientific data that supports the devices' safety, efficacy, and performance. If data meets the device's desirable safety, efficacy, and performance, then the device is suitable for use.

While innovative medical devices require to prove their performance and safety by conducting the clinical investigation on the human subjects to prove the claims of intended applications [10].

11.2.2 Pre-Clinical Evaluation

Pre-clinical evaluation is a primary assessment of the device for safety and efficacy, including before the clinical investigation [12].

Pre-clinical evaluation of medical devices consists of the various examination of the devices according to standards like ISO 10093 and ASTM F748. Some of the evaluations are physicochemical characterization, in vitro cytotoxicity, irritation, skin sensitization, intra-cutaneous reactivity, material pyrogenicity, systemic toxicity, and implantation test genotoxicity, carcinogenicity, reproductive toxicity [8, 13].

Pre-clinical evaluation of medical device classification is a risk-based class requirement. Table 11.2 represents the categories of the devices and related evaluation [8].

Table 11.2 Pre-clinical test requirements of medical devices in contrast to their nature of contact and duration

Medical device categorization			Endpoints of biological evaluation														
Nature of body contact		**Contact duration**	**Physical and/or chemical information**	**Cytotoxicity**	**Sensitization**	**Irritation activity**	**Material mediated pyrogenicity**[a]	**Acute systemic toxicity**[b]	**Subacute toxicity**[b]	**Subchronic toxicity**[b]	**Chronic toxicity**[b]	**Implantation effects**[b,c]	**Hemocompatibility**	**Genotoxicity**[d]	**Carcinogenicity**[d]	**Reproductive/ developmental toxicity**[d,e]	**Degradation**[f]
Category	**Contact**	A – Limited (≤24 h) B – Prolonged (≥24 h to 30 d) C – Long term (>30 d)															
Surface medical device	Intact skin	A	N[g]	Y[h]	Y	Y											
		B	N	Y	Y	Y											
		C	N	Y	Y	Y											
	Mucosal membrane	A	N	Y	Y	Y											
		B	N	Y	Y	Y		Y	Y			Y					
		C	N	Y	Y	Y		Y	Y	Y	Y	Y		Y			
	Breached or compromised surface	A	N	Y	Y	Y	Y	Y									
		B	N	Y	Y	Y	Y	Y	Y			Y					
		C	N	Y	Y	Y	Y	Y	Y	Y	Y	Y		Y	Y		
Externally Communicating medical device	Blood path, indirect	A	N	Y	Y	Y	Y	Y					Y				
		B	N	Y	Y	Y	Y	Y	Y				Y				
		C	N	Y	Y	Y	Y	Y	Y	Y	Y	Y	Y	Y	Y		
	Tissue/ bone/ dentin[e]	A	N	Y	Y	Y	Y	Y									
		B	N	Y	Y	Y	Y	Y	Y			Y		Y			
		C	N	Y	Y	Y	Y	Y	Y	Y	Y	Y		Y	Y		
	Circulating blood	A	N	Y	Y	Y	Y	Y					Y	Y[i]			
		B	N	Y	Y	Y	Y	Y	Y			Y	Y	Y			
		C	N	Y	Y	Y	Y	Y	Y	Y	Y	Y	Y	Y	Y		
Implant medical device	Tissue/bone[j]	A	N	Y	Y	Y	Y	Y									
		B	N	Y	Y	Y	Y	Y	Y			Y		Y			
		C	N	Y	Y	Y	Y	Y	Y	Y	Y	Y		Y	Y		

	Blood	A	N	Y	Y	Y	Y	Y				Y	Y	Y			
		B	N	Y	Y	Y	Y	Y	Y			Y	Y	Y			
		C	N	Y	Y	Y	Y	Y	Y	Y	Y	Y	Y	Y	Y		

[a]ISO 10993-11:2017, Annex F

[b]Data extracted from assessments that include acute systemic toxicity, subacute toxicity, subchronic toxicity, and/or chronic toxicity may be sufficient if sufficient animals and time points are included and evaluated. Therefore, these studies are not always mandatory for acute, subacute, subchronic, and chronic toxicity

[c]Site specific implantation should be considered

[d]The carcinogenic, mutagenic, and/or toxic to reproduction prone medical devices (material) should be considered in the risk assessment

[e]Needs to assess reproductive and developmental toxicity of novel materials and medical devices with relevant target populations (e.g. pregnant women) and/or where there is the high risk potential for reproductive organs

[f]Degradation analysis required to generate for any medical device, component of medical device, and materials remaining within the patient

[g]N denotes prerequisite examination needed for a risk assessment

[h]Y denotes endpoints to be evaluated in the risk assessment

[i]All devices intended for extracorporeal circuits

[j]Medical devices contact with tissues, contain tissue fluids or subcutaneous spaces need to be tested as per device-specific standards for biocompatibility examination

11.3 Needs of Clinical Evaluation of Medical Devices

The clinical evaluation is the regulatory requirement of a device to enter into a market. Each country has its guidelines for the assessment of the safety and effectiveness of the devices.

Regulatory requirements like in India, Medical Devices Rules (MDR) 2017; USA, Code of Federal Regulations Title 21 (USFDA); Europe, European Commission; United Kingdom, Medicines and Healthcare Products Regulatory Agency; Japan, Pharmaceutical and Medical Devices Agency; Australia, Therapeutic Goods Administration, Global-International Organization for Standardization (ISO 13485, ISO 14155), etc. should follow to enter their respective markets [11]. The basic needs of clinical evaluation are to prove the medical devices' safety and performance by conducting the clinical evaluation either by scientific or clinical investigation data. Intended use of a new device possesses specific claim like unique features toward the application needs to prove the performance by full clinical investigations. Various markets have their documented norms for clinical investigations and some are listed below:

- India, MDR 2017, manufacturers have to submit clinical evidence to demonstrate the conformity of the essential principle of design.
- USFDA manufacturers need to submit clinical equivalence by scientific data by literature or conducting a clinical trial as per ISO 14155.
- EU, Medical Device Directives 93/42/EEC manufacturers need to conduct the clinical evaluation by literature or perform the clinical investigation as requirements of MEDEV 2.7 rev.4.followed by ISO 14155.
- Japan, Pharmaceutical Affair Law (PAL) needs to conduct the clinical evaluation by literature or perform clinical investigations as PAL requirements.
- ATG, administration needs to conduct the clinical evaluation by literature or perform clinical investigations.

For innovative medical devices, it needs to conduct the clinical investigation to understand the safety, performance, and effectiveness. A device similar to marketed product may not need to perform any clinical investigation since predicated data is available based on the physicochemical, biological, and technological characteristics. For instance, a newly developed device with unique design features and functions needs clinical investigation in human subjects (ISO 14155) to prove its performance and safety.

11.4 Type of Clinical Evaluation

11.4.1 Clinical Investigation

Clinical investigation of medical devices is classified into two distinct types: clinical trials (clinical investigation) and clinical evaluation by literature data. Clinical trials

are classified into two more categories based on the study's nature, i.e., pilot and pivot studies. Whereas the clinical evaluation is performed by collecting and analyzing the data published in the literature.

Clinical investigations are the regulatory requirements for developed medical devices. The clinical investigation for the devices is performed when sufficient scientific data is not available for particular medical devices. Moreover, the predicate medical devices must prove the devices' safety and effectiveness [12, 14, 15].

For instance, according to USFDA, for newly developed pacemakers or cardiac stent drug-eluting stent requires clinical evaluation with clinical trial data before releasing the products. Besides this, all high-risk Class III devices require clinical trial in the USA as regulatory requirements PMA (premarket approval) of USFDA. Similarly, the EU also requires clinical investigations to prove the safety and effectiveness of high-risk devices [16].

Steps Involved in Clinical Investigations

There are several steps involved in the clinical investigation of the new medical devices, Fig.11.1. The process of clinical investigation of the new medical devices is summarized as follows:

- The newly developed device, which does not have similar legally marketed devices, needs to prove its characteristics like clinical indication and intended purpose, technical—specification, design and biological—biocompatibility, etc.
- To define the plan for clinical evaluation
- Identification of the clinical data from the literature search or a clinical experience. The data could be either published or unpublished.
- Appraisal of data sets by scientific validity, suitability, demonstration of safety, clinical performance, and/or effectiveness of clinical data. Also, sample size, inclusion–exclusion criteria concerning age, medical condition, severity, prognostic factors, etc. Follow-up and outcome of the clinical data.

  Analysis of clinical data: a literature review of clinical data by using different analysis methods like sound methods, comprehensive analysis, additional pre-clinical evaluation, and clinical investigations or other measures is required for safety, effectiveness, and risk/benefit analysis.
- Is this clinical evidence sufficient to declare conformity with relevant essential principal consideration of novelty of device, risk level, and risk–benefit analysis?
- If yes, these are fulfilling all essential principal requirements, then no further clinical data needed (clinical investigation not needed).
- If no, these are not fulfilling all essential principal requirements, then additional clinical data required.
- Is the additional data available? If yes, then generate the new or additional data by the literature search; if no, then conduct the clinical investigation.
- Clinical investigation is needed to declare the safety and effectiveness of the device. Clinical investigation steps are:
  - Sponsor of clinical investigation
  - Institute performing the clinical investigation

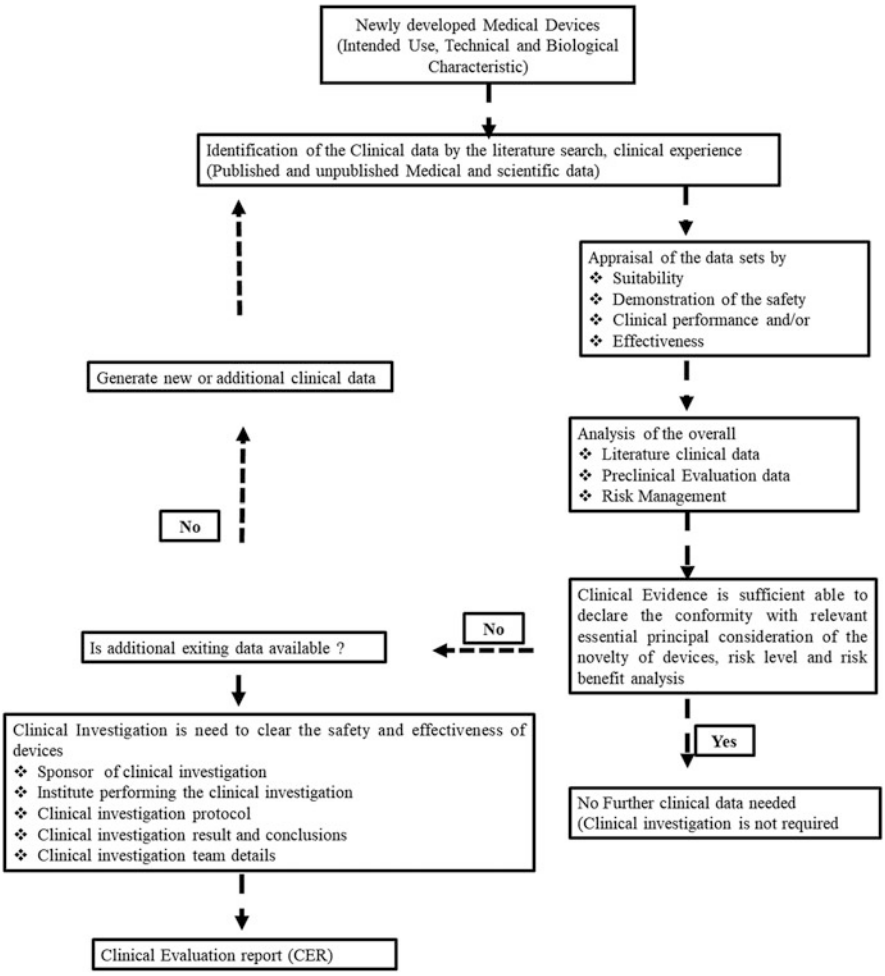

Fig. 11.1 The steps involved in the clinical investigation of new medical devices

  - Clinical investigation protocol (objectives, subjects, methods)
  - Clinical investigations results and conclusions
  - Clinical investigation team details

- Finally, the clinical evaluation report concludes the fate of the device by considering safety and effectiveness.

11.4.2 By Literature Way

Clinical evaluations by literature way are also regulatory requirements for substantially equivalent devices. The safety and effectiveness can be established by

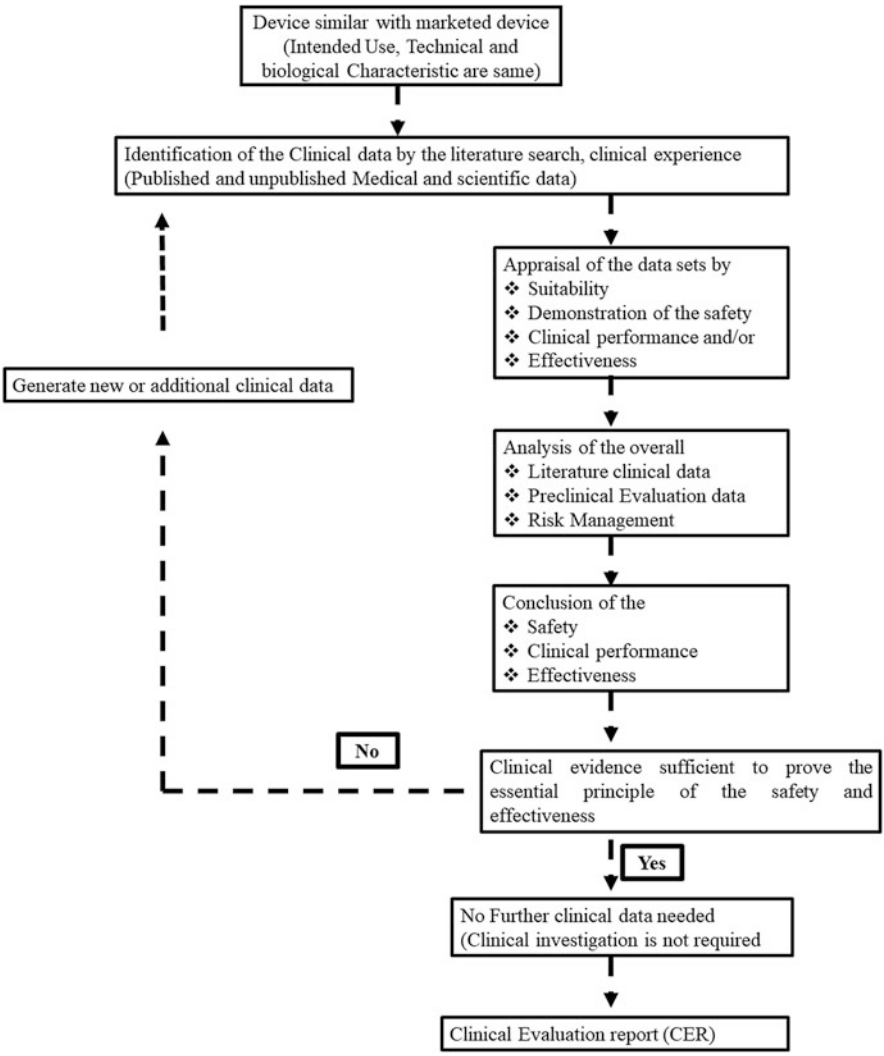

Fig. 11.2 The steps involved in the clinical investigation of the medical devices by literature route

conducting a literature search related to available clinical data (published and unpublished medical-scientific data) of exited devices. When predicate clinical data is insufficient, it needs to pass in clinical investigations for safety and effectiveness [10, 17]. The detailed flow of evolution is presented in Fig. 11.2.

Class II or lower-risk devices like wound dressing devices (hemostatic) or bone fixation devices (screws) do not require clinical trial, but it should be clinically equivalent as that of existing one [16].

Steps Involved in Clinical Evaluation by Literature Way

- The developed device is similar to legally marketed devices with characteristics such as clinical characteristic—indication and intended purpose, technical characteristic—specification and design, biological characteristic—material biocompatibility.
- Define the plan for clinical evaluation **Identification of the potential threat from the previous research** works and clinical experience from published and unpublished clinical data.
- Appraisal of data sets by scientific **justification**, suitability, **criteria** of safety, clinical performance, and/or effectiveness of clinical data. Besides, sample size, inclusion–exclusion criteria concerning age, medical condition, severity, prognostic factors, etc. Follow-up and outcome of the clinical data.
- Analysis of clinical data: a literature review of clinical data by using different analysis methods like sound methods, comprehensive analysis, additional pre-clinical evaluation, and clinical investigations or other measures is required for safety, effectiveness, and risk/benefit analysis. Besides, it needs to determine the post-market clinical follow-up when any risk remains from risk analysis and then describe residual risks and any other information.
- The gathering of clinical evidence is sufficient to prove the essential principle of safety and effectiveness.
- Is this clinical evidence sufficient to declare conformity with relevant essential principal consideration of intended use, risk level, and risk–benefit analysis?
- If yes, these fulfill all essential principal requirements, then no further clinical data is needed to complete a clinical evaluation report.
- If no, these are not fulfilling all essential principal requirements, then additional clinical data required.
- Generate new or additional data or conduct the clinical study.
- Prepare a clinical evaluation report.

The devices are developed based on the predicated devices so that all the characteristic features should be similar to predicates devices. The specifications such as clinical indication, technical performance, design, and biological aspect must be similar to that of the predicate devices.

Make a clinical evaluation plan and define the scope, contents of the clinical evaluation like description and characteristic of device, clinical background state of the art, whether the device under evaluation and clinical equivalence, identification, analysis, and appraisal of clinical data. Further, it needs to document the summary of clinical data, safety-related data, and conclusion.

Identification of clinical data from databases like PubMed, Medscape, Prospero, Cochrane, Clinical Trials database, incident report on the MAUDE database, DAEN, and MHRA database by defining the search term or defining keyword.

Analysis of clinical data—literature clinical data review by using different analysis methods like—sound methods, comprehensive analysis, additional pre-clinical evaluation, and clinical investigations or other measures are required for safety, effectiveness, and risk/benefit analysis, determine needs of the post-market clinical follow-up when any risk is remaining from risk analysis, then describe residual risks any other information.

Inclusion–exclusion criteria concerning age, medical condition, severity, and prognostic factors, etc. Follow-up and outcome of the clinical data.

Final appraisal of data sets by scientific validity, suitability, demonstration of safety, clinical performance, and/or effectiveness of clinical data. Appraisal criteria are based on level 1, level 2, level 3 data.

If clinical evidence from the literature is sufficient to prove the essential principle of safety and effectiveness of the devices, then no further clinical data needed to complete the clinical evaluation report. Whereas if data fail to prove the principle requirement, then need to generate the new additional data or perform the clinical trial and generate the clinical evaluation report. Figure 11.2 depicts the overall process of literature route for the clinical investigation of medical devices.

11.5 Clinical Validation According to the Type of Devices

11.5.1 Clinical Validation

Clinical validation of medical devices will be carried by their application with consideration of their risk factor. The classification of medical devices will majorly rely on the safety of the end-user. The major markets classified the medical devices in almost the same fashion with consideration of risk and named differently. Based on the devices' classification, the regulation is formulated for clinical validation to understand the safety and efficacy before entering into the market. Understanding clinical validation of medical devices by class is essential and here, the validation procedure is presented based on USFDA.

According to the Clinical Laboratory Improvement Act (CLIA) of the USA, Validation is the confirmation by investigation and provision of objective evidence that proves the medical device meets the user's need and intended use [18].

The validation can be classified as:

I. Process validation: It must be conducted before the production to ensure that the devices' manufacturing procedure does not affect the overall safety and performance of the devices.
II. Design validation: It must be completed before delivering the product to ensure that the device confirmation or the handling does not affect the device performance.

It is also remembered that the route of process validation and design validation changes from country to country as well as device to device, as medical devices are

used for a wide range of applications. Here we tried to give a glimpse of the process: design validation and in vitro diagnostics as taking the USA as a reference.

11.5.2 Process Validation

Process validation is defined in the FDA's 21 CFR part 820 (quality system regulation) subpart (G) 820.75. Process validation is defined as establishment of evidence for an objective by a process that consistently produces a result to meet predetermined specifications. The results of a particular process will be fully verified by subsequent inspections and tests. Prior to that, the process needs to be validated with a high degree of assurance and approved according to established procedures [18]. It must consider the key set of protocols with installation qualification (IQ), performance qualification (PQ), and operational qualification (OQ).

Regulatory Requirements for Process Validation
(a) Requirements of ISO 13485
(b) Further relevant national and international provisions: GHTF (now International Medical Device Regulators Forum (IMDRF))
(c) Requirements of the FDA (21 CFR part 820.75)

Key Points for the Control of Validated Processes
(a) Monitoring and control methods and data
(b) Date performed
(c) Individual(s) performing the process, where appropriate
(d) Major equipment used, where appropriate

Tips for Validating a Process
(a) Validate only relevant parameters
(b) Validating a validation process
(c) Verifying instead of validating
(d) Process validation and PQ, IQ, and OQ

11.5.3 Revalidation

It is a part of the process validation; whenever aberrations are observed in the processes of manufacturing, immediate review process is needed for the process validation.

Various validations are performed in process validation, for instance, prospective validation, concurrent validation, retrospective validation, and laboratory and pilot-scale validation.

(a) Prospective validation is a pre-planned validation.
(b) Concurrent validation is the data collected in a manufacturing facility during the actual study process.
(c) Retrospective validation is where the production has been started but has not been validated according to the prospective, and concurrent protocol is not a realistic option.
(d) Laboratory and pilot-scale validation: The planned manufacturing processes cannot be carried out in a manufacturing facility.

11.5.4 Design Validation

Design validation is also addressed by FDA's 21 CFR part 820.30, and additional details were specified in FDA's Design Control Guidance for Medical Devices [1].

Following nine criteria are required for design validation:

1. User friendly device designs and operations that are self-manifest and blunder proof.
2. Device safety, efficiency, working, and performance.
3. The variety of envisioned user populaces. These include the variety of users with miscellaneous physical properties and abilities (height, size, dexterity, flexibility, vision, hearing, and tactile compassion, etc.), cultural circumstances and languages, learning skills, and emotional and intellectual capabilities. The level of information and understanding and exercise can also affect how well a user can network with a specific medical device.
4. The planned patient populaces should contain neonates, children, young adults, adults, and the elderly.
5. They use surroundings, ranging from operating rooms (ORs), emergency rooms (ERs), to standard hospital rooms, clinics, and homes. The clinical atmosphere is an intricate system of medical and support personnel and patients. They can household a huge sum of diverse medical devices and supportive equipment. The surroundings in a clinical situation are well controlled related to the atmosphere of a home. Factors like humidity, temperature, vibration, noise, space, lighting, compatibility with other devices, radiofrequency interference, electrical-electromagnetic interference, and atmospheric pressure must be built into the design validation.
6. Clear, comprehensible IFUs that can be effortlessly followed and recollected when users return after an interval to use the device once more. Methods of directives must be geared toward intended user populaces. Electronic directions such as videos may be more effective for a certain demographic of users than the physical user manuals. Additionally, approaches to writing the directives, i.e., illustrative versus straight text, can also affect usability.
7. Efficacy of use can be measured by the total number of steps done acceptably divided by the total number of steps. This points to use errors and the frequency of those errors during use.

8. Efficiency of use can be obtained by the total time taken to complete the tasks versus a targeted goal.
9. User approval and acceptability of use for each task and the overall serviceability and operation of the device can be measured using the survey (questionnaires) with a Likert-type scale and subsequently analyzing it.

- **Software validation**: It is a part of the design validation of a finished product that confirms the intended use's software specifications.

The International Medical Device Regulators Forum (IMDRF) is a group of medical device regulators globally joined together to harmonize medical products' regulatory requirements that diverge from one country to the other. The World Health Organization (WHO) acts as an official spectator. The Asia Pacific Economic Cooperation (APEC), Regulatory Harmonization Steering Committee (RHSC), Life Sciences Innovation Forum's (LSIF), the Asian Harmonization Working Party (AHWP), and the Pan American Health Organization (PAHO) are the regional harmonization initiatives with IMDRF [19].

According to all the regulatory bodies and forums, medical devices' clinical validation and clinical evaluation come under Quality System (QS) regulation 21 CFR part 820.

11.6 Clinical Validation for each Class of Medical Devices

The following are common examples of processes that should be validated during the manufacturing of the medical device.

(a) Sterilization and sterile packaging sealing
(b) Cleanroom ambient conditions
(c) Aseptic filling
(d) Lyophilization
(e) Heat treating, plating, welding, soldering, painting, etc.
(f) Plastic injection molding

These are steps of validation involved in the processing of a medical device of all the three classes according to USFDA.

Class I
Class I devices are considered low-risk devices and are subjected to only general controls alone. The duration of device contact with the body is < 24 hours. Class I devices are mostly non-invasive devices. This class is exempt from premarket notification 510(k) and premarket approval (PMA). Examples of Class I medical devices include bandages, surgical instruments, wheelchairs, etc.

Class I medical devices are further divided into three classes: Class 1 s, 1r, and 1 m. This subclass of Class I medical devices requires 510(k).

(a) 1 s: Devices that are placed on the market in a sterile condition
(b) 1r: Reusable surgical instruments (r stands for "reusable")
(c) 1 m: Devices with a measuring function

If the medical devices fall under any of the subclass of Class 1 among 1 s, 1r, and 1 m, the device undergoes various clinical validation steps as mentioned in the GHTF, and it may also require 510(k) [20]. The clinical validation of medical devices step-by-step flow chart is shown in Fig.11.1.

Class II

Class II devices are considered as minimal risk devices and are subjected to general controls and special controls. The duration of device contact with the body ranges from 24 hours to 30 days. Blood collection tubes come under Class II devices; these are the minimally invasive devices. This Class II device requires premarket notification 510(k). Examples of Class II devices include infusion pumps for intravenous medication and computed tomography.

Often the blood collection tubes (BCTs) are underrecognized or ignored variable in the preanalytical phase of clinical laboratory studies. BCTs validation considerations are according to Clinical Laboratory Standards Institute (CLSI) GP34-A guidelines [21]. The clinical validation of Class II medical devices step-by-step flow chart is shown in Fig.11.1.

Class III

Class III devices include most of the implants, and these are considered high risk, which are subjected to the most stringent standards. Class III devices pass through number of pathways to reach the market for premarket approval (PMA) [22]. In this class, the implants or biomaterial intended to use will contact the body for more than 30 days; it would be regarded as high risk. Examples of Class III medical devices include a pacemaker, cardiac stents, brain stimulators, etc.

Joint prosthesis comes under the Class III high-risk devices category. The typical clinical failure scenarios reported for epiphyseal stem in joint prosthesis include aseptic loosening, mechanical failure, and sub-capital dislocation. It is essential to develop precise and reliable metrics to understand the functional aspects, which identify how well the patient recovered after the operation. Until then, the verdict of a claimed assistance's clinical relevance remains entirely on the clinical experts. However, it is the accountability of the pre-clinical validation to assess if the claimed benefit can be measured; if this is not the case, the introduction of a new design is unethical [23]. The clinical validation of Class III medical devices step-by-step flow chart is shown in Fig. 11.3. The clinical validation and clinical evaluation process are stringent in Class III medical devices as they fall under the high-risk category.

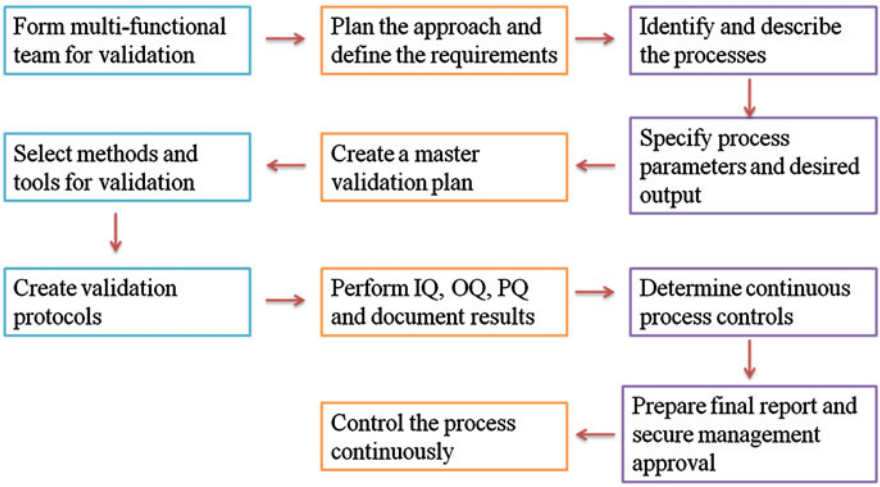

Fig. 11.3 Basic steps in medical devices process validation from GHTF

11.7 Clinical and Analytical Validations of Biosensors Based IVDs

In the twenty-first century, the biosensor based diagnostic devices open a new dimension for the manufacturer, as it gives rapid, high-throughput clinical data regarding the intended application [24]. Thus, the regulation and clinical validation of these types of devices become a general mandatory requirement to control and ensure the devices' safety and performance feasibility for launching them to the market. Biosensors are usually considered a diagnosing system to predict, measure, or monitor any physiological entity's presence or upregulation in terms of different signaling processes like electrical, optical, and thermal [25, 26]. According to the International Union of Pure and Applied Chemistry (IUPAC), the "biosensors" are defined as "a device that uses specific biochemical reactions mediated by isolated enzymes, immune-systems, tissues, organelles, or whole cells to detect chemical compounds usually by electrical, thermal or optical signals" [27]. Now, as per the 21 CFR 809.3 of USFDA regulation, the in vitro diagnostic products (IVD) are entitled to "reagents, instruments, and systems intended for use in the diagnosis of a disease or other conditions, including a determination of the state of health, to cure, mitigate, treat, or prevent disease or its sequelae" [28, 29]. Considering the above two definitions from the two well-established statutory bodies, one can consider that "biosensor" as an in vitro diagnostic product. Though there is no specified regulatory pathway that is reported for clinical validation of biosensors, some countries where the regulatory framework is deep-rooted regulate and validate biosensors' safety and clinical performance as per the in vitro diagnostic devices regulations. Besides that, some de facto agencies like the International Standardization Organization (ISO),

ASTM, IMDRF developed some regulations and strategies for controlling and validating biosensors' crucial parameters.

It is important to note that as the arena of biosensors is so-vast and their uses, detection strategies also versatile in nature, for that the ultimate clinical validation of these types of devices depends on their intended application, claimed analytical characteristics, and efficacy of detection systems [30]. The clinical performance evaluation procedure or validation of sensors is principally based upon the two main parameters, they are analytic performance validation and clinical performance validation [29, 31]. **The following illustration depicts the key considerations involved in the validation of biosensors.**

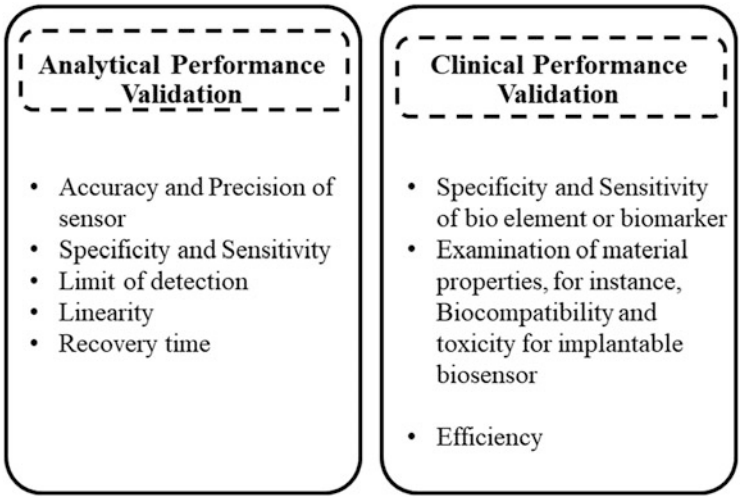

The projected value for each parameter correlates with a certain standard to satisfy or validate the product. ISO/TS 21412:2020 is one such standard that provides specification limits of characteristics and measurement methods of the materials associated with the electrochemical biosensors [32]. Another well-established standard is ISO/TR 19693:2018; this standard's scope is for characterization, the method, and strategies of surface functionalization of the silane-based group for sensing the biological elements upon paper-based or glass slides [33]. This particular standard is related to all those types of sensors where the sensor's surface is modified to immobilization or generation of electrical signals. One remarkable difference between the analytical performance validation of qualitative and quantitative sensor is that for qualitative sensors, the manufacturer or applicant should submit the evaluation report related to its specificity/sensitivity and limit of detection (LOD) only, whereas, for quantitative sensors, the applicant should submit all the reports accordance with sensitivity, specificity, LOD, accuracy, reusability, measuring range, etc. [34]In recent times, the World Health Organization (WHO) proposed some prerequisite requirements for the qualification of the in vitro diagnostic tests [35]. It ensures the safety and performance of the device and makes clinical data

more reliable to healthcare professionals. **The following illustration reflects an overall procedure of the pre-qualification program by the WHO** [36].

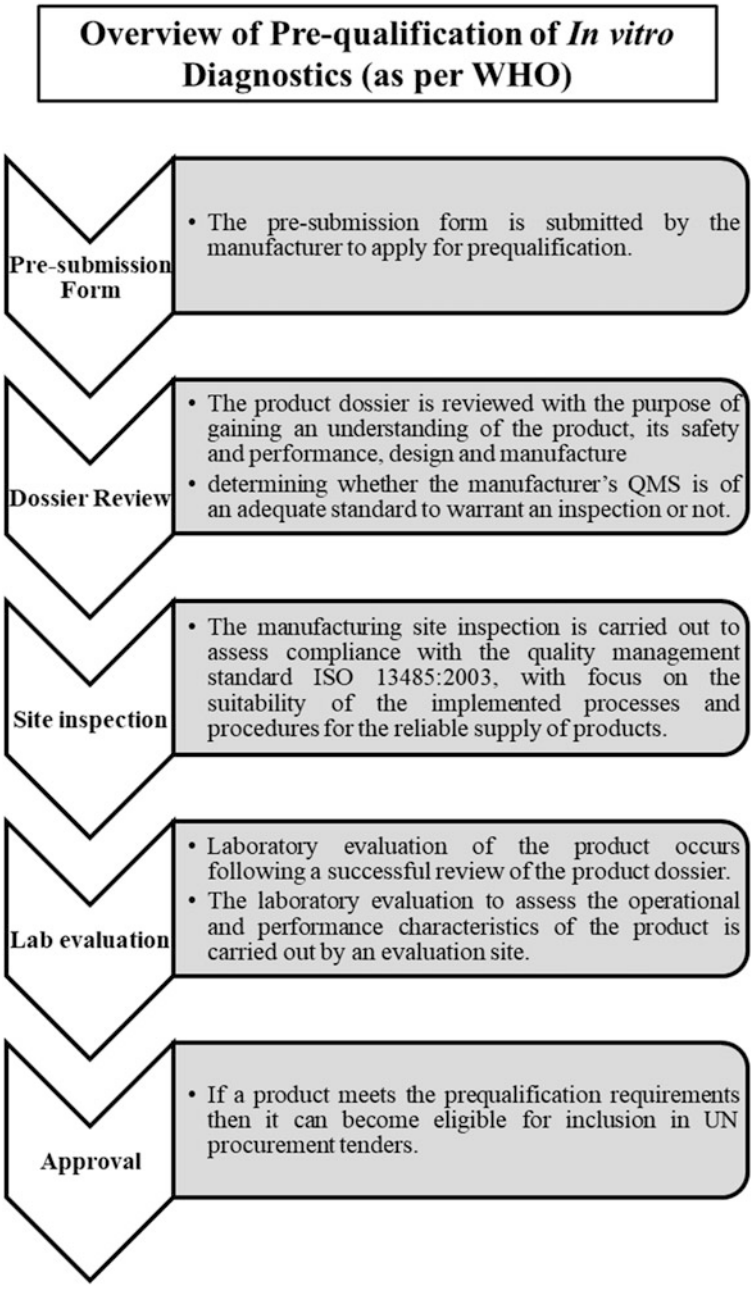

Recently, CDSCO classified the notified in vitro diagnostic devices into three categories: IVD analyzer (53 types), IVD instruments (18 types), and IVD software (9 types) [37]. According to this amendment, all the POC biosensors are regulated as IVD analyzers, as they analyze certain physiological biomarker levels. For other non-invasive wearable devices such as continuous glucose monitoring systems, two separate clinical evaluation reports are needed for the implanted part and software part, respectively. All the biosensors associated with any software or computer system should be regulated distinctively for the clinical validation of software as a medical device. For the other simple POC diagnostic systems, the applicant should submit a performance evaluation report issued by the central medical devices testing laboratory or a medical device testing laboratory registered under rule 83 or by any laboratory accredited by the National Accreditation Board for Testing and Calibration Laboratories or by any hospital accredited by National Accreditation Board for Hospitals and Healthcare Providers [38].

In conclusion, we can say that for the clinical validation of sensor-based diagnostic devices, both the analytical performance verification and clinical performance evaluation are necessary by following respective standards to demonstrate the overall performance and reliability of the sensor-generated data for commercialization of the product. Recently some regulatory bodies like USFDA, IMDRF proposed or encouraged the applicant or manufacturers to consult the tests' necessity and justify the results directly with the regulatory authority for faster and smooth commercialization of the product.

11.8 The Regulatory Perspective of the Medical Device in Consideration with Clinical Validation

11.8.1 Medical Device Rules (MDR)-2017, India

Medical devices are regulated as "drugs" in India. The CDSCO acts as the highest authority for the regulation of medical devices and in vitro diagnostic devices. The Government of India gazette two different notifications on February 11, 2020, for a revised definition of medical devices and the medical devices regulations (Amendment), 2020. Previously, only 37 types of medical devices were regulated or notified to be regulated in India. The revised regulations cover all medical devices to determine their quality, safety, and efficacy. According to the new medical device rules, Chapter VII, published by CDSCO, deals with medical devices' clinical investigation and clinical performance evaluation of new in vitro diagnostics. Several medical device testing laboratories have been developed to cross-check and ensure the products' quality, safety, and efficacy. The governing bodies of the MDR also enlisted rule 49 to rule 62 for the same. MDR also separates medical devices' guidelines into some accompanying legislation such as clinical investigation, import, manufacturing, sales, and distribution. Based on the device classification, the

requirement of a clinical investigation or testing protocols is also classified in a detailed manner. As per the MDR, Class A devices need the least clinical testing, and Class D devices require more accurate clinical validation data.

Chapter seven of MDR contains all the regulatory compliances required for getting the authorization to import or manufacture investigational medical devices for clinical studies. A few numbers of forms are also mandated to validate and control the clinical investigation. Some of the forms, namely MD-12, MD-16, MD-22, and MD-24, are mandatory to submit irrespective of device class. For getting the clinical investigation's approval, the application of Class A and B should be submitted to the State Licensing Authority (SLA) and for Class C and D to the Central Licensing Authority (CLA). All the application submission and the grant of permission/approval licenses are revised through the online portal of CDSCO (https://cdscomdonline.gov.in). All the required compliances for the Indian market are given in Fig.11.4. As per the Indian regulations, the clinical studies are carried out in two phases: the pilot and pivotal clinical investigations to validate safety and efficacy. The pilot clinical investigation is done for determining the preliminary device performance, checking the eligibility aspects and their applications. The pivotal study's goal is to determine the unavoidable adverse event, explore the device mechanism, and establish a process to determine an outcome measure. Pivotal studies have been mandatory for a new custom based investigational medical device that does not have a substantially equivalent device but gets approved for marketing in any country except India, to get the confirmation regarding the devices' performance upon the Indian ethnicity.

- **Submission of clinical data with the application**

1. Design analysis data including:
   (a) Documents of design input and design output;
   (b) Results of mechanical and electrical tests;
   (c) Reliability tests;
   (d) Authentication of device software;
   (e) Other performance tests (if any);
   (f) Ex vivo studies.
2. The agreement between the sponsor and principal and coordinating investigator (s).
3. The appropriate insurance certificate, if any.
4. Forms for reporting any adverse event and serious adverse event.
5. Report of biocompatibility tests along with the rationale for selecting these tests, including a summary report.
6. Results of the risk analysis.
7. Animal performance study data.
8. Clinical investigational plan, investigator's brochure, case report form, informed consent form, investigator's undertaking, and ethics committee clearance.
9. Pilot and pivotal clinical investigation data include clinical data that may carry out in other countries.

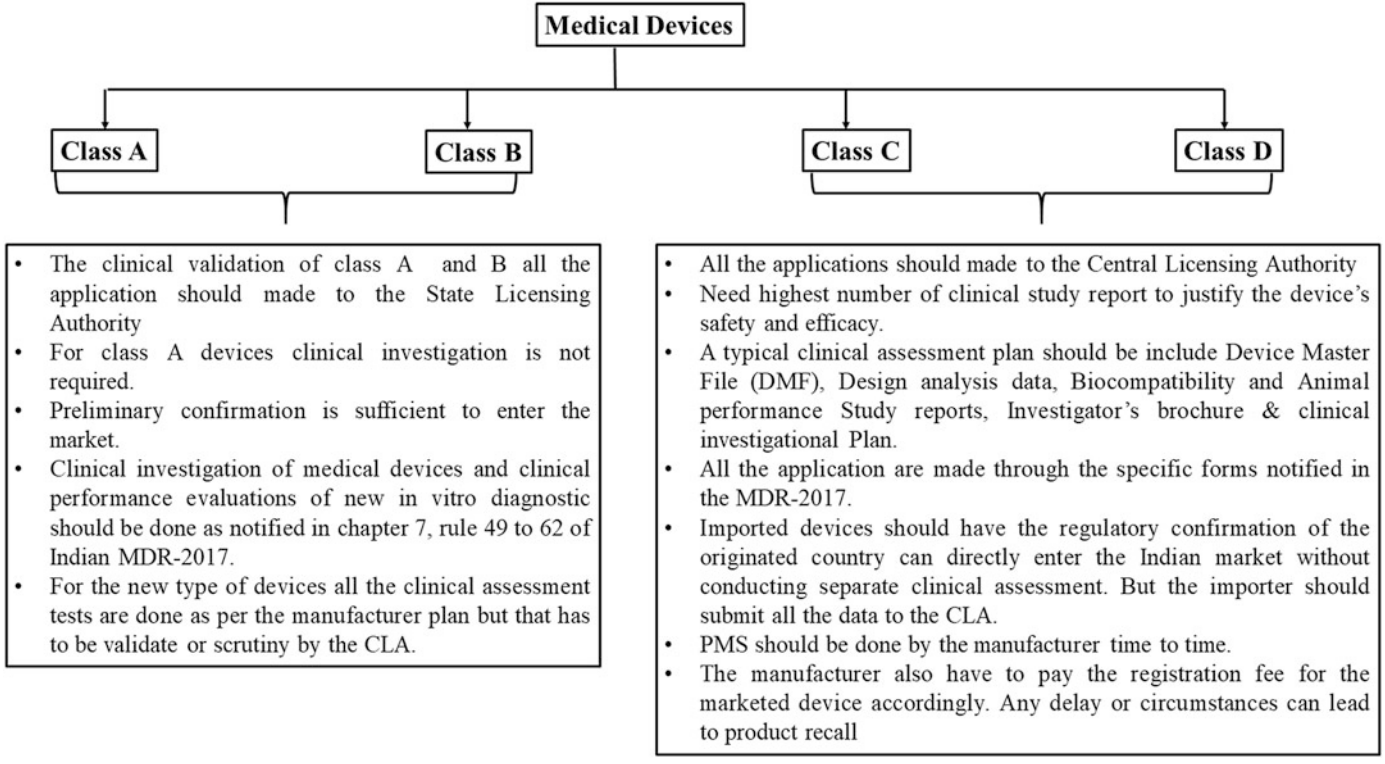

Fig. 11.4 Regulatory compliances required for the clinical validation of medical device in India as per the Indian MDR 2017

10. Regulatory status and restriction on use in other countries, if any, where marketed or approved.
11. Proposed instructions for use and labels.

The regulation is also implemented for the devices which contain drugs. If the drug is already approved or has proof of human safety, some clinical examinations can be skipped by the manufacturer.

MDR states that to perform the clinical evaluation of any devices, importers or the manufacturers will need to follow any of the performance standards imposed by the Bureau of Indian Standards (BIS) or given by the Ministry of Health and Family Welfare in the Central Government. It also proposed, where there are no pertinent standards recommended by BIS, then the manufacturer can do the clinical studies in accordance with the standards released by the International Organization for Standardization (ISO) or the International Electro-Technical Commission (IEC), or by any other standard agency. It also claimed that if no such standards have been found, then the manufacturer can design his protocol and validate it accordingly [39].

11.8.2 Food and Drug Administration USA

Within FDA, the Center for Devices and Radiological Health (CDRH) is primarily accountable for medical device regulation and clinical validation. According to the FDA's 3-tier risk-based classification, Class I devices are exempted from the clinical validation or the confirmatory assessment test; only the minimum device safety report has to be submitted. Class II devices have some amount of more risk factors than Class I, so these devices are needed some special concern about the packaging, labeling, user guidance along with the premarket notification (PMN), which is needed to market this product. Class III devices require the highest number of regulatory compliances regarding clinical validation and risk assessment testing. It is also suggested that any manufacturer or the sponsors can also validate the clinical testing data with any other internationally accepted standards for ensuring the device's safety and efficacy. In a proposal to CDRH, the FDA suggests that sponsors include their risk assessment at the start of the segment on biocompatibility testing. According to the FDA, it is also recommended that they have to give a proper reason for explaining any toxicities and adverse effects identified in their biocompatibility testing or other clinical evaluations study. As per the amendment of the CDRH, the manufacturers also follow some de facto standards to support their risk assessment program. Some of such standards like ISO 10993-5 "Biological evaluation of medical devices—Part 5: Tests for in vitro cytotoxicity testing, ISO 10993-18 "Biological evaluation of medical devices—Part 18: Chemical characterization of materials" or ISO/TS 10993–19 "Biological evaluation of medical devices—Part 19: Physio-chemical, morphological and topographical characterization of materials" must be followed for Class III devices [29]. All the essential compliance is given in Fig.11.5 for the USFDA clinical validation. However, the guidelines are well

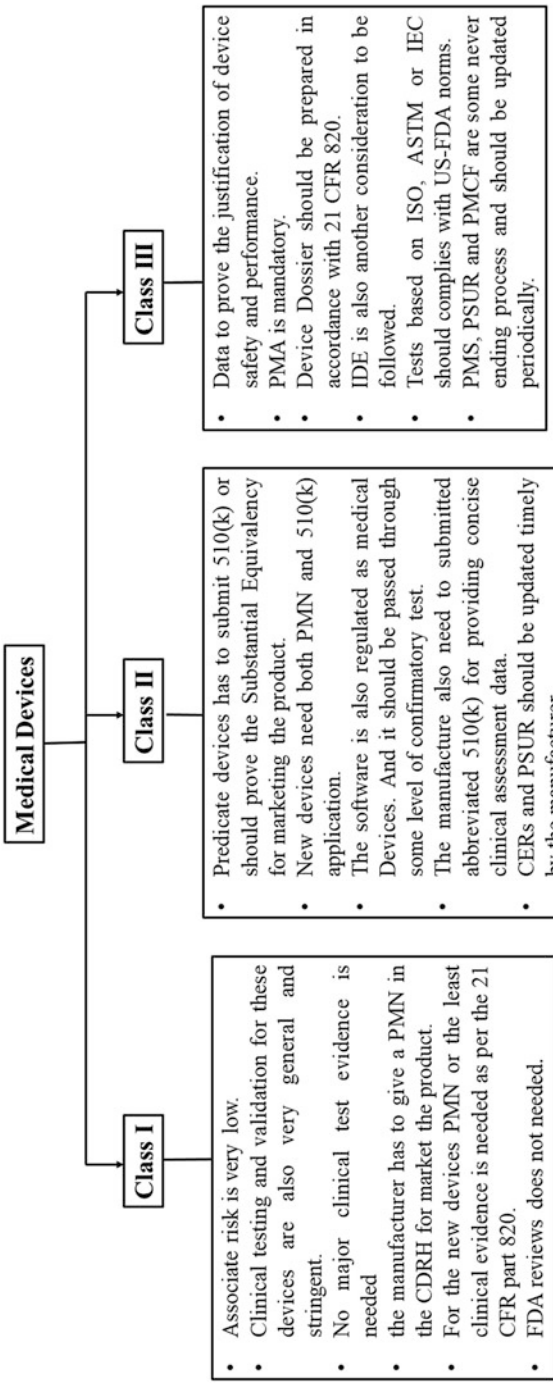

Fig. 11.5 The chart depicts the required regulatory compliances for the clinical validation as per the USFDA

designed for clinical validation of medical devices. However, it is essential to comply with the local (country) regulations to introduce a product. To support the safety validation, the explanation of selecting the standards and their protocols needs to provided so that the FDA can review the process. Generally, the FDA asks for the clinical evaluation data with their testing protocols related to device safety requirements [40].

Another mandatory clinical, regulatory compliance is PMS, which is needed for high-risk devices (i.e., Class II and III) after the FDA approval and marketing. The federal Safe Medical Devices Act of 1990 and the FDA Modernization Act of 1997 (FDAMA) permitted the FDA to required essential PMS for these classes of devices to obtain some goals such as reporting of any serious adverse events (SAE) or the device failure and tracking the devices or for the product recall.

As per the new amendment, for notifying the updated information regarding the device quality, safety, and efficacy, a Periodic Safety Update Report (PSUR) has to be submitted to the CDRH once after the market share devices [34]. **The PSURs should be updated every six months' interval for the first two years after the medical device's approval even more for the next two years.** For getting the clinical validation of a Humanitarian Device Exemption (HDE), the clinical pieces of evidence related to the device's effectiveness and lack of significant risk have to acquiesce with the HDE application. One of the main differences between the application of HDE and PMA is that in the case of HDE, the manufacturer only required the clinical shreds of evidence related to devising safety. However, for PMA, both the device safety and efficacy consideration are needed, from the point of clinical justification [41].

11.8.3 Medical Devices Clinical Validation Process in EU

In the EU, three medical device legislations have been implemented such as Medical Device Directive (MDD) 90/385/EEC for active implantable medical devices, MDD 93/42/EEC regarding medical devices, and directive of in vitro diagnostic medical devices 98/79/EC [16]. Considering these three MDDs, a new Medical Device Rules (MDR)-2017/745 (amendment) has been published for medical device regulation and MDR 2017/746 for in vitro diagnostic devices. The newly published MDR comprises 10 chapters, with 123 articles and 17 annexes, and it also covers all the clinical assessment tests and examinations for the EU certification, contingent upon the kind of support (commercial, non-commercial, and academic). Chapter 6 of the MDR deals with the clinical evaluation and their validation for the product aiming to market in the EU. By concerning MDD 93/42/EC, the lower-risk devices, i.e., Class I and IIa, should have Clinical Evaluation Reports (CERs) and higher-risk devices such as Class IIb and III, the manufacturer needed to compile clinical data on device dossier. The clinical evaluation should be conducted on MDR following Article 61 and Part A of Annex XIV [7]. Also, a public summary of safety and clinical performance (Article 32 of EU-MDR) must be submitted by the manufacturer for a

certain category of devices. To be precise, the manufacturer must have a documented plan to conduct a clinical evaluation, confirm conformity with general safety and performance requirements, evaluate for unwanted adverse effects, and estimate the benefit–risk ratio's acceptability Fig. 11.6 represents the neccessary documents for clincal assesment of Medical Devices under EU. Article 61 [1] of the MDR and Article 56 [1] of the IVDR state that "The manufacturer shall specify and justify the level of clinical evidence necessary to demonstrate conformity with relevant general safety and performance requirements." **Finally, a clinical evaluation assessment report (CEAR) authorized by the notified body is needed, which gives the inference of the clinical studies.** It is one of the core requirements of the Medical Device Regulation (EU) 2017/745 (MDR) [34].

The clinical evaluation results shall be documented in a Clinical Evaluation Report (CER), which should include the clinical data related to the evaluation of scientific literature, key findings of clinical investigations, and a consideration of available alternative key measures. It is also important to remember that the clinical evaluation and its documentation shall be updated throughout the device life cycle with clinical data obtained from PMCF and PMS. The EU-MDR also mandate Unique Device Identification (UDI) and European Databank on Medical Devices (EUDAMED) for tracing the ADE reporting and facilitating tracing of the device. EUDAMED is developed under the consideration of Article 33 of MDR. It was expected to go live on March 25, 2020, for an application on May 26, 2020. But as per the latest information from the EU is that EUDAMED will be delayed until May 2022. The authorities anyway planned this situation. If its implementation is delayed, the manufacturers will have six months to fill the database after working.

Another key component for the EU approval is CE certification of the products. By submitting CE certification with the other clinical evidence, the manufacturer can increase the device's safety, which is further help to get the final approval. CE certification also facilitated the customer preference and free movement of the product in the EU's respective countries. According to the new legislation of MDR 2017/745, the Medical Device Software (MDSW) also needs to be clinically validated with an intended purpose. It is also stated that if a software is controlling more than one medical device, an independent ***Clinical Evaluation (MDR) or Performance Evaluation (IVDR)*** is required for each predicted and clinically viable software-device combination [42].

11.8.4 Clinical Confirmatory Process in Australia

In Australia, the Therapeutic Goods Administration (TGA) regulates medical device registration, manufacturing, and sales. It also acts as a governing body for reviewing and updating the Australian Regulatory Guidelines for Medical Devices (ARGMD). As per Regulation 4.1 of the Therapeutic Goods (Medical Devices) Regulations 2002, the conformity assessment test is mandatory for getting clinical acceptance regarding its safety and performance as a premarket assessment [43]. After submitting all the performance evaluation tests, the results have to be submitted to the TGA,

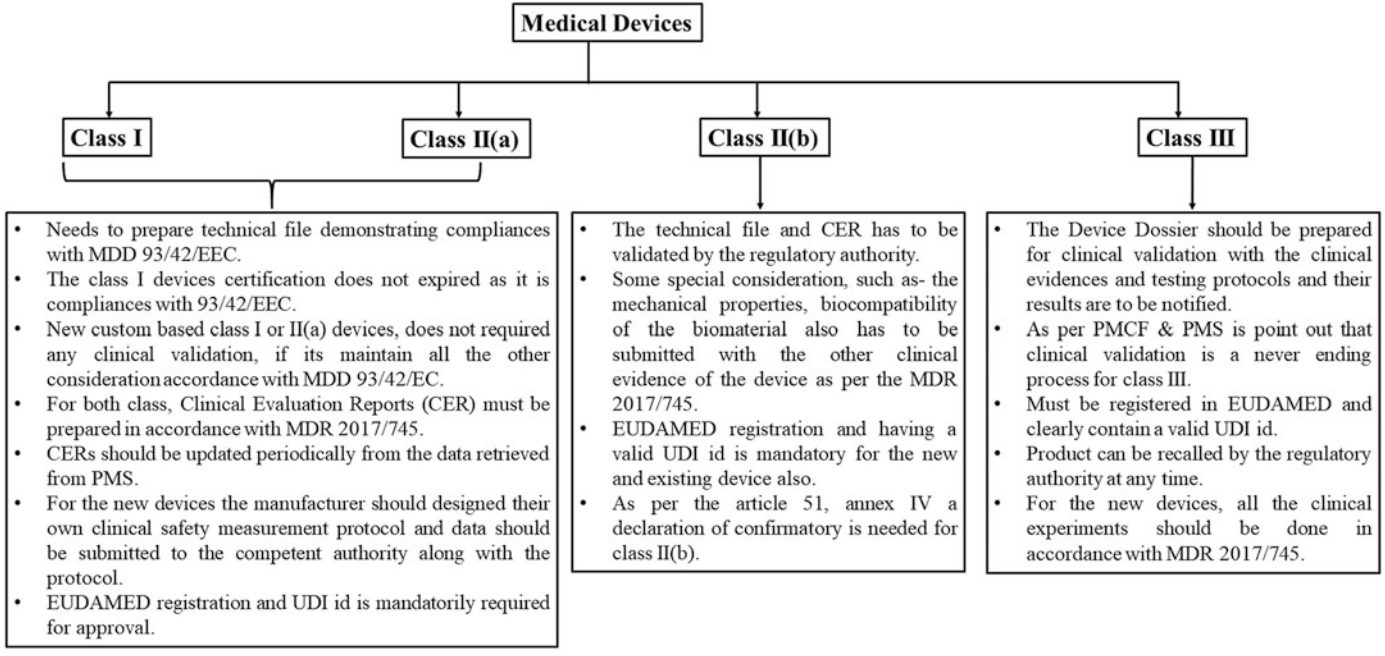

Fig. 11.6 The chart shows the technical documents needed for the clinical assessment in the EU

and then they issued a TGA conformity assessment certificate after cross-checking all the clinical data. The assessment certificate is mandatory for getting permission for the marketing and sales of the device. Usually, TGA follows regulatory compliances same as the EU-MDR. But any manufacturer who wants to market their products in the Australian market must have the TGA approval listing number, and the device must also be included on the Australian Register of Therapeutic Goods (ARTG) unless the device is exempt or excluded from the market. TGA also claims that the clinical evidence data should be updated from time to time by the manufacturer, and TGA can review the data at any time. The regulation also states that CER should be reviewed in each five-year interval relying upon the gadget's oddity and risk, as per MEDDEV 2.7/1 revision 428 (page 12) [44]. Post Marketing Clinical Follow-up (PMCF) is another important criterion that has to be done by the manufacturer to prove strong evidence regarding the safety and efficacy of the device. The degree of conformity assurance required must suit the extent and complexity of using the device, ranging from vendor self-evaluation for low-risk devices to assurance of the manufacturer's quality control framework and analysis by a notified body highest-risk devices of the specification of the individual product [45].

11.8.5 Medical Devices Clinical Validation in China

In China, the National Medical Product Administration (NMPA), previously known as China Food and Drug Administration (CFDA), regulates the regulatory compliance requirements for the Medical Devices and in vitro diagnostic devices. Although China's government decided to make their market more harmonized by adopting a 3-tier risk-based classification system, now some burden is still existing for the Western device manufacturer to get regulatory approval for the Chinese market. This may be because of the complexity of the device registration and the overhauled medical device regulation [46]. According to the NMPA jurisdiction, all the devices must fulfill all the criteria notified in the China Good Clinical Practice requirements (GCP). On November 17, 2017, NMPA published some new regulations regarding accepting foreign clinical evidence data. However, it is also stated that the manufacturer or the Person Responsible for Regulatory Compliance (PRRC) for the Chinese market should be notified to the NMPA for the use of foreign clinical testing data before the application. Generally, NMPA reviews the gap between ethnicity and the clinical confirmatory testing pathway for the foreign clinical evaluation data. While the CFDA testing labs should justify home manufacturer of the China, the clinical validation of the device although self-clinical study reports (CSR) will also be acceptable and should be satisfactory [47]. The degree of clinical evaluation report data varies with the device's risk, for example, the higher risk associated devices like Class III devices will need some additional supplementary device dossier along with the general clinical evidence data [48].

Table 11.3 Some of the internationally acceptable de facto *s*tandards for clinical validation of medical devices

Standards	Description of use
ISO 14971:2007	"It covers aspects including risk management, design control during product development, and verification and validation systems"
ISO 10993-1:2009	"Biological evaluation of medical devices—Part 1: Evaluation and testing within a risk management process. It is the most widely used standard for assessing medical devices' biocompatibility and materials and provides a framework for determining the appropriate biocompatibility steps for planning a biological evaluation"
IEC 62366–1:2015	"Medical devices—Part 1: Application of usability engineering to medical devices"
IEC 60601–1:2005	"It deals with the basic safety and essential performance requirements of medical electrical equipment and serves to ensure that no single electrical, mechanical, or functional failure shall pose an unacceptable risk to patients and/or operators"
ISO 11135 ISO 11137 ISO 17665	"Requirements for the development, validation, and routine control of sterilization processes for medical devices and other healthcare products. • For ethylene oxide sterilization • For radiation sterilization • For moist heat sterilization"
ISO 14644	"It states all the criteria for cleanroom environments for medical devices"
ASTM F2150–13	"It contains the standard guideline for characterization and testing of biomaterial scaffolds used in tissue-engineered medical devices"
ASTM F2027–16	"It deals with the standard guideline for characterization and testing of raw or starting materials for tissue-engineered devices"

[a]All the above standards must be compared and then complied with the formal mandated standards validated by the target country's regulatory authorities for marketing

Although various countries have their own formulated regulations for medical devices, still some de facto standards are frequently adopted to examine the safety performance and quality of medical devices. Table 11.3 provides a little glimpse about the de facto standards for different devices testing protocols, which are quietly acceptable in various markets.

11.9 Conclusions

The clinical evaluation of medical devices and their validation is one of the uttermost essential regulatory compliance to ensure the three important dimensions of any devices, i.e., quality or performance, safety, and efficacy. Another important aspect of the clinical validation is the quality of the data and its formatting. Recently, IMDRF, under the monitoring of GHTF, is tried to bring all the major regulatory bodies under one roof to facilitate and justify all the necessary criteria or guidelines for clinical validation and its acceptance. Currently, the Summary of Technical Documentation (STED) format is well accepted in different countries, which follows

the IMDRF over clinical data formatting. Some countries like India and Brazil also accept the clinical evaluation data produced outside of the country and may not be asked to be repeated depending on the quality of the data and the credentials of the laboratory where such data has been generated. So, it seems that all are trying to make the clinical data evaluation pathways more stringent and more effective over the device classes. The execution of EUDAMED or UDI suggests that the effective implementation of such regulatory submission can make a leap forward to a stringent clinical validation process and increase customer compliance. Thus, the requirement of clinical validation is needed for regulatory approval and needed for the user's satisfaction throughout the device lifetime.

References

1. https://fas.org/sgp/crs/misc/R42130.pdf 2020 [cited 2020 08-08-2020]. Available from: https://fas.org/sgp/crs/misc/R42130.pdf
2. Gupta, S. K. (2016). Medical device regulations: A current perspective. *Journal of Young Pharmacists, 8*(1).
3. Saini, K., Kaushik, A., Anil, B., & Rambabu, S. (2010). Harmonized medical device regulation: Need, challenges, and risks of not harmonizing the regulation in Asia. *Journal of Young Pharmacists, 2*(1), 101–106.
4. https://www.diva-portal.org/smash/get/diva2:121327/FULLTEXT01.pdf 2020 [cited 2020 07-08-2020]. Available from: https://www.diva-portal.org/smash/get/diva2:121327/FULLTEXT01.pdf
5. Jardaneh, M. A.-TN, Shaqlous, R., & Kawar, R. (2010). *Medical devices: Regulations & requirements in Europe, USA, Jordan & Saudi Arabia*.
6. Maak, T. G., & Wylie, J. D. (2016). Medical device regulation: A comparison of the United States and the European Union. *The Journal of the American Academy of Orthopaedic Surgeons, 24*(8), 537–543.
7. Sethi, R., Popli, H., & Sethi, S. (2017). Medical devices regulation in United States of America, European Union and India: A comparative study. *Pharm Regul Aff, 6*(179), 2.
8. Goldsack, J. C., Coravos, A., Bakker, J. P., Bent, B., Dowling, A. V., Fitzer-Attas, C., et al. (2020). Verification, analytical validation, and clinical validation (V3): The foundation of determining fit-for-purpose for biometric monitoring technologies (BioMeTs). *NPJ Digital Medicine, 3*, 55.
9. https://www.accessdata.fda.gov/scripts/cdrh/cfdocs/cfRES/res.cfm 2020 [cited 2020 28-07-2020]. Available from: https://www.accessdata.fda.gov/scripts/cdrh/cfdocs/cfRES/res.cfm
10. Group MDCEW. (2019). Clinical Evaluation. In F. IMDR (Ed.), *International Medical Device Regulators Forum*.
11. Ogrodnik, P. J. (2013). Chapter 9–Evaluation (validation and verification). In P. J. Ogrodnik (Ed.), *Medical device design* (pp. 201–253). Oxford: Academic Press.
12. Park, J. C., Lee, D. H., & Suh, H. (1999). Preclinical evaluation of prototype products. *Yonsei Medical Journal, 40*(6), 530–535.
13. https://www.iso.org/obp/ui/#iso:std:iso:14155:ed-2:v1:en 2020 [cited 2020 11-08-2020]. Available from: https://www.iso.org/obp/ui/#iso:std:iso:14155:ed-2:v1:en
14. https://ec.europa.eu/docsroom/documents/10336/attachments/1/translations/en/renditions/native [cited 2020 08-08-2020]. Available from: https://ec.europa.eu/docsroom/documents/10336/attachments/1/translations/en/renditions/native
15. https://www.astm.org/Standards/F748.htm [cited 2020 07-08-2020]. Available from: https://www.astm.org/Standards/F748.htm

16. Kaushik, D., Rai, S., Dureja, H., Mittal, V., & Khatkar, A. (2013). Regulatory perspectives on medical device approval in global jurisdictions. *The Journal of Gene Medicine, 10*(3–4), 159–171.
17. http://www.imdrf.org/docs/imdrf/final/technical/imdrf-tech-191010-mdce-n57.pdf [cited 2020 07-08-2020]. Available from: http://www.imdrf.org/docs/imdrf/final/technical/imdrf-tech-191010-mdce-n57.pdf
18. Code of Federal Regulations. In: Administration FaD, editor. U.S.A: 21; 01.04.2020
19. Gagliardi, J. (2009). The global harmonization task force: What you need to know. *Biomedical Instrumentation & Technology, 43*(5), 403–405.
20. Class 1 Medical Devices. (2020) [cited 2020 28.07.2020]. Available from: https://www.johner-institute.com/articles/regulatory-affairs/and-more/class-1-medical-devices/
21. Bowen, R. A., & Adcock, D. M. (2016). Blood collection tubes as medical devices: The potential to affect assays and proposed verification and validation processes for the clinical laboratory. *Clinical Biochemistry, 49*(18), 1321–1330.
22. Morrison, R. J., Kashlan, K. N., Flanangan, C. L., Wright, J. K., Green, G. E., Hollister, S. J., et al. (2015). Regulatory considerations in the design and manufacturing of implantable 3D-printed medical devices. *Clinical and Translational Science, 8*(5), 594–600.
23. Viceconti, M., Affatato, S., Baleani, M., Bordini, B., Cristofolini, L., & Taddei, F. (2009). Pre-clinical validation of joint prostheses: A systematic approach. *Journal of the Mechanical Behavior of Biomedical Materials, 2*(1), 120–127.
24. Suman, P., & Chandra, P. (2020). *Immunodiagnostic technologies from laboratory to point-of-care testing*. Springer.
25. Chandra P,. Nanobiosensors for personalized and onsite biomedical diagnosis: The Institution of Engineering and Technology; 2016
26. Purohit, B., Kumar, A., Mahato, K., & Chandra, P. (2020). Smartphone-assisted personalized diagnostic devices and wearable sensors. *Current Opinion in Biomedical Engineering, 13*, 42–50.
27. McNaught, A. D., & Wilkinson, A. (1997). *Compendium of chemical terminology*. Oxford: Blackwell Science.
28. https://www.fda.gov/media/71075/download. US-FDA; [cited 2020 15-12-2020]. Available from: https://www.fda.gov/media/71075/download
29. Purohit, B., Vernekar, P. R., Shetti, N. P., & Chandra, P. (2020). Biosensor nanoengineering: Design, operation, and implementation for biomolecular analysis. *Sensors International, 1*, 100040.
30. Sergeev, N. V., Herold, K. E., & Rasooly, A. (2008). Regulatory and validation issues for biosensors and related bioanalytical technologies. In *Handbook of Biosensors and Biochips*. Wiley.
31. Standards NCfCL. (2005). Molecular diagnostic methods for infectious diseases: Proposed guideline: NCCLS.
32. https://www.iso.org/standard/70874.html. [cited 2020 15-12-2020]. Available from: https://www.iso.org/standard/70874.html
33. https://www.iso.org/standard/66037.html. 2020 [cited 2020 15-12-2020]. Available from: https://www.iso.org/standard/66037.html
34. https://clsi.org/media/1435/ep09a3_sample.pdf. 2020 [cited 2020 12-12-2020]. Available from: https://clsi.org/media/1435/ep09a3_sample.pdf
35. https://www.who.int/diagnostics_laboratory/evaluations/en/. 2020 [cited 2020 12-12-2020]. Available from: https://www.who.int/diagnostics_laboratory/evaluations/en/
36. https://apps.who.int/iris/bitstream/handle/10665/259403/WHO-EMP-RHT-PQT-2017.02-eng.pdf;jsessionid=387D24F53BDCAA88F4DBA8BFD1B8DBF1?sequence=1. 2020 [cited 2020 12-12-2020]. Available from: https://apps.who.int/iris/bitstream/handle/10665/259403/WHO-EMP-RHT-PQT-2017.02-eng.pdf;jsessionid=387D24F53BDCAA88F4DBA8BFD1B8DBF1?sequence=1

37. https://cdsco.gov.in/opencms/opencms/en/Medical-Device-Diagnostics/Medical-Device-Diagnostics/. [cited 2020 13-12-2020]. Available from: https://cdsco.gov.in/opencms/opencms/en/Medical-Device-Diagnostics/Medical-Device-Diagnostics/
38. list.pdf hcgioosmCWedfdjniMCwtl. [cited 2020 08-12-2020]. Available from: https://cdsco.gov.in/opencms/opencms/system/modules/CDSCO.WEB/elements/download_file_division.jsp?num_id=MTkwNA== /Category wise testing laboratory list.pdf
39. https://www.emergobyul.com/sites/default/files/india-medical-devices-rules-2017.pdf 2017 [cited 2020 07-08-2020]. Available from: https://www.emergobyul.com/sites/default/files/india-medical-devices-rules-2017.pdf
40. Pritchard, G. (2017). Clinical evaluation reports from the medical writer's perspective. *Medical Writing, 26*(2), 14–19.
41. Van Norman, G. A. (2016). Drugs, devices, and the FDA: Part 2: An overview of approval processes: FDA approval of medical devices. *JACC: Basic to Translational Science, 1*(4), 277–287.
42. Commisison, E. (2020). *MDCG 2020–1 Guidance on clinical evaluation (MDR) / Performance evaluation (IVDR) of Medical device software*. In: Commisison E, editor.
43. Governement A. *Australian regulatory guidelines for medical devices (ARGMD).* In: Administration TG, editor.
44. Govenment A. [cited 2020 08-08-2020]. Available from: https://www.tga.gov.au/book-page/part-1-general-requirements
45. Government A. *Overview of medical devices and IVD regulation* [cited 2020 08-08-2020]. Available from: https://www.tga.gov.au/sme-assist/medical-devices-regulation-introduction
46. Health S. *Regulatory requirements for medical devices in China* [cited 2020 07-08-2020]. Available from: https://www.syneoshealth.com/sites/default/files/documents/Syneos%20Health_Med%20Device%20Diagnostics_Med%20Devices%20in%20China.pdf
47. Administration NMP. http://english.nmpa.gov.cn/ [cited 2020 07-8-2020]. Available from: http://english.nmpa.gov.cn/
48. Clinical evaluation assessment report template 2020. [cited 2020 08-08-2020]. Available from: https://ec.europa.eu/health/sites/health/files/md_sector/docs/mdcg_clinical_evaluationtemplate_en.pdf

Chapter 12
Dried Blood Patterns for Diagnosis of Non-Communicable and Infectious Diseases

Jijo Easo George and Debjani Paul

12.1 Introduction

Over the years, the human race has been under the relentless attack of infectious and non-infectious diseases. The history and civilization of the human race, to an extent, are shaped by these fatal diseases [1]. Globalization plays a key role in the spread of infectious diseases [2, 3]. The Global Burden of Disease reports that populations of affluent nations are more likely to succumb to non-communicable diseases (NCD) [4]. On the contrary, the scenario is different for middle- and low-income nations where the major causes of death are infectious diseases, namely, respiratory tract infections, diarrhoea, human immunodeficiency virus (HIV), tuberculosis, influenza, and malaria [5, 6]. These infectious diseases have a greater impact on the global exchequer and public healthcare systems compared to non-communicable diseases. For instance, the global economy [7] is expected to nosedive to an all-time low due to the emergence of a new betacoronavirus called severe acute respiratory syndrome–coronavirus 2 (SARS-CoV-2), leading to the coronavirus disease 2019 (COVID-19) [8, 9]. This spread of the virus across the globe resulted in a pandemic [10]. Till now, the death toll due to COVID-19 has exceeded 500,000 globally and is expected to rise further. In a conventional healthcare system, diagnosis involves time-consuming, labour-, and resource-intensive steps including sample collection and transportation, analytical phase, result intimation, and batching practices [11]. This will altogether consume a lion's share of time that could result in delayed treatment or even treatment failure. To improve the healthcare systems, scientists across the world are perpetually looking for rapid and affordable diagnostic platforms [12]. Such platforms are indispensable to mitigate the overall fatalities and

J. E. George (✉) · D. Paul
Department of Biosciences and Bioengineering, Indian Institute of Technology Bombay, Mumbai, India
e-mail: jijo.george@iitb.ac.in

V. Borse et al. (eds.), *BioSensing, Theranostics, and Medical Devices*,
https://doi.org/10.1007/978-981-16-2782-8_12

economic burdens caused by infectious and non-communicable diseases [13]. Globally, the technology that can revolutionize the healthcare system is the Point-of-Care (POC) diagnostic platform [14]. Under the aegis of Bill and Melinda Gates Foundation and the National Institute of Health (NIH), developing POC devices for infectious disease diagnosis is recognized as one of the "Grand Challenges for Global Health" [15].

Although a universally accepted definition for POC testing does not exist, it generally refers to the analytical testing in proximity to the patient, away from a central lab where one can make a rapid and accurate therapeutic intervention [16]. In other words, decentralizing diagnostic testing could facilitate early diagnosis and hence prevent infectious disease outbreaks [17, 18]. The test can be done conveniently in a doctor's office, or at a healthcare centre, or even at home. In 2004, the World Health Organization (WHO) has put forward the "ASSURED" criteria for POC tests. The acronym stands for affordability, sensitivity, specificity, user friendliness, rapid and robust, and equipment-free [19, 20]. The POC tests have several advantages, for instance, reducing the time required to diagnose critical illnesses, avoiding the necessity of sample storage, plugging loopholes in healthcare practice where patients do not need to come back to get the test results and hence lowering the travel expenses associated with diagnosis [14, 21, 22]. Owing to the aforementioned advantages, both developed and developing countries would embrace POC testing as a promising primary form of diagnostic testing [23]. The advent of smartphones has improved the global connectivity and has the potential to reform the healthcare sector by coupling diagnostic testing with communication of test results from areas with limited resources [24–26]. The motivation behind manufacturing such affordable POC devices is to enable an untrained layman (end-user) to perform and interpret the result of the diagnostic tests [27]. Such rapid and low-cost POC diagnostics play crucial roles in healthcare strategies including detection, therapy, health management, economy, and surveillance [28, 29].

The field of POC diagnostic devices made significant inroads with the advent of microfluidic "Lab on a Chip" (LOC) platforms [30, 99]. It offers miniaturization, integration, and automation of fluid flow on chips, thus enabling a set of complex plumbing functions, which is usually performed in research laboratories, to be performed in a resource-limited environment in a time-saving and cost-effective manner [31, 32]. The advances in the field of microfluidics, nanotechnology, and material science had added impetus to the field of POC devices [33, 34]. Most of the POC devices developed by researchers in the laboratories could not reach the market due to their cumbersome chip design and the requirement of extensive supplementary instrumentation. From an industrial perspective, there are logistical, commercial, and organizational impediments towards developing compatible and efficient diagnostic tools for the developing world [35]. Another major problem is the lack of a proper understanding of the requirements of a resource-limited environment. The availability of clinical trial sites that follow the highest standards slows down translation of these devices [35]. Lastly, the ambiguity in international regulatory affairs hampers the commercialization of diagnostic technologies. Often, the absence of harmonized global regulatory standards leads to the appearance of counterfeit and

ineffective tests in the market and the health department may lack the resources to identify the legitimate and illicit tests [20, 35].

In the coming sections, we introduce a low cost, chip-free approach with promising results that could complement the existing diagnostic technologies. In this chapter, we discuss how an evaporated pattern formed by blood drops can be used as a diagnostic tool for infectious and non-infectious diseases. Later, we shed some light on the physics behind drop formation, with focus on spreading, wetting, evaporation, crack formation, etc. We then enumerate the benefits of using blood drops for disease diagnosis compared to other existing approaches. We also describe some of the published studies on dried blood patterns in detail. We further explain how drying patterns of whole blood leads to better diagnosis compared to the blood plasma. Finally, we explore the challenges faced and the prospects of this new diagnostic field.

12.2 Whole Blood and its Physical Properties

Biofluids refer to biological fluids that can be secreted (bile), excreted (sweat), obtained with a needle (blood), or developed due to pathological process (cyst fluid) from the human body. The functions of a biofluid depend on its constituents [36]. Here, we primarily focus on the biofluid "whole blood" as a diagnostic tool over blood plasma for detecting communicable and non-communicable diseases. Human blood accounts for approximately 7% of the bodyweight [37]. Whole blood is a multi-component biological fluid comprising of plasma (55% of blood volume) as the continuous medium and blood cells as the colloidal phase [38]. Plasma is a Newtonian fluid composed of 92% water. Plasma also contains macromolecular proteins (<10%) including albumins (80%), globulin (16%), and fibrinogen (4%) [39, 40]. The colloidal phase is composed of three different blood cells, namely, the red blood cells (RBC), the white blood cells (WBC), and the platelets. Around 45% of the total blood volume is composed of RBCs and help in the transport of gases. On the other hand, WBCs and platelets are critical for the immune response of the body. The platelets are responsible for clotting of blood [41].

The ratio of RBC volume to the total volume of blood is called the haematocrit level. It affects the density and viscosity of blood. The density of the whole blood ranges from 1020 to 1060 kg/m^3 depending on the haematocrit value [38]. Blood has a surface tension (γ) of 69.8 mN/m. Whole blood behaves as a non-Newtonian liquid, i.e. its viscosity decreases with high shear rates [42]. The apparent viscosity of whole blood depends on haematocrit value, plasma viscosity, and the aggregation as well as the mechanical properties of RBCs. Any substantial change in the aforementioned parameters results in the haemorheological variations [43]. Further, the high deformability of RBCs can affect the elastic and viscoelastic properties of blood. Thus, the wetting and spreading properties of a blood drop on artificial surfaces are greatly affected by the physical properties of its different components.

12.3 Physics of Pattern Formation

The formation of evaporation patterns of colloidal drops can be seen in our everyday life [44, 45]. The study of the physical phenomena behind the interaction of blood with artificial surfaces is a challenging area with potential applications in medical diagnosis [46], archaeology [47, 48], DNA microarray printing [49, 50], and forensic science [51, 52]. The formation of intricate patterns as a result of evaporation of whole blood or plasma is attributed to the spatial and temporal evolution of the three-phase contact line, the gradual generation of capillary flow and Marangoni flow, transport of suspended matter, relaxation of internal stresses, interplay of the surfaces forces, and salt crystallization [42, 53–58]. These dried patterns show a wide range of morphologies, including a solid ring along the perimeter of the drop, multiple cracks, and crystal formation within the dried residual pattern (Fig. 12.1). The intricacy in the morphology of drying blood drops is due to the interaction between the cells in addition to the molecular interactions. The changes in the cellular and macromolecular components of blood, for instance, due to ailments, could alter the resulting evaporation pattern. Such morphological disparity could be exploited as a diagnostic platform to monitor one's health [59]. The method applies to dried blood patterns from livestock as well [60]. Nevertheless, the fundamental physics of the pattern formation is still an open area of research.

The spreading and morphological evolution of drops can be divided into three phases such as pre-gelation phase, gelation phase, and post-gelation phase [42]. The evaporation rate of a liquid drop depends on the wettability of the solid surface on which it is deposited. For instance, blood drop on a hydrophilic surface has higher rate of evaporation at the contact line than the bulk of the liquid. This disparity in the evaporation rate induces a capillary flow towards the contact perimeter to compensate for the liquid loss due to evaporation. Subsequently, the solute present in the liquid will move along with the solvent molecules resulting in a "coffee ring" [61, 62]. This capillary flow transfers macromolecules, cells (mainly RBCs), and other dissolvable solutes to the contact rim, causing a reorganization of materials [63]. This is the pre-gelation phase [40, 64, 65]. Concomitantly, the interaction of RBC and macromolecular proteins with the solid substrate results in their adhesion. The rise in the concentration of RBCs and proteins above a critical value results in an increase in the local viscosity of the plasma, initiating a glass transition to the gel phase (solid) [66]. The appearance of the porous gel structure at the contact perimeter alters the initial high evaporative flux [67]. Thus, the liquid adjacent to the gel phase exhibits a high evaporative flux. This is the gelation phase [68, 69].

The interplay between the gel adhesion and shrinkage due to plasma evaporation induces a tensile stress on the dried deposit. The dehydration of blood drop shrinks the RBCs carried to the contact line. This deforming strain is stored as elastic energy. The release of excess energy stored as elastic energy (stress) results in the appearance of cracks and folds in the dried pattern [70]. Firstly, the nucleation of cracks occurs at the solid (gel) phase of the contact perimeter. Secondly, the cracks propagate inward since the motion of the plasma drop front induces stretching of

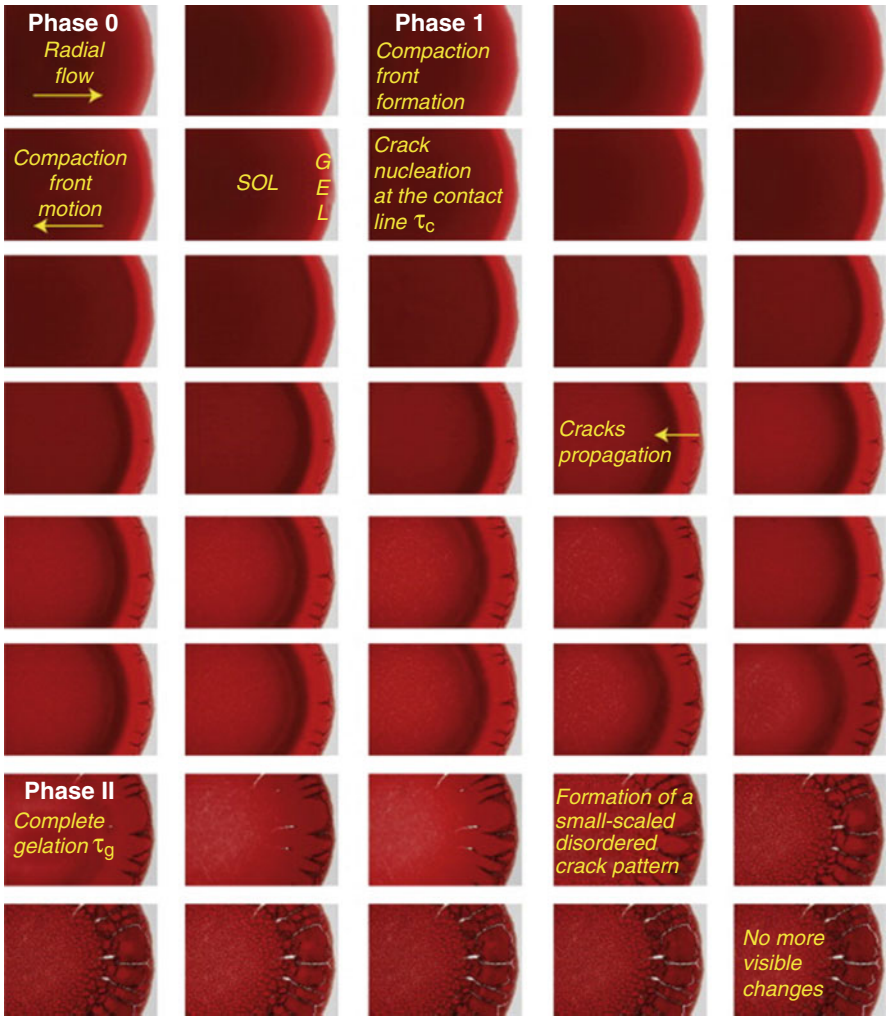

Fig. 12.1 Pattern evolution of a whole blood drop of radius 3 mm under ambient conditions. Reproduced with permission from [42]. © 2014 Elsevier

the gel [71]. In the central region, rapid gelation of the plasma occurs in the central part of the drop at the end. Once the gelation process is complete, the cracks continuously emerge until the evaporation of the solvent molecules ceases. Radially, the cracks continue to form small scale disordered fractures at the centre, resulting in the post-gelation phase [72]. The parameters such as macromolecular concentration, ionic strength, presence of a surfactant, and the elasticity and cell dimension influence pattern morphology. Furthermore, the appearance of crystalline structures in the central region is attributed to the crystallization of macromolecular proteins and inorganic salts [73]. As the evaporation progresses, there is a heterogeneous

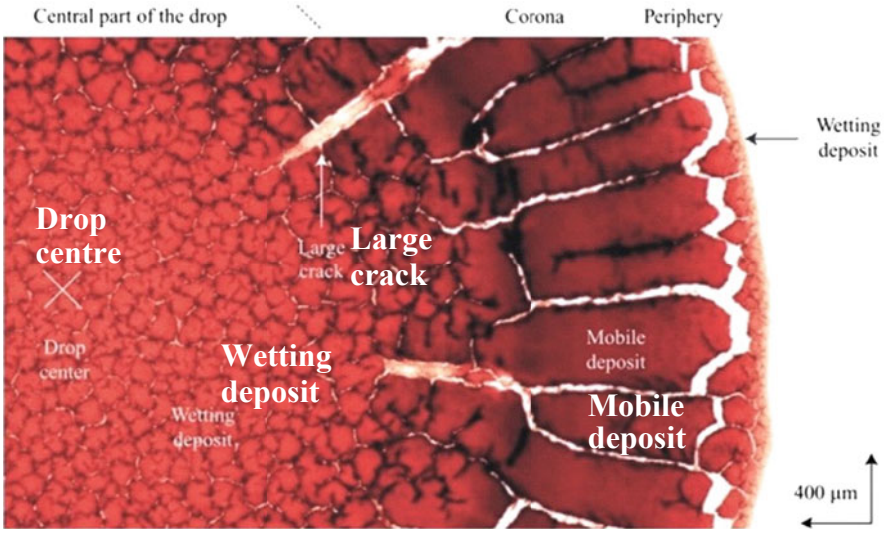

Fig. 12.2 Image of a dried pattern of whole blood on a hydrophilic glass slide at 22 °C. Reproduced with permission from [40]. © 2011 Cambridge University Press

distribution of ions and proteins in the central part [74]. The increased ionic concentration diminishes the electrostatic double layer and promotes protein aggregation and crystallization [75]. In short, the dehydration of a blood drop leads to internal capillary flow, adhesion, self-organization of macromolecules, solidification, and emergence of cracks. The morphology of blood drop of a healthy person on a hydrophilic substrate has three regions; a fine peripheral region with orthoradial cracks followed by a corona region with larger cracks, and a middle region populated with small and random cracks [36, 40] (Fig. 12.2).

In the peripheral region, the retreating of the solvent phase from the peripheral region induces radial internal stresses. This oriented radial stress increases as the evaporation progresses. Consequently, the release of the dominant radial stress results in the formation of orthoradial cracks, which is symmetrical about the drop centre [76]. Unlike the peripheral region, the coronal region is thicker and water molecules remain underneath the gelation film in this region. The continuous evaporation of solvent from the gelled film enhances the orthoradial stress resulting in radial cracks in the coronal region [76]. Moreover, the central region with the most water content happens to have a flat liquid–air interface such that a uniform local evaporative flux is observed. Thus, the absence of an oriented local stress results in the appearance of random cracks in the central region [36]. However, under the same environmental conditions, the patterns formed by plasma or serum (plasma without fibrinogen) are dissimilar to that of the whole blood patterns. Even though the physical process of pattern formation involves protein aggregation, gelation, crack formation, and salt crystallization; the absence of cellular components of blood would substantially affect pattern formation.

12.4 Factors Affecting the Pattern Formation

The factors affecting the pattern formation of blood on a substrate not only depend on the ambient conditions, for instance, relative humidity (RH) and temperature, but also on the wettability of the substrate. In addition, the morphology of the pattern depends on the biological composition of the blood drop.

The studies on the evaporation of whole blood on glass slides confirm that the relative humidity influences the evaporation rate at a constant temperature [77] (Fig. 12.3). It is observed that as the relative humidity increases, the evaporation rate decreases. This prolongs the lifetime of the liquid phase (plasma phase) in the blood drop and thus facilitates the adhesion [78]. The enhanced longevity of the liquid phase is believed to affect the coronal plaque formation. The relative humidity also affects the apparent contact angle of the blood drop on a hydrophilic surface. Higher the humidity, lower will be the apparent contact angle. Thus, greater will be the spread diameter and the peripheral area of the dried pattern [64, 79].

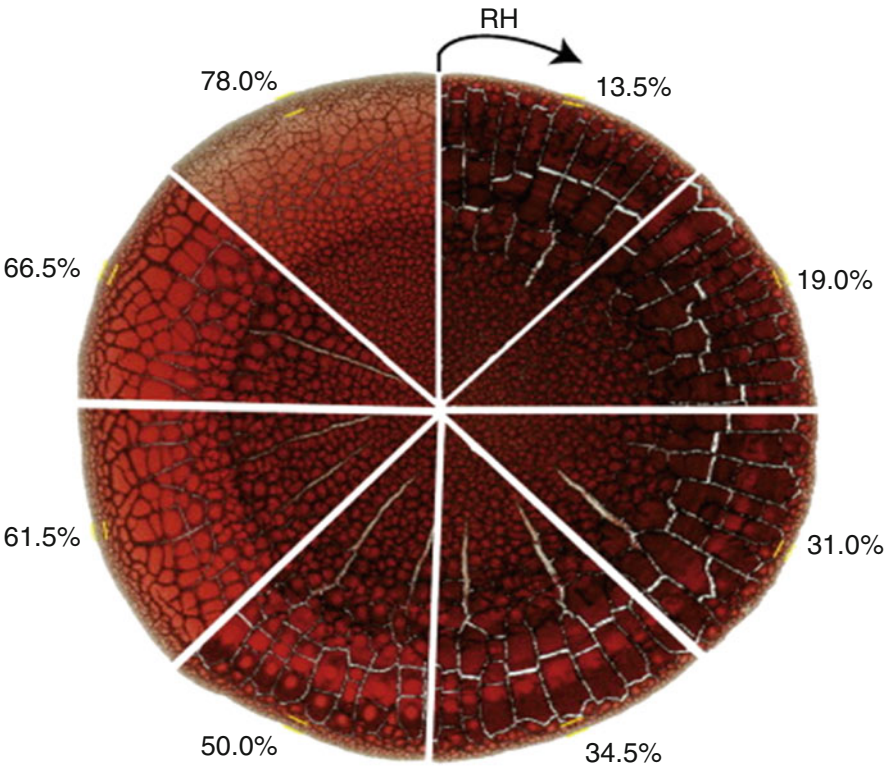

Fig. 12.3 Images of different morphologies of whole blood patterns under different relative humidity conditions varying from 13.5% to 78%. Reproduced with permission from [Bou-[78]]. © 2013 Elsevier

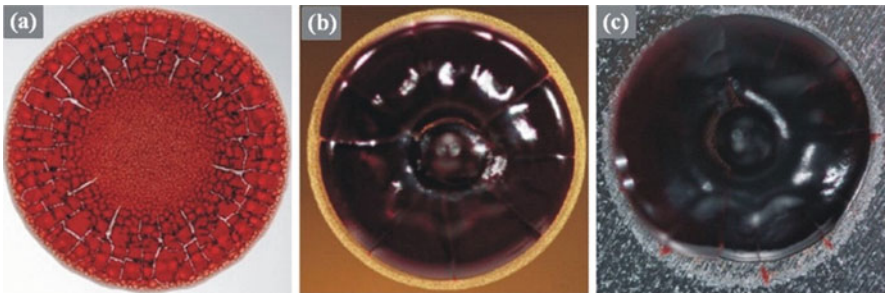

Fig. 12.4 Images of different morphologies of dried blood drops formed on: (**a**) hydrophilic glass (**b**) hydrophobic gold (**c**) hydrophobic aluminium. Reproduced with permission from [43]. © 2012 American Society of Mechanical Engineers

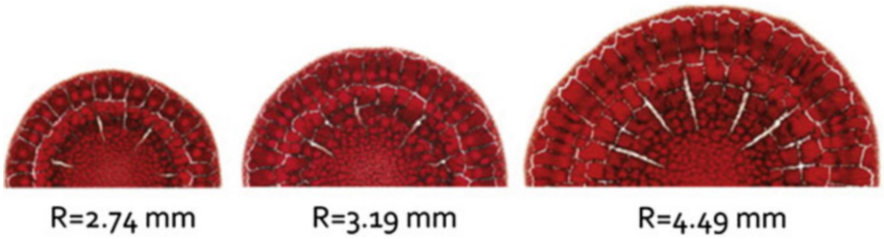

Fig. 12.5 Images of crack formation as a function of the drop radius. Reproduced with permission from [42]. © 2014 Elsevier

Furthermore, the wettability of the substrate affects the evaporation dynamics and yields a morphologically different pattern (Fig. 12.4). The contrast in the patterns formed on a hydrophilic and a hydrophobic surface is attributed to the differential evaporation rate at different regions of the drop [64]. This differential flux is maximum for a hydrophilic surface and minimum for the hydrophobic surface. On the contrary, Laplace pressure induced by RBC network and the liquid menisci formed by the neighbouring RBCs induces warping of the structures. The haematocrit value is a determining factor for the switching from warping to cracking pattern, which, in turn, affects the evaporation dynamics [80].

Further, it is observed that decrease in the wettability of the drying surface decreases the width of the peripheral region and vice-versa. In the case of the coronal region of the dried pattern, the density of radial cracks is inversely related to the contact angle, while the scale of the cracks remains unaffected [43]. In the central region, the plaque size is proportional to droplet contact angle [36]. However, the number of plaques and random cracks has an inverse correlation to wettability of the surface. On the other hand, volume of the droplet also influences the final dried pattern [40]. In the case of coronal region, the crack density increases with the contact perimeter of the drop [81]. But, the crack spacing and the length of the cracks are a function of droplet height [42] (Fig. 12.5).

The concentration of inorganic salts and proteins is critical in the pattern formation of the sessile blood drop [82, 83]. A study based on metal chlorides revealed the importance of cations in the diversity of the morphology [82, 84]. The concentration of the salt influences the evaporation rate of the sessile drop. Higher salt concentration leads to greater evaporation flux at the centre of the droplets. On the contrary, the evaporation rate is higher near the periphery for low concentration of inorganic salts [75]. The protein concentration is also critical in the morphology variation of the dried drop. The studies based on bovine serum albumin (BSA) and human serum albumin (HSA) proteins displayed a plethora of patterns ranging from layered porous micelles, dendrites, fractals to glassy matrix [12, 85].

12.5 Disease Diagnosis Using the Dried Pattern of Blood Plasma and Serum

Although the study of blood for disease diagnosis dates back to the 1950s [36], the research on dried blood pattern as a diagnostic tool has gained momentum only at the beginning of the twenty-first century. Most of the reported studies initially employed blood plasma or serum dried patterns to decipher the health of the person in question. In 2002, Rapis was able to diagnose metastatic carcinoma from the dried pattern of human blood plasma. The patients with metastatic carcinoma showed an altered phase transition. There is a stark contrast between the morphologies of dried plasma films of a healthy and an ailing person (carcinoma) as a result of protein self-assembly and symmetry [86]. Later, Yakhno et al. investigated the dried serum patterns of people suffering from hepatitis B, burn disease, Waldenstrom's macroglobulinaemia (abnormal increase in WBC), and paraproteinemic haemoblastosis (excess of myeloma protein). They observed a regular 3D liquid-crystal protein structure of varying size. Upon drying, it undergoes gelation and the rest experiences a transition to crystalline structures. The solid crystal structure is analogous to immunoglobulin M (IgM). The observed differential behaviour of blood serum of healthy and diseased individuals is attributed to the presence of excess IgM due to endogenous intoxication [87].

Another study by Yakhno et al. used blood serum from patients with breast cancer, hepatitis, lung cancer, and paraproteinaemia. They also investigated the serum samples of women at different stages of gestation. The morphological patterns of serum samples were unique to the disease identified. In addition, they used acoustic-mechanical impedance (AMI) [88, 89] measurements to inquire about the dynamics of the phase transition of the serum drop during evaporation [90].

Further, it was demonstrated by Kimovich et al. that the crystallogenesis characteristics of blood serum can be used for diagnostic purposes. The study performed free and induced crystallization of blood serum from healthy people and hepatitis (B, C) patients [91].

Subsequently, Buzoverya et al. observed interesting and distinct dried patterns of human plasma. They observed differentiable patterns for healthy individuals and patients with cardiovascular pathology. The serum pattern of a healthy person is regular with radial cracks. The pattern from a patient with the pathological condition has a chaotic and random structure. Furthermore, the authors pointed out that pathological information of a serum sample can be extracted from the cracking patterns. They attribute the formation of triactinal cracks to disruption in the venous outflow along with congestive events. Inflammation and chronic hypoxia are believed to result in tourniquet shaped cracks. The dished cracks hint to the early stages of encephalopathy. The crackscan (large-sized) indicates dehydration (water loss) and dysproteinaemia [92, 93].

Another group led by Muravlyova et al. studied the implications of chronic pulmonary lung disease on the morphological pattern of blood plasma. The plasma samples from patients with interstitial lung fibrosis (ILF) and idiopathic interstitial pneumonia (IIP) were studied [94]. The authors ascribe the incongruence in the patterns to the ratio of oxidized to a reduced form of proteins (mainly albumin) and extracellular nucleic acids.

Recently, Baranov et al. investigated the influence of donor immunity on the self-assembled patterns formed by the evaporated blood serum. They used laser correlation spectroscopy to study the serum protein agglomeration and optical microscopy to study the pattern formed. The authors found the patterns of serum from two healthy donors to be different. Upon addition of diphtherial toxoid, the structure of the serum pattern did not change much for the first donor. However, the presence of diphtheria toxoid made the pattern of the second donor appear short with fewer bifurcations. The authors attribute this difference in the pattern of serum to the different protein combinations, and hence to a different degree of immunity [95].

Based on the available literature, dried plasma or serum patterns appear to have a strong potential as a POC diagnostic tool for the detection of certain infectious and non-infectious diseases.

12.6 Disease Diagnosis Using the Dried Pattern of Whole Blood

While researchers across the world have extensively looked into the characteristics of dried patterns exhibited by blood plasma and serum droplets, there are only a few reports available on the whole blood patterns as a means of medical diagnosis [43]. Whole blood offers the possibility of gaining better insights into the medical condition of a person since it accounts for variations at both cellular and molecular levels. Studies on plasma or serum require pre- or post-processing of blood samples.

In 2010, Brutin et al. reported a study on the pattern formed by whole blood from patients with anaemia (low haemoglobin content) and hyperlipidaemia (elevated quantity of lipids, e.g. triglycerides) [40]. The study showcases the efficiency of

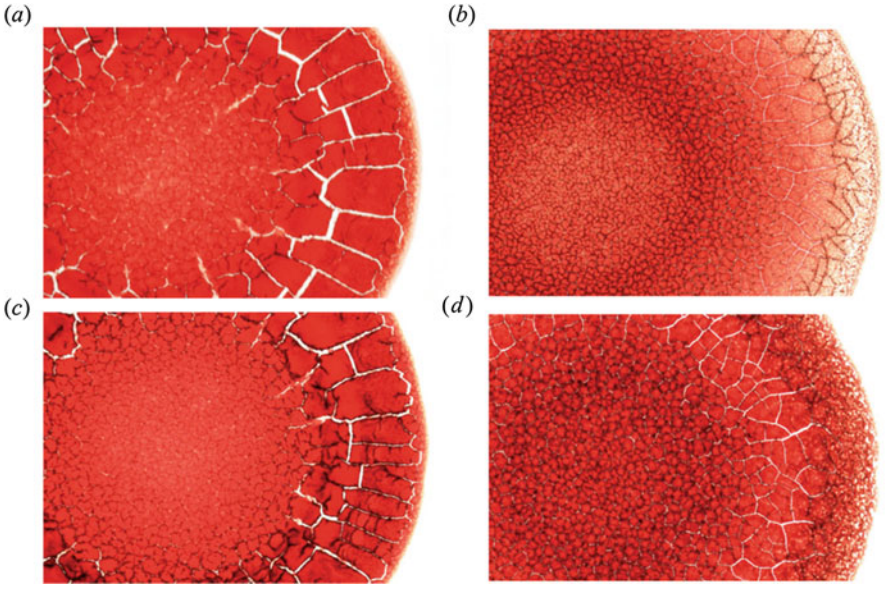

Fig. 12.6 Images of patterns of whole blood from (**a**) healthy woman (**b**) anaemic patient (**c**) healthy man (**d**) hyperlipidaemic patient. Reproduced with permission from [40]. © 2011 Cambridge University Press

whole blood pattern as a diagnostic tool. The dried blood pattern of the anaemic individual had light-coloured corona compared to the central region and small-sized plaques in the centre (Fig. 12.6), which clearly distinguished the diseased pattern from the healthy one.

Later, Sikarwar et al. developed a software tool to recognize the patterns of dried whole blood patterns. They performed the study on the blood samples from patients suffering from tuberculosis and anaemia [96]. It turns out that the peripheral ring and cracks in the dried pattern of healthy individuals are thicker than the patterns of TB and anaemic patients. They averaged the dried pattern of healthy individuals and subtracted it from the corresponding image from ailing individuals. It was observed that the image difference is maximum for TB patients, slightly less for anaemic patients and least for healthy ones (Fig. 12.7). This image difference parameter can be employed as an indicator of disease severity.

Recently, Bahmani et al. compared the blood patterns of thalassaemia and neonatal jaundice patients (Fig. 12.8). Their observations suggest the presence of two thick rings near the periphery of the dried pattern of healthy and jaundice group. However, the thalassaemia group had a single thin ring near the contact rim. The authors probed the role of different parameters including haematocrit, bilirubin, and the plasma viscosity as a function of cracking. The study indicates that the ratio of stacking pressure (here RBC) and curvature pressure is the major factor that controls the crack formation.

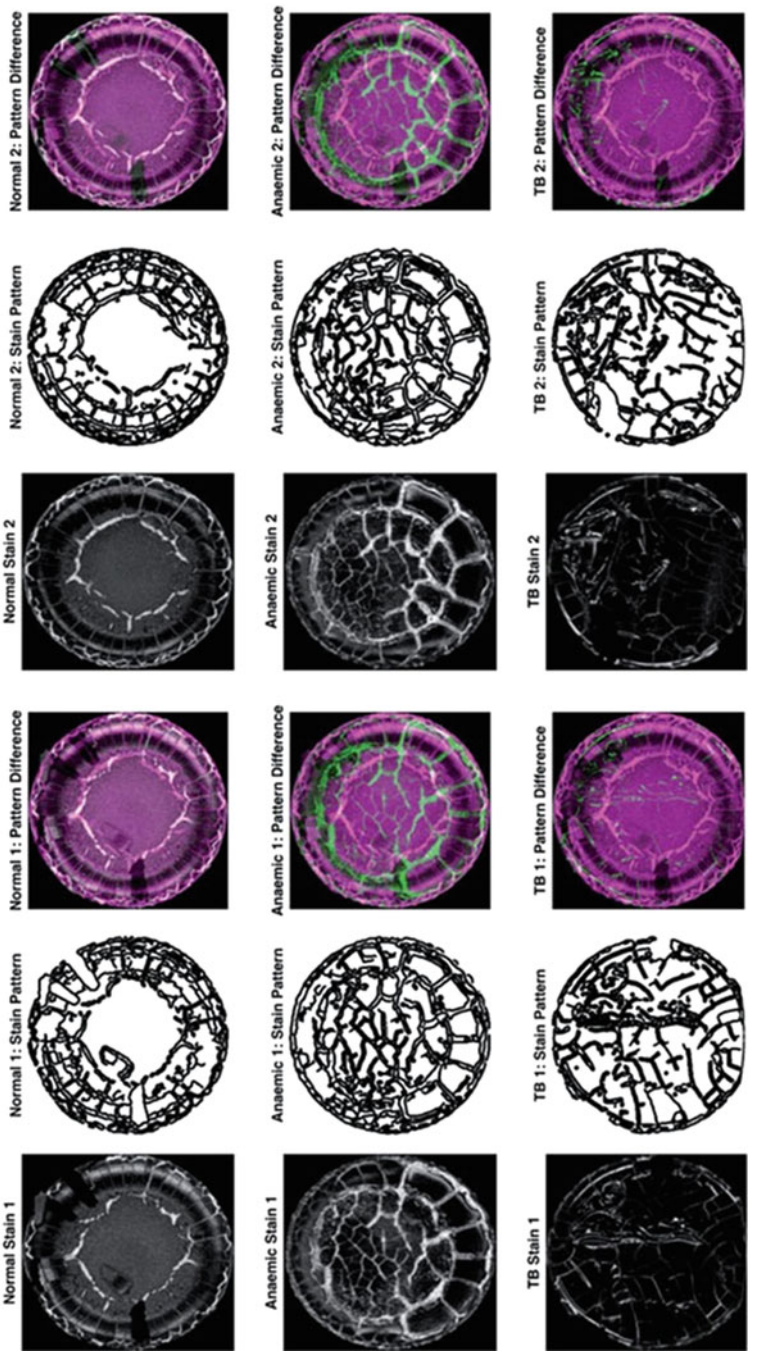

Fig. 12.7 Different morphologies of whole blood from healthy, anaemic, and TB infected donors. The contour images and their absolute difference are shown subsequently. Reproduced with permission from [96]. © 2016 Informa UK Limited, trading as Taylor & Francis Group

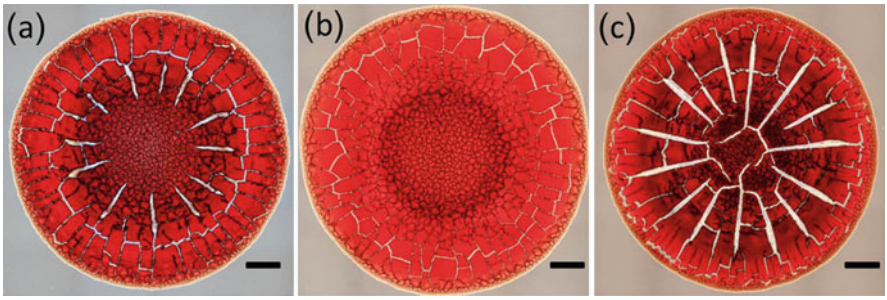

Fig. 12.8 Morphologies of blood drop of (**a**) a healthy male (**b**) a male thalassaemia patient, and (**c**) a male infant with jaundice. The scale bar is 1 mm. Reproduced with permission from [97]. © 2016 Elsevier

This pressure ratio depends on the plasma viscosity. When the ratio is low, crack formation is promoted. Also, the ratio has an inverse proportion to the length of cracks. The study confirms that a high pressure ratio results in the disappearance of large cracks in the thalassaemia patients. The large cracks in the jaundice patients are related to the bilirubin level [97].

Based on the aforementioned literature reports, it is evident that the patterns formed by the evaporation of whole blood contain more information compared to drops of plasma and serum.

12.7 Challenges and Future Outlook

Based on the available literature, dried blood patterns appear to be a promising diagnostic tool. The deployment of these patterns for the diagnosis of infectious and non-communicable diseases can bring us one step closer to realizing affordable and rapid diagnostics.

However, accurate clinical interpretation of these patterns needs controlled drying conditions as the morphology of the pattern depends on the ambient conditions including temperature and relative humidity. Also, the blood composition and haematocrit value vary from person to person [98]. The visual perception of a technician can introduce subjectivity in the interpretation of the pattern. This limitation can be overcome by introducing computer-based image processing and artificial intelligence techniques.

Dried blood pattern-based diagnosis is still in its nascent stage. A considerable amount of research needs to be done for a complete understanding of the physics principles behind pattern formation of blood. Also, a complete understanding of the factors affecting the pattern formation and how a certain disease affects blood composition need further research.

Acknowledgement J.E.G. acknowledges the institute postdoctoral fellowship from IIT Bombay.

References

1. Sherman, I. W. (2007). *Twelve diseases that changed our world* (p. 60). Wiley.
2. Collin, N., & Briand, S. (2009). Influenza vaccine: Globalization of public health stakes. *Médecine tropicale : revue du Corps de santé, 69*, 322–322.
3. Garrett, L., & Fidler, D. P. (2007). Sharing H5N1 viruses to stop a global influenza pandemic. *PLoS Medicine, 4*.
4. World Health Organization. (2004). *The world health report: 2004: Changing history*. WHO.
5. Morens, D. M., Folkers, G. K., & Fauci, A. S. (2004). The challenge of emerging and re-emerging infectious diseases. *Nature, 430*, 242–249.
6. Zarei, M. (2018). Infectious pathogens meet point-of-care diagnostics. *Biosensors & Bioelectronics, 106*, 193–203.
7. Sułkowski, Ł. (2020). Covid-19 pandemic; recession virtual revolution leading to de-globalization? *Journal of International Management, 12*, 1–11.
8. Rothan, H. A., & Byrareddy, S. N. (2020). The epidemiology and pathogenesis of coronavirus disease (COVID-19) outbreak. *Journal of Autoimmunity, 102433*.
9. Sohrabi, C., Alsafi, Z., O'Neill, N., Khan, M., Kerwan, A., Al-Jabir, A., & Agha, R. (2020). World Health Organization declares global emergency: A review of the 2019 novel coronavirus (COVID-19). *International Journal of Surgery, 76*, 71–76.
10. World Health Organization. (2020). WHO director-General's remarks at the media briefing on 2019-nCoV. WHO.
11. Schimke, I. (2009). Quality and timeliness in medical laboratory testing. *Analytical and Bioanalytical Chemistry, 393*, 1499.
12. Bissonnette, L., & Bergeron, M. G. (2012). Infectious disease management through point-of-care personalized medicine molecular diagnostic technologies. *Journal of Personalized Medicine, 2*, 50–70.
13. Faulstich, K., & Haberstroh, K. (2009). Handheld and portable test systems for decentralized testing: From lab to marketplace. *Optics and Photonics in Global Homel Secu V and Biomet Tech for Human Ident VI, 7306*, 73060.
14. Zarei, M. (2017b). Portable biosensing devices for point-of-care diagnostics: Recent developments and applications. *TrAC, 91*, 26–41.
15. Mabey, D., Peeling, R. W., Ustianowski, A., & Perkins, M. D. (2004). Diagnostics for the developing world. *Nature Reviews Microbiology, 2*, 231.
16. College of American Pathologists. (2001). *Point-of-care testing section 30*. Northfield IL: College of American Pathologists.
17. Nichols, J. H. (2007). Point of care testing. *Clinics in Laboratory Medicine, 27*, 893–908.
18. Rajan, A., & Glorikian, H. (2009). Point-of-care diagnostics: Market trends and growth drivers. *Expert Opinion on Medical Diagnostics, 3*, 1–4.
19. Kettler, H., White, K., & Hawkes, S. J. (2004). *Mapping the landscape of diagnostics for sexually transmitted infections: Key findings and recommendations*. Geneva: WHO.
20. Peeling, R. W., Smith, P. G., & Bossuyt, P. M. (2006). A guide for diagnostic evaluations. *Nature Reviews Microbiology, 4*, S2–S6.
21. Dincer, C., Bruch, R., Kling, A., Dittrich, P. S., & Urban, G. A. (2017). Multiplexed point-of-care testing–xPOCT. *Trends in Biotechnology, 35*, 728–742.
22. Zarei, M. (2017a). Advances in point-of-care technologies for molecular diagnostics. *Biosensors & Bioelectronics, 98*, 494–506.
23. Nasseri, B., Soleimani, N., Rabiee, N., Kalbasi, A., Karimi, M., & Hamblin, M. R. (2018). Point-of-care microfluidic devices for pathogen detection. *Biosensors & Bioelectronics, 117*, 112–128.
24. Fan, Y., Liu, J., Wang, Y., Luo, J., Xu, H., Xu, S., & Cai, X. (2017). A wireless point-of-care testing system for the detection of neuron-specific enolase with microfluidic paper-based analytical devices. *Biosensors & Bioelectronics, 95*, 60–66.

25. Purohit, B., Kumar, A., Mahato, K., & Chandra, P. (2020a). Smartphone-assisted personalized diagnostic devices and wearable sensors. *Current Opinion in Biomedical Engineering, 13*, 42–50.
26. Purohit, B., Vernekar, P. R., Shetti, N. P., & Chandra, P. (2020b). Biosensor nanoengineering: Design, operation, and implementation for biomolecular analysis. *Sensors International*, 100040.
27. Yetisen, A. K., Akram, M. S., & Lowe, C. R. (2013). Based microfluidic point-of-care diagnostic devices. *Lab on a Chip, 13*, 2210–2251.
28. Amukele, T. K., Street, J., Carroll, K., Miller, H., & Zhang, S. X. (2016). Drone transport of microbes in blood and sputum laboratory specimens. *Journal of Clinical Microbiology, 54*, 2622–2625.
29. Nayak, S., Blumenfeld, N. R., Laksanasopin, T., & Sia, S. K. (2017). Point-of-care diagnostics: Recent developments in a connected age. *Analytical Chemistry, 89*, 102–123.
30. Walsh, I. I. I. D. I., Kong, D. S., Murthy, S. K., & Carr, P. A. (2017). Enabling microfluidics: From clean rooms to makerspaces. *Trends in Biotechnology, 35*, 383–392.
31. Huang, G., Huang, Q., Xie, L., Xiang, G., Wang, L., Xu, H., & Jin, X. (2017). A rapid low-cost and microfluidic chip-based system for parallel identification of multiple pathogens related to clinical pneumonia. *Scientific Reports, 7*, 1–10.
32. Huckle, D. (2006). Point-of-care diagnostics: Will the hurdles be overcome this time? *Expert Review of Medical Devices, 3*, 421–426.
33. Chin, C. D., Linder, V., & Sia, S. K. (2012). Commercialization of microfluidic point-of-care diagnostic devices. *Lab on a Chip, 12*, 2118–2134.
34. Sia, S. K., & Kricka, L. J. (2008). Microfluidics and point-of-care testing. *Lab on a Chip, 8*, 1982–1983.
35. Azhar, M., & Dendukuri, D. (2017). Microfluidic platforms for point of care (POC) medical diagnostics. *Medical Biosensors for Point of Care (POC) Applications*, 255–273.
36. Chen, R., Zhang, L., & Shen, W. (2018). Controlling the contact angle of biological sessile drops for study of their desiccated cracking patterns. *Journal of Materials Chemistry B, 6*, 5867–5875.
37. Bruce, A., Alexander, J., Julian, L., Martin, R., Keith, R., & Peter, W. (2002). Molecular biology of the cell. *Garland Science, 4*, 1313–1362.
38. Thiriet, M. (2008). Biology and mechanics of blood flows: Part I: biology. *CRM Ser Mathl Phy Springer NY, 34*, 35–36.
39. Brust, M., Schaefer, C., Doerr, R., Pan, L., Garcia, M., Arratia, P. E., & Wagner, C. (2013). Rheology of human blood plasma: Viscoelastic versus Newtonian behavior. *Physical Review Letters, 110*, 078305.
40. Brutin, D., Sobac, B., Loquet, B., & Sampol, J. (2011). Pattern formation in drying drops of blood. *Journal of Fluid Mechanics, 667*, 85–95.
41. Li, L., Huang, X., Liu, W., & Shen, W. (2014). Control performance of paper-based blood analysis devices through paper structure design. *ACS Applied Materials & Interfaces, 6*, 21624–21631.
42. Sobac, B., & Brutin, D. (2014). Desiccation of a sessile drop of blood: Cracks folds formation and delamination. *Colloids and Surfaces A: Physicochemical and Engineering Aspects, 448*, 34–44.
43. Brutin, D., Sobac, B., & Nicloux, C. (2012). Influence of substrate nature on the evaporation of a sessile drop of blood. *Journal of Heat Transfer, 134*, 061101.
44. Duggal, R., Hussain, F., & Pasquali, M. (2006). Self-assembly of single-walled carbon nanotubes into a sheet by drop drying. *Advanced Materials, 18*, 29–34.
45. Kaya, D., Belyi, V. A., & Muthukumar, M. (2010). Pattern formation in drying droplets of polyelectrolyte and salt. *The Journal of Chemical Physics, 133*, 114905.
46. Shatokhina, S. N., Shabalin, V. N., Buzoverya, M. E., & Punin, V. T. (2004). Bio-liquid morphological analysis. *Scientific World Journal, 4*, 657–661.

47. Rowell, R. M., & Barbour, R. J. (1989). *Archaeological wood: Properties chemistry and preservation*. ACS.
48. Wilson, A. S., Brown, E. L., Villa, C., Lynnerup, N., Healey, A., Ceruti, M. C., & Taylor, T. (2013). Archaeological radiological and biological evidence offer insight into Inca child sacrifice. *The Proceedings of the National Academy of Sciencesi, 110*, 13322–13327.
49. Nima, Z. A., Mahmood, M., Xu, Y., Mustafa, T., Watanabe, F., Nedosekin, D. A., & Basnakian, A. G. (2014). Circulating tumor cell identification by functionalized silver-gold nanorods with multicolor super-enhanced SERS and photothermal resonances. *Scientific Reports, 4*, 4752.
50. Smalyukh, I. I., Zribi, O. V., Butler, J. C., Lavrentovich, O. D., & Wong, G. C. (2006). Structure and dynamics of liquid crystalline pattern formation in drying droplets of DNA. *Physical Review Letters, 96*, 177801.
51. Atwater, C. S., Durina, M. E., Durina, J. P., & Blackledge, R. D. (2006). Visualization of gunshot residue patterns on dark clothing. *Journal of Forensic Sciences, 51*, 1091–1095.
52. Hortolà, P. (2002). Red blood cell haemotaphonomy of experimental human bloodstains on techno-prehistoric lithic raw materials. *Journal of Archaeological Science, 29*, 733–739.
53. Giorgiutti-Dauphiné, F., & Pauchard, L. (2014). Elapsed time for crack formation during drying. *The European Physical Journal E, 37*, 39.
54. Hirsh, S. L., McKenzie, D. R., Nosworthy, N. J., Denman, J. A., Sezerman, O. U., & Bilek, M. M. (2013). The Vroman effect: Competitive protein exchange with dynamic multilayer protein aggregates. *Colloids and Surfaces. B, Biointerfaces, 103*, 395–404.
55. Kokornaczyk, M. O., Dinelli, G., Marotti, I., Benedettelli, S., Nani, D., & Betti, L. (2011). Self-organized crystallization patterns from evaporating droplets of common wheat grain leakages as a potential tool for quality analysis. *Scientific World Journal, 11*, 1712–1725.
56. Krumpfer, J. W., & McCarthy, T. J. (2010). Contact angle hysteresis: A different view and a trivial recipe for low hysteresis hydrophobic surfaces. *Faraday Discussions, 146*, 103–111.
57. Savino, R., Paterna, D., & Favaloro, N. (2002). Buoyancy and Marangoni effects in an evaporating drop. *Journal of Thermophysics and Heat Transfer, 16*, 562–574.
58. Yunker, P. J., Still, T., Lohr, M. A., & Yodh, A. G. (2011). Suppression of the coffee-ring effect by shape-dependent capillary interactions. *Nature, 476*, 308–311.
59. Chen, R., Zhang, L., Zang, D., & Shen, W. (2016a). Blood drop patterns: Formation and applications. *Advance in Colloid and Interface Science, 231*, 1–14.
60. Yakhno, T. A., Sanin, A. A., Ilyazov, R. G., Vildanova, G. V., Khamzin, R. A., Astascheva, N. P., & Yakhno, V. G. (2015). Drying drop technology as a possible tool for detection leukemia and tuberculosis in cattle. *Journal of Biomedical Science and Engineering, 8*, 1.
61. Deegan, R. D., Bakajin, O., Dupont, T. F., Huber, G., Nagel, S. R., & Witten, T. A. (1997). Capillary flow as the cause of ring stains from dried liquid drops. *Nature, 389*, 827–829.
62. Deegan, R. D., Bakajin, O., Dupont, T. F., Huber, G., Nagel, S. R., & Witten, T. A. (2000). Contact line deposits in an evaporating drop. *Physical Review E, 62*, 756.
63. Denkov, N. D., Velev, O. D., Kralchevsky, P. A., Ivanov, I. B., Yoshimura, H., & Nagayama, K. (1993). Two-dimensional crystallization. *Nature, 361*, 26–26.
64. Hu, H., & Larson, R. G. (2002). Evaporation of a sessile droplet on a substrate. *The Journal of Physical Chemistry B, 106*, 1334–1344.
65. Popov, Y. O. (2005). Evaporative deposition patterns: Spatial dimensions of the deposit. *Physical Review E, 71*, 036313.
66. Bodiguel, H., & Leng, J. (2010). Imaging the drying of a colloidal suspension. *Soft Matter, 6*, 5451–5460.
67. Zheng, R. (2009). A study of the evaporative deposition process: Pipes and truncated transport dynamics. *The European Physical Journal E, 29*, 205–218.
68. Okuzono, T., Kobayashi, M., & Doi, M. (2009). Final shape of a drying thin film. *Physical Review E, 80*, 021603.
69. Sobac, B., & Brutin, D. (2011). Structural and evaporative evolutions in desiccating sessile drops of blood. *Physical Review E, 84*, 011603.

70. Chen, R., Zhang, L., Zang, D., & Shen, W. (2016b). Wetting and drying of colloidal droplets: Physics and pattern formation. *Advances in Colloid Science*, 3–25.
71. Annarelli, C. C., Fornazero, J., Bert, J., & Colombani, J. (2001). Crack patterns in drying protein solution drops. *The European Physical Journal E, 5*, 599–603.
72. Vella, D., Adda-Bedia, M., & Cerda, E. (2010). Capillary wrinkling of elastic membranes. *Soft Matter, 6*, 5778–5782.
73. Leckband, D., & Sivasankar, S. (1999). Forces controlling protein interactions: Theory and experiment. *Colloids and Surfaces. B, Biointerfaces, 14*, 83–97.
74. Pauchard, L., Parisse, F., & Allain, C. (1999). Influence of salt content on crack patterns formed through colloidal suspension desiccation. *Physical Review E, 59*, 3737.
75. Chen, G., & Mohamed, G. J. (2010). Complex protein patterns formation via salt-induced self-assembly and droplet evaporation. *The European Physical Journal E, 33*, 19–26.
76. Chen, R., Zhang, L., Zang, D., & Shen, W. (2017). Understanding desiccation patterns of blood sessile drops. *Journal of Materials Chemistry B, 5*, 8991–8998.
77. Zeid, W. B., Vicente, J., & Brutin, D. (2013). Influence of evaporation rate on cracks' formation of a drying drop of whole blood. *Colloids and Surfaces A: Physicochemical and Engineering Aspects, 432*, 139–146.
78. Zeid, W. B., & Brutin, D. (2013). Influence of relative humidity on spreading pattern formation and adhesion of a drying drop of whole blood. *Colloids and Surfaces A: Physicochemical and Engineering Aspects, 430*, 1–7.
79. Bou-Zeid, W., & Brutin, D. (2014). Effect of relative humidity on the spreading dynamics of sessile drops of blood. *Colloids and Surfaces A: Physicochemical and Engineering Aspects, 456*, 273–285.
80. Iqbal, R., Shen, A. Q., & Sen, A. K. (2020). Understanding of the role of dilution on evaporative deposition patterns of blood droplets over hydrophilic and hydrophobic substrates. *Journal of Colloid and Interface Science, 579*, 541–550.
81. Esmonde-White, K. A., Esmonde-White, F. W., Morris, M. D., & Roessler, B. J. (2014). Characterization of biofluids prepared by sessile drop formation. *Analyst, 139*, 2734–2741.
82. Yakhno, T. (2008). Salt-induced protein phase transitions in drying drops. *Journal of Colloid and Interface Science, 318*, 225–230.
83. Yakhno, T. A., Kazakov, V. V., Sanina, O. A., Sanin, A. G., & Yakhno, V. G. (2010). Drops of biological fluids drying on a hard substrate: Variation of the morphology, weight, temperature, and mechanical properties. *Technical Physics, 55*, 929–935.
84. Annarelli, C. C., Reyes, L., Fornazero, J., Bert, J., Cohen, R., & Coleman, A. W. (2000). Ion and molecular recognition effects on the crystallisation of bovine serum albumin–salt mixtures. *Crystal Engineering, 3*, 173–194.
85. Tarasevich, Y. Y., & Ayupova, A. K. (2003). Effect of diffusion on the separation of components in a biological fluid upon wedge-shaped dehydration. *Technical Physics, 48*, 535–540.
86. Rapis, E. (2002). A change in the physical state of a nonequilibrium blood plasma protein film in patients with carcinoma. *Technical Physics, 47*, 510–512.
87. Yakhno, T. A., Sedova, O. A., Sanin, A. G., & Pelyushenko, A. S. (2003). On the existence of regular structures in liquid human blood serum (plasma) and phase transitions in the course of its drying. *Technical Physics, 48*, 399–403.
88. Yakhno, T., Sanin, A., Pelyushenko, A., Kazakov, V., Shaposhnikova, O., Chernov, A., & Johnson, B. (2007). Uncoated quartz resonator as a universal biosensor. *Biosensors & Bioelectronics, 22*, 2127–2131.
89. Yakhno, T. A., Sanin, A. G., Vacca, C. V., Falcione, F., Sanina, O. A., Kazakov, V. V., & Yakhno, V. G. (2009). A new technology for studying multicomponent liquids using a quartz crystal resonator: Theory and applications. *Technical Physics, 54*, 1423.
90. Yakhno, T. A., Yakhno, V. G., Sanin, A. G., Sanina, O. A., Pelyushenko, A. S., Egorova, N. A., & Yashukova, E. V. (2005). The informative-capacity phenomenon of drying drops. *IEEE Engineering in Medicine and Biology Magazin, 24*, 96–104.

91. KIMOVICH, M. A., Zimin, Y., & Bochkareva, A. (2007). Morphology of dried blood serum specimens of viral hepatitis. *Hepatitis*, 207–210.
92. Buzoverya, M. E., Shcherbak, Y. P., & Shishpor, I. V. (2012a). Experimental investigation of the serum albumin fascia microstructure. *Technical Physics, 57*, 1270–1276.
93. Buzoverya, M. E., Shcherbak, Y. P., Shishpor, I. V., & Potekhina, Y. P. (2012b). Microstructural analysis of biological fluids. *Technical Physics, 57*, 1019–1024.
94. Muravlyova, L. Y., Molotov-Luchanskiy, V. B., Bakirova, R. Y., Zakharova, Y. E., Klyuyev, D. A., Bakenova, P. A., & Suleimenova, S. B. (2014). Structure-forming properties of blood plasma of patients with interstitial lung diseases. *World Journal of Medical Sciences, 10*, 478–483.
95. Baranov, M., Savchenko, E., & Nepomnyashchaya, E. (2019). The study of the self-organized blood serum films for medical diagnostics of human immunity. *International Conference App Opt Phot, 11207*, 112072Y.
96. Sikarwar, B. S., Roy, M., Ranjan, P., & Goyal, A. (2016). Automatic disease screening method using image processing for dried blood microfluidic drop stain pattern recognition. *Journal of Medical Engineering & Technology, 40*, 245–254.
97. Bahmani, L., Neysari, M., & Maleki, M. (2017). The study of drying and pattern formation of whole human blood drops and the effect of thalassaemia and neonatal jaundice on the patterns. *Colloids and Surfaces A: Physicochemical and Engineering Aspect, 513*, 66–75.
98. Sefiane, K. (2010). On the formation of regular patterns from drying droplets and their potential use for bio-medical applications. *Journal of Biological Engineering, 7*, S82–S93.
99. Shafiee, H., Warkiani, M. E., Draz, M. S., & Pandya, H. J. (2017). Rapid diagnosis of infectious diseases using microfluidic systems. *Diagn Dev Microflu*, 167–184.

Chapter 13
Theranostics: Principles, Materials, and Technical Advancements

Sri Amruthaa Sankaranarayanan, Surya Prakash Singh, and Aravind Kumar Rengan

13.1 Introduction to Principles of Theranostics

Personalized medicine remains the backbone of theranostics. Most of the clinical trials are limited to their outcomes because of the differential drug response in individuals. This is due to the varied genetic composition when considered in many patients. Thus, personalized medicine or individualized medicine has emerged as a promising strategy to overcome such limitations in most disease treatments [1]. One crucial challenge faced in personalized medicine is the variable pharmacokinetics of drugs or therapeutics in individuals. Real-time monitoring of the drug's pharmacokinetics will help plan further treatment strategy and reduce the disease/drug-associated adverse side effects. A combination of diagnostics and therapeutics, theranostics aims to minimize the delay in treatment after diagnosis. It includes early diagnosis, molecular imaging, the right treatment at the right time and right dose, and real-time monitoring of treatment efficacy [1].

In this perspective, Nanotechnology plays a vital role in overcoming the problems and limitations of conventional therapies. It deals with nanoparticles of size 1–100 nm in any one dimension since the nano-sized materials have unusual, unique physical, optical, and chemical characteristics compared to their bulk counterparts. The applications of nanomedicine and nanotechnology are widely explored in the treatment of various diseases. The essential functions of nanomaterials that play a significant role in medical applications are small size, higher surface area to volume ratio, surface energy, aspect ratio, etc. Due to the small size, these nanoparticles can interact with biological membranes and enter into the cells. Upon internalization, depending on the carrier type or the functional materials loaded, these nanoparticles

S. A. Sankaranarayanan · S. P. Singh · A. K. Rengan (✉)
Department of Biomedical Engineering, Indian Institute of Technology Hyderabad, Sangareddy, India
e-mail: aravind@bme.iith.ac.in

V. Borse et al. (eds.), *BioSensing, Theranostics, and Medical Devices*,
https://doi.org/10.1007/978-981-16-2782-8_13

can mingle with the cellular components such as DNA, proteins, surface receptors and can also help in diagnostics and therapeutics of various diseases [2, 3].

Nanotheranostic systems deal with various nanomaterials comprising three crucial components: a therapeutic agent, an imaging agent, and a carrier to deliver the imaging and therapeutic agent to the targeted site. Funkhouser coined the term theranostics in the year 2002 owing to integrating two modalities, therapy and imaging, in a single nanomaterial to understand and analyze the variations in biodistribution and efficacy of these systems. Though the concept was initially focused mostly on cancer treatment, it was later extended to multiple diseases such as inflammatory diseases, cardiovascular diseases, autoimmune diseases, and neurological disorders. Using an engineered multifunctional theranostic material helps in simultaneous diagnosis and treatment with monitoring of therapeutic efficacy using various imaging techniques such as MRI, CT, PET, or fluorescence imaging. The enhanced therapeutic efficacy of these theranostic nanosystems can be achieved by using smart and novel biomaterials capable of longer blood circulation, evading the immune response, and reducing toxicity. These nanomaterials can be engineered to be responsive to external stimuli such as pH, temperature or presence of targeting moiety. This in turn will aid in control and regulation of system-specific drug delivery and reduced toxicity to surrounding normal tissues [4]. A successful translation of any theranostic system requires an enhanced and selective accumulation of these NPs in the targeted site. Generally, most of the NPs reach the target site by passive targeting due to the EPR effect and this depends mainly on the size, shape, surface charge, and surface functionalization of the NPs. The efficacy of theranostic systems-based diagnosis and therapeutic can be significantly enhanced via targeted delivery using targeting moieties such as antibodies, ligands, peptides, aptamers, etc. Several types of nanomaterials have been developed as theranostic agents and will be discussed in detail in this chapter.

13.2 Materials for Cancer Theranostics

13.2.1 Gold-Based Nanosystems

Gold-based NPs are the most commonly used nanosystems for diagnosis, imaging, and targeting applications attributing to their unique physical, optical, and chemical properties exhibited by gold nanoparticles compared to their bulk counterpart. The ease of synthesis of gold NPs from 1 nm to 100 nm, the different shapes displayed by gold NPs such as spheres, rods, nanostars, nanoshells, etc., intensive light absorption and scattering, efficient photothermal conversion, ease of surface functionalization, biocompatibility, etc., also contribute to the unique properties of gold NPs [5]. The optical properties of gold NPs differ with an increase in size. Excitation of NPs in size range of 20 nm is due to absorption, whereas NPs of size 40 nm is due to scattering and for NPs of size 80 nm to excite due to scattering and absorption. Therefore, the optimal size of NPs is desired, depending on the type of biomedical

application. For example, in imaging, gold NPs of larger size are preferred due to their higher scattering efficiency. In contrast, in photothermal therapy, small-sized NPs are preferred due to their enhanced absorption resulting in enhanced photothermal conversion of light [6]. Au NPs offer an advantage of easy surface functionalization to load both therapeutic and diagnostic agents. Au NPs can be modified using several ligands such as PEG, biotin and also drugs such as Paclitaxel and Doxorubicin.

Belonging to the class of noble metals, gold in its nano-size is an good imaging agent due to the strong electric fields exerted on their surface, leading to strong scattering. Gold NPs absorb and scatter light in the 650–900 nm range depending on size and minimize the light extinction by intrinsic chromophores. Au NPs have been used as potentially effective alternatives of contrast agents for CT imaging compared to Iodine. This is attributed to their high atomic number and exhibit 5.7 times enhanced X-ray absorption compared to Iodine. Also, gold NPs have lesser toxicity and faster elimination and clearance [7]. Several studies have reported that the coating of PEG over gold NPs' surface has significantly increased the blood circulation time when injected in rat animal models with hepatoma. Also, high contrast was obtained in groups treated with Au NPs, which resulted in a clear distinction between normal and tumor liver tissues [8]. Different forms of gold NPs, such as nanorods, nanoshells, nanospheres, silica gold, etc., exhibit different optical properties depending on their shape, size, and chemical composition. Among the various structures of gold NPs, nanoshells and nanorods are reported to be extensively used for in vivo applications attributing to their tunable optical properties in the NIR region [9]. Au NPs conjugated with gadolinium chelates have been reported to be excellent contrast agents with enhanced clearance from the body. Gadolinium ions enhance MRI contrast, whereas the presence of Au atoms increases X-ray imaging contrast [10]. Such bio-conjugated NPs are promising for diagnostics, imaging, and therapeutics of various diseases such as HIV, Alzheimer's, diabetes, and significantly across multiple cancer types [11].

Au NPs are mostly used for their efficient photothermal conversion properties in photothermal therapies wherein they absorb the incident light and convert into heat resulting in thermal ablation of cells. The efficacy of such treatments could be synergistically enhanced by combining with chemotherapy and targeted delivery. Studies have reported the use of Au NPs as multifunctional nanocarriers conjugated with PSMA (Prostate specific membrane antigen) co-loaded with Doxorubicin resulting in enhanced targeted delivery and PTT mediated tumor damage [12]. Au NPs are also involved in PDT, wherein upon absorption of the incident light, the photosensitizer generates free reactive oxygen radicals causing cancer cell death. Nano-sized gold was used as a site-specific photosensitizer in cervical cancer cells, and it was found to induce cell death via apoptosis in the presence of light [13].

Aurolase, a theragnostic agent consisting of silica–coated gold nanoshells has entered into clinical trials with an FDA approved pilot study for application in photothermal therapy of solid tumors. The initial trials were conducted in the patients with recurrent head and neck cancer and subsequently, the trials were extended to patients with metastatic lung tumors. More recently, Nu-0129, a nucleic

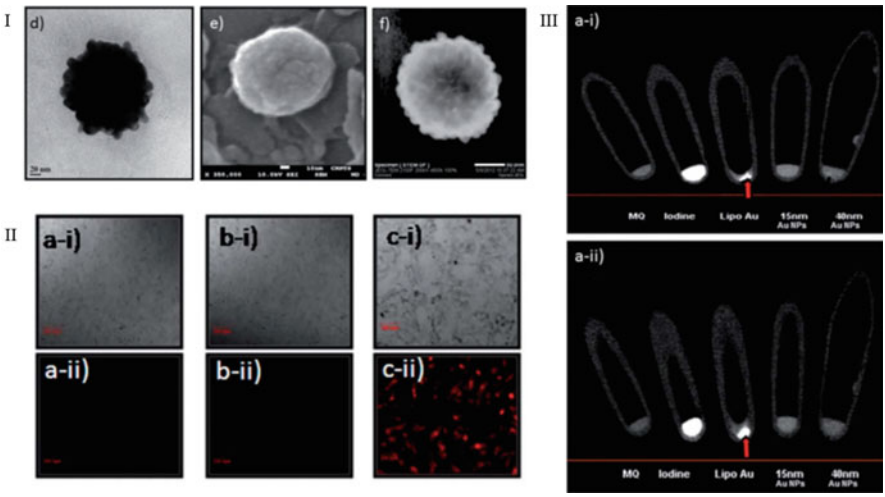

Fig. 13.1 (**I**) (d) FEG-TEM (e) FEG-SEM (f) STEM (scanning transmission electronmicroscopy) image of LiposAuNP showing the hollow central region with dark contrast. (Bare liposomes were used as controls in (a) and (b); scale bars: (d) 20 nm, (e) 10 nm, (f) 50 nm). (II) Photothermal cytotoxicity (qualitative analysis) (i) differential scanning images of (a) cells incubated with LiposAuNPs only (b) cells irradiated for 7.5 min with 750 nm laser (c) cells incubated with LiposAuNPs and irradiated for 7.5 min with 750 nm laser (a–c), (**II**) corresponding CLSM images exhibiting PI stain (dead cells) in red. (**III**) (a) X-ray CT imaging (LiposAuNPs) at (i) 70 kVp and (ii) 90 kVp. Reprinted with copyright permission from reference [14]. Source: A.K. Rengan et al., Nanoscale. 6 (2014) 916–923

acid nanoplatform consisting of a nucleic acid residue functionalized on the surface of small and spherical gold NPs, has entered into the clinical trials for patients suffering from recurrent glioblastoma multiforme. The developed nanomedicine was reported to cross the blood–brain barrier and as the nanomedicine reaches the tumor site, the nucleic acid component could target a specific gene, Bcl2L12, which is found to be selectively expressed in higher levels in glioblastoma multiforme. Though efficient as imaging agents, the size and biodegradability of these nanosystems play a significant role for use in photothermal treatment. Size $<$5–6 nm, in case of inorganic metal system is required for an effective renal clearance through the glomerular basement membrane. Hence, development of multifunctional nanosystems capable of effective clearance via both the hepato-biliary and renal routes with effective photothermal transduction is of utmost importance. NIR light responsive gold-coated liposomes (LiposAu) NPs were developed and reported to exhibit EPR mediated non-invasive targeting in different cancer models. Further, the pharmacokinetics studies in mouse models revealed in situ degradation of NPs in hepatocytes and clearance via the hepato-biliary and renal routes. NIR laser irradiation resulted in ablation of the tumor mass completely with prolonged disease-free survival [14, 15] (Figs. 13.1 and 13.2).

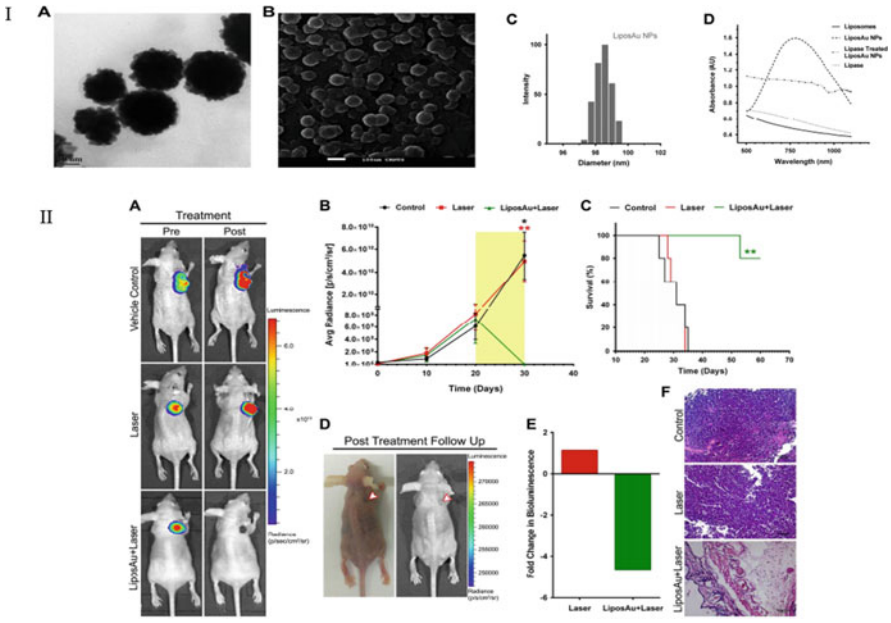

Fig. 13.2 (**I**) Characterization of LiposAu NPs. (A) TEM image of LiposAu NPs. (B) SEM image of LiposAu NPs. (C) DLS size distribution of LiposAu NPs. (D) UV-Vis absorbance (**II**) In vivo photothermal ablation by LiposAu NPs in tumor xenograft. (A) Representative pre- and post-treatment in vivo bioluminescence images of mice bearing HT1080-*fluc2-turboFP* tumor xenografts. (B) Quantitative assessment of bioluminescence to demonstrate the increase in tumor volume. (C) Kaplan–Meier survival curve of the tumor-bearing mice (D) Representative photographic and bioluminescence image of LiposAu NPs and laser treated mouse post 6 months of treatment reveals no signs of regression. (E) Bar diagram represents the fold change in bioluminescence between the laser and LiposAu NPs + laser treated tumors. (F) Hematoxylin and Eosin (H&E) stained histological evaluation of tumor tissue after PTT. Reprinted with copyrights permission from reference [15]. Source: A.K. Rengan et al., Nano Letters. 15 (2015) 842–848

13.2.2 Iron Oxide-Based Nanosystems

Having unique properties like super-paramagnetism, high magnetic susceptibility, high coercivity, stability, biocompatibility, and easy surface modification, magnetic iron oxide nanoparticles have been used in biological applications such as MRI contrast agent, bio-separation, bio-detection and diagnosis, magnetic hyperthermia, and targeted drug delivery. In the presence of an external magnetic field, SPIONs exhibit magnetic properties and are of three classes, namely, maghemite, magnetite, and hematite. SPIONs can be easily functionalized or conjugated with different types of material such as biopolymers, silica, or metal NPs, Cd/Se, organic dye molecules, or protein-peptides depending on the application [16]. Several studies have reported the use of peptide functionalized iron oxide NPs for in vitro and in vivo targeting applications. Most of the times, the use of iron oxide NPs is limited due to their poor

stability and reduced biocompatibility. Iron oxides NPs coated with PEG were found to be more biocompatible and safer for use in in vivo applications [17]. SPIONs exhibit unique magnetic properties with strong relaxation pathways in both transverse (T2) and longitudinal (T1). Conjugation of SPIONs with specific targeting ligands or contrast agents acts as excellent contrast agents in MR imaging for disease detection in early stages. Also, with the aid of magnetic field-based imaging, the drug responses can also be monitored when SPIONs are used as theranostic carriers. Several studies have reported the use of multifunctional SPIONs for specific targeting in transgenic mouse models and for MR imaging. In one study, the surface of iron oxide NPs was functionalized with a copolymer of PEG and chitosan and the surface was functionalized with anti-HER2/new monoclonal antibody for specifically targeting metastatic breast cancer. The nanosystem was also labeled with a fluorescent dye to aid in optical imaging. Compared to the control, the targeted SPIONs showed enhanced cellular uptake. Also, the uptake of SPIONs by non-targeted body organs revealed the possibility of potential metastatic infection to secondary organs [18]. Several hybrid NPs system incorporated with iron SPIONs have been developed for theranostic applications. Magnetic core–shell NPs made up of PLGA core loaded with docetaxel and SPIONs and surface functionalized with Folate–chitosan shell were evaluated for their anti-cancer therapeutic efficacy and MRI contrast. The biocompatible hybrid NPs enabled receptor-based targeting to cancer cells with controlled release of docetaxel and SPIONs for anti-cancer treatment and MR imaging, respectively. Enhancement of cellular uptake was observed in folate expressing cancer cells and hence caused significantly increased cytotoxicity. The aggregation of SPIONs within the core of the NPs reduced the overall T2 relaxation time and thereby enhanced the NP relaxivity for better MRI contrast [19]. Most of Nanotheranostics agents are limited to their poor targeting ability, drug leakage, insensitive detection leading to reduced treatment efficacy. In a recent study, a hierarchical tumor acidic pH-responsive magnetic nanobomb (HTAMN) was synthesized for effective cancer theranostics involving image guided photodynamic therapy. The nanobombs were developed through self-assembly of photosensitizer Ce6 functionalized on SPIONs through a modified PEG copolymer. The study revealed enhanced imaging, effective tumor targeting and accumulation, and superior photodynamic therapeutic efficacy of HTAMNs [20] (Fig. 13.3).

13.2.3 Other Metallic Nanosystems

In addition to the conventional metal NPs used, several researches have shown great interest in the use of other metallic nanoparticles systems made up of Copper, Palladium, Platinum, Cadmium, Selenium, etc., for theranostic applications. Due to simple synthesis procedures, copper nanoparticles have been extensively used in theranostic applications. This could also be attributed to their enhanced photothermal conversion, low cost, and stable optical properties. A study reported that use of copper oleate with lipid surfactants generated photoacoustic contrast and

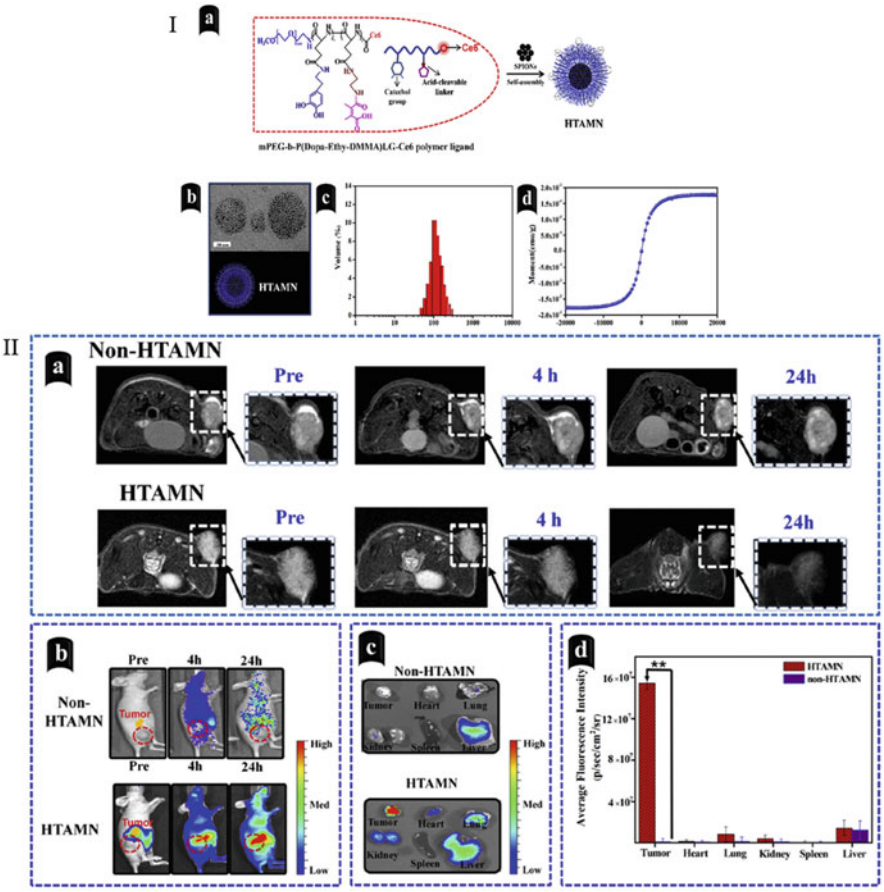

Fig. 13.3 (**I**) Construction and characterization of hierarchical tumor acidity-responsive magnetic nanotheranostics (HTAMN) for tumor-acidity activation; (a) Schematic representation of polymer ligand-assisted fabrication of self-assembled magnetic nanotheranostics; (b) HRTEM images of HTAMNs at pH 7.4; (c) The size distribution of HTAMNs by DLS assays at pH 7.4 (average diameter of ~100 nm); (d) The magnetization curve of the HTAMNs at 300 K. (**II**) In vivo MRI and NIRF tumor imaging of the HTAMN. (a) T2-weighted MR imaging of tumor at 4 h and 24 h after intravenous injection of HTAMN or non-HTAMN into mice bearing HepG2 tumor; (b) In vivo NIRF imaging of HepG2 tumor-bearing mice after intravenous injection of the HTAMN or non-HTAMN before, 4 h and 24 h after injection. Ex vivo NIRF imaging (c) and the relative fluorescence signal intensities (d) of tumor and main organs extracted 24 h post-treatment. Reprinted with copyrights permission from [20]. Source: H.Y. Yang et al., J. Control. Release. 301 (2019) 157–165

a four-fold higher signals in the NIR window than blood. The surface of Cu NPs can also be easily functionalized with targeting agents such as folic acid for applications in PET imaging and PET guided PTT [21]. Palladium NPs exhibit excellent catalytic and optical properties for use in theranostic applications. Several studies have

reported the use of Pd NPs as photothermal agents, prodrug activator, in anti-cancer and anti-microbial therapies [22]. Platinum NPs are also efficient theranostic agents mostly used in radiotherapies. A novel receptor targeted theranostic platform was developed with Platinum NPs for enhanced radio-sensitization in Her2 positive breast cancer. Pt NPs were conjugated with fluorescent dye Cy5 and functionalized with anti HER2 protein to enhance specific site targeting. The results revealed a significant inhibition of the growth of tumor cells compared to the healthy cells [23]. Cadmium and Selenium NPs are least frequently used in theranostic applications due to the associated toxicity.

13.2.4 Carbon-Based Nanosystems

Among the number of nanomaterials being currently studied for their applications in biomedicine, carbon-based nanosystems have emerged as a promising one at a remarkable speed. The most important advantage of using carbon-based materials is the high aspect ratio and the surface area they provide for easy surface functionalization with theranostic moieties such as imaging (radioisotopes or fluorescent dyes) or targeting agents (antibodies or peptides). The surface of carbon-based nanomaterials can also be easily functionalized with polymers such as PEG to increase their hydrophilicity and biocompatibility. Carbon-based nanomaterials are available in various dimensions such as Fullerene (in 0D), Carbon nanotubes (in 1D), or graphene (2D). Carbon dots are nanoclusters of amorphous form of carbon with 0D [24]. Fullerenes, C60, is unique in their photophysical and photochemical properties and hence the key feature of C60 is that they act as good photosensitizers in photodynamic therapy for the generation of reactive oxygen species. The low water solubility of water can be addressed by functionalization of fullerene surface with various hydrophilic groups. The cage like structure of Fullerene nanosystems provides a large surface area for encapsulation of different molecules and drugs. Fullerenes can be loaded with Gadolinium or SPIONs for MRI contrast agents due to their enhanced relaxivity. Additionally, Fullerenes are also capable of forming self-assembled vesicles called fullerosomes, which are one of the promising drug delivery carriers with targeting abilities [25, 26]. Carbon nanotubes (CNTs) consists of cylinders of graphene sheets and are classified either as Single walled or Multi walled based on the number of layers. Functionalized CNTs with either metals, polymers, peptides, etc., increase their biocompatibility and have been used in various biomedical applications such as sensing, therapeutics, diagnostics, etc. Also, their intrinsic spectroscopic properties such as Raman scattering and photoluminescence assist in biomedical detection and imaging of diseases [27, 28]. Various graphene-based biosensors have been developed based on their unique optical, electrical, and chemical properties to detect biomolecules with high sensitivity. Graphene oxide-based nanocarriers have gained immense importance in drug delivery and imaging modalities due to their high specific surface area, which is double than most of the nanomaterials used. This enables efficient drug loading and delivery to the targeted site. Graphene oxide has high stability and dispersity in water

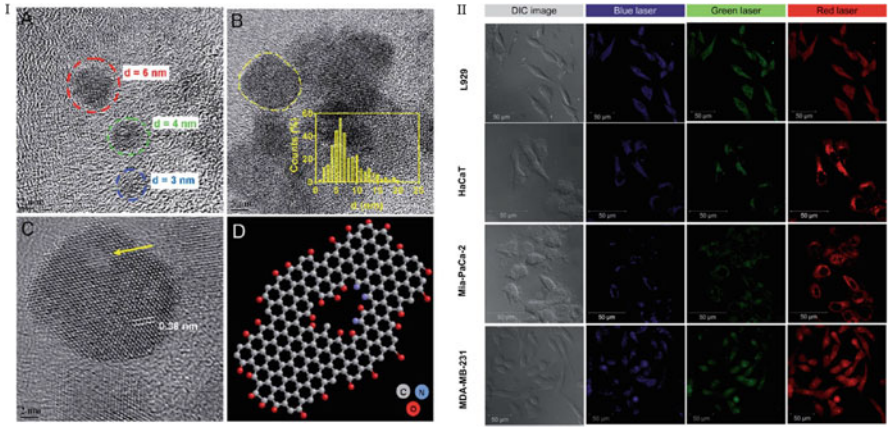

Fig. 13.4 (**I**) Morphological analysis of GQDs from withered leaves. TEM image showing (A) ultra-small GQDs of diameter: 3 nm, 4 nm, and 6 nm (color labeled) and (B) the existence of GQDs in cluster form within set showing size distribution. (C) HRTEM of a single crystalline GQD (marked in B) (D) Ball and stick model indicating the defect in a typical structure of GQD with self-passivated functional groups sketched using ChemSketch and visualized using RasWin.(**II**) Multi-color CLSM imaging of L929 cells, HaCaT cells, Mia-PaCa-2 cells, and MDA-MB-231 cells labeled with GQDs. Reprinted with copyrights permission from reference [31]. Source: M. Thakur et al., RSC Adv. 7 (2017) 5251–5261

which adds to the advantage [29, 30]. A one-step facile synthesis of graphene dots from withered leaves of plants was reported to synthesize NPs with NIR light responsive properties. The dots, capable of self-assembly, were biocompatible with high fluorescence intensity and thus they were used as in situ labeling probes in both normal and cancer cells. Upon laser irradiation with 808 nm laser, there was a concentration dependent increase in cytotoxicity and ROS production in cancer cells. Also, the cell death could be traced using the fluorescence properties of the Graphene dots even after laser illumination, proving the photostability of such nanomaterials compared to organic dyes that undergo photobleaching [31, 32]. Carbon dots or carbon quantum dots are small nanoparticles of size <10 nm. The quantum size and photoluminescence exhibited by these dots were first reported in 2007. Carbon dots have the advantage that it can be synthesized from various sources like plant extracts, organic materials like polymers, amino acids, etc. The fluorescence properties of C-dots can be tuned depending on their size, chemical modifications, and surface tailoring [33] (Fig. 13.4).

13.2.5 Silica-Based Nanosystems

In most of the nanomaterials, the properties change as their size reduces to nanoscale and the number of atoms present at the surface becomes significant. The use of silica-

based nanosystems in theranostic applications is attributed to the constant physical properties of silica NPs irrespective of size and only the total surface area increases with decrease in size. Also, their well-defined tunable nanostructures due to their siloxane chemistry pave the way to develop NPs with desired functionalization for diagnostic or therapeutic purposes. The use of silica NPs in theranostic applications is also attributed to their ease of surface functionalization and their ability to form porous structures. The porous silica NPs offer greatly enhanced surface area and also different topographies for synergistic application such as for co-delivery of therapeutics and also incorporation of imaging or contrast agents within their porous structures [34].

Silica NPs, owing to their biocompatibility, in vivo stability, ease to functionalization, excretability, chemical inertness, tailorability, and diverse morphology are well suited for theranostic application. Most of the in situ diagnosis and disease staging application require incorporation of contrast agents within the nanostructures suitable for an imaging technique chosen [35–37]. Currently, several studies have employed silica NPs to incorporate Gadolinium, manganese, and iron oxide for MRI imaging [38, 39] and for incorporation of radio-labeled ^{18}F-FDG for use in PET scan [40], for use in SPECT by incorporating radionuclides such as Iodine123 and Iodine 131, for use in CT imaging by incorporating gold, Iodine, and barium, and finally for use in optical imaging by incorporating fluorophores and dyes such as ICG, FITC, or Alexa fluor [41–44].

The surface of Silica NPs can be functionalized for therapeutic applications such as nucleic acid-based cancer therapy, chemotherapy, PDT also radioisotopes based oncological therapies. This is done by incorporation of siRNAs, DNA plasmids, oligonucleotides, incorporation of drugs such as Paclitaxel, Doxorubicin, cisplatin, etc., incorporation of photosensitizer dyes such as porphyrin, Zinc (II) phthalocyanine dyes, and by incorporation of radionuclides used in therapeutics such as yttrium-90, Iodine-131, and strontium-89 [42, 45]. A bio responsive mesoporous silica nanoparticle DOX and capped with green fluorescent carbon dots were developed for cancer theranostics application. The dual functionality of the developed nanosystem was well enhanced with good control on controlled drug release and excellent bioimaging of cancer cells. Further functionalization with folic acid would enable efficient targeting to cancer cells overexpressing folic acid receptors [46].

13.2.6 Quantum Dots-Based Nanosystems

Most of the conventional nanoparticles-based delivery systems such as liposomes, polymers, gold, or iron oxide do not generate any contrast inherently. They require a contrast agent to be incorporated within their nanostructures. One of the limitations faced with such exogenous attachment of contrast agents is that they can promote non-targeted interactions and also it can alter the physicochemical properties of the NPs and subsequently their therapeutic efficacy. Thus, to avoid such drawbacks, it is

desirable to develop a nanosystem that possesses inherent optical contrast to help in enhanced imaging and diagnostic applications [47, 48].

Quantum dots are semiconductor nanomaterials of size <10 nm with a light responsive luminescence property. When a photon of light excites a quantum dot, the electron in the valence band shifts to the conduction band forming an electron–hole pair. Based on the type of semiconductor material used in QD synthesis, the de-excitation of electron–hole pair leads to release of photon of light. The wavelength of the released photons depends on the size and chemical composition of the QDs. In addition to the endogenous ability to generate contrast, QDs also offer an enhanced functional surface area for incorporation of therapeutic moieties [49, 50].

13.2.7 Polymer-Based Nanosystems

One of the main requirements in nanotechnology-based medicine is the development of biocompatible and biodegradable NPs delivery system. Polymers offer an advantage of being biodegradable into their monomers upon metabolism and easily removed from the body. Depending on the source, natural or synthetic, polymers NPs can be synthesized and stabilized using techniques like conjugation, grafting, etc. Polymer NPs have ease of surface modification and functionalization with different molecules depending on the application. Biodegradation and controlled release of drug/molecules from polymer systems can be achieved based on the physicochemical properties of the polymers (For example, molecular weight, hydrophilicity/hydrophobicity, dispersity index, etc.) used. These properties also influence the pharmacokinetics, biodistribution, and pharmacodynamics of the NPs inside the system. Polymeric systems are known for their ability to deliver variety of classes of drugs into the targeted site along with sustained and controlled delivery. This is due to the large surface area they provide for easy encapsulation of therapeutic moieties. PLGA, PLA, PEG, Chitosan are some of the common polymeric nanosystems used in theragnostic applications [51].

Of the numerous polymers, the most successful ones were the nanocarriers with poly ethylene glycol (PEG) which leads to escape from RES of the blood thereby reduced immunogenicity and antigenicity and also increases blood circulation time and stability. For that reason, nanoparticles coated with PEG were defined as stealth nanoparticles. PEG is also reported to shield the core of nanocarriers from degradation due to steric hindrance thereby reducing renal clearance. This is due to increase in hydrodynamic size of nanocarriers functionalized with PEG and increase in solubility due to the hydrophilicity of PEG. One study reported that the PEG could be converted into fluorescent PEG (FL-PEG) in a facile one-step synthesis method which would eliminate the need for other additional fluorescent moieties for tracking and imaging purposes. This FL-PEG synthesized could be used to coat metals such as gold and silver for various biomedical applications such as antibacterial NPs and photothermal therapy [52].

Several polymeric formulations have been approved by the FDA and some have entered in to the clinical trials. The first polymeric NPs approved by FDA is a PLGA-based NPs encapsulating leuprolide named Eligard for the treatment of prostate cancer in 2002. Following this several polymeric nanocarriers for cancer therapy have entered into clinical trials phase II and III. Of these, Doxorubicin transdrug, i.e., Doxorubicin loaded poly alkyl cyanoacrylate developed against multi drug resistant hepatocellular carcinoma is currently in clinical trials phase III. Also, a polymer-drug conjugate of polyglutamic acid and paclitaxel named poliglumex is in phase III of clinical trials and have shown significantly enhanced survival in patients suffering from non-small cell lung cancer.

A biodegradable multifunctional polymer-based nanosystem was developed to encapsulate hydrophobic drug for triggered release in cancer theranostics. A potential anti-cancer plant extract was loaded into PLGA-based nanoparticles and was combined with IR-780 dye to make it photo-responsive. The inherent fluorescence properties of the plant extract due to the presence of chlorophyll was utilized for understanding the cellular uptake and drug release. The photo thermal efficacy of IR-780 was also synergistically enhanced when loaded into a polymeric nanosystem. The combinatorial approached resulted in synergistic toxicity in skin cancer theranostics [53].

In another study, a single nanoplatform was developed to combine NIR laser induced Nitric oxide therapy/PTT using semi-conducting polymer nanoparticles (SPNs, PFTDPP) in combination with nitric oxide donor, s-nitrosothiol groups (SNAP). SPNs help in achieving enhanced photothermal conversion to convert into heat with generation of nitric oxide. The structural and spectral features of the semi-conducting polymers used provide NIR window II and photoacoustic imaging for guiding the combined nitric oxide/Photothermal therapy [54] (Fig. 13.5).

Polymeric micelles are a type of nanosystems mostly used in encapsulation and delivery of hydrophobic drugs. Several studies have reported the use of polymeric micelles in theranostic applications such as contrast agents or MR imaging with the help of radioactive nuclides or SPIONs. Based on the theranostic application, the micelles can be easily modified with the type of block copolymer used to make the system responsive to external stimuli such as pH, temperature, light, or sound that would enable controlled and sustained drug release [55]. A type of multifunctional pH-responsive micellar NPs delivery system was developed using star copolymers made up of β-cyclodextrin core loaded with DOX and MRI contrast agents for combined targeted cancer cell drug delivery and enhanced contrast for MR imaging. The study revealed that the NPs system exhibited controlled DOX release in acidic pH environment and also expressed augment T1 relativity with enhanced contrast [56].

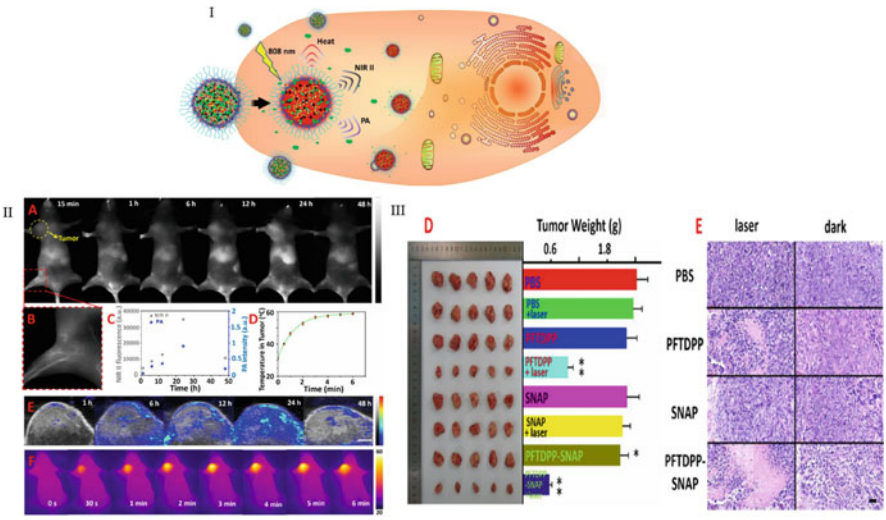

Fig. 13.5 (**I**) Schematic illustrating NIR II/photoacoustic imaging-guided photothermal initiated NO/photothermal therapy. (**II**) The dual-mode imaging property of PFTDPP-SNAP NPs in vivo. (A) The whole-body NIR II imaging of MCF-7 tumor-bearing (yellow circle) nude mice. (B) The enlarged imaging of hind limb region in (A) at 15 min. (C) Variation of the NIR II fluorescence (gray dots) and PA (blue dots) signal intensity at tumor region within 48 h. (D) Temperature at tumor region with 808 nm laser irradiation (1 W/cm2) (E) The photoacoustic (PA) imaging of the tumor region by loading PFTDPP-SNAP NPs in PBS solution (PFTDPP 1 mg/mL and SNAP 0.5 mg/mL) with 808 nm laser irradiation. (F) The thermal imaging of tumor region after treatment. (**III**) (D) Photograph and tumor weights of tumors after excision from each group. (E) The representative image of the tumor sections examined by H&E staining in dark and with 808 nm laser irradiation. Reprinted with copyrights permission from reference [54]. Source: J. Li et al., Biomaterials. 217 (2019) 119304

13.2.8 Lipid-Based Nanosystems

Lipids-based NPs represent one of the most efficient and successful carriers used in biomedical applications due to their mimicking nature of natural cell membranes. Among the different types of lipid-based NPs, liposomes are the first forms and mostly used in the field of theranostics. These NPs are made up of spherical vesicles of lipid bilayer ranging from 50 nm to 500 nm held together by hydrophobic interactions. The most important advantage of using liposomal NPs is that they can carry and deliver both hydrophobic and hydrophilic drugs molecules within their core. Based on the source of lipids, either natural or synthetic, the properties of the formed NPs vary. The composition of the bilayer influences the properties of the liposomes formed such as surface charge, permeability, circulation time, etc. Most of the times, liposome NPs are recognized by the immune system and cleared by the macrophages. Hence, several studies have reported the use of PEG to coat over the surface of liposomes to prolong the circulation time in blood [57–59]. Liposomal nanoformulations were the first nanomedicines to be approved by FDA and

clinically translated. Doxil, a liposomal formulation of Doxorubicin was the first FDA approved nanomedicine in 1995 against Kaposi's sarcoma and also ovarian cancer and multiple myeloma in the subsequent years. The success of this nano-formulation was due to the coating of methoxy-PEG which contributed to the hydrophilicity and hence greater stability and longer circulation time and reduced cardiotoxicity compared to conventional Doxorubicin [60, 61].

Despite successful clinical outcomes, liposomes are limited to their poor stability in blood and poor drug solubility and uncontrolled drug release profiles in vivo. To overcome this, solid lipid nanoparticles (SLNs) have emerged as a potential alternative delivery system due to their controlled drug release and delivery profile. They offer several advantages such as tolerability, reduced toxicity, biodegradability, and stable drug encapsulation. However, SLNs are also limited to their reduced loading of hydrophilic drugs [62, 63]. Several multifunctional liposomal formulations have entered into clinical trials, Thermodox is a thermosensitive lipid bilayer encapsulated with Doxorubicin which releases Dox when combined with high energy radiofrequency. Several targeted liposomal formulations have also been developed [64].

Liposomal NPs combined with targeting ligands such as RGD peptide and Transferrin help to increase tumor uptake and also enable enhanced permeability across blood–brain barrier and combined with Paclitaxel help in synergistic treatment of glioma [65]. NIR light responsive nanoliposomes encapsulating NIR photosensitizer IR780 and anti-cancer bioactive plant extract were developed for efficient and selective cancer theranostics. The developed nanosystems exhibited concentration dependent increased cytotoxicity and ROS generation selectively in cancer cells while the normal cells were healthy and unaffected. The synergistic activation of ROS generation leads to cancer cell death via autophagy and provides a useful strategy for enhancing the theranostic potential of such therapies [66] (Fig. 13.6).

13.3 Advanced Theranostic Nanomedicine Platforms for Clinical Applications

13.3.1 Photodynamic and Photothermal Therapy

Use of light to treat diseases dates back to centuries ago. Several plant extracts have been used in combination with sunlight to treat several skin diseases such as leukoderma and vitiligo about 3500 years ago. In the modern era, photodynamic therapy is based on the same principle, where in a photosensitizer dye is used to absorb the incident light of a particular wavelength and releases reactive oxygen species (ROS) resulting in cell death. The combination of light and photosensitizer results in synergistic damage or death of tissues. The generated ROS causes oxidative stress to the cellular machinery thereby causing cytotoxic effects. The exerted

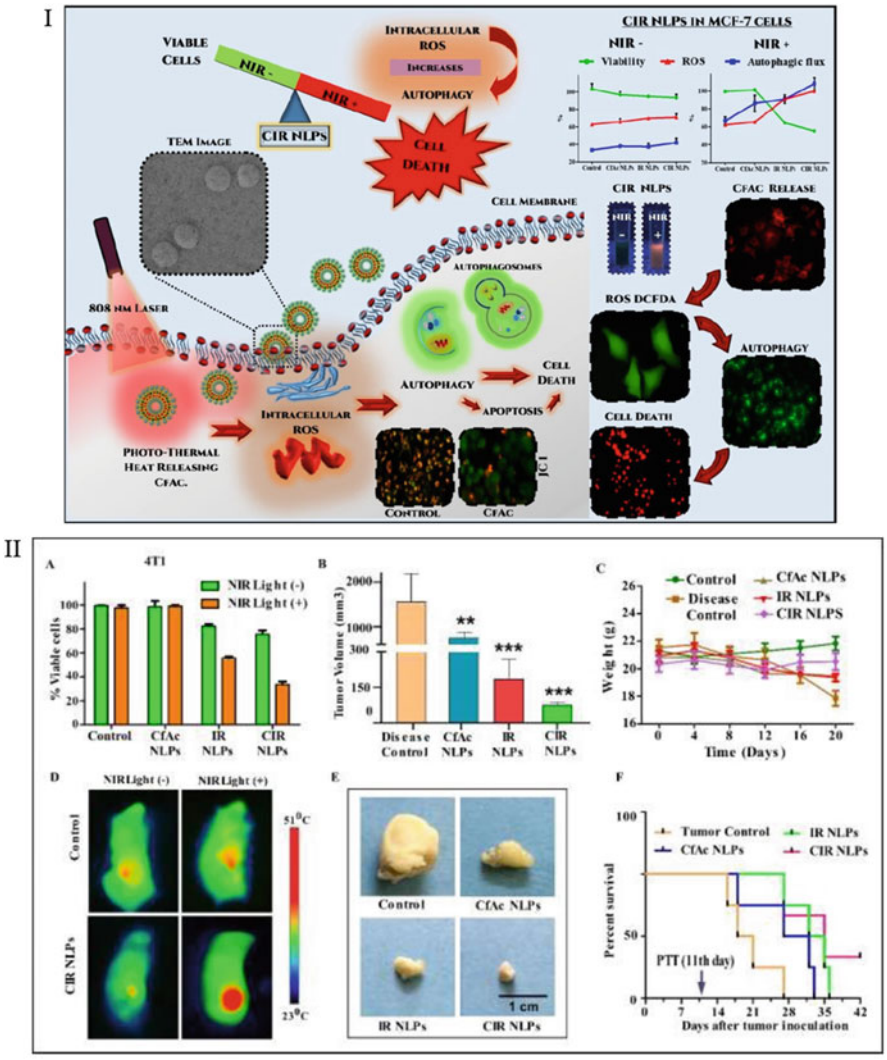

Fig. 13.6 (**I**) Schematic showing the ROS dependent autophagy induced by bioactive nanoliposomes. (**II**) in vivo studies. (A) NIR light mediated cytotoxicity in 4 T1 cells using NLPs. (B) Tumor volumes recorded upon treatment with NLPs and NIR irradiation. (C) Changes in body weight recorded during the study period. (D) Thermal images of animals upon treatment with CIR NPs and NIR irradiation. (E) Images of tumor inoculated in xenograft models of different groups. (F) Survival profile of the animals upon treatment with various NLPs. Reprinted with copyrights permission from reference. Source: T. Appidi et al., Nanoscale. 12 (2020) 2028–2039

effect is localized to the photosensitizer accumulated tissue thereby reducing off target damage and lesser side effects [67, 68]. PDT has been successful in the treatment of various dermal, ocular, and cancer management [69, 70]. Photothermal

therapy, a form of light-based therapy which utilizes molecules or nanoparticles that absorb the incident light leading to thermal ablation of tissues. The spatial control of PTT is similar to that of PDT, where in only the localized environment is affected. However, PTT had an additional advantage that it does not require oxygen in case of hypoxic conditions. Most commonly used PTT agents are plasmonic NPs of gold. With the development of laser fibers, pilot studies in clinical trials of imaged guided PTT have begun to evaluate the potential of such NPs in this modality. The practical and clinical limitations of Photo-therapies is mainly the limited penetration of visible light into living tissues due to the presence of absorbers like oxygenated hemoglobin in blood. However, this has been overcome by using NPs that absorb in the NIR region (650–900 nm). The advantage of using NIR window is that the excitation wavelength is higher than that of the absorption of hemoglobin and below than that of water. Also, light in NIR window can penetrate in to several depths in tissues and also NIR light has reduced autofluorescence due to the optimized signal-background ratio of inherent fluorophores of body [71–73].

13.3.2 Imaging

The differences in optical properties of different tissues like absorption, fluorescence, scattering, etc., have led to emergence of various imaging modalities. Imaging involves a multi-disciplinary field to create a visual representation of the target. In medical field, imaging plays an important role to provide information about a disease using non-invasive methods such as MRI, ultrasonography, CT, PET, SPET, etc. Bioimaging is promising during the early stages of drug delivery and diagnosis. It is also sensitive and used for monitoring of treatment efficacy in real time. The development of various novel probes has enhanced the scope of using light for medicinal applications by reducing complete dependence on endogenous chromophore for imaging. NP-based labeling system provides much effective results compared to the conventional imaging systems [74]. For a bioimaging purpose, the NPs used should be stable, biocompatible, easy for surface functionalization, and sensitive to external stimulus. Apart from bioimaging, molecular imaging also helps to identify and detect various biological changes within an organism at the molecular level. This usually required advanced instrumentation and molecular probes using image contrast agents. Most of the spatial and temporal biodistribution analysis of NPs is obtained using this technique. Molecular imaging is also a quantitative technique, used to monitor specific genes, functions, interactions, and various pathways involved of a gene and it can be done both in vitro and in vivo studies. The important function of an imaging agent is to enhance the signals of the particular subject of interest w.r.t their surroundings. Characteristic properties such as penetration depth, temporal resolution, detection threshold of the probes used also play a major role in the type of modality used for imaging. The advantages of using NPs as imaging agents include high surface area to volume ratio, better penetration into biological barriers, easy to functionalize, good stability, and most importantly highly

resistant to photobleaching. But, the biocompatibility, toxicity, clearance, accumulation, and uptake by RES limit the advantages of using NPs as imaging agents. Endogenous imaging agents such as GFP or luciferase are mostly involved in the molecular imaging processes. Exogenous imaging agents include the organic fluorophores, metal NPs, and magnetic nanoparticles such as Quantum dots, gold NPs, and iron oxide nanoparticles [75–77].

13.3.3 Nanobiosensors

Detection of biomarkers or analytes with sensitivity is an important requisite for clinical diagnosis. Though these clinical markers act as a sign of onset of the disease, their levels are too low at the earlier stages of disease progression. With the advancements in the field of nanomaterials and nanotechnologies, several novel biosensors are being developed to detect accurately very low concentrations of such biomarkers. Several nanomaterials have been used in the design and development of novel biosensors for sensing various biomarkers for an effective point of care and onsite diagnosis. The size, shape, surface properties, and the type of nanomaterials, for example, metallic or carbon or polymer, etc., influence the efficiency of biosensors. Use of nanotechnology also helps to miniaturize the detection device fabrication rendering a portable device with comparable sensitivity of that of the conventional sophisticated instruments. Gold NPs are one of the mostly commonly used metallic nanosystems in biosensors due to their unique size dependent electronic and optical properties. Owing to their easy surface functionalization, often gold NPs are conjugated with various antibodies or aptamers to develop efficient bio-affinity based nanosensors. Also, metal oxide NPs of mainly Fe, ZN, Mn, etc., are also commonly used in biosensing applications. Several carbon-based nanomaterials, in particular graphene oxide and reduced graphene oxide are used in biosensors due to its unique electrical and optical properties. Polymers are generally used in the development of low cost, biocompatible nanobiosensors due to its surface functionalization and biocompatibility. Conducting polymers are most commonly used in development of electrochemical sensors. Of late, the recent technological advancements in smart phones processors and camera have been highly utilized in integrating with biosensing applications for the development of portable diagnostic devices [74, 78–80].

13.3.4 Magnetic Hyperthermia

Magnetic hyperthermia involves the use of externally applied high frequency magnetic field converted into thermal energy to kill targeted cells. SPIONs are class of magnetic NPs that renders the cells sensitive to external magnetic field. They could convert the external high energy magnetic field to thermal heat in an localized

environment. Presence of SPIONs could help to elevate the temperature in the tumor core upon exposure to magnetic field resulting in tumor inhibition. This has been reported in case of human head and neck cancer xenograft model. SPIONs mediated hyperthermia have also been translated into clinics for human trials due to the superior advantage of tissue penetration and reduced skin toxicity as compared to the photo triggered therapies. However, efficiency of the magnetic-heat conversion has been limited in most of the cases which can be overcome by combining with other radio/chemo therapies [81–83].

13.3.5 Multimodal Image Guided Therapy

One of the important goals of nanomedicine is to improve and enhance the biodistribution of the NPs formulations and accumulation at the targeted site upon systemic administration. This requires a non-invasive imaging modality to analyze the biodistribution and pharmacokinetics of the administered drug. For this purpose, different types of nanomedicines have been developed where certain imaging agents are also co-loaded with therapeutic moieties. In some cases, radionuclides or fluorescent dyes are used. It has been evident in various animal studies and clinical trials that use of such image guided therapeutics has substantially assisted in enhancing the understanding of biodistribution and in prediction of therapeutic efficacy of targeted nanomedicine.

13.3.6 Treatment of Cardiovascular Diseases

Globally, CVD remains one of the leading causes of serious public ill health. Nanotheranostics in CVD were developed for addressing the non-invasive real-time monitoring of cardiac health and some of them were successful in the preclinical trials. However, there is no standardized procedure to analyze the role of NPs based theranostics in specific for CVD [84]. One of the first studies involving theranostics for CVD was the use of ultra-small SPIONs for non-invasive imaging to evaluate the drug response in patients suffering from atherosclerosis [85]. Targeted theranostic microbubbles have been developed to bind to the platelets for in vivo ultrasound imaging of thrombi. Nanotheranostics can be used to enhance and accelerate the development of novel approaches to monitor the success of either fibrinolytic or thrombolytic therapies for CVD [86].

13.3.7 Treatment of Central Nervous System Related Diseases

Diseases of the central and peripheral nervous system present a significant challenge in modern society. Conventional treatment or techniques are limited to alleviate or diagnose the signs and symptoms of the disease. However, the development of therapeutic and imaging contrast probes that can cross the blood–brain barrier has emerged as significant solutions. In this perspective, nanotechnology and Nanotheranostics can be developed as efficient tools to improve the imaging of CNS and to investigate the deeply diseased conditions. MRI remains the most important tool of imaging brain disorders. Similarly, PET has been used in monitoring the pathophysiology of Alzheimer's disease to improve understanding of the disease conditions. Several radiolabeled ligands have been developed for this purpose. Nanotheranostics can facilitate solutions for understanding of complete mechanism underlying the neurodegenerative disease that limit the clinical outcomes of existing treatment modalities [87, 88].

13.4 Commercialization and Translational Challenges of Theranostic Nanosystems

During the initial stages of development, nanoparticles were designed and developed either for therapeutic or imaging applications. With the limitations of existing modalities and need for combinational therapeutics, there has been a shift of interest towards the development of multifunctional theranostic nanomaterials. With nanoparticles being used as drug delivery systems, several imaging moieties such as for MRI or optical imaging, various NPs such as gold, iron oxide, mesoporous silica, and carbon-based NPs are also being used as templates for the development of theranostic nanoparticles. One of the crucial challenges faced in clinical translation of these theranostic systems is the nano-bio interaction. The potential toxic outcomes upon nanoparticle interaction with biological interface include immune responses, inflammation, and related diseases. However, the toxicity depends mainly on the size, charge, and solubility of these nanosystems. The physicochemical properties of these nanosystems also influence their interaction with proteins, leading to corona formation on their surface. This corona formation, subsequently leads to altered size, solubility, stability, biodistribution, clearance, and pharmacokinetics of the nanosystem. Hence, the compatibility profile of theranostic system for human applications still remains a significant concern in view of clinical translation [89].

Another critical challenge faced in the commercialization of theranostic systems is designing a highly controllable and reproducible synthesis procedures for a significant scale up production. Though these particle systems have shown promising potential for practical applications, there is still a lack of information regarding the scale up production of these nanoparticles and commercialization of these theranostic systems in clinical use. At present, these nanosystems are being prepared

in a laboratory scale small batch. The production quality depends on the type of particle being used and the reaction scale is generally in grams. The purification of the synthesized systems is necessary to remove the impurities present and reaction by products. Several methods like centrifugation, solvent evaporation, dialysis, ultrafiltration, etc., are generally used for purification. The major challenges faced during large-scale production are the effects and process limitations of preparative methods. First, the characteristics of the NPs is said to be affected like the particle size, drug loading, morphology, and stability. Some studies have reported that the scale up production reduces the percentage of drug loading capacity of the NPs. Second, other process limitations include the stability and availability of raw materials used in the production and usage of solvents like chloroform and DMSO owing to their toxicity. Therefore, novel methods involving aqueous solvents with reduced toxicity must be developed for large-scale production by pharmaceutical industries. Two potential nanomedicines have been approved by the FDA, namely, Doxil (Liposomal formulation of Doxorubicin) in 1995 and Abraxane (Albumin NPs bound Paclitaxel) in 2005 for the treatment of ovarian and breast cancer, respectively. Despite such clinical success, nanoformulations suffer from various limitations like systemic toxicities, immune response, stability issues, etc. Thus, clinical translation of such nanoformulations is majorly limited by their scale up production. Therefore, it seeks much attention from the science researchers regarding the successful development of large-scale production of these nanomedicines. Upon achieving successful scale up production, these nanoformulations will serve as better alternatives for a myriad of diseases compared to the existing ones [90].

Till date, no theranostic nanomaterials have been approved by the FDA for commercialization. This is mainly due to the above-discussed challenges related to the heterogeneity in synthesis, design, safety, and efficacy in clinical trials of these nanosystems. Hence, future research has to be more focused on effectively improving the clinical efficacy and translational probability of these nanotheranostic agents given each material's advantages and limitations. Emphasis on a better understanding of these material's pharmacokinetics and pharmacodynamics in human applications is the need of the hour with combined efforts from interdisciplinary experts. Overall, it is believed strongly that the development of several theranostic systems will provide a promising revolutionary potential in various clinical needs by improving the population's quality of life [91].

13.5 Conclusion

Personalized medicine or individualized medicine has emerged as a promising strategy to overcome limitations in most of disease treatments and remains the backbone of theranostics. However, the genetic variability and associated pharmacokinetics of drugs or therapeutics remain a major challenge. Recent advancements in nanotechnology have paved way to combine diagnosis, treatment, prevention, and cure for the deadly diseases in a single platform. In this chapter, recent developments

in nanotheranostic systems have been discussed in detail. Nanotheranostics act as an attractive platform allowing to integrate multiple treatment modalities in general for cancer therapeutics, aiming to enhance the biocompatibility and stability of the existing systems. Specific targeting and controlled release of therapeutic moieties also enable effective tackling of multi drug resistance and adverse side effects of the existing modalities. Nanotheranostics offer potential advantage in personalized medicine and image guided therapy to handle various diseases. Therefore, nanotheranostics have an inevitable role in paving way for better health care in future.

Acknowledgments The authors would like to thank Dept. of Science and Technology (DST), Dept. of Biotechnology (DBT), Ministry of Education (MoE), Govt. of India for funding the following projects DST-Inspire (DST/INSPIRE/04/2015/000377), DST-AMT (DST/TDT/AMT/2017/227), IITH ID BME/MSME grant and MoE IMPRINT (4291). Author SAS would like to thank DST and PMRF for funding her fellowship. Financial support from the DBT-RA Program in Biotechnology and Life Sciences is gratefully acknowledged by author SPS.

References

1. Hood, L. (2013). Systems biology and P4 medicine: past, present, and future. *Rambam Maimonides Medical Journal, 4*, e0012. https://doi.org/10.5041/rmmj.10112.
2. Moghimi, S. M., Hunter, A. C., & Murray, J. C. (2005). Nanomedicine: current status and future prospects. *FASEB Journal, 19*, 311–330. https://doi.org/10.1096/fj.04-2747rev.
3. Muthu, M. S., Leong, D. T., Mei, L., & Feng, S. S. (2014). Nanotheranostics - application and further development of nanomedicine strategies for advanced theranostics. *Theranostics, 4*, 660–677. https://doi.org/10.7150/thno.8698.
4. Shi, J., Kantoff, P. W., Wooster, R., & Farokhzad, O. C. (2017). Cancer nanomedicine: Progress, challenges and opportunities. *Nature Reviews Cancer, 17*, 20–37. https://doi.org/10.1038/nrc.2016.108.
5. Khlebtsov, N., Bogatyrev, V., Dykman, L., Khlebtsov, B., Staroverov, S., Shirokov, A., Matora, L., Khanadeev, V., Pylaev, T., Tsyganova, N., & Terentyuk, G. (2013). Analytical and theranostic applications of gold Nanoparticles and multifunctional nanocomposites. *Theranostics, 3*, 167–180. https://doi.org/10.7150/thno.5716.
6. Sharma, G., Sharma, A. R., Nam, J. S., Doss, G. P. C., Lee, S. S., & Chakraborty, C. (2015). Nanoparticle based insulin delivery system: the next generation efficient therapy for type 1 diabetes. *Journal of Nanbiotechnology, 13*, 1–13. https://doi.org/10.1186/s12951-015-0136-y.
7. Kim, D., Kim, J. W., Jeong, Y. Y., & Jon, S. (2009). Antibiofouling polymer coated gold@iron oxide nanoparticle (GION) as a dual contrast agent for CT and MRI. *Bulletin of the Korean Chemical Society, 30*, 1855–1857. https://doi.org/10.5012/bkcs.2009.30.8.1855.
8. Murphy, C. J., Gole, A. M., Stone, J. W., Sisco, P. N., Alkilany, A. M., Goldsmith, E. C., & Baxter, S. C. (2008). Gold nanoparticles in biology: beyond toxicity to cellular imaging. *Accounts of Chemical Research, 41*, 1721–1730.
9. Jain, P. K., Lee, K. S., El-sayed, I. H., & El-sayed, M. A. (2006). Calculated absorption and scattering properties of gold nanoparticles of different size, shape, and composition: applications in biological imaging and biomedicine. *Journal of Physical Chemistry B, 110*, 7238–7248.
10. Alric, C., Taleb, J., Le Duc, G., Mandon, C., Billotey, C., Le Meur-herland, A., Brochard, T., Vocanson, F., Janier, M., Perriat, P., Roux, S., Tillement, O., & Lyon, C. B. (2008). Gadolinium

chelate coated gold nanoparticles as contrast agents for both x-ray computed tomography and magnetic resonance imaging. *Journal of the American Chemical Society, 130*, 5908–5915.
11. Boisselier, E., & Astruc, D. (2009). Gold nanoparticles in nanomedicine: preparations, imaging, diagnostics, therapies and toxicity. *Chemical Society Reviews, 38*, 1759–1782. https://doi.org/10.1039/b806051g.
12. Kim, D., Jeong, Y. Y., & Jon, S. (2010). A drug-loaded aptamer - gold nanoparticle bioconjugate for combined ct imaging and therapy of prostate cancer. *ACS Nano, 4*, 3689–3696. https://doi.org/10.1021/nn901877h.
13. Pedrosa, P., Vinhas, R., Fernandes, A., & Baptista, P. V. (2015). Gold nanotheranostics: proof-of-concept or clinical tool? *Nanomaterials, 5*, 1853–1879. https://doi.org/10.3390/nano5041853.
14. Rengan, A. K., Jagtap, M., De, A., Banerjee, R., & Srivastava, R. (2014). Multifunctional gold coated thermo-sensitive liposomes for multimodal imaging and photo-thermal therapy of breast cancer cells. *Nanoscale, 6*, 916–923. https://doi.org/10.1039/c3nr04448c.
15. Rengan, A. K., Bukhari, A. B., Pradhan, A., Malhotra, R., Banerjee, R., Srivastava, R., & De, A. (2015). In vivo analysis of biodegradable liposome gold nanoparticles as efficient agents for photothermal therapy of cancer. *Nano Letter, 15*, 842–848. https://doi.org/10.1021/nl5045378.
16. Mahmoudi, M., Sant, S., Wang, B., Laurent, S., & Sen, T. (2011). Superparamagnetic iron oxide nanoparticles (SPIONs): development, surface modification and applications in chemotherapy. *Advanced Drug Delivery Reviews, 63*, 24–46. https://doi.org/10.1016/j.addr.2010.05.006.
17. Hervé, K., Douziech-Eyrolles, L., Munnier, E., Cohen-Jonathan, S., Soucé, M., Marchais, H., Limelette, P., Warmont, F., Saboungi, M. L., Dubois, P., & Chourpa, I. (2008). The development of stable aqueous suspensions of PEGylated SPIONs for biomedical applications. *Nanotechnology, 19*, 465608. https://doi.org/10.1088/0957-4484/19/46/465608.
18. Kievit, F. M., Stephen, Z. R., Veiseh, O., Arami, H., Wang, T., Lai, V. P., Park, J. O., Ellenbogen, R. G., Disis, M. L., & Zhang, M. (2012). Targeting of primary breast cancers and metastases in a transgenic mouse model using rationally designed multifunctional SPIONs. *ACS Nano, 6*, 2591–2601. https://doi.org/10.1021/nn205070h.
19. Shanavas, A., Sasidharan, S., Bahadur, D., & Srivastava, R. (2017). Magnetic core-shell hybrid nanoparticles for receptor targeted anti-cancer therapy and magnetic resonance imaging. *Journal of Colloid and Interface Science, 486*, 112–120. https://doi.org/10.1016/j.jcis.2016.09.060.
20. Yang, H. Y., Jang, M. S., Li, Y., Fu, Y., Wu, T. P., Lee, J. H., & Lee, D. S. (2019). Hierarchical tumor acidity-responsive self-assembled magnetic nanotheranostics for bimodal bioimaging and photodynamic therapy. *Journal of Controlled Release, 301*, 157–165. https://doi.org/10.1016/j.jconrel.2019.03.019.
21. Zhou, M., Song, S., Zhao, J., Tian, M., & Li, C. (2015). Theranostic CuS nanoparticles targeting folate receptors for PET image-guided photothermal therapy. *Journal of Materials Chemistry B, 3*, 8939–8948. https://doi.org/10.1039/c5tb01866h.
22. Dumas, A., & Couvreur, P. (2015). Palladium: a future key player in the nanomedical field? *Chemical Science, 6*, 2153–2157. https://doi.org/10.1039/c5sc00070j.
23. Yue, Y., Wagner, S., Medina-Kauwe, L., Cui, X., Zhang, G., Shiao, S., Sandler, H., & Fraass, B. (2016). WE-FG-BRA-11: theranostic platinum nanoparticle for radiation sensitization in breast cancer radiotherapy. *Medical Physics, 43*, 3826–3826. https://doi.org/10.1118/1.4957911.
24. Patel, K. D., Singh, R. K., & Kim, H. W. (2019). Carbon-based nanomaterials as an emerging platform for theranostics. *Materials Horizons, 6*, 434–469. https://doi.org/10.1039/c8mh00966j.
25. Wang, M., Nalla, V., Jeon, S., Mamidala, V., Ji, W., Tan, L. S., Cooper, T., & Chiang, L. Y. (2011). Large femtosecond two-photon absorption cross sections of fullerosome vesicle nanostructures derived from a highly photoresponsive amphiphilic C 60-light-harvesting fluorene dyad. *Journal of Physical Chemistry C, 115*, 18552–18559. https://doi.org/10.1021/jp207047k.

26. Zhang, J., Ye, Y., Chen, Y., Pregot, C., Li, T., Balasubramaniam, S., Hobart, D. B., Zhang, Y., Wi, S., Davis, R. M., Madsen, L. A., Morris, J. R., Laconte, S. M., Yee, G. T., & Dorn, H. C. (2014). Gd3N@C84(OH)x: a new egg-shaped metallofullerene magnetic resonance imaging contrast agent. *Journal of the American Chemical Society, 136*, 2630–2636. https://doi.org/10.1021/ja412254k.
27. Karimi, M., Solati, N., Ghasemi, A., Estiar, M. A., Hashemkhani, M., Kiani, P., Mohamed, E., Saeidi, A., Taheri, M., Avci, P., Aref, A. R., Amiri, M., Baniasadi, F., & Hamblin, M. R. (2015). Carbon nanotubes part II: a remarkable carrier for drug and gene delivery. *Expert Opinion on Drug Delivery, 12*, 1089–1105. https://doi.org/10.1517/17425247.2015.1004309.
28. Niyogi, S., Hamon, M. A., Hu, H., Zhao, B., Bhowmik, P., Sen, R., Itkis, M. E., & Haddon, R. C. (2002). Chemistry of single-walled carbon nanotubes. *Accounts of Chemical Research, 35*, 1105–1113. https://doi.org/10.1021/ar010155r.
29. Cao, X., He, Q., Shi, W., Li, B., Zeng, Z., Shi, Y., Yan, Q., & Zhang, H. (2011). Graphene oxide as a carbon source for controlled growth of carbon nanowires. *Small, 7*, 1199–1202. https://doi.org/10.1002/smll.201100071.
30. Mohanty, N., & Berry, V. (2008). Graphene-based single-bacterium resolution biodevice and DNA transistor: interfacing graphene derivatives with nanoscale and microscale biocomponents. *Nano Letter, 8*, 4469–4476. https://doi.org/10.1021/nl802412n.
31. Thakur, M., Kumawat, M. K., & Srivastava, R. (2017). Multifunctional graphene quantum dots for combined photothermal and photodynamic therapy coupled with cancer cell tracking applications. *RSC Advances, 7*, 5251–5261. https://doi.org/10.1039/c6ra25976f.
32. Kumawat, M. K., Thakur, M., Gurung, R. B., & Srivastava, R. (2017). Graphene quantum dots for cell proliferation, nucleus imaging, and photoluminescent sensing applications. *Scientific Report, 7*, 1–16. https://doi.org/10.1038/s41598-017-16025-w.
33. Sun, Y. P., Zhou, B., Lin, Y., Wang, W., Fernando, K. A. S., Pathak, P., Meziani, M. J., Harruff, B. A., Wang, X., Wang, H., Luo, P. G., Yang, H., Kose, M. E., Chen, B., Veca, L. M., & Xie, S. Y. (2006). Quantum-sized carbon dots for bright and colorful photoluminescence. *Journal of the American Chemical Society, 128*, 7756–7757. https://doi.org/10.1021/ja062677d.
34. Chen, N. T., Cheng, S. H., Souris, J. S., Chen, C. T., Mou, C. Y., & Lo, L. W. (2013). Theranostic applications of mesoporous silica nanoparticles and their organic/inorganic hybrids. *Journal of Materials Chemistry B, 1*, 3128–3135. https://doi.org/10.1039/c3tb20249f.
35. Hu, J. J., Liu, L. H., Li, Z. Y., Zhuo, R. X., & Zhang, X. Z. (2016). MMP-responsive theranostic nanoplatform based on mesoporous silica nanoparticles for tumor imaging and targeted drug delivery. *Journal of Materials Chemistry B, 4*, 1932–1940. https://doi.org/10.1039/c5tb02490k.
36. Bharti, C., Gulati, N., Nagaich, U., & Pal, A. (2015). Mesoporous silica nanoparticles in target drug delivery system: a review. *International Journal of Pharmaceutical Investigation, 5*, 124. https://doi.org/10.4103/2230-973x.160844.
37. Nakamura, T., Sugihara, F., Matsushita, H., Yoshioka, Y., Mizukami, S., & Kikuchi, K. (2015). Mesoporous silica nanoparticles for 19F magnetic resonance imaging, fluorescence imaging, and drug delivery. *Chemical Science, 6*, 1986–1990. https://doi.org/10.1039/c4sc03549f.
38. Iqbal, M. Z., Ma, X., Chen, T., Zhang, L., Ren, W., Xiang, L., & Wu, A. (2015). Silica-coated super-paramagnetic iron oxide nanoparticles (SPIONPs): a new type contrast agent of T1 magnetic resonance imaging (MRI). *Journal of Materials Chemistry B, 3*, 5172–5181. https://doi.org/10.1039/c5tb00300h.
39. Carniato, F., Tei, L., & Botta, M. (2018). Gd-based mesoporous silica nanoparticles as MRI probes. *European Journal of Inorganic Chemistry, 2018*, 4936–4954. https://doi.org/10.1002/ejic.201801039.
40. Norregaard, K., Jørgensen, J. T., Simón, M., Melander, F., Kristensen, L. K., Bendix, P. M., Andresen, T. L., Oddershede, L. B., & Kjaer, A. (2017). 18F-FDG PET/CT-based early treatment response evaluation of nanoparticle-assisted photothermal cancer therapy. *PLoS One, 12*, e0177997. https://doi.org/10.1371/journal.pone.0177997.
41. Portilho, F. L., Helal-Neto, E., Cabezas, S. S., Pinto, S. R., dos Santos, S. N., Pozzo, L., Sancenón, F., Martínez-Máñez, R., & Santos-Oliveira, R. (2018). Magnetic core mesoporous

silica nanoparticles doped with dacarbazine and labelled with 99mTc for early and differential detection of metastatic melanoma by single photon emission computed tomography. *Artificial Cells, Nanomedicine, and Biotechnology, 46*, 1080–1087. https://doi.org/10.1080/21691401.2018.1443941.

42. Shi, S., Chen, F., Goel, S., Graves, S. A., Luo, H., Theuer, C. P., Engle, J. W., & Cai, W. (2018). In vivo tumor-targeted dual-modality PET/optical imaging with a yolk/Shell-structured silica nanosystem. *Nano-Micro Letters, 10*, 1–11. https://doi.org/10.1007/s40820-018-0216-2.
43. Caltagirone, C., Bettoschi, A., Garau, A., & Montis, R. (2015). Silica-based nanoparticles: a versatile tool for the development of efficient imaging agents. *Chemical Society Reviews, 44*, 4645–4671. https://doi.org/10.1039/c4cs00270a.
44. Accomasso, L., Rocchietti, E. C., Raimondo, S., Catalano, F., Alberto, G., Giannitti, A., Minieri, V., Turinetto, V., Orlando, L., Saviozzi, S., Caputo, G., Geuna, S., Martra, G., & Giachino, C. (2012). Fluorescent silica nanoparticles improve optical imaging of stem cells allowing direct discrimination between live and early-stage apoptotic cells. *Small, 8*, 3192–3200. https://doi.org/10.1002/smll.201200882.
45. Liberman, A., Mendez, N., Trogler, W. C., & Kummel, A. C. (2014). Synthesis and surface functionalization of silica nanoparticles for nanomedicine. *Surface Science Reports, 69*, 132–158. https://doi.org/10.1016/j.surfrep.2014.07.001.
46. Prasad, R., Aiyer, S., Chauhan, D. S., Srivastava, R., & Selvaraj, K. (2016). Bioresponsive carbon nano-gated multifunctional mesoporous silica for cancer theranostics. *Nanoscale, 8*, 4537–4546. https://doi.org/10.1039/c5nr06756a.
47. Chan, W. C. W., Maxwell, D. J., Gao, X., Bailey, R. E., Han, M., & Nie, S. (2002). Luminescent quantum dots for multiplexed biological detection and imaging. *Current Opinion in Biotechnology, 13*, 40–46. https://doi.org/10.1016/S0958-1669(02)00282-3.
48. Medintz, I. L., Uyeda, H. T., Goldman, E. R., & Mattoussi, H. (2005). Quantum dot bioconjugates for imaging, labelling and sensing. *Nature Materials, 4*, 435–446. https://doi.org/10.1038/nmat1390.
49. Gao, X., Cui, Y., Levenson, R. M., Chung, L. W. K., & Nie, S. (2004). In vivo cancer targeting and imaging with semiconductor quantum dots. *Nature Biotechnology, 22*, 969–976. https://doi.org/10.1038/nbt994.
50. Sanford, S., Voura, E., Jaiswal, J., & Mattoussi, H. (2004). Spectral imaging of quantum dots in mice. *Journal of Histochemistry and Cytochemistry, 52*, S19–S19.
51. Ali, I., Alsehli, M., Scotti, L., Scotti, M. T., Tsai, S. T., Yu, R. S., Fa Hsieh, M., & Chen, J. C. (2020). Progress in polymeric nano-medicines for theranostic cancer treatment. *Polymers (Basel), 12*, 598. https://doi.org/10.3390/polym12030598.
52. Thomas, A., Appidi, T., Jogdand, A. B., Ghar, S., Subramaniyam, K., Prabusankar, G., Mohanty, J. R., & Rengan, A. K. (2020). Facile synthesis of fluorescent polymer encapsulated metal (PoeM) nanoparticles for imaging and therapeutic applications. *ACS Applied Polymer Materials, 2*, 1388–1397. https://doi.org/10.1021/acsapm.0c00017.
53. Pemmaraju, D., Appidi, T., Minhas, G., Singh, S. P., Khan, N., Pal, M., Srivastava, R., & Rengan, A. K. (2018). Chlorophyll rich biomolecular fraction of A. cadamba loaded into polymeric nanosystem coupled with photothermal therapy: a synergistic approach for cancer theranostics. *International Journal of Biological Macromolecules, 110*, 383–391. https://doi.org/10.1016/j.ijbiomac.2017.09.084.
54. Li, J., Jiang, R., Wang, Q., Li, X., Hu, X., Yuan, Y., Lu, X., Wang, W., Huang, W., & Fan, Q. (2019). Semiconducting polymer nanotheranostics for NIR-II/photoacoustic imaging-guided photothermal initiated nitric oxide/photothermal therapy. *Biomaterials, 217*, 119304. https://doi.org/10.1016/j.biomaterials.2019.119304.
55. Oerlemans, C., Bult, W., Bos, M., Storm, G., Nijsen, J. F. W., & Hennink, W. E. (2010). Polymeric micelles in anticancer therapy: targeting, imaging and triggered release. *Pharmaceutical Research, 27*, 2569–2589. https://doi.org/10.1007/s11095-010-0233-4.
56. Liu, T., Li, X., Qian, Y., Hu, X., & Liu, S. (2012). Multifunctional pH-disintegrable micellar nanoparticles of asymmetrically functionalized β-cyclodextrin-based star copolymer covalently

conjugated with doxorubicin and DOTA-Gd moieties. *Biomaterials, 33*, 2521–2531. https://doi.org/10.1016/j.biomaterials.2011.12.013.
57. Li, S., Goins, B., Zhang, L., & Bao, A. (2012). Novel multifunctional theranostic liposome drug delivery system: construction, characterization, and multimodality MR, near-infrared fluorescent, and nuclear imaging. *Bioconjugate Chemistry, 23*, 1322–1332. https://doi.org/10.1021/bc300175d.
58. Lee, W., & Im, H. J. (2010). Theranostics based on liposome: looking back and forward. *Nuclear Medicine and Molecular Imaging, 53*(2019), 242–246. https://doi.org/10.1007/s13139-019-00603-z.
59. Chang, H.-I., & Cheng, M.-Y. (2012). Clinically-proven liposome-based drug delivery: formulation, characterization and therapeutic efficacy. *Journal of Nanomedicine and Biotherapeutic Discovery, 01*, 1–8. https://doi.org/10.4172/scientificreports.195.
60. James, N. D., Coker, R. J., Tomlinson, D., Harris, J. R. W., Gompels, M., Pinching, A. J., & Stewart, J. S. W. (1994). Liposomal doxorubicin (Doxil): an effective new treatment for Kaposi's sarcoma in AIDS. *Clinical Oncology, 6*, 294–296. https://doi.org/10.1016/S0936-6555(05)80269-9.
61. Gibbs, D. D., Pyle, L., Allen, M., Vaughan, M., Webb, A., Johnston, S. R. D., & Gore, M. E. (2002). A phase I dose-finding study of a combination of pegylated liposomal doxorubicin (Doxil), carboplatin and paclitaxel in ovarian cancer. *British Journal of Cancer, 86*, 1379–1384. https://doi.org/10.1038/sj.bjc.6600250.
62. Lin, C. H., Chen, C. H., Lin, Z. C., & Fang, J. Y. (2017). Recent advances in oral delivery of drugs and bioactive natural products using solid lipid nanoparticles as the carriers. *Journal of Food and Drug Analysis, 25*, 219–234. https://doi.org/10.1016/j.jfda.2017.02.001.
63. Adhikari, P., Pal, P., Das, A. K., Ray, S., Bhattacharjee, A., & Mazumder, B. (2017). Nano lipid-drug conjugate: an integrated review. *International Journal of Pharmaceutics, 529*, 629–641. https://doi.org/10.1016/j.ijpharm.2017.07.039.
64. May, J. P., & Li, S. (2013). Hyperthermia-induced drug targeting. *Expert Opinion on Drug Delivery, 10*, 511–527.
65. Qin, L., Wang, C. Z., Fan, H. J., Zhang, C. J., Zhang, H. W., Lv, M. H., & De Cui, S. (2014). A dual-targeting liposome conjugated with transferrin and arginine-glycine-aspartic acid peptide for glioma-targeting therapy. *Oncology Letters, 8*, 2000–2006. https://doi.org/10.3892/ol.2014.2449.
66. Appidi, T., Pemmaraju, D. B., Khan, R. A., Alvi, S. B., Srivastava, R., Pal, M., Khan, N., & Rengan, A. K. (2020). Light-triggered selective ROS-dependent autophagy by bioactive nanoliposomes for efficient cancer theranostics. *Nanoscale, 12*, 2028–2039. https://doi.org/10.1039/c9nr05211a.
67. Brown, S. B., Brown, E. A., & Walker, I. (2004). The present and future role of photodynamic therapy in cancer treatment. *Lancet Oncology, 5*, 497–508. https://doi.org/10.1016/S1470-2045(04)01529-3.
68. Babilas, P., & Szeimies, R. M. (2011). Photodynamic therapy. *Laser and IPL Technology in Dermatology and Aesthetic Medicine, 90*, 357–375. https://doi.org/10.1007/978-3-642-03438-1_28.
69. Kunzi-Rapp, K. (2015). Photodynamic therapy in dermatology. *Photonics & Lasers in Medicine, 4*, 378–379. https://doi.org/10.1201/b15582-45.
70. Bressler, N. M., & Bressler, S. B. (2000). Photodynamic therapy with verteporfin (visudyne): impact on ophthalmology and visual sciences. *Investigative Ophthalmology and Visual Science, 41*, 624–628.
71. Jin, C. S., Lovell, J. F., Chen, J., & Zheng, G. (2013). Ablation of hypoxic tumors with dose-equivalent photothermal, but not photodynamic, therapy using a nanostructured porphyrin assembly. *ACS Nano, 7*, 2541–2550. https://doi.org/10.1021/nn3058642.
72. Huang, X., El-Sayed, I. H., Qian, W., & El-Sayed, M. A. (2006). Cancer cell imaging and photothermal therapy in the near-infrared region by using gold nanorods. *Journal of the American Chemical Society, 128*, 2115–2120. https://doi.org/10.1021/ja057254a.

73. Huang, X., Jain, P. K., El-Sayed, I. H., & El-Sayed, M. A. (2008). Plasmonic photothermal therapy (PPTT) using gold nanoparticles. *Lasers in Medical Science, 23*, 217–228. https://doi.org/10.1007/s10103-007-0470-x.
74. Kumar, A., Roy, S., Srivastava, A., Naikwade, M. M., Purohit, B., Mahato, K., Naidu, V. G. M., & Chandra, P. (2019). *Nanotherapeutics*. Amsterdam: Elsevier. https://doi.org/10.1016/B978-0-12-818823-1.00010-7.
75. Curry, T., Kopelman, R., Shilo, M., & Popovtzer, R. (2014). Multifunctional theranostic gold nanoparticles for targeted CT imaging and photothermal therapy. *Contrast Media & Molecular Imaging, 9*, 53–61. https://doi.org/10.1002/cmmi.1563.
76. Van Schooneveld, M. M., Cormode, D. P., Koole, R., Van Wijngaarden, J. T., Calcagno, C., Skajaa, T., Hilhorst, J., 'T Hart, D. C., Fayad, Z. A., Mulder, W. J. M., & Meijerink, A. (2010). A fluorescent, paramagnetic and PEGylated gold/silica nanoparticle for MRI, CT and fluorescence imaging. *Contrast Media & Molecular Imaging, 5*, 231–236. https://doi.org/10.1002/cmmi.376.
77. Janib, S. M., Moses, A. S., & MacKay, J. A. (2010). Imaging and drug delivery using theranostic nanoparticles. *Advanced Drug Delivery Reviews, 62*, 1052–1063. https://doi.org/10.1016/j.addr.2010.08.004.
78. Mahato, K., Maurya, P. K., & Chandra, P. (2018). Fundamentals and commercial aspects of nanobiosensors in point-of-care clinical diagnostics. *3 Biotech, 8*, 149. https://doi.org/10.1007/s13205-018-1148-8.
79. Purohit, B., Kumar, A., Mahato, K., & Chandra, P. (2020). Smartphone-assisted personalized diagnostic devices and wearable sensors. *Current Opinion in Biomedical Engineering, 13*, 42–50. https://doi.org/10.1016/j.cobme.2019.08.015.
80. Purohit, B., Vernekar, P. R., Shetti, N. P., & Chandra, P. (2020). Biosensor nanoengineering: design, operation, and implementation for biomolecular analysis. *Sense Internationa, 1*, 100040. https://doi.org/10.1016/j.sintl.2020.100040.
81. Liu, X., Zhang, Y., Wang, Y., Zhu, W., Li, G., Ma, X., Zhang, Y., Chen, S., Tiwari, S., Shi, K., Zhang, S., Fan, H. M., Zhao, Y. X., & Liang, X. J. (2020). Comprehensive understanding of magnetic hyperthermia for improving antitumor therapeutic efficacy. *Theranostics, 10*, 3793–3815. https://doi.org/10.7150/thno.40805.
82. Maier-Hauff, K., Ulrich, F., Nestler, D., Niehoff, H., Wust, P., Thiesen, B., Orawa, H., Budach, V., & Jordan, A. (2011). Efficacy and safety of intratumoral thermotherapy using magnetic iron-oxide nanoparticles combined with external beam radiotherapy on patients with recurrent glioblastoma multiforme. *Journal of Neuro-Oncology, 103*, 317–324. https://doi.org/10.1007/s11060-010-0389-0.
83. Chandrasekharan, P., Tay, Z. W., Hensley, D., Zhou, X. Y., Fung, B. K. L., Colson, C., Lu, Y., Fellows, B. D., Huynh, Q., Saayujya, C., Yu, E., Orendorff, R., Zheng, B., Goodwill, P., Rinaldi, C., & Conolly, S. (2020). Using magnetic particle imaging systems to localize and guide magnetic hyperthermia treatment: tracers, hardware, and future medical applications. *Theranostics, 10*, 2965–2981. https://doi.org/10.7150/thno.40858.
84. Fitzgerald, K. T., Holladay, C. A., McCarthy, C., Power, K. A., Pandit, A., & Gallagher, W. M. (2011). Standardization of models and methods used to assess nanoparticles in cardiovascular applications. *Small, 7*, 705–717. https://doi.org/10.1002/smll.201001347.
85. Kool, M. E., Cappendijk, V. C., Cleutjens, K. B. J. M., Kessels, A. G. H., Kitslaar, P. J. E. H. M., Borgers, M., Frederik, P. M., Daemen, M. J. A. P., & Van Engelshoven, J. M. A. (2003). Accumulation of ultrasmall superparamagnetic particles of iron oxide in human atherosclerotic plaques can be detected by in vivo magnetic resonance imaging. *Circulation, 107*, 2453–2458. https://doi.org/10.1161/01.CIR.0000068315.98705.CC.
86. Wang, X., Gkanatsas, Y., Palasubramaniam, J., Hohmann, J. D., Chen, Y. C., Lim, B., Hagemeyer, C. E., & Peter, K. (2016). Thrombus-targeted theranostic microbubbles: a new technology towards concurrent rapid ultrasound diagnosis and bleeding-free fibrinolytic treatment of thrombosis. *Theranostics, 6*, 726–738. https://doi.org/10.7150/thno.14514.

87. Alam, M. I., Beg, S., Samad, A., Baboota, S., Kohli, K., Ali, J., Ahuja, A., & Akbar, M. (2010). Strategy for effective brain drug delivery. *European Journal of Pharmaceutical Sciences, 40*, 385–403. https://doi.org/10.1016/j.ejps.2010.05.003.
88. Nordberg, A., Rinne, J. O., Kadir, A., & Lngström, B. (2010). The use of PET in Alzheimer disease. *Nature Reviews Neurology, 6*, 78–87. https://doi.org/10.1038/nrneurol.2009.217.
89. Singh, D., Dilnawaz, F., & Sahoo, S. K. (2020). Challenges of moving theranostic nanomedicine into the clinic. *Nanomedicine, 15*, 111–114. https://doi.org/10.2217/nnm-2019-0401.
90. Muthu, M. S., & Wilson, B. (2012). Challenges posed by the scale-up of nanomedicines. *Nanomedicine, 7*, 307–309. https://doi.org/10.2217/nnm.12.3.
91. Wong, X. Y., Sena-Torralba, A., Álvarez-Diduk, R., Muthoosamy, K., & Merkoçi, A. (2020). Nanomaterials for nanotheranostics: tuning their properties according to disease needs. *ACS Nano, 14*, 2585–2627. https://doi.org/10.1021/acsnano.9b08133.

Chapter 14
Nanotheranostics: Nanoparticles Applications, Perspectives, and Challenges

Atul Kumar Ojha, Ragavi Rajasekaran, Anurag Kumar Pandey, Abir Dutta, Venkata Sundeep Seesala, Subrata K. Das, Koel Chaudhury, and Santanu Dhara

14.1 Introduction

Diagnostic and therapeutic aspects in recent times are emerging as a key area of research in the field of healthcare. Smart health care requires a single platform where a combination of therapeutic and diagnostic strategies comes together for personalized medicine [1]. With the advancement of nanotechnology, theranostics is attributing to precision medical treatment [2]. Theranostics has changed conventional disease treatment into modern translational medicine through integrated practice approaches. These approaches enable one to evaluate the actual therapeutic drug position at the targeted site and its expression [3]. Effectiveness of theranostic drug is dependent upon heterogeneity at cell specified target and is not recommended for a broader range of patients due to its nature of personalized treatment [4]. As of December 2016, according to World Health Organization, 40.5 million total number of deaths were reported out of 56.9 million worldwide deaths for non-communicable diseases (NCDs). Among NCDs, CVD, cancer, diabetes, and chronic lung diseases were four leading life style diseases causing 79% of the total mortality.

A. K. Ojha
Biomaterials and Tissue Engineering Laboratory, School of Medical Science and Technology (SMST), Indian Institute of Technology Kharagpur, Kharagpur, India

Clinical Biomarkers Research Laboratory, School of Medical Science and Technology (SMST), Indian Institute of Technology Kharagpur, Kharagpur, India

R. Rajasekaran · A. K. Pandey · A. Dutta · V. S. Seesala · S. K. Das · S. Dhara (✉)
Biomaterials and Tissue Engineering Laboratory, School of Medical Science and Technology (SMST), Indian Institute of Technology Kharagpur, Kharagpur, India
e-mail: sdhara@smst.iitkgp.ac.in

K. Chaudhury
Clinical Biomarkers Research Laboratory, School of Medical Science and Technology (SMST), Indian Institute of Technology Kharagpur, Kharagpur, India

V. Borse et al. (eds.), *BioSensing, Theranostics, and Medical Devices*,
https://doi.org/10.1007/978-981-16-2782-8_14

Interestingly it can be noted that in the past decade, the emphasis was given to nanotheranostics for early diagnosis and treatment. Nanoparticles play a vital role in theranostics is the use of nanoparticles; its wide applications in therapeutic areas of healthcare. Furthermore, utilizing the physiochemical properties of nanoparticles give different advantages in various fields like environment, energy harvesting, drugs, manufacturing, and biomedical applications [5, 6].

Most of the reported scientific documents have discussed theranostics applications in the field of cancer and its more extensive applications. Few of the articles have considered the nanotechnological applications in cancer. However, the gap persists concerning the compilation of such claims in single documents—the same collection and recent updates along with critical perspectives have been highlighted in this chapter. Here, in this book chapter, we have tried to focus on different nanotheranostics approaches with applications ranging from CVD, cancer, neurodegenerative diseases (NDD), antimicrobial resistance, and some orthopedic diseases.

14.2 Approaches Towards Nanotheranostics

Different platforms are being reported in the field of nanotheranostics for biomedical applications. These range from the use of polymers, colloids, emulsions, liposomes, metallic nanoparticles, inorganic nanoparticles, and carbon nanotubes [7]. The use of different nanoparticles generally contributes to a lot of confusion for authors to choose the best available platform for theranostics. Here, we have simplified and categorized different approaches based on different synergistic approaches (Fig. 14.1.) We categorized theranostics platform into four easily recognizable divisions, namely solid, liquid, dry, and biomolecular approaches. These are further subdivided into 11 categories for understanding their applications.

14.2.1 Solid/Particles Approach

14.2.1.1 Quantum Dots

QDs are defined as three dimensional confined nanocrystal having the size in range 2–10 nm with fluorescence emission capability on excitation with light sources. Nanocrystal might be composed of either semiconductor or carbonaceous materials that give birth to semiconductor quantum dot (SQDs) and carbon quantum dot (CQDs)/graphene quantum dot (GQD). Based on descending toxicity in bio-applications, QDs are further divided into different groups. They are labeled as cadmium (Cd) and lead (Pb) containing II–VI groups >Cd and Pb free III–V and I–III–VI groups >CQDs IV group, materials of the periodic table [8, 9]. Their optical and electronics properties like fluorescence spectra, band-gap could be altered by varying sizes and composition of selected materials, respectively. Issues like

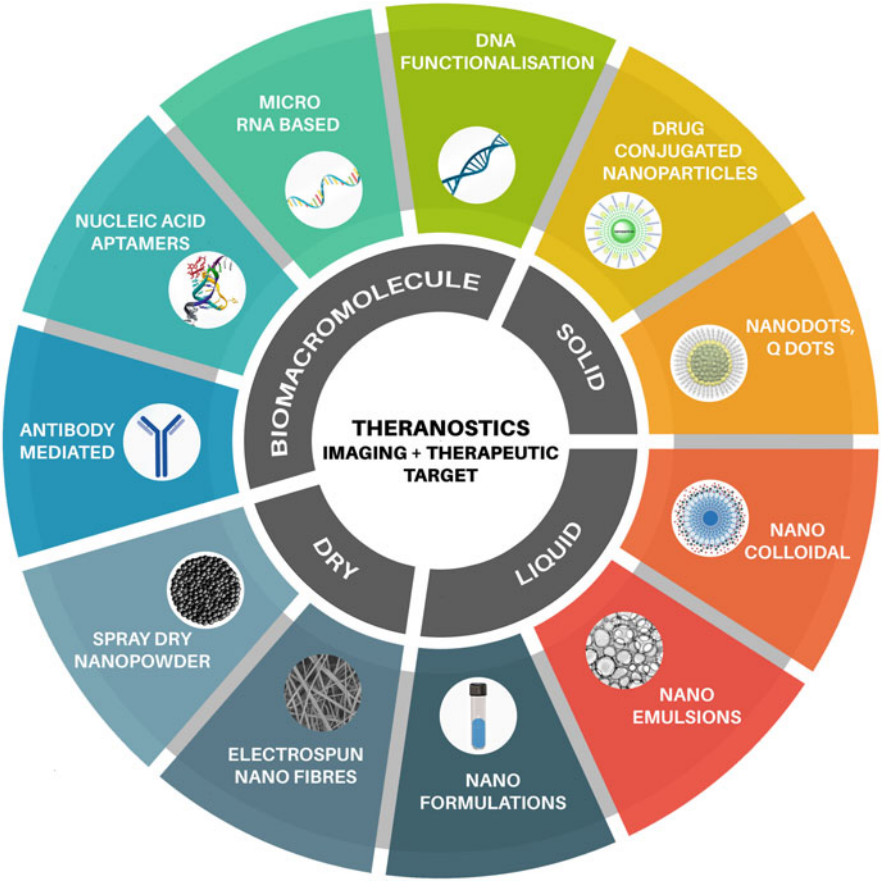

Fig. 14.1 Nanotheranostics: solid, liquid, dry, and biomolecule based nanosystem for management of bioimaging, cardiovascular diseases, cancer, and antimicrobial resistance

aqueous solubility and toxicity limit their use in biomedical applications. Surface functionalization, passivation are two essential modifications that enable them to rectify the above-mentioned issues [10].

SQDs have gained more attention in biological applications due to their high quantum yield, size-tunable light emission, and excellent chemical and photostability over organic dye. The first bio-applicable SQDs were reported in 1988 for *in vitro* imaging of cancer cell [11, 12]. Moreover, a lot of effort has been made for SQD to explore its capability in various bio-applications like imaging, early-stage cancer diagnosis, drug delivery, and photodynamic therapy (PDT), to name a few [13]. The discovery of CQDs dots by Xu.et al. (in 2004) brought a

revolution in the field of biology due to its additional property of low toxicity and aqueous solubility over SQDs with/without any further surface modifications [14].

Synthesis and Modification of SQDs and CQDs for Bio-Applications

Synthesis and modification of SQDs in comparison to CQDs are more complicated due to its possible integration in organic solutions, making them insoluble in water. SQDs core can be passivated with the wide band-gap semiconductor or with surfactant/ligands to overcome challenges. There are numerous examples like 3-mercaptopropionic acid (MPA), mercaptoacetic acid, thioglycolic acid (TGA), polysaccharide copolymers/thioglycolic acid, cysteamine or polyethylene glycol (PEG), with which passivation happens. It promotes aqueous solubility, core stability, long-wavelength fluorescence emission, ease bio-conjugation, and prevents core materials from leaching [15]. As CQDs have low toxicity, efficient water dispersibility, and good fluorescent properties, they require no additional passivation step. The smallest size and large surface area of SQDs and CQDs with proper functional groups help to tag biomolecules such as peptides, antibodies, and proteins to form bioconjugated-QDs (B-QDs). These B-QDs are very potent as nanotheranostics in biomedical research fields like *in vivo* and *in vitro* imaging, diagnostics, drug delivery, and photodynamic therapy application.

14.2.2 Liquid Approach

14.2.2.1 Liquid Metal Approach

Recently liquid metal approach drawn much attention owing to its theranostics possibility [16]. Despite its genesis in nuclear medicine decades ago, the domain is newly emerging for detailed research due to several disadvantages with traditional approaches. The incapability of quick diagnosis and conventional techniques used for both diagnostics and therapeutics for cancer is still a serious threat. In this regard, the metals are explored in forms of radioactive nanoparticles for imaging as well as detection purposes (as the core of the system) and an outer shell composed by organic polymers or drugs for further dealing with the environment within the body while serving its purpose of protection of the core as well as delivering the targeted drugs. An avenue opening work was done by Rosenberg and his team in 1965, leading to the discovery of Cisplatin as a positive inorganic metal moiety for targeting cancer-affected areas. In terms of detection purposes, extensive efforts have been devoted towards developing targeted near-infrared and surface enhanced Raman scattering imaging probes for quick and precise diagnosis of tiniest possible affected areas under scan [17]. However, the appropriate distribution of the drugs

promptly into the body is also another challenge for these liquid-based metal approach in theranostics.

14.2.3 Dry Approach

Recently, the nanotheranostic platform is enabled and demonstrated to be a promising smart technique for diagnosis, therapeutic, monitoring, and plan for the secondary treatments, especially for personalized and precision medicine for cancer theranostic (Fig. 14.2) [18–20]. Such rapidly evolving technologies along with dry approaches such as electrospun nanofibers, spray nanopowder, spray dry nanopowder emerged as a promising tool for theranostics [21].

14.2.3.1 Electrospun Nanofibres

Electrospun nanofiber occurred as an advanced nanostructure in biosensors and therapeutic applications due to its various benefits such as cost-effectiveness, high surface area to volume, tailorable nanostructure, porosity, and biocompatibility [22, 23]. Electrospun sheets could be placed in the body through different ways such as oral, sublingual, rectal, buccal, topical, ocular, etc., due to its high surface-to-volume ratio and high drug loading capability makes the process superior as a drug carrier.

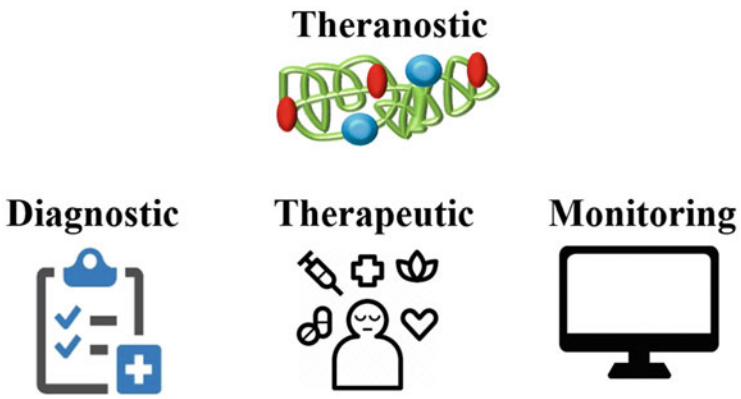

Fig. 14.2 Schematic image of nanotheranotics for health care applications

14.2.4 Biomacromolecule Based Approaches

14.2.4.1 Functionalized DNA with Nanoparticle

Gene therapy has been considered as the direct passing of hereditary elements of genes to the building blocks of our body, i.e., cells and tissues for treatment of those diseases with defective gene expression [24–26]. This approach involves the introduction of a therapeutic gene inside the cells followed by RNA expression and translation of deficient protein in other conditions, and the therapeutic gene can inhibit the RNA expression of defective genes. These therapeutic genes are comprised of mainly nucleic acids, antisense oligonucleotides (ASO), small interfering RNAs (siRNAs), and microRNA (miRNA), which enable replacement of a damaged gene or inhibition of undesired genes [27].

A suitable carrier/vector can effectively bind with negatively charged nucleic acid, cross through the negatively charged cell membrane to desire destination facilitating *endosomal escape,* provide protection against various exo or endonuclease, and release it in the cytoplasm or in nucleus. Some nucleic acids are chemically modified for high cellular uptake, nuclease resistance, and efficient binding capacity with the target. Two significant types of vector for therapeutic gene delivery, namely viral and nonviral vectors, are currently under clinical trials. However, owing to elevated transfection efficiency of viral vectors, the nonviral carriers have advantages like easy to prepare, low production cost, less immunogenic, manipulation of polymer properties, no potential of virus recombination. The nonverbal vector can be organic (lipid-mediated, polymer-based) and inorganic (magnetic nanoparticle, quantum dot, carbon nanotubes, gold nanoparticle) [28].

Liposome (Lipofectamine 2000/3000, Lipofectin and Lipofectace) has been successfully used to deliver DNA in culture media, in animals, and in patients enrolled in phase I and II clinical trials [29, 30]. Therapeutic nucleic acids with cationic liposomes target the vasculature of tumors selectively as antiangiogenic therapy [31]. Liposomes are also used as carriers for CRISPR/Cas9 delivery [32]. *In vitro* cholesterol-rich, lipid-mediated nanoparticles are also used for the transfection of Cas9/sgRNA plasmids [33]. DOTAP: cholesterol nanoparticles encapsulating a TUSC2 expression plasmid (DOTAP: chol-TUSC2) showed an efficient transfer ofTUSC2 gene into lung cancer cells and evidenced as anti-cancer therapy, and phase I and phase II trial along with erlotinib has been completed. Polyethylenimine as polymer-based systems has been established as an excellent avenue for the successful facilitation of gene delivery to the lung [34, 35].

The severe side effect of chemotherapeutic agents is a significant problem in cancer treatments. An intra-arterial chemofilter device based on covalently attached genomic DNA/iron oxide particle combination has been developed to capture chemotherapeutic agents (doxorubicin, cisplatin, and epirubicin) from the bloodstream [36]. Rapid and sensitive nucleic acid testing from complex biological samples are essential in clinical diagnostics. Virus specific reporter probes (oligonucleotides) coupled with POEGMA-N3-co-OEGMA-OH polymer brushes have

been developed to identify target DNA by direct hybridization in point-of-care settings as amplification-free nucleic acid testing, saving assay time and resource [37].

14.2.4.2 Antisense Oligonucleotides (ASOs)

In universal gene expression DNA encode messenger RNA (mRNA) and finally transcribe into protein. As altered expression affects disease, recognition of disease gene or its encoded mRNA has excellent potential for drug development. Therapeutic antisense oligonucleotides (ASOs) ranging from 18 to 30 bp single-stranded DNA can bind to mRNA target by recognizing complementary base pairing. ASOs can modify target mRNA expression either by altering splice switching or recruiting RNA cleaving enzyme, RNase H leading to target degradation. The mode of ASO action is based on its chemical modification and binding location. The modifications of oligos improve mainly nuclease resistance enhancing intercellular stability and specificity to target mRNA. Most of ASO modifications are phosphorothioate (PS) [38] in the phosphodiester bond. The high binding property of charged PS modifications to plasma protein in circulation is thought to be the accessibility to cells. ASO with 2'-O-alkyl modifications (MOE) of the ribose sugar has been developed as RNAse H-resistance, which is potentially utilized as Splice-switching ASOs. Recently, two ASO with MOE modification (nusinersen for spinal muscular atrophy and inotersen for familial amyloid polyneuropathy) got approval clinically by the FDA, and many others are in clinical trial.

Phosphoramidate morpholino-oligomer (PMO) is the most widely used modified ASO. Here, a neutral phosphorodiamidate linkage is replaced by negatively charged phosphodiester linkage, which increases target specificity and nuclease resistance. It has been popularly accepted approach for successful modification of splicing. Morpholino eteplirsen, a 30 base morpholino drug for the treatment of Duchene muscular dystrophy was approved by the FDA. PMO has reduced protein binding affinity that needs a proper carrier to deliver in vivo. Morpholinos conjugated with dendrimer (vivo morpholino) enhances cellular uptake [39]. Also, cyclic RGD peptide (cRGD) promoted morpholino-oligomer accumulation in CNV following tail vein injection in mouse [40].

Locked nucleic acid (LNA), a most biologically stable ASO, contains a 2'-O, 4'-C methylene bridge, and has been used for clinical and diagnostic purposes. Single-stranded LNA oligonucleotide has a superior efficacy of downregulating target mRNA *in vivo* as it has outstanding RNA binding affinity and specificity and resistance to enzymatic degradation. A series of LNA based drug candidates has been developed clinically against cancer and metabolic diseases [41]. LNA hybridization-ligation ECL ELISA was developed, aiming to detect and quantify siRNA therapeutics from biological sample [42].

14.2.4.3 Small RNA Mediated Therapeutics

Modulation of gene expressions employing small non-coding RNAs (ncRNAs) that do not code protein is an attractive domain for therapeutic development. Most popular classes of small ncRNAs are namely siRNAs, and micro-RNAs (miRNAs) have been reported for the treatment of various ailments like cancer and infections. Therapeutic approaches based on siRNA involve the introduction of a synthetic dsRNA (21–23 bp) into the target cells or organism, thereby showing the expression of a specific target mRNA to facilitate a gene silencing effect by the mechanism known as RNA interference (RNAi). siRNA-lipid based formulation is approved by the United States Food and Drug Administration (FDA) for human usage and commercially available as Onpattro™.

Surprisingly, it has been found that dsRNA targeting gene promoters can also activate gene expression, a mechanism termed "RNA activation" (RNAa). RNAa can be used as a therapeutic approach to restore loss of function, which is associated with a pathological condition [43]. Micro-RNAs are approximately 20–25 nucleotides in length, generally bind to the 3'-UTR of target mRNAs and regulate expression of multiple genes either by blocking the translation or by degrading the mRNA directly. The miRNA-based treatment involves either by restoring using the introduction of synthetic double-stranded miRNAs/miRNA overexpression vector [44] or repressing miRNAs expression using synthetic modified anti-miR oligonucleotides. The chemical modifications include phosphorothioates containing oligonucleotides [45], MOE oligonucleotides [46], locked nucleic acids (LNA) [47], peptide nucleic acids [48], other changes [49]. Unusual expression of miRNA in various diseases, including cancer, neurodegenerative disorders, and CVD makes it for the development of biomarkers in diagnostics and treatment [50].

Unmodified miRNAs conjugated with cysteamine-functionalized gold nanoparticles (AuNPs) were delivered in cancer cells showing the highest payload, lowest toxicity, fastest endosomal escape, and increased half-lives [51]. Nanoparticles AuNP-miR-145 in prostate and breast cancer [52], AuNP-miR-375 in hepato-carcinoma [53], AuNP-miR-29b in myeloid cell leukemia [54] have been studied as higher cellular accessibility of miRNA and the anti-cancerous activity.

14.3 Applications

14.3.1 Quantum Dots

Nowadays, QDs are being used in various applied medical and theranostics field. These areas are very broad and here, we have summarized its applications briefly in areas like *in vivo* and *in vitro* imaging, diagnostics, drug delivery, and photodynamic therapy application (Fig. 14.3).

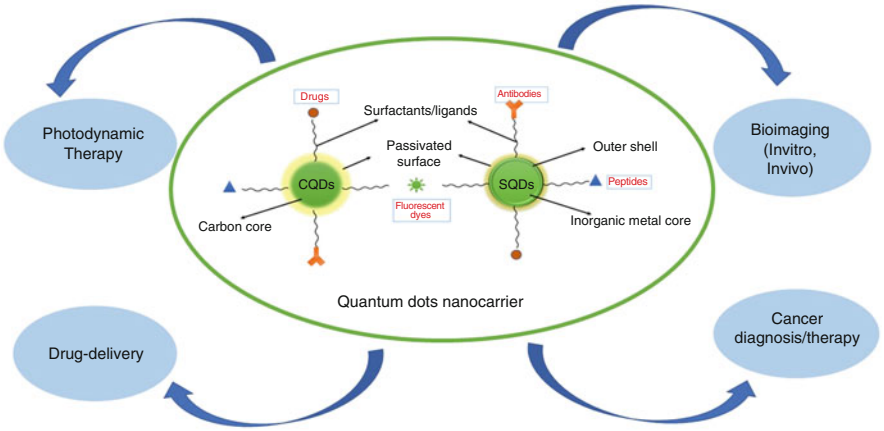

Fig. 14.3 The role of bio-conjugated quantum dots nanocarrier as multifunctional nanotheronastic agents

14.3.1.1 Bioconjugate-QDs (B-QDs) for Cancer Diagnostic

Cancer diagnosis helps to detect the location of the malignancy source and types of cells involved. Diagnosis of macroscopic tumors require noninvasive and invasive techniques such as computed tomography (CT), magnetic resonance imaging (MRI), positron emission tomography (PET) and immunohistochemistry (IHC), tissue biopsy, respectively. However, they are limited due to its lower specificity, sensitivity, inability to detect smaller tumors, and early-stage cancer. To overcome the above issues, B-SQDs and B-CQDs have emerged as an efficient alternate candidate due to its better properties over organic dye as a contrast agent in cancer imaging techniques. These B-SQD and B-CQDs with multiplex capability can be used as an imaging probe to label various cancer biomarkers (in vitro and in vivo) to identify and detect cancer at its nascent stage.

14.3.1.2 In Vitro Imaging

The first SQD-IHC base multiplex imaging probe was developed by Wu.et al. in 2003 [55]. Here, immunoglobulin and streptavidin based B-SQD were used to label breast cancer markers to detect two targets (HER2 and antigen in the nucleus) with a single excitation wavelength. Similar work was carried out to identify five different cellular markers concurrently on the same segment of formalin-fixed paraffin-embedded tissues [56] and six biomarkers for predicting the risk of colorectal cancer [57]. Furthermore, various general/specific cancer biomarkers were labeled using B-SQDs, B-CQDs in fixed cells and tissue for diagnosis of different cancers such as breast cancer [58, 59], gastro-intestinal [57, 60], brain cancer [61, 62], and ovarian

cancer [63, 64]. B-SQDs and B-CQDs also made adequate progress in the fix and live-cell imaging of various components in cells, cell surface receptors [65, 66], and intracellular target [67, 68].

14.3.1.3 In Vivo Imaging

Nanomaterials for in vivo imaging have to follow criteria of low toxicity, blood compatibility, biocompatibility, small hydrodynamic diameter, and rapid clearance from the body. SQDs and CQDs have been explored for in vivo imaging due to its EPR (enhanced permeability and retention) and targeted molecular imaging features. This allows leakage of nanocarrier from the circulatory system to tumor tissue, which further allows them for imaging and treatment of cancer. Some targeted and non-targeted SQDs also have been studied for vascular imaging [69, 70], sentinel lymph node (SLN) mapping [71], and cell trafficking [72], needed near-infrared imaging (NIR) QDs. Due to NIR emission capability, lower toxicity and rapid clearance from the body, Cd and Pb free QDs are widely used as compared to Cd and Pb based QDs. The high specificity of both quantum dots uptake by the reticuloendothelial system (RES) is necessary to maximize active targeting. So, SQDs and CQDs passivation with polyethylene glycol have seen improvement in its circulation time [72, 73]. However, limitation still exists due to larger hydrodynamic size due to passivation directly affecting clearance.

14.3.1.4 B-QDs for Drug Delivery

Targeted drug delivery has to gain more attention over the traditional chemotherapy approach due to its high specificity, better drug efficacy, and minimal side effect [74]. B-SQDs and B-CQDs loaded with drugs can be used as a dual nanocarrier system for cancer diagnosis and therapy on the same platform. Bagalkot et al. (in 2007) [75] reported aptamer-based B-QDs loaded with Dox (doxorubicin) drugs for cancer imaging, therapy, and drug delivery sensing on the prostate cancer cell. Here, drug release between QDs and Dox was observed. Moreover, SQDs and CQDs targeted bioconjugate of aptamer, peptide, antibody, and ligand loaded with the different drugs have been reported for diagnosis and therapy of various cancers [76, 77]. To overcome the issue of drug leakage and nonspecific delivery, hybrid quantum dot using polymers, proteins, polysaccharides, and lipids also has been studied [78]. CQDs have emerged as a substitute to semiconductor SQDs that suffer from some shortcomings like poor solubility, high toxicity, and insufficient loading capacity for drugs doxorubicin (DOX) and optical imaging ability.

14.3.1.5 Photodynamic Therapy (PDT)

Photodynamic therapy is a promising tool for cancer treatment by targeting photosensitizing material in diseased tissue followed by light irradiation, which produces reactive singlet oxygen species (ROS) that causes infected cell death without damaging healthy cells ideally. SQDs and CQDs both have great potential in PDT, either as photosensitizer [79, 80] or as carrier [81, 82]. But the remaining molecules after treatment create problems in daylight exposure, which can be overcome by enclosing dye molecules in porous nanoparticles [83]. The main issue that limits SQDs in PDT applications is toxicity due to the use of heavy metal. Recently, CQDs are used as a multifunctional therapeutic system for cancer [84].

14.3.2 Neurodegenerative Diseases (NDD)

14.3.2.1 Parkinson's Disease (PD)

Parkinson's disease (PD) is the second most abundant progressive neurodegenerative disease after the most prevalent AD (Alzheimer's disease) that is followed by a decrease in striatal dopamine (DA) level [85] in substantia nigra of midbrain. In the initial phase of PD, tremor, hypokinesia, rigidity and postural instability are the most apparent phenotypic symptoms, which further progresses into loss of motor control and nonmotor functions [86]. Pathophysiological studies have revealed that this disease arises due to intra-neuronal inclusions formation of Lewy bodies (LB) [87, 88]. LB are the result of misfolding, fibrillar aggregates and mismatched mutation of α-synuclein protein. α-synuclein is an important major component of LB which mediates the regulation of synaptic vesicle and dopamine secretion. PD happens due to LB accumulation and has no cure till now [89–91]. However, various therapeutic approaches have been recognized, ranging from levodopa, dopaminergic agonists, catechol-o-methyl transferase (COMT) inhibitors, monoamine oxidase (MAO-B inhibitors), and anticholinergic drugs [92, 93].

14.3.2.2 Theranostics Approaches for the Treatment of PD

Theranostics meditated treatment for neurodegenerative diseases constitutes of imaging of brain regions followed by therapeutic drug delivery to localized, targeted sites. The former approach mainly relies on single-photon emission computed tomography (SPECT), PET, CT, and MRI, which attributes to the diagnosis of brain lesions differentiating it from other diseases like cancer [94]. The latter therapeutic treatment includes the use of various drug conjugated NPs like nuclear medicine, Qdots, polymeric nanoparticles, metal NPs [95].

Specific nanoparticles, biomolecules, when targeted at specific sites, lead to disintegrate themselves, attributing to specific protein aggregates, which are the

leading cause of neurodegenerative diseases [96]. This process is accompanied by a variety of challenges that decide the theranostics personalized medicine approach for NDD. Issues like, removal of protective layers (lipid coating), degradation of drug conjugates, crossing blood-brain barrier are major prime concerns which are under research.

14.3.3 Electrospun Nanofibers Application

As shown in Fig. 14.4, the overview of nanocarrier or nanomedicine using electrospun sheet to treat cancer is briefly discussed in the following:

14.3.3.1 Cancer Cell Capture

Cancer is one of the major life-threatening diseases globally and required extremely challenging treatment strategies [97]. Various treatments and approaches are being established and studied for effective action, whereas nanomedicine using polymeric based nanocarriers proved to be active in both diagnosis and treatment [97, 98]. Nanofibers could effectively capture cancer cells due to its topographical

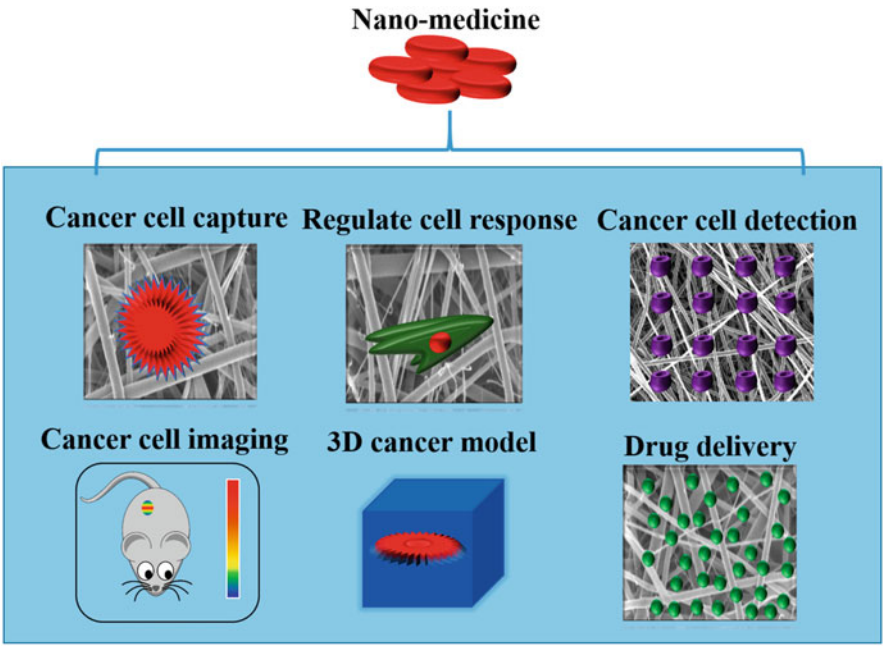

Fig. 14.4 Overview of nanomedicine on cancer theranostic research

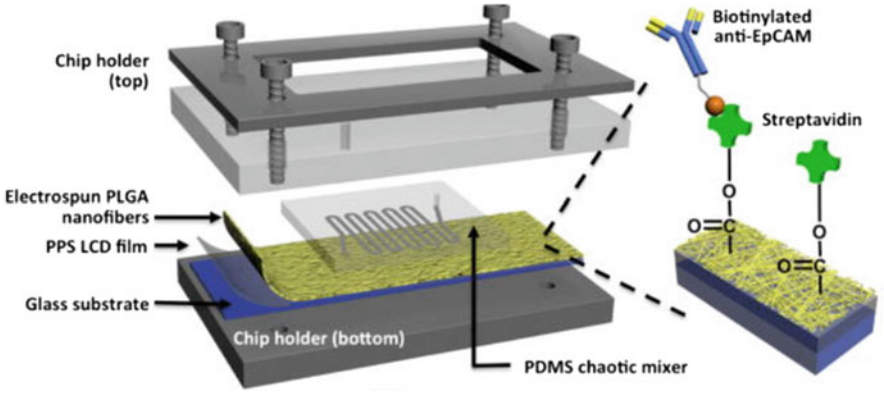

Fig. 14.5 Structure of embedded PLGA nanofiber in NanoVelcro Chip (Copyright © 2013 WILEY-VCH Verlag GmbH & Co. KGaA, Weinheim) [104]

features such as surface-immobilized targeting molecules by incubating the blood samples [99]. Both static or dynamic with various types of nanofiber enabled cancer cell capturing applications are available with multiple approaches such as polymer molecule-mediated conjugation, covalent conjugation, and biotin–avidin interaction. Further, to detect circulating tumor cells (CTCs), integrating nanofibers with microfluidic chip presented high sensitivity, rapid diagnosis, and improved efficiency [100].

Static Condition Fan et al. developed folic acid (FA) surface modified on poly (vinyl alcohol) (PVA)/polyethyleneimine (PEI) polymer electrospun nanofiber for cancer cell capturing [101]. HeLa or U87MG cancer cells were suspended with culture medium and incubated for 10–240 min. The cell counting, confocal microscopy, and scanning electron microscopy (SEM) observation proved effective capturing of up to 85.0% on the surface-modified nanofiber [101]. Zhao et al. fabricated electrospun cellulose acetate (CA) assembled with a bilayer of poly (diallyldimethylammonium chloride) (PDADMAC) and polyacrylic acid (PAA) to create a dendrimer modified with FA to capture cancer cells [102]. The KB cells were seeded and incubated for (10–60 min), whereas the result showed capture up to 82.7% at 60 min [102]. Zhang et al. fabricated electrospun TiO_2 nanofibers developed from titanium n-butoxide (TBT)/polyvinyl pyrrolidone (PVP) nanofibers [103]. The study was performed using HCT116, BGC823, HeLa, K562 cells and results showed promising with 45% of spiked HCT116 cells from artificial bold samples and CTCs ranging from 0 to 19 CTCs per 0.5 mL in colorectal and gastric cancer patients blood samples [103]. However, dynamic conditions could present a more rapid and effective detection of CTCs.

Dynamic Condition One of the most responsive and practical approaches for the dynamic condition of microfluidics is to capture and analyze the CTCs due to its size and amount of sample required [100]. Zhao et al. designed a NanoVelcro chip embedded with poly(lactic-co-glycolic acid) (PLGA) nanofiber [104]. As shown in

Fig. 14.5, the chip is composed of superimposed PDMS chaotic mixer chip and tri-layer of electrospun PLGA immobilized the anti-EpCAM followed by polyphenylene sulfide (PPS) laser capture microdissection (LCM) for segregating the seized CTCs from the scaffold using 355 nm UV laser source and glass substrate to support the layers. The study was conducted with blood samples at a different flow rate to capture CTCs from a prostate cancer patient, and at 0.5 mL $h^{-1}$the study showed 82% of efficiency [104]. Xu et al. fabricated PLGA nanofiber and surface functionalized by hyaluronic acid (HA) embedded in a microfluidic chamber to capture cancer cell. The study was conducted using CD44 receptor positive carcinoma cells with different flow rates, and the result showed effective capture over 80% at the flow rate 1.0 mL h^{-1} [105]. Compared to static conditions, the dynamic system proved to be more operative and rapid with less amount of sample. Further functionalized electrospun scaffolds could enhance efficacy with more effectiveness.

14.3.3.2 Regulate Cell Response

For monitoring the cancer cells towards the progression of the disease, understanding the phenotypic changes with the migration of metastasis cells plays a vital role [106]. Jain et al. studied the migration of MCF-7 and MDA-MB-231 cells on the different electrospun nanofiber orientations. The study showed metastatic cells migrated up to approximately (2–5) fold distance on aligned nanofibers than that of the randomly arranged fibers. Further, MDA-MB-231 showed to have more rate migration than that of MCF-7. Hence highly metastatic cells are more prone to migrate than the less metastatic cell. Saha *et al.* studied the nanofiber orientation on cancer cells to evaluate the effect of topographical cues on tumor development. The randomly oriented nanofiber mimics the native extracellular matrix (ECM), and the study conducted using H605, NMuMG, and MCF-7 cells resulted in elongated spindle-shaped cell morphology on aligned fibers whereas the flat stellar shape as evidenced on random orientation [107] of fibers. Conversely, the complication of in vivo or native system is difficult to understand, especially the native structure of ECM and other cues that trigger or control cancer cells. Further, such studies on chemoresistance, stimuli-responsive systems, and therapeutic strategy could be studied by relocating and inhibiting the cancer cells on nanofiber substrate.

14.3.3.3 Cancer Cell Detection

Effective and sensitive biosensor for detection of cancer biomarkers plays widespread attention. Paul et al. reported multiwalled carbon nanotubes (MWCNT) embedded with highly oriented zinc oxide (ZnO) using electrospinning as immune sensor to detect cancer cells. The electrochemical biosensor platform was fabricated by calcination of electrospun fibers as an electrode that is immobilized with anti-CA125 antibodies and immunoelectrode study carried by carcinoma antigen −125 (10 UmL^{-1}) in vitro with the outstanding outcome of detection limit up to

0.00113 U/mL concentration with remarkable sensitivity of 90.14μA/(U/mL)/cm^2 and wide range of detection 0.001 U/mL −1 kU/mL [108]. Ali et al. reported a microfluidic-based immunosensor embedded with electrospun carbon-doped titanium dioxide nanofibers ($nTiO_2$) and modified porous hierarchical graphene foam (GF) further, immobilized with anti-ErbB2 for prompt detection of EGFR2 or ErbB2m proteins. The result exhibited excellent sensitivity with 0.585μA/μM/cm^2 in a range of concentration from 1×10^{-15} M (1.0 fM) to 0.1×10^{-6} M (0.1μM) to target ErbB2 antigen [109].

14.3.3.4 Cancer Cell Imaging

In the theranostic cancer paradigm, nanotechnology offers a safe multifunctional platform for diagnosis, therapeutic, and monitoring of the progress by imaging [110]. Whereas materials such as graphene oxide, iron oxide have potential in MRI as a contrast agent, luminescence or photosensitizer could also bring added advantages along with imaging capabilities [111]. Hou et al. prepared a porous and upconversion (UC) luminescent electrospun nanofiber composite of $NaYF_4$:Yb^{3+}, Er^{3+}@SiO_2 [112]. Along with drug delivery for anti-cancer drug (doxorubicin hydrochloride (DOX)) in a pH sensitive manner, the release of drug and bioimaging of HeLa cells was presented successfully [112]. Li *et al.* demonstrated self-assembled nanoparticle of hyaluronic acid (HA)-cystamine-cholesterol (HSC) conjugate for tumor targeting dual mode of imaging and programmed photoactive therapy (PPAT) [113]. Such electrospun nanofibers could be useful in multifunctional cancer theranostic; however, further research is required for limitations such as safety issues, the complexity of nanostructure, and drug-releasing kinetics.

14.3.3.5 Drug Delivery

Nanofibers could produce tailorable drug-releasing kinetics and, along with targeted specific therapies, improve the therapeutic performance in cancer patients [22]. Nanoplatform with drug delivery and imaging is recently well explored by the researchers for advanced cancer nanomedicine. Several ongoing investigations (Table 14.1) have explored the drug-loaded nanofiber scaffolds and targeted cancer therapies to improve the efficiency by combining imaging with diagnostic components. The result could provide a localized and controlled release of drugs directly on the tumor site to radically improve the prognosis of recurrent tumors. Further multiple drugs could also be loaded with tailorable drug release kinetics towards futuristic nanomedicine with multiple platforms combining diagnostics and therapeutics [120].

Despite these advantageous steps in cancer detection, restricting its grasp towards severely jeopardizing the structural support system of our body, i.e., bones are still inevitable for clinicians. In this regard, how theranostics based approach could be

Table 14.1 Recently reported few nanofibers based localized drug delivery for different cancer types

S. no	Modes	Polymer	Drug	Target cancer	In vitro studies	In vivo studies	Ref
1.	Oral	PVA and TPGS	Phloretin	Oral cancer	Artificial saliva fluid	N/A	[114]
2.	Surgically	PCL/PLGA	Epirubicin	Upper tract urothelial carcinoma (UTUC)	Artificial urine solution	BALB/c mice	[115]
3.	Surgically	SF coated on PDO	CUR and 5-fluorouracil (5-FU)	Colorectal cancer	HCT116, NCM460 cells	BALB/c nude mice	[116]
4.	Surgically	HB/PVP (core–shell)	Artemisinin	Prostate cancer	DU145	N/A	[117]
5.	Surgically	PLA-hyaluronic acid (HA)	Gemcitabine	Pancreatic cancer	PANC-1 and 3 T3 cells	Xenograft tumor model	[118]
6.	Surgically	PLGA-PLA-PCL	Temozolomide	Glioma	Artificial cerebrospinal fluid	Rat model	[119]

PVA poly(vinyl alcohol), *TPGS-d-α* tocopheryl polyethylene glycol succinate, *PCL* poly(ε-caprolactone), *PLGA* poly(lactide-co-glycolide), *SF* silk fibroin, *PDO* polydioxanone stent, *CUR* curcumin, *HB* hyperbranched poly(butylene adipate), *PVP* Poly(vinylpyrrolidone)

utilized with the conventional treatment strategies deserves a brief discussion. Cancer has spread into society in such depth that the traditional ways of treatments have been in a continuous surge of improvements in terms of precision and ability of early diagnosis in a time-efficient manner [121]. Bone is the support structure of the human body. It is very evident in many cases of lung, prostate, breast, or other types of cancers that induce several metastases in the bone structures of patients. It is still a gray area of interdisciplinary research to identify the root causes of these metastases.

Conversely, the elderly population in many cases, survivors of first or second phase cancers, suffer from various types of degenerative diseases such as osteoporosis and arthritis, which get worse with age. The requirement of early diagnosis and application of appropriate therapeutic agents to minimize the spread of the disease has led to the vast but impressive domain called theranostics. Application of theranostics based approach towards skeletal issues like bone cancers or metastases has offered few specific advantages: (1) hydrophobic drug delivery system, (2) sustained drug delivery system to serve the purpose of disease treatment, and (3) effectively decreasing the chances of non-specific medications under differential pathological assumptions [122]. Radiotherapeutic agents is not a very new aspect of therapy. It dates back to almost 70 years [123, 124], while several types of radioactive Iodine were used (124I for diagnosis and 131I for treatment) for treatment of thyroid cancer. 90Y silicate has been used for joint arthritis treatment. Lexidronam is another drug that has been approved by FDA in the year 1997 for the treatment of bone metastases. The basic structure–function opted for radiotheranostics using radioactive isotopes follows ligand-linker-radioisotope design. The targeted ligand functions as an integrator which enhances the reach of the radioisotope to the diseased zones in the body. In typical cases, peptides are known to be the targeting ligands. In Lexidronam (Quadramet), 153Sm is the therapeutic isotopic agent, and 99Tc and 18NaF are imaging agents for bone metastases. Though in earlier 1993, Strontium89 (Metastron), having 89Sr as a therapeutic isotopic agent and only 18NaF as imaging isotopic agent, was approved successfully for its application in relieving bone pain by inducing neo-bone formation.

Later in 2013, an advanced theranostic drug, Radium223 (Xofigo) was approved, which has the same combination of imaging agents as of Lexidronam and 223Ra as a therapeutic agent. An interesting fact about these approved drugs is that these drugs do not have any particular ligands for them. Several developed drugs are also under clinical trials. 223Ra is a bone-affinitive alpha-emitter that finds higher amounts of bone apposition due to the presence of metastatic bone lesions. Radiation dosages are delivered by this to the affected area to improve the condition [125]. Notable among those is Apamistamab, for which antibody acts as a ligand. 131I is utilized as a therapeutic agent, whereas CD45 is the target to treat bone marrow ablation. Currently, this drug is undergoing phase 3 clinical trials. The main advantages of these radiotheranostic drugs are its simple procedural steps that are tolerable for the patients, compared to those conventional approaches involving chemotherapy or other radiotherapies. The adverse effects are also reported to be limited to only nausea and fatigue except for few stranded cases with complications or failure of the therapeutic drugs. However, high development costs of these radiotheranostic drugs

is an issue yet to be solved. Prolonged time to get the approval of newer drugs due to exhaustive clinical trials is also an obstacle towards establishing this approach for the treatment of patients.

The inability to identify tiny lesions, tumors, and multiple metastases using conventional approaches like X-Ray, CT scan, or MRI in bones led to delayed diagnosis of the patient. It is one of the few key reasons which has increased the morbidity rate of patients worldwide. A combination of *in vivo* tracking by imaging along with a targeted drug delivery system like mesoporous silica-coated upconversion nanoparticles (UCNP-MSs, UCMSs), which can convert the near IR radiations into visible lights, has become another popular theranostic method for treatment [126]. Deep light penetration depth, excellent chemical and photostability, negligible damage to biological substances are some of the critical aspects of these groups of particles. Moreover, using gadolinium (III) (Gd) doping within these groups of nanoparticles enables to structure a multimodal therapy platform. However, UCMS system's enhanced bone targeting is a drawback compared to its definite advantages in the treatment of early stages of cancers.

Along with these nanoparticles to diagnose the early stage bone metastases, bisphosphonate drugs can be utilized as a potent drug delivery agent in treating the bone lesions. Rheumatoid arthritis is another growing challenge in the elderly population. Liposomes, gold-based nanoparticles, polymeric nanoparticles, silica-based nanoparticles, and metal oxides are found to be excellent for diagnosing arthritis in patients due to their intrinsic moieties and huge surface availability to incorporate different drugs. However, the distribution of the nanoparticles in a proper homogenized way is still a challenge, which affects the diagnostic precision negatively. Notable among many is Metal-BODIPY (4, 4-difluoro-4-bora-3a,4a-diaza-s-indacene), which is the current choice for theranostics based approaches to treat arthritis [127]. New nanogel matrixes have also been developed having photosensitizers aiming to targeted delivery of drugs into the affected bone joints. In a recent development, a colloidal nanogel has been developed using chitosan and penta sodium triphosphate with hyaluronic acid on the surfaces of chitosan. Hyaluronic acid is an excellent agent in identifying the CD44 receptors, which are overexpressed during rheumatoid arthritis. No cytotoxicity was reported during successful application of this formulation.

14.3.4 Cardiovascular Diseases

Cardiovascular diseases (CVD) are a group of symptoms most prevalent in the modern world and closely related to changes in lifestyle and eating habits. CVD accounts for 45% of all deaths in Europe and 37% of all deaths in the EU [128]. Atherosclerosis is the most frequently documented cause of CVD related deaths where cholesterol accumulates in macrophages resulting in the formation of plaques in walls of coronary arteries. These symptoms are hard to identify in early stages and do

not manifest until the sudden onset of disease, often leading to decreased response to therapeutic agents.

Vikas nandwana et al. developed Fe_3O_4magnetic nanostructures coated with 1,2-dipalmitoyl-sn-glycerol-3-phosphocholine (DPPC) and Apoprotein 1 as HDL mimicking theranostic nanostructures. In clinical therapeutics, this HDL and apo 1 trigger reverse cholesterol transport (RCT) from lipid-laden macrophages to the liver. RCT is a key mechanism protecting from CVD and triggering this with HDL mimics. At the same time, imaging in MRI helps in early diagnosis and treatment of macrophage and cholesterol-rich atherosclerotic plaques. Furthermore, from the diagnostic perspective, these particles show significantly higher MR contrast enhancement than FDA approved Ferumoxytol [129].

Jason R. McCarthy et al. investigated crosslinked dextran based iron oxide nanoparticles for theranostics of atherosclerotic lesions. These particles were modified with NIR fluorophore for imaging and a chlorine-based sensitizer for ablative action. Macrophages have shown an intrinsic affinity towards these particles, and local irradiation with particular wavelength has shown to disrupt the plaque. Further, hysteresis heating of magnetic iron oxide nanoparticles could be used for inducing hypothermia. This synergistic effect has helped in reducing extraneous toxicity, but it was also observed that healthy cells like endothelial and smooth muscle cells in the vicinity were also ablated. This could increase the risk of sudden stroke due to the rupture of lesion and thrombosis. However, these magnetic nanostructures could be used for MRI imaging and catheter intervention by a see and treat approach [130].

Stenosis of blood vessels due to atherosclerosis is clinically treated by balloon dilation and stent placement. However, restenosis at the dilated site and associated complexities have prompted doctors to use drug-eluting stents, but they could interfere with endothelial healing causing late stent thrombosis [131]. For such cases, Cyrus et al. developed αvβ3-integrin targeted paramagnetic nanoparticles loaded with rapamycin, which showed reduced restenosis without effecting endothelial healing [132]. Similarly, Chorny et al., used paclitaxel loaded magnetic nano particles and used the magnetic properties of stent and external magnetic field to achieve high local concentration of drug in stented areas [133].

Apoptosis of myocardial cells resulting from ischemia induces oxidative stress is another important aspect of CVD where theranostics can play a long-term defensive role. It was shown that blocking annexin V, which is usually secreted by an apoptotic cell, has reduced the cellular damage [134]. Howard H. Chen et al. developed AnxCLIO-Cy5.5 nano particles, which contain annexin V conjugated with fluorescent nanoparticle CLIO-Cy5.5 (CLIO = cross-linked iron oxide) for diagnosis. They documented that cell membrane rupture was significantly downregulated in cells exposed to AnxCLIO-Cy5.5 and demonstrated that direct stabilization of cell membranes by the nanoparticles within a critical time period after injury was responsible for this protective effect. This effect was limited when compared to the therapeutic agent like caspase inhibitors. Still, any small therapeutic effect by a diagnostic agent is noteworthy, and further study was required to understand the exact mechanism [135]. As discussed above, Ferumoxytol is FDA approved long-circulating analogue of CLIO and has the potential to become a successful theranostics agent.

However, it is essential to choose a proper animal model and assess reliability for testing theranostic treatments as the pathology and physiology of CVD are very different in humans. Since the pathology of CVD in humans is mostly associated with lifestyle, smoking, alcohol, and food intake, it is challenging and non-ethical to develop a similar in vivo model. Also, arterial anatomy is very different in mice and other animal models compared to humans, which raises doubts about the clinical applicability of theranostics nanoparticles [136].

14.3.5 Antimicrobial Drug Resistance

Multi-drug resistance in microbes has been increasing due to inappropriate prescriptions, insufficient diagnostic facilities as well as increased agricultural use. Superbugs are threatening the healthcare system and prompting pharmaceuticals to produce new and more potent drugs. During replication, microbes develop resistance to drugs by mutations and gene transfer. Nanotechnology offers an innovative solution in the form of theranostics, where identifying and destroying the microbes can be done selectively with minimized dosage. An exciting work by Kelly group [137] revealed that Ru^{II} complexes are efficient as both a probe for detecting non-canonical DNA structures and are active against Gram +ve drug-resistant bacteria.

Further studies by Kirsty L. Smitten et al. [138]. on Ruthenium tetrapyridophenazine, complex revealed dual bioimaging and antibacterial theranostic effect against gram –ve strains. Primarily they explored the X-ray crystal structure and their mechanism of action against bacteria where both DNA and cell membrane were effected. Imaging by TEM reveals that these complex effects both cell wall and membrane within 20 min of exposure associated with rapid cell death. However, in the case of gram +ve stains, it was found that this compound binds electrostatically to the teichoic acid and lipotechoic acid in the cell wall, decreasing its efficacy. Methicillin resistant Staphylococcus Aureus (MRSA) is another dreaded clinical strain often referred to as superbug, which is responsible for sepsis and acute endocarditis. Zhao et al. [139] performed computer simulation of poly(allylamine)-coated silica nanoparticles (SiO2/PAH) interacting with bacteria to develop a nanotheranostic probe that is independent of bacterial enzyme molecules. They developed a silica nanotheranostic probe that could be activated in the presence of MRSA for NIR imaging and PTT. This probe is based on silica nanoparticles coated with vancomycin-modified polyelectrolyte-cypate complexes (SiO2-Cy-Van), which is activated by an interesting phenomenon of bacteria-responsive dissociation of the polyelectrolyte from silica nanoparticles. They demonstrated that MRSA can destabilize the complex due to its affinity for vancomycin and draw them onto their own surface. This changes the state of cypate complex from off (aggregation) to on (disaggregation) leading to near-infrared fluorescence (NIRF) and photothermal action against bacterial cell wall and membrane.

Copper is a well-known antibacterial material, but the nanoparticles in *in vitro* and *in vivo* were found to be toxic due to excessive generation of reactive oxygen species. Das et al. explored theranostic application of these Cu nanoparticles by doping them in carbon nanodots (CND) to regulate the ROS effect *in vitro*. The underlying mechanism of downregulation of ROS involves the formation of carbonate and bicarbonate ions by reaction between produced ROS and carbon from CND [140]. This composite also showed a dual mode imaging by both SERS and fluorescence, which could be explored for live-cell tracking. Further, both gram –ve and +ve strains were found to be highly sensitive to this composite. The main application could be seen in preventive antibacterial coating for implants and wound bed dressings. Dai et al. explored magnetic iron nanoparticles coated with gold and attached monoclonal antibody specific to multi-drug-resistant salmonella DT 104. PEGylation reduced further toxicity of gold, targeting, imaging. PDT was achieved by methylene blue coating. Gold coating served two purposes of stabilizing magnetic Fe nanoparticles in blood and optical nanoheater in NIR range for PTT. Iron core serves the purpose of separating nanoparticles conjugated with bacteria. These multifunctional nanoplatforms have shown a bacterial capture efficacy of 97% and have a potential for clinical translation with specific or multiple bacterial targets [141].

Magdiel I. Setyawati, et al. [142], utilized Watson-Crick base pairing to tailor DNA nanopyramids scaffolds that can integrate both antimicrobial compounds and gold nano-clusters for theranostics. To achieve theranostics the DP scaffold was designed to carry ultra-small red emissive gold nano-clusters of ~2 nm with glutathione coating. Actinomycin D was loaded into the scaffold by aligning phenoxanone aromatic rings parallel to the guanine base pairs of DP. Figure 14.6 shows schematic of formation of DPAu/AMD structures. Due to the presence of DNA base pairs in the DP scaffold, they were readily internalized by bacterial cells like S. Aureus and E. Coli. Also presence of DNase enzyme in the bacterial cell facilitated the dissolution of the DP scaffold and immediate release of the entire drug to the interior of the cell. By incorporating targeting moieties to these DP, they can be made theranostic by differentiating mammalian cell from bacterial cells. In a similar fashion Kevin Ferreira et al. [143] targeted the iron intake mechanism in bacterial cells by preparing drug conjugates with siderophores. They have a high affinity for iron and are secreted by bacteria to satisfy their iron requirement. Multiple transporters are available in bacterial wall to facilitate both endogenous and xenosiderophores. Tetrapodal 1,4,7,10-tetraazacyclododecane-1,4,7,10-tetraacetic amide (DOTAM) moiety was explored with three arms conjugated with catechol moieties for iron binding and one arm with fluorophore malachite green using various linkers. It has been reported that these multifunctional complexes could be used for both diagnosis and treatment owing to their ability to cross the gram –ve cell wall. They further found the uptake of these complexes by E. coli and P. Auregenosa strains, which cannot synthesize their endogenous siderophores and depend on xenosiderophores for their iron uptake. Thus they can be used to treat multiple bacterial strains *in vivo*. Many studies have explored luminogens [144] with aggregation-induced emission (AIEgen) as fluorescent probes for turn-on sensing of

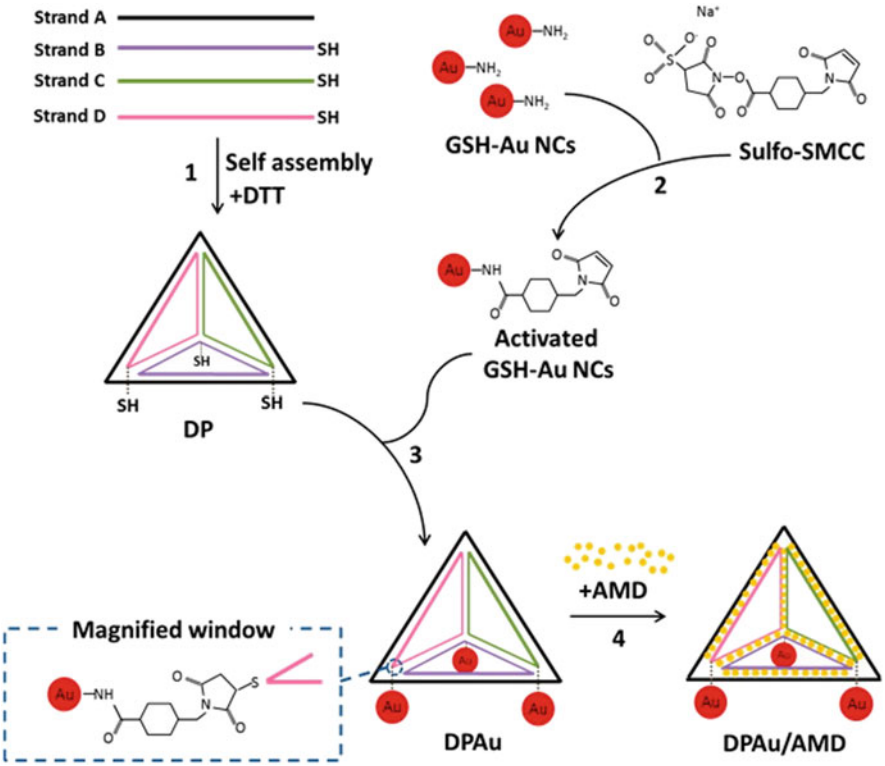

Fig. 14.6 Schematic representation of nanotheranostic DPAu/AMD synthesis. (1) DNA nanopyramid (DP) is self-assembled from four complementary oligonucleotides and DTT is added to fully reduce the thiol groups on the DP. (2) At the same time, GSH-protected Au NCs are activated with sulfo-SMCC to allow (3) the conjugation of Au NCs on the DP (DPAu) via maleimide bonds (magnified window). (4) Then, the Actinomycin D (AMD) is let to intercalate into the DPAu structure and the nanotheranostic DPAu/AMD structure is formed. Reprinted (adapted) with permission from (Setyawati, Magdiel I., et al. "Novel theranostic DNA nanoscaffolds for the simultaneous detection and killing of Escherichia coli and Staphylococcus aureus." *ACS applied materials & interfaces* 6.24 (2014): 21822–21,831). Copyright (2014) American Chemical Society [142]

pathogens with high sensitivity and specificity. Peptides, polymers, micelles, metal complexes, nanoparticles, etc., could be used as AIEgen driven systems. Also due to aggregation, these nanostructures exhibited excellent photodynamic inactivation (PDI) activity offering great potential for both diagnosis of pathogen and image-guided PDI therapy for pathogenic infection. Their unique turn-on fluorescent properties with large stokes' shift, luminosity, photobleach resistance, emission tunability in NIR range make them excellent choices for multiple pathogenic identifications and long-term infection monitoring ranging from *in vitro* to *in vivo*.

14.4 Challenge and Perspective

In recent years, various nanotheranostic medicines have been explored with their unique capability for concurrent detecting, imaging, and treatment of early-stage cancer but there are still challenges associated with their clinical translation by duplicating an in-vivo system. The recent developments of various approach to form theranostic nanomedicine such as solid approach (drug conjugated nanoparticles and nanodots), liquid approach (nanocolloids, nanoemulsions, and nanoformulation), dry approach (spray dry nanopowder, electrospun nanofiber), and biomacromolecule approach (DNA functionalization, micro-RNA based, and antibody mediated) have been studied to understand their effects and limitations for future via step-by-step processing. There are different criteria for clinical translation of nanomaterials, which depend on the selection of the best nanoplatforms for personalized treatment. Nanotheranostic efficiency is dependent upon simple synthetic techniques with higher reproducibility and lower cost. Furthermore, the challenges remain in the development approach for in vivo applications at the preclinical and clinical levels. However, the development of theranostic nanomedicine has advantages over conventional medicines in terms of many factors. These include multiplex, multiple imaging agent capabilities, stimulus (pH, magnetism, and temperature) based responsive drug release, multimodal ability, and efficient drug delivery. The development of versatile and smart theranostic applications is highly needed, which may help researchers, clinicians for various precision-based therapeutic strategies.

Meanwhile, it has disadvantages that need to overcome that include toxicity and lower colloidal stability of heavy metal-based upconversion nanoparticles. Here, the above-mentioned queries attribute to troubleshoot SQDs of which high cost, oxidative stress formation in gold/silver nanoparticles, the low sensitivity of magnetic nanoparticles, non-biodegradable nature of carbon nanotube are the primary focus. Bio-inspired and biomimetic systems based on CQDs might be promising to resolve the obstacles of the present nanotheranostics system like short circulation time, volatility in a complex biological system, and comparatively low tumor-targeting sensitivity through the EPR effect. Therefore, regular and long-term studies are still needed to explore their biological effects comprehensively. Moreover, various factors like distribution, circulation half-life, translocation, metabolism, bio-degradation, and the pharmacokinetics of various approaches mentioned above should be investigated in detail that might emerge as promising directions for nanomedicines.

Semiconductor and metallic based nanoparticles in cancer therapy will need more optimization for their clinical applications. Efforts seeking better B-QDs strategies will continue to develop effective and efficient cancer nanotheranostics. Macromolecule, dry approaches require unique nanomedicine technology and knowledge for their cost-effective delivery, therapy to avoid non-specific site accumulation of drug, crossing BBB, a narrow therapeutic strategy. With the rapid development of CQDs, we expect its more favorable use in various fields like agriculture, environment, and

energy, including nanomedicine. We rely on these above-mentioned unresolved concerns that will be encouraged and challenging for additional studies and develop various nanotheranostics based biomedical applications.

References

1. Shetty, Y., Prabhu, P., & Prabhakar, B. (2019). Emerging vistas in theranostic medicine. *International Journal of Pharmaceutics, 558*, 29–42.
2. Navalkissoor, S., Gnanasegaran, G., & Baum, R. (2018). Theranostics and precision medicine special feature. *The British Journal of Radiology, 91*(1091), 20189004.
3. Moek, K. L., Giesen, D., Kok, I. C., de Groot, D. J. A., Jalving, M., Fehrmann, R. S., Lub-de Hooge, M. N., Brouwers, A. H., & de Vries, E. G. (2017). Theranostics using antibodies and antibody-related therapeutics. *Journal of Nuclear Medicine, 58*(Supplement 2), 83S–90S.
4. Jo, S. D., Ku, S. H., Won, Y.-Y., Kim, S. H., & Kwon, I. C. (2016). Targeted nanotheranostics for future personalized medicine: recent progress in cancer therapy. *Theranostics, 6*(9), 1362.
5. Khan, I., Saeed, K., & Khan, I. (2019). Nanoparticles: properties, applications and toxicities. *Arabian Journal of Chemistry, 12*(7), 908–931.
6. Kumar, A., Roy, S., Srivastava, A., Naikwade, M. M., Purohit, B., Mahato, K., Naidu, V., & Chandra, P. (2019). Nanotherapeutics: a novel and powerful approach in modern healthcare system. In *Nanotechnology in modern animal biotechnology* (pp. 149–161). Amsterdam: Elsevier.
7. Muthu, M. S., Leong, D. T., Mei, L., & Feng, S.-S. (2014). Nanotheranostics· application and further development of nanomedicine strategies for advanced theranostics. *Theranostics, 4*(6), 660.
8. Matea, C. T., Mocan, T., Tabaran, F., Pop, T., Mosteanu, O., Puia, C., Iancu, C., & Mocan, L. (2017). Quantum dots in imaging, drug delivery and sensor applications. *International Journal of Nanomedicine, 12*, 5421.
9. Sun, Y.-P., Zhou, B., Lin, Y., Wang, W., Fernando, K. S., Pathak, P., Meziani, M. J., Harruff, B. A., Wang, X., & Wang, H. (2006). Quantum-sized carbon dots for bright and colorful photoluminescence. *Journal of the American Chemical Society, 128*(24), 7756–7757.
10. Wang, J., Han, S., Ke, D., & Wang, R. (2012). Semiconductor quantum dots surface modification for potential cancer diagnostic and therapeutic applications. *Journal of Nanomaterials, 2012*, 129041.
11. Bruchez, M., Moronne, M., Gin, P., Weiss, S., & Alivisatos, A. P. (1998). Semiconductor nanocrystals as fluorescent biological labels. *Science, 281*(5385), 2013–2016.
12. Chan, W. C., & Nie, S. (1998). Quantum dot bioconjugates for ultrasensitive nonisotopic detection. *Science, 281*(5385), 2016–2018.
13. Chandra, P., & Pandey, L. M. (2020). *Biointerface engineering: prospects in medical diagnostics and drug delivery*. Singapore: Springer.
14. Xu, X., Ray, R., Gu, Y., Ploehn, H. J., Gearheart, L., Raker, K., & Scrivens, W. A. (2004). Electrophoretic analysis and purification of fluorescent single-walled carbon nanotube fragments. *Journal of the American Chemical Society, 126*(40), 12736–12737.
15. Bailey, R. E., Smith, A. M., & Nie, S. (2004). Quantum dots in biology and medicine. *Physica E: Low-dimensional Systems and Nanostructures, 25*(1), 1–12.
16. Pandey, A., Kulkarni, S., & Mutalik, S. (2020). Liquid metal based theranostic nanoplatforms: application in cancer therapy, imaging and biosensing. *Nanomedicine: Nanotechnology, Biology and Medicine, 26*, 102175.
17. Li, C. (2014). A targeted approach to cancer imaging and therapy. *Nature Materials, 13*(2), 110–115.

18. Sneider, A., VanDyke, D., Paliwal, S., & Rai, P. (2017). Remotely triggered nano-theranostics for cancer applications. *Nanotheranostics, 1*(1), 1.
19. Kim, T. H., Lee, S., & Chen, X. (2013). Nanotheranostics for personalized medicine. *Expert Review of Molecular Diagnostics, 13*(3), 257–269.
20. Purohit, B., Kumar, A., Mahato, K., Roy, S., & Chandra, P. (2019). Cancer cytosensing approaches in miniaturized settings based on advanced nanomaterials and biosensors. In *Nanotechnology in modern animal biotechnology* (pp. 133–147). Amsterdam: Elsevier.
21. Perecin, C., Cerize, N., Chitta, V., Gratens, X., Léo, P., de Oliveira, A., & Yoshioka, S. (2016). Magnetite nanoparticles encapsulated with PCL and poloxamer by nano spray drying technique. *Nanoscience and Nanotechnology, 6*(4), 68–73.
22. Cleeton, C., Keirouz, A., Chen, X., & Radacsi, N. (2019). Electrospun nanofibers for drug delivery and biosensing. *ACS Biomaterials Science & Engineering, 5*(9), 4183–4205.
23. Chandra, P., & Prakash, R. (2020). *Nanobiomaterial engineering*. Singapore: Springer.
24. Rapti, K., Chaanine, A. H., & Hajjar, R. J. (2011). Targeted gene therapy for the treatment of heart failure. *Canadian Journal of Cardiology, 27*(3), 265–283.
25. Pouton, C. W., & Seymour, L. W. (2001). Key issues in non-viral gene delivery. *Advanced Drug Delivery Reviews, 46*(1–3), 187–203.
26. Robbins, P. D., & Ghivizzani, S. C. (1998). Viral vectors for gene therapy. *Pharmacology & Therapeutics, 80*(1), 35–47.
27. Chery, J. (2016). RNA therapeutics: RNAi and antisense mechanisms and clinical applications. *Postdoc Journal: A Journal of Postdoctoral Research and Postdoctoral Affairs, 4*(7), 35.
28. Mabrouk, M., Rajendran, R., Soliman, I. E., Ashour, M. M., Beherei, H. H., Tohamy, K. M., Thomas, S., Kalarikkal, N., Arthanareeswaran, G., & Das, D. B. (2019). Nanoparticle-and nanoporous-membrane-mediated delivery of therapeutics. *Pharmaceutics, 11*(6), 294.
29. Dass, C. R. (2002). Biochemical and biophysical characteristics of lipoplexes pertinent to solid tumour gene therapy. *International Journal of Pharmaceutics, 241*(1), 1–25.
30. Even-Chen, S., Cohen, R., & Barenholz, Y. (2012). Factors affecting DNA binding and stability of association to cationic liposomes. *Chemistry and Physics of Lipids, 165*(4), 414–423.
31. Dass, C. R. (2003). Improving anti-angiogenic therapy via selective delivery of cationic liposomes to tumour vasculature. *International Journal of Pharmaceutics, 267*(1–2), 1–12.
32. Fan, J., Liu, Y., Liu, L., Huang, Y., Li, X., & Huang, W. (2019). A multifunction lipid-based CRISPR-Cas13a genetic circuit delivery system for bladder Cancer gene therapy. *ACS Synthetic Biology, 9*(2), 343–355.
33. Hosseini, E. S., Nikkhah, M., & Hosseinkhani, S. (2019). Cholesterol-rich lipid-mediated nanoparticles boost of transfection efficiency, utilized for gene editing by CRISPR-Cas9. *International Journal of Nanomedicine, 14*, 4353.
34. Di Gioia, S., & Conese, M. (2008). Polyethylenimine-mediated gene delivery to the lung and therapeutic applications. *Drug Design, Development and Therapy, 2*, 163.
35. Dass, C. R., DeCruz, E. E., Walker, T. L., & Burton, M. A. (1997). Barriers to liposomal gene transfer into solid tumours. *Australasian Biotechnology, 7*, 155–159.
36. Blumenfeld, C. M., Schulz, M. D., Aboian, M. S., Wilson, M. W., Moore, T., Hetts, S. W., & Grubbs, R. H. (2018). Drug capture materials based on genomic DNA-functionalized magnetic nanoparticles. *Nature Communications, 9*(1), 1–7.
37. Thomson, D. A., Tee, E. H., Tran, N. T., Monteiro, M. J., & Cooper, M. A. (2012). Oligonucleotide and polymer functionalized nanoparticles for amplification-free detection of DNA. *Biomacromolecules, 13*(6), 1981–1989.
38. Miller, C. M., & Harris, E. N. (2016). Antisense oligonucleotides: treatment strategies and cellular internalization. *RNA & Disease (Houston, TX), 3*(4), e1393.
39. Uehara, H., Cho, Y., Simonis, J., Cahoon, J., Archer, B., Luo, L., Das, S. K., Singh, N., Ambati, J., & Ambati, B. K. (2013). Dual suppression of hemangiogenesis and

lymphangiogenesis by splice-shifting morpholinos targeting vascular endothelial growth factor receptor 2 (KDR). *The FASEB Journal, 27*(1), 76–85.
40. Uehara, H., Muddana, S. K., Zhang, X., Das, S. K., Bhuvanagiri, S., Liu, J., Wu, Y., Choi, S., Carroll, L. S., & Archer, B. (2017). Targeted delivery of FLT-morpholino using cyclic RGD peptide. *Translational Vision Science & Technology, 6*(3), 9–9.
41. Frieden, M., & Orum, H. (2006). The application of locked nucleic acids in the treatment of cancer. *IDrugs: The Investigational Drugs Journal, 9*(10), 706–711.
42. Thayer, M. B., Lade, J. M., Doherty, D., Xie, F., Basiri, B., Barnaby, O. S., Bala, N. S., & Rock, B. M. (2019). Application of locked nucleic acid oligonucleotides for siRNA preclinical bioanalytics. *Scientific Reports, 9*(1), 1–9.
43. Choi, S., Uehara, H., Wu, Y., Das, S., Zhang, X., Archer, B., Carroll, L., & Ambati, B. K. (2018). RNA activating-double stranded RNA targeting FLT-1 promoter inhibits endothelial cell proliferation through soluble FLT-1 upregulation. *PLoS One, 13*(3), e0193590.
44. Mishra, P. J., & Merlino, G. (2009). MicroRNA reexpression as differentiation therapy in cancer. *The Journal of Clinical Investigation, 119*(8), 2119–2123.
45. Crooke, S. T., Graham, M. J., Zuckerman, J. E., Brooks, D., Conklin, B. S., Cummins, L. L., Greig, M. J., Guinosso, C. J., Kornbrust, D., & Manoharan, M. (1996). Pharmacokinetic properties of several novel oligonucleotide analogs in mice. *Journal of Pharmacology and Experimental Therapeutics, 277*(2), 923–937.
46. Yoo, B. H., Bochkareva, E., Bochkarev, A., Mou, T. C., & Gray, D. M. (2004). 2′-O-methyl-modified phosphorothioate antisense oligonucleotides have reduced non-specific effects in vitro. *Nucleic Acids Research, 32*(6), 2008–2016.
47. Wahlestedt, C., Salmi, P., Good, L., Kela, J., Johnsson, T., Hökfelt, T., Broberger, C., Porreca, F., Lai, J., & Ren, K. (2000). Potent and nontoxic antisense oligonucleotides containing locked nucleic acids. *Proceedings of the National Academy of Sciences, 97*(10), 5633–5638.
48. Hyrup, B., & Nielsen, P. E. (1996). Peptide nucleic acids (PNA): synthesis, properties and potential applications. *Bioorganic & Medicinal Chemistry, 4*(1), 5–23.
49. Pallan, P. S., Greene, E. M., Jicman, P. A., Pandey, R. K., Manoharan, M., Rozners, E., & Egli, M. (2011). Unexpected origins of the enhanced pairing affinity of 2′-fluoro-modified RNA. *Nucleic Acids Research, 39*(8), 3482–3495.
50. Hayes, J., Peruzzi, P., & Lawler, S. (2014). MicroRNAs in cancer: biomarkers, functions and therapy. *Trends in Molecular Medicine, 20*(8), 460–469.
51. Ghosh, R., Singh, L. C., Shohet, J. M., & Gunaratne, P. H. (2013). A gold nanoparticle platform for the delivery of functional microRNAs into cancer cells. *Biomaterials, 34*(3), 807–816.
52. Ekin, A., Karatas, O. F., Culha, M., & Ozen, M. (2014). Designing a gold nanoparticle-based nanocarrier for microRNA transfection into the prostate and breast cancer cells. *The Journal of Gene Medicine, 16*(11–12), 331–335.
53. Crew, E., Rahman, S., Razzak-Jaffar, A., Mott, D., Kamundi, M., Yu, G., Tchah, N., Lee, J., Bellavia, M., & Zhong, C.-J. (2012). MicroRNA conjugated gold nanoparticles and cell transfection. *Analytical Chemistry, 84*(1), 26–29.
54. Xue, H.-Y., Liu, Y., Liao, J.-Z., Lin, J.-S., Li, B., Yuan, W.-G., Lee, R. J., Li, L., Xu, C.-R., & He, X.-X. (2016). Gold nanoparticles delivered miR-375 for treatment of hepatocellular carcinoma. *Oncotarget, 7*(52), 86675.
55. Wu, X., Liu, H., Liu, J., Haley, K. N., Treadway, J. A., Larson, J. P., Ge, N., Peale, F., & Bruchez, M. P. (2003). Immunofluorescent labeling of cancer marker Her2 and other cellular targets with semiconductor quantum dots. *Nature Biotechnology, 21*(1), 41–46.
56. Fountaine, T. J., Wincovitch, S. M., Geho, D. H., Garfield, S. H., & Pittaluga, S. (2006). Multispectral imaging of clinically relevant cellular targets in tonsil and lymphoid tissue using semiconductor quantum dots. *Modern Pathology, 19*(9), 1181–1191.
57. Bostick, R. M., Kong, K. Y., Ahearn, T. U., Chaudry, Q., Cohen, V., & Wang, M. D. (2006). Detecting and quantifying biomarkers of risk for colorectal cancer using quantum dots and

novel image analysis algorithms. In *2006 international conference of the IEEE engineering in medicine and biology society* (pp. 3313–3316). IEEE.
58. Chen, C., Sun, S.-R., Gong, Y.-P., Qi, C.-B., Peng, C.-W., Yang, X.-Q., Liu, S.-P., Peng, J., Zhu, S., & Hu, M.-B. (2011). Quantum dots-based molecular classification of breast cancer by quantitative spectroanalysis of hormone receptors and HER2. *Biomaterials, 32*(30), 7592–7599.
59. Liu, M.-X., Chen, S., Ding, N., Yu, Y.-L., & Wang, J.-H. (2020). A carbon-based polymer dot sensor for breast cancer detection using peripheral blood immunocytes. *Chemical Communications, 56*(20), 3050–3053.
60. Wang, T., Zhang, W., Zhang, X., Qiqige, X., Qimuge, W., Qimuge, A., Wang, H., Baila, B., Qimuge, A., & Yuan, M. (2017). Synthesis of fluorescent carbon dots by gastrointestinal fluid treatment of Mongolia Har Gabur. *Journal of Nanomaterials, 2017*, 8575162.
61. Wang, J., Yong, W. H., Sun, Y. H., Vernier, P. T., Koeffler, H. P., Gundersen, M. A., & Marcu, L. (2007). Receptor-targeted quantum dots: fluorescent probes for brain tumor diagnosis. *Journal of Biomedical Optics, 12*(4), 044021.
62. Zheng, M., Ruan, S., Liu, S., Sun, T., Qu, D., Zhao, H., Xie, Z., Gao, H., Jing, X., & Sun, Z. (2015). Self-targeting fluorescent carbon dots for diagnosis of brain cancer cells. *ACS Nano, 9*(11), 11455–11461.
63. Hamd-Ghadareh, S., Salimi, A., Fathi, F., & Bahrami, S. (2017). An amplified comparative fluorescence resonance energy transfer immunosensing of CA125 tumor marker and ovarian cancer cells using green and economic carbon dots for bio-applications in labeling, imaging and sensing. *Biosensors and Bioelectronics, 96*, 308–316.
64. Liu, Y.-S., Sun, Y., Vernier, P. T., Liang, C.-H., Chong, S. Y. C., & Gundersen, M. A. (2007). pH-sensitive photoluminescence of CdSe/ZnSe/ZnS quantum dots in human ovarian cancer cells. *The Journal of Physical Chemistry C, 111*(7), 2872–2878.
65. Chu, T. C., Shieh, F., Lavery, L. A., Levy, M., Richards-Kortum, R., Korgel, B. A., & Ellington, A. D. (2006). Labeling tumor cells with fluorescent nanocrystal–aptamer bioconjugates. *Biosensors and Bioelectronics, 21*(10), 1859–1866.
66. Liu, T. C., Wang, J. H., Wang, H. Q., Zhang, H. L., Zhang, Z. H., Hua, X. F., Cao, Y. C., Zhao, Y. D., & Luo, Q. M. (2007). Bioconjugate recognition molecules to quantum dots as tumor probes. *Journal of Biomedical Materials Research Part A, 83*(4), 1209–1216.
67. Kim, B. Y., Jiang, W., Oreopoulos, J., Yip, C. M., Rutka, J. T., & Chan, W. C. (2008). Biodegradable quantum dot nanocomposites enable live cell labeling and imaging of cytoplasmic targets. *Nano Letters, 8*(11), 3887–3892.
68. Yezhelyev, M. V., Qi, L., O'Regan, R. M., Nie, S., & Gao, X. (2008). Proton-sponge coated quantum dots for siRNA delivery and intracellular imaging. *Journal of the American Chemical Society, 130*(28), 9006–9012.
69. Stroh, M., Zimmer, J. P., Duda, D. G., Levchenko, T. S., Cohen, K. S., Brown, E. B., Scadden, D. T., Torchilin, V. P., Bawendi, M. G., & Fukumura, D. (2005). Quantum dots spectrally distinguish multiple species within the tumor milieu in vivo. *Nature Medicine, 11*(6), 678–682.
70. Cai, W., Shin, D.-W., Chen, K., Gheysens, O., Cao, Q., Wang, S. X., Gambhir, S. S., & Chen, X. (2006). Peptide-labeled near-infrared quantum dots for imaging tumor vasculature in living subjects. *Nano Letters, 6*(4), 669–676.
71. Kim, S., Lim, Y. T., Soltesz, E. G., De Grand, A. M., Lee, J., Nakayama, A., Parker, J. A., Mihaljevic, T., Laurence, R. G., & Dor, D. M. (2004). Near-infrared fluorescent type II quantum dots for sentinel lymph node mapping. *Nature Biotechnology, 22*(1), 93–97.
72. Gao, X., Cui, Y., Levenson, R. M., Chung, L. W., & Nie, S. (2004). In vivo cancer targeting and imaging with semiconductor quantum dots. *Nature Biotechnology, 22*(8), 969–976.
73. Yang, S.-T., Cao, L., Luo, P. G., Lu, F., Wang, X., Wang, H., Meziani, M. J., Liu, Y., Qi, G., & Sun, Y.-P. (2009). Carbon dots for optical imaging in vivo. *Journal of the American Chemical Society, 131*(32), 11308–11309.

74. Hola, K., Zhang, Y., Wang, Y., Giannelis, E. P., Zboril, R., & Rogach, A. L. (2014). Carbon dots—emerging light emitters for bioimaging, cancer therapy and optoelectronics. *Nano Today, 9*(5), 590–603.
75. Bagalkot, V., Zhang, L., Levy-Nissenbaum, E., Jon, S., Kantoff, P. W., Langer, R., & Farokhzad, O. C. (2007). Quantum dot− aptamer conjugates for synchronous cancer imaging, therapy, and sensing of drug delivery based on bi-fluorescence resonance energy transfer. *Nano Letters, 7*(10), 3065–3070.
76. Pardo, J., Peng, Z., & Leblanc, R. M. (2018). Cancer targeting and drug delivery using carbon-based quantum dots and nanotubes. *Molecules, 23*(2), 378.
77. Mingqian, T., & Aiguo, W. (2016). *Nanomaterials for tumor targeting theranostics: a proactive clinical perspective*. Singapore: World Scientific.
78. Zayed, D. G., AbdElhamid, A. S., Freag, M. S., & Elzoghby, A. O. (2019). Hybrid quantum dot-based theranostic nanomedicines for tumor-targeted drug delivery and cancer imaging. *Nanomedicine (London), 14*(3), 225–228.
79. Bakalova, R., Ohba, H., Zhelev, Z., Nagase, T., Jose, R., Ishikawa, M., & Baba, Y. (2004). Quantum dot anti-CD conjugates: are they potential photosensitizers or potentiators of classical photosensitizing agents in photodynamic therapy of cancer? *Nano Letters, 4*(9), 1567–1573.
80. Tao, H., Yang, K., Ma, Z., Wan, J., Zhang, Y., Kang, Z., & Liu, Z. (2012). In vivo NIR fluorescence imaging, biodistribution, and toxicology of photoluminescent carbon dots produced from carbon nanotubes and graphite. *Small, 8*(2), 281–290.
81. Wu, F., Yue, L., Su, H., Wang, K., Yang, L., & Zhu, X. (2018). Carbon dots@ platinum porphyrin composite as Theranostic Nanoagent for efficient photodynamic Cancer therapy. *Nanoscale Research Letters, 13*(1), 357.
82. Samia, A. C., Chen, X., & Burda, C. (2003). Semiconductor quantum dots for photodynamic therapy. *Journal of the American Chemical Society, 125*(51), 15736–15737.
83. Solanki, A., Kim, J. D., & Lee, K.-B. (2008). Nanotechnology for regenerative medicine: nanomaterials for stem cell imaging. *Nanomedicine (London, England), 3*(4), 567–578.
84. Li, X., Vinothini, K., Ramesh, T., Rajan, M., & Ramu, A. (2020). Combined photodynamic-chemotherapy investigation of cancer cells using carbon quantum dot-based drug carrier system. *Drug Delivery, 27*(1), 791–804.
85. Obeso, J. A., Rodriguez-Oroz, M. C., Goetz, C. G., Marin, C., Kordower, J. H., Rodriguez, M., Hirsch, E. C., Farrer, M., Schapira, A. H., & Halliday, G. (2010). Missing pieces in the Parkinson's disease puzzle. *Nature Medicine, 16*(6), 653–661.
86. Mueller, J. C., Fuchs, J., Hofer, A., Zimprich, A., Lichtner, P., Illig, T., Berg, D., Wüllner, U., Meitinger, T., & Gasser, T. (2005). Multiple regions of α-synuclein are associated with Parkinson's disease. *Annals of Neurology, 57*(4), 535–541.
87. Koch, J., Bitow, F., Haack, J., d'Hedouville, Z., Zhang, J., Tönges, L., Michel, U., Oliveira, L., Jovin, T., & Liman, J. (2015). Alpha-Synuclein affects neurite morphology, autophagy, vesicle transport and axonal degeneration in CNS neurons. *Cell Death & Disease, 6*(7), e1811–e1811.
88. Langston, J. W., Schüle, B., Rees, L., Nichols, R. J., & Barlow, C. (2015). Multisystem Lewy body disease and the other Parkinsonian disorders. *Nature Genetics, 47*(12), 1378.
89. Fonseca-Ornelas, L., Eisbach, S. E., Paulat, M., Giller, K., Fernández, C. O., Outeiro, T. F., Becker, S., & Zweckstetter, M. (2014). Small molecule-mediated stabilization of vesicle-associated helical α-synuclein inhibits pathogenic misfolding and aggregation. *Nature Communications, 5*(1), 1–11.
90. Bendor, J. T., Logan, T. P., & Edwards, R. H. (2013). The function of α-synuclein. *Neuron, 79*(6), 1044–1066.
91. Zondler, L., Miller-Fleming, L., Repici, M., Gonçalves, S., Tenreiro, S., Rosado-Ramos, R., Betzer, C., Straatman, K., Jensen, P. H., & Giorgini, F. (2014). DJ-1 interactions with α-synuclein attenuate aggregation and cellular toxicity in models of Parkinson's disease. *Cell Death & Disease, 5*(7), e1350–e1350.

92. Jankovic, J., & Aguilar, L. G. (2008). Current approaches to the treatment of Parkinson's disease. *Neuropsychiatric Disease and Treatment, 4*(4), 743.
93. Thomas, B. (2009). Parkinson's disease: from molecular pathways in disease to therapeutic approaches. *Antioxidants & Redox Signaling, 11*(9), 2077–2082.
94. Li, Y., Liu, R., Ji, W., Li, Y., Liu, L., & Zhang, X. (2018). Delivery systems for theranostics in neurodegenerative diseases. *Nano Research, 11*(10), 5535–5555.
95. Kumar, A., Chaudhary, R. K., Singh, R., Singh, S. P., Wang, S.-Y., Hoe, Z.-Y., Pan, C.-T., Shiue, Y.-L., Wei, D.-Q., & Kaushik, A. C. (2020). Nanotheranostic applications for detection and targeting neurodegenerative diseases. *Frontiers in Neuroscience, 14*, 305.
96. Lee, S.-J., Lim, H.-S., Masliah, E., & Lee, H.-J. (2011). Protein aggregate spreading in neurodegenerative diseases: problems and perspectives. *Neuroscience Research, 70*(4), 339–348.
97. Ali, I., Alsehli, M., Scotti, L., Tullius Scotti, M., Tsai, S.-T., Yu, R.-S., Hsieh, M. F., & Chen, J.-C. (2020). Progress in polymeric nano-medicines for theranostic cancer treatment. *Polymers, 12*(3), 598.
98. Rampado, R., Crotti, S., Caliceti, P., Pucciarelli, S., & Agostini, M. (2019). Nanovectors design for theranostic applications in colorectal cancer. *Journal of Oncology, 2019*, 2740923.
99. Xiao, Y., Shen, M., & Shi, X. (2018). Design of functional electrospun nanofibers for cancer cell capture applications. *Journal of Materials Chemistry B, 6*(10), 1420–1432.
100. Jackson, J. M., Witek, M. A., Kamande, J. W., & Soper, S. A. (2017). Materials and microfluidics: enabling the efficient isolation and analysis of circulating tumour cells. *Chemical Society Reviews, 46*(14), 4245–4280.
101. Fan, Z.-Y., Zhao, Y.-L., Zhu, X.-Y., Luo, Y., Shen, M.-W., & Shi, X.-Y. (2016). Folic acid modified electrospun poly (vinyl alcohol)/polyethyleneimine nanofibers for cancer cell capture applications. *Chinese Journal of Polymer Science, 34*(6), 755–765.
102. Zhao, Y., Zhu, X., Liu, H., Luo, Y., Wang, S., Shen, M., Zhu, M., & Shi, X. (2014). Dendrimer-functionalized electrospun cellulose acetate nanofibers for targeted cancer cell capture applications. *Journal of Materials Chemistry B, 2*(42), 7384–7393.
103. Zhang, N., Deng, Y., Tai, Q., Cheng, B., Zhao, L., Shen, Q., He, R., Hong, L., Liu, W., & Guo, S. (2012). Electrospun TiO2 nanofiber-based cell capture assay for detecting circulating tumor cells from colorectal and gastric cancer patients. *Advanced Materials, 24*(20), 2756–2760.
104. Zhao, L., Lu, Y. T., Li, F., Wu, K., Hou, S., Yu, J., Shen, Q., Wu, D., Song, M., & OuYang, W. H. (2013). High-purity prostate circulating tumor cell isolation by a polymer nanofiber-embedded microchip for whole exome sequencing. *Advanced Materials, 25*(21), 2897–2902.
105. Xu, G., Tan, Y., Xu, T., Yin, D., Wang, M., Shen, M., Chen, X., Shi, X., & Zhu, X. (2017). Hyaluronic acid-functionalized electrospun PLGA nanofibers embedded in a microfluidic chip for cancer cell capture and culture. *Biomaterials Science, 5*(4), 752–761.
106. Jain, A., Betancur, M., Patel, G. D., Valmikinathan, C. M., Mukhatyar, V. J., Vakharia, A., Pai, S. B., Brahma, B., MacDonald, T. J., & Bellamkonda, R. V. (2014). Guiding intracortical brain tumour cells to an extracortical cytotoxic hydrogel using aligned polymeric nanofibres. *Nature Materials, 13*(3), 308–316.
107. Saha, S., Duan, X., Wu, L., Lo, P.-K., Chen, H., & Wang, Q. (2012). Electrospun fibrous scaffolds promote breast cancer cell alignment and epithelial–mesenchymal transition. *Langmuir, 28*(4), 2028–2034.
108. Paul, K. B., Singh, V., Vanjari, S. R. K., & Singh, S. G. (2017). One step biofunctionalized electrospun multiwalled carbon nanotubes embedded zinc oxide nanowire interface for highly sensitive detection of carcinoma antigen-125. *Biosensors and Bioelectronics, 88*, 144–152.
109. Ali, M. A., Mondal, K., Jiao, Y., Oren, S., Xu, Z., Sharma, A., & Dong, L. (2016). Microfluidic immuno-biochip for detection of breast cancer biomarkers using hierarchical composite of porous graphene and titanium dioxide nanofibers. *ACS Applied Materials & Interfaces, 8*(32), 20570–20582.

110. Ruman, U., Fakurazi, S., Masarudin, M. J., & Hussein, M. Z. (2020). Nanocarrier-based therapeutics and theranostics drug delivery systems for next generation of liver cancer nanodrug modalities. *International Journal of Nanomedicine, 15*, 1437.
111. Sasikala, A. R. K., Thomas, R. G., Unnithan, A. R., Saravanakumar, B., Jeong, Y. Y., Park, C. H., & Kim, C. S. (2016). Multifunctional nanocarpets for cancer theranostics: remotely controlled graphene nanoheaters for thermo-chemosensitisation and magnetic resonance imaging. *Scientific Reports, 6*, 20543.
112. Hou, Z., Li, C., Ma, P. A., Cheng, Z., Li, X., Zhang, X., Dai, Y., Yang, D., Lian, H., & Lin, J. (2012). Up-conversion luminescent and porous NaYF4: Yb3+, Er3+@ SiO2 nanocomposite fibers for anti-cancer drug delivery and cell imaging. *Advanced Functional Materials, 22*(13), 2713–2722.
113. Li, X., Wang, X., Zhao, C., Shao, L., Lu, J., Tong, Y., Chen, L., Cui, X., Sun, H., & Liu, J. (2019). From one to all: self-assembled theranostic nanoparticles for tumor-targeted imaging and programmed photoactive therapy. *Journal of Nanobiotechnology, 17*(1), 23.
114. Nam, S., Lee, S. Y., & Cho, H.-J. (2017). Phloretin-loaded fast dissolving nanofibers for the locoregional therapy of oral squamous cell carcinoma. *Journal of Colloid and Interface Science, 508*, 112–120.
115. Wang, J., Wang, G., Shan, H., Wang, X., Wang, C., Zhuang, X., Ding, J., & Chen, X. (2019). Gradiently degraded electrospun polyester scaffolds with cytostatic for urothelial carcinoma therapy. *Biomaterials Science, 7*(3), 963–974.
116. Xie, X., Zheng, X., Han, Z., Chen, Y., Zheng, Z., Zheng, B., He, X., Wang, Y., Kaplan, D. L., & Li, Y. (2018). A biodegradable stent with surface functionalization of combined-therapy drugs for colorectal cancer. *Advanced Healthcare Materials, 7*(24), 1801213.
117. Bonadies, I., Maglione, L., Ambrogi, V., Paccez, J. D., Zerbini, L. F., e Silva, L. F. R., Picanço, N. S., Tadei, W. P., Grafova, I., & Grafov, A. (2017). Electrospun core/shell nanofibers as designed devices for efficient artemisinin delivery. *European Polymer Journal, 89*, 211–220.
118. Xia, G., Zhang, H., Cheng, R., Wang, H., Song, Z., Deng, L., Huang, X., Santos, H. A., & Cui, W. (2018). Localized controlled delivery of gemcitabine via microsol electrospun fibers to prevent pancreatic cancer recurrence. *Advanced Healthcare Materials, 7*(18), 1800593.
119. Ramachandran, R., Junnuthula, V. R., Gowd, G. S., Ashokan, A., Thomas, J., Peethambaran, R., Thomas, A., Unni, A. K. K., Panikar, D., & Nair, S. V. (2017). Theranostic 3-dimensional nano brain-implant for prolonged and localized treatment of recurrent glioma. *Scientific Reports, 7*, 43271.
120. Yohe, S. T., Herrera, V. L., Colson, Y. L., & Grinstaff, M. W. (2012). 3D superhydrophobic electrospun meshes as reinforcement materials for sustained local drug delivery against colorectal cancer cells. *Journal of Controlled Release, 162*(1), 92–101.
121. Ferlay, J., Soerjomataram, I., & Ervik, M. (2013). *GLOBOCAN 2012 v1.0 Cancer incidence and mortality worldwide: IARC CancerBase no. 11 [internet]*. Lyon: International Agency for Research on Cancer.
122. Nadar, R. A., van den Beucken, J. J., & Leeuwenburgh, S. C. (2020). Pharmacological interventions targeting bone diseases in adjunction with bone grafting. In *Dental implants and bone grafts* (pp. 251–280). Amsterdam: Elsevier.
123. Herrmann, K., Schwaiger, M., Lewis, J. S., Solomon, S. B., McNeil, B. J., Baumann, M., Gambhir, S. S., Hricak, H., & Weissleder, R. (2020). Radiotheranostics: a roadmap for future development. *The Lancet Oncology, 21*(3), e146–e156.
124. Seidlin, S., Marinelli, L., & Oshry, E. (1946). Radioactive iodine therapy: effect on functioning metastases of adenocarcinoma of the thyroid. *Journal of the American Medical Association, 132*(14), 838–847.
125. Etchebehere, E., Brito, A. E., Rezaee, A., Langsteger, W., & Beheshti, M. (2017). Therapy assessment of bone metastatic disease in the era of 223 radium. *European Journal of Nuclear Medicine and Molecular Imaging, 44*(1), 84–96.

126. Qiao, H., Cui, Z., Yang, S., Ji, D., Wang, Y., Yang, Y., Han, X., Fan, Q., Qin, A., & Wang, T. (2017). Targeting osteocytes to attenuate early breast cancer bone metastasis by theranostic upconversion nanoparticles with responsive plumbagin release. *ACS Nano, 11*(7), 7259–7273.
127. Madav, Y., Barve, K., & Prabhakar, B. (2020). Current trends in theranostics for rheumatoid arthritis. *European Journal of Pharmaceutical Sciences, 145*, 105240.
128. Allender, S., Scarborough, P., Peto, V., Rayner, M., Leal, J., Luengo-Fernandez, R., & Gray, A. (2008). European cardiovascular disease statistics. *Eur Heart Netw, 3*, 11–35.
129. Nandwana, V., Ryoo, S.-R., Kanthala, S., McMahon, K. M., Rink, J. S., Li, Y., Venkatraman, S. S., Thaxton, C. S., & Dravid, V. P. (2017). High-density lipoprotein-like magnetic nanostructures (HDL-MNS): theranostic agents for cardiovascular disease. *Chemistry of Materials, 29*(5), 2276–2282.
130. McCarthy, J. R., Korngold, E., Weissleder, R., & Jaffer, F. A. (2010). A light-activated theranostic nanoagent for targeted macrophage ablation in inflammatory atherosclerosis. *Small, 6*(18), 2041–2049.
131. O'Brien, B., & Carroll, W. (2009). The evolution of cardiovascular stent materials and surfaces in response to clinical drivers: a review. *Acta Biomaterialia, 5*(4), 945–958.
132. Cyrus, T., Zhang, H., Allen, J. S., Williams, T. A., Hu, G., Caruthers, S. D., Wickline, S. A., & Lanza, G. M. (2008). Intramural delivery of rapamycin with αvβ3-targeted paramagnetic nanoparticles inhibits stenosis after balloon injury. *Arteriosclerosis, Thrombosis, and Vascular Biology, 28*(5), 820–826.
133. Chorny, M., Fishbein, I., Yellen, B. B., Alferiev, I. S., Bakay, M., Ganta, S., Adamo, R., Amiji, M., Friedman, G., & Levy, R. J. (2010). Targeting stents with local delivery of paclitaxel-loaded magnetic nanoparticles using uniform fields. *Proceedings of the National Academy of Sciences, 107*(18), 8346–8351.
134. Rentrop, K. P., & Feit, F. (2015). Reperfusion therapy for acute myocardial infarction: concepts and controversies from inception to acceptance. *American Heart Journal, 170*(5), 971–980.
135. Chen, H. H., Feng, Y., Zhang, M., Chao, W., Josephson, L., Shaw, S. Y., & Sosnovik, D. E. (2012). Protective effect of the apoptosis-sensing nanoparticle AnxCLIO-Cy5.5. *Nanomedicine: Nanotechnology, Biology and Medicine, 8*(3), 291–298.
136. Tang, J., Lobatto, M. E., Read, J. C., Mieszawska, A. J., Fayad, Z. A., & Mulder, W. J. (2012). Nanomedical theranostics in cardiovascular disease. *Curr Cardiovasc Imaging Rep, 5*(1), 19–25.
137. Kirsch-De Mesmaeker, A., Jacquet, L., & Nasielsi, J. (1988). Ruthenium(II) complexes of 1,4,5,8-tetraazaphenanthrene (TAP) and 2,2′-bipyridine (bpy). Ground- and excited-state basicities of Ru2+(bpy)n(TAP)3-n (n = 0,1,2): their luminescence quenching by organic buffers. *Inorganic Chemistry, 27*, 4451–4458.
138. Smitten, K. L., Fairbanks, S. D., Robertson, C. C., de la Serna, J. B., Foster, S. J., & Thomas, J. A. (2020). Ruthenium based antimicrobial theranostics–using nanoscopy to identify therapeutic targets and resistance mechanisms in Staphylococcus aureus. *Chemical Science, 11*(1), 70–79.
139. Zhao, Z., Yan, R., Yi, X., Li, J., Rao, J., Guo, Z., Yang, Y., Li, W., Li, Y.-Q., & Chen, C. (2017). Bacteria-activated theranostic nanoprobes against methicillin-resistant Staphylococcus aureus infection. *ACS Nano, 11*(5), 4428–4438.
140. Das, B., Dadhich, P., Pal, P., Thakur, S., Neogi, S., & Dhara, S. (2020). Carbon nano dot decorated copper nanowires for SERS-fluorescence dual-mode imaging/anti-microbial activity and enhanced angiogenic activity. *Spectrochimica Acta Part A: Molecular and Biomolecular Spectroscopy, 227*, 117669.

141. Dai, X., Fan, Z., Lu, Y., & Ray, P. C. (2013). Multifunctional nanoplatforms for targeted multidrug-resistant-bacteria theranostic applications. *ACS Applied Materials & Interfaces, 5* (21), 11348–11354.
142. Setyawati, M. I., Kutty, R. V., Tay, C. Y., Yuan, X., Xie, J., & Leong, D. T. (2014). Novel theranostic DNA nanoscaffolds for the simultaneous detection and killing of Escherichia coli and Staphylococcus aureus. *ACS Applied Materials & Interfaces, 6*(24), 21822–21831.
143. Ferreira, K., Hu, H. Y., Fetz, V., Prochnow, H., Rais, B., Müller, P. P., & Brönstrup, M. (2017). Multivalent siderophore–DOTAM conjugates as theranostics for imaging and treatment of bacterial infections. *Angewandte Chemie International Edition, 56*(28), 8272–8276.
144. He, X., Xiong, L.-H., Zhao, Z., Wang, Z., Luo, L., Lam, J. W. Y., Kwok, R. T. K., & Tang, B. Z. (2019). AIE-based theranostic systems for detection and killing of pathogens. *Theranostics, 9*(11), 3223.